AD_____

Award Number: DAMD17-96-1-6306

TITLE: Genetic and Dynamic Analyses of Murine Peak Bone Density

PRINCIPAL INVESTIGATOR: Wesley G. Beamer, Ph.D.

CONTRACTING ORGANIZATION: The Jackson Laboratory
Bar Harbor, Maine 04609-1500

REPORT DATE: October 2001

TYPE OF REPORT: Final

PREPARED FOR: U.S. Army Medical Research and Materiel Command
Fort Detrick, Maryland 21702-5012

REPORT DOCUMENTATION PAGE

Form Approved
OMB No. 074-0188

1. AGENCY USE ONLY (Leave blank)	2. REPORT DATE	3. REPORT TYPE AND DATES COVERED
	October 2001	Final (27 Sep 96 - 26 Sep 01)

4. TITLE AND SUBTITLE
Genetic and Dynamic Analyses of Murine Peak Bone Density

5. FUNDING NUMBERS
DAMD17-96-1-6306

6. AUTHOR(S)
Wesley G. Beamer, Ph.D.

7. PERFORMING ORGANIZATION NAME(S) AND ADDRESS(ES)
The Jackson Laboratory
Bar Harbor, Maine 04609-1500

E-Mail: wgb@jax.org

8. PERFORMING ORGANIZATION REPORT NUMBER

9. SPONSORING / MONITORING AGENCY NAME(S) AND ADDRESS(ES)
U.S. Army Medical Research and Materiel Command
Fort Detrick, Maryland 21702-5012

10. SPONSORING / MONITORING AGENCY REPORT NUMBER

11. SUPPLEMENTARY NOTES

12a. DISTRIBUTION / AVAILABILITY STATEMENT
Approved for Public Release; Distribution Unlimited

12b. DISTRIBUTION CODE

13. ABSTRACT ***(Maximum 200 Words)***

A comprehensive genetic assessment was undertaken for Quantitative Trait Loci (QTLs) that regulate acquisition of peak bone density using the low density C57BL/6J (B6) and the high density CAST/EiJ (CAST) and C3H/HeJ (C3H) inbred strains. Genome wide analyses of (B6 x CAST)F2 and (B6 x C3H)F2 progeny yielded 8 QTLs in the B6CAST-F2 F2 and 10 QTLs in the B6C3H-F2 progenies, respectively. Heritability of BMD ranged from 57 to 87%, demonstrating the strong genetic basis for this trait. Locations of the QTLs (LOD scores > 2.9) were established, major effects and modes of inheritance were established, and B6 background congenic strains were established to pursue biological and fine mapping/cloning of genes. Genes common to femurs and to vertebrae were found, in addition to genes unique to each bone site. Biological studies of the progenitor B6, C3H, and CAST inbred strains reveal that there are both formation and resorption processes actively in place that contribute to the differences in bone mineral density, microstructure and strength differences in these strains. Studies of QTL gene locations, structure, biomechanical, microarchitectural, and process of bone turn-over are currently being pursued as well as being planned for the future.

14. SUBJECT TERMS
Osteoporosis, Quantitative traits, Mouse

15. NUMBER OF PAGES
185

16. PRICE CODE

17. SECURITY CLASSIFICATION OF REPORT	18. SECURITY CLASSIFICATION OF THIS PAGE	19. SECURITY CLASSIFICATION OF ABSTRACT	20. LIMITATION OF ABSTRACT
Unclassified	Unclassified	Unclassified	Unlimited

Table of Contents

Page No.

Cover.....1

SF 298.....2

Table of Contents.....3

Introduction.....4

Body.....4

Key Research Accomplishments.....15

Reportable Outcomes.....15

Conclusions.....19

References.....19

Appendices.....20

Final Report

Introduction.

The subject of this research effort was to undertake genetic analyses of the acquisition of peak bone density that is recognized as an important predictor of osteoporotic fracture in humans. Given that these studies are extremely difficult in humans due to the need for prohibitively large populations of sib pairs, we utilized an animal model system consisting of low bone density C57BL/6J and high bone density C3H/HeJ inbred strains of mice. F2 progeny were produced and genome-wide analyses for genetic loci regulating bone mineral density of the femur and the vertebrae were conducted. Furthermore, numerous studies were conducted to establish the bone formation and bone resorption parameters that accounted for the differences in BMD of these two strains of mice. Homologous relationships between the genomes of humans and mice are being utilized to predict the location of human genes that might also regulate human BMD. Finally, new technologies associated with microarchitecture assessment and biomechanical tests of bone strength parameters are now a part of this on-going bone genetics research program. The details of our studies are summarized in the following text.

Body

Specific Aim A. To map genes that regulate the difference in peak bone density between C3H/HeJ (high BMD) and C57BL/6J (low BMD) inbred strains of mice.

Strategy for genetic analyses of BMD as a quantitative trait. Our genetic analyses utilized a variety of mating systems including F2 intercrosses, BXH RI strains, and congenic strains to locate QTLs responsible for differences in BMD between progenitor strains: B6, CAST, and C3H.

- Experiment 1: a (B6 x CAST)-F2 cross was undertaken to gain proof of principle that the complex phenotype of BMD could be successfully analyzed by quantitative trait analysis methods. Since B6 and CAST are known to be highly polymorphic (genomes 95% different), we predicted that genes would be easier to locate in this cross than between strains which are more closely related.
- Experiment 2: the B6 x C3H-F2 cross was undertaken to exploit the largest known difference (50%) in the BMD among inbred strains of mice that we surveyed.
- Experiment 3: the 12 existing BXH Recombinant Inbred (RI) strains, created for mapping traits driven by single polymorphic genes differing between B6 and C3H strains, were tested for BMD differences to determine the possibility of mapping major gene effects.
- Experiment 4: our newly developed congenic strains were tested for effects on BMD of different QTL alleles discovered in the B6CAST-F2 and in the B6C3H-F2 intercrosses.

Experiment 1. Proof of principle - B6CAST-F2 analyses. **Appendix 6.**

We established the polygenic nature and heritability (H^2 = 57%) of femoral BMD in F2 mice derived from intercross matings of (B6 x CAST)F1 parents. The B6 and CAST/Ei progenitors differ in body size, femur length and volume, and mid-diaphyseal circumference. Importantly, the cortical thickness was greater in CAST, resulting in more mineral per unit volume and 35% higher BMD than in B6. F1 hybrid BMDs are intermediate between the progenitors (**Table 1** below).

Developmental data for ages 2 to 24 months showed that femoral peak BMD was achieved by 4 months of age in the progenitor strains. Thus, F2 progeny were raised to 4 months of age, then femurs were isolated from females and BMD data were obtained by pQCT. (Jointly housed F2 males were lethally aggressive, and were not kept.) Genotype data were obtained from genomic DNA for the 19 autosomes by PCR assays for 127 selected polymorphic markers (4-9 markers, mean genetic interval, 12-13 cM/chromosome). Genome wide scans for correlation of genetic marker data with high or low BMD revealed loci on eight different chromosomes, four of which (Chrs 1, 5, 13, & 15) achieved conservative statistical criteria for suggestive (LOD score = 2.8) or significant (LOD score = 4.3) linkage with BMD (34). Main effects on BMD associated with marker having the highest LOD score on each of the 8 chromosomes are shown in **Figure 1** below.

Table 1. Data for femurs from B6, CAST, and F1 females aged 4 months. Total density data are for entire femur; periosteal circumference, cortical thickness, and cortical density data are from mid-point

of the diaphysis. Mean ± SEM; no. in ( ) = mice/group. Bold letter gives significance ($p < 0.05$) of CAST and F1 vs B6 (**a**), and then CAST vs F1(**b**).

Strain	Body wt. (g)	Femur length (mm)	Total femur BMD (mg/mm^3)	Periosteal circum. (mm)	----- Cortical ------ thickness (mm)	density (mg/mm^3)
B6 (14)	21.9 ± 0.8	16.03 ± 0.08	0.458 ± 0.004	4.862 ± 0.042	0.312 ± 0.003	0.663 ± 0.009
CAST (17)	15.7± 0.3^{a}	13.55 ± 0.09^{a}	0.616 ± 0.013^{a}	4.242 ± 0.033^{a}	0.406 ± 0.006^{a}	0.653 ± 0.005
F1 (8)	19.6± 0.3^{a,b}	15.76± 0.16^{a,b}	0.563± 0.006^{a,b}	4.540^{a,b}± 0.014	0.375± 0.003^{a,b}	0.675± 0.006^{a,b}

Figure 1 . Main effects on femoral BMD in B6CAST-F2 mice associated with homozygosity for CAST (*ca/ca*) or B6 (*b6/b6*) or with heterozygous allelic combination. Bold letters indicate if mean BMD for *ca/b6* (**a**) differed from *ca/ca* or if *b6/b6* (**b**) differed from *ca/ca* . MIT marker with greatest effect is shown in each graph and identifies the chromosomal location of the bone regulatory region.

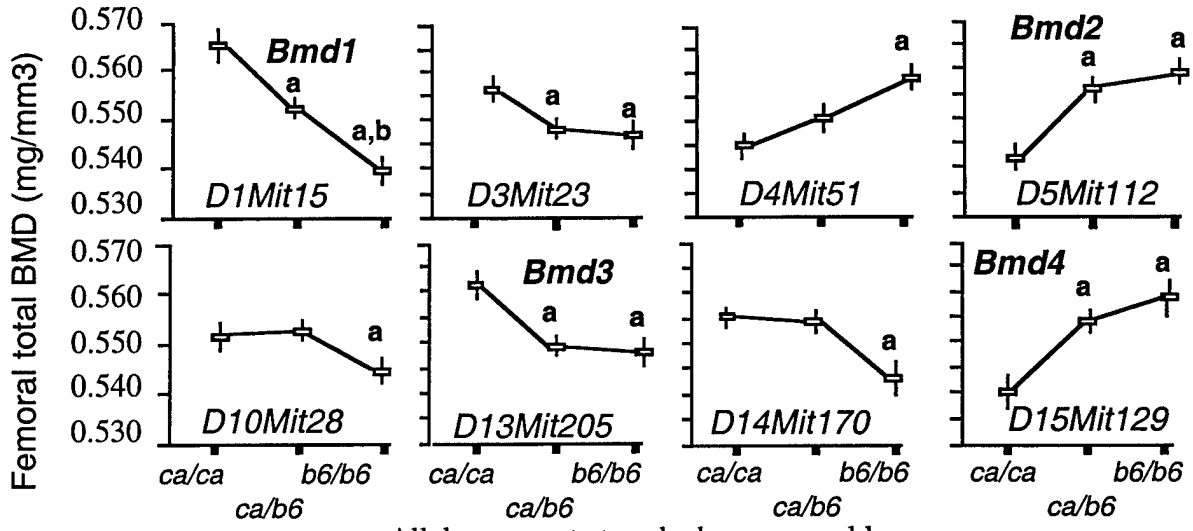

The four best QTLs were named *Bmd1* (Chr 1), *Bmd2* (Chr 5), *Bmd3* (Chr 13), and *Bmd4* (Chr 15). Additive effects were observed for *Bmd1*, recessive for *Bmd3* and dominant effects for *Bmd2* and *Bmd4*. The low BMD B6 strain contributed alleles (*b6*) on Chrs 4, 5, and 15 that increased BMD! None of the 4 named *Bmd* loci exhibited significant pairwise interaction effects detectable by ANOVA, and the summed QTL variances explained a moderate 13.1% of the F2 population variance in BMD. The chromosomal regions represented by the 4 *Bmd* QTLs share homologous linkage relationships with several human chromosomal regions (e.g., *D1Mit15* with 1q21-42). We recognize that mouse regions must be reduced from current size of 6-31 cM with as many as 2000 genes before pursuit of candidate genes is justified. Thus, the B6CAST-F2 progeny provided proof-of-principle for the QTL analytic approach, revealing at least 4 to 8 loci regulating BMD in this cross.

Experiment 2: B6C3H-F2 analyses.

Among the 33 inbred strains examined to date, the B6 and C3H strains differ the most in pQCT BMD due to increased mineral content and size of the cortical compartment **Appendix 12**. In young adults, the C3H femur is 50% more dense than B6, while the C3H vertebra is a moderate 9% greater in density. Body weights and femur dimensions are similar, whereas the C3H vertebrae are approximately one-third larger than B6. Data from four month old B6, C3H, and F1 hybrid females are shown in **Tables 2A & B**. In addition, the remaining isolated lumbar spinal columns (L2-L4) were assessed by DEXA using a PIXImus instrument (LUNAR Corp., Madison, WI) to obtain QTL data for areal BMD for comparison with the pQCT volumetric BMD data.

Table 2A. C3H, B6, and F1 data from 4 month old females. Length and density for the entire femur. Periosteal, cortical thickness, and cortical density data are from the mid-diaphysis. Mean ± SEM; bold letter gives significance ($p < 0.05$) of C3H and F1 vs B6 (**a**), and then C3H vs F1(**b**).

Strain (n)	Body wt. (g)	femur length (mm)	Femoral total BMD (mg/mm^3)	periosteal circum. (mm)	cortical thickness (mm)	cortical density (mg/mm^3)
B6 (8)	22.64±0.46	15.54±0.05	0.487±0.005	4.720±0.021	0.312±0.003	0.616±0.004
C3H (8)	23.06±1.89	15.24±0.14**a**	0.738±0.006**a**	4.384±0.013**a**	0.509±0.008**a**	0.781±0.006**a**
F1 (10)	27.48±0.58**a,b**	16.3 ±0.78**a,b**	0.614±0.006**a,b**	4.488±0.069**a,b**	0.388±0.002**a,b**	0.714±0.003**a,b**

Table 2B. pQCT data for lumbar vertebrae (L5) from C3H, B6, and F1 females from lumbar L5 vertebrae. Areal BMD (DEXA) are from L2-L4. Mean ± SEM; no. in ( ) = mice/group. Mean ± SEM; bold letter gives significance ($p < 0.05$) of C3H and F1 vs B6 (**a**), and then C3H vs F1(**b**).

Mouse strain	total L5 mineral (mg)	total L5 volume (mm^3)	total L5 density (mg/mm^3)	Cortical mineral (mg)	Areal BMD (g/cm^2)	Areal BMC (g)
B6 (8)	3.80±0.07	13.69±0.23	0.278±0.003	1.65±0.06	0.056±0.002	0.015±0.001
C3H (12)	5.69±0.18**a**	18.82±0.47**a**	0.302±0.003**a**	3.16±0.16**a**	0.066±0.001**a**	0.018±0.001**a**
F1 (8)	5.22±0.18**a,b**	16.74±0.44**a,b**	0.312±0.004**b**	2.85±0.15**a,b**	nd	nd

Developmental data from 1-24 months of age showed that both peak femoral and vertebral BMDs were achieved by four months in progenitor strains. Accordingly, 1000 F2 females were bred, aged to four months, necropsied to obtain femurs and vertebrae, then BMD measured by pQCT and DEXA. Heritability (h^2) calculations for pQCT BMD yielded estimates of 83% for femurs and 87% for vertebrae. Genotype data were obtained for the 19 autosomes by screening F2 progeny for 110 PCR-based SSLP markers discriminating B6 and C3H alleles (methodology detailed in Appendices 5 & 9). The results of the genome wide scan for each chromosome, with critical thresholds for 'p' levels of 0.05 and 0.01 corrected for multiple tests, are presented for femoral and vertebral BMD in **Figure 2A** and **B**.

Figure 2. Genome wide scan for femoral BMD QTLs (**A**) and vertebral BMD QTLs (**B**).

These complex scans are best viewed in **Appendix 12.**

Genetic analyses of pQCT data: The summary of best markers and LOD scores from those genetic analyses for femur and vertebral density data are found in **Table 3** below. We found femoral BMD QTLs on 9 chromosomes (signif. linkage -> Chrs 1, 4, 6, 11, 13, 14, 16, 18; suggest. linkage -> Chr 12) contributing to differences between B6 and C3H mice. This rich array of loci was further increased by Chrs 1 and 13, each of which has two QTLs for femoral BMD separated by 45 and 20 cM, respectively. We found vertebral BMD QTLs on 7 chromosomes (signif. linkage -> Chrs 1, 4, 7, 9, 14, 18; suggest. linkage -> Chr 11) contribute to differences between B6 and C3H mice. The best markers on Chrs 1, 4, 13, 14, and 18 were common to both femur and vertebral sites, while Chrs 6, 11, 12 and 16 were unique to femurs, and Chrs 7 and 9 were unique to the vertebrae. The second femoral QTLs on Chr 1 and 13 were not detected at any level of significance for vertebrae.

Genetic analysis of DEXA PIXImus data. The genetic analysis of spinal data obtained by PIXImus revealed QTLs on 5 Chrs (significant linkage -> Chrs 1, 4, 14, 18; suggestive linkage -> Chr 16) contributing to areal density differences between B6 and C3H mice. Four of the five DEXA QTLs were common to those detected for vertebrae by pQCT, indicative of excellent agreement between measurement systems when the phenotypic differences are large enough. The vertebral QTLs detected on Chr 7, 9, and 13 with pQCT data were not detected by DEXA measurements.

Table 3. Summary of genome wide scans of B6C3H-F2 mice for density QTLs. Femoral and L5 vertebral volumetric BMD obtained by pQCT; lumbar spine areal BMD by DEXA PIXImus. LOD scores are given for the best marker (LOD score > 2.8 suggestive linkage; >4.3 significant linkage). ns = not significant.

Chromosome and locus	MGD map position (cM)	F-BMD LOD score	% variance	V-BMD LOD score	% variance	DEXA spine LOD score
Major QTLs						
D1Mit282	36.9	11.0	--	ns	--	ns
D1Mit14	81.6	20.3	10.3	12.5	5.8	8.3
D4Mit124	57.4	16.5	7.5	13.8	6.7	15.0
D18Mit36	24.0	13.1	6.0	4.0	6.9	5.3
Minor QTLs						
D6Mit150	51.0	4.6	2.4	ns	--	ns
D7Mit332	65.6	ns	--	6.5	2.4	ns
D9Mit196	48.0	ns	--	4.0	2.5	ns
D11Mit242	31.0	6.3	3.2	ns	ns	ns
D12Mit215	2.0	3.6	1.5	ns	ns	ns
D13Mit266	16.0	6.4	--	ns	ns	ns
D13Mit13	35.0	9.0	3.0	2.9	ns	ns
D14Mit160	40.0	4.4	2.0	4.1	2.5	6.9
D16Mit12	27.6	4.3	2.0	ns	--	2.8

Collectively, the 9 femoral QTLs accounted for 37.9% of the F2 femur BMD variance, with the major QTLs on Chrs 1, 4, and 18 accounting for nearly 2/3 of that population variance. Likewise, the 7 vertebral QTLs accounted for 25.6% of the F2 vertebral BMD variance, with the best QTLs on Chrs 1, 4, and 18 accounting for 3/4 of that population variance. As was true for the B6CAST-F2 data, extensive pairwise marker analyses by ANOVA for interaction between loci was remarkable in that no significant interactions among QTLs for either bone site were detected. From a statistical perspective, femoral and vertebral BMD result from the sum of the individual effects of alleles at each locus.

Analyses of allele effects. The main effects of alleles for each QTL found in the B6C3H-F2 progeny proved predominantly additive, since the *b6/c3* allelic combination was intermediate in BMD and significantly different from either homozygous combination (*b6/b6* or *c3/c3*). Exceptions appeared to be Chr 12 (*D12Mit215*) and Chr 16 (*D16Mit12*), where C3H alleles acted in a recessive manner. Only two of the QTLs, Chr 6 and 12, decreased femoral BMD as the number of C3H alleles increased, whereas for each of the other QTLs C3H alleles increased BMD. Graphs, in descending size of the QTL LOD score, depicting each QTL's effects are shown in **Figure 3** shown on the next page, along with the proposed names of each QTL (*Bmd*).

Figure 3. Main effects of QTLs on femoral BMD in F2 progeny; LOD scores > 3.6. Mean values are indicated by filled circles; SEM varied from 0.4-0.5% of the means and are not shown. Letters indicate comparison ($p < 0.005$), **a** = signif. differ. from *b6/b6* and **b** signif. differ from *b6/c3*.

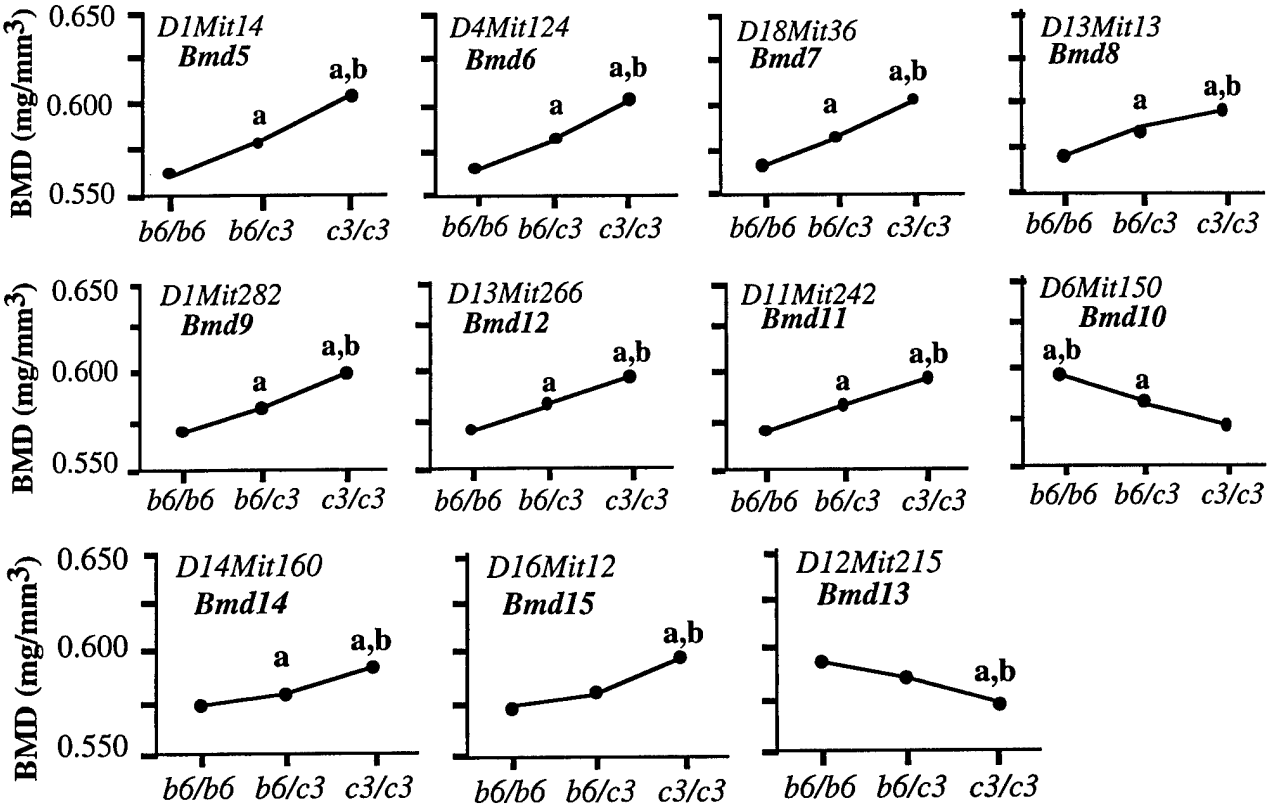

Alleles at each chromosomal locus

Benefits & limitations of QTL analyses. QTL analyses yield insights about the number of genes supporting BMD, identify regions likely to contain BMD loci (95% confidence intervals), and lead to the estimated variance of BMD for which these loci can account. Although this approach will not identify candidate genes because the markers are surrogates and rarely lie within a gene, further genetic manipulations can narrow QTL regions in preparation for candidate gene analyses, as well as for cloning. One must be aware that LOD scores assess strength of association between genetic markers and BMD, and not a QTL's effect on BMD. Better mathematical tools are needed to address multigenic interactions and to discriminate whether more than one locus resides within a QTL region. An important issue is the likelihood that Type II errors associated with the stringent significance levels proposed by Lander and Kruglyak (1995), leading to incomplete appreciation of the genes supporting a polygenic trait. An example of this is addressed below in the discussion of the congenic strains. Nevertheless, given substantial F2 intercross progenies, the QTL methodology has provided insights and knowledge of BMD genetics not addressable by any other method and pointed toward fruitful directions of discovery.

Experiment 3: BXH RI strain analyses. **Appendix 19.** The second form of genetic cross proposed for analyses of BMD loci was the BXH Recombinant Inbred (RI) strains. This set of 12 inbred strains was derived from intercrosses of (B6 x C3H)F1 parents to produce F2 progeny, then inbreeding individual F2 x F2 matings to obtain new strains of mice. At F20, each is a new strain with half of its genome from B6 and half from C3H, and each new strain has a different combination of genes from the B6 and C3H progenitors. The BXH RI have been typed by other laboratories for more than 600 polymorphic genes and SSLPs representing all autosomes and sex chromosomes. In theory, any trait dependent on 1-2 genes that differs between B6 and C3H can be quickly mapped to a chromosome by phenotyping a few mice from each BXH RI strain to obtain the strain distribution pattern (SDP). This new pattern is compared to all other SDPs for genes of known chromosomal location to find the linkage.

Virgin BXH RI strain females with mature bone density were necropsied at 8 months to obtain femurs and vertebrae. Femurs were isolated and measured in groups of 6-14 females by pQCT for

density and linear properties described for B6C3H-F2 progeny.

Results. Data are summarized in **Table 4** below, wherein mean values for RI strains are compared with the progenitors. Body weights and femur lengths were similar for B6 and C3H. In contrast, five of the RI strains had lower body weights than B6, and many of the RI strains had shorter femurs than either progenitor. As expected, the B6 and C3H progenitors differed for femur and vertebral BMD. All BXH RI means for femur BMD were intermediate between B6 and C3H. On the other hand, vertebral BMD displayed a broad range of values that were lower, intermediate or higher than the B6 and C3H progenitors. Only the high femur density of C3H was not recapitulated in at least one of the BXH RI strains. BXH-2 developed early leukemia and have been excluded from the table.

Table 4. Body weight, femoral and vertebral pQCT parameters from B6, C3H, and BXH R I strains. Mean ± SEM (n= 6-14 mice/group); **b** = different from B6, **h** = different from C3H ($p < 0.01$).

Strain	Body Weight (g)	Length (mm)	Femur BMD (mg/mm3)	Vertebral BMD (mg/mm3)
Progenitors				
B6	28.2±0.9	16.9±0.2	0.459±0.009**h**	0.228±0.007**h**
C3H	31.9±3.9	16.6±0.1	0.680±0.010**b**	0.240±0.007**b**
BXH RI strains				
-3	25.6±1.0**h,h**	16.0±0.1**b,h**	0.511±0.013**b,h**	0.189±0.008**b,h**
-4	31.4±1.3**b**	17.2±0.1**h**	0.601±0.006**b,h**	0.246±0.008
-6	25.7±1.3**b,h**	16.0±0.1**b,h**	0.602±0.012**b,h**	0.220±0.006
-7	26.9±2.3	15.9±0.1**b,h**	0.524±0.012**b,h**	0.200±0.009**b,h**
-8	24.3±1.3**b,h**	16.1±0.1**b,h**	0.548±0.016**b,h**	0.213±0.007**b,h**
-9	31.9±1.9	16.4±0.1**b**	0.585±0.007**b,h**	0.229±0.006
-10	26.6±0.7**h**	15.1±0.1**b,h**	0.551±0.004**b,h**	0.188±0.004**b,h**
-11	24.5±1.8**b,h**	16.4±0.1**h**	0.522±0.008**b,h**	0.189±0.005**b,h**
-12	28.9±2.5	16.0±0.1**h**	0.594±0.008**b,h**	0.226±0.007
-14	27.4±1.5**h**	16.5±0.1**h**	0.613±0.013**b,h**	0.279±0.010**b,h**
-19	21.7±0.4**b,h**	16.2±0.1**b,h**	0.604±0.008**b,h**	0.256±0.010B

The traits of femoral and vertebral BMD are demonstrably inherited among the BXH RI strains, with each bone displaying different inheritance patterns. However, genetic linkage analysis with these BXH RI strain data was not pursued. Clearly, these phenotypes did not segregate in the BXH RI strains as either B6-like or C3H-like, but rather as complex traits with numerous genetic determinants. With respect to femoral BMD, failure to identify a BXH RI strain with a C3H-like femur density meant that there were not enough RI strains for the unique combination of genetic alleles for C3H-like BMD to be reassembled in a single 'new' strain. Assigning RI strains to phenotypic classes necessarily would be based on subjective (e.g., intermediate high; extremely low) rather than objective criteria (strain mean BMD). In essence, this limited set of 12 RI strains is not optimum for such a polygenic trait. This point is reinforced by the data presented above for the B6C3H-F2 progeny indicating that 9 to 11 QTLs support the femoral BMD difference between B6 and C3H mice.

However, there are two BXH RI strains that allow us to reduce the size of the Chr 1 QTL region (**Figure 4** below). The net effect of QTLs on Chr 1, 4, 6, and 18 on femoral BMD was examined for BXH-3 and BXH-19 strains. These strains were chosen because BXH-3 has the lower part of Chr 1 QTL region homozygous for C3H whereas BXH-19 has the upper part of Chr 1 QTL region homozygous for C3H. Published Strain Distribution Pattern (SDP) data for polymorphic loci were used to define whether C3H or B6 genes were predominant in the QTL regions on Chr 1, 4, 6, and 18. The stick diagrams below show that BXH-3 and BXH-19 both have similar SDPs on Chr 6 and on Chr 18, whereas BXH-3 differs from BXH-19 by the absence of C3H genes in the critical region of the Chr 4 BMD QTL. Although it is tempting to suggest that the femur BMD of BXH-3 (0.511±0.013) is lower than in BXH-19 (0.604±0.008) because of the differences in alleles at Chr 1 QTL, the difference is better explained by the presence of C3H alleles in the Chr 4 QTL region. If the bone regulatory gene resides in the distal part of the Chr 1 QTL in BXH-3, then addition of these 4

QTL effects (7% + 0% + 0% + 3.1% = 10.1%) should, and does, approximate the 11.3% difference between BXH-3 and B6 (see Table 4 above). In contrast, if the bone regulatory gene is in the proximal region of the Chr 1 QTL in BXH-19, then addition of these 4 QTL effects (7% + 8.9% + 0% + 3.1% = 19%) should, but does not, approximate the 31.6% difference between BXH-19 and B6 (see Table 4 above). Thus, comparison of BMDs between BXH-3 and BXH-19 predicts that the bone regulatory gene in Chr 1 QTL region is in the distal part bounded by markers *D1Mit217or 416* (63.1 cM) and *D1Mit14* (81.6 cM). The BXH RI strain data has allowed us to reduce the size of the Chr 1 QTL region from 40 to 20 cM. The distal location of the Chr 1 QTL was predicted by the original B6C3H-F2 study (distal marker had greatest LOD score) and confirmed by the BXH-19 data. Unfortunately, there are no BXH RI strains suitable for similar analyses of the QTL regions on Chr 4, 6, or 18.

Figure 4. The B6.C3H-1 congenic region (all C3H alleles) compared with the regions of Chrs-1, -4, -6, and -18 in BXH-3 and BXH-19 strains and their strain distribution patterns of C3H genes in the regions with BMD QTLs.

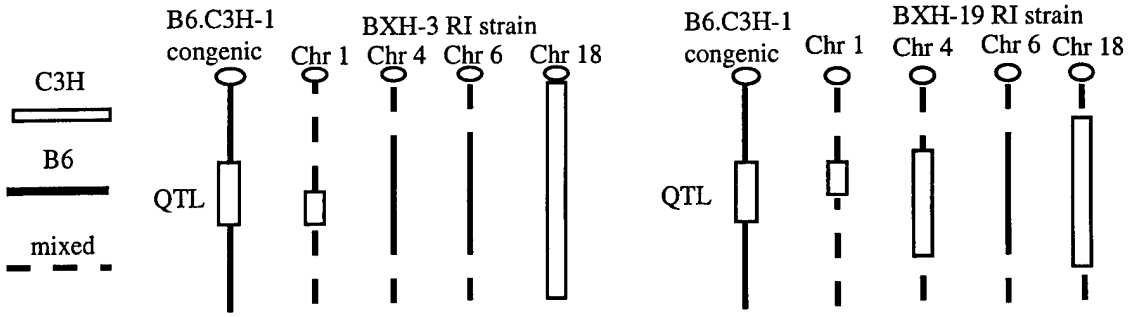

Experiment 4: Congenic strains. Recombinant Congenic strains were originally proposed for testing putative QTLs associated with BMD identified in F2 analyses, assuming that small sets of QTLs might be required to detect differences in BMD. A simpler, less complex alternative is that of congenic strains, each of which carries a single chromosomal region-containing a density regulatory locus donated from another strain. We have chosen the latter approach to isolate QTLs and to define their biological contributions.

Preliminary femoral genetic analyses were utilized for choosing chromosomes with BMD QTLs suitable for congenic strain development. The congenic strains were developed: a) to prove that BMD QTLs contained biologically active genes, b) to determine if predictions from B6C3H-F2 data for relationships between statistical LOD scores and biological effects, direction of allele effects, and modes of action would be born out in phenotypic data, and c) for fine mapping of each BMD QTL. Congenic strains were made by crossing either CAST (Chr 1, 3, 5, 13, & 14) or C3H (Chr 1, 4, 6, 11, 13, & 18) QTL regions into the B6 strain with 6 cycles of backcrossing (N6F1). The choice of B6 as the recipient background was based upon ensuring comparability of data from both B6.CAST and B6.C3H congenic strains, and initial uncertainty about whether a strain could have a lower BMD than B6 and remain healthy and viable. CAST or C3H donor chromosomal segments were followed by flanking polymorphic SSLP markers during the backcrossing procedure. Then (N6F1 x N6F1) matings produced N6F2 littermate mice that were genotyped to identify homozygotes for: a) CAST (*ca/ca*) or B6 (*b6/b6*), and b) C3H (*c3/c3*) or B6 (*b6/b6*) in the donated chromosomal segments. Heterozygous progeny were not retained for testing. At 4 months of age, F2 mice were necropsied for tissue and bone specimens. Results for femoral BMD are in **Table 5A** and **B** on the next page.

Table 5A. Femur data for female B6.CAST congenic strains (n = 11-18/ group); **a** = 'p' < 0.05

Congenic strain	Alleles present	Body wt (g)	Length (mm)	Total density (mg/mm3)	% diff. in BMD
B6.CAST-1	*ca/ca*	20.7±0.5	15.5±0.1	0.536±0.007[a]	8.1%
	b6/b6	21.8±0.8	15.4±0.2	0.496±0.006	
B6.CAST-3	*ca/ca*	21.1±0.2	15.2±0.1	0.508±0.005[a]	2.8%
	b6/b6	20.8±0.5	15.3±0.1	0.494±0.003	
B6.CAST-5	*ca/ca*	21.9±0.6	15.4±0.2	0.455±0.006[a]	-4.8%
	b6/b6	21.9±0.4	15.4±0.1	0.478±0.004	
B6.CAST-13	*ca/ca*	21.4±0.5	16.0±0.1[a]	0.506±0.008[a]	3.3%
	b6/b6	20.8±0.5	15.4±0.1	0.489±0.004	
B6.CAST-14	*ca/ca*	19.7±0.3[a]	15.7±0.1	0.513±0.005[a]	5.6%
	b6/b6	21.1±0.4	15.7±0.1	0.486±0.006	

We found significant alterations in femoral BMD in each of the B6.CAST congenic strains. CAST alleles were dominant to B6 for Chr 1, 3, 13, and 14, increasing BMD by 2.8 to 8.1%. On the other hand, B6 alleles were dominant to CAST for Chr 5, increasing BMD; a result predicted from the F2 analyses (see **Fig 1** above). The B6.CAST-3 congenic is valuable because the femoral QTL on Chr 3 did not achieve statistical significance by strict criteria. Nevertheless, the congenic BMD argues for a real gene on Chr 3 that increases femoral density when CAST alleles are present. Body weights were constant and B6-like, except for a small decline in B6.CAST-14. A small increase in femur length of B6.CAST-13 mice occurred when *ca/ca* alleles were present. Interestingly, vertebral BMD means were not different for B6 and CAST mice at either 4 or 12 months of age. Vertebral data for the B6.CAST congenics have not yet been acquired. It is unknown whether any of the QTLs for femoral BMD discovered in the B6CAST-F2 analyses will also affect vertebral BMD values.

Table 5B. B6.C3H female congenic data at 4 months of age (n = 10-16 per group); * ='p' < 0.01

Congenic strain	Alleles present	Body wt (g)	Length (mm)	Femoral BMD (mg/mm3)	% diff. in BMD	Vertebral BMD	% diff. in BMD
B6.C3H-1	*c3/c3*	23.2±0.7*	15.3±0.2	0.507±0.007*	7.0%	0.245±0.006	7.5%
	b6/b6	20.3±0.9	14.8±0.2	0.474±0.005		0.228±0.008	(p = .077)
B6.C3H-4T	*c3/c3*	21.8±0.5	15.8±0.1*	0.527±0.012*	8.9%	0.251±0.004*	7.5%
	b6/b6	22.2±0.7	15.4±0.1	0.484±0.004		0.236±0.005	(p = .012)
B6.C3H-4A	*c3/c3*	21.6±0.3	15.6±0.1	0.513±0.004*	2.4%	0.253±0.003*	8.6%
	b6/b6	22.7±0.6	15.6±0.1	0.501±0.005		0.233±0.005	(p = .001)
B6.C3H-6	*3/c3*	19.9±0.4*	14.8±0.1	0.470±0.005*	-3.4%	0.212±0.004*	-6.1%
	b6/b6	22.8±0.8	15.3±0.1	0.486±0.006		0.227±0.004	(p = .009)
B6.C3H-13	*c3/c3*	21.9±0.9	15.3±0.1*	0.505±0.005*	4.1%	0.237±0.005	4.9%
	b6/b6	22.0±0.6	15.6±0.1	0.485±0.004		0.226±0.006	(p = .182)
B6.C3H-18	*c3/c3*	22.8±0.7*	15.5±0.2	0.505±0.006*	3.1%	0.249±0.008	5.5%
	b6/b6	20.6±0.7	15.2±0.2	0.490±0.005		0.236±0.004	(p = .147)

Significant alterations in femoral BMD were found when C3H alleles for QTLs were transferred into the B6 background. C3H alleles for Chr 1, 4T, 4A, 13, and 18 QTLs increased BMD in the B6 background. On the other hand, the C3H alleles for the QTL on Chr 6 significantly reduced femoral BMD. This result was also predicted from the main effects analyses in the B6C3H-F2 progeny (**Figure 3 above**). The percent changes in femoral BMD ranged from 2.4 to 8.9% and were similar

to those observed for the B6.CAST congenics. With respect to vertebral BMD, we found that C3H alleles for the QTLs on Chrs 4 (T and A) increased L5 BMD, whereas chr 6 significantly decreased densities. C3H alleles in Chr 1 nearly achieved significance, whereas Chr 13 and 18 did not. Again, the variation in vertebral BMD among *b6/b6* littermate groups was not significant by ANOVA test.

We noted that the mean femoral BMD values of the *b6/b6* littermates in each of the 11 congenic strain sets varied from 0.474 to 0.501 mg/mm^3; ANOVA did not reveal a significant 'treatment' effect. From archival data on 12 sets of B6 female femurs, 4-5 months old, the grand mean±SEM was 0.485±0.004 mg/mm^3 (min. value = 0.476, max. value = 0.505). It is possible that the variation in control groups may be due to residual modifier loci linked to the transferred QTLs, modifying genes in the B6 background, gene-environmental interactions, or multiple gene interactions for which adequate statistical tools are lacking. Likewise, we are cognizant of experimental error that may be induced by machine variation, operator actions, etc. Nevertheless, we believe that the variation in BMD of the *b6/b6* genotype littermates noted among the congenics is most likely a sampling issue, and that littermate controls accurately reveal QTL effects.

The two sets of F2 mice show femoral BMD QTLs on Chrs 1, 4, 13, and 14, raising the question, "Are these the same genes?" Although we do not yet have definitive data to answer this question, the BMD QTL 1 regions do not overlap and thus represent separate loci. On the other hand, the QTL regions for Chrs 4, 13, and 14 do overlap sufficiently such that B6, CAST, and C3H could have unique alleles at each of these bone regulatory loci. In this application, we will concentrate resources and efforts on the B6.C3H congenic strains as the most judicious choice to capitalize on preliminary data and publications.

In summary, our genetic analyses have demonstrated: 1) BMD is a polygenic trait with a substantial number of genes supporting this bone parameter; 2) many of the individual QTLs are sufficiently strong, biologically, to change density if introduced one at a time into a suitable genetic background; 3) alleles may be additive or dominant recessive in actions; 4) the adult peak bone density in a given strain is the net result of QTLs with both positive and negative effects on BMD; 5) there appear to be QTLs acting on multiple bone sites, as well as QTLs with site specific effects; and 6) the congenics are going to be powerful tools for biological investigation of bone as well as fine mapping and candidate gene testing.

Specific Aim B. To identify the bone modeling mechanisms that characterize the skeletal phenotypes of C57BL/6J and C3H/HeJ mice. The goal of the following studies was to determine what biochemical mechanisms contribute to the BMD differences between B6 and C3H during development.

DEVELOPMENT OF BMD DIFFERENCE BETWEEN B6 AND C3H MICE

We previously established that the acquisition of peak bone density typically occurs by 4 months of age across many inbred strains of mice, and capitalized upon that feature for the genetic studies outlined above. Two studies were undertaken to define the development of adult bone: a) initially, between 4 and 26 weeks of age, b) then, from 1 to 8 weeks of age to conduct more detailed examination of changes associated with puberty.

• Development of adult BMD. Fundamental measurements of bone size and formation rates were gathered at 4, 8, 12, 16 and 26 weeks of age via histomorphometry on dual tetracycline labeled, undecalcified sections from tibias and femurs harvested from both B6 and C3H females. We found that at all ages: a) C3H had a greater bone formation rates at the periosteal and, especially, at endosteal surfaces when compared to B6, b) C3H acquired a greater cortical bone area in both tibia and femur sites, and c) C3H had smaller medullary cross-sectional areas (**Appendix 5**). The greater cortical bone compartment is one major reason for the increased BMD in C3H mice. These differences (**Figure 5**) were interpreted to be the consequences of genetic differences between the two strains, making this a suitable system for analyses of genes regulating bone formation rates.

Figure 5 **A-D** Standard light and fluorescent microscopic images of mid-diaphyseal sections of femurs from C3H and B6 females at 2 month of age.

These images are found in Sheng et al (**Appendix 5**)

• Development of BMD during puberty. The follow-up study then focused on differences between B6 and C3H strains in bone formation rates during the pubertal growth (**Appendices 9, 10**). Volumetric and geometric parameters were measured at the femoral mid-diaphyses, plus biochemical markers of bone turnover were measured in B6 and C3H mouse serum and bone extracts at weekly intervals from 1-8 weeks of age by Richman et al. (2000). Morphologic parameters indicated that the periosteal circumference at the mid-diaphysis changed in a similar fashion and was not different between the two strains of mice through 8 weeks. On the other hand, the cortical thickness increased much faster in C3H femurs than in B6 femurs. The data further showed that C3H mice began to acquire bone mineral earlier and faster than the age-matched B6 mice. Serum alkaline phosphatase, IGF-I, and osteocalcin were found to be higher in C3H compared with B6 at most all of the ages examined. Bone osteocalcin levels in extracts were less clearly associated with increasing mineral in the two strains. These findings point to increased endosteal bone formation, but not decreased bone resorption, as a major contributor to the higher BMD in C3H compared with B6 mice.

DEMONSTRATION OF ENHANCED BONE FORMATION RATES IN C3H MICE

The outcome of our developmental studies called for more detailed analyses of biochemical correlates indicative of bone formation as well as investigation of stimuli that may be critical to higher formation rates in C3H compared with B6 mice.

• Serum and skeletal IGF-I. An important first study into a mechanism associated with increased bone mass in C3H was to determine if circulating and skeletal IGF-I levels were greater than in B6. Rosen et al. (1997-98; 2000) (**Appendices 1,2,11**) demonstrated that C3H mice had significantly higher serum IGF-I compared with B6 from 1 through 10 months of age (i.e., at 4 month, C3H = 525±22 and B6 = 350±15 ng/ml). Serum IGF-I levels in F1 hybrids were intermediate between C3H and B6, while IGF-I serum levels in small groups of F2 mice correlated with high or low BMD. Conditioned media from B6 and C3H neonatal calvarial cells showed low and high IGF-I levels respectively, as did skeletal extracts from B6 and C3H mice. Finally, serum alkaline phosphatase (ALP) - a good marker of bone formation - was significantly higher in C3H versus B6, and serum ALP levels correlated well with increasing serum IGF-I levels. Thus, evidence of increased bone formation in C3H is in hand, and a possible mechanism contributing to the differences in peak BMD could be related to synthesis of IGF-I.

• Osteoprogenitor cells and ALP. We investigated the hypothesis that the increased BMD in C3H was a response to increased bone formation (**Appendix 3**). Accordingly, increased numbers of osteoprogenitor cells as well as ALP were correlated with the enhanced peak BMD in C3H vs B6 mice. Serum ALP levels again were higher in C3H compared with B6 at 6 (118 vs 100 u/L) and 32 (22.2 vs 17.2 U/L) weeks of age. A similar increase in ALP levels in conditioned media from C3H vs B6 bone organ and single cell cultures was also observed. Furthermore, increased ALP-positive CFU production from C3H vs B6 bone marrow stromal cell cultures was observed at 6 and 14 weeks of donor age. These data support the concept that enhanced bone formation is a major contributor to the high BMD of C3H mice.

BONE RESORPTION DIFFERS IN B6 AND C3H MICE

It is important to recognize that the B6 and C3H mice may reveal independent mechanisms resulting in their respective low or high BMDs. The genetic analyses cited above unquestionably supports the polygenic nature of BMD, hence multiple points of regulation. Two studies aimed at bone resorption functions in B6 and C3H yielded somewhat differing conclusions that need resolution.

• Osteoclast number and activity. We examined the hypothesis that bone resorption might be greater in B6 than in C3H mice by TRAP staining and counts of multi-nucleated cells (**Appendix 3**). Linkhart et al. showed that osteoclast numbers on bone surfaces of the distal humerus secondary spongiosa was 2-fold higher in pubertal B6 than in age matched C3H mice. In addition, B6 bone marrow derived cells co-cultured with Swiss Webster osteoblasts consistently generated more osteoclasts than did C3H bone marrow cells cultured in a like fashion. Spleen cultures from B6 also formed more osteoclasts than spleens from C3H mice. Reciprocal co-cultures with marrow and calvarial osteoblast cells from B6 and C3H mice did not indicate that osteoblast source affected the numbers of osteoclasts formed from marrow cells. Importantly, the B6 bone marrow cells formed 2.5-fold more pits on dentin slices than did such cells from C3H mice. These data suggest that genes

affecting bone marrow osteoclast precursor population number and activity may contribute to BMD differences between B6 and C3H mice.

• Osteoprotegerin (OPG) and osteoprotegerin-ligand (OPG-L). Alternatively, new data on osteoclastogenesis has recently come to light that may bear directly upon the difference in bone mass between B6 and C3H mice (Janet Rubin, et al. ASBMR Ann. Mtng. abst, Toronto 2000). The slow bone resorption of C3H was investigated by preparing marrow stromal cell cultures with macrophages removed. Remarkably, the C3H osteoblastic progenitor cells out-grew the similarly treated B6 marrow cells! OPG mRNA, via RNase protection assay, was significantly elevated in C3H subcultured cells compared with B6 subcultured cells, while OPG-L mRNA levels were not different between strains in the presence or absence of 1,25-Vit D3. These new data suggest that C3H osteoblasts are over-producing OPG protein and that this molecule could be blocking normal osteoclastogenesis and differentiation of C3H mice. These data are interpreted to mean that reduced bone resorption in C3H is likely to be one of the determinants of their high bone mass. An important question is whether the *Opg* gene or a critical regulatory factor for *Opg* resides in one of the QTL regions currently 'captured' within a B6.C3H congenic strain. Finally, the issue of whether B6 osteoclastic resorption activity is constituitively greater than that of C3H osteoclasts is currently under additional investigation with Dr. Rubin.

STIMULI REGULATING BONE FORMATION IN B6 AND C3H MICE

A provocative hypothesis that might account for the markedly higher peak BMD in C3H versus B6 mice would be that the two strains differ in response to loads placed on bone. Thus, two investigations have focused on mechanical stimuli as a possible determinant of the marked difference in BMD of B6 mice versus C3H.

• Unloading of bone. The first study was undertaken to mechanically unload the tibia through unilateral denervation (sciatic, femoral and obturator neurectomy) of the left hind limb (**Appendix 4**). Kodama et al. surgically neurectomized or sham treated groups of mice at 8 weeks of age, then necropsied 4 weeks later to obtained treated and control tibial specimens for histomorphometry and serum for assay of biochemical markers of bone formation. No significant changes were found in serum alkaline phosphatase or osteocalcin levels between neurectomized and sham treated B6 or C3H mice. However, histomorphometry performed at the tibiofibular junction and at the proximal tibia of B6 bone showed decreasing length of endosteal bone forming perimeter and increased medullary cavity area. Such changes were also observed in the C3H bone sites but the decrease in endosteal bone formation was much smaller and no change in medullary area was found. These findings were interpreted to indicate that the B6 mice are more sensitive to endosteal bone loss in the immobilized bone than are C3H mice.

• Loading of bone. The alternative approach to addressing the effect of biomechanics on BMD between B6 and C3H mice was to apply additional biological loading to the appendicular skeleton (**Appendix 7**). This experimental approach also was undertaken by Kodama et al. (1999) to examine the hypothesis that the C3H mice were less sensitive than B6 to mechanical loading. The loading stimuli were induced by 4 weeks of daily jumping exercise for both B6 and C3H mice. Serum levels of osteocalcin, ALP, and IGF-I were assayed as indices of bone formation, while biomechanical tests of tibial strength were measured by 3 point bending tests. The serum results showed that: a) serum IGF-I levels increased with jump testing only in C3H, and b) no changes in serum osteocalcin or ALP levels were observed in either strain. B6 mice but not C3H mice showed increased tibial strength (mN/g b wt) as a result of jump testing. The C3H mice did not respond to jump testing with histological evidence of change, whereas the B6 mice increased total bone area, periosteal perimeter, periosteal mineral apposition rate, and periosteal bone formation. No effects of bone resorption were observed in either strain. These data were interpreted to mean that C3H bones are insensitive to mechanical loading stimuli compared with the bone of B6 mice.

• Calcium challenge. The hypothesis that calcium metabolism has a role in determining the difference in BMD between B6 and C3H was investigated using a regimen of dietary depletion and repletion lasting two weeks each phase (**Appendix 9**). We found in the depletion studies that: a) femur dry weight declined and serum ALP and PTH levels increased similarly in both strains, b) that tibial marrow cavity increased in both strains, c) endosteal bone formation declined in both strains, but no changes were seen in the periosteal formation, and d) marrow osteoclast progenitor cells decreased in number in both B6 and C3H mice (2000). Repletion of dietary calcium corrected all changes. These

data indicate that the higher BMD of C3H versus B6 mice is independent of low calcium as a resorptive stimuli.

BONE PROPERTIES: MASS, MICROSTRUCTURE, STRENGTH

Correlation of heritable variation in BMD, morphology, and strength. In addition to BMD, properties of morphology and quality are classic components of bone strength. We addressed the hypothesis that genetic differences in bone mass of B6 and C3H would also be reflected in differences in bone microstructure and biomechanical parameters at clinically important sites **(Appendix 8)**. Accordingly, Turner et al. (2000) examined the femur neck and lumbar vertebrae by microCT (Scanco Medical AG, MicroCT 20), femoral strength by biomechanical testing (Vitrodyne 2000) and femoral cortical mineral packing density by back-scattering electron images (using a Link Tetra BSE detector) of bone specimens from 4 month old B6 and C3H females. Micro CT data confirmed that C3H have thicker cortical bone at femoral neck and lumbar vertebral bodies. Cortical mineralization by BSE was significantly greater in C3H than in B6 femurs. In comparison with B6, the C3H mice had fewer trabeculae in vertebral bodies, femoral neck, and greater trochanter. Trabecular spacing was much expanded in C3H vertebrae. The C3H femurs had greater resistance to bending than B6 femurs, but the vertebrae were not different in resistance to compression loading, presumably because the thicker cortex of C3H was combined with poor trabecular structure. Collectively, the results demonstrate a) that morphological and strength differences are also associated with the differences in BMD between B6 and C3H, and b) that C3H mice benefit from alleles that enhance femoral strength but are deficient in trabecular bone structure in the vertebrae.

Lastly, in the year Sept 2000 to Sept 2001, a special supplement of $240,000 was awarded for the purpose of obtaining equipment for preparation of undecalcified sections of bone and for X-ray based imaging of cancellous bone at high resolution (see **Appendix 19**). Accordingly, we purchased a Polycut Model SM2500E sliding microtome (manufactured by Leica) for sectioning of undecalcified bone for the purpose of studying bone cell types (osteoblasts and osteoclasts) their locations on periosteal, endosteal, and trabecular surfaces, plus dynamic rates of bone formation and bone resorption using fluorochrome label incorporation methodology. In addition, we purchased a state-of-the-art MicroCT 40 (SCANCO AG, Switzerland) for imaging and analyses of bone at resulotion levels as low as 6 microns. These instruments arrived in late spring and late Summer of 2001. These instruments are just beginning to be put to use and are expected to provide vital biological measurements related to the genes for bone density, structure, and strength captured in the congenic strains desctibed above. Our first publications are being prepared at this time in the Fall of 2001.

Key Accomplishments.

- QTLs for bone mineral density located, named, and major effects described
- QTLs unique to femurs and to vertebrae, as well as common to both bone sites described
- Heritabilities for BMD established in both F2 crosses; found to be similar to that in humans
- Both bone resorption and bone formation processes were found to differ in C57BL/6J and C3H/HeJ strains that contribute to the differences in BMD between the strains
- New research grants have been obtained to expand studies based upon initial work support by this DAMD grant
- QTLs have been transferred into individual new congenic strains of mice with the common genetic background of C57BL/6J. There are providing the next generation of in vivo research tools for biological studies of what individual QTLs are doing and for fine mapping and cloning of QTLs to identify (at the DNA Level) each gene. these will serve as pharmaceutical targets for osteoporosis or even other bone disease amelioration.

Reportable Outcomes

Publications directly related to the Specific Aims

1. Rosen CJ, Dimai H P, Verault D, Donahue LR, Beamer WG, Farley J, Linkhart S, Linkhart T, Mohan S, & Baylink DJ. 1997. Circulating and skeletal insulin-like growth factor-I (IGF-I) concentrations in two inbred strains of mice with different bone mineral densities. Bone. 21: 217-223.

2. Dimai HP, Linkhart TA, Linkhart SG, Donahue LR, Beamer WG, Rosen CJ, Farley JR, Baylink DJ. 1998. Alkaline phosphatase levels and osteoprogenitor cell number suggest that bone formation may contribute to peak bone density differences between two inbred strains of mice. Bone 22: 211-216.

3. Linkhart TA, Linkhart SG, Kodama Y, Farley JR, Dimai HP, Wright KR, Wergedal JE, Sheng MA, Beamer WG, Donahue LR, Rosen CJ, and Baylink DJ. 1999. Osteoclast formation in bone marrow cultures from two inbred strains of mice with different bone densities. J. Bone Miner Res. 14: 39-46.

4. Kodama Y, Dimai HP, Wergedal J, Sheng M, Malpe S, Kutilek S, Beamer WG, Rosen CJ, Donahue LR, Baylink DJ, Farley J. 1999. Cortical tibial bone volume in two strains of mice: A study of the effect of sciatic neurectomy and the genetic regulation of the bone response to mechanical loading. Bone 25:183-190.

5. Sheng MC-H, Baylink DJ, Beamer WG, Donahue LR, Rosen CJ, Lau K-HW, and Wergedal JE. 1999. Phenotype studies show that bone formation and bone mineral apposition rate are greater in C3H/HeJ (high density) than in C57BL/6J (low density) mice during growth. Bone 25: 421- 429.

6. Beamer WG, Shultz KL, Churchill GA, Frankel WN, Baylink DJ, Rosen CJ, Donahue LR. 1999. Quantitative trail loci for bone density in C57BL/6J and CAST/EiJ inbred mice. Mamm. Genome 10: 1043-1049.

7. Kodama Y, Umemura Y, Nagasawa S, Beamer WG, Donahue LR, Rosen CJ, Baylink DJ, Farley JR. 1999. Exercise and mechanical loading increase periosteal bone formation in C57BL/6J mice, but not in C3H/HeJ mice. Calcif. Tissue Int. 66:298-306.

8. Turner CH, Hsieh Y-F, Mueller R, Bouxsein ML, Baylink DJ, Rosen CJ, Grynpas MD, Donahue LR, Beamer WG. 2000. Genetic regulation of cortical and trabecular bone strength and microstructure in inbred strains of mice. J Bone Miner Res. 15: 1126-1131.

9. Kodama Y, Miyakoshi N, Linkhart TL, Wergedal J, Srivastava A, Beamer WG, Donahue LR, Rosen CJ, Baylink DJ, Farley JR. 2000. Effects of dietary calcium depletion and repletion on dynamic determinants of tibial bone volume in two inbred strains of mice. Bone. 27:445-452.

10. Richman C, Kutilek S, Myakoshi N, Srivastava AK, Beamer WG, Donahue LR, Rosen CJ, Wergedal JE, Baylink DJ, Mohan S. 2000. Postnatal and pubertal skeletal changes contribute predominantly to the differences in peak bone density between C3H/HeJ and C57BL/6J mice. J. Bone Miner Res 16: 386-397.

11. Rosen CJ, Churchill GA, Donahue LR, Shultz KL, Burgess JK, Powell DR, and Beamer WG. 2000. Mapping quantitative trait loci (QTLs) for serum insulin-like growth factor-I (IGF-I) levels in mice.Bone 27:521-528.

12. Beamer WG, K Shultz, L Donahue, G Churchill, W Frankel, J Wergedal, D Baylink & Clifford J. Rosen. 2000. Quantitative trait loci for femoral and lumbar vertebral bone mineral density in C57BL/6J and C3H/HeJ inbred strains of mice. J Bone Miner Res. 16:1195-1206.

Publications Relevant to Genes and Bone

13. Rogers J, Mahaney MC, Beamer WG, Donahue LR, Rosen CJ. 1997. Beyond one gene-One disease: Alternative strategies for deciphering genetic determinants of osteoporosis. Calcif. Tissue Int'l. 60: 225-228.

14. Rosen CJ, Donahue LR, Beamer WG, Adler RA, Kurland ES, and Bilezikian JP. 1998. IGF-I and Osteoporosis: Lessons from mice and men. In, "Nutritional Aspects of Osteoporosis" (Eds.) P. Burkhardt, B. Dawson-Hughes, & R. Heaney, Springer Verlag, New York, pp135-141.

15. Umeda S, Beamer WG, Takagi K, Naito M, Hayashi S-I, Yonemitsu H, Yi T, Shultz LD. 1999. Deficiency of SHP-1 protein-tyrosine phosphatase activity results in heightened osteoclast function and decreased bone density. Amer. J. Pathol.: 155:223-233.

16. Beamer WG, Rosen CJ, Baylink DJ, Bronson RT, Weikuan Gu, Donahue LR, Richman, CC, Crawford-Sharpe G, Barker JE. 2000. Spontaneous Fracture (*sfx*): A mouse model of defective peripubertal bone formation. Bone 27: 619-626.

17. Parhami F, Tintut Y Gharavi N, Beamer WG, Goodman W, Demer LL. 2001. High fat diet reduced mineral content and density in mice. J Bone Miner Res, 16: 182-188.

18. Mohan S, Kutilek S, Zhang C, Shen H G, Kodama Y, Srivastava A K, Wergedal J E, Beamer W G, and Baylink, D J. 2000. Comparison of the site specific effects of PTH (1-34) and PTH (1-31) on bone formation in mice. Bone 27:471-478.

19. Turner CH, Hsieh Y-F, Mueller R, Bouxsein ML, Rosen CJ, McCrann ME, Donahue LR, Beamer WG. 2001. Variation in bone biomechanical properties and microstructure in BXH recombinant inbred mice. J Bone Mineral Res. J Bone Miner Res. 16: 206-213.

20. Murray EJB, Beamer WG, Duarte ME, Behnam K, Grisanti MS, Murray SS. 2001. Effects of dietary restriction on appendicular bone in the SENCAR mouse. Metabolism 50: 436-442.

21. Bikle D, Majumdar S, Laib A, Powell-Braxton L, Rosen CJ, Beamer WG, Nauman E, Leary C, Halloran B. 2001. The skeletal structure of insulin-like growth factor-I deficient mice. J Bone Miner Res. in press Fall 2001.

22. Beamer WG, Donahue LR, & Rosen CJ. 2000. Insulin-like growth factor I and bone: From mouse to man. Growth Hormone & IGF Res. Suppl B, S103-S105.

Abstracts presented at meetings

1. Beamer WG, Shultz KL, Frankel WN, Donahue LR, Baylink DJ, & Rosen CJ. Genetic loci for cortical bone density density in inbred strains of mice. 1997. J Bone Miner Res 12, Suppl 1, abst # (Cincinnati).

2. Beamer WG, Shultz KL, Frankel WF, Donahue LR, Baylink DJ, & Rosen CR. 1997. Genetic loci for cortical bone density in inbred mice J. Bone Miner Res. 12, suppl. 1, abst #292.

3. Beamer WG, Rosen CJ, Donahue LR, Frankel WN, Churchill GA, Shultz KL, & Baylink DJ. 1998. Location of genes regulating volumetric bone mineral density in C57BL/6J (low) and C3H/HeJ (high) inbred strains of mice. Bone 23 (Suppl) abst. 1056.

4. Donahue LR, Rosen CJ, & Beamer WG. 1999. Comparison of Bone Mineral Content and Bone Mineral Density in C57BL/6J and C3H/HeJ Female Mice by pQCT (Stratec XCT 960M) and DEXA (PIXImus). Bone 23 (Suppl) abst. abst # ?.

5. Beamer WG, Donahue LR, Churchill GA, Powell DR, Ackert CL, Shultz KL, Beamer WG. 1999. Identification of four QTLs for serum IGF-I in Mice and their functional relationship to bone. J Bone Miner Res. 15, suppl 1, abst 1191.

6. Beamer WG, Donahue LR, Shultz KL, Rosen CJ, Churchill GA, Baylink DJ. 1999. Genetic regulation of BMD in low density C57BL/6J carrying donated QTLs from high density C3H/HeJ mice. J Bone Miner Res 15 suppl 1, abst # 1192.

7. Richman C, Kutilek S, Miyakoshi N, Beamer WG, Wergedal JE, Baylink DJ, Mohan S.1999. Evidence that prepubertal and pubertal skeletal changes contribute to the extreme differences in peak bone density between C3H/HeJ(C3) and C57BL/6J(B6) strains of mice. J Bone Miner Res 15 suppl 1, abst # Su096.

8. Beamer WG, Donahue LR, Shultz KL, Rosen CJ, Churchill GA, & Baylink DJ. 2000. Genetic regulation of BMD in low density C57BL/6J mice carrying donated QTLs from high density C3H/HeJ mice. J Bone Miner Res., 15, suppl 1, abst #1192.

9. Beamer WG, Sen S, Churchill GA, Rosen CJ, Donahue LR, Shultz KL, Mytar JO, Turner CH, Müller R, Uchiyama T, & Bouxsein ML. 2001. Genetic relationships among bone phenotypes regulated by sets of quantitative trait loci (QTL) in B6C3F2 mice. J. Bone Miner Res. 16 suppl 1, abst #F114 .

10. Wergedal JE , Sheng HM , Donahue LR, Baylink DJ, & Beamer WG. 2000. Studies in Inbred Strains of Mice Show that Bone Size (Periosteal Perimeter) is Genetically Determined and Positively Correlated with Breaking Strength. J. Bone Miner Res. suppl. 1, abst # F140.

11. Turner, Q.Sun, M.L. Bouxsein, C.J. Rosen, L.R. Donahue, K.L. Shultz, W.G. Beamer. 2001. Major Genetic Influence on Bone Stiffness and Strength Identified on Mouse Chromosome 4. J Bone Miner Res. suppl 1, 16, abst 1126.

12. Bouxsein ML, Mueller R, Uchiyama T, Mytal JO, Turner CH, Donahue LR, Rosen CJ, Beamer WG. 2001 Assessing the genetic determinants of vertebral bone density and microarchitecture in mice. J Bone Miner. Res. 16, suppl 1, abst #1066.

13. Ackert CL, Donahue LR, Turner CH, Turner RT, Bouxsein ML, Mueller R, Beamer WG, Shultz KL, Rosen CJ. 2001. Testing in vivo effects of a genetic determinant of IGF-I expresion on bone phenotypes in a new congenic strain. J Bone Miner. Res. 16, suppl 1, abst # F112.

14. Gu W, Edderkaoui B, Beamer WG, Shultz KL, Li X, Sheng H-CM, Wergedal JE, Lau K-HW, Donahue LR, Rosen CJ, Mohan S, Baylink DJ. 2001. Studies Using Congenic Mice Reveal That Chromosome 1 QTL Locus in Cast/EiJ Mouse Contributes to 30% Variation in BMD Difference Between Cast and C57BL Mice. J Bone Miner. Res. 16, suppl 1, abst #109.

15. Donahue LR, Beamer WG, Bouxsein ML, Müller R, Turner CH, Shultz KL, Rosen CJ. 2001. Genetic effects on bone mineral density independent of growth hormone and IGF-I regulation. J Bone Miner. Res. 16, suppl 1, abst #F122.

16. Rubin J, Murphy T, Fan X, Gewant H, Beamer WG, Donahue LR, and Rosen CJ. 2000. OPG/OPGL ratios are increased in bone stromal cells from C3H (high bone density) compared to C57BL/6 (low bone density) mice. J. Bone Miner Res. Suppl. abst #SA141.

17. Turner CH, Sun Q, Schriefer J, Bouxsein ML, Rosen CJ, Donahue LR, Shultz KL & Beamer WG. 2002. Genetic insluences on bone density and geometry affect femoral bone strength. Orthopedic Res Soc. 48th Ann. Mtng, 10-13 Feb 2002, Dallas, TX.

18. Turner CH, Sun Q, Schriefer J, Pitner N, Price R, Bouxsein ML, Rosen CJ, Donahue LR, Shultz KL & Beamer WG. 2002. Congenic mouse strains reveal gender-specific genetic regulation of bone structure. Orthopedic Res Soc. 48th Ann. Mtng, 10-13 Feb 2002, Dallas, TX.

Patents and licenses.

None

Degrees obtained from research support

None

Development of cell lines, tissue or serum repositories.

None

Informatics and animal models

Set of congenic strains of mice (B6.CAST andB6.C3H) are present in our research colony and are being freely shared with the scientific community. Details are in Body of Report given above.

Funding applied for based upon work supported by this award.

Source: NIAMS (AR45433). PI: CJ Rosen. Title: Genetic Regulation of IGF-I in Peak Bone Density of Mice

Source: NIAMS (AR46530). PI: CH Turner. Title: Genetic Analysis of Vertebral Strength.

Source: NIAMS (AR43618-05 renewal). PI: WG Beamer. Title: Genetic and Dynamic Analyses of Murine Peak Bone Density.

Employment or research opportunities applied for based upon this research support.

None

Conclusions.

In summary, functional comparisons of C3H vs B6 show that there are marked differences in both bone formation and bone resorption cell types and processes accounting for marked differences in BMD, again supporting the polygenic regulation of the BMD phenotype. In view of the findings that B6 and C3H differ with respect to BMD, key bone morphologies, and biomechanical indices of strength, we are pursuing collaborative studies with Drs. C. Turner, University of Indiana, and M. Bouxsein and R. Mueller, Beth Israel Hospital, Boston. These co-operative investigations will include measurements of phenotypes related to biomechanical strength and morphology of femurs and vertebrae from our B6.C3H congenic strains. The congenic strains of mice created by transfer of individual CAST or C3H QTLs into the C57BL/6J genetic background provide proof that the QTLs exert independent effects on bone mineral density, and in addition are being found to also regulate bone microarchitectural and geometric properties. Studies of these QTLs in the congenic background will demonstrate which genes regulate formation and resorption functions critical to production and maintenance of biomechanically strong or weak bones.

References

All are listed in the **Reportable Outcomes** section cited above that stem from this research support. There are 22 published manuscripts and 18 abstracts.

APPENDICES

Appendix 1 - 22 Copies of all publications supported by the USAMRMC

Appendix 23 Copy of Request for Extension and Supplement for equipment dated 31 August 2000

ELSEVIER

Bone Vol. 21, No. 3
September 1997:217–223

ORIGINAL ARTICLES

Circulating and Skeletal Insulin-like Growth Factor-I (IGF-I) Concentrations in Two Inbred Strains of Mice With Different Bone Mineral Densities

C. J. ROSEN,[1] H. P. DIMAI,[2] D. VEREAULT,[1] L. R. DONAHUE,[3] W. G. BEAMER,[3] J. FARLEY,[2] S. LINKHART,[2] T. LINKHART,[2] S. MOHAN,[2] and D. J. BAYLINK[2]

[1] *St. Joseph Hospital, Bangor, ME, USA*
[2] *J. L. Pettis VA Hospital Medical Center, Loma Linda, CA, USA*
[3] *Jackson Laboratory, Bar Harbor, ME, USA*

Recent work has demonstrated differences in femoral bone mineral density between two common inbred strains of mice, C3H/HeJ (C3H) and C57BL/6J (B6), across a wide age range. To investigate one possible mechanism that could affect acquisition and maintenance of bone mass in mice, we studied circulatory and skeletal insulin-like growth factor-I (IGF-I) and femoral bone mineral density (F-BMD) by pQCT in C3H and B6 progenitor strains, as well as serum IGF-I obtained from matings between these two strains and mice bred from subsequent F_1 intercrosses (F_2). Serum IGF-I measured by radioimmunoassay was more than 35% higher in virgin progenitor C3H than virgin B6 at 1, 4, 8, and 10 months of age, and in 8-month-old C3H compared with B6 retired breeders ($p < 0.001$). In the progenitors, there was also a strong correlation between serum IGF-I and serum alkaline phosphatase ($r = 0.51$, $p = 0.001$). In the 4 month F_1 females IGF-I levels and F-BMD were intermediate between C3H and B6 progenitors. In contrast, groups of F_2 mice with the highest or lowest BMD also had the highest or lowest serum IGF-I ($p = 0.0001$). IGF-I accounted for >35% of the variance in F-BMD among the F_2 mice. Conditioned media from newborn C3H calvarial cultures had higher concentrations of IGF-I than media from B6 cultures, and cell layer extracts from C3H calvariae exhibited greater alkaline phosphatase activity than cultures from B6 calvarial cells ($p < 0.0001$). The skeletal content of IGF-I in C3H tibiae, femorae, and calvariae (6–14 weeks of age) was also significantly higher than IGF-I content in the same bones of the B6 mice ($p < 0.05$). These data suggest that a possible mechanism for the difference in acquisition and maintenance of bone mass between these two inbred strains is related to systemic and skeletal IGF-I synthesis. (Bone 21:217–223; 1997)

Key Words: Insulin-like growth factors; Femoral bone density.

Address for correspondence and reprints: C. J. Rosen, St. Joseph Hospital, 360 Broadway, Bangor, ME 04401. E-mail:crosen@maine.maine.edu

Introduction

Recent studies from our laboratory have demonstrated large differences (50%) in femoral bone density, measured by peripheral quantitative computed tomography (pQCT), between C3H/HeJ(C3H) and C57BL/6J(B6), two common inbred strains of mice.[2] These strain differences are noted as early as 4 weeks of age, a time during peak bone mass acquisition, and are maintained through at least 12 months of age.[2,10] Moreover, differences in bone density are not limited to the femur, since C3H mice compared to B6 mice have consistently higher bone mass (both cortical and trabecular) at other skeletal sites including the tibia, vertebrae, and phalanges.[2] Although the mechanisms responsible for a greater bone mineral density in C3H mice have yet to be clearly defined, changes in bone resorption or bone formation must underlie differences in the acquisition of peak bone mass between these two strains. Preliminary histomorphometrical and biochemical evidence from our laboratory suggests that bone formation is increased significantly at the time of acquisition of peak bone mass in C3H mice (Baylink et al., unpublished observation).

Osteoblasts mediate bone formation through a series of events that are regulated by hormonal and skeletal growth factors.[1] Several of these regulatory factors are also operative during acquisition of bone mass. These include insulin-like growth factors (IGF-I and -II), transforming growth factor-β (TGF-β), bone morphogenic proteins (BMPs), fibroblast growth factors, numerous interleukins, tumor necrosis factor (TNF), and various prostaglandins.[1] Several lines of evidence suggest that IGFs are important mitogenic and differentiative factors for bone cells. First, these peptides are found in very high concentrations within the skeletal matrix.[1] Second, calciotropic hormones such as parathyroid hormone (PTH), 1,25-dihydroxyvitamin D, and growth hormone may mediate their effects on osteoblasts in part by regulating the synthesis of IGFs and/or their binding proteins.[14,19] Third, studies of growth hormone-deficient patients have found that serum IGF-I concentrations closely correlate with reduced bone density, and that growth hormone replacement increases both serum IGF-I and bone mineral density.[4,13] Fourth, age-associated declines in circulating IGF-I parallel similar drops in skeletal levels of IGF-I.[3,17] Fifth, several cross-sectional studies have demonstrated a strong linear relationship between serum IGF-I and bone mineral density in postmenopausal women.[5,16] These points suggest that IGF-I may play an important

8756-3282/97/$17.00
PII S8756-3282(97)00143-9

Bone Vol. 21, No. 3
September 1997:217–223

role in normal remodeling and may have pathophysiological significance in certain osteopenic states.

The possibility that IGF-I, an important bone growth factor, may be critical in determining peak bone mass in mice has recently emerged from studies in our laboratory on bone mineral density of the *little* mutant (*lit*), a growth hormone- and IGF-I-deficient mouse.[7] This strain is characterized by low levels of serum IGF-I and growth hormone owing to a point mutation in the hypothalamic growth hormone-releasing hormone receptor.[10] These mice also have low bone mineral density.[8] Based on developmental and histomorphometrical data from C3H mice and *lit/lit* homozygotes, as well as historical data that growth hormone levels in C3H mice are significantly higher than other strains, we hypothesized that differences in femoral BMD (F-BMD) between C3H and B6 mice might be related to changes in the skeletal and/or circulatory levels of IGF-I.[20,21] We therefore examined the relationship between this skeletal growth factor and F-BMD in two inbred strains of mice as well as F_1 mice and F_2 progeny of $F_1 \times F_1$ matings.

Materials and Methods

Animals

The two inbred strains of mice used for this study were raised and housed at the Jackson Laboratory and in the Animal Research Facility of the Jerry L. Pettis Memorial Veterans Medical Center. All studies had been approved by the animal research committee of the institutions where they were conducted. Females (ages 1–12 months) from the C3H and B6 strains were maintained in groups of three or four in polycarbonate boxes (130 cm^2) on bedding of sterilized white pine shavings under conditions of 14 h light:10 h darkness and an ambient temperature of 20 ± 2°C. Water (acidified with HCl, pH 2.8–3.2) and an autoclaved pelleted diet (National Institutes of Health 31 diet: 18% protein, 6% fat, 1.27% Ca, 0.92% P, trace mineral and vitamin fortified; Purina, Madison, WI) were available ad libitum. Eight-month-old mice were obtained from the Jackson Laboratory's Animal Resources as retired breeders at 5–7 months of age and placed on the above diet until necropsy at 8 months of age. B6 females were mated to C3H males and groups of their (B6C3)F_1 progeny were set aside for data collection. $F_1 \times F_1$ matings were established to produce F_2 female progeny for serum and bone mineral density analyses at 4 months of age.

At the specified ages, groups of nonfasted mice (up to six) were decapitated and trunk blood was collected on ice. Blood was clotted for 4 h at 4°C, then separated and stored frozen at −15°C for future study. A partial carcass preparation was derived from each mouse and preserved in 95% ethanol. Subsequent dissection and storage of the left rear limb was described previously.[2]

F-BMD

Total F-BMD was assessed by pQCT with a Stratec XCT 960M (Norland Medical Systems, Ft. Atkinson, WI) specifically modified for use on small bone specimens to measure bone mineral and volume.[2] Isolated femurs were scanned at 2 mm intervals over their entire lengths and the unit volume within which mineral was measured was set at 0.1 mm^3. F-BMD (which represents almost exclusively cortical bone) at the midpoint of the femur measured eight times reveals a precision error of 1.2% with this machine. The resolution of detection of the machine is 0.05 mm.

Preparation of Serum Samples

Whole-blood samples from individual nonfasting female progenitor B6 and C3H mice ages 1, 4, 8, and 10 months were obtained as described above (total samples from mice: n = 92). In addition, 19 B6C3 F_1 female mice (ages 8 and 12 months) and 51 F_2 female mice (age 4 months) had whole-blood samples obtained. For assay characterization, 30 sets of pooled serum samples from retired breeders (aged 8 months) of each strain were also obtained (pools consisted of serum from two female C3H progenitor mice and three female B6 progenitors). Fifteen pools of each strain were allocated and frozen. The replicate samples of each pool were analyzed independently at two different laboratories (Maine and California) using the methodologies noted below. Samples were stored at −15°C prior to thawing, and assays were performed immediately after the first defrost. However, to assess whether repetitive defrosting of mouse serum contributed to variance in the radioimmunoassay (RIA), acid-ethanol cryoprecipitation (AEC) followed by RIA was performed after repeated freeze-thaws from several pools of C3H and B6 sera.

IGF-I RIA After Removal of IGF Binding Proteins (IGFBPs)

Two methods were employed to remove IGFBPs prior to measurement of serum IGF-I by RIA in mouse sera. Each method has been used previously in assays of mouse sera, and the differences between the two relate to the method of removing IGFBPs prior to RIA. AEC was performed according to the procedures developed by Brier et al.[6] and Grogean et al.[11] One volume of 100 μL of serum was pipetted to the bottom of a 12 × 75 mm high-density polyethylene (HDPE) RIA tube. Four hundred microliters of acid ethanol solution [87.5% ethanol (ETOH), 12.5% 2N HCl, v/v] was added to the tube. The mixture was vortexed and then incubated for 30 min at room temperature. The sample was then centrifuged for 35 min at 3000g at 4°C. Two hundred fifty microliters of supernatant was removed from the tube and mixed with 100 μL of cold 0.855 mol/L Tris (tris [hydroxymethyl] aminomethane, pH 10) in a second HDPE tube. This mixture was vortexed, then incubated for 60 min at −20°C. The sample was then centrifuged for 35 min at 3000g, at 4°C. One hundred microliters of supernatant was taken from this tube and diluted with 1400 μL of PBS. Extracted samples were stored for 1–7 days at 4°C before analysis by RIA. All AEC extractions were done in duplicate. Recovery of recombinant human IGF-I (rhIGF-I) from pooled mouse serum ranged from 95% to 104%. Assays were performed in duplicate using a polyclonal antibody and a commercially available RIA kit from Nichols Institute (San Juan Capistrano, CA). Cross-reactivity with rhIGF-II in this assay is <1%. The interassay coefficient of variation was 5.7%; the intra-assay coefficient of variation (CV) was 3.2%. The detection limit with this method in mouse serum is 12 ng/mL, and linearity was established at several different dilutions after extraction.

A second method for separating IGF-I from its binding proteins has recently been reported using a biospin column separation technique (BSPC).[6,17] To prepare the columns, 10 g of Bio-Gel P-10 (BioRad, Hercules, CA) was allowed to hydrate in 150 mL, 1 mol/L acetic acid containing 0.1 mol/L NaCl (in the absence or presence of 10 g/L bovine serum albumin [BSA]) overnight at room temperature and degassed for 10–15 min. The gel was then allowed to settle, 30 mL of supernatant containing fine particles was removed, and 3 cm^3 gel slurry was poured into the empty biospin columns to a packed column bed height of 4 cm. Serum samples (10 μL) were diluted with 40 μL of 1.25 mol/L acetic acid, 0.125 mol/L NaCl, and applied to the biospin columns as described.[16] IGF-I by RIA was determined after

column extraction using rhIGF-I (Ciba Geigy, NJ) as a tracer and standard, and rabbit polyclonal antiserum as previously described.[16] The sensitivity of this assay was 2–5 ng/mL. The cross-reactivity of IGF-II in the IGF-I RIA was <0.5%. Intra- and interassay coefficients of variation were <10%. Serum IGF-I by RIA in the same samples using different extraction methods correlated closely ($r = 0.80$, $p < 0.001$).

IGF-I Concentrations in Skeletal Samples

Mouse calvariae were demineralized, extracted with guanidine-HCl, and dialyzed using Spectrapor 3 with a method adopted from a previous protocol.[16] For extraction of IGF-I from cortical bone, tibiae were separated from femur and fibula, and muscle was carefully removed from the bones. Bones were cut and washed for 24 h in 1 mL of a protease inhibitor containing 5 mmol/L benzamidine HCl, 100 mmol/L of ε-amino caproic acid, and 1 mmol/L phenylmethyl-sulfonyl fluoride. After removal from the protease inhibitor, bones were allowed to dry at room temperature, and dry weights of bones were determined. Individual bones then were transferred to precoated polypropylene tubes, and 1 mL of extraction buffer containing 0.5 mmol/L ethylenediaminetetraacetic acid and 4 mmol/L guanidine HCl in protease inhibitor solution was added to each of the bones. Bones were extracted for 24 h at 4°C with constant shaking. The extraction procedure was repeated four times for each bone, and the extracts were combined and stored at 4°C. The pooled extracts then were desalted by dialysis (Spectra/Por 3 Tubing; Spectrum Medical Industries, Houston, TX) against 20 mmol/L acetic acid (HAC) at 4°C. To avoid binding of growth factors to the dialysis membranes, these were soaked in BSA prior to use. Each dialyzed extract was transferred to a precoated polypropylene tube and concentrated by vacuum centrifugation. Pellets were reconstituted in 150 μL of 1 mmol/L HAC and kept frozen at −20°C until separation of IGF from binding proteins by BSPC.

To determine whether differences in serum or skeletal IGF-I might be related to IGF-I production by bone cells, mouse calvarial cells were prepared from calvaria of newborns of each strain and cultured for 48 h in six-place-well dishes containing 2 mL/well of serum-free Dulbecco's modified Eagle's medium. IGF-I was measured by RIA in the cell-conditioned medium after BSPC separation from IGFBPs. Replicate cultures (n = 6/strain) were used, and the results are expressed as mean ± standard errors of the mean (SEM).

Alkaline Phosphatase (ALP) Activity in Cell Extracts and Serum

Alkaline phosphatase-specific activity was measured by a calorimetric assay in Triton X100 extracts of cells prepared as described previously.[9] Results are reported as milliunits of ALP per milligram of protein. Extract protein concentration was determined by the Bradford assay using a commercial kit (Bio-Rad, Richmond, CA). Total serum ALP was measured in pooled serum from the 8-month-old retired breeders with the same assay used for calvarial cultures with the exception that 10 mmol of phenylalanine was added to the reaction. Results in serum were reported in units per liter.

Statistical Methodology

All results are reported as mean ± SEM. Strain differences for IGF-I and ALP in serum (pooled and individual samples) and in culture media were analyzed by a Student's *t*-test for unpaired samples. Differences across ages and strains for serum IGF-I were analyzed by two-way analysis of variance (ANOVA), while strain differences in skeletal IGF-I were analyzed by a nonparametric sign test. Regressions for IGF-I vs. ALP activity were reported as Pearson correlations. Differences were considered significant if $p < 0.05$.

Results

Data from seven groups of female C3H and B6 mice ages 1, 4, and 10 months are presented in **Figure 1.** There were significant strain differences ($p < 0.001$) for serum IGF-I in mice across all

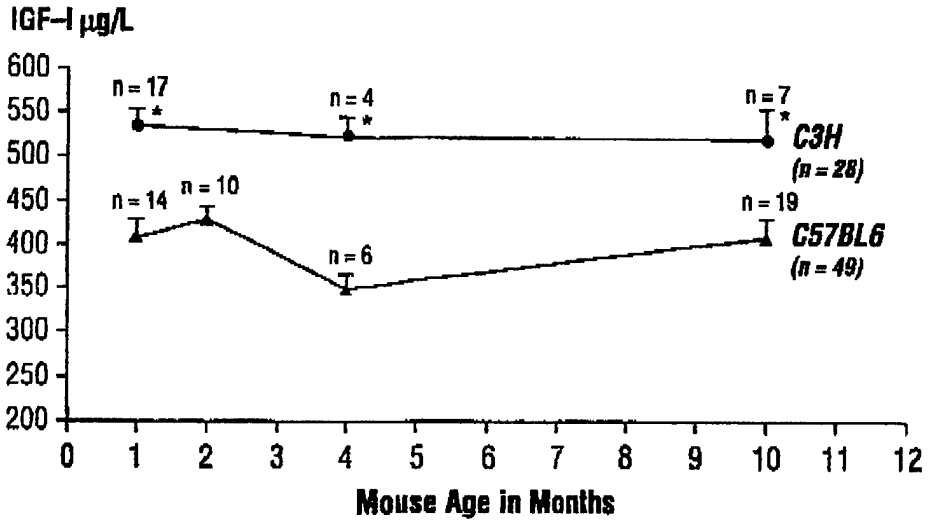

Figure 1. Female C3H/HeJ(C3H) and C57BL/6J(B6) mice ages 1, 4, and 10 months had serum levels of IGF-I measured by RIA following acid-ethanol cryoprecipitation to remove IGFBPs. Two-month-old female B6 were also included. Samples were obtained from nonfasting animals on a standard diet that were decapitated; samples were frozen immediately after being spun. All measurements were performed in a single run using a polyclonal antibody to IGF-I after extraction to assure minimal assay variation. The differences between strains in IGF-I were statistically significant for each age group at $p < 0.001$ (by two-way ANOVA [strain and age]). IGF-I did not differ by age of the animal within a particular strain (by ANOVA). Seventy-seven samples were assayed.

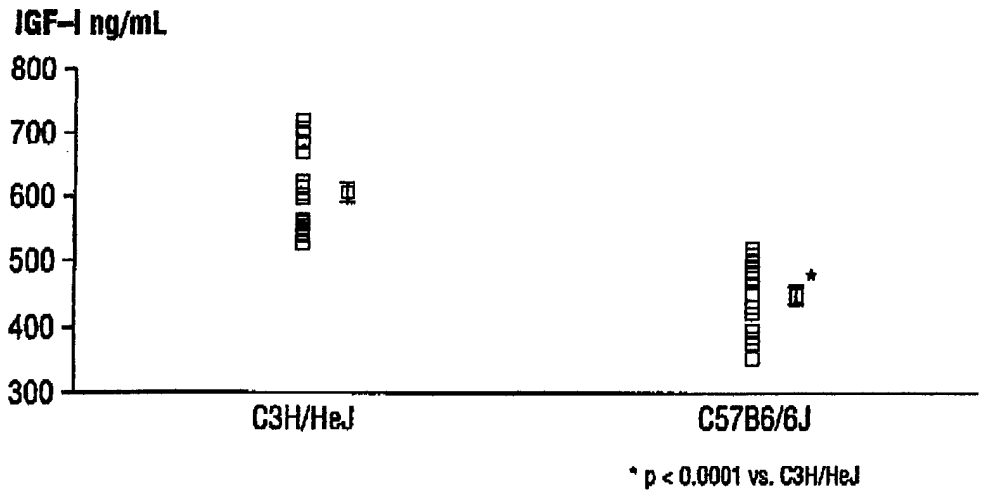

Figure 2. Individual samples (n = 15) from 8-month-old retired breeders of each strain were assayed for IGF-I after acid-ethanol cryoprecipitation to separate IGFBPs from IGF-I. As noted, there was minimal overlap in IGF-I concentrations between the two strains.

age groups. Furthermore, pooled or individual serum samples from 8-month-old retired breeders assayed for IGF-I either after extraction with AEC (n = 15) or after BSPC (n = 19) revealed minimal interstrain overlap (**Figure 2**). Samples from seven C3H and seven B6 retired breeders were also analyzed individually after extraction with AEC. **Table 1** summarizes differences between C3H and B6 retired breeders for (a) IGF-I in both pooled and individual samples, (b) ALP activity in individual serum samples, and (c) F-BMD. It is worth noting that actual values for F-BMD in these 8-month-old B6 and C3H females are virtually the same as those in our previous report on 12-month-old mice.[1] Moreover, the magnitude of differences in F-BMD between these strains corresponds to the degree of interstrain differences in circulating and skeletal IGF-I.

For B6C3F$_1$ progeny (n = 19), serum IGF-I was intermediate between the two progenitors: 522 ± 48 and 490 ± 40 ng/mL for 8- and 12-month-old mice, respectively. There was a direct correlation between serum IGF-I and F-BMD in the F$_1$ mice (r = 0.65, p = 0.007). Two sets of data from F$_2$ mice are presented in **Table 2**. In set 1 high and low F-BMD were tested, whereas in set 2 serum from three groups of 4-month-old female mice representing low, intermediate, and high F-BMD were assayed for IGF-I. Table 2 shows that F$_2$ progeny with the highest F-BMD also had the highest IGF-I levels, whereas the F$_2$ progeny with the lowest F-BMD had low IGF-I levels in both sets. Combining both data sets, more than 35% of the variance in F-BMD for F$_2$ mice could be attributed to serum IGF-I (**Figure 3**).

To determine whether strain-dependent differences in serum IGF-I were associated with corresponding differences in skeletal levels of IGF-I, we measured the content of IGF-I in nine paired groups of bones (i.e., calvariae, tibiae, and femorae) obtained from groups of age- and sex-matched C3H and B6 mice (n = 8–10/group) between the ages of 6 and 14 weeks. IGF-I was measured in extracts of individual bones, expressed as nanograms of IGF-I per milligram of dry weight of bone, and analyzed for differences between the two strains. Of the nine groups of matched bone extracts, eight showed higher levels of IGF-I in bones obtained from C3H compared to B6 mice, and the ninth group showed no difference. Absolute values for IGF-I content ranged from 2.96 ± 0.54 to 10.88 ± 1.52 ng IGF-I/mg dry weight of bone. There were no within-strain or site- or sex-specific differences in the IGF-I content of the bones; however, the mean difference in skeletal IGF-I between the C3H and B6 strains was +32% ($p < 0.05$ by nonparametric sign test). The magnitude of this difference was very similar to the strain differences in serum IGF-I for the pooled samples (+34%, $p < 0.0001$) and the individual sera obtained from 8-month-old animals (+26%, $p < 0.001$).

As noted in Table 1, there were also significant differences in

Table 1. Strain differences in 8 month retired breeder mice

Strain	C3H/HeJ	C57BL/6J
Body weight (g) (n = 15)	30.3 ± 0.9	32.6 ± 0.9
Total femoral bone density (n = 16) (mg/mm^3 [pQCT])	0.699 ± 0.009	0.443 ± 0.004*
IGF-I (AEC) (n = 15) (ng/mL)	609.3 ± 16.0	455 ± 14.0*
IGF-I pooled (BSPC) (n = 19) (ng/mL)	708.5 ± 20.5	457 ± 15†
Alkaline phosphatase activity (U/L) (n = 19)	22.0 ± 0.8	17.2 ± 0.8†

*$p < 0.001$ vs. C3H/HeJ.
†$p < 0.0001$ vs. C3H/HeJ.

Table 2. Serum IGF-I and femoral bone density (F-BMD) in 51 F$_2$ mice

Data set	n	F-BMD (mg/cm^3)	IGF-I (ng/mL)
1			
F$_2$ low density	12	0.529 ± 0.004*	385 ± 21†
F$_2$ high density	14	0.613 ± 0.011	510 ± 20
2			
F$_2$ low density	11	0.523 ± 0.006‡	352 ± 38‡
F$_2$ intermediate density	12	0.586 ± 0.008§	437 ± 19§
F$_2$ high density	12	0.653 ± 0.009	479 ± 23

Neither intermediate F-BMD nor IGF-I was different from the high F-BMD group.
*$p < 0.0002$ vs. high density for F-BMD.
†$p < 0.0001$ vs. high density for IGF-I.
‡$p < 0.0001$ vs. high density for both F-BMD and IGF-I.
§$p < 0.03$ vs. low density for both F-BMD and IGF-I.

Bone Vol. 21, No. 3
September 1997:217–223

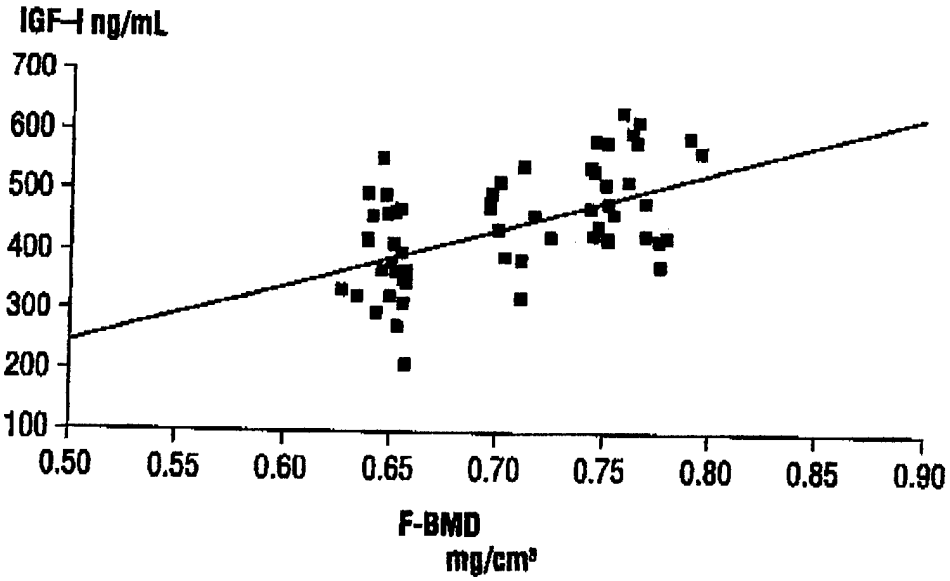

Figure 3. Three groups of 4-month-old F_2 female mice representing low, intermediate, and high F-BMD were measured for IGF-I in one assay (set 2). There was a strong correlation between IGF-I and F-BMD for both sets of samples ($r = 0.60$, $r^2 = 0.36$, $p < 0.001$).

serum ALP activity between the two strains. Serum levels of ALP activity showed positive correlations with serum IGF-I levels ($r = 0.51$, $p = 0.001$) (Figure 3). To assess whether a similar pattern of differences in skeletal IGF-I and ALP existed in bone cells derived from C3H and B6 mice, conditioned media and cell layer extracts from newborn calvarial cells were assayed for both IGF-I and ALP, respectively. C3H calvarial cultures yielded consistently higher levels of IGF-I in the conditioned medium than B6 cultures (0.695 ± 0.03 ng/mL vs. 0.512 ± 0.02 ng/mL; $p = 0.0001$). This pattern also held for ALP activity measured in cell layer extracts (C3H = 0.058 ± 0.004 vs. B6 = 0.011 ± 0.001 mU/mg protein; $p = 0.0001$).

Discussion

In this study, we have demonstrated large differences in serum IGF-I between C3H and B6 inbred strains of mice across a wide age range. In addition, we have provided evidence that both the skeletal content of IGF-I and in vitro bone cell production of IGF-I differ between the two inbred strains. Because differences in IGF-I concentrations in cell culture and in serum for these two strains were proportional to differences in ALP activity, our data suggest that strain differences in osteoblast number and/or activity may be associated with variation in bone mineral density. Finally, data from B6C3F$_1$ progeny and subsequent F_2 progeny

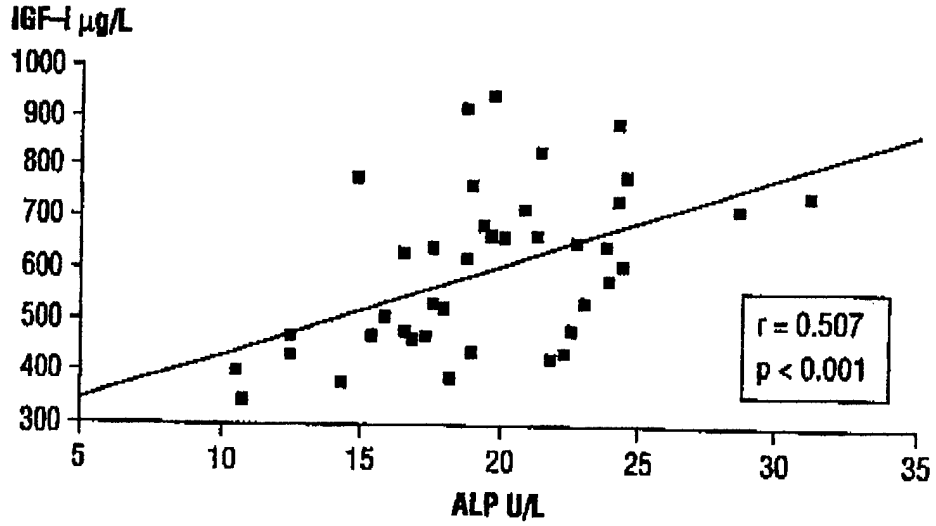

Figure 4. Total serum alkaline phosphatase activity was measured in C3H and B6 8-month-old retired breeders on the same pool of serum used to determine serum IGF-I concentrations after BSPC extraction. There was a strong linear correlation between IGF-I and ALP activity ($r = 0.51$, $r^2 = 0.26$, $p = 0.001$).

support the hypothesis that IGF-I is genetically associated with cortical BMD in the femur. Nevertheless, definitive evidence supportive of a causal relationship between serum IGF-I and skeletal bone density will have to await more extensive functional studies using the B6 and C3H progenitor strains.

Notwithstanding future studies, several lines of evidence currently provide support for the thesis that IGF-I may play a significant role in the regulation of bone density. First, IGF-I has been considered an important skeletal growth factor that acts as a weak mitogen but an inducer of osteoblastic differentiation.[12] In mice, IGF-I is necessary for longitudinal growth, maintenance of lean body mass, and normal bone turnover.[7,10] More important, IGF-I is synthesized and secreted by chrondrocytes and osteoblasts, which in turn are regulated by both local and systemic factors.[1,11,14,18] Since IGF-I is stored in large quantities within the skeletal matrix and has been hypothesized to be released during active bone resorption, this growth factor may serve to couple osteoblasts and osteoclasts.[12] Hence, it is not surprising that differences in bone mass could in part be related to perturbations in either the skeletal or circulatory IGF system. Recent findings in the growth hormone-deficient mutant, the *little* mouse, which has low serum IGF-I concentrations, small body size, increased total fat content, and markedly reduced F-BMD, further support a major role for IGF-I in the regulation of bone mineral density.[7,8]

Second, in recent human studies, circulating levels of IGF-I have been found to be associated with bone mineral density. At least two groups have reported low serum IGF-I levels in males with idiopathic osteoporosis.[15,18] Other investigators have noted that IGF-I levels correlate closely with lumbar bone mineral density in postmenopausal women with and without osteoporosis.[10,16,17] Also, in humans there is a significant age-associated decrease in serum IGF-I which parallels a decline in bone mineral density with age and a similar decrease in cortical bone content of IGF-I and TGF-β.[3,17] Since bone loss in later life is associated with a marked impairment in osteoblast function (coupled with increased bone resorption), it is possible that perturbations in skeletal and systemic IGF-I may play a causal role in senile osteoporosis.

Studies of the IGF regulatory system in mouse strains offer several distinct advantages over human models. First, since circulating IGF-I in mammals is a function of several hormonal factors (growth hormone, testosterone, insulin, thyroxine, estrogen, and cortisol), as well as environmental determinants (nutrient intake, physical activity, and sunlight exposure), many of these variables can be controlled in mice. Second, an inbred strain represents a virtually unlimited set of genetically identical twins. This significantly reduces intrastrain variation for many phenotypes (including serum IGF-I and bone mineral density) as well as enhancing the likelihood of defining specific gene–gene interactions. Finally, a large body of literature for both B6 and C3H strains is available to investigators for development of strategies to assess mechanisms responsible for the phenotype under study.

From this study alone, we cannot define the mechanisms that produce high serum and cortical IGF-I levels in C3H mice. One obvious possibility is an alteration in growth hormone secretion between the two strains. In fact, two previous studies highlight the importance of earlier investigations which defined the hormonal status of these inbred strains of mice. Sinha et al.[20] reported that 7-month-old C3H/St female mice had serum growth hormone levels 50% higher than C57BL6/St females (22 ± 4 vs. 13 ± 2 ng/mL).[20] In a subsequent study, the same group reported an even greater difference in growth hormone levels between 3-month-old female C3H/HeJ and similarly aged C57BL/6J mice (20.3 ± 2.4 vs. 8.2 ± 1.1 ng/mL).[21] Those earlier studies are consistent with findings reported here, even though the mechanism of enhanced GH secretion (e.g., increased growth hormone releasing hormone secretion or decreased somatostatin production) in C3H mice cannot be determined from this study. Still, it is somewhat surprising to note that neither body weight nor length of the long bones was different between C3H and B6, despite differences in growth hormone and IGF-I levels. Further studies will be required to assess this paradox.

In conclusion, we have shown that serum and skeletal levels of IGF-I differ between two inbred strains of mice. These IGF-I strain differences may provide one clue as to the mechanism of increased bone mineral content in C3H compared to B6 mice. In addition, these changes imply that components of the growth hormone/IGF system contribute to the regulation of peak bone mass. Finally, these data point to the need for more studies to fully elucidate the pathophysiological significance of alterations in the growth hormone/IGF regulatory system, especially with respect to the adult mammalian skeleton.

Acknowledgments: This work was supported in part by grants from the National Institutes on Aging (AG10942-0451 [C.J.R.], from the NIH (Nos. AR-43618 [W.G.B., L.R.D., and C.J.R.] and CA-34196 [W.G.B.]) and from the U.S. Army Medical Research Acquisition Activity (DAMD17-96-1-6306 [W.G.B. and D.J.B.], and by medical research grants from the Department of Veterans Affairs (T.A.L., J.R.F., and D.J.B.).

References

1. Baylink, D. J., Finkelman, R. D., and Mohan, S. Growth factors to stimulate bone formation. J Bone Miner Res 8(Suppl.):S565–S572; 1993.
2. Beamer, W. G., Donahue, L. R., Rosen, C. J., and Baylink, D. J. Genetic variability in adult bone density among inbred strains of mice. Bone 18:397–403; 1996.
3. Bennett, A. E., Heinz, W. W., Riggs, B. L., and Hintz, R. IGF-I and II: Aging and bone density in women. J Clin Endocrinol Metab 59:701–704; 1984.
4. Bing-You, R. G., Denis, M. C., and Rosen, C. J. Low bone mineral density in adults with previous hypothalamic-pituitary tumors: Correlations with serum GH responses to GHRH, IGF-I and IGFBP-3. Calcif Tissue Int 52:183–187; 1993.
5. Boonen, S., Lesaffre, E., Dequeker, J., Aerssens, J., Nijs, J., Pelemans, W., and Bouillon, R. Relationship between basal IGF-I and femoral bone density in women aged over 70 years: Potential implications for the prevention of age-related bone loss. J Am Geriatr Soc 44:1301–1306; 1996.
6. Brier, R. H., Ballaher, B. W., and Gluckman, P. D. Radioimmunoassay for IGF-I: Solutions to some potential problems and pitfalls. J Endocrinol 128: 347–357; 1991.
7. Donahue, L. R. and Beamer, W. G. Growth hormone deficiency in *little* mice results in aberrant body composition, reduced IGF-I and IGFBP-3 but does not affect IGFBP-2, -1, or -4. J Endocrinol 136:91–104; 1993.
8. Donahue, L. R., Beamer, W. G., and Rosen, C. J. Parathyroid hormone (PTH) improves bone density in mice with growth hormone (GH) deficiency and insulin-like growth factor (IGF-I) deficiency. J Bone Miner Res 10(Suppl): 1995.
9. Farley, J. R., Hill, S. L., Tanner, M. A., and Wegedal, J. E. Specific activity of skeletal alkaline phosphatase in human osteoblast like cells is regulated by phosphate, phosphate esters and phosphate analogs and release of alkaline phosphatase activity is inversely regulated by calcium. J Bone Miner Res 9:497–508; 1994.
10. Godfrey, P., Rahal, J. O., Beamer, W. G., Copeland, N. G., Jenkins, N. A., and Mayo, K. E. GHRH receptor of *little* mice contains a missense mutation in the extracellular domain that disrupts receptor function. Nat Genet 4:227–232; 1993.
11. Grogean, T., Vercault, D., Millard, P. S., Kiel, D., MacLean, D., Orwoll, E., Greenspan, S., and Rosen, C. J. A comparative analysis of methods to measure IGF-I in human serum. Endocrinol Metab 4:109–114; 1997.
12. Hayden, J. M., Mohan, S., and Baylink, D. J. The insulin-like growth factor system and the coupling of formation to resorption. Bone 17(Suppl.):93S–98S; 1995.

13. Jorgensen, J. O. L., Thuesen, L., Ingemann-Hansen, T., Pedersen, S. A., Jorgensen, J. O., Skakkebaek, N. E. S., and Christiansen, J. S. Beneficial effects of GH treatment in GH deficient adults. Lancet i:1221–1225; 1989.
14. Linkhart, T. A. and Mohan, S. PTH stimulates release of IGF-I and IGF-II from neonatal mouse calvaria in organ culture. Endocrinology 125:1484–1491; 1989.
15. Ljunghall, S., Johansson, A. G., Bornane, P., Kampe, O., Lindh, E., and Karlsson, F. A. Low plasma levels of IGF-I in male patients with idiopathic osteoporosis. J Intern Med 232:59–64; 1992.
16. Mohan, S., and Baylink, D. J. Development of a simple valid method for the complete removal of IGF-binding proteins from IGFs in human serum and other biological fluids: Comparison with acid-ethanol treatment and C18 Sep-Pak separation. J Clin Endocrinol Metab 80:637–647; 1995.
17. Nicholas, V., Prewett, A., Bettieu, P., Mohan, S., Finkleman, R. D., Baylink, D. J., and Farley, J. R. Age related decreases in IGF-I and transforming growth factor-β in femoral cortical bone from both men and women: Implications for bone loss in aging. J Clin Endocrinol Metab 78:1011–1016; 1994.
18. Reed, B. Y., Zerwekh, J. E., Sakhaee, K., Breslau, N. A., Gottschalk, F., and Pak, C. Y. C. Serum IGF-I is low and correlated with osteoblastic surface in idiopathic osteoporosis. J Bone Miner Res 10:1218–1224; 1995.
19. Rosen, C. J., Donahue, L. R., and Hunter, S. J. Insulin-like growth factors and bone: The osteoporosis connection. Proc Soc Exp Biol Med 206:83–102; 1994.
20. Sinha, Y. N., Salnicks, C. B., and Vanderlaan, W. P. Prolactin and growth hormone levels in different inbred strains of mice: Patterns in association with estrous cycle, time of day and perphenazine stimulation. Endocrinology 97: 1112–1122; 1975.
21. Sinha, Y. N., Vlahakis, G., and Vanderlaan, W. P. Serum, pituitary and urine concentrations for prolactin and growth hormone in eight strains of mice with varying incidence of mammary tumors. Int J Cancer 24:430–437; 1979.

Date Received: March 31, 1997
Date Revised: May 19, 1997
Date Accepted: June 6, 1997

ELSEVIER

Bone Vol. 22, No. 3
March 1998:211–216

Alkaline Phosphatase Levels and Osteoprogenitor Cell Numbers Suggest Bone Formation May Contribute to Peak Bone Density Differences Between Two Inbred Strains of Mice

H. P. DIMAI,[1] T. A. LINKHART,[1,2] S. G. LINKHART,[1] L. R. DONAHUE,[3] W. G. BEAMER,[3] C. J. ROSEN,[4] J. R. FARLEY,[1,2] and D. J. BAYLINK[1,2]

[1] *J. L. Pettis Memorial Veterans Medical Center, Loma Linda, California, USA*
[2] *Loma Linda University, Loma Linda, California, USA*
[3] *Jackson Laboratories, Bar Harbor, Maine, USA*
[4] *St. Joseph Hospital, Bangor, Maine, USA*

Previous studies have shown that C3H/HeJ (C3H) mice have higher peak bone density than C57BL/6J (B6) mice, at least in part because of differences in rates of bone resorption. The current studies were intended to examine the alternative, additional hypothesis that the greater bone density in C3H mice might also be a consequence of increased bone formation. To that end, we measured two presumptive, indirect indices of bone formation and osteoblast number in these inbred strains of mice: alkaline phosphatase (ALP) activity in serum, bones, and bone cells; and the number of ALP-positive colony-forming units (CFU) in bone marrow stromal cell cultures. We found that C3H mice had higher serum levels of ALP activity than B6 mice at 6 (118 vs. 100 U/L, $p < 0.03$) and 32 weeks of age (22.2 vs. 17.2 U/L, $p < 0.001$). Tibiae from C3H mice also contained higher levels of ALP activity than tibiae from B6 mice at 6 (417 vs. 254 mU/mg protein, $p < 0.02$) and 14 weeks of age (132 vs. 79 mU/mg protein, $p < 0.001$), as did monolayer cultures of bone-derived cells from explants of 7.5-week-old C3H calvariae and femora (8.2 times more, $p < 0.02$, and 4.6 times more, $p < 0.001$, respectively). Monolayer cell cultures prepared by collagenase digestion of calvariae from newborn and 6-week-old mice also showed similar strain-dependent differences in ALP-specific activity ($p < 0.001$ for each). Our studies also showed more ALP-positive CFU in bone marrow stromal cell cultures from 8-week-old C3H mice, compared with B6 mice (72.3 vs. 26.1 ALP-positive CFU/culture dish, $p < 0.001$). A similar result was seen for ALP-positive CFU production at 6 and 14 weeks of age, and the difference was greatest for the CFU that contained the greatest numbers of ALP-positive cells. Because skeletal ALP activity is a product of osteoblasts and has been shown to correlate with rates of bone formation, and because the number of ALP-positive CFU is believed to reflect the number of osteoprogenitor cells, the current data are consistent with the general hypothesis that bone formation may be greater in C3H than B6 mice because of a difference in osteoblast number. Our data further suggest that peak bone density may be greater in C3H mice than B6 mice due to a combination of decreased bone resorption and increased bone formation. (Bone 22:211–216; 1998)

Key Words: Bone density; Genetics; Mice; Alkaline phosphatase; Osteoblasts.

Introduction

Recent studies indicate that genetics may determine up to 70% of peak bone density,[11,17,18,26] which is presumed to be a polygenic trait. We have developed an animal model for quantitative trait locus (QTL) analysis[1,3,4] of genes associated with peak bone density differences between two inbred strains of mice. Adult C3H/HeJ (C3H) and C57BL/6J (B6) mice are of similar size and body weight and have femora of similar size (i.e., by external dimensions), but femoral bone density is 53% greater in C3H, compared with B6, mice.[4] To complement the QTL analysis, we have also planned a strategy of histomorphometric and biochemical studies to identify the mechanistic differences (i.e., in rates of bone formation and resorption) that result in the density difference between these strains of mice. Data from previous studies have shown that B6 femora have much larger medullary cavities than C3H femurs,[2,4] and suggested that the rate of endosteal bone resorption is lower in the femora of C3H, compared with B6, mice.[2] More recent in vitro studies have supported this hypothesis: Marrow cells from B6 mice produce more presumptive osteoclasts than marrow cells from C3H mice.[21]

Therefore, we have proposed that developmental differences in rates of bone resorption could account for the difference in peak bone density, if the rates of bone formation are equivalent. The current studies were intended to assess the alternative, but not mutually exclusive, possibility that the greater peak bone density in C3H mice might also be a consequence of differences in rates of bone formation. In other words, we sought to test the specific hypothesis that the rate of bone formation would be higher in C3H mice than in B6 mice and, as an approach to that end, we measured alkaline phosphatase (ALP) activity—in serum, and extracts of bone cells and bones—as a presumptive

Address for correspondence and reprints: John Farley, Ph.D., c/o Research Service (151), J. L. Pettis Memorial Veterans Medical Center, 11201 Benton Street, Loma Linda, CA 92357.

8756-3282/98/$19.00
PII S8756-3282(97)00268-8

Bone Vol. 22, No. 3
March 1998:211–216

index of the number and/or activity of bone-forming osteoblasts.[7,10,12–14,20,23,24,34,36] We also measured the number of ALP-positive colony forming units (CFU)—in marrow stromal cell cultures—as a presumptive index of the number of osteoblast-line progenitor cells.[19,22,25,27,30] A similar analysis of marrow stromal CFU as an index of osteoprogenitor cell number was included as one aspect of a combined histomorphometric, densitometric, and in vitro cell cell culture study of the SAMP6 strain of mice,[16] which exhibit accelerated senescence with attendant osteopenia. Although SAMP6 mice are not closely related to either C3H or B6 mice, the aforementioned study[16] is relevant to our investigations in three important respects: first, because it showed a strain-dependent difference in CFU formation; second, because it demonstrated an association between low bone mineral density and decreased osteoblastogenesis; and finally, because it will provide a phenotypic/mechanistic correlate for QTL analysis to identify the genes that determine senescent osteopenia in SAMP6 mice.[5] The current studies are one aspect of our coordinate phenotypic/genotypic studies to identify the genes that determine peak bone density in C3H and B6 mice.

Materials and Methods

Materials

Dulbecco's minimal essential medium (DMEM) was obtained from Mediatech Inc. (Herndon, VA), collagenase was from Boehringer-Mannheim (Indianapolis, IN), and α-MEM and trypsin-EDTA were from Gibco Life Sciences (Grand Island, NY). Calf serum (CS) and fetal bovine serum were from Hyclone (Logan, VT). *p*-Nitrophenylphosphate (PNPP), 1,25-dihydroxyvitamin D_3 [1,25-$(OH)_2D_3$], Triton X-100, Naphthol AS-TR, and Fast-Red Violet LB were from Sigma Chemicals (St. Louis, MO). Tissue culture dishes were from Corning (Corning, NY). Protein dye-binding reagent was purchased from Bio-Rad (Hercules, CA). Sodium azide and buffers were purchased from Fisher Scientific (Pittsburgh, PA).

Animals

Inbred mice of strains C57BL/6J and C3H/HeJ were obtained from the Jackson Laboratory (Bar Harbor, ME). All mice used in these studies were female and were housed in an accredited facility (in the J. L. Pettis Memorial Veterans Medical Center) for at least 1 week before euthanasia for collection of serum and/or skeletal tissues. Acidified water (HCl, pH 2.8–3.2) and autoclaved, pelleted diet (NIH 31: 18% protein, 6% fat, 1.27% calcium, 0.92% phosphate, trace minerals, vitamin fortified; Purina, Madison, WI) were freely available. At the specified ages, groups of mice were killed by decapitation, using ethrane anesthesia. Blood samples were allowed to clot, and centrifuged for the preparation of serum. Sera were kept in frozen storage (−20°C) for subsequent assessments of skeletal ALP activity. For the preparation of osteoblast-lineage cell cultures, bones (femora and calvariae) were removed aseptically and monolayer cell cultures derived from either: (i) femur marrow cells; (ii) outgrowth from bone fragments; or (iii) incubation of bone fragments with collagenase. Additional bones (femora, tibiae, calvariae) were dissected free of adherent tissue (without removing the periosteum) and used for extraction of ALP activity. All protocols were reviewed and approved by the animal studies subcommittee of the J. L. Pettis Memorial Veterans Medical Center.

Extraction of Bones

As in our previous studies,[13,14] tibiae were freed of adherent tissue and the long bones were cut into two pieces (near the midshaft) before an overnight incubation in phosphate-buffered saline (PBS) containing 0.01% sodium azide, at 4°C (1.5 mL/bone), to remove the marrow and contaminating serum. Each sample was then transferred to a solution of 0.01% Triton X-100, containing 0.01% sodium azide in 25 mmol/L $NaHCO_3$ buffer (pH 7.4) for a 72 h extraction at 4°C (1.5 mL/bone). The extracts were then centrifuged to remove insoluble material, and ALP and protein concentration[6] were determined in each extract. The extracted bones were transferred to 70% ethanol (1 mL/bone) for a 24 h incubation at 37°C, then dried for 18 h at 37°C for determination of dry weight (Cahn Microbalance, Model 7500, Cahn Instruments, Cerritos, CA).

Preparation and Culture of Bone-Derived Cells

Cells released from bone by collagenase digestion. Osteoblast-line cells were prepared by sequential collagenase digestion of calvariae dissected from newborn and 4-week-old mice. After an initial 15 min incubation at 37°C, with 1 mg/mL collagenase A in DMEM (from which the cell-containing supernatant was discarded), the calvariae were incubated with fresh collagenase A for 90 min. The cells released during this interval were collected by centrifugation and grown in monolayer cultures in DMEM + 10% CS until they reached confluence. The confluent cells were passaged (with trypsin-EDTA) and plated in replicate cultures (24-place multiwell tissue-culture dishes, n = 6/strain at each age) in DMEM + 10% CS for 4 days [with or without 10 nmol/L 1,25$(OH)_2D_3$], then changed to serum-free DMEM, containing 0.1% BSA [±1,25$(OH)_2D_3$ as before] for an additional 24 h. The cell layers were rinsed four times with PBS and extracted with 0.10 mL of a 0.01% solution of Triton X-100 in 25 mmol/L $NaHCO_3$ buffer (pH 7.5) for assessment of ALP specific activity.

Cells derived from bone explants. Calvariae and femora were dissected from 7.5-week-old mice under aseptic conditions and rinsed in α-MEM. The calvariae were cut into pieces (about 2–3 mm on a side) and incubated in DMEM + 10% CS in a six-place multiwell tissue-culture plate. Calvariae from two mice of the same strain were combined in each well and a total of four wells were prepared from each strain. The femora were used as a source of marrow for the preparation of osteoclast-lineage cells[21] by removing the ends of bones and flushing the marrow from the midshaft with a 25 gauge needle and cold α-MEM.[15,33] The marrowless femora were cut into fragments and incubated in DMEM + 10% CS in six-place multiwell tissue-culture plates. Fragments of femora from two mice of the same strain were combined in each well, as just described. The culture media was changed every 2–3 days. After 12 days, the bone fragments were removed from the cultures. After 17 days, the cell layers were rinsed four times with PBS (to remove CS) and extracted with 0.25 mL of a 0.01% solution of Triton X-100 in 25 mmol/L $NaHCO_3$ buffer (pH 7.5) for assessment of ALP specific activity.

Assessment of ALP-Positive Colony Forming Units From Marrow Cell Preparations

Bone marrow stromal cells were obtained from femora of 6- and 8-week-old female mice by modification of the procedure described previously.[15,33] Femora were aseptically removed, placed on ice in α-MEM, and dissected free of soft tissues. The ends of the bones were removed and the marrow was flushed from the midshaft with a syringe and a 25 gauge needle using

cold α-MEM. Marrow cells were washed, resuspended in α-MEM containing 10% fetal bovine serum, 10 nmol/L dexamethasone, penicillin, and streptomycin, and the number of nucleated cells was determined. Cells were plated at 10^6 nucleated cells per 6-cm-diameter culture dish. Because preliminary studies showed more ALP-positive CFU in marrow stromal cell cultures from CH3 than B6 mice, we prepared more B6 cell cultures (i.e., n = 6 and n = 10 dishes for B6, n = 3 for CH3). After 24 h, unattached cells were removed and the medium was replaced. The medium was changed at 3 days and 6 days and, at the last medium change, $1,25(OH)_2D_3$ was added at 10 nmol/L. On day 10 of culture the cells were stained for ALP activity, using Naphthol AS-TR substrate and Fast-Red Violet LB coupler.[35] We counted: (a) the number of ALP-positive colonies in each dish; and (b) the number of ALP-positive cells in each colony.

ALP Activity

ALP activity was assessed by the time-dependent formation of *p*-nitrophenolate (which absorbs light of 405 nm in an alkaline solution) from PNPP. Our standard protocols used 5 μL of serum or 25 μL of bone or cell layer extract in a total volume of 0.3 mL containing 10 mmol/L PNPP, 1 mmol/L $MgCl_2$, and, for the serum samples, 10 mmol/L L-phenylalanine (to inhibit any circulating intestinal ALP activity), in 150 mmol/L Na_2CO_3 buffer (pH 10.3) in the individual wells of a 96-place microtiter plate.[20,36] Each sample was measured in duplicate. Reactions were initiated by the addition of substrate (PNPP) and the time-dependent increase in absorbance at 405 nm was measured on a microtiter plate spectrophotometer (Labinstruments, Model EAR400/340AT, Vienna, Austria). ALP activity was calculated as units per liter of serum, milliunits per milligram of protein, or milliunits per milligram of dry weight of bone, where 1 U is defined by the conversion of 1 μmol of substrate to product per minute at room temperature (25°C). Protein was measured by the dye-binding method of Bradford,[25] using a commercial preparation of the dye reagent (Bio-Rad).

Statistical Analyses

Data are presented as the averages of replicate samples in each group (usually as mean ± SEM). Analytic methods included analysis of variance (ANOVA), linear regression, and Pearson correlation, using SYSTAT statistical software (Systat Inc., Evanston, IL).

Results

Consistent with previous studies,[4] we found that female C3H mice did not differ from female B6 mice, with respect to body weight, at 6, 8, 14, or 32 weeks of age. These results are shown in **Table 1**. The same studies also showed that C3H mouse serum contained higher levels of ALP activity than B6 mouse serum, between the ages of 6 and 32 weeks—18% more at 6 weeks ($p < 0.003$), 31% more at 8 weeks ($p < 0.002$), and 29% more at 32 weeks ($p < 0.001$). Although previous studies have suggested that mouse serum ALP is primarily derived from bone,[13,24] the serum ALP assay that was used in the present study was not isoenzyme-specific (i.e., our assay would have measured both skeletal and hepatic ALP isoenzyme activities, if both were present).

To test the hypothesis that the higher levels of serum ALP activity in C3H mice, compared with B6 mice, reflected higher levels of skeletal ALP activity in bone, we measured ALP activity in Triton X-100 extracts of tibiae obtained from some (but not all) of the mice that we had used for measurements of serum ALP. As summarized in **Table 2**, the results of these studies showed: (a) that the dry weight of the tibiae from female C3H mice was greater than the dry weight of tibiae from female B6 mice at 8 and 14 weeks of age, but not at 6 weeks of age; and (b) that C3H tibial extracts contained higher levels of ALP activity than B6 tibial extracts, at 6, 8, and 14 weeks of age.

An initial correlation showed that the level of (skeletal) ALP activity in the extracts of tibiae was proportional to the amount of ALP activity in serum, when the data from all of the mice were combined (i.e., irrespective of age and strain). This is shown in **Figure 1**. Further analysis showed that the correlation between serum ALP activity and tibial ALP activity (combining data from both strains of mice) was significant at 8 weeks ($r = 0.485$, $p < 0.05$) and 14 weeks ($r = 0.579$, $p < 0.02$), but not at 6 weeks of age ($r = 0.02$). This is not surprising, inasmuch as tibial ALP decreased consistently with time in both strains ($r = -0.78$ and $r = -0.81$ for C3H and B6 mice, respectively, $p < 0.001$ for each), whereas serum ALP did not. Although our data revealed

Table 1. Age- and strain-dependent differences in body weight and serum ALP activity

Age (wk)	Parameter	Value of parameter in indicated strain: C3H	Value of parameter in indicated strain: B6	Significance of difference
6	weight	16.3 ± 0.3	16.8 ± 0.4	n.s.
8	weight	18.5 ± 0.5	18.9 ± 0.5	n.s.
14	weight	20.3 ± 0.3	21.8 ± 0.5	n.s.
32	weight	30.3 ± 0.9	32.6 ± 0.9	n.s.
6	serum ALP	117.7 ± 4.0	99.8 ± 5.0	$p < 0.003$
8	serum ALP	138.2 ± 9.1	105.4 ± 7.5	$p < 0.002$
14	serum ALP	56.1 ± 3.0	49.1 ± 3.2	n.s.
32	serum ALP	22.2 ± 0.9	17.2 ± 0.9	$p < 0.001$

Serum collected from C3H and B6 mice of the indicated ages. Group size ranged from 8 to 20 as follows: 20 mice of each strain at 6 weeks; 16 C3H and 14 B6 mice at 8 weeks; 9 CH3 and 8 B6 mice at 14 weeks; and 20 mice of each strain at 32 weeks. Body weight is shown in grams and ALP activity in milliunits per milliliter of mouse serum and the data are expressed as mean ± SEM for each group. n.s. indicates no significance (i.e., $p > 0.05$). Two-way ANOVA shows effects of both age and strain on serum ALP activity ($p < 0.001$ for each).

Table 2. Age-and strain-dependent differences in tibial dry weight and tibial ALP activity

Age (wk)	Parameter	Value of parameter in indicated strain: C3H	Value of parameter in indicated strain: B6	Significance of difference
6	dry weight	26.0 ± 0.5	25.2 ± 0.7	n.s.
8	dry weight	31.8 ± 0.8	26.1 ± 0.7	$p < 0.02$
14	dry weight	39.4 ± 1.0	35.2 ± 0.9	$p < 0.01$
6	ALP SA	417 ± 15	254 ± 17	$p < 0.02$
8	ALP SA	204 ± 14	143 ± 18	$p < 0.04$
14	ALP SA	132 ± 11	79 ± 17	$p < 0.001$

Tibiae were dissected from C3H and B6 mice at the indicated ages. Group size ranged from 8 to 10 as follows: 8 mice of each strain at 6 weeks and 8 weeks; 10 C3H and 9 B6 mice at 14 weeks. Tibiae were extracted with Triton X-100 (as described in *Materials and Methods*) for measurement of ALP activity and protein and then dried for determination of weight. Tibial dry weight is shown in grams and ALP specific activity (SA) in milliunits per milligram of protein. All data are expressed as mean ± SEM. n.s. indicates no significant difference. Two-way ANOVA shows effects of both age and strain on tibial ALP specific activity ($p < 0.001$ for each).

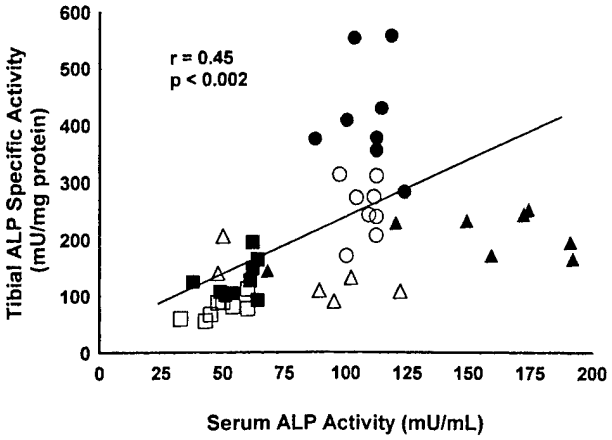

Figure 1. Correlation of ALP specific activity in extracts of tibiae with ALP activity in serum, using data summarized in Tables 1 and 2 for C3H (solid symbols) and B6 (open symbols) mice at 6 weeks (triangles), 8 weeks (circles), and 14 weeks (squares) of age. Linear regression analysis shows a significant relationship with $r = 0.45$, $p < 0.002$ (n = 51 mice).

an overall negative correlation between serum ALP activity and age in both B6 ($r = -0.76$, $p < 0.001$) and C3H ($r = -0.33$, $p < 0.03$) mice, this relationship was determined by the large net decrease in serum ALP activity between 6 and 32 weeks. Serum ALP did not decrease in either strain between the ages of 6 and 8 weeks, and, in fact, serum ALP increased at between 6 and 8 weeks of age in the C3H mice ($p < 0.05$).

Additional ALP studies revealed that monolayer cultures of calvarial cells (prepared by collagenase digestion) from newborn and 6-week-old CH3 mice contained 3.6–12 times more ALP activity per milligram of cell protein than B6 calvarial cells ($p < 0.001$ for each). Although the addition of $1,25(OH)_2D_3$ to the culture medium increased ALP specific activity in the cells from 6-week-old C3H calvariae ($p < 0.02$), it did not affect the level of ALP activity in parallel cultures of cells from 6-week-old B6 calvariae, or in calvarial cells prepared from newborn mice of either strain. Bone cells derived from explants of femora and calvariae from 7-week-old mice also showed similar differences—cells from C3H femora and calvariae had 8.2- and 4.6-fold higher levels of ALP activity (i.e., ALP activity per milligram of cell protein, $p < 0.001$ and $p < 0.002$, respectively) than cells derived from the femora and calvariae of B6 mice. The results of these cell culture studies are summarized in **Table 3**. Although the relative level of ALP activity per milligram of cell protein varied widely between the tested cell cultures [e.g., from a low of 0.01 mU/mg for B6 femur explant cells to a high of 35.5 mU/mg for $1,25(OH)_2D_3$-treated C3H calvarial cells—presumably reflecting differences in osteoblastic differentiation], the C3H cells always had much higher levels of ALP activity than the parallel cultures of B6 cells.

To determine whether the higher levels of ALP activity in the bone cell cultures prepared from C3H mice, compared to B6 mice, were associated with corresponding differences in the

Table 3. Strain-dependent difference in ALP activity in monolayer cell cultures

Source of cells (±D)	Method of preparation/age	ALP specific activity (mU/mg)		Significance of difference
		C3H	B6	
Calvaria (−D)	collagenase/newborn	26.3 ± 1.2	7.25 ± 0.5	$p < 0.001$
Calvaria (+D)	collagenase/newborn	35.5 ± 4.5	6.93 ± 0.35	$p < 0.001$
Calvaria (−D)	collagenase/6 weeks	5.06 ± 1.09	0.65 ± 0.07	$p < 0.001$
Calvaria (+D)	collagenase/6 weeks	10.75 ± 1.42	0.82 ± 0.10	$p < 0.001$
Femurs (−D)	explants/7 weeks	0.082 ± 0.009	0.010 ± 0.002	$p < 0.001$
Calvaria (−D)	explants/7 weeks	0.248 ± 0.069	0.054 ± 0.023	$p < 0.002$

Replicate cultures prepared from bones of C3H and B6 mice (of the indicated ages) by collagenase digestion (n = 6) and by outgrowth from bone fragments (explants, n = 4). After culture in DMEM + 10% FCS [with or without 10 nmol/L $1,25(OH)_2D$, as indicated], the cell layers were rinsed four times with PBS (to ensure removal of serum) and then extracted with a solution of 0.01% Triton X-100 in 25 mmol/L $NaCO_3$ buffer (pH 7.5). ALP activity and protein were determined in each extract. ALP specific activity was calculated as milliunits per milligram of protein (shown as mean ± SEM).

Table 4. ALP-positive colony forming units

Number of cells per colony	Type of colonies counted	Number colonies observed for indicated strain of mice	
		C3H	B6
3–10 ALP-positive cells	ALP-positive colonies	22.7 ± 3.2	19.7 ± 1.4
11–20 ALP-positive cells	ALP-positive colonies	19.3 ± 2.6	5.3 ± 1.5[b]
>20 ALP-positive cells	ALP-positive colonies	13.3 ± 2.0	0.8 ± 0.4[b]
>3 ALP-positive cells	ALP-positive colonies	55.3 ± 5.0	25.8 ± 2.4[a]
3–10 cells	all colonies	90.7 ± 12.7	39.3 ± 2.9[b]
11–20 cells	all colonies	77.3 ± 10.4	10.7 ± 2.9[b]
>20 cells	all colonies	53.3 ± 8.1	1.7 ± 0.8[b]
>3 cells	all colonies	221.3 ± 19.8	51.7 ± 4.8[b]

Replicate marrow cell cultures from 6-week old C3H (n = 3) and B6 (n = 6) mice were scored for: number of ALP-positive colonies/dish; number of ALP-positive cells/colony (i.e., 3–10, 11–20, and >20 ALP-positive cells/colony); total number of colonies/dish (including ALP-negative colonies); and total number of cells/colony (including ALP-negative cells). Data shown as mean ± SEM. Two-way ANOVA shows effects of both strain and percentage of ALP-positive cells on the number of ALP-positive colonies seen ($p < 0.001$).
[a]Significant difference between C3H and B6, $p < 0.005$.
[b]$p < 0.001$.

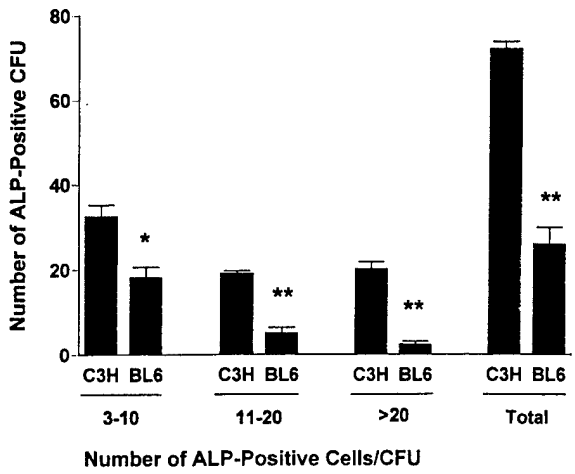

Figure 2. ALP-positive CFU prepared from marrow stromal cell cultures of 8-week-old C3H and B6 mouse femurs. Data shown as the number of ALP-positive CFU observed per culture dish, mean ± SEM (n = 10 dishes for B6, n = 3 for C3H) for CFU that contained the indicated numbers of ALP-positive cells. Asterisk: significant difference between C3H and B6, $p < 0.005$; double asterisk: $p < 0.001$. Two-way ANOVA shows effects of both strain and number of ALP-positive cells on the number of ALP-positive CFU observed ($p < 0.001$ for each).

number of bone marrow stromal cells with osteoblastic potential, we determined the numbers of ALP-positive colony forming units (CFUs) that could be obtained from marrow stromal cell cultures. We first prepared stromal cell cultures from the femora of 6-week-old C3H and B6 mice. As summarized in **Table 4**, we found that marrow stromal cells from CH3 mice produced more CFU of all sizes ($p < 0.001$), and more ALP-positive CFU (i.e., with 11–20 and >20 ALP-positive cells/CFU, $p < 0.001$ for each) than marrow stromal cells from B6 mice. Consistent with these findings, a follow-up study revealed: (i) that marrow stromal cells from 8-week-old C3H mice produced 2.7 times more ALP-positive CFU than marrow stromal cells from 8-week-old B6 mice, $p < 0.001$; (ii) that the ALP-positive CFU derived from C3H mouse marrow contained a greater percentage of ALP-positive cells than the B6 CFU, $p < 0.005$ at 3–10 ALP-positive cells per CFU and $p < 0.001$ at 11–20 and <20 ALP-positive cells per CFU; and (iii) that this difference became more pronounced as the size of the CFU increased, $p < 0.001$ by two-way ANOVA. These results are shown in **Figure 2**.

Discussion

The results of our studies allow two conclusions: first, that CH3 mice have higher levels of ALP activity than B6 mice, in serum and extracts of bone cells and bones; and second, that bone marrow stromal cell cultures prepared from C3H femurs produce more ALP-positive colonies than marrow stromal cell cultures from B6 femora. Because previous studies have shown that the amount of skeletal ALP activity in serum (and in bone) can provide an index of the rate of bone formation, in humans[10,20,36] and in rodents,[7,13,14,23,24] and that the number of ALP-positive CFU in bone marrow stromal cell cultures can provide an index of the number of osteoprogenitor cells, and therefore the osteogenic potential,[19,22,25,27,30] our observations are consistent with the general hypothesis that bone formation is greater in C3H mice than in B6 mice because the former are producing more osteoblasts.

We should note, however, that these interpretations are contingent on successful resolution of the following two issues. First, we need to know why serum ALP activity did not correlate more closely with tibial ALP in both strains, at all ages. Although we have interpreted the strain-dependent differences in serum ALP activity as reflective of differences in skeletal ALP and, by extension, differences in the systemic average rate of bone formation, serum ALP activity was not correlated with tibial ALP activity in the 8-week-old mice. An inspection of our data shows that serum ALP activity increased in the C3H mice, between 6 weeks and 8 weeks of age, and then decreased at 14 and 32 weeks, whereas tibial ALP activity consistently decreased from 6 to 8 to 14 weeks of age. Although we may speculate that the disparity could be due to: (a) a larger contribution to serum skeletal ALP from other (nontibial) skeletal sources between 6 and 8 weeks of age; or (b) a transient relative increase in hepatic ALP activity in serum (the onset of puberty may also be a factor), further studies are required to resolve this issue. Additional studies are also required to determine whether our observations of strain-specific differences in ALP activity and osteoprogenitor pool size are actually indicative of strain-specific differences in rates of bone formation. For example, differences in bone formation should result in proportional, or at least parallel, differences in ALP activity, osteocalcin, and type I collagen synthesis.

With regard to mechanism, previous studies have suggested that bone formation may be higher in the C3H mice, compared with B6 mice, because of higher levels of growth hormone. C3H mice have higher serum levels of growth hormone than B6 mice[31,32] and we found higher levels of IGF-I in the serum and bones of C3H mice, compared with B6 mice.[29] Finally, more recent studies have shown a genetic association between femoral bone density and serum levels of IGF-I in the F_2 progeny of a C3H × B6 cross,[28] but association is not evidence of causative linkage. Other strain-dependent differences may also contribute to (or be determinants of) the observed differences in ALP activity and CFU formation. For example, previous studies have shown that C3H mice have higher basal levels of parathyroid hormone and $1,25(OH)_2D_3$ than B6 mice, a higher proportion of occupied vitamin D receptors, and a corresponding higher rate of intestinal Ca absorption.[8,9]

In summary, the current studies indicate that C3H mice have higher levels of ALP activity (in serum and in bone) than B6 mice and that C3H mice can produce more ALP-positive CFU than B6 mice and, together, these observations suggest that C3H mice produce more osteoblastic cells (and have a greater osteogenic potential) than B6 mice. This is consistent with the recent observation of an apparent link between decreased osteoblastogenesis and low bone mineral density in the unrelated SAMP6 strain of mice.[16] Our observations are also consistent with the general hypothesis that the greater peak bone density in C3H mice, compared with B6 mice, is a multifactorial consequence of both decreased bone resorption[2,4,21] and increased bone formation.

Acknowledgments: The authors thank the secretarial staff of the Loma Linda University Mineral Metabolism Research Unit (which is located in the J. L. Pettis Memorial Veterans Medical Center) for assistance in the preparation of this manuscript. These studies were supported by: the National Institutes of Health, Grants #AR-43618 and CA-34196 (W.G.B); a subcontract from U.S. Army Medical Research Acquisition Activity Grant DAMD17-96-1-6306 (W.G.B. and D.J.B.); medical research grants from the Department of Veterans Affairs (T.A.L., S.G.L., J.R.F., and D.J.B.); the Government of Austria (HPD); and Loma Linda University (T.A.L., J.R.F., and D.J.B.).

References

1. Baylink, D. J., Donahue, L., Rosen, C. J., Gruber, H., Lee, J. E. S., Farley, J., and Beamer, W. Novel genetic model of peak bone density: A polygenic trait. Tenth International Congress of Endocrinology, Program and Abstracts, Vol. 1, Abstract #P1-945; 1996.
2. Baylink, D., Jarley, J., Donahue, L., Rosen, C. J., Barr, B., Lee, J. E. S., and Beamer, W. Evidence that high peak bone density is due to decreased resorption not increased formation in a murine model [abstract #344]. J Bone Mineral Res 10(Suppl.):S338; 1995.
3. Beamer, W. G., Donahue, L. R., Baylink, D. J., and Rosen, C. J. Mapping genes for normal bone density in inbred mice by quantitative trait locus analysis. J Bone Miner Res 11(Suppl. 1):S176; 1996.
4. Beamer, W. G., Donahue, L. R., Rosen, C. J., and Baylink, D. J. Genetic variability in adult bone density among inbred strains of mice. Bone 18:397–403; 1996.
5. Benes, H., Dennis, R., Zheng, W., Weinstein, R. S., Shelton, R., Jilka, R. L., Roberson, P., Manolagas, S. C., and Shmookler, R. J. Genetic mapping of osteopenia-associated loci using crosses between closely related mouse strains with differing bone mineral density [abstract #F598]. J Bone Miner Res 12(Suppl. 1):S375; 1997.
6. Bradford, M. M. A rapid and sensitive method for the quantitation of microgram amounts of protein, utilizing the principle of protein-dye binding. Anal Biochem 72:248–255; 1976.
7. Canalis, E. Effect of hormones and growth factors on alkaline phosphatase activity and collagen synthesis in cultured rat calvariae. Metabolism 32:14–20; 1983.
8. Chen, C. and Kalu, D. N. Strain differences in calcium absorption, serum $1,25(OH)_2D$ and serum parathyroid hormone in response to dietary calcium restriction in C3H/HeJ and C57BL/6J mice [abstract #F595]. J Bone Miner Res 12(Suppl. 1):S375; 1997.
9. Chen, C., Noland, K. A., and Kalu, D. N. Strain differences in bone density, calcium absorption, and intestinal calcium transport between C3H/HeJ and C57BL/6J mice [abstract F594]. J Bone Miner Res 12(Suppl. 1):S374; 1997.
10. Clark, L. C. and Beck, E. Serum alkaline phosphatase and growth in adolescent children. J Pediatr 36:335–341; 1950.
11. Evans, R. A., Marel, G. M., Lancaster, E. K., Kos, S., Evans, M., and Wong, Y. P. Bone mass is low in relatives of osteoporotic patients. Ann Intern Med 109:870–873; 1988.
12. Farley, J. R. and Baylink, D. J. Skeletal alkaline phosphatase as a bone formation index in vitro. Metabolism 35:563–571; 1986.
13. Farley, J. R., Hall, S. L., Herring, S., and Tarbaux, N. M. Two biochemical indices of mouse bone formation are increased, in vivo, in response to calcitonin. Calcif Tissue Int 50:67–73; 1992.
14. Farley, J. R., Hall, S. L., and Tarbaux, N. M. Calcitonin (but not calcitonin gene-related peptide) increases mouse bone cell proliferation in a dose-dependent manner, and increases mouse bone formation, alone and in combination with fluoride. Calcif Tissue Int 45:214–221; 1989.
15. Jilka, R. L., Hangoc, G., Girasole, G., Passeri, G., Willians, D. C., Abrams, J. S., Boyce, B., Broxmeyer, H., and Manolagas, S. C. Increased osteoclast development after estrogen loss: Mediation by interleukin-6. Science 257:88–91; 1992.
16. Jilka, R. L., Weinstein, R. S., Takahashi, K., Parfitt, A. M., and Manolagas, S. C. Linkage of decreased bone mass with impaired osteoblastogenesis in a murine model of accelerated senescence. J Clin Invest 97:1732–1740; 1996.
17. Jouanny, P., Guillemin, F., Kuntz, C., Jaendel, C., and Pourel, J. Environmental and genetic factors affecting bone mass. Similarity of bone density among members of healthy families. Arthritis Rheum 38:61–67; 1995.
18. Kelly, P. J. and Harris, M. Genetic regulation of peak bone mass. Acta Paediatr Scand 411(Suppl.):24–29; 1995.
19. Kuznetsov, S. and Robey, P. G. Species differences in growth requirements for bone marrow stromal fibroblast colony formation in vitro. Calcif Tissue Int 59:265–270; 1996.
20. Lauffenburger, T., Olah, A. J., Dambacher, M. A., Guncaga, J., Lentner, C., and Haas, H. G. Bone remodeling and calcium metabolism: A correlated histomorphometric, calcium kinetic, and biochemical study in patients with osteoporosis and Paget's disease. Metabolism 26:589–597; 1977.
21. Linkhart, T., Linkhart, S., Farley, J., Dimai, H. P., Beamer, W., Donahue, L. R., Rosen, C., Gruber, H., and Baylink, D. J. Genetic model of murine peak bone density: Strain specific differences in peak bone density, osteoclast number and interleukin-6 production [abstract P221]. J Bone Miner Res 11(Suppl. 1):S146; 1996.
22. Long, M. W., Robinson, J. A., Ashcraft, E. A., and Mann, K. G. Regulation of human bone marrow-derived osteoprogenitor cells by osteogenic growth factors. J Clin Invest 95:881–887; 1995.
23. Marie, P. J. and Travers, R. Continuous infusion of 1,25-dihydroxyvitamin D stimulates bone turnover in the normal young mouse. Calcif Tissue Int 35:418–425; 1983.
24. Menahan, L. A., Sobocinski, K. A., and Austin, B. P. The origin of plasma alkaline phosphatase activity in mice and rats. Comp Biochem Physiol 79B: 279–283; 1984.
25. Nishida, S., Yamaguchi, A., Tanizawa, T., Endo, N., Mashiba, T., Uchiyama, Y., Suda, T., Yoshiki, S., and Takahashi, H. E. Increased bone formation by intermittent parathyroid hormone administration is due to the stimulation of proliferation and differentiation of osteoprogenitor cells in bone marrow. Bone 6:717–723; 1994.
26. Pocock, N. A., Eisman, J. A., Hooper, J. L., Yeates, M. G., Sambrook, P. N., and Ebert, S. Genetic determinants of bone mass in adults. J Clin Invest 80:706–710; 1987.
27. Quarto, R., Thomas, D., and Liang, C. T. Bone progenitor cell deficits and the age-associated decline in bone repair capacity. Calcif Tissue Int 56:123–129; 1995.
28. Rosen, C. J., Dimai, H. P., Vereault, D., Donahue, L. R., Beamer, W. G., Farley, J., Linkhart, S., Linkhart, T., Mohan, S., and Baylink, D. J. Serum IGF-I segregates with femoral bone density in the F_2 progeny of C3 (high bone density) and B6 (low bone density) crosses [abstract P292]. J Bone Miner Res 12(Suppl. 1):S174; 1977.
29. Rosen, C. J., Dimai, H. P., Vereault, D., Donahue, L. R., Beamer, W. G., Farley, J., Linkhart, S., Linkhart, T., Mohan, S., and Baylink, D. J. Circulating and skeletal insulin-like growth factor-I (IGF-I) concentrations in two inbred strains of mice with different bone densities. Bone. In press.
30. Scutt, A. and Bertram, P. Bone marrow cells are targets for the anabolic actions of prostaglandin E_2 on bone: Induction of a transition from nonadherent to adherent osteoblast precursors. J Bone Miner Res 10:474–487; 1995.
31. Sinha, Y. N., Salocks, C. B., and Vanderlaan, W. P. Prolactin and growth hormone levels in different inbred strains of mice: Patterns in association with estrous cycle, time of day and perphenazine stimulation. Endocrinology 97: 1112–1122; 1975.
32. Sinha, Y. N., Vlahakis, G., and Vanlerlaan, W. P. Serum, pituitary and urine concentrations for prolactin and growth hormone in eight strains of mice with varying incidence of mammary tumors. Int J Cancer 24:430–437; 1979.
33. Takahashi, N., Yamana, H., Yoshiki, S., Roodman, G. D., Mundy, G. R., Jones, S. J., Boyde, A., and Suda, T. Osteoclast-like cell formation and its regulation by osteotropic hormones in mouse bone marrow cultures. Endocrinology 122:1373–1382; 1988.
34. Weiss, M., Cole, D., Ray, K., Whyte, M. P., Lafferty, M. A., Mulivor, R. A., and Harris, H. A missense mutation in the human liver-bone-kidney ALP gene causing a lethal form of hypophosphatasia. Proc Natl Acad Sci USA 85:1766–1769; 1988.
35. Wergedal, J. E. and Baylink, D. J. Characterization of cells isolated and cultured from human bone. Proc Soc Exp Biol Med 176:60–69; 1984.
36. Van Straalen, J. P., Sanders, E., Prummel, M. F., and Santers, G. T. B. Bone alkaline phosphatase as indicator of bone formation. Clin Chim Acta 201:27–34; 1991.

Date Received: September 18, 1997
Date Revised: October 28, 1997
Date Accepted: October 28, 1997

JOURNAL OF BONE AND MINERAL RESEARCH
Volume 14, Number 1, 1999
Blackwell Science, Inc.

Osteoclast Formation in Bone Marrow Cultures from Two Inbred Strains of Mice with Different Bone Densities*

THOMAS A. LINKHART,[1,2,3] SUSAN G. LINKHART,[1] YOSHIAKI KODAMA,[1] JOHN R. FARLEY,[1,2,4] H. PETER DIMAI,[1] KENNETH R. WRIGHT,[5] JON E. WERGEDAL,[1,2,4] MATILDA SHENG,[1] WESLEY G. BEAMER,[6] LEAH RAE DONAHUE,[6] CLIFFORD J. ROSEN,[7] and DAVID J. BAYLINK[1,2,4]

ABSTRACT

For the purpose of identifying genes that affect bone volume, we previously identified two inbred mouse strains (C57BL/6J and C3H/HeJ) with large differences in femoral bone density and medullary cavity volume. The lower density and larger medullary cavity volume in C57BL/6J mice could result from either decreased formation or increased resorption or both. We recently reported evidence suggesting that bone formation was increased in vivo and that osteoblast progenitor cells are more numerous in the bone marrow of C3H/HeJ compared with C57BL/6J mice. In the present study, we determined whether osteoclast numbers in vivo and osteoclast formation from bone marrow cells in vitro might also differ between the two mouse strains. We have found that the number of osteoclasts on bone surfaces of distal humerus secondary spongiosa was 2-fold higher in 5.5-week-old C57BL/6J mice than in C3H/HeJ mice of the same age ($p < 0.001$). Bone marrow cells of C57BL/6J mice cocultured with Swiss/Webster mouse osteoblasts consistently produced more osteoclasts than did C3H/HeJ bone marrow cells at all ages tested from 3.5–14 weeks of age ($p < 0.001$). Osteoclast formation was also greater from spleen cells of 3.5-week-old C57BL/6J mice than C3H/HeJ mice. The distribution of nuclei per osteoclast and the 1,25-dihydroxyvitamin D_3 dose dependence of osteoclast production from bone marrow cells were similar. Osteoclasts that developed from both C57BL/6J and C3H/HeJ marrow cells formed pits in dentin slices. Cultures from C57BL/6J marrow cells formed 2.5-fold more pits than cultures from C3H/HeJ marrow cells ($p < 0.02$). We compared the abilities of C57BL/6J and C3H/HeJ osteoblasts to support osteoclast formation. When bone marrow cells from either C57BL/6J or C3H/HeJ mice were cocultured with osteoblasts from either C57BL/6J or C3H/HeJ newborn calvaria, the strain from which osteoblasts were derived did not affect the number of osteoclasts formed from marrow cells of either strain. Together, these observations suggest that genes affecting the bone marrow osteoclast precursor population may contribute to the relative differences in bone density that occur between C3H/HeJ and C57BL/6J mouse strains. (J Bone Miner Res 1999;14:39–46)

INTRODUCTION

BONE DENSITY IS KNOWN to be determined by many factors, including age, calcium balance, exercise, and genetics.[1–9] Although the role of genetics in determining bone density is well established, specific genes that affect bone density have not been identified. Previous studies have shown significant differences in bone mineral content and bone size among different mouse strains.[10] To identify genes affecting bone density, a murine model has been developed for the purpose of investigating differences in bone density among inbred strains of mice.[11] Eleven strains of mice were screened using peripheral quantitative computerized tomography, and two were selected with widely different femoral bone densities. Mice of the strain C3H/HeJ have a mean femoral peak bone density of 0.69 ± 0.03 mg/

*Parts of this work were presented in an abstract presentation at the 18th Annual Meeting of the American Society for Bone and Mineral Research, Seattle, WA, U.S.A., 1996.

[1]J.L. Pettis VA Medical Center, Loma Linda University, Loma Linda, California, U.S.A.
[2]Department of Biochemistry, Loma Linda University, Loma Linda, California, U.S.A.
[3]Department of Pediatrics, Loma Linda University, Loma Linda, California, U.S.A.
[4]Department of Medicine, Loma Linda University, Loma Linda, California, U.S.A.
[5]Department of Anatomy, Loma Linda University, Loma Linda, California, U.S.A.
[6]The Jackson Laboratory, Bar Harbor, Maine, U.S.A.
[7]St. Joseph Hospital, Bangor, Maine, U.S.A.

mm^3, while mice of the strain C57BL/6J have a mean femoral peak density of 0.45 ± 0.01 mg/mm^3, $p < 0.001$ at 12 months of age. C3H/HeJ and C57BL/6J mice have significantly different femoral bone densities at all ages tested from 2–12 months. Bone densities of vertebrae and metacarpals were also higher in C3H/HeJ mice than C57BL/6J mice, indicating apparent differences between strains in both cortical and trabecular bone density. Although there were no differences in the external perimeter or length of the femur, the C3H/HeJ mouse femurs had greater cortical bone volume and smaller medullary cavity volume (0.82 ± 0.02 and 7.8 ± 0.09 mm^3, respectively) compared with C57BL/6J (0.61 ± 0.01 and 14.1 ± 0.4 mm^3, respectively, $p < 0.001$). These apparent differences in endosteal bone volume regulation might arise from different rates of bone resorption or bone formation or both.

Recently, we found that alkaline phosphatase activity in serum and bones of C3H/HeJ was higher than in C57BL/6J mice,[12] which is consistent with our observations that bone formation was increased in C3H/HeJ compared with C57BL/6J mice.[13] Furthermore, we found that the number of ALP-positive colonies produced in vitro per 10^6 bone marrow cells was greater in C3H/HeJ compared with C57BL/6J mice, which suggests that osteoblastic progenitor cells are more numerous in the bone marrow of C3H/HeJ mice. This observation leads to the question of whether osteoclastic progenitor cell numbers might also differ between C3H/HeJ and C57BL/6J mice. Preliminary observations that urine pyridinoline/creatinine excretion was lower in C3H/HeJ mice (451 ± 61 ng/mg) than in C57BL/6J mice (595 ± 167 ng/mg, $p < 0.05$, respectively),[14] suggest that the C57BL/6J mice have an increased rate of resorption compared to C3H/HeJ mice.

The current study was undertaken to test the specific hypotheses that in vivo osteoclast numbers and in vitro osteoclast formation from bone marrow cells are quantitatively different between C57BL/6J and C3H/HeJ mice; to assess bone resorption by the osteoclasts that develop in vitro; and to determine possible differences in capacities of osteoblasts from these two mouse strains to support osteoclast formation.

MATERIALS AND METHODS

Materials

Alpha minimal essential medium (α-MEM) and fetal bovine serum for marrow cell osteoblast cocultures were purchased from GIBCO BRL (Gaithersburg, MD, U.S.A.). Dulbecco's minimal essential medium (DMEM) and Fe-supplemented bovine calf serum for osteoblast cultures were purchased from Mediatech (Herndon, VA, U.S.A.) and Hyclone (Logan, UT, U.S.A.), respectively. Penicillin and streptomycin were purchased from Gemini Bio-Products (Calabasas, CA, U.S.A.). Dexamethasone (Sigma, St. Louis, MO, U.S.A.) and 1,25-dihydroxyvitamin D_3 ($1,25(OH)_2D_3$) (kindly provided by Hoffman LaRoche, Nutley, NJ, U.S.A.) were made as anhydrous ethanol stocks then diluted in marrow cell media. Final concentrations of ethanol were < 0.01%. Synthetic salmon calcitonin (Sigma) was used to inhibit osteoclast formation in vitro.

Animals

C57BL/6J and C3H/HeJ mice were obtained at different postweanling ages or as pregnant females from The Jackson Laboratory (Bar Harbor, ME, U.S.A.). Pregnant Swiss Webster mice were obtained from B&K Universal Ltd. (Freemont, CA, U.S.A.). All mice were housed at least 1 week before being used as sources of bone marrow or calvaria cells. All protocols were reviewed and approved by the Institutional Animal Care and Use Committees of the appropriate institutions.

Osteoclast numbers in vivo

Analysis of osteoclasts in demineralized bone sections is based on previously described procedures.[15] Mice were euthanized at 5.5 weeks of age by urethane injection. The right distal femur was fixed in neutral buffered 10% formalin for 24 h, demineralized, and prepared for parafin sectioning. Midcoronal sections (2 μm thick) of the distal femurs were stained for tartrate-resistant acid phosphatase (TRAP) as described[15] except that counterstaining was by Harris hematoxylin. Osteoclasts were identified as TRAP positive cells on bone surfaces. Bone surface length, number of osteoclasts, and fraction of bone surface occupied by osteoclasts were measured in the secondary spongiosa of the distal femur using a color video microscopy imaging system and Osteomeasure 2.31 program (OsteoMetrics, Inc., Atlanta, GA, U.S.A.). The sampling site was defined as the area between endosteal cortical bone surfaces extending from 0.3 mm to 0.78 mm proximal of the distal femur midepiphyseal plate. All contiguous optical fields within this area were analyzed at a magnification of ×1400.

Osteoclast formation in vitro

Mice for bone marrow and spleen cell preparations were euthanized by CO_2 inhalation. Femurs were aseptically removed, placed on ice in α-MEM, and dissected free of soft tissues. The ends of the bones were removed and the marrow was flushed from the midshaft with a syringe and 25 guage needle using cold α-MEM.[14] Marrow cells from two to five female mice per strain were washed and resuspended in α-MEM containing 10% fetal bovine serum, 100 U/ml penicillin, and 100 μg/ml streptomycin. The washed marrow cells (5×10^5/well) were cocultured with neonatal calvaria cells (1×10^4/well) from outbred Swiss/Webster mice or from inbred (C3H/HeJ or C57BL/6J) mice in 24-well plates (Corning, Corning, NY, U.S.A.) in a final volume of 1 ml. Cultures were fed with media containing 10 nM $1,25(OH)_2D_3$ and 10 nM dexamethasone and were changed at day 3 by removing 0.5 ml of media and replacing it with fresh media. The marrow/osteoblast cultures were stopped at day 6. Groups of six replicate wells were used for

each incubation condition. Spleen cells from 3.5-week-old mice were prepared as described previously[16] and were cocultured with calvaria cells as described above for bone marrow cells.

Osteoblast cells used for coculturing with marrow cells were isolated by collagenase digestion from calvariae of newborn mice. Mice 1–2 days of age were euthanized by CO_2 inhalation, and calvariae were dissected free from adhering soft tissue. The calvariae were digested for 15 minutes at 37°C with 1 mg/ml collagenase A (Boehringer Mannheim, Indianapolis, IN, U.S.A.) in DMEM, then the supernatant was discarded and the calvaria were digested further in collagenase A for 90 minutes. The cells released were washed in DMEM + 10% calf serum and plated in the same media in 100 mm plates. Cells were grown until confluence and frozen in aliquots for subsequent bone marrow or spleen coculture studies. The calvarial cells were thawed 24 h prior to use, so all experiments were performed with cells at passage two.

Osteoclast identification in cocultures

Cultures were rinsed, fixed, and stained for TRAP following kit directions (Sigma, St. Louis, MO, U.S.A.). Cells were counted as osteoclasts if they were both TRAP positive and had three or more nuclei per cell. As reported previously in studies of similar mixed culture preparations,[17,18] osteoclasts that developed in the cocultures formed resorption pits on mineralized dentin slices. Other studies have demonstrated that similar cultures express calcitonin receptors.[19,20] We found that cultures maintained without $1,25(OH)_2D_3$ had very few TRAP positive multinucleated cells, and that addition of calcitonin to cultures containing $1,25(OH)_2D_3$ prevented formation of TRAP positive multinucleated cells and pit formation on dentin slices (see Results), supporting the conclusion that these cells are osteoclasts. There were no TRAP positive adherent cells 24 h after plating and some TRAP positive mononucleated cells but no multinucleated cells at 3 days. We observed TRAP positive multinucleated cells only at 6 days, suggesting that they developed between 4 and 6 days of culture and were not already present in the marrow cell population.

We analyzed six replicate wells per incubation condition unless otherwise noted, and, when osteoclast number was high, numbers of osteoclasts were estimated by counting cells in random fields comprising 15% of the well surface. Estimated cell counts were highly reproducible and compared closely with counts of entire wells. To minimize effects of interassay variation, statistical comparisons were limited, unless otherwise noted, to assessment of differences within each experiment. All observations were repeated at least twice. Statistical analysis was performed by one-ay analysis of variance (ANOVA) using the SYSTAT program (Systat, Inc., Evanston, IL, U.S.A.). Data are expressed as mean ± SEM.

Pit formation on sperm whale dentin slices was determined by modification of the procedure described by Takada et al.[21] Marrow cells from 4.5-week-old C3H/HeJ or C57BL/6J (5×10^5/well) were cocultured with neonatal calvaria cells (1×10^4/well) from Swiss Webster mice, on 1-mm-thick, 1.5 cm^2 dentine slices in 1.9 cm^2 wells and cultured as for TRAP positive osteoclast formation. At 6 days, the cells were removed from the dentin by brief sonication in 0.01 M NaOH. Pits were then stained with 1% toluidine blue in 1% sodium borate or in acid hematoxylin (Sigma Chemical Co.). Pits stained with acid hematoxylin had more well defined edges and were used for area measurements. Random optical fields observed by transmitted light microscopy were digitized using a color video camera, and pit areas were determined using the Sigma Scan/Image program (Jandel Scientific, San Rafael, CA, U.S.A.).

RESULTS

In vivo characteristics of C3H/HeJ and C57BL/6J mice

Previous studies comparing inbred mouse strains have determined that bone length and animal weight did not differ between the C3H/HeJ and C57BL/6J strains of mice.[11] Since differences in total body weight could influence bone density based on weight bearing, in this study we confirmed that the average animal weight at each age examined was not significantly different between the two mouse strains. The mean weights for C3H/HeJ and C57BL/6J mice at 7 weeks of age, for example, were 15.80 ± 0.19 g and 15.75 ± 0.21 g, respectively (n = 8/group).

Osteoclast numbers in vivo in C3H/HeJ and C57BL/6J mice

Distal femur trabecular bone in the secondary spongiosa of 5.5-week-old female C57BL/6J mice contained approximately twice as many osteoclasts compared with C3H/HeJ mice (Table 1). C57BL/6J mice had a slightly higher bone surface length but this was not statistically significant. Numbers of osteoclasts were significantly greater ($p < 0.001$) in C57BL/6J than C3H/HeJ whether the numbers were expressed per bone surface length or per total area analyzed.

Osteoclast formation in vitro

When marrow cells from C3H/HeJ and C57BL/6J mice were cocultured with Swiss Webster osteoblasts in the presence of 10^{-8} M $1,25(OH)_2D_3$, multinucleated, TRAP positive osteoclasts formed by 6 days. In a representative experiment, C57BL/6J cultures had 907 ± 110 osteoclasts/well and C3H/HeJ cultures had 243 ± 36 osteoclasts/well. In the same experiment, addition of calcitonin (10 mU/ml) reduced osteoclast formation more than 95% to 38 ± 7 osteoclasts/well and 7 ± 4 osteoclasts/well, in C57BL/6J and C3H/HeJ cultures, respectively ($p < 0.001$ for each). Osteoclast formation was also dependent on $1,25(OH)_2D_3$ (Fig. 1). These characteristics, together with our observations (below) that mixed bone marrow cultures formed pits in dentine slices, support the assumption that the TRAP positive

TABLE 1. OSTEOCLAST NUMBERS IN SECONDARY SPONGIOSA OF DISTAL FEMUR OF 5.5-WEEK-OLD FEMALE C57BL/6J AND C3H/HEJ MICE WERE DETERMINED AS DESCRIBED IN THE MATERIALS AND METHODS

	C57BL/6J (n = 7)	*C3H/HeJ* (n = 6)	p *value*
Total area (mm^2)	0.889 ± 0.031	0.826 ± 0.026	NS
Osteoclasts per mm^2 total area	249 ± 13	103 ± 18	<0.001
Bone surface (mm)	14.7 ± 1.6	11.4 ± 1.4	NS
Osteoclasts per mm bone surface	15.6 ± 1.0	7.5 ± 1.0	<0.001
Osteoclast surface/bone surface	0.348 ± 0.028	0.171 ± 0.016	<0.001

The sample area was from 0.3–0.78 mm proximal to the distal growth plate cartilage. Data are presented as mean ± SEM. Significant differences between mouse strains were tested by one-way ANOVA. NS, not significant.

multinucleated cells observed in the cocultures are osteoclast-like cells.

Comparison of osteoclast formation in vitro

There was a significantly greater number of osteoclasts generated per 10^6 marrow cells from C57BL/6J compared with C3H/HeJ femurs at all ages tested from 3–14 weeks of age, as summarized in Table 2. These experiments were repeated with marrow cells from female mice of different ages and with marrow cells from both male and female mice at 8 weeks of age. In 11 out of 12 cell preparations, the number of osteoclasts per 10^6 bone marrow cells was significantly higher for C57BL/6J mice than the C3H/HeJ mice. To assess the variation from animal to animal and verify that the differences between mouse strains were not simply due to errors in counting cells of the bone marrow preparations, an experiment was conducted comparing four replicate groups from each strain. Each group contained marrow cells pooled from the femurs of two mice. Cells of each group were counted separately and osteoclast formation was determined in three culture wells per group (Table 3). These data demonstrated that, in all mice tested, C57BL/6J marrow cells gave rise to more osteoclast formation in vitro than C3H/HeJ marrow cells.

To ascertain whether the differences in osteoclast formation observed in female mice also occurred in male mice, an experiment was done with marrow cells from male C3H/HeJ and C57BL/6J mice. Within the same strain, male and female femur marrow cells produced comparable numbers of osteoclasts. Osteoclast formation from male C57BL/6J mice was significantly higher than from male C3H/HeJ mice (Table 2).

In one experiment with the youngest mice (3.5-week-old), we isolated cells from the spleen as well as bone marrow. In cocultures with Swiss Webster osteoblasts, spleen and bone marrow cells from C57BL/6J mice produced more osteoclasts compared with C3H/HeJ mice (Table 2).

Previous studies of mouse bone marrow and osteoblast cocultures normally treated the cultures with $1,25(OH)_2D_3$ at 10^{-8} M. One possible explanation for the difference in osteoclast formation between C3H/HeJ and C57BL/6J mice is that osteoprogenitor cells in the two strains are differentially dependent on $1,25(OH)_2D_3$ concentration. To test this possibility, we treated cocultures with $1,25(OH)_2D_3$ doses from 10^{-7} to 10^{-11} M. The maximal number of osteoclasts formed at 10^{-9} M $1,25(OH)_2D_3$ in cultures from bone marrow cells of both mouse strains (Fig. 1). At all doses tested, the C57BL/6J bone marrow cell population produced more osteoclasts than the C3H/HeJ bone marrow cell population.

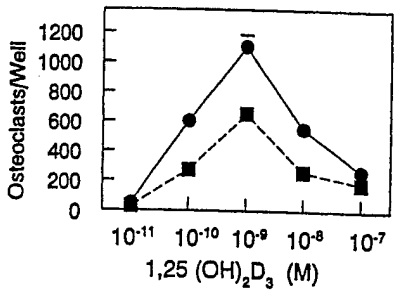

FIG. 1. $1,25(OH)_2D_3$ dose response for C3H/HeJ and C57BL/6J marrow osteoclast formation. Cocultures were established with Swiss Webster osteoblasts and femoral marrow cells as described in the Materials and Methods. Data points are mean ± SEM. The error bars are obscured by the symbols in all but one point. The C57BL/6J (circles) cultures had significantly more osteoclasts from 10^{-10} to 10^{-7} M $1,25(OH)_2D_3$ ($p < 0.001$ at 10^{-10} to 10^{-8} M and $p < 0.05$ at 10^{-7} M) than the C3H/HeJ mice (squares). $n = 6$ replicates per dose.

Not only were there more osteoclasts formed in vitro per 10^6 marrow cells in the C57BL/6J mice, but at all ages examined, from 3.5 to 14 weeks, the number of nucleated marrow cells per femur was higher in the C57BL/6J mice, probably as a result of the larger medullary cavity. In the experiment described in Table 2, for example, 6.5- to 7-week-old C3H/HeJ mice had 4.25 ± 0.34 × 10^6 nucleated marrow cells per femur, while C57BL/6J mice had 7.08 ± 0.30 × 10^6 cells per femur. Thus, with 83 ± 2 and 498 ± 79 osteoclasts formed per 10^6 nucleated marrow cells, the C3H/HeJ and C57BL/6J mice formed 353 ± 9 and 3530 ± 43 osteoclasts per femur, respectively.

To determine whether osteoclast size might vary between the two mouse strains, TRAP positive cells formed in vitro were divided into three groups based on the number of

TABLE 2. OSTEOCLAST FORMATION IN COCULTURES OF NEWBORN SWISS WEBSTER OSTEOBLASTS AND EITHER C57BL/6J OR C3H/HEJ MARROW CELLS OR SPLEEN CELLS

Experiment	*Age of mice (weeks)*	*Osteoclast source*	*C57BL/6J osteoclasts*	*C3H/HeJ osteoclasts*	p *value*
1	4.5	Bone marrow	907 ± 110	243 ± 36	<0.001
2	6.5	Bone marrow	249 ± 32	42 ± 8	<0.001
2	6.5 (males)	Bone marrow	237 ± 54	82 ± 38	<0.05
3	6	Bone marrow	1544 ± 137	681 ± 104	<0.001
3	13	Bone marrow	1139 ± 137	696 ± 118	<0.05
4	7.5	Bone marrow	206 ± 31	121 ± 11	<0.05
5	9	Bone marrow	617 ± 52	272 ± 28	<0.001
6	7.5	Bone marrow	435 ± 44	246 ± 45	<0.05
7	6	Bone marrow	173 ± 44	118 ± 40	NS
8	14	Bone marrow	656 ± 106	337 ± 19	<0.01
9	3.5	Bone marrow	1029 ± 80	613 ± 87	<0.01
9	3.5	Spleen	822 ± 67	128 ± 18	<0.01
10	4.5	Bone marrow	939 ± 103	564 ± 43	<0.05

Cultures were established as specified in the Materials and Methods, in different experiments with marrow cells (0.5×10^6/well) from mice ages 3.5–14 weeks at the time of the experiment. Except where noted, all animals were female. Numbers are expressed as osteoclast per well ± SEM, six replicates per group. Combined ANOVA indicated that the difference between C57BL/6J and C3H/HeJ is highly significant ($p < 0.001$).

TABLE 3. VARIATION IN OSTEOCLAST FORMATION BETWEEN ANIMALS OF THE SAME STRAIN

	Osteoclasts/well	
Group	*C57BL/6J*	*C3H/HeJ*
1	242 ± 69	40 ± 24
2	327 ± 24	44 ± 27
3	264 ± 116	43 ± 30
4	162 ± 48	40 ± 5
Strain average	249 ± 32	42 ± 8

Two 6.5-week-old female mice were used as a source of marrow cells for each group and cells were then plated with Swiss Webster calvaria cells as described in the Materials and Methods. Results are expressed as mean ± SEM. Strain averages are based on group means of three wells/group, four groups per strain. There were no significant differences between groups of the same strain (by ANOVA), while the difference between the strains is statistically significant ($p < 0.001$). Results of strain averages are also included in Table 2 as experiment 2.

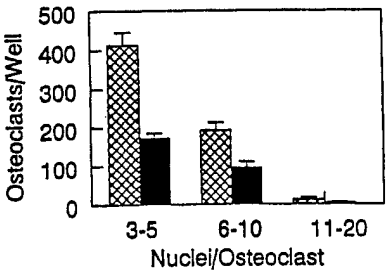

FIG. 2. Distribution of nuclei per osteoclast. Cocultures were established with Swiss Webster osteoblasts as described in the Materials and Methods. TRAP positive cells with one or two nuclei were not counted. The numbers of TRAP positive osteoclasts (mean ± SEM) with 3–5, 6–10, and 11–20 nuclei/cell were significantly greater in C57BL/6J (hatched bars) than in C3H/HeJ (solid bars) cultures, $p < 0.001$ for each. The average number of nuclei per osteoclast was 5.55 ± 0.13 for C3H/HeJ cultures and 5.46 ± 0.05 for C57BL/6J cultures (NS, $n = 6$ replicates per group).

nuclei per cell (Fig. 2). In all three size classes, osteoclasts from C57BL/6J mice were more numerous than osteoclasts from C3H/HeJ mice ($p < 0.001$). There was no significant difference between mouse strains in the number of osteoclast nuclei per cell. C3H/HeJ marrow-derived osteoclasts had, on average, 5.55 ± 0.13 nuclei, while C57BL/6J marrow derived osteoclasts had 5.46 ± 0.05 nuclei per cell ($n = 6$). Because there were more osteoclasts per well in C57BL/6J marrow derived cultures, the total number of osteoclast nuclei per culture well was greater in C57BL/6J than in C3H/HeJ cultures.

Osteoclasts that developed from C57BL/6J and C3H/HeJ bone marrow cells in cocultures with Swiss/Webster osteoblasts resorbed pits in dentin slices. Pits stained by toluidine blue or by acid hematoxylin exhibited characteristic morphologies described previously. C57BL/6J bone marrow cell cultures from 4.5-week-old mice produced 2.5-fold as many pits per dentin slice as were produced by C3H/HeJ cultures ($p < 0.01$; Table 4). In the same experiment, the number of TRAP positive multinucleated osteoclasts that formed in plastic wells was also greater for C57BL/6J than C3H/HeJ cultures. Addition of 10 mU/ml calcitonin decreased the number of pits formed by osteoclasts to < 3% (Table 4). Areas of the pits formed in cultures from both strains of mice had a broad range. The mean pit area in C3H/HeJ cultures was 16% higher than the mean area in C57BL/6J cultures but was not significantly different. When pit area values were log transformed, however, the transformed values exhibited a normal distribution (Fig. 3) and were statistically different ($p < 0.05$).

TABLE 4. PIT FORMATION IN MARROW CELL OSTEOBLAST COCULTURES PLATED ON DENTINE SLICES

	Media	*C57BL/6J*	*C3H/HeJ*	p
Osteoclasts/cm^2	1,25(OH)$_2$D$_3$	499 ± 61 (5)*	301 ± 29 (5)	<0.02
Pits/cm^2	1,25(OH)$_2$D$_3$	859 ± 138 (4)	340 ± 55 (4)	<0.01
Pits/cm^2	1,25(OH)$_2$D$_3$ + CT	13 ± 2 (2)	9 ± 1 (2)	
Pit area (μm^2)†	1,25(OH)$_2$D$_3$	4830 ± 280 (473)	5640 ± 360 (392)	<0.05

C57BL/6J or C3H/HeJ marrow cells from 4.5-week-old mice were cocultured with newborn Swiss Webster osteoblasts on either plastic (experiment 10 of Table 2) or dentine slices in 24-well plates. Media contained 10 nM 1,25(OH)$_2$D$_3$ or 1,25(OH)$_2$D$_3$ + 10 mU/ml human calcitonin. At 7 days, the cells on plastic were stained for TRAP and the dentine slices were stained with acid hematoxylin to reveal resorption pits. Osteoclast production was assessed in parallel cultures plated in plastic wells. Significant differences between C57BL/6J and C3H/HeJ, determined by ANOVA, are indicated in the far right column. Data are presented as osteoclasts or pits per square centimeter of surface, mean ± SEM, because the surface areas of the plastic wells and the dentine slices were different (1.9 cm^2 and 1.6 cm^2, respectively).

* The number of wells or pits per group is shown in parentheses.

† Pit areas were significantly different only after log transformation.

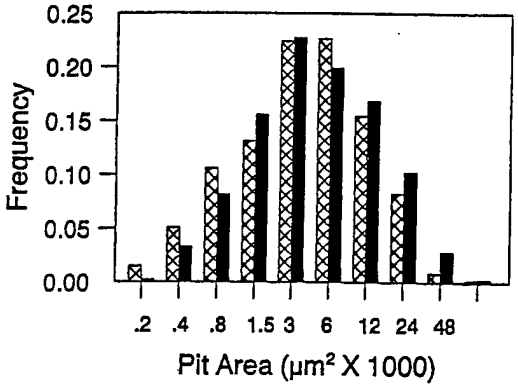

FIG. 3. Areas of pits formed in dentin slices by C57BL/6J and C3H/HeJ osteoclasts. Areas were determined in a random sample of pits (473 from C57BL/6J, 392 from C3H/HeJ) formed by mixed cultures of 4.5-week-old C57BL/6J (hatched bars) or C3H/HeJ (solid bars) marrow cells and newborn Swiss/Webster osteoblasts. Histogram classes are powers of two. The mean area of C3H/HeJ pits, shown in Table 3, was significantly different ($p < 0.05$) from the mean area of C57BL/6J pits when areas were log transformed.

Since there were virtually no osteoclasts formed in the absence of osteoblasts in our experiments, and previous studies have demonstrated the importance of osteoblasts in inducing osteoclast formation, we hypothesized that osteoblasts in the marrow or on the endosteum of C57BL/6J and C3H/HeJ mice may influence the relative amount of osteoclast formation. Although our experiments using osteoblasts from a third unrelated mouse strain (Swiss Webster) suggested that differences in osteoclast formation between C57BL/6J and C3H/HeJ marrow arise from differences in the marrow cells, these experiments do not rule out possible effects of osteoblast genotype on the induction of osteoclast formation. To assess whether the number of osteoclasts generated in vitro was determined by the strain from which the osteoblasts were derived, experiments were performed using neonatal osteoblastic cells from either C57BL/6J or C3H/HeJ calvariae, with marrow cells from either the same strain or from the heterologous strain. Surprisingly, there was no effect of the osteoblast cells to alter numbers of osteoclasts formed from either mouse strain (Fig. 4). Whether Swiss Webster, C57BL/6J, or C3H/HeJ cells were used as the osteoblast source, there were always more osteoclasts formed from C57BL/6J marrow than from C3H/HeJ marrow.

DISCUSSION

C57BL/6J mice had more osteoclasts on endosteal bone surfaces compared with C3H/HeJ mice. The site in the humerus that we investigated is an area of active bone remodeling in which relative rates of bone formation and resorption determine the amount of trabecular bone present. We speculate that the increased number of osteoclasts in C57BL/6J bone results in increased resorption compared with C3H/HeJ mice. This supports previous evidence for increased resorption in C57BL/6J mice that was based on increased pyridinoline excretion.[14]

Osteoclast formation in vitro was significantly greater from C57BL/6J than C3H/HeJ marrow cells at all ages tested. This suggests that the difference in osteoclast formation was not caused simply by a developmental delay of osteoclast precursor populations in C3H/HeJ mice which would eventually "catch up" to C57BL/6J mice. Osteoclast formation from spleen cells was also greater in C57BL/6J mice compared with C3H/HeJ mice, suggesting that possible differences in osteoclast precursor populations are not restricted to the bone marrow microenvironment but might be influenced by systemic factors that differ quantitatively between the mouse strains. One possible factor is circulating 1,25(OH)$_2$D$_3$. However, in a preliminary report,[22] circulating 1,25(OH)$_2$D$_3$ levels were lower in C57BL/6J than in C3H/HeJ mice, suggesting either that the sensitivity of C57BL/6J osteoclast precursor cells to 1,25(OH)$_2$D$_3$ might be greater in C57BL/6J mice or that different 1,25(OH)$_2$D$_3$

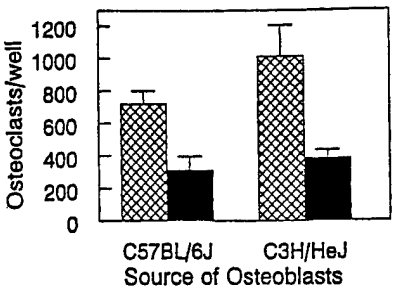

FIG. 4. Osteoclast formation in cocultures with C57BL/6J and C3H/HeJ osteoblasts. Marrow cells from 9-week-old mice were cocultured with osteoblasts from either newborn C57BL/6J or C3H/HeJ calvariae. The C57BL/6J marrow cells (hatched bars) produced more osteoclasts compared with C3H/HeJ marrow cells (solid bars), whether they were plated with C57BL/6J or C3H/HeJ osteoblasts, $p < 0.001$ for each. Values are mean ± SEM, $n = 6$ per group.

levels in vivo cannot account for different osteoclast formation in vitro. Our data from $1,25(OH)_2D_3$ dose-response experiments suggest that the difference in osteoclast formation in vitro between C3H/HeJ mice and C57BL/6J mice is not due to differential sensitivity to $1,25(OH)_2D_3$. Another possible systemic difference between the mouse strains is circulating estrogen or androgen levels. However, osteoclast production was not dependent on the sex of the mice from which the bone marrow cells were isolated. This result suggests that potential differences in sex steroid levels or cell sensitivity to sex steroids (or other sex-related differences) cannot account for the differences in osteoclast formation that occur between the two mouse strains. Last, circulating growth hormone and insulin-like growth factor (IGF) levels, which are positively associated with bone resorption and osteoclast formation,[23] might differ between C3H/HeJ and C57BL/6J mice. C3H/HeJ mice have higher circulating levels of growth hormone and IGF-I,[24] which may contribute to the higher bone formation that occurs in C3H/HeJ mice.[13] Higher IGF-I levels, however, would give rise to higher numbers of osteoclasts, so IGFs cannot account for the lower osteoclast numbers in C3H/HeJ mice.

Osteoclasts from C3H/HeJ and C57BL/6J mice resorbed pits in dentin slices, as described previously in studies using the same mixed culture model with different mouse strains.[17,18] The number of pits was greater in cultures from C57BL/6J than C3H/HeJ mice and was roughly proportional to the number of osteoclasts formed in the same experiment. The size of resorption pits was nearly the same in C3H/HeJ and C57BL/6J cultures and was statistically different only when pit areas were log transformed. Whether meaningful differences exist in the abilities of osteoclasts from the two strains to resorb bone cannot be determined from the present data. The data do indicate, however, that the reduced number of pits formed in C3H/H3J cultures does not result from defective pit formation.

Since it is well established that osteoblastic stromal cells are important regulators of osteoclastogenesis from bone marrow precursor cells, we initially considered the corollary hypothesis that differences in osteoclast formation from C3H/HeJ compared with C57BL/6J mouse marrow cells result from differences in the capacities of the stromal cells from the respective mouse strains to stimulate or support osteoclast formation. The stromal cells not only secrete soluble factors such as macrophage colony-stimulating factor (M-CSF), which stimulate osteoclast differentiation, but cell contact between stromal cells and osteoclast progenitor cells may also be necessary for osteoclast formation.[25] In the SAMP6 mouse genetic model for accelerated aging, decreased osteoclast formation in SAMP6 bone marrow culture was attributed to defective stromal cells rather than defective osteoclasts.[26] Results of the present study, however, do not support a difference in the ability of osteoblasts to support osteoclast formation in vitro. The results are consistent with the hypothesis that C3H/HeJ and C57BL/6J mouse strains differ in the number of bone marrow osteoclast progenitor cells, or in the ability of osteoblastic cells to differentiate into mature osteoclasts in the coculture system, or in both characteristics.

We found that C57BL/6J osteoblasts produced higher levels of IL-6 and granulocyte M-CSF compared with C3H/HeJ osteoblasts.[27] Although these differences in osteoblast cytokine production cannot account for the differences in osteoclast formation observed between the mouse strains (because in the present study C57BL/6J osteoblasts did not support increased osteoclast formation from marrow cells of either strain compared with C3H/HeJ osteoblasts) it is possible that differential cytokine signaling in the bone marrow in vivo results in increased numbers of osteoclast progenitor cells in C57BL/6J mice compared with C3H/HeJ mice.

Interestingly, we have observed differences between C3H/HeJ and C57BL/6J mice in osteoblast properties, osteoblast formation from marrow cell precursors in vitro,[12] and bone formation in vivo.[13] Osteoblasts isolated from femurs and calvariae of C3H/HeJ mice had higher ALP activities compared with osteoblasts from C57BL/6J mice, and the number of ALP positive stromal cell colonies formed per 10^6 marrow cells was greater in C3H/HeJ mice compared with C57BL/6J mice. In vivo studies found that endosteal bone mineral apposition rate and relative bone formation rate were significantly higher in C3H/HeJ mice than C57BL/6J mice. Thus, different genes affecting resorption and formation could contribute to the difference in bone density between C3H/HeJ and C57BL/6J mice. Furthermore, our findings indicate that bone marrow populations from C3H/HeJ and C57BL/6J mice have an inverse relationship between osteoblast and osteoclast progenitor cell numbers. Although these observations do not indicate a causal relationship, one could speculate that the increased osteoblast progenitor cell population and increased bone formation that are apparent in C3H/HeJ bone may create an environment that is inhibitory to osteoclast progenitor cell formation. However, how this mechanism could account for differences in osteoclast formation from spleen cells of the two mouse strains is currently unclear.

In summary, our data suggest that there are differences in osteoclast precursor populations of the bone marrow between C3H/HeJ and C57BL/6J mice. These differences could contribute to the differences in bone density observed

between these two inbred mouse strains. The ultimate goal of our studies is to identify genes that can account for the difference in bone density between the C3H/HeJ and C57BL/6J mice. The results of the previous and the present study together suggest that genes that regulate osteoclast lineage cells, as well as genes that regulate osteoblast lineage cells, may contribute to the difference in bone densities which exists between the two inbred mouse strains.

ACKNOWLEDGMENTS

The authors thank Ms. Angela Eason and Ms. Sarán Wilkins for expert technical assistance. We thank Dr. Helen Gruber of Carolinas Medical Center for consultation on histologic and histochemical methods. Funding for this work was supplied by grants from the National Institutes of Health #AR-43618 and #CA-34196 (W.G.B.), by a subcontract from U.S. Army Medical Research Acquisition Activity Grant DAMD17-96-1-6306 (W.G.B. and D.J.B.), by Medical Research grants from the Department of Veterans Affairs (T.A.L., J.R.F., D.J.B.), and by the Loma Linda University School of Medicine Research Support Fund.

REFERENCES

1. Takeshita T, Yamagata Z, Iijima S, Nakamura T, Ouchi Y, Orimo H, Asaka A 1992 Genetic and environmental factors of bone mineral density indicated in Japanese twins. Gerontology 38:43–49.
2. Kelly PJ, Harris M 1995 Genetic regulation of peak bone mass. Acta Paediatr 411:24–29.
3. Alekal L, Clasey JL, Fehling PD, Weigel RM, Boileau RA, Erdman JW, Stillman R 1995 Contributions of exercise, body composition, and age to bone mineral density in premenopausal women. Med Sci Sports Exerc 27:1477–1485.
4. Jouanny P, Guillemin F, Kuntz C, Jeandel C, Pourel J 1995 Environmental and genetic factors affecting bone mass. Similarity of bone density among members of healthy families. Arthritis Rheum 38:61–67.
5. Livshits G, Vainder M, Pavlovsky O, Kobyliansky E 1996 Population biology of human aging: Ethnic and climatic variation of bone age scores. Hum Biol 68:293–314.
6. Matkovic V 1996 Nutrition, genetics and skeletal development. J Am Coll Nutr 15:556–569.
7. Ralston SH 1997 The genetics of osteoporosis. QJM 90:247–251.
8. Ferrari S, Rizzoli R, Slosman D, Bonjour JP 1998 Familial resemblance for bone mineral mass is expressed before puberty. J Clin Endocrinol Metab 83:358–361.
9. Hopper JL, Green RM, Nowson CA, Young D, Sherwin AJ, Kaymakci B, Larkins RG, Wark JD 1998 Genetic, common environment, and individual specific components of variance for bone mineral density in 10- to 26-year-old females: A twin study. Am J Epidemiol 147:17–29.
10. Murray EJ, Song MK, Laird EC, Murray SS 1993 Strain-dependent differences in vertebral bone mass, serum osteocalcin, and calcitonin in calcium-replete and -deficient mice. Proc Soc Exp Biol Med 203:64–73.
11. Beamer WG, Donahue LR, Rosen CJ, Baylink DJ 1996 Genetic variability in adult bone density among inbred strains of mice. Bone 18:397–403.
12. Dimai HP, Linkhart TA, Linkhart SG, Donahue LR, Beamer WG, Rosen CJ, Farley JR, Baylink DJ 1998 Alkaline phosphatase levels and osteoprogenitor cell numbers suggest that bone formation may contribute to peak bone density differences between two inbred strains of mice. Bone 22:211–216.
13. Sheng MH-C, Beamer WG, Donahue LR, Rosen CJ, Baylink DJ, Wergedal JE 1998 Phenotype studies show that endosteal bone formation is greater in C3 (high density) than B6 (low density) mice during growth. FASEB J 12:A508 (abstracts).
14. Baylink D, Farley J, Donahue L, Rosen CJ, Barr B, Lee JES, Beamer W 1995 Evidence that high peak bone density is due to decreased resorption not increased formation in a murine model. J Bone Miner Res 10 (Suppl):338.
15. Boyce BF, Wright K, Reddy SV, Koop BA, Story B, Devlin R, Leach RJ, Roodman GD, Windle JJ 1995 Targeting simian virus 40 T antigen to the osteoclast in transgenic mice causes osteoclast tumors and transformation and apoptosis of osteoclasts. Endocrinology 136:5751–5759.
16. Takahashi N, Akatsu T, Udagawa N, Sasaki T, Yamaguchi A, Moseley JM, Martin TJ, Suda T 1988 Osteoblastic cells are involved in osteoclast formation. Endocrinology 123:2600–2602.
17. Jimi E, Nakamura I, Amano H, Taguchi Y, Tsurakai T, Tamura M, Takahashi N, Suda T 1996 Osteoclast functions is activated by osteoblastic cells through a mechanism involving cell-to-cell contact. Endocrinology 137:2187–2190.
18. Girasole G, Passeri B, Jilka RL, Manolagas SC 1994 Interleukin-11: A new cytokine critical for osteoclast development. J Clin Invest 93:1516–1524.
19. Udagawa N, Takahashi N, Katagiri T, Tamura T, Wada S, Findlay DM, Martin TJ, Hirota H, Taga T, Kishimoto T, Suda T 1995 Interleukin (IL)-6 induction of osteoclast differentiation depends on IL-6 receptors expressed on osteoblastic cells but not on osteoclast progenitors. J Exp Med 182:1461–1468.
20. Takahashi N, Udagawa N, Akatsu T, Tanaka H, Shionome M, Suda T 1991 Role of colony-stimulating factors in osteoclast development. J Bone Miner Res 6:977–985.
21. Takada Y, Kusuda M, Hiura K, Sato T, Mochizuki H, Nagao Y, Tomura M, Yahiro M, Hakeda Y, Kawashima H, Kumegawa M 1992 A simple method to assess osteoclast-mediated bone resorption using unfractionated bone cells. Bone Miner 17:347–359.
22. Chen C, Beamer WG, Donahue LR, Kalu DN 1996 Strain differences in serum $1,25(OH)_2$ levels and in intestinal vitamin D receptor occupancy between C3H/HeJ and C57BL/6J mice. J Bone Miner Res 11 (Suppl 1):S316 (abstract M537).
23. Mochizuki H, Hakeda Y, Wakatsuki N, Usui N, Akashi S, Sato T, Tanaka K, Kumegawa M 1992 Insulin-like growth factor-I supports formation and activation of osteoclasts. Endocrinology 131:1075–1080.
24. Rosen CJ, Dimai HP, Vereault D, Donahue LR, Beamer WG, Farley J, Linkhart S, Linkhart T, Mohan S, Baylink DJ 1997 Circulating and skeletal insulin-like growth factor-I (IGF-I) concentrations in two inbred strains of mice with different bone mineral densities. Bone 21:217–223.
25. Suda T, Udagawa N, Nakamura I, Miyaura C, Takahashi N 1995 Modulation of osteoclast differentiation by local factors. Bone 17:87S–91S.
26. Jilka RL, Weinstein RS, Takahashi K, Parfitt AM, Manolagas SC 1996 Linkage of decreased bone mass with impaired osteoblastogenesis in a muring model of accelerated senescence. J Clin Invest 97:1732–1740.
27. Linkhart T, Linkhart S, Farley J, Dimai HP, Quian H-Y, Horowitz M, Beamer W, Donahue LR, Rosen C, Baylink DJ 1996 Osteoblast production of osteolytic cytokines: Differences between low peak bone density C57BL/6J mice and high peak bone density C3H/HeJ mice. J Bone Miner Res 11 (Suppl 1):S167 (abstract S309).

Address reprint requests to:
Thomas A. Linkhart, Ph.D.
Research Service (151)
J.L. Pettis VA Medical Center
11201 Benton Street
Loma Linda, CA 92357 U.S.A.

Received in original form November 24, 1997; in revised form September 4, 1998; accepted September 18, 1998.

ELSEVIER

Bone Vol. 25, No. 2
August 1999:183–190

Cortical Tibial Bone Volume in Two Strains of Mice: Effects of Sciatic Neurectomy and Genetic Regulation of Bone Response to Mechanical Loading

Y. KODAMA,[1] H. P. DIMAI,[1] J. WERGEDAL,[1,2] M. SHENG,[1,2] R. MALPE,[1,2] S. KUTILEK,[1] W. BEAMER,[3] L. R. DONAHUE,[3] C. ROSEN,[4] D. J. BAYLINK,[1,2] and J. FARLEY[1,2]

[1]*Jerry L. Pettis Memorial Veterans Medical Center, Loma Linda, CA, USA*
[2]*Department of Medicine, Loma Linda University, Loma Linda, CA, USA*
[3]*The Jackson Laboratory, Bar Harbor, ME, USA*
[4]*Maine Center for Osteoporosis Research, St. Joseph Hospital, Bangor, ME, USA*

Although C3H/HeJ (C3H) and C57BL/6J (B6) mice are similar in body size (and adult weight), and have bones of similar external size, C3H mice have higher peak bone densities than B6 mice (e.g., 53% higher peak bone density in the femora). The current studies were intended to assess the role of mechanical loading/unloading as a possible determinant of the bone density difference between these inbred strains of mice and, specifically, to assess the effect of sciatic neurectomy on histomorphometric indices of bone formation and resorption in the tibiae of female C3H and B6 mice. Groups of 10 mice of each strain were subjected to left-side sciatic neurectomy (left hindlimb immobilization) or a sham procedure. The contralateral (right) legs of each mouse were used as controls. Four weeks of immobilization produced no systemic changes in bone formation indices in either strain of mice (i.e., no change in serum alkaline phosphatase or serum osteocalcin). However, histomorphometric assessments at the tibiofibular junction showed that 4 weeks of immobilization caused a time-dependent decrease in the length of the endosteal bone forming perimeter (e.g., 14% of control single-labeled, noneroded surface at 4 weeks, $p < 0.005$) with a concomitant increase in the length of the endosteal bone resorbing perimeter (i.e., 424% of control eroded surface at 4 weeks, $p < 0.005$), in the B6 mice. These effects were associated with an increase in medullary area (132% of control, $p < 0.05$) at this site, in the B6 mice. The pattern of response was different in the tibiae of the C3 mice—a much smaller decrease in bone forming perimeter (88% of control at 4 weeks, $p < 0.05$), with no associated increase in bone resorbing perimeter, and no change in medullary area. Similar effects were seen at a second cross-sectional sampling site, in the proximal tibia. Together, these findings indicate that B6 mice are more sensitive to endosteal bone loss from hindlimb immobilization than C3H mice. (Bone 25:183–190; 1999)

Key Words: Bone; Mechanical Loading; Mouse; Bone resorption; Bone formation.

Address for correspondence and reprints: Dr. John Farley, c/o Research Service (151), J. L. Pettis Memorial Veterans Medical Center, 11201 Benton Street, Loma Linda, CA 92357.

Introduction

Osteoporosis is characterized by an age-dependent decrease in bone density and a consequent increase in the risk of skeletal fracture.[11,29] Adult bone density can be defined in terms of peak bone density (usually achieved in young adulthood), and the subsequent rate of net loss and, from this definition, it follows that peak bone density is a physiological determinant of the age-dependent risk of osteoporotic fracture.[11,29] Previous studies have estimated that as much as 70% of peak bone density is determined by genetic factors,[10,15,17,24] and we have developed an animal model for quantitative trait locus (QTL) analysis that will allow us to identify the genes responsible for the peak bone density difference between two inbred strains of mice.[2,3,5,6,9,21,25]

Adult C3H/HeJ (C3H) and C57BL/6J (B6) mice are similar in body size and weight and their bones are of similar external size; however, the C3H mice have a greater peak bone density than the B6 mice (e.g., 53% greater peak bone density in the femora). This difference in density can be attributed to a difference in medullary space—the medullary cavity is larger in the B6 mice.[6] Preliminary QTL analyses have estimated the genetic component of the femoral density difference to be at least 70%, and histological, biochemical, and in vitro cell culture studies[2,3,5,6,9,21,25] have revealed cytological-mechanistic differences that could contribute to the bone density difference between C3H and B6 mice.

Our previous studies have shown that the rate of bone resorption is greater in young B6 mice than in C3H mice[2,3] and, conversely, that the rate of bone formation is greater in young C3H mice than in B6 mice.[3] Our previous studies have also revealed a larger population of osteoclastic progenitor cells in the marrow of B6 compared with C3H mice,[21] and a larger population of alkaline phosphatase-positive, osteoblast-lineage cells in the marrow of C3H compared with B6 mice.[9] Finally, our previous studies have shown increased levels of the skeletal growth factor IGF-I, and of the bone-specific enzyme, skeletal ALP, in the serum and the bones of C3H compared with B6 mice.[25] Together, these observations have led to the hypothesis that developmental differences in the rates of bone formation and resorption may be responsible (at least in part) for the greater peak bone density in C3H compared with B6 mice.

The current studies were intended to extend those observations, by beginning an assessment of the role of mechanical loading as another possible determinant of the bone density difference between

8756-3282/99/$20.00
PII S8756-3282(99)00155-6

Bone Vol. 25, No. 2
August 1999:183–190

CH3 and B6 mice. Our rationale for these studies was based on the following two observations. Previous studies have shown that immobilization can increase bone resorption and/or decrease bone formation in experimental animals and humans.[1,12,16,20,26,27,32] Previous studies have also revealed that mechanical loading can increase bone formation and/or decrease bone resorption[13,16,18,19,30] and increase the local production of skeletal growth factors, including the insulin-like growth factors (IGFs).[22,31] Because we have found evidence for strain-specific differences in (a) the osteoclast and osteoblast-progenitor pool populations of C3H and B6 mice, (b) the serum and skeletal levels of IGF-I, and (c) the osteoblastic production of IGF-I,[9,21,25] we considered the possibility that C3H and B6 mice might show different responses to the effects of immobilization. For instance, B6 mice might be more efficient at recruiting osteoclasts in response to immobilization, resulting in a differential increase in resorption, and/or IGF production in response to mechanical loading, (e.g., C3H osteoblast-line cells might produce more IGF-I synthesis in response to mechanical loading than B6 osteoblast-line cells, resulting in a differential increase in formation). Thus, we hypothesized that CH3 mice might be less sensitive to immobilization (i.e., suffer less net loss of bone from such a reduction in loading) and/or more sensitive to mechanical loading (i.e., form more bone in response to the same degree of loading), compared with B6 mice. The current studies were specifically intended to test the effects of hindlimb immobilization caused by sciatic neurectomy.

Methods

Animals and Treatment

Female C3H/HeJ (C3H) and C57BL/6J (B6) mice were purchased from the Jackson Laboratory (Bar Harbor, ME). The mice were maintained on a 12 h light/dark cycle in our accredited facility and fed standard laboratory chow. A preliminary study was conducted to assess the feasibility of the procedure, followed by the formal study. There were no significant problems associated with the procedures (i.e., other than the self-mutilation observed in the preliminary study, which was, subsequently, prevented by taping) and no differences in body weight between the treatment groups. Serum and tissue samples were collected at the time of killing. Sera were frozen (−20°C) for measurements of ALP activity and osteocalcin. Bones were used for histological analysis or extraction. All protocols were reviewed and approved by the animal studies subcommittee (of the research and development committee) of the J. L. Pettis Memorial Veterans Medical Center.

Preliminary Study

Sciatic neurectomy[26,27,32] was performed on the left legs of seven C3H and eight B6 mice (8 weeks of age) and the right legs were used as controls. During the following week, we observed some of the mice chewing on (and mutilating) their immobilized limbs. To prevent this behavior, we wrapped the neurectomized hindlimbs in cotton gauze and several layers of duct tape, affixing the hindlimb to the tail in the process. This procedure reduced (but did not prevent) the incidence of gnawing and completely prevented self-mutilation (i.e., the mice could still gnaw on their hindlimbs, but could not inflict the same degree of overt damage). Although we found no anatomical or histomorphometrical evidence of hindlimb damage caused by the taping procedure (e.g., restricted blood flow from to soft tissues and/or bones), our studies were not designed to assess this possibility. After 3 weeks of immobilization (an arbitrary time, selected with reference to previous studies with rats[27,32]), the mice were killed (CO_2 gas and decapitation) and the tibiae were dissected for analysis of cross-sectional areas at the tibiofibular junction (syndesmosis[4,20,27,32]).

Sciatic Neurectomy Study

Thirty 7-week-old mice of each strain (i.e., C3H and B6) were used for this study. After 2 weeks of acclimation, the mice were randomly divided into three groups of ten for each strain: a baseline control group to be killed on day 0; a sham-operated control group; and a sciatic neurectomized group. The mice were approximately 9 weeks of age at the start of the study. The mice in the surgical groups were anesthesized by an intraperitoneal injection with ketamine 100 mg/kg body weight (b.w.) and xylocaine 15 mg/kg b.w. The left leg sciatic nerve was exposed, a 3–4 mm length of the nerve was resected (i.e., removed), and the skin was stitched closed with surgical thread. The sciatic nerve resection (confirmed visually by two observers at the time of surgery) effectively denervated all regions of the hindlimb served by the sciatic nerve and its branches (e.g., the tibial and fibular nerves), immobilizing the tibia and fibula and most of the femur (i.e., excluding the proximal femur, which could still have been affected by some muscles in the buttocks). For the sham-operated animals, the sciatic nerve was exposed (but not resected) and then the skin was closed. Immediately after the operation, cotton gauze and duct tape were used to immobilize the neurectomized left leg by fixing it to the tail. No duct tape was applied to the sham-operated group. Because the gauze padding could still be compressed through the tape, we assumed that the taping did not constrict the soft tissues. To assess the rates of bone formation and mineralization, the mice were injected intraperitoneally with 20 mg/kg acromycine on day 0, 5 mg/kg calcein on day 12, 20 mg/kg declomycin on day 19, and 5 mg/kg calcein on day 26. On day 28, all the mice were killed with CO_2 gas, followed by decapitation and collection of blood from the neck and body. The tibiae from both legs of each mouse were dissected free of adherent tissue and ground sections were prepared at the tibiofibular junction, for histomorphometrical analysis. The femora were extracted, as described in what follows.

Histomorphometric Analysis

Undecalcified ground cross sections of 30 μm thickness were prepared just above the tibiofibular junction (i.e., the syndesmosis) for histomorphometric analysis.[4] Undecalcified ground cross sections were also prepared at a site in the proximal tibia, 6 mm distal to the proximal end of the tibia. This second site was assessed because periosteal woven bone formation was observed in more than half of the cross sections prepared at the tibiofibular junction in the bones from neurectomized mice. The periosteal woven bone formation (which we have attributed to the neurectomized animal's gnawing on their numb hindlimb) was not observed in the cross sections prepared at the proximal tibial site. The tibial sampling sites are shown schematically in **Figure 1**, and the appearance of the ground sections is illustrated in **Figure 2**. Undecalcified ground sections were used in these studies for the following three reasons: (a) the method is rapid (i.e., compared with procedures required for the preparation and analysis of thin sections—decalcification, fixation, embedding, staining, etc.); (b) we were familiar with this method and this sampling site from previous studies with rats[4] and mice;[2,3,6] and (c) although we understood that the histomorphometric data derived from this procedure would be limited (i.e., compared with thin section data from sagittal sections), the method allows measurements of medullary area and both forming and resorbing surfaces (i.e., fluorescent-labeled and eroded perimeters, respectively), and we believed that such data would be sufficient for an initial test of our hypothesis. From the ground sections, we determined

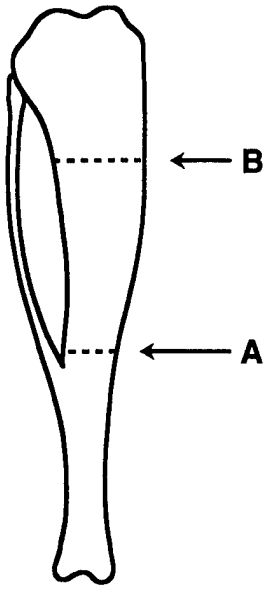

Figure 1. Schematic illustration of the two tibial sampling sites used for preparation of undecalcified ground sections. The first site (A) was located at the tibiofibular junction and the second site (B) was 6 mm distal to the proximal end of the tibia.

total bone area (B.Ar; i.e., total cross-sectional area within the periosteal perimeter) and total medullary area (Ma.Ar). We also measured the endosteal bone forming perimeter as the absolute length of the noneroded, single-labeled perimeter (sL.Pm) and as the ratio of noneroded, single-labeled perimeter to total endosteal perimeter (sL.Pm/B.Pm). Endosteal bone resorbing perimeter was determined as the absolute length of the eroded surface (E.Pm) and as the ratio of eroded perimeter to total endosteal perimeter (E.Pm/B.Pm). The mineral apposition rate (MAR) was

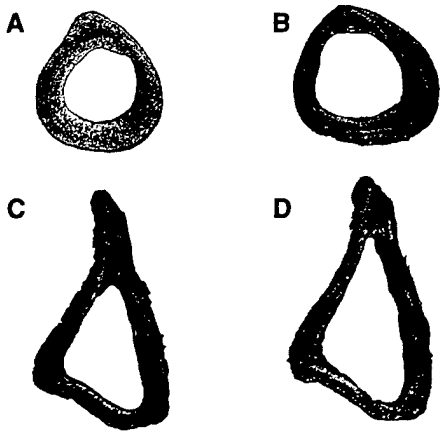

Figure 2. Representative photographs of undecalcified ground sections prepared from B6 mice, at each of the sampling sites. (A) and (B) are sections prepared at the tibiofibular junction from control and neurectomized B6 mice, respectively. Note the apparent increase in medullary area in the sample prepared from the B6 neurectomized mouse. Also, note the appearance of periosteal woven bone in the B6 neurectomized section (this phenomenon of new periosteal bone was observed in some, but not all of the sections prepared at this site from the neurectomized animals). (C) and (D) are sections prepared at the proximal tibial site (6 mm from the distal end of the tibia) from control and neurectomized B6 mice, respectively.

calculated as the mean distance between fluorescent labels, divided by the interval (i.e., in days) between them. Histomorphometric indices were based on nomenclature recommended by the American Society of Bone and Mineral Research.[23] Histomorphometric measurements were made using the OsteoMeasure system (OsteoMetrics Inc., Atlanta, GA). A more detailed description of the methods related to the preparation and measurement of ground cross sections of bone at the tibiofibular junction was provided in a previous report of histomorphometric analyses of rat bone at this sampling site.[4]

Extraction of Femora

As in our previous studies,[9,25] femora were freed of adherent tissue, cut near the midshaft, and incubated overnight in phosphate-buffered saline containing 0.01% azide at 4°C (1.5 mL/bone) to remove marrow and contaminating serum. Each bone was then transferred to 1.5 mL of 25 mmol/L $NaHCO_3$ (pH 7.4) containing 0.01% azide and 0.01% Triton X-100 for a 72 h extraction at 4°C. Each extract was centrifuged to remove insoluble material and used for quantitation of alkaline phosphatase (ALP) activity and osteocalcin, as described in what follows. The extracted bones were dehydrated during a 24 h incubation in 70% ethanol (1 mL/bone at 37°C), then dried (18 h at 37°C) for measurement of bone dry weight (Cahn microbalance, Model 7500, Cahn Instruments, Cerritos, CA).

Measurement of ALP Activity in Serum and Extracts of Femora

ALP activity[9,25] was measured by the time-dependent formation of *p*-nitrophenolate from paranitrophenyl phosphate (PNPP) (i.e., increased absorption of light at 405 nm) in alkaline solution, using a microtiter plate spectrophotometer (EAR400/340AT, Labinstruments, Vienna, Austria). Reactions were initiated by the addition of 0.005–0.025 mL of serum or bone extract, to a total reaction volume of 0.3 mL (in 96 place microtiter plate wells) containing 10 mmol/L PNPP, 1 mmol/L $MgCl_2$, and 150 mmol/L carbonate buffer (pH 10). The reaction mixtures for the serum assays also contained 10 mmol/L L-phenylalanine, to inhibit circulating intestinal ALP activity. ALP activity was calculated as units per liter of serum and milliunits per milligram dry weight of bone, where 1 U is defined by the conversion of 1 μmol of substrate to product per minute at room temperature (25°C).

Measurement of Osteocalcin in Serum and Extracts of Femora

Osteocalcin was measured in serum and extracts of femora by radioimmunoassay (RIA), as in our previous studies, using kit components purchased from Biomedical Technologies (Stoughton, MA). Duplicate aliquots of each serum sample and bone extract were measured and the average value was used for the analyses. Serum osteocalcin is expressed as milligrams per liter of serum, and bone extract osteocalcin expressed as nanograms per milligram of dry weight of bone.

Statistical Analysis

Data are presented as the averages of replicate samples in each group (usually as mean ± SEM). Analytical methods include analysis of variance (ANOVA), Pearson correlation, paired comparisons (e.g., for right vs. left legs from the same animal), and nonparametric analyses, using SYSTAT statistical software (Systat Inc., Evanston, IL).

Bone Vol. 25, No. 2
August 1999:183–190

Table 1. Results of preliminary study: cross-sectional areas at the tibiofibular junction

Mouse strain (n)	Treatment group	Cross-sectional area (mm^2)	
		Total area (B.Ar)	Medullary area (Ma.Ar)
C3H (8)	Neurectomy-right	0.930 ± 0.025	0.120 ± 0.007
C3H (8)	Neurectomy-left	0.959 ± 0.039	0.125 ± 0.009
B6 (7)	Neurectomy-right	0.871 ± 0.016	0.259 ± 0.016[a]
B6 (7)	Neurectomy-left	0.911 ± 0.035	0.325 ± 0.032[a]

Cross-sectional areas were measured at the tibiofibular junction of C3H and B6 mice subjected to sciatic neurectomy (the left leg, neurectomy-left), compared with the contralateral control (the right leg, neurectomy-right), 21 days after the procedures. Data are presented as mean ± SEM (n = 7 or 8 mice per group, as indicated).

[a]Significant difference, compared with C3H mice, $p < 0.001$. There were no significant effects of the sciatic neurectomy on either cross-sectional area.

Results

Our preliminary (feasibility) study of sciatic neurectomy in C3H and B6 mice showed a greater medullary area at the tibiofibular junction in B6 mice compared with C3 mice, but no effects of neurectomy. These results are summarized in **Table 1**. Although the procedure was effective (i.e., the leg was denervated by the resection), the immobilization was without apparent effect (i.e., the −25% measured difference in the medullary area in the B6-neurectomized leg, compared with the contralateral control, was not significant). Reasoning that a time-dependent effect might become more evident with a longer postoperative period and that a greater number of mice in each group would increase our power to detect a smaller significant difference, we planned a second, longer study, with an increased number of mice in each group. We also amended the study design to include two additional groups of sham-operated mice (one for each strain) as an additional control for the immobilized legs. We anticipated that these additional control groups would allow us to compare the right (control) legs of the neurectomized and sham groups to determine whether the left leg immobilization resulted in compensatory right leg overloading, distorting our interpretation of the effects of immobilization (i.e., if the right legs of the neurectomized mice were not different from the right legs of the sham-operated mice, we would discount the possibility of compensatory overloading).

Table 2 summarizes the results of the sciatic neurectomy study, with respect to body weight and two presumptive indices of the (systemic average) rate of bone formation—serum ALP activity and serum osteocalcin. Although the body weights of both strains of mice were increased during the study (i.e., as the mice grew between 9 and 13 weeks of age), there were no significant differences in final body weight between the neurectomized and sham-control mice or between the C3H and B6 mice in either treatment group. We observed significant decreases in serum ALP activity, between 9 and 13 weeks of age, in both strains of mice, but, again, no effects of neurectomy on this systemic index of the rate of bone formation. The only significant change in serum osteocalcin was a decrease in the B6 sham-surgical group, compared with the basal controls. Although these data demonstrate that 4 weeks of hindlimb immobilization, following sciatic neurectomy, did not produce changes in body weight, serum ALP activity, or serum osteocalcin, further studies may be required to assess more carefully the possibility of changes in serum osteocalcin (i.e., timed collection of serum and feeding restrictions can reduce the effects of diurnal variation on serum osteocalcin).

Our bone extraction studies (summarized in **Table 3**) revealed significant differences in femur dry weight, ALP per milligram bone, and osteocalcin per milligram bone, between the 9-week-old basal control groups and the 13-week-old sham and neurectomized groups of each strain. In addition, our measurements of femur dry weight showed the anticipated differences between the bones of C3H and B6 mice, in every treatment group, but no effects of neurectomy. There were no differences in ALP activity per milligram dry weight of bone between the C3H and B6 mice or between the neurectomized and sham-operated mice of either strain. There were, however, differences in extractable osteocalcin (expressed as nanograms per milligram dry weight) between the C3H and B6 mice at 13 weeks of age.

Table 2. Alkaline phosphatase (ALP) and osteocalcin in serum

Strain—treatment (number of samples)	Final body weight (g)	Weight gain (g)	ALP activity in serum (U/L)	Osteocalcin in serum (mg/L)
C3H—basal (10)	18.5 ± 0.4	—	195 ± 6	35.6 ± 4.8
C3H—sham (8)	20.4 ± 0.6[a]	2.4 ± 0.3	147 ± 8[b]	34.5 ± 5.0
C3H—neurectomy (10)	19.7 ± 0.2[a]	3.0 ± 0.2	166 ± 8[a]	22.1 ± 4.1
B6—basal (10)	18.3 ± 0.2	—	208 ± 10	54.8 ± 6.6
B6—sham (10)	21.1 ± 0.3[b]	3.0 ± 0.2	148 ± 4[b]	29.0 ± 3.3[b]
B6—neurectomy (10)	20.5 ± 0.2[b]	2.5 ± 0.3	162 ± 11[b]	37.8 ± 3.7

Sera used for measurements of ALP activity and osteocalcin as described in *Methods* (two sera from the C3H sham group were lost). Final body weights determined at 9 weeks for the basal group and 13 weeks for treatment groups. Weight gain reflects the treatment interval of 9–13 weeks. All data shown as mean ± SEM. There were no significant differences between C3H and B6 mice receiving the same treatment (i.e., basal, sham, or neurectomized). There were no significant differences between the neurectomized and sham-surgical control groups of either strain (i.e., no effects of neurectomy).

Different from the basal control group of the same strain (i.e., C3H or B6), at [a]$p < 0.05$ or [b]$p < 0.005$.

Table 3. Alkaline phosphatase (ALP) and osteocalcin in extracts of femora

Strain—treatment	Right (control) femur			Left (neurectomized) femur		
	Weight	ALP	Osteocalcin	Weight	ALP	Osteocalcin
C3H—basal	34.6 ± 1.6	15.6 ± 1.5	0.20 ± 0.02	35.0 ± 0.9	21.3 ± 1.1	0.14 ± 0.02
C3H—sham	43.9 ± 1.1[b]	7.1 ± 0.6[b]	0.28 ± 0.05	43.1 ± 1.2[b]	8.0 ± 0.8[b]	0.33 ± 0.06[b]
C3H—neurectomized	44.8 ± 0.9[b]	5.4 ± 0.3[b]	0.24 ± 0.03[c]	43.4 ± 0.9[b]	6.3 ± 0.5[b]	0.34 ± 0.05[b]
B6—basal	30.2 ± 1.6	18.5 ± 1.6	0.23 ± 0.05	28.0 ± 2.0[d]	21.8 ± 2.9	0.20 ± 0.03
B6—sham	36.5 ± 0.5[ad]	9.2 ± 0.8[b]	0.18 ± 0.02	35.5 ± 1.1[bd]	9.5 ± 0.8[b]	0.20 ± 0.03
B6—neurectomized	35.8 ± 1.2[ad]	7.2 ± 0.6[b]	0.12 ± 0.02	34.3 ± 1.5[ad]	8.7 ± 0.8[b]	0.16 ± 0.02[d]

The left (neurectomized) and right (control) femora from each mouse (n = 10/group) were extracted for measurements of ALP activity, dry weight, and osteocalcin, as described in *Methods*. ALP activity and osteocalcin expressed as milliunits per milligram dry weight and nanograms per milligram dry weight, respectively. All data shown as mean ± SEM. There were no significant differences between the neurectomized (left) legs and the contralateral controls in the neurectomized mice or between the neurectomized (left) legs and the sham-surgical (left) legs of either strain (i.e., no effects of neurectomy).

Different from basal control group (right or left leg, as appropriate) of the same strain at [a]$p < 0.05$ or [b]$p < 0.005$.

Different from C3H mice receiving the same treatment (i.e., basal control, sham surgery, or neurectomized, comparing right or left leg, as appropriate) at [c]$p < 0.05$ or [d]$p < 0.005$.

We found no effects of neurectomy on femur dry weight, ALP activity per milligram dry weight, or extractable osteocalcin per milligram dry weight.

Our histological measurements of ground sections prepared at the tibiofibular junction showed that the 9-week-old basal control mice had similar total bone areas (B.Ar = 0.829 ± 0.012 mm^2 for C3H mice, compared with 0.827 ± 0.018 mm^2 for B6 mice), but differed greatly with respect to medullary area. (See Figure 2 for exemplary photographs of the ground sections prepared at this sampling site.) The medullary area in B6 mice (0.341 ± 0.017 mm^2) was about 94% greater than in C3H mice (0.176 ± 0.005 mm^2, $p < 0.001$). As summarized in **Table 4,** these studies also revealed a neurectomy-dependent increase in medullary area at the tibiofibular junction of the B6 mice. This difference was also significant compared with sham-operated controls.* In contrast to these results, we found no effect of neurectomy on medullary area at the tibiofibular junction in the C3H mice.

There were two noteworthy findings from our histomorphometric measurements of ground sections prepared from the tibiae of sham-operated mice. First, we found no difference in any measured parameter between the left (sham-surgical) and right (sham contralateral control) tibiae in either C3H or B6 mice (i.e., between-legs variations in the sham-surgical mice were less than or equal to within-leg variations). Therefore, we combined the data from the left and right legs of these animals and report average values, for the sham-surgical mice, in Table 4 and **Table 5** and in Figures 1 and 2 and **Figure 3.** Second, we found no difference in any measured parameter between the right (contralateral control) legs of the neurectomized and sham-surgical groups of either strain of mice. (In other words, we found no evidence of compensatory overloading in the right leg of the neurectomized mice.)

Our assessments of endosteal resorbing (i.e., eroded) perimeter showed neurectomy-dependent increases in both strains of mice. As shown in Table 4 and Figure 3, we found that the length of endosteal eroded perimeter (E.Pm) was increased in the neurectomized (left) legs of C3H mice, compared with both the contralateral (right) legs and the average values for both legs of the sham-operated controls. This apparent effect of neurectomy was even more pronounced in the B6 mice. Our histological assessments at the tibiofibular junction also revealed that the length of the endosteal bone forming

*Although the appearance of irregular periosteal woven bone formation in some (but not all) of the ground sections prepared from the neurectomized mice (i.e., at the tibiofibular junction) precluded accurate measurements of total bone area, we estimated total bone area by excluding the new periosteal bone from our measurements. These estimates indicate no differences in total bone area at this sampling site—either between the two strains of mice or between the treatment groups. These estimates also suggest that the neurectomy-dependent increase in medullary area in the B6 mice was associated with a decrease in cortical bone area from 63.8% to 57.1% of total bone area, $p < 0.5$ (i.e., from 0.551 ± 0.21 mm^2 to 0.517 ± 0.20 mm^2).

Table 4. Histologic measurements at the tibiofibular junction

Mouse strain	Treatment group	Medullary area (Ma.Ar, mm^2)	Eroded perimeter (E.Pm/tot.Pm, %)	Labeled perimeter (sL.Pm/tot.Pm, %)	Mineral apposition rate (MAR, μm/day)
C3H	Sham surgery	0.157 ± 0.006	31.1 ± 1.2	59.8 ± 3.2	—
C3H	Neurectomy-right	0.138 ± 0.009[a]	30.8 ± 1.7	69.2 ± 1.7	1.38 ± 0.07
C3H	Neurectomy-left	0.126 ± 0.017[a]	47.2 ± 4.9[ad]	52.8 ± 4.9[c]	1.33 ± 0.10
B6	Sham surgery	0.294 ± 0.009[f]	20.8 ± 1.8	0.673 ± 0.044	—
B6	Neurectomy-right	0.313 ± 0.020[f]	16.8 ± 2.9[e]	78.3 ± 3.4	1.11 ± 0.07[e]
B6	Neurectomy-left	0.388 ± 0.019[acf]	88.3 ± 2.9[bdf]	9.6 ± 3.1[bdf]	0.64 ± 0.18[ef]

Ground sections prepared at the tibiofibular junction of bones from the immobilized (neurectomy, left) and contralateral control legs (neurectomy, right) of the neurectomized mice, and from both legs of the sham-surgical mice (n = 10 for each). All data shown as mean ± SEM. Endosteal eroded (resorbing) and noneroded, single-labeled (forming, using the second calcein marker) perimeter lengths expressed as percent of total endosteal perimeter length.

Different from sham-surgical controls at [a]$p < 0.05$ or [b]$p < 0.005$.

Different from neurectomy-right (control) at [c]$p < 0.05$ or [d]$p < 0.005$.

Different from C3H mice receiving the same treatment at [e]$p < 0.01$ or [f]$p < 0.001$.

Bone Vol. 25, No. 2
August 1999:183–190

Table 5. Histologic measurements in the proximal tibia

Mouse strain (sL.Pm/tot.Pm) (n)	Treatment group	Absolute lengths of perimeters		Relative lengths of perimeters	
		Eroded (E.Pm, mm)	Labeled (sL.Pm, mm)	Eroded (%) (E.Pm/tot.Pm, %)	Labeled (%)
C3H (7)	Sham	0.360 ± 0.030	1.66 ± 0.05	17.5 ± 1.6	79.0 ± 1.9
C3H (8)	Neurectomy-right	0.368 ± 0.047	1.78 ± 0.06	16.8 ± 1.9	81.7 ± 2.3
C3H (8)	Neurectomy-left	0.439 ± 0.038	1.58 ± 0.079	21.0 ± 1.8	75.8 ± 3.3
B6 (8)	Sham	0.157 ± 0.033	3.16 ± 0.07[d]	4.0 ± 0.9[d]	95.1 ± 1.2[c]
B6 (8)	Neurectomy-right	0.158 ± 0.038	3.20 ± 0.09[d]	4.6 ± 1.1[d]	93.2 ± 1.7
B6 (8)	Neurectomy-left	1.15 ± 0.13[abd]	2.13 ± 0.02[abd]	32.9 ± 3.8[abd]	61.0 ± 5.6[abc]

Ground sections (30 μm) prepared 6 mm distal to the proximal end of tibiae from immobilized (neurectomy-left), and control (neurectomy-right) legs of neurectomized mice, and sham-surgical controls (sham). (n = 7 or 8 for each group, all intact bones were analyzed, see *Methods*). Data shown as mean ± SEM. Endosteal eroded (resorbing) and noneroded, single-labeled (forming, using the second calcein marker) perimeters measured as absolute lengths (mm) and also expressed as percent of total endosteal perimeter.
[a]Different from sham-surgical controls at $p < 0.005$. [b]Different from neurectomy-right (control) at $p < 0.005$. [c]Different from C3H mice receiving same treatment at $p < 0.05$ or [d]$p < 0.005$.

perimeter (measured as the noneroded length of endosteal perimeter stained with the final calcein label, given 2 days before killing [sL.Pm]) was decreased dramatically by neurectomy in B6 mice, but was unchanged in C3H mice. These results are shown in Table 4 and **Figure 4**. The time dependence of the effect of sciatic neurectomy to decrease the length of the endosteal bone forming perimeter (i.e., sL.Pm) in B6, but not C3H mice, is shown in **Figure 5**. Finally, the effect of sciatic neurectomy to decrease the rate of endosteal mineral apposition (MAR) in B6, but not C3H, mice is summarized in Table 4.

We did not assess the effects of sciatic neurectomy on total bone area at the tibiofibular junction, because we observed irregular periosteal woven bone formation in more than half of the immobilized legs (see the example in Figure 2B). Although we postulated that the mice gnawing on their numb hindlimbs caused this periosteal formation, we could not dismiss the possibility that this periosteal formation also affected our measurements at the endosteal surface. To address this possibility, we made additional measurements of ground sections prepared from a secondary site—in the proximal metaphysis—which was free of such irregular periosteal formation. (Exemplary photographs of ground sections prepared at this proximal tibial site are also shown in Figure 2.) These supplemental studies showed that both total bone area and medullary area were greater at this anatomical site in the B6 sham-operated mice (1.45 ± 0.02 mm^2 and 0.636 ± 0.13 mm^2, respectively), compared with the C3H sham-operated mice (1.07 ± 0.02 mm^2 and 0.285 ± 0.009 mm^2, $p < 0.001$ for each). Again, we found no difference, in any measured parameter, between the sham-operated left leg and the contralateral right leg of the sham-operated mice of either strain and, therefore, we combined the data from both legs of the sham-operated mice. Our histomorphometrical measurements at this proximal tibial site showed no effect of neurectomy on either total bone area or medullary area in either strain of mice; the results of our measurements of endosteal forming (noneroded, single-labeled) and resorbing (eroded) perimeters are summarized in Table 5. Although we found no effect of sciatic neurectomy on the length of either perimeter at this proximal tibial sampling site in the C3H mice, we found a neurectomy-dependent increase in the length of eroded (resorbing) perimeter and a neurectomy-dependent decrease in the length of single-labeled (forming) perimeter in the B6 mice.

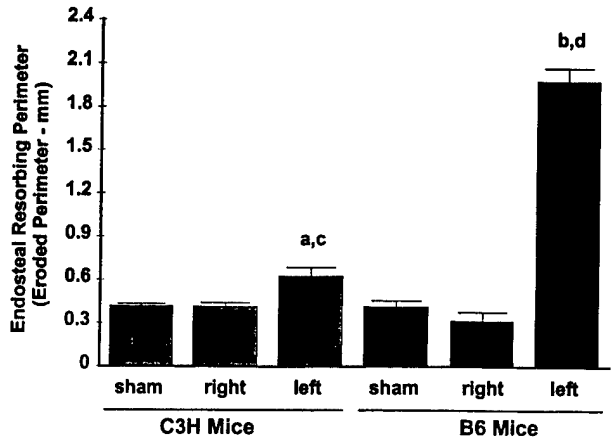

Figure 3. Effect of immobilization on endosteal resorbing surface in C3H and B6 mice. Length of endosteal eroded perimeter (mm), measured at 28 days, in ground sections prepared at the tibiofibular junction. Data shown as mean ± SEM for the neurectomized (left) legs of neurectomized C3H and B6 mice ("left"), the contralateral control legs of neurectomized mice ("right") and sham-surgical controls ("sham"). [a]Different, compared with "sham" of the same strain, at $p < 0.05$ or [b]$p < 0.001$. [c]Different, compared with the "right" legs of the same strain at $p < 0.05$ or [d]$p < 0.001$.

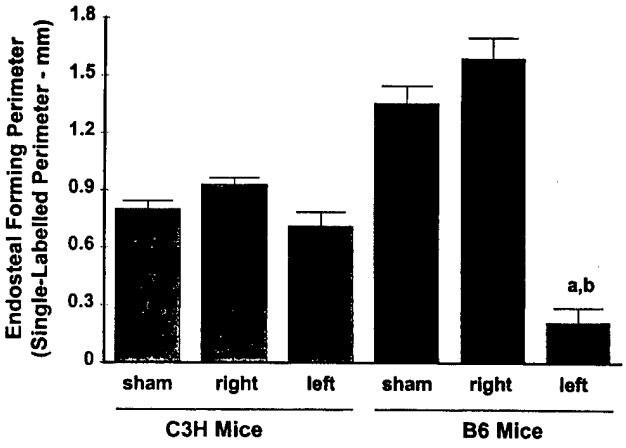

Figure 4. Effect of immobilization on endosteal forming surface in C3H and B6 mice. Length of endosteal, noneroded, single-labeled perimeter (mm), measured at 28 days, in ground sections prepared at the tibiofibular junction. Data shown as mean ± SEM for the neurectomized (left) legs of neurectomized C3H and B6 mice ("left"), the contralateral control legs of neurectomized mice ("right"), and sham-surgical controls ("sham"). [a]Different, compared with "sham" of the same strain, at $p < 0.001$. [b]Different, compared with "right" legs of the same strain, at $p < 0.001$.

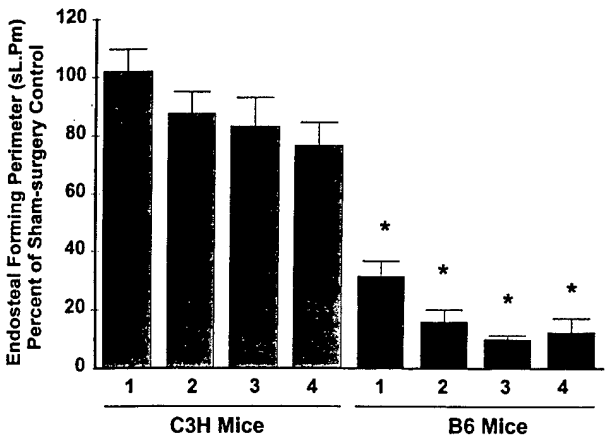

Figure 5. Time-dependent effect of immobilization on endosteal forming surface in C3H and B6 mice. Length of endosteal, noneroded, single-labeled perimeter, measured in ground sections prepared at the tibiofibular junction, for each fluorescent label—labled 1, 2, 3, and 4 (see *Methods* for labeling schedule). Average values observed in neurectomized (left) legs of neurectomized mice are expressed as the percent of values observed in the sham-surgical controls of the same strain. Data shown as mean ± SEM (n = 10) for each group. *Different, compared with the sham-surgical controls, at $p < 0.001$. Two-way ANOVA revealed effects of neurectomy and time ($p < 0.001$ for each).

Discussion

The results of the current studies indicate that sciatic neurectomy had differential effects on bone formation and resorption in the tibiae of C3H, compared with B6, mice. The left-side denervation decreased bone formation indices in the tibiae of B6 mice, but had no such effect in the tibiae of C3H mice. Although sciatic neurectomy increased the length of the endosteal bone resorbing (eroded) perimeter in the tibiae of both strains, the effect was greater (both in absolute and relative terms) in the B6 mice. We did not observe a systemic response (i.e., in serum ALP or serum osteocalcin), nor did we see a difference in ALP or osteocalcin in extracts of femora, suggesting that the skeletal effects of immobilization were localized and greatest in the most distal regions of the hindlimb skeleton.

The effect of sciatic neurectomy to increase bone resorption at the tibiofibular junction in the B6 mice (e.g., a 325% increase in eroded perimeter/total endosteal perimeter, $p < 0.001$) was consistent with effects observed at the proximal tibial site (e.g., a 722% increase in eroded perimeter/total endosteal perimeter, $p < 0.001$) and with previous reports of the effects of immobilization to increase bone resorption.[12,16,26,27,32] In contrast, our studies showed a relatively small effect of sciatic neurectomy to increase bone resorption at the tibiofibular junction of the C3H mice (e.g., a 51% increase in eroded surface/total endosteal surface, $p < 0.05$) and no significant effect on bone resorption in the proximal tibial site. It is of interest to speculate that these differences in the effects of immobilization to increase bone resorption in the bones of C3H and B6 mice may be related to differences in the availability and/or responsiveness of osteoclast progenitor cells. (We have recently reported that the marrow of B6 femora contains more osteoclast progenitors than the marrow of C3H femora.[21]) Further studies are required to address this new hypothesis.

Further studies are also required to address a parallel hypothesis concerning the differential effects of immobilization on bone formation indices in these two inbred strains of mice. The effects of sciatic neurectomy to inhibit bone formation at the tibiofibular junction of the B6 mice (e.g., an 86% decrease in noneroded, single-labeled perimeter/total endosteal perimeter, $p < 0.001$) was consistent with decreases seen in the proximal tibial site (e.g., a 36% decrease in noneroded, single-labeled perimeter/total endosteal perimeter, $p < 0.05$) and with previous reports of immobilization-dependent decreases in formation.[1] Although our studies show that immobilization had no such effect to inhibit endosteal bone formation in the tibiae of C3H mice, our data also indicate that the effect of sciatic neurectomy to decrease the length of the endosteal bone forming perimeter in the tibiae of B6 mice was time-dependent. Therefore, it is possible that a longer study would reveal a similar decrease in the length of the endosteal bone forming perimeter in the tibiae of C3H mice. With regard to mechanism, it is of interest to speculate that this unexpected difference may be related to differences in the availability and/or activity of osteoblast-line cells in C3H, compared with B6, mice.[9] This hypothesis would be consistent with previous studies showing that differences in the recruitment and/or differentiation of osteoblast and osteoclast progenitor cells were associated with (and may be responsible for) peak bone density differences between C3H and B6 mice[2,3,5,6,9,21,25] and the low bone density of SAMP6 mice.[7,14] It is also of interest to speculate that differences in the recruitment and activity of bone forming and resorbing cells in C3H and B6 mice may be related to differences in circulating levels of growth hormone, IGF-I, or 1,25-dihydroxyvitamin D. Previous studies have shown that serum growth hormone levels are higher in C3H mice than in B6 mice,[28] as are circulating and skeletal levels of IGF-I,[24] and that circulating levels of 1,25-dihydroxyvitamin D are higher in B6 mice compared with C3H mice.[8]

With regard to the unexpected (and troublesome) observation of irregular woven bone formation on the periosteum of the immobilized tibiae of many (about 70%) of the neurectomized mice, we believe that it was caused by gnawing and not by neurectomy. The periosteal formation was irregular and localized to a variable region just adjacent to the tibiofibular junction, and the following two observations suggest that it did not compromise the interpretation of the endosteal changes that we reported. First, we observed the same patterns of neurectomy-dependent and mouse-strain-specific endosteal changes in both forming and resorbing perimeter lengths at the tibiofibular junction (where the periosteal formation was observed) and at a second endosteal site, at the proximal end of the tibia (where periosteal formation was not observed in any of the mice). Second, the periosteal formation was variable, both in occurrence and degree, yet the pattern of the endosteal changes (e.g., the neurectomy-dependent changes in the lengths of forming and resorbing perimeters in the B6 mice) was similar in all the animals (i.e., there was no association between the degree of periosteal formation and the degree of endosteal change). Although these findings support our contention that the endosteal changes reported in response to sciatic neurectomy were dependent on the periosteal formation, we cannot dismiss that possibility. Further studies (e.g., using hard plastic sheathing to protect the immobilized hindlimb from gnawing) will be necessary to resolve this issue.

Further studies will also be required for a more extensive histomorphometrical analysis (using decalcified thin sections) of the skeletal responses of C3H and B6 mice to hindlimb immobilization by sciatic neurectomy. We believe that such studies are warranted, because the current data indicate that histomorphometry provides the most sensitive index of neurectomy-dependent changes in the rates of bone formation and resorption. (The current studies revealed immobilization-dependent changes in histomorphometric indices of bone formation and resorption, without concomitant changes in serum or bone extract indices of either process.) Furthermore, thin sections will allow for specific identification of osteoblasts and osteoclasts (i.e., by staining for ALP and acid phosphatase activity, respectively), as well as quantitation of osteoid and mineralized bone. Finally, sagittal thin sections of tibial metaphysis will allow us to determine whether the effects of sciatic neurectomy that we

observed in endosteal cortical bone are similarly evident in cancellous (trabecular) bone.

In summary, the current studies indicate that B6 mice are more sensitive to bone loss from hindlimb immobilization than C3H mice. Because these are highly inbred strains, this observation suggests that the effects of immobilization to increase bone resorption and to decrease bone formation are genetically determined and, thus, may be amenable to QTL analysis. Further studies are required to test the new hypothesis that C3H and B6 mice will show analogous (i.e., opposing) strain-specific differences in their skeletal responses to supplemental mechanical loading. Further studies will also be required to determine whether the genetic and cellular mechanisms that determine peak bone density in C3H and B6 mice are also determinants of the effects of immobilization and loading.

Acknowledgments: The authors thank the secretarial staff of the Loma Linda University Mineral Metabolism Research Unit (which is located in the Jerry L. Pettis Memorial Veterans Medical Center) for assistance in the preparation of this manuscript. These studies were supported by: the National Institutes of Health, Grants AR-43618 and CA-34196 (W.B.); a subcontract from U.S. Army Medical Research Acquisition Activity Grant DAMD17-96-1-6306 (W.B. and D.J.B.); medical research grants from the Government of Austria (H.P.D.); the Japan–North America Medical Exchange Foundation (Y.K.); the Jackson Laboratory (W.B. and L.R.D.); Loma Linda University (M.S., S.K., and R.M.); and the Veterans Administration (D.J.B. and J.F.).

References

1. Barou, O., Palle, S., Vico, L., Alexandre, C., and Lafage-Proust, M. H. Hindlimb unloading in rat decreases preosteoblast proliferation assessed in vivo with BrdU incorporation. Am J Physiol 274:E108–114; 1998.
2. Baylink, D. J., Donahue, L., Rosen, C. J. et al. Novel genetic model of peak bone density: A polygenic trait. Tenth International Congress of Endocrinology. Bethesda, MD; The Endocrine Society Press; 1996; Abstract P1–945.
3. Baylink, D., Farley, J., Donahue, L. et al. Evidence that high peak bone density is due to decreased resorption not increased formation in a murine model [abstract]. J Bone Miner Res 10(Suppl.):S338; 1995.
4. Baylink, D., Stauffer, M., Wergedal, J., and Rich, C. Formation, mineralization, and resorption of bone in vitamin D-deficient rats. J Clin Invest 49:1122–1129; 1970.
5. Beamer, W. G., Donahue, L. R., Baylink, D. J., and Rosen, C. J. Mapping genes for normal bone density in inbred mice by quantitative trait locus analysis [abstract]. J Bone Miner Res 11(Suppl. 1):S176; 1996.
6. Beamer, W. G., Donahue, L. R., Rosen, C. J., and Baylink, D. J. Genetic variability in adult bone density among inbred strains of mice. Bone 18:397–403; 1996.
7. Benes, H., Dennis, R., Zheng, W. et al. Genetic mapping of osteopenia-associated loci using crosses between closely related mouse strains with differing bone mineral density [abstract F598]. J Bone Miner Res 12(Suppl. 1):S375; 1997.
8. Chen, C. and Kalu, D. N. Strain differences in calcium absorption, serum $1,25(OH)_2D$ and serum parathyroid hormone in response to dietary calcium restriction in C3H/HeJ and C57BL/6J mice [abstract F595]. J Bone Miner Res 12(Suppl. 1):S375; 1997.
9. Dimai, H. P., Linkhart, T. A., Linkhart, S. G. et al. Alkaline phosphatase levels and osteoprogenitor cell numbers suggest bone formation may contribute to peak bone density differences between two inbred strains of mice. Bone 22:211–216; 1998.
10. Evans, R. A., Marel, G. M., Lancaster, E. K., Kos, S., Evans, M., and Wong, Y. P. Bone mass is low in relatives of osteoporotic patients. Ann Intern Med 109:870–873; 1988.
11. Glaser, D. L. and Kaplan, F. S. Osteoporosis. Definition and clinical presentation. Spine 22(Suppl.):12S–16S; 1997.
12. Globus, R. K., Bikle, D. D., and Morey-Holton, E. Effects of simulated weightlessness on bone mineral metabolism. Endocrinology 114:2264–2270; 1984.
13. Gross, T. S., Edwards, J. L., McLeod, K. J., and Rubin, C. T. Strain gradients correlate with sites of periosteal bone formation. J Bone Miner Res 12:982–988; 1997.
14. Jilka, R. L., Weinstein, R. S., Takahashi, K., Parfitt, A. M., and Manolagas, S. C. Linkage of decreased bone mass with impaired osteoblastogenesis in a murine model of accelerated senescence. J Clin Invest 97:1732–1740; 1996.
15. Jouanny, P., Guillemin, F., Kuntz, C., Jaendel, C., and Pourel, J. Environmental and genetic factors affecting bone mass. Arthrit Rheum 38:61–67; 1995.
16. Kaneps, A. J., Stover, S. M., and Lane, N. E. Changes in canine cortical and cancellous bone mechanical properties following immobilization and remobilization with exercise. Bone 21:419–423; 1997.
17. Kelly, P. and Harris, M. Genetic regulation of peak bone mass. Acta Paediat Scand 411(Suppl.):24–29; 1995.
18. Kerr, D., Morton, A., Kick, I., and Prince, R. Exercise effects on bone mass in postmenopausal women are site-specific and load-dependent. J Bone Miner Res 11:218–225; 1996.
19. Klein-Nulend, J., Veldhuijzen, J. P., van Strien, M. E., de Jong, M., and Burger, E. H. Inhibition of osteoclastic bone resorption by mechanical stimulation in vitro. Arthrit Rheum 33:66–72; 1990.
20. Kodama, Y., Nakayama, K., Fuse, H. et al. Inhibition of bone resorption by pamidronate cannot restore normal gain in cortical bone mass and strength in tail-suspended rapidly growing rats. J Bone Miner Res 12:1058–1067; 1997.
21. Linkhart, T., Linkhart, S., Farley, J. et al. Osteoclast formation in bone marrow cultures from two inbred strains of mice with different bone densities. J Bone Miner Res 14:40–47; 1998.
22. Malpe, R., Baylink, D. J., Linkhart, T. A., Wergedal, J. E., and Mohan, S. Insulin-like growth factor (IGF)-I, -II, IGF binding proteins-3, -4, and -5 levels in the conditioned media of normal human bone cells are skeletal site-dependent. J Bone Miner Res 12:423–430; 1997.
23. Parfitt, A. M., Drezner, M. K., Glorieux, F. H. et al. Bone histomorphometry: Standardization of nomenclature, symbols, and units. Report of the ASMBR Histomorphometry Nomenclature Committee. J Bone Miner Res 2:595–610; 1987.
24. Pocock, N. A., Eisman, J. A., Hooper, J. L., Yeates, M. G., Sambrook, P. N., and Ebert, S. Genetic determinants of bone mass in adults. J Clin Invest 80:706–710; 1987.
25. Rosen, C. J., Dimai, H. P., Verault, D. et al. Circulating and skeletal insulin-like growth factor-I concentrations in two inbred strains of mice with different bone mineral densities. Bone 21:217–223; 1997.
26. Sakai, A., Nakamura, T., Tsurukami, H. et al. Bone marrow capacity for bone cells and trabecular bone turnover in immobilized tibia after sciatic neurectomy in mice. Bone 18:479–486; 1996.
27. Shen, V., Liang, X. G., Birchman, R. et al. Short-term immobilization-induced cancellous bone loss is limited to regions undergoing high turnover and/or modeling in mature rats. Bone 21:71–78; 1997.
28. Sinha, Y. N., Vlahakis, G., and Vanlerlaan, W. P. Serum, pituitary and urine concentrations for prolactin and growth hormone in eight strains of mice with varying incidence of mammary tumors. Int J Cancer 24:430–437; 1979.
29. Washnich, R. D. Epidemiology of osteoporosis. In: Favus, M. J., Ed. Primer on the Metabolic Bone Diseases and Disorders of Mineral Metabolism, 3rd Ed. New York: Lippincott-Raven; 1996; 249–251.
30. Westerlind, K. C., Wronski, T. J., Ritman, E. L. et al. Estrogen regulates the rate of bone turnover but bone balance in ovariectomized rats is modulated by prevailing mechanical strain. Proc Natl Acad Sci USA 94:4199–4204; 1997.
31. Zaman, G., Suswillo, R. F., Cheng, M. Z., Tavares, I. A., and Lanyon, L. E. Early responses to dynamic strain change and prostaglandins in bone-derived cells in culture. J Bone Miner Res 12:769–777; 1997.
32. Zeng, Q. Q., Jee, W. S., Bigornia, A. E. et al. Time responses of cancellous and cortical bones to sciatic neurectomy in growing female rats. Bone 19:13–21; 1996.

Date Received: November 10, 1998
Date Revised: April 13, 1999
Date Accepted: April 13, 1999

ELSEVIER

Bone Vol. 25, No. 4
October 1999:421–429

Histomorphometric Studies Show That Bone Formation and Bone Mineral Apposition Rates Are Greater in C3H/HeJ (High-Density) Than C57BL/6J (Low-Density) Mice During Growth

M. H.-C. SHENG,[1] D. J. BAYLINK,[1] W. G. BEAMER,[2] L. R. DONAHUE,[2] C. J. ROSEN,[3] K.-H. W. LAU,[1] and J. E. WERGEDAL[1]

[1]*Musculoskeletal Disease Center, Jerry L. Pettis Memorial VA Medical Center and Departments of Medicine and Biochemistry, Loma Linda University, Loma Linda, CA, USA*
[2]*Jackson Laboratories, Bar Harbor, ME, USA*
[3]*Maine Center for Osteoporosis Research, Bangor, ME, USA*

High-density C3H/HeJ (C3H) and low-density C57BL/6J (B6) mice, with femoral bone density differing by 50%, were chosen as a model to investigate the mechanisms controlling peak bone density and to map peak bone density genes. The present longitudinal study was undertaken to further establish the bone biologic phenotypes of these two inbred strains of mice. To evaluate phenotypic differences in bone formation parameters in C3H and B6 mice between the ages of 6 and 26 weeks, undecalcified ground sections from the diaphyses of the tibia and femur were prepared from mice receiving two injections of tetracycline. Histomorphometric analyses revealed that the cortical bone area was significantly greater (16%–56%, $p < 0.001$) in both the femur and tibia of the C3H mice than in the B6 mice at all timepoints. This difference in cortical bone area was due to significantly smaller medullary areas in the C3H mice than in the B6 mice. The bone formation rates (BFR) at the endosteum in both the femur and tibia were significantly greater (28%–117%, $p < 0.001$) in the young C3H mice (6–12 weeks old) than in B6 mice. The higher bone formation in C3H mice was associated with higher values of the bone mineral apposition rate (25%–94%, $p < 0.001$), and was not associated with higher values of the forming surface length as measured by tetracycline label length. Similar interstrain differences in mineral apposition and bone formation rates were observed in the periosteum of the femur and tibia. In conclusion, the greater bone area in the high-density C3H mice vs. the low-density B6 mice was, in part, due to the greater periosteal and endosteal bone formation rates during growth in the C3H mice. Because the C3H and B6 mice were maintained under identical environmental conditions (diet, lighting, etc.), the observed interstrain differences in bone parameters were the result of the action of genetic factors. Consequently, these two inbred strains of mice are suitable as a model to identify genetic factors responsible for high bone formation rates. (Bone 25: 421–429; 1999)

Key Words: Bone density; Bone formation; Bone histomorphometry; Cortical bone; Inbred mice.

Introduction

Peak bone mass is an important determining factor of future fracture risks in humans. There is an abundance of evidence in humans indicating that genetic factors can determine up to 70% of variation in peak bone mass.[3,5,6,11,16] Accordingly, it is essential to understand the contribution of genetic factors to peak bone mass. With the exception of identical twins, the genetic background in humans varies significantly from one individual to another, making studies of genetic involvement in a given bone phenotype in humans difficult. Inbred mice, which possess identical genetic backgrounds, provide excellent animal models for assessing the involvement of genetic factors in the determination of a given phenotype and, therefore, would be ideal for investigating genetic contributions to peak bone mass.

We have recently demonstrated that two inbred strains of mice, namely C3H/HeJ (C3H) and C57BL/6J (B6), display a profound difference in peak bone density. The femur density (measured by peripheral quantitative computed tomography, or pQCT) in the adult C3H mice is 53% higher than that of the B6 mice.[2] The difference in femur bone density is not due to differences in body size, because these mice do not differ significantly in body weight. Therefore, these two mouse strains have been selected as the basis of an animal model to assess genetic regulation of peak bone mass.

Bone mass is regulated by the balance of bone formation and resorption rates. Our recent studies with biochemical markers revealed that the C3H mice (high-bone-density mice) exhibited a significantly higher level of alkaline phosphatase activity in serum and in bone extracts, than did the B6 mice.[4] The C3H mice possessed higher insulin-like growth factor (IGF-1) levels in serum and bone extracts than the B6 mice.[12] These biochemical studies raise the strong possibility that the bone formation rate in the C3H mice was elevated compared with the B6 mice and, as such,

Address for correspondence and reprints: Dr. Matilda H.-C. Sheng, Musculoskeletal Disease Center (151), Jerry L. Pettis Memorial VA Medical Center, 11201 Benton Street, Loma Linda, CA 92357. E-mail: shengm@llvamc.va.gov

8756-3282/99/$20.00
PII S8756-3282(99)00184-2

Bone Vol. 25, No. 4
October 1999:421–429

suggesting that the phenotype of increased bone density in the C3H mice may be due, in part, to a greater bone formation rate.

Previous pQCT data also indicate that the difference in femoral density between the C3H and B6 mice could be detected by as early as 8 weeks of age. Thus, it is conceivable that the gene(s) responsible for the phenotype of an increased femoral density may be expressed at an early age. Moreover, there is also evidence that the difference between strains in bone density is seen in the vertebrae, phalanges, and tibia,[2] raising the possibility that the phenotype of high bone density in C3H mice is not unique to the femur.

The present study sought to test three hypotheses using bone histomorphometry: (1) the C3H mice have a greater bone formation rate than the B6 mice; (2) the difference in bone formation between strains is seen in endosteal and periosteal bone sites of both tibia and femur; and (3) the difference in bone formation rate between strains occurs during the early development of peak bone mass. To test these three hypotheses, and to further establish the bone biologic phenotypes of these inbred mice, we conducted a longitudinal study to evaluate differences in histomorphometric bone formation parameters in the C3H and B6 inbred mice at the ages of 6, 8, 12, 16, and 26 weeks. These age groups are appropriate for assessing phenotypic differences during peak bone mass development in these mice, because it has been shown that these inbred mice reach peak bone mass at approximately 16 weeks of age.[2] Due to the fact that the majority of bone in the femur and tibia is cortical rather than trabecular, we concentrated on evaluating the cortical bone using ground sections of the diaphysis. Measurement of tetracycline labels on bone surfaces in this study provided the histomorphometric data that revealed large differences between C3H and B6 mice in bone formation rate at both periosteal and endosteal surfaces. The differences in bone formation rates were due largely to different mineral apposition rates (MAR), rather than to different forming surface lengths, as assessed by tetracycline-labeled surface (TLS). Finally, the differences in these bone formation parameters were seen only in the young, growing mice of 6–12 weeks of age, but not in the older, mature animals.

Methods and Materials

Animals

Female C3H/HeJ (C3H) and C57BL/6J (B6) inbred mice of 6, 8, 12, 16, and 26 weeks of age, respectively (n = 6–11 per group), were used in this experiment. The mouse colonies were maintained and housed in an accredited animal care facility at the Jackson Laboratory (Bar Harbor, ME). The mice for each age were randomly selected from several litters (average litter size did not differ between strains) and housed in a controlled environment in groups of three or four from weaning until necropsy. The mice were fed an autoclaved NIH 31 diet (modified to 6% fat content) obtained from Purina Mills, Inc. (St. Louis, MO) and given acidified (HCl, pH 2.8–3.1) water. The bedding provided was autoclaved white pine shavings. Each animal was first labeled with achromycine (20 mg/kg) and then with demeclocycline (20 mg/kg) with a 6 day interval. One day after the second label, the mice were killed and both tibiae and femora were removed (with muscle) from each animal. The bones were fixed with 10% cold neutral buffered formalin for 4–5 h, rinsed to remove extra formalin, placed in 70% ethanol, and were then immediately shipped to the Jerry L. Pettis Memorial VA Medical Center. The bones were stored at 4°C until processing for analysis. The animal protocol was reviewed and approved by the animal care and use committee of the Jackson Laboratory.

Preparation of Bone Samples

The femora and tibiae were defleshed and a thin cross section (0.5 mm thickness) was removed from the middiaphysis of the femur (1 mm distal to the midpoint between the greater trochanter and the distal end) or from the tibial diaphysis just proximal to the fibular junction, respectively, with a low-speed saw (Isomet, Buehler, Lake Bluff, IL). The cross sections were then ground to 30 μm in thickness, mounted in aqueous Fluoromount-G (Fisher Scientific, Pittsburgh, PA), and examined under an Olympus BH-2 fluorescence/bright-field microscope.

Histomorphometric Measurements

All bone histomorphometric parameters were measured with the OsteoMeasure system equipped with a digitizing tablet (OsteoMetrics, Atlanta, GA) and a color video camera (Sony, Japan). Tetracycline measurements were made at a total magnification of 600× (20× microscope objective and 30× camera magnification), whereas the measurements of bone area were made at a total magnification of 60× (2× microscope objective and 30× camera magnification). Cortical bone area was calculated by subtracting the medullary area from the total cross-sectional bone area. The tetracycline-labeled surface (TLS, in millimeters) was calculated as the sum of the length of double labels (dL) plus one half of the length of single labels (sL) along the entire endosteal or periosteal bone surfaces; that is, TLS = dL + 0.5sL.[7] The mineral apposition rate (MAR, in microns per day) was determined by dividing the mean of the width of the double labels by the interlabel time (6 days). The bone formation rate (BFR) was calculated by multiplying MAR by TLS and was expressed in $mm^2 \times 10^{-3}$/day. The methodological coefficients of variation for each parameter, which were determined by analysis of variance (ANOVA) of three repeated measurements on five different bone specimens, were as follows: area, 0.78%–1.86%; perimeter, 0.57%–1.36%; label length, 6.44%; and label width, 4.98%.

Data Presentation and Statistical Analysis

Because there was a difference in size between the two strains of mice, the bone formation data were presented in two alternative ways; that is, using a bone surface referent (BFR/BS and TLS/BS) and using a total cross-sectional referent (BFR/TCS and TLS/TCS). The data are expressed as mean ± SEM. Two-way ANOVA was used to analyze independent effects of mouse strain and age, and also the interaction between mouse strain and age. The difference between mouse strains at a given age was analyzed using the Tukey honestly significant difference (HSD) post hoc multiple comparison test. All statistical analyses were performed with SYSTAT statistical software (Systat, Evanston, IL) on a personal computer. Differences were considered statistically significant when $p < 0.05$. Because the pattern of interstrain differences was not the same for young (6–12-week-old) mice and mature (16–26-week-old) mice, the statistical analysis was done separately for young and mature mice.

Results

Total Cortical Bone Area

Femur. Gross morphometric analysis of the ground sections from the middiaphysis of the femur indicated that the femoral cortical bone area in high-density C3H mice was significantly ($p < 0.001$, ANOVA) larger than that of low-density B6 mice (**Figures 1** and **2A**). The difference in cortical bone area between C3H and B6 increased with age (i.e., by 16% at 6 weeks, 16% at 8 weeks, 31%

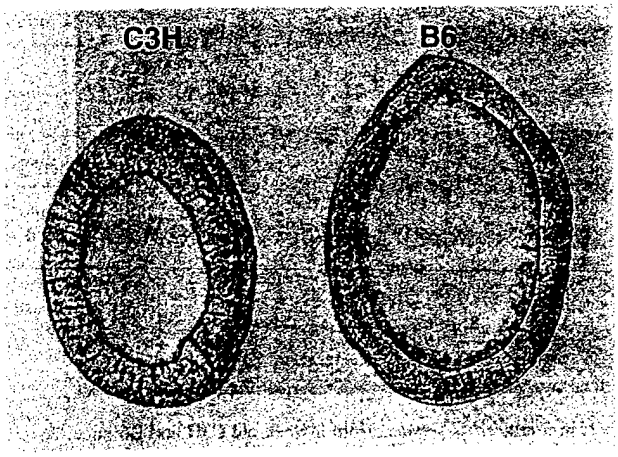

Figure 1. Photomicrograph (35×) comparing the diaphyseal cross section from the femur of an 8-week-old B6 mouse with the cross section from a C3H mouse.

at 12 weeks, 36% at 16 weeks, and 56% at 26 weeks, respectively). Consequently, these findings indicate that C3H mice, in addition to having a higher femoral bone density,[2] also had a larger femoral cortical bone volume. The medullary area in C3H mice was also significantly less (by approximately 50%) than that in B6 mice of each test age (Figure 2B). Because the total bone cross-sectional area was smaller in the C3H mice than in the B6 mice (Figure 2C), the difference in medullary area was primarily responsible for the

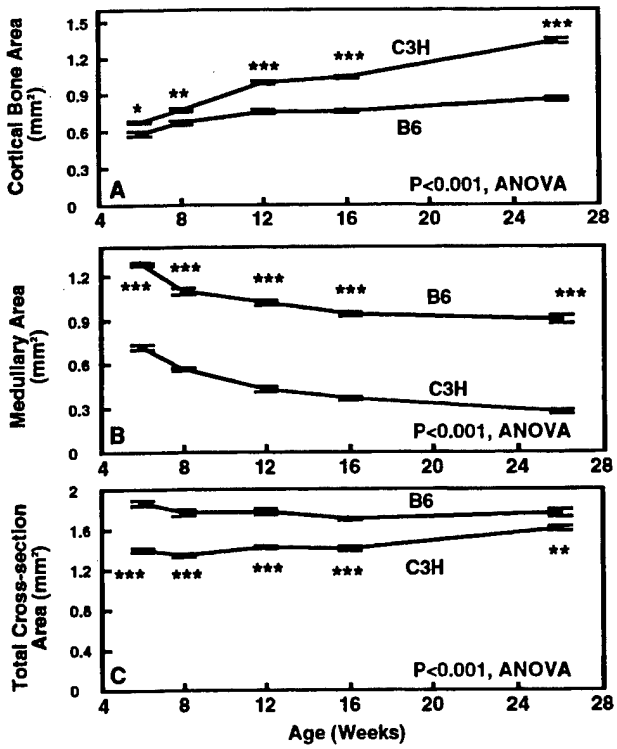

Figure 2. Plot of cortical bone area, medullary area, and total cross-sectional area for C3H and B6 mice aged 6–26 weeks (n = 7–11) at middiaphysis of the femur. ANOVA showed that the C3H mice had a greater cortical bone area, smaller medullary area, and smaller total cross-sectional area than the B6 mice. Data given as mean ± SEM. $*p < 0.05$; $**p < 0.01$; $***p < 0.001$, by Tukey's HSD posthoc test.

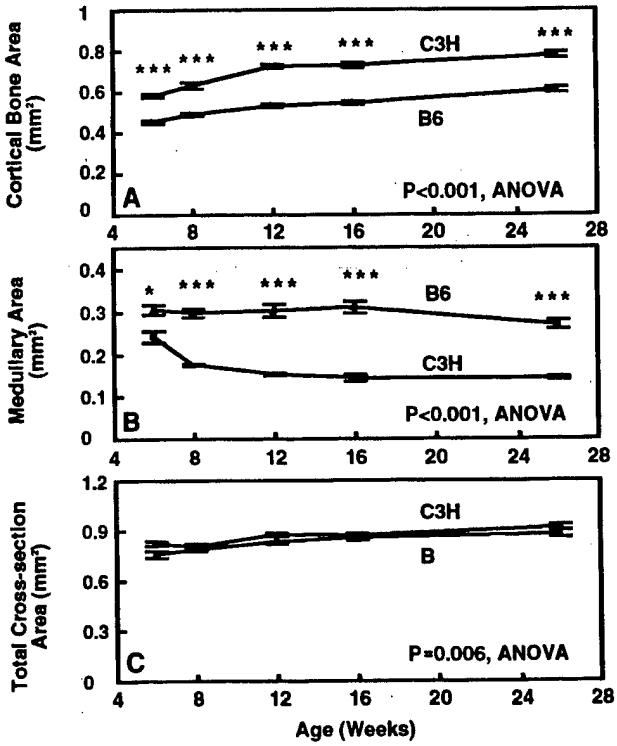

Figure 3. Plot of cortical bone area, medullary area, and total cross-sectional area for C3H and B6 mice aged 6–26 weeks (n = 7–11) at the tibiofibular junction of the tibia. ANOVA indicated that the C3H mice had a larger cortical bone area, smaller medullary area, and greater total cross-sectional area than the B6 mice. Data given as mean ± SEM. $*p < 0.05$; $**p < 0.01$; $***p < 0.001$ by Tukey's HSD post hoc test.

larger cortical bone area in the C3H mice. However, with increasing age, the cross-sectional area increased faster in the C3H mice. Consequently, this difference in growth in circumference contributed to the increasing difference in cortical area with increasing age. These findings clearly indicate that C3H mice, in addition to having a higher bone density in the femur than B6 mice,[2] also have a higher cortical bone area in the femur.

Tibia. To test whether the differences in bone area seen in femur could also be detected in tibia, the tibial total cross-sectional area, medullary area, and cortical bone area were measured at the tibiofibular junction (**Figure 3**). In the tibia (as in the femur), the cortical bone area was significantly ($p < 0.001$, ANOVA) larger in the C3H mice than it was in the B6 mice (i.e., by 28% at 6 weeks, 29% at 8 weeks, 36% at 12 weeks, 33% at 16 weeks, and 28% at 26 weeks of age, respectively) (Figure 3A). Furthermore, the high cortical bone area in the tibia of the C3H mice was associated with a smaller medullary cavity ($p < 0.001$, ANOVA), and the medullary cavity decreased with age faster in the C3H than in the B6 mice (Figure 3B). Because the total cross-sectional areas of the tibia were only slightly different (although statistically significant) between the two strains (Figure 3C), the differences in cortical bone area in the tibia were also primarily due to differences in medullary area. Accordingly, the difference between strains in cortical bone area was not unique to the femur, but was also present in the tibia.

Endosteal Bone Formation

Femur. To evaluate the hypothesis that the difference in cortical bone area seen in these two mouse strains was, at least in part,

Bone Vol. 25, No. 4
October 1999:421–429

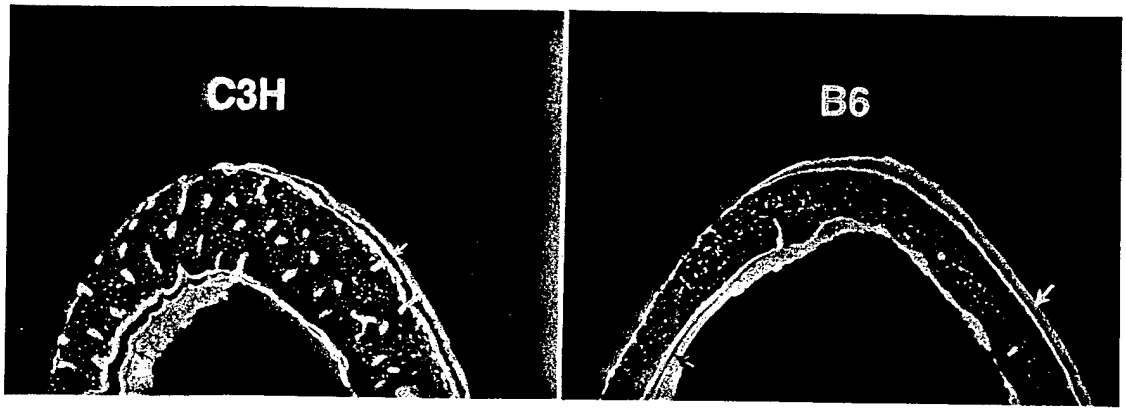

Figure 4. Photomicrograph (40×) illustrating the presence of tetracycline labels in femur cross sections from 8-week-old C3H and B6 mice. Arrows indicate double tetracycline labels at the periosteal (white arrows) and endosteal (gray arrows) surfaces.

due to a difference in bone formation, we measured the histomorphometric bone formation parameters in these mice. **Figure 4** illustrates the tetracycline labels measured in these studies. **Table 1** compares the bone formation parameters at the femoral endosteum for C3H and B6 mice. There was no statistically significant difference in the endosteal BFR/TCS per femur cross section between the C3H and B6 mice and the young mice. However, when BFR was normalized against the total endosteal surface, the endosteal BFR (i.e., BFR/BS) in the femur of the young C3H mice (i.e., between 6 and 12 weeks of age) was significantly ($p < 0.001$, ANOVA) greater than that of B6 mice of the same age (by 28% at 6 weeks, 92% at 8 weeks, and 51% at 12 weeks of age, respectively). Thus, these findings indicate that the endosteal BFR/BS in the femur of young C3H mice was greater than in B6 mice of corresponding age. Statistical analysis by two-way ANOVA showed that there was no significant interaction between age and mouse strain on either endosteal BFR/TCS or BFR/BS in the young, growing mice (6–12 weeks of age), suggesting that the effects of mouse strain and developmental growth on BFR were independent of each other. These observations are consistent with the interpretation that C3H mice had a greater endosteal BFR than the B6 mice had in the femur and that this led to a higher cortical bone area.

Consistent with a higher BFR/BS in the young C3H mice,

Table 1. Bone formation data[a] from the femoral endosteum of C3H and B6 mice aged 6–26 weeks (n = 6–11)

	Bone surface referent			Total cross-sectional referent	
Age/strain	BFR/BS ($mm^2 \times 10^{-3}$/mm per day)	MAR (μm/day)	TLS/BS (mm/mm)	BFR/TCS ($mm^2 \times 10^{-3}$/TCS per day)	TLS/TCS (mm/TCS)
Young mice					
6 weeks					
C3H	5.954 ± 0.142[c]	6.010 ± 0.165[c]	0.992 ± 0.015	18.48 ± 0.42	3.080 ± 0.055[d]
B6	4.643 ± 0.527	4.808 ± 0.546	0.968 ± 0.024	19.45 ± 2.29	4.050 ± 0.122
8 weeks					
C3H	3.967 ± 0.210[c]	4.367 ± 0.190[c]	0.907 ± 0.027[c]	11.04 ± 0.59	2.525 ± 0.081
B6	2.071 ± 0.461	2.597 ± 0.406	0.753 ± 0.070	8.37 ± 2.00	3.002 ± 0.331
12 weeks					
C3H	2.220 ± 0.098	2.749 ± 0.113	0.812 ± 0.035	5.518 ± 0.332	2.015 ± 0.110[c]
B6	1.467 ± 0.128	1.773 ± 0.109	0.819 ± 0.026	5.652 ± 0.487	3.161 ± 0.108
p value (6–12)[b]					
Strain	<0.001	<0.001	n.s.	n.s.	<0.001
Age	<0.001	<0.001	<0.001	<0.001	<0.001
Strain × age	n.s.	n.s.	n.s.	n.s.	n.s.
Mature mice					
16 weeks					
C3H	0.975 ± 0.104	1.294 ± 0.079	0.739 ± 0.041	2.258 ± 0.247[d]	1.714 ± 0.104[c]
B6	1.002 ± 0.107	1.336 ± 0.109	0.740 ± 0.034	3.847 ± 0.416	2.835 ± 0.134
26 weeks					
C3H	0.296 ± 0.031[d]	0.788 ± 0.075	0.385 ± 0.028[c]	0.585 ± 0.056[c]	0.768 ± 0.059[c]
B6	0.714 ± 0.071	1.022 ± 0.076	0.691 ± 0.026	2.561 ± 0.275	2.473 ± 0.114
p value (16–26)[b]					
Strain	0.008	n.s.	<0.001	<0.001	<0.001
Age	<0.001	<0.001	<0.001	<0.001	<0.001
Strain × age	0.019	n.s.	<0.001	n.s.	0.007

KEY: BFR, bone formation rate; BS, bone surface; MAR, mineral apposition rate; TCS, total cross section; TLS, tetracycline-labeled surface.
[a]Data shown as mean ± SEM.
[b]Two-way ANOVA.
[c]$p < 0.05$ vs. B6; [d]$p < 0.01$ vs. B6; [e]$p < 0.001$ vs. B6; n.s., not significant, $p > 0.05$.

Table 2. Bone formation data[a] from the tibial endosteum of C3H and B6 inbred mice aged 6–26 weeks (n = 6–11)

	Bone surface referent			Total cross-sectional referent	
Age/strain	BFR/BS ($mm^2 \times 10^{-3}$/mm per day)	MAR (μm/day)	TLS/BS (mm/mm)	BFR/TCS ($mm^2 \times 10^{-3}$/TCS per day)	TLS/TCS (mm/TCS)
Young mice					
6 weeks					
C3H	1.656 ± 0.184[c]	2.574 ± 0.334[c]	0.652 ± 0.018	3.012 ± 0.417	1.165 ± 0.035
B6	1.054 ± 0.133	1.703 ± 0.171	0.619 ± 0.051	2.161 ± 0.292	1.263 ± 0.105
8 weeks					
C3H	1.944 ± 0.149[c]	2.475 ± 0.140[d]	0.781 ± 0.028	3.077 ± 0.260	1.226 ± 0.041[e]
B6	1.386 ± 0.046	1.604 ± 0.046	0.864 ± 0.012	2.848 ± 0.096	1.779 ± 0.042
12 weeks					
C3H	1.659 ± 0.066[e]	2.155 ± 0.110[e]	0.777 ± 0.021	2.445 ± 0.115[c]	1.144 ± 0.041
B6	0.764 ± 0.039	1.108 ± 0.038	0.701 ± 0.045	1.485 ± 0.056	1.362 ± 0.076
p value (6–12)[b]					
Strain	<0.001	<0.001	n.s.	0.001	<0.001
Age	0.001	0.005	<0.001	<0.001	<0.001
Strain × age	n.s.	n.s.	n.s.	n.s.	0.003
Mature mice					
16 weeks					
C3H	1.013 ± 0.082	1.136 ± 0.043	0.885 ± 0.048	1.385 ± 0.114	1.210 ± 0.066[c]
B6	0.729 ± 0.067	0.968 ± 0.056	0.742 ± 0.039	1.485 ± 0.056	1.499 ± 0.076
26 weeks					
C3H	0.428 ± 0.057[e]	0.878 ± 0.098	0.491 ± 0.026[e]	0.617 ± 0.086[e]	0.698 ± 0.041[e]
B6	0.963 ± 0.073	1.154 ± 0.075	0.836 ± 0.040	1.792 ± 0.123	1.557 ± 0.058
p value (16–26)[b]					
Strain	n.s.	n.s.	0.024	<0.001	<0.001
Age	0.029	n.s.	0.001	n.s.	0.003
Strain × age	<0.001	0.009	<0.001	<0.001	<0.001

See Table 1 for abbreviations.
[a]Data shown as mean ± SEM.
[b]Two-way ANOVA.
[c]$p < 0.05$ vs. B6; [d]$p < 0.01$ vs. B6; [e]$p < 0.001$ vs. B6; n.s., not significant, $p > 0.05$.

C3H mice also exhibited a greater ($p < 0.001$) endosteal MAR than the B6 mice (by 25% at 6 weeks, 68% at 8 weeks, and 55% at 12 weeks, respectively). For forming surface measurements, the picture was different. The endosteal TLS/TCS (an index of forming surface) was significantly ($p < 0.001$) less in C3H mice than in B6 mice (by 24% at 6 weeks, 16% at 8 weeks, 36% at 12 weeks, and 40% at 16 weeks). Because the total endosteal surface was also lower in the C3H than in the B6 mice, expression of labeled surface as a function of the endosteal surface (i.e., TLS/BS) resulted in equivalent values for C3H and B6. Consequently, the higher BFR/BS in young C3H mice in the femur appears to be due to a higher MAR, rather than due to a higher forming surface.

In the mature mice (16 and 26 weeks of age), the high BFR/BS values at the femoral endosteum decreased in the C3H mice, whereas the rates in the B6 mice did not change. MAR in the C3H decreased until it became equivalent to that of the B6 mice, and the TLS/BS of the C3H mice decreased so that it was lower than that of the B6. Thus, in mature mice, the pattern of interstrain differences in endosteal formation changed from that of the young mice.

Tibia. **Table 2** compares the endosteal bone formation parameters from the tibiae of C3H and B6 mice. The pattern of endosteal bone formation in the tibia was the same as that seen in the femur. In the tibia of the young mice, the BFR/TCS and the BFR/BS were significantly higher in the C3H mice than they were in B6 mice of the same age ($p \leq 0.001$, ANOVA).

Corresponding to a greater tibial endosteal BFR/TCS in the young C3H mice, C3H mice of 12 weeks of age or younger showed a significantly higher MAR ($p < 0.001$, ANOVA) than B6 mice of the same respective age. As was the case in the femur, the tibial endosteal TLS/TCS in C3H mice was significantly lower than that in B6 mice. However, TLS/BS of the C3H mice was no different from that of the B6 mice. Thus, these findings demonstrate that, in the tibia, like the femur, endosteal bone formation and MAR, but not labeled surface, were higher in C3H mice than in B6 mice in young animals.

In mature mice, the high BFR/TCS of the young C3H mice, as compared with the B6 mice, was reversed. As in the femur the MAR of the C3H dropped to levels comparable to the B6 and the TLS/BS decreased to values lower than the B6. Thus, the pattern of formation during remodeling in the older animal may be different from the pattern present during development of peak bone mass.

Periosteal Bone Formation

Femur. Because there appeared to be a difference in cross-sectional area in the femur, periosteal bone formation parameters in the C3H and B6 mice were also evaluated. The femoral periosteal bone formation parameters from C3H and B6 mice are shown in **Table 3**. Consistent with endosteal values, two of the three timepoints in young mice showed significantly higher periosteal values for BFR/BS in C3H mice compared with B6 mice. In addition, the periosteum of the femur exhibited a significantly ($p < 0.001$, ANOVA) higher MAR at all timepoints in the young C3H mice than in the B6 mice of the same age (by 70% at 6 weeks, 45% at 8 weeks, and 47% at 12 weeks, respectively). At the periosteum, the TLS/BS was higher in the C3H at two of the three early timepoints. These findings indicate

Bone Vol. 25, No. 4
October 1999:421–429

Table 3. Bone formation data[a] from the femoral periosteum of C3H and B6 mice aged 6–26 weeks (n = 6–11)

	Bone surface referent			Total cross-sectional referent	
Age/strain	BFR/BS ($mm^2 \times 10^{-3}$/mm per day)	MAR (μm/day)	TLS/BS (mm/mm)	BFR/TCS ($mm^2 \times 10^{-3}$/TCS per day)	TLS/TCS (mm/TCS)
Young mice					
6 weeks					
C3H	1.201 ± 0.145[d]	2.176 ± 0.230[c]	0.546 ± 0.017[c]	5.151 ± 0.604[c]	2.346 ± 0.072
B6	0.544 ± 0.095	1.277 ± 0.179	0.421 ± 0.029	2.687 ± 0.446	2.090 ± 0.137
8 weeks					
C3H	1.380 ± 0.087	2.472 ± 0.159[c]	0.563 ± 0.023	5.829 ± 0.364	2.385 ± 0.112[d]
B6	1.071 ± 0.159	1.703 ± 0.189	0.617 ± 0.025	5.320 ± 0.756	3.073 ± 0.108
12 weeks					
C3H	0.934 ± 0.056[c]	1.697 ± 0.077	0.550 ± 0.017[c]	4.071 ± 0.241	2.398 ± 0.076
B6	0.483 ± 0.048	1.156 ± 0.051	0.419 ± 0.042	2.392 ± 0.239	2.077 ± 0.212
p value (6–12)[b]					
Strain	<0.001	<0.001	0.004	<0.001	n.s.
Age	<0.001	0.001	<0.001	<0.001	<0.001
Strain × age	n.s.	n.s.	0.001	n.s.	<0.001
Mature mice					
16 weeks					
C3H	0.689 ± 0.055[d]	1.383 ± 0.090[d]	0.498 ± 0.015	3.001 ± 0.229[d]	2.170 ± 0.063
B6	0.394 ± 0.025	1.000 ± 0.069	0.394 ± 0.012	1.902 ± 0.124	1.902 ± 0.062
26 weeks					
C3H	0.550 ± 0.037[c]	1.038 ± 0.050	0.532 ± 0.029[e]	2.509 ± 0.174[c]	2.428 ± 0.148[d]
B6	0.319 ± 0.065	0.903 ± 0.081	0.337 ± 0.044	1.548 ± 0.322	1.631 ± 0.221
p value (16–26)[b]					
Strain	<0.001	0.002	<0.001	<0.001	0.001
Age	0.034	0.006	n.s.	n.s.	n.s.
Strain × age	n.s.	n.s.	n.s.	n.s.	n.s.

See Table 1 for abbreviations.
[a]Data shown as mean ± SEM.
[b]Two-way ANOVA.
[c]$p < 0.05$ vs. B6; [d]$p < 0.01$ vs. B6; [e]$p < 0.001$ vs. B6; n.s., not significant, $p > 0.05$.

that the differences between strains in BFR and MAR in the femur were evident at the periosteum as well as the endosteum, but that this involved differences in forming surface length as well as differences in MAR.

This high periosteal bone formation in the C3H mice continued in the mature mice. This is in contrast to the endosteum where bone formation dropped in the older C3H mice. The continued high values in the C3H are consistent with the increasing differences between strains in cortical bone with age (Figure 2A).

Tibia. The differences in periosteal bone formation parameters in the tibia between C3H and B6 mice (**Table 4**) were similar to those found in the femur periosteum. Accordingly, in the tibia, periosteal BFR/TCS of young C3H mice was significantly ($p <$ 0.001, ANOVA) higher than BFR/TCS of B6 mice (by 29% at 6 weeks, 93% at 8 weeks, and 290% at 12 weeks, respectively). Periosteal BFR/BS was also significantly greater in the C3H than B6 mice at 6–12 weeks ($p < 0.001$, ANOVA) (by 26% at 6 weeks, 96% at 8 weeks, and 279% at 12 weeks, respectively). The MAR in tibial periosteum was also significantly higher ($p <$ 0.001, ANOVA) in young C3H mice than that in young B6 mice (by 34% at 6 weeks, 63% at 8 weeks, and 135% at 12 weeks, respectively). These data show that the same differences in periosteal BFR and MAR (higher values in young C3H mice) were present in the tibia as were present in femur.

In the mature mice, the differences between strains in periosteal BFR and MAR decreased. This contrasts with the femur and is consistent with the lack of difference between strains in the periosteal circumference (Figure 2C) in the mature mice.

Discussion

This study represents the first evaluation and comparison of the effects of developmental growth on histomorphometric bone formation parameters in high-density C3H and low-density B6, two inbred mouse strains that have marked differences in peak bone density.[2] Our morphometric analysis of the ground section of either femur at the middiaphysis or tibia at the tibiofibular junction indicated that C3H mice had a significantly larger cortical bone area that was accompanied by a significantly smaller medullary area than B6 mice at both bone sites. These differences between strains were seen in mice as young as 6 weeks old, and maximal differences were attained between the age of 16 and 26 weeks, during which time these animals attained peak bone mass.[1] Accordingly, these observations suggest that the physiological changes, which led to the observed phenotypic differences in cortical peak bone area (or volume) in these two mouse strains, might have occurred during early developmental growth (i.e., young age). Because it is likely that a greater bone volume may be related to a greater bone density, these findings are consistent with previous pQCT data that C3H mice had a greater peak bone density than B6 mice.[2]

Three major histomorphometric findings in this study provide strong, albeit circumstantial, evidence for our three hypotheses. First, the BFR/TCS and/or BFR/BS in C3H mice were significantly higher than that in B6 mice. These observations (along with the past observations that C3H mice exhibited increased serum levels of alkaline phosphatase activity[4] and IGF-I,[12] compared with B6 mice) are entirely consistent with our first hypothesis that the greater peak bone mass in C3H mice may be at least

Table 4. Bone formation data[a] from the tibial periosteum of C3H and B6 mice aged 6–26 weeks (n = 6–11)

	Bone surface referent			Total cross-sectional referent	
Age/strain	BFR/BS ($mm^2 \times 10^{-3}$/mm per day)	MAR (μm/day)	TLS/BS (mm/mm)	BFR/TCS ($mm^2 \times 10^{-3}$/TCS per day)	TLS/TCS (mm/TCS)
Young mice					
6 weeks					
C3H	2.596 ± 0.125[c]	3.212 ± 0.142[c]	0.814 ± 0.045	8.538 ± 0.365[d]	2.675 ± 0.126
B6	2.063 ± 0.189	2.394 ± 0.193	0.858 ± 0.017	6.609 ± 0.612	2.748 ± 0.058
8 weeks					
C3H	1.807 ± 0.106[c]	2.741 ± 0.066[c]	0.660 ± 0.037	5.873 ± 0.337[c]	2.143 ± 0.114
B6	0.923 ± 0.105	1.677 ± 0.079	0.552 ± 0.062	3.049 ± 0.346	1.823 ± 0.204
12 weeks					
C3H	1.175 ± 0.062[c]	2.172 ± 0.134[c]	0.543 ± 0.010[d]	3.989 ± 0.236[c]	1.841 ± 0.036[d]
B6	0.310 ± 0.045	0.926 ± 0.041	0.326 ± 0.039	1.024 ± 0.143	1.079 ± 0.124
p value (6–12)[b]					
Strain	<0.001	<0.001	0.009	<0.001	0.003
Age	<0.001	<0.001	<0.001	<0.001	<0.001
Strain × age	n.s.	n.s.	0.015	n.s.	0.013
Mature mice					
16 weeks					
C3H	0.438 ± 0.010	0.811 ± 0.027	0.543 ± 0.016[d]	1.463 ± 0.034	1.813 ± 0.060[c]
B6	0.356 ± 0.086	0.921 ± 0.115	0.355 ± 0.051	1.215 ± 0.296	1.210 ± 0.188
26 weeks					
C3H	0.338 ± 0.036	0.708 ± 0.034	0.470 ± 0.038	1.172 ± 0.125	1.630 ± 0.133
B6	0.291 ± 0.027	0.704 ± 0.037	0.409 ± 0.018	0.985 ± 0.088	1.386 ± 0.054
p value (16–26)[b]					
Strain	n.s.	n.s.	0.003	n.s.	0.003
Age	n.s.	0.017	n.s.	n.s.	n.s.
Strain × age	n.s.	n.s.	n.s.	n.s.	n.s.

See Table 1 for abbreviations.
[a]Data shown as mean ± SEM.
[b]Two-way ANOVA.
[c]$p < 0.05$ vs. B6; [d]$p < 0.01$ vs. B6; [e]$p < 0.001$ vs. B6; n.s., not significant, $p > 0.05$.

in part due to a higher bone formation rate compared with B6 mice.

An intriguing observation regarding bone formation is that the higher BFR/BS in C3H mice seemed to be associated with a higher MAR without a significantly higher TLS/BS compared with B6 mice. Akhter et al.[1] also noted a higher MAR in the tibia of C3H mice compared with that of B6 mice. However, because the mice used in their study were 16-week-old adult mice, and because we demonstrated in this study that a significant difference in MAR was seen only in the young mice (i.e., <16 weeks old), the difference in MAR reported in their study did not reach a statistically significant level. Nevertheless, their study is consistent with our observations that C3H mice had a higher MAR. In this respect, MAR is generally interpreted as a measure of the activity of osteoblasts.[10–12,14,15,18] This would indicate that the C3H osteoblasts are more active than the B6 osteoblasts. However, it is possible that there may be greater numbers of osteoblasts per unit-forming surface in the C3H mice, a difference that could possibly account for the higher MAR. Therefore, it will be necessary to measure and compare the number of osteoblasts per forming surface between the two inbred strains of mice to establish that the interpretation of higher activity per osteoblast in C3H mice is correct. In further support of the premise that MAR is an important parameter of bone mass, it was shown, in the mouse senescence model (SAM-P/2, SAM-R1, and SAM-P6 mice), that higher endosteal MAR was associated with greater bone mass.[17] These findings may have an important implication with respect to our efforts of finding gene(s) that control peak bone mass, if our conclusion is confirmed that osteoblast activity (i.e., MAR) plays a more essential role than osteoblast proliferation (i.e., TLS) in determining the peak bone mass. Accordingly, it may be speculated that the genes that help to determine peak bone mass in these mice may be those that are involved in regulating osteoblast differentiation and/or activity.

Second, this study provides evidence that significant differences between strains in MAR were detected primarily in the younger mice (i.e., 6–12 weeks old). Thus, the differences occurred during growth and modeling rather than during adult bone remodeling. Furthermore, differences between strains were already evident at 6 weeks of age. These findings support our second hypothesis that a majority of the differences between strains in bone formation rate may occur during an early age. We should point out animals <6 weeks old were not tested in this study. Thus, we do not know whether significant differences in bone mass and BFR (or MAR) can also be detected in animals <6 weeks of age. However, we should note that the biggest differences in MAR and BFR between these two mouse strains were seen with animals between the ages of 6 and 12 weeks. Thus, we favor the possibility that phenotype differences among C3H and B6 mice, regarding bone formation parameters, may also occur at <6 weeks. Accordingly, because mice typically undergo puberty at between 4 and 5 weeks of age, we tentatively conclude that additional phenotypic differences between strains most likely occur during puberty. If this conclusion is confirmed, it can be speculated that the gene(s) which contribute to the differences in bone formation rate and in peak bone mass in these mice are expressed predominantly during puberty. This information is very important in relation to our continuing efforts to find gene(s) that are involved in peak bone mass determination. If this

Bone Vol. 25, No. 4
October 1999:421–429

conclusion is valid, it would be essential for us to use animals during puberty to search for genes that regulate peak bone mass.

Third, we have evidence that differences in BFR and/or MAR are present at both periosteal as well as endosteal bone sites. Moreover, differences in bone area and BFR were also observed at both the tibia and femur. Consequently, these observations are entirely consistent with our third hypothesis that the strain-associated difference in bone formation and bone mass is not specific for a particular weight-bearing bone site. These findings are consistent with previous observations that the strain-related difference in bone density is evident in the vertebrae, proximal phalanges, femur, and tibia.[2]

In this study, we have also showed that, at the fibular junction site of the tibia, there was essentially no difference in cross-sectional area between strains. However, in the femoral midshaft, there was a difference in cross-sectional area with the B6 mice having a larger cross-sectional area, indicating that there are some site-specific differences. Nevertheless, bone area and bone formation were higher in the C3H mice at both sites, consistent with the differences in phenotype of these two strains. Akhter and coworkers reported that, at a more proximal tibial site than the fibular junction, they found a greater response to mechanical loading in the B6 mice than in the C3H mice[1]; they suggested that the larger cross-sectional area of the B6 mice may be due to a stronger adaptive response to mechanical loading. If this is correct, the adaptive response is more important during rapid growth because the differences in femur cross-sectional area decrease with age.

There was also a difference in the formation pattern between the periosteum and endosteum in mature mice. Formation dropped at the endosteum in the C3H mice. Because the C3H mice have blood levels of red and white blood cells[13] that are among the lowest values for inbred mouse strains, it can be speculated that the great reduction in marrow space in the C3H mice may have triggered a response (decreased formation) to increase marrow size and blood cell production.

Differences in cortical bone area can be due to differences in bone resorption as well as differences in bone formation. In this regard, there is evidence suggesting that C3H mice might also have a lower bone resorptive capability than B6 mice in that bone marrow cells derived from C3H mice produced significantly less resorptive cytokines and osteoclasts than those of B6 mice in vitro.[8,9] Moreover, we have previously shown that there are fewer osteoclasts in the trabecular bone of the distal femur in C3H mice. Accordingly, we believe that it is likely that the greater peak bone mass in C3H mice may be caused by a combination of an increased bone formation rate and a reduced bone resorption rate. We further note that bone resorption parameters have not been evaluated in this study. Therefore, the precise quantitative role of bone resorption in the diaphysis needs further study.

Finally, we emphasize that the C3H and B6 inbred mice were housed under well-defined and identical environmental conditions. Accordingly, these mice were fed an identical diet, received identical lighting, occupied the same amount of living space with an identical type of bedding and with same housing density in the same room, and were maintained by the same laboratory personnel. Therefore, we conclude that the observed differences between strains in these histomorphometric bone formation parameters were not due to environmental factors, but rather were the consequence of genetic factors. Consequently, these findings further confirm our contention that the C3H/B6 inbred mouse model is an appropriate animal model for searching for the genes that contribute to high peak bone density (or peak bone area). Moreover, the genes affecting peak bone density in this model include, at least, genes regulating osteoblast activity.

In summary, we have presented the first bone histomorphometric evidence to support the conclusion that C3H mice have a greater peak bone mass than B6 mice. We have also demonstrated, for the first time, that the larger peak bone mass in C3H mice may be associated, at least in part, with a greater bone formation rate, which is mediated primarily through a higher MAR. Regardless of whether a lower bone resorption rate is involved in the greater peak bone mass in C3H mice, this study strongly suggests that the phenotype differences responsible for the marked difference in bone mass between the two mouse strains are most likely to occur at early age of the animal (i.e., puberty).

Acknowledgment: This work was supported in part by research grants from NIH (RO1 AR-43618) and Army (DAMD17-96-1-6306). The authors acknowledge the assistance of the media development staff at the Jerry L. Pettis Memorial VA Medical Center in the preparation of the manuscript.

References

1. Akhter, M. P., Cullen, D. M., Pedersen, E. A., Kimmel, D. B., and Recker, R. R. Bone response to in vivo mechanical loading in two breeds of mice. Calcif Tissue Int 63:442–449; 1998.
2. Beamer, W. G., Donahue, L. R., Rosen, C. J., and Baylink, D. J. Genetic variability in adult bone density among inbred strains of mice. Bone 18:397–403; 1996.
3. Christian, J. C., Yu, P. L., Slemenda, C. W., and Johnston, C. C. Heritability of bone mass: A longitudinal study in aging male twins. Am J Human Genet 44:429–433; 1989.
4. Dimai, H. P., Linkhart, T. A., Linkhart, S. G., Donahue, L. R., Beamer, W. G., Rosen, C. J., Farley, J. R., and Baylink, D. J. Alkaline phosphatase levels and osteoprogenitor cell numbers suggest bone formation may contribute to peak bone density differences between two inbred strains of mice. Bone 22:211–216; 1998.
5. Hansen, M. A., Hassager, C., Jensen, S. B., and Christiansen, C. Is heritability a risk factor for postmenopausal osteoporosis. J Bone Miner Res 7:1037–1043; 1992.
6. Kelly, P. J., Nguyen, T., Hooper, J., Pocock, N., Sambrook, P., and Eisman, J. Changes in axial bone density with age. J Bone Miner Res 8:11–17; 1993.
7. Keschawarz, N. M. and Recker, R. R. The label escape error: Comparison of measured and theoretical fraction of total bone-trabecular surface covered by single label in normals and patients with osteoporosis. Bone 7:83–87; 1986.
8. Linkhart, T., Linkhart, S., Farley, J., Dimai, H. P., Quian, H.-Y., Horowitz, M., Beamer, W., Donahue, L. R., Rosen, C., and Baylink, D. Osteoblast production of osteolytic cytokines: Differences between low peak bone density C57BL/6J mice and high peak bone density C3H/HeJ mice [abstract S309]. J Bone Miner Res 11(Suppl. 1):S167; 1996.
9. Linkhart, T. A., Linkhart, S. G., Kodama, Y., Farley, J. R., Dimai, H. P., Wright, K. R., Wergedal, J. E., Sheng, M., Beamer, W. G., Donahue, L. R., Rosen, C. J., and Baylink, D. J. Osteoclast formation in bone marrow cultures from two inbred strains of mice with different bone densities. J Bone Miner Res 14:39–46; 1999.
10. Morey, E. R. and Baylink, D. J. Inhibition of bone formation during space-flight. Science 201:1138–1141; 1978.
11. Pocock, N. A., Eisman, J. A., Hopper, J. L., Yeates, M. G., Sambrook, P. N., and Eberl, S. Genetic determinants of bone mass in adults: A twin study. J Clin Invest 80:706–710; 1987.
12. Rosen, C. J., Dimai, H. P., Vereault, D., Donahue, L. R., Beamer, W. G., Farley, J., Linkhart, T., Linkhart, S., Mohan, S., and Baylink, D. J. Circulating and skeletal insulin-like growth factor-I (IGF-I) concentrations in two inbred strains of mice with different bone densities. Bone 21:217–223; 1997.
13. Russell, E. S., Neufeld, E. F., Higgins, C. T. Comparison of normal blood forming pictures of young adults from 18 inbred strains of mice. Proc Soc Exp Biol Med 78:761–776, 1951.
14. Schmidt, I. U., Dobnig, H., and Turner, R. T. Intermittent parathyroid hormone treatment increases osteoblast number, steady state messenger ribonucleic acid

levels for osteocalcin, and bone formation in tibial metaphysis of hypophysectomized female rats. Endocrinology 136:5127–5134; 1995.
15. Schnitzler, C. M., Biddulph, S. L., Mesquita, J. M., and Gear, K. A. Bone structure and turnover in the distal radius and iliac crest: A histomorphometric study. J Bone Miner Res 11:1761–1768; 1996.
16. Smith, D. M., Nance, W. E., Kang, K. W., Christian, J. C., and Johnston, C. C. Genetic factors in determining bone mass. J Clin Invest 52:2800–2808; 1973.
17. Tsuboyama, T., Takahashi, K., Matsushita, M., Okumura, H., Yamamuro, T., Umezawa, M., and Takeda, T. Decreased endosteal formation during cortical bone modelling in SAM-P/6 mice with a low peak bone mass. Bone Miner 7:1–12; 1989.
18. Wronski, T. J. and Morey, E. R. Inhibition of cortical and trabecular bone formation in the long bones of immobilized monkeys. Clin Orthopaed Rel Res 181:269–276; 1983.

Date Received: January 5, 1999
Date Revised: June 14, 1999
Date Accepted: June 15, 1999

Original Contributions

Beamer, WG
DAMD17-96-1-6306
Appendix 6

Mammalian Genome
Incorporating Mouse Genome

Mammalian Genome 10, 1043–1049 (1999).

Quantitative trait loci for bone density in C57BL/6J and CAST/EiJ inbred mice

Wesley G. Beamer,[1] Kathryn L. Shultz,[1] Gary A. Churchill,[1] Wayne N. Frankel,[1] David J. Baylink,[2] Clifford J. Rosen,[1,3] Leah Rae Donahue[1]

[1]The Jackson Laboratory, 600 Main Street, Bar Harbor, Maine 04609, USA
[2]J.L. Pettis VA Medical Center, 11201 Benton Street, Loma Linda, CA 92357, USA
[3]Maine Center for Osteoporosis, Research & Education, 268 Center Street, Bangor, ME 04401, USA

Received: 5 May 1999 / Accepted: 22 June 1999

Abstract. Genetic analyses for loci regulating bone mineral density have been conducted in a cohort of F_2 mice derived from intercross matings of (C57BL/6J × CAST/EiJ)F_1 parents. Femurs were isolated from 714 4-month-old females when peak adult bone density had been achieved. Bone mineral density (BMD) data were obtained by peripheral quantitative computed tomography (pQCT), and genotype data were obtained by Polymerase Chain Reaction (PCR) assays for polymorphic markers carried in genomic DNA of each mouse. Genome-wide scans for co-segregation of genetic marker data with high or low BMD revealed loci on eight different chromosomes, four of which (Chrs 1, 5, 13, and 15) achieved conservative statistical criteria for suggestive, significant, or highly significant linkage with BMD. These four quantitative trait loci (QTLs) were confirmed by a linear regression model developed to describe the main effects; none of the loci exhibited significant interaction effects by ANOVA. The four QTLs have been named *Bmd1* (Chr 1), *Bmd2* (Chr 5), *Bmd3* (Chr 13), and *Bmd4* (Chr 15). Additive effects were observed for *Bmd1*, recessive for *Bmd3*, and dominant effects for *Bmd2* and *Bmd4*. The current large size of the QTL regions (6→31 cM) renders premature any discussion of candidate genes at this time. Fine mapping of these QTLs is in progress to refine their genetic positions and to evaluate human homologies.

Introduction

In humans, peak bone density in both sexes is achieved at the end of the second decade of life after pubertal growth ceases and adult rates of bone turnover have been established (Glastre et al. 1990; Haapasalo et al. 1996; Kroger et al. 1993; Teegarden et al. 1995; Theintz et al. 1992). Low peak bone density is considered to be a risk factor for osteoporotic fracture in elderly adults, on the basis of numerous studies with a variety of measurement methodologies (Genant et al. 1996). A long-term effort by many investigators has resulted in identifying major regulatory factors supporting the adult skeletal system. These include environmental variables such as nutrition, exercise, exposure to sunlight, and pharmacologic agents, plus endogenous variables such as reproductive status, aging, disease states (cancer, diabetes, hyperparathyroidism), serum hormone and mineral levels.

An individual's genomic complement orchestrates the effect of all such factors to achieve the final adult bone physiologic homeostasis. Our knowledge about the extent of genetic regulation of the normal adult skeleton is primarily based on investigative efforts with twin studies, multi-generational family studies, and sib pair analyses (Arden et al. 1996; Barthe et al. 1999; Christian et al. 1989; Cohen-Solal et al. 1998; Danielson et al. 1999; Eisman et al. 1993; Ferrari et al. 1998; McKay et al. 1994; Seeman et al. 1989; Slemenda et al. 1991; Smith et al. 1973). Collectively, such studies have shown that 60–70% of the normal variability in bone density is genetically determined. Even though much has been learned from rare heritable bone diseases, identifying genes participating in regulation of the normal adult skeleton is at an early stage. Population studies have implicated genetic polymorphisms for the vitamin D receptor (Morrison et al. 1994), collagen 1A1 (Uitterlinden et al. 1998), serum IGF-I (Rosen et al. 1998), apolipoprotein E (Shiraki et al. 1997), calcitonin receptor (Masi et al. 1998), bone-specific alkaline phosphatase (Harris et al. 1998), transforming growth factor β-1 (Langdahl et al. 1997), α 2HS-glycoprotein (Zmuda et al. 1998), and estrogen receptor (Deng et al. 1998) to be related to low bone mineral density (BMD) associated with osteoporosis. In spite of the preliminary and often controversial status of the evidence for such genes, it is clear from the wide range of factors influencing bone density that it is a quantitative trait dependent upon the action of numerous genes. The search for and functional analysis of such genes can be efficiently pursued in animal models wherein control over environmental factors improves the power to identify heritable regulation of bone density.

Inbred strains of mice that differ in their bone mineral densities are amenable to genetic analyses of this polygenic trait via the experimental design of quantitative trait loci (QTL) analysis (Lander and Botstein 1989). Within each strain all genetic loci are homozygous, while crosses between strains allow unambiguous association between genotype and the bone density phenotype of individuals. More than 6000 molecular markers have been shown to be polymorphic among inbred strains of mice, allowing accurate genotyping of progeny; thus, by segregation analyses, genes underlying a trait can be assigned to chromosomal regions (Dietrich et al. 1996). Of critical importance to such genetic analyses is the availability of methodology with marked sensitivity and precision to accurately assign the bone density phenotype. Peripheral computed tomography (pQCT) has provided the necessary tool to undertake such an analysis. In this report, we present genetic data on QTLs for differences in adult peak BMD derived from an F_2 intercross of C57BL/6J and CAST/EiJ mice.

The Jackson Laboratory is fully accredited by the American Association for Laboratory Animal Care. Experimental protocols have been reviewed and approved by the Institutional Animal Care and Use Committee.

Correspondence to: W.G. Beamer

Materials and methods

Mice. Mice were produced and maintained in our research colony under 14:10 h light:dark cycles. Autoclaved diet NIH-31 with 6% fat (Purina Mills, Inc; 18% protein, Ca:P 1:1, vitamin and mineral fortified) and HCl acidified water (pH 2.8–3.2) were provided ad libitum. Females were housed in groups of four or five within polycarbonate boxes of 51 sq. in. area, on sterilized shavings of Northern White Pine as bedding.

The inbred strains selected for QTL analyses of femoral BMD were C57BL/6J (B6) and CAST/EiJ (CAST). We have reported that these strains have markedly different cortical and total bone densities (Beamer et al. 1997), and others have demonstrated that these strains are highly polymorphic for genetic differences at more than 95% of simple sequence length polymorphic loci (Dietrich et al. 1996). F_2 progeny for genetic analyses of BMD were produced by mating low-density B6 females to high-density CAST males, then intercrossing these (B6 × CAST)F_1 hybrids to produce F_2 offspring. We retained 714 F_2 females for bone and genetic analyses; F_2 males were not kept because of lethally aggressive behavior when group housed.

The parental strains were evaluated at 1, 2, 4, 8, and 12 months of age to characterize the acquisition of adult bone density. The F_2 progeny were analyzed at 4 months of age when the acquisition of adult bone was completed. Body weights were recorded at necropsy, and a partial carcass preparation was derived from each mouse (lumbar spine, pelvis, plus rear limbs) and preserved in 95% ethanol. Subsequently, femurs were isolated and their lengths measured by digital calipers (Stoelting, Wood Dale, IL) prior to densitometry. Kidneys and spleens from each mouse were frozen in liquid N_2 and stored at –60C for later extraction of genomic DNA.

Bone densitometry. Briefly, isolated femurs were assessed by pQCT with a Stratec XCT 960M (Norland Medical Systems, Ft. Atkinson, Wis.) as previously described (Beamer et al. 1996). Femurs were scanned at 2-mm intervals over their entire lengths, utilizing an x-ray attenuation threshold of 2.000 units to define high-density bone, a threshold of 1.300 to define low-density bone, and a unit volume for measurement of mineral set at 0.1 mm^3. A manufacturer-supplied software program, designated "XMICE v5.1", analyzes the X-ray attenuation data to generate values for an array of bone parameters including mineral content, volume, and periosteal circumference. The precision of this instrument for densitometry of mouse bones has been determined to be 1.2% by repeated placement and measurement of a single femur. Calibration of the densitometer was done with a set of hydroxy apatite standards (0.050–1.000 mg/mm^3), yielding a correlation of 0.997 between standards and pQCT estimation of density.

Femoral density was selected for genetic analysis because of the precision with which the mineral could be measured, because the majority of the mineral resides in its cortical compartment, and because it is a target of processes leading to osteoporotic fracture. To assure that the inbred strain differences in bone density were demonstrable by alternative methods, pQCT total femoral BMD data were compared with data obtained from the absolute ethanol volume displacement by separate pools of B6 and CAST femurs that were then ashed at 600°C for 18 h. At 8 months of age (see Fig. 1), the total femoral BMD of B6 (0.462 mg/mm^3) was 74% of CAST (0.622 mg/mm^3) by pQCT. By ash weight/ethanol volume displacement, B6 (0.545 mg/mm^3) was 70% of CAST (0.782 mg/mm^3). Finally, we compared the periosteal perimeter measurements obtained from mid-diaphysis for several inbred strains by pQCT and by histomorphometry and found a correlation of $r = 0.908$, indicating good agreement of methodologies.

Genetic analyses. Genomic DNA was prepared from kidneys or spleens of mice by standard chloroform:phenol methodology. Genotyping of individual mouse DNAs was accomplished by PCR with oligonucleotide primer pairs from Research Genetics (Birmingham, Ala.). Primer pairs identifying SSLPs that discriminate between alleles from B6 versus CAST were selected from more than 6000+ available (Dietrich et al. 1996). Details of PCR reactions have been previously described (Shultz et al. 1996; Svenson et al. 1995). DNAs from B6, CAST, and (B6 × CAST)F_1 hybrids were used as electrophoretic standards in every gel to identify the genotype of PCR products derived from F_2 mice {i.e., homozygous B6 (*b/b*) or CAST (*c/c*); and heterozygous (*b/c*)}.

We chose groups of 70–75 F_2 mice from the extreme tails of the density distribution ($n = 714$) as described for heritable traits (Lander and Botstein 1989). The 19 autosomes in the 145 F_2 progeny were assessed for associations of PCR-based molecular markers with bone density data. Chr X alleles were not assessed because reciprocal $F_1 \times F_1$ matings would be required to yield all possible allelic combinations necessary for meaningful genetic evaluation. Four to nine microsatellite DNA polymorphic markers were selected for testing each autosome at approximately 12 to 15-cM intervals from centromere to telomere. Given the F_2 sample size, the 15-cM genetic distance is adequate to detect major loci for bone density in this experimental design. In total, 711 F_2 mice were included in the final data analyses; tissues from three mice could not be located. Mice appearing in either extreme of the BMD distributions were genotyped for 127 markers, then these data were assessed for correlations between segregating alleles and density. DNA from the remaining 566 F_2 mice was prepared and genotyped for nine selected markers previously indicated by mapping of the extremes to be correlated with femoral BMD data.

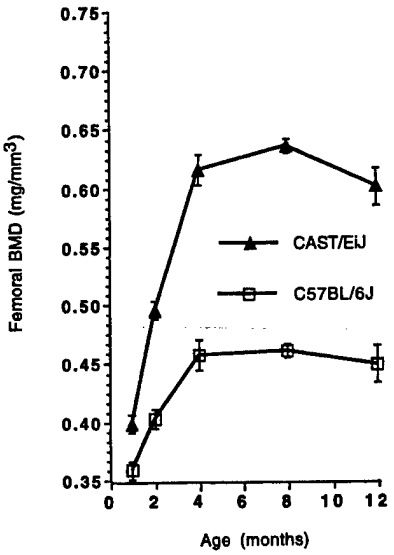

Fig. 1. Development of femoral BMD for the C57BL/6J and CAST/EiJ progenitor strains from 1 to 12 months of age. Pattern of increasing density with plateauing at approximately 4 months is similar for both strains; however, values for peak BMD are markedly different. Data points represent means ± SEM for groups of $n = 7–17$.

Statistical analyses. Statistical analyses of parental and hybrid strain femoral densities were performed with StatView 4.5 software for Macintosh (Abacus Concepts, Berkeley, Calif.). These density data were analyzed first by ANOVA to detect major strain effects. Individual strain means were assessed for significant differences by Fisher's Protected LSD test. Differences were judged statistically significant when $p < 0.05$.

Initial detection of significant association between bone densities and marker loci for QTLs in F_2 progeny was carried out by computing unconstrained regression analyses for each marker in the genome with the computer programs MATLAB (Mathworks, Inc Natick, Mass.) and MapMaker QTL (Lander et al. 1987) for an F_2 population with Free Genetics (two degrees of freedom). The unconstrained regressions have two degrees of freedom (for F_2 data) and will fit any mode of inheritance. Permutation critical values for the maximal F-statistic (Churchill and Doerge 1994; Doerge and Churchill 1996) provided a guide for selecting chromosomes with statistically significant effects on the bone density phenotypes. Permutation testing provides a genome-wide type I error level for each genome scan. Markers were judged highly significant, significant, or suggestive with respect to linkage with BMD as recommended by Lander and Kruglyak (1995).

Results

Preliminary inspection of pQCT data from the F_2 mouse femurs suggested the possibility of two related density measurements. One was termed total BMD and was derived from all measurable mineral divided by the total bone volume. The second excluded the marrow cavity and was termed apparent cortical BMD and was

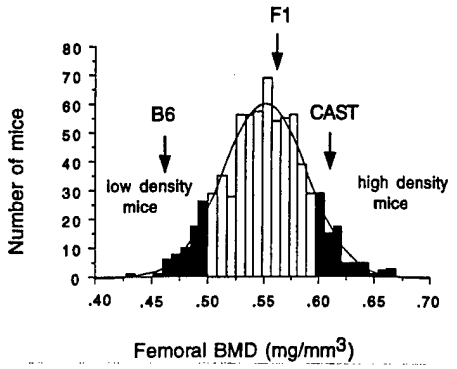

Fig. 2. Distribution of femoral BMD in 714 female B6CAST-F_2 mice at 4 months of age. The shaded areas show the two groups of mice with low or high BMD chosen for initial genetic analyses. Positions of mean BMDs for the progenitor and F_1 parents are indicated by arrows, while the bell-shaped line depicts the theoretical normal distribution.

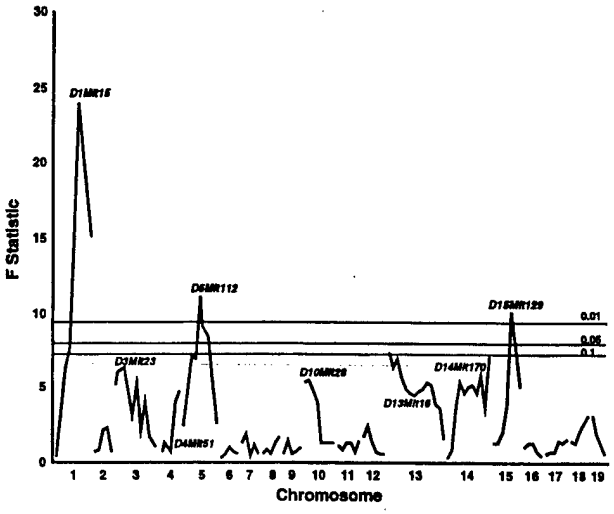

Fig. 3. Summary of genome-wide scans of regression F statistics for an unconstrained model are shown for tested polymorphic markers on all 19 autosomes. Dashed lines represent critical values from permutation tests (correcting for multiple tests) for the F statistic at 99% ($p < 0.01$), 95% ($p < 0.05$), and 90% ($p < 0.10$) for association with BMD.

derived from the mineral exceeding the threshold (2.000 attenuation units) for cortical bone divided by the volume occupied by that mineral. In this report, we have focused on total BMD (hereafter, BMD) as the phenotypic measure of the entire femur. Accordingly, femoral BMD data for the B6 and CAST progenitor strain females obtained between the ages of 1 and 12 months are presented in Fig. 1, where BMD values differed between B6 and CAST at all ages. The rapid rate of acquisition of BMD plateaued at about 4 months, resulting in significantly higher ($p < 0.0001$) density values in CAST females compared with B6 values at 4, 8, and 12 months of age. These data are similar to our initial report that the acquisition of adult peak bone density in inbred mice is complete at approximately 4 months of age (Beamer et al. 1996).

The distribution of BMD for all B6CAST-F_2 females is presented in Fig. 2. Shaded areas identify the mice in the extreme tails of the distribution chosen for initial genotyping. The Gaussian distribution of density in F_2 mice supports the hypothesis that the BMD phenotype is the consequence of polygenic regulation, with a calculated heritability of 57% (Jenkins 1990). At 4 months of age, the mean BMD value ± SEM for the B6 mice (n = 14) was 0.458 ± 0.004 mg/mm^3, and for the CAST mice (n = 17) was 0.616 ± 0.013 mg/mm^3 (arrows, Fig. 2). The mean BMD value for eight F_1 females (4 months old) was 0.563 ± 0.006 mg/mm^3; this was statistically different ($p < 0.01$) from BMD of B6 and CAST progenitors. The distribution of BMD in F_2 females also shows that very few F_2 mice had densities below that of the low density B6 progenitor, whereas there are many more F_2 mice with densities higher than that of the high-density CAST progenitor. This occurrence of transgressive segregation indicates that a gene(s) with alleles contributing to increased BMD may be present in the 'low density' B6 progenitor.

Body weights of the two progenitor strains at 4 months were significantly different (B6 = 22.6 ± 0.5 g; CAST = 15.7 ± 0.3 g; $p < 0.0001$). The B6 femurs were morphologically similar to those of CAST mice, although longer (B6 = 16.03 ± 0.08 mm; CAST = 13.55 ± 0.09 mm; $p < 0.0001$). When all 714 F_2 progeny were examined for correlations between BMD and body weights or femur lengths, a significant but weak relationship was found with body weight (r = 0.112; $p = 0.0028$; $r^2 = 0.013$), whereas no correlation was observed with femur length (r = 0.021; p = ns).

The regression analyses for genome-wide scans of BMD extremes for all 127 molecular markers are summarized in Fig. 3. Tests at individual markers are based on the F-statistic for an unconstrained mode of inheritance (degrees of freedom = 2; 651) and are shown on the ordinate. Chromosomal assignments for the markers are indicated on the abscissa. Dashed lines represent permutation based thresholds for genome-wide significance at levels of 'p' = 0.10, 0.05, and 0.01. The genome-wide scan analyses

Table 1. Summary of regression analyses for femoral total BMD on SSLP markers for four chromosomes from genome-wide scan of B6CAST-F2 female mice. Chromosomes with loci having permutation p-values < 0.1 are designated *B*one *m*ineral *d*ensity (*Bmd*) 1–4.

Locus Name	Chromosome Best Marker	QTL Region Interval (cM)	F Statistic	Nominal p-value	Permutation p-value
Bmd1	Chr 1 *D1Mit15*	*D1Mit14→D1Mit17* (23)	23.94	8.7×10^{-11}	<< 0.01
Bmd2	Chr 5 *D5Mit112*	*D5Mit254→D5Mit89* (7)	10.92	2.1×10^{-5}	< 0.01
Bmd3	Chr 13 *D13Mit16*	centromere→*D15Mit15* (6)	7.30	7.3×10^{-4}	< 0.10
Bmd4	Chr 15 *D15Mit29*	*D15Mit115→D15Mit35* (31)	10.19	4.3×10^{-5}	< 0.01

revealed numerous chromosomal regions characterized by variable strength of statistical association with BMD. Table 1 summarizes details from the genome-wide scan for chromosome markers associated with BMD. Data for four candidate density QTLs are presented, including: a) proposed locus names (*B*one *m*ineral *d*ensity; *Bmd1–4*), b) the most significant Mit marker, c) flanking Mit markers that define the QTL-containing region and estimated size, and d) statistical assessments (nominal and permutation p-values). The four QTLs with the strongest permutation test statistical support are: Chr 1 ($p < 0.001$), 5 ($p < 0.01$), 13 ($p < 0.10$) and 15 ($p < 0.01$). Fig. 4 presents interval maps for the named QTLs that include all markers tested along with a dashed lined indicating the threshold LOD score of 2.8 for suggestive linkage of marker with BMD. The ordinates for the interval maps depicting LOD scores are scaled with respect to each other for comparative purposes.

The results of fitting a multiple regression model to the best marker in 694 F_2 mice for the four chromosomes harboring BMD QTLs are summarized in Table 2. In these analyses, the QTLs are assumed to have additive effects across each of the loci. The p-values are nominal and are *not* adjusted for the genome-wide search. Individual QTL variances ranged from 1.7% to 6.0%. The summed model variances explain 13.1% of the F_2 population variance in BMD. The value, 13.1%, accounts for BMD variance in all F_2 mice and is considered to be a conservative estimate, as indicated in the Discussion below. It is important to note that each of the QTLs remains significant after adjusting for effects of the other three and, furthermore, that the direction and magnitudes of the estimated effects are similar in adjusted and unadjusted analyses.

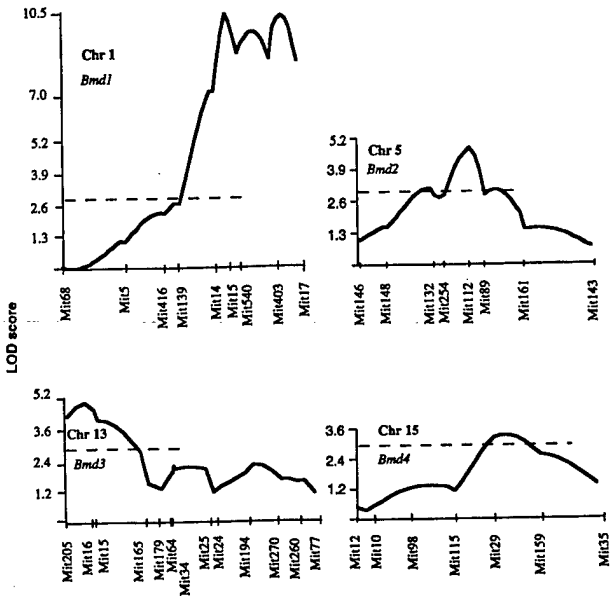

Fig. 4. Interval maps for Chrs 1, 5, 13, and 15 shown to carry QTLs for BMD. Statistical analyses are presented as LOD scores calculated for molecular markers beginning with the centromeric end of each chromosome on the left and extending toward the telomeric end.

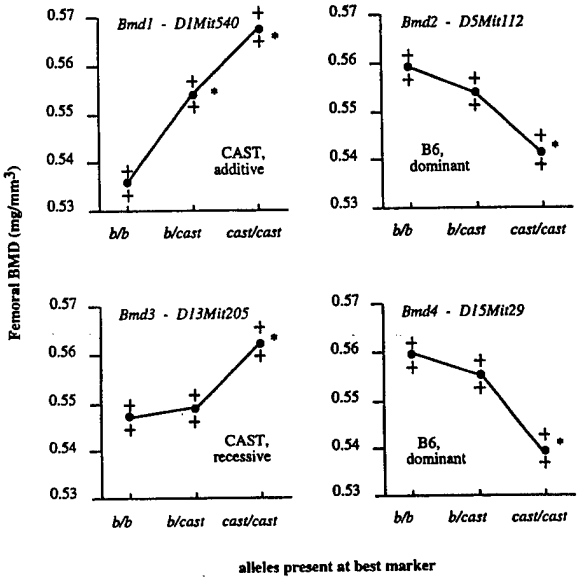

Fig. 5. The effect of genotypes for markers most closely associated with femoral BMD on Chrs 1, 5, 13, and 15. Data are presented as means ± SEM (n = 127–336). For each panel, the observed mean values are presented for mice that are homozygous for the C57BL/6J allele (*b/b*), heterozygous (*cast/b*), and homozygous for the CAST/EiJ allele (*cast/cast*). The asterisks (*) denote when the mean for the genotype *cast/b* or *c/c* is significantly different from that of *b/b* genotype mice. The source of the allele yielding the highest BMD and the allele's mode of action are listed for each QTL.

Table 2. Summary of regression analyses for femoral total BMD on Mit markers for four chromosomes from B6CAST-F_2 female femoral data. F statistics are adjusted to account for effects of other markers on BMD; % variance of phenotypic trait calculated on all F_2 data available for each marker.

Chromosome and Marker	F_2; 694 statistic	Adj. F test *p*-value	% Variance by marker
D1Mit15	25.86	1.5×10^{-11}	6.0
D5Mit112	13.47	1.8×10^{-6}	3.1
D13Mit16	7.38	6.7×10^{-4}	1.7
D15Mit29	9.67	7.2×10^{-5}	2.3
		Total	13.1%

Table 3. Homologous linkage relationships between mouse chromosomal regions with QTLs for femoral BMD and human chromosomal regions.

Optimum mouse QTL Marker	Locus name	MGD map position (cM)	QTL region size (cM)	Region of human chromosome homology
D1Mit15	*Bmd1*	95.8	23	1q21-q42
D5Mit112	*Bmd2*	24.5	7	4p15-q32
D13Mit16	*Bmd3*	10.0	6	1q42-q43; 7p15-p13; 6p25-p21
D15Mit29	*Bmd4*	42.8	31	8q22-qter; 22q13-q22

A genome-wide search for pairwise interaction effects between markers was carried out with the two-way ANOVA F-test (results not shown). The analysis failed to reveal significant interactions when the test statistics were compared with genome-wide permutation threshold.

An important issue is that of what effect on bone density can be detected for each of the four loci identified by regression analyses described above. The large numbers of mice in this cross and the measurement precision permit testing for allele effects, even though the variance in BMD accounted for is small. Main effects of alleles (homozygous: *b/b* = B6, *cast/cast* = CAST; heterozygous *b/cast*) on BMD were calculated for each *Bmd* locus and presented in Figure 5. On the basis of significance of individual terms in the multiple regression, we propose that: a) CAST alleles increase BMD and are additive for Chr 1; b) B6 alleles increase BMD and are dominant for Chrs 5 and 15; and c) CAST alleles increase BMD and are recessive for Chr 13.

Table 3 presents all QTL regions, together with Mouse Genetic Database (MGD) map locations for the best markers. The approximate size of the genetic region containing each QTL, ranging from 6 to 31 cM in length, was estimated from a 1-LOD reduction from the peak LOD score generated by MapMakerQT. Inspite of the large size of the QTL regions, we searched MGD for linkage homology between regions found in the four mouse chromosomes and regions found in the human genome. Adopting a region encompassing 10 cM on either side of the best mouse genetic marker, we found two chromosomes in the human genome of particular interest—Chr 1 and Chr 4. The region with mouse *Bmd1* is entirely contained within human Chr 1q21-42 and, similarly, *Bmd2* within Chr 4p15-q32. On the other hand, *Bmd3* and *Bmd4* QTLs span multiple human chromosomal regions.

Discussion

The quantitative trait loci analyses for bone density were undertaken with B6 and CAST strains to exploit their genetic diversity as well as their divergent femoral BMD. The high degree of genetic polymorphisms enhanced the number of markers available with which to systematically analyze each chromosome for association with femoral bone density. The femur was selected as a model site for genetic analyses because the majority of mineral is present in one bone compartment—cortical bone—and because femoral BMD data correlate well with such data from other sites (vertebrae, phalanges, tibia (Beamer et al. 1996)). We chose pQCT as the method for measuring the phenotype of peak femoral bone density in progenitor, F_1, and F_2 mice because of its ability to accurately and precisely measure mineral mass and bone volume. pQCT-based measurements have been found to correlate very closely with histomorphometric volume determinations and with total mineral ash weight in rats (Rosen et al. 1995a, 1995b) and in our mice. Comparison of pQCT total mineral density with density derived from traditional Archimedes principles yielded very similar relative differences wherein B6 femurs were 70–74% of CAST femoral density. The consistent finding of a large relative differ-

ence in density between the two strains provided the basis for undertaking a genetic analysis of this trait.

Our genetic analyses with F_2 progeny from B6 and CAST progenitors indicate that numerous loci are associated with femoral BMD. Four chromosomes (Chrs 1, 5, 13, and 15) contained loci that achieved conservative statistical criteria which corrected for multiple tests conducted across the genome. These results support the hypothesis that bone density is a quantitative trait that can be partitioned into its genetic components. However, it is likely that the loci associated with femoral density identified in the cross between B6 and CAST represent only a beginning in the quest for locating bone density genes. Although B6 and CAST are highly polymorphic for PCR-based SSLP markers that identify anonymous DNA segments, strain differences for alleles coding for true genes are not as abundant. Thus, alleles for femoral BMD genes that B6 and CAST share would not be detected. Given that the biochemical processes underlying bone morphology and function are exquisitely complex, other crosses are required to provide a more complete picture of loci regulating even one aspect of skeletal biology.

The size of each identified QTL varies from approximately 6 to 31 cM in length. Silver (1995) estimates that 1 cM of genetic distance in the mouse contains approximately 60–70 genes. Thus, the smallest QTL region on Chr 13 could contain as many as 400 genes. The current large size of the QTL regions renders premature any discussion of candidate genes at this time. Likewise, the homologies found with human Chrs 1 and 4 should be considered tentative until QTL regions are reduced in size. In order to identify the bone density regulatory gene(s) within each QTL region, it is necessary to reduce the size of the QTL region so that fewer candidate genes need be considered and gene cloning can be undertaken. We are approaching this task through development of congenic strains that isolate QTLs in the B6 genetic background. These congenic strains will facilitate positional cloning, investigation of single and interactive gene effects, and provide in vivo models for biological studies.

We found that the QTLs on four chromosomes accounted for 13% of the variance in 694 B6CAST-F_2 femoral BMD. It is likely the QTL-related variances are modestly underestimated, owing to recombination between the true QTL and the marker loci used to represent them in the regression model. On the other hand, when the percentage variances accounted for were calculated for the 145 mice in the 'extremes' groups, the values were severalfold higher. This difference in amount of variance accounted for is owing to fact that the whole population variance is not assessed in the 'extreme' selection designs. The overestimate can be significant, i.e., severalfold, and depends on a number of factors including the severity of 'extreme' selection, the size of the phenotypic effect, and the error variation. Independent of the actual variance accounted for by these four QTLs, the data raise questions of what other factors contribute to the difference in BMD of B6 and CAST progenitors documented in this report. At this time, our statistical analyses did not support gene-gene interaction as a major explanation. Nevertheless, this does not imply absence of interaction effects because 1) the genome threshold criterion is so stringent when all pairs of loci are tested that real QTLs may be eliminated, and 2) the ANOVA F-test is not specific and may have low statistical power even with the sample sizes used here. Another factor, measurement error, has been partially assessed by showing precision of measurement by a single operator is 1.2%; multiple operator error has not been evaluated. The remaining obvious factors are biological (litter number and litter size), as well as environment and associated environment-gene interaction, which have not been experimentally analyzed in this cross.

Recently, Klein and associates (1998) reported nine different chromosomes with QTLs for areal BMD by comparison mapping with the BXD RI strain set utilizing DEXA methodology. The unique nature of RI strains that facilitates single polymorphic gene mapping—all loci are homozygous for alleles from one or the other progenitor strain—presents challenges for polygenic quantitative trait analyses. Critical issues for RI strain analyses include detection of gene interactions that yield phenotypes identical to actions of other loci, assignment of intermediate phenotypes to progenitor classes, and decisions about how to classify RI strains with novel phenotypes (i.e., RI strain significantly different from both progenitors). Although a large number of loci for areal BMD make intuitive sense, putative loci need confirmation regardless of the biologic system employed for initial detection.

Comparison of genetic loci derived from pQCT-based data and loci derived from DEXA-based data can be made, while recognizing differences in methodologies. With respect to the methodologies, both pQCT and DEXA are X-ray based methodologies that share the attributes of accurate and precise assessment of mineral. These methodologies differ in that pQCT estimates the volume containing that mineral for calculation of density, whereas DEXA utilizes the two-dimensional size of the skeletal specimen as a denominator for calculation of density. The problem of 'small skeletal size equals low areal BMD' continues to challenge interpretation of DEXA data (Carter et al. 1992), and indeed is also a factor in the BXD RI strain data set (Klein et al. 1998). Thus, mineral data could be comparable, but the indices of mass/unit "volume" are not, leading to the conclusion that the genetic analyses derived from different phenotypes are likely to reflect different bone properties. The same can be said about bone mass phenotypes derived from other methodologies (single x-ray absorptiometry, roentgenography, ultrasonography, magnetic resonance imaging, cortical thickness index) and consequent genetic data. Genes so identified are going to be those associated with the phenotype being measured, and differences should be anticipated. Nevertheless, our belief is that some of these densitometry phenotypes will share the same genetic regulation. Support for this position stems from the finding that the Chr 15 QTL detected by pQCT in B6CAST-F_2 analyses and by DEXA in BXD RI strain analyses are within 2 cM of each other (Klein et al. 1998).

Other investigators are pursuing different models and approaches for genetic analyses of bone regulatory genes. The Senescence Accelerated Mouse strains, designated SAM, were developed as models for studies of aging and spontaneous osteopenia (Okamoto et al. 1995; Tsuboyama et al. 1993). Recently, Shimizu et al. (1999) reported an F_2 intercross between osteopenic SAM-P6 and normal bone mass SAM-P2 with QTLs for femoral cortical thickness index (surrogate for peak bone mass) on Chrs 11 and 13, with a possible third locus on Chr X. We note with interest that the SAM-P6 Chr 13 locus is virtually identical in location to the *Bmd3* locus on Chr 13 described in this report. Further familial studies in two different primates have recently identified bone regulatory loci. In a colony of pedigreed baboons, genetic studies reported by Mahaney et al. (1997) have located the first QTL for DEXA-derived areal BMD on baboon Chr 11. In a group of closely related human families, Johnson et al. (1997) reported finding a gene that results in high bone mass (*HBM*) linked to Chr 11q12-13, also using areal BMD. In the same region of Chr 11q, Koller et al. (1998) have reported linkage for another locus that contributes to normal variation in femoral neck areal BMD. Although the relationship between these loci remains to be defined, Chr 11q12-q13 represents a valuable discovery in the search for relevant bone regulatory genes. At this time, none of the eight loci identified in these B6CAST-F_2 mice are homologous regions with either human or baboon Chr 11q loci. Nevertheless, these collective findings are vital initial steps in locating single genes that regulate normal bone density.

In summary, the F_2 intercross is a powerful experimental design that, combined with molecular genetic analyses, demonstrated QTLs on four different chromosomes associated with BMD differences between B6 versus CAST inbred mice. Genetic marker-based regression analyses detected and characterized the effects of

bone density QTLs. This computationally efficient procedure allowed us to use permutations to correct for multiple comparisons and to conservatively assess the significance of associations. From these conservative and rigorous analyses, we have designated four loci as *Bmdl–4*, within which allelic differences account for a moderate percentage of variance in femoral bone density. Congenic strains (containing QTLs from donor strains in a common background) will facilitate both molecular genetic efforts at cloning and cell biology studies to determine the effects and interactions among these genes.

Acknowledgments. The authors thank Drs. K. Johnson and B. Taylor for critical review of this manuscript. We appreciate the dedicated assistance provided by R. Donahue, V. Haynes, K. Leibwohl, T. Leidy, K. Smith, and C. Wishcamper in the pursuit of this work. The research was supported by grants from the National Institutes of Health (AR43618, RR08911-5, CA34196), the US Army (DAMA17-94-J-4016), and the S.D. Bechtel Foundation.

References

Arden NK, Baker J, Hogg C, Spector TD (1996) The heritability of bone mineral density, ultrasound of the calcaneus and hip axis length: A study of postmenopausal twins. J Bone Miner Res 11, 530–534

Barthe N, Basse-Cathalina B, Meiunier PJ, Ribot C, Marchandise X et al. (1999) Measurement of bone mineral density in mother-daughter pairs for evaluating the family influence on bone mass acquisition: A GRIO survey. Osteoporos Int 8, 379–384

Beamer WG, Donahue LR, Rosen CJ, Baylink DJ (1996) Genetic variability in adult bone density among inbred strains of mice. Bone 18, 397–403

Beamer WG, Shultz KL, Frankel WF, Donahue LR, Baylink DJ (1997) Genetic loci for cortical bone density in inbred mice. J Bone Miner Res 12, Suppl 1, abst # P292: S174

Carter DR, Bouxsein ML, Marcus R (1992) New approaches for interpreting projected bone densitometry data. J Bone Miner Res 7, 137–145

Christian JC, Yu PL, Slemenda CW, Johnston CCJ (1989) Heritability of bone mass: a longitudinal study in aging male twins. Am J Hum Genet 44, 429–433

Churchill GA, Doerge RW (1994) Empirical threshold values for quantitative trait mapping. Genetics 138, 963–971

Cohen-Solal ME, Baudin C, Omouri M, Kuntz D, De Vernejoul MC (1998) Bone mass in middle-aged osteoporotic men and their relatives: familial effect. J Bone Miner Res 13, 1909–1914

Danielson ME, Cauley JA, Baker CE, Newman AB, Dorman JS et al. (1999) Familial resemblance of bone mineral density (BMD) and calcaneal ultrasound attenuation: the BMD in mothers and daughters study. J Bone Miner Res 14, 102–110

Deng HW, Li J, Li JL, Johnson M, Gong G et al. (1998) Change of bone mass in postmenopausal Caucasian women with and without hormone replacement therapy is associated with vitamin D receptor and estrogen receptor genotypes. Hum Genet 103, 576–585

Dietrich WF, Miller J, Steen R, Merchant MA, Damron-Boles D et al. (1996) A comprehensive genetic map of the mouse genome. Nature 380, 149–152

Doerge RW, Churchill GA (1996) Permutation tests for multiple loci affecting a quantitative character. Genetics 142, 285–294

Eisman JA, Kelly PJ, Morrison NA, Pocock NA, Yeoman R et al. (1993) Peak bone mass and osteoporosis prevention. Osteoporos Int 3, 56–60

Ferrari S, Rizzoli R, Slosman D, Bonjour JP (1998) Familial resemblance for bone mineral mass is expressed before puberty. J Clin Endocrinol Metab 83, 358–361

Genant HK, Engleke K, Fuerst T, Gluer G-C, Grampp S et al. (1996) Noninvasive assessment of bone mineral and structure: State of the art. J Bone Miner Res 11, 707–730

Glastre C, Braillon P, Cochat P, Meunier PJ, Delmas PD (1990) Measurement of bone mineral content of the lumbar spine by DEXA in normal children: correlations with growth parameters. J Clin Endocrinol Metab 70, 1330–1333

Haapasalo H, Kannus P, Sievanen H, Pasanen M, Uusi-Rasi K et al. (1996) Development of mass, density, and estimated mechanical characteristics of bones in Caucasian females. J Bone Miner Res 11, 1751–1760

Harris M, Nguyen TV, Howard GM, Kelly PJ, Eisman JA (1998) Genetic and environmental correlations between bone formation and bone mineral density: a twin study. Bone 22, 141–145

Jenkins JB (1990) *Human Genetics.* (New York: Harper Collins)

Johnson ML, Gong G, Kimberling W, Recker SM, Kimmel DB et al. (1997) Linkage of a gene causing high bone mass to human Chromosome 11 (11q12-13). Am J Hum Genet 60, 1326–1332

Klein RF, Mitchell SR, Phillips TJ, Belknap JK, Orwoll ES (1998) Quantitative trait loci affecting peak bone mineral density in mice. J Bone Miner Res 13, 1648–1656

Koller DL, Rodriquez LA, Christian JC, Slemenda CW, Econs MJ et al. (1998) Linkage of a QTL contributing to normal variation in bone mineral density to Chromosome 11q12-13. J Bone Miner Res 13, 1903–1908

Kroger H, Kotaniemi E, Kroger L, Alhava E (1993) Development of bone mass and bone density of the spine and femoral neck: a prospective study of 65 children and adolescents. Bone Miner 23, 171–182

Lander ES, Botstein D (1989) Mapping Mendelian factors underlying quantitative traits using RFLP linkage maps. Genetics 121, 185–199

Lander E, Kruglyak L (1995) Genetic dissection of complex traits: guidelines for interpreting and reporting results. Nat Genet 11, 241–247

Lander ES, Green P, Abrahamson J, Barlow A, Daly MJ et al. (1987) MAPMAKER: an interactive computer package for constructing primary genetic linkage maps of experimental and natural populations. Genomics 1, 174–181

Langdahl BL, Knudsen JY, Jensen HK, Gregersen N, Eriksen EF (1997) A sequence variation: 713-8delC in the transforming growth factor-β 1 gene has higher prevalence in osteoporotic women than in normal women and is associated with very low bone mass in osteoporotic women and increased bone turnover in both osteoporotic and normal women. Bone 20, 289–294

Mahaney MC, Morin P, Rodriguez LA, Newman DE, Rogers J (1997) A quantitative trait locus on Chromosome 11 may influence bone mineral density at several sites: linkage analysis in pedigreed baboons. J Bone Miner Res 12: S37

Masi L, Becherini L, Colli E, Gennari L, Mansani R et al. (1998) Polymorphisms of the calcitonin receptor gene are associated with bone mineral density in postmenopausal Italian women. Biochem Biophys Res Commun 248, 190–195

McKay HA, Bailey DA, Wilkinson AA, Houston CS (1994) Familial comparison of bone mineral density at the proximal femur and lumbar spine. Bone Miner 24, 95–107

Morrison NA, Qi JC, Tokita A, Kelly PJ, Crofts L et al. (1994) Prediction of bone density from vitamin D receptor alleles. Nature 367, 284–287

Okamoto Y, Takahashi K, Toriyama K, Takeda N, Kitagawa K et al. (1995) Femoral peak bone mass and osteoblast number in an animal model of age-related spontaneous osteopenia. Anat Rec 242, 21–28

Rosen HN, Chen V, Citadini A, Greenspan SL, Douglas PS et al. (1995a) Treatment with growth hormone and IGF-1 in growing rats increases bone mineral content but not bone mineral density. J Bone Miner Res 10, 1352–1358

Rosen HN, Tollin S, Balena R, Middlebrooks VL, Beamer W et al. (1995b) Differentiating between orchiectomized rats and controls using measurements of trabecular bone density: a comparison among DXA, histomorphometry, and peripheral quantitative computerized tomography. Calcif Tissue Int 57, 35–39

Rosen CJ, Kurland ES, Vereault D, Adler RA, Rackoff PJ et al. (1998) Association between serum insulin-like growth factor-I (IGF-I) and a simple sequence repeat in IGF-I gene: implications for genetic studies of bone mineral density. J Clin Endocrinol Metab 83, 2286–2290

Seeman EJ, Hopper JL, Bach LA, Cooper ME, Parkinson E et al. (1989) Reduced bone mass in daughters of women with osteoporosis. N Engl J Med 320, 554–558

Shimizu M, Higuchi K, Bennett B, Xia C, Tsuboyama T et al. (1999) Identification of peak bone mass QTL in a spontaneously osteoporotic mouse strain. Mamm Genome 10, 81–87

Shiraki M, Shiraki Y, Aoki C, Hosoi T, Inoue S et al. (1997) Association of bone mineral density with apolipoprotein E phenotype. J Bone Miner Res 12, 1438–1445

Shultz KL, Svenson KL, Cheah Y-C, Paigen B, Beamer WG (1996) Strain distribution pattern for SSLP markers in the SWXJ recombinant inbred strain set: Chromosomes 7 to X. Mamm Genome 7, 526–532

Silver LM (1995) *Mouse Genetics.* (New York: Oxford University Press)

Slemenda CW, Christian JC, Williams CJ, Norton JA, Johnston CCJ (1991) Genetic determinants of bone mass in adult women: a reevaluation of the twin model and the potential importance of gene interaction on heritability estimates. J Bone Miner Res 6, 561–567

Smith DM, Nance WE, Kang KW, Christian JC, Johnston CC (1973) Genetic factors in determining bone mass. J Clin Invest 52, 2800–2808

Svenson KL, Cheah Y-C, Shultz KL, Mu JL, Paigen B et al. (1995) Strain distribution pattern for the SSLP markers in the SWXJ recombinant inbred strain set: Chromosomes 1 to 6. Mamm Genome 6, 867–872

Teegarden D, Proulx WR, Martin BR, Zhao J, McCabe GP et al. (1995) Peak bone mass in young women. J Bone Miner Res 10, 711–715

Theintz G, Buchs B, Rizzoli R, Slosman D, Clavien H et al. (1992) Longitudinal monitoring of bone mass accumulation in healthy adolescents: evidence for a marked reduction after 16 years of age at the levels of lumbar spine and femoral neck in female subjects. J Clin Endocrinol Metab 75, 1060–1065

Tsuboyama T, Takahashi K, Yamamuro T, Hosokawa M, Takeda T (1993) Cross-mating study on bone mass in the spontaneously osteoporotic mouse (SAM-P/6). Bone Miner 23, 57–64

Uitterlinden AG, Burger H, Huang Q, Yue F, McGuigan FE et al. (1998) Relation of alleles of the collagen type I α1 gene to bone density and the risk of osteoporotic fractures in postmenopausal women. N Engl J Med 338, 1016–1021

Zmuda JM, Eichner JE, Ferrell RE, Bauer DC, Kuller LH et al. (1998) Genetic variation in alpha 2HS-glycoprotein is related to calcaneal broadband ultrasound attenuation in older women. Calcif Tissue Int 63, 5–8

Calcif Tissue Int (2000) 66:298–306

Exercise and Mechanical Loading Increase Periosteal Bone Formation and Whole Bone Strength in C57BL/6J Mice but Not in C3H/Hej Mice

Y. Kodama,[1,2] Y. Umemura,[3] S. Nagasawa,[3] W. G. Beamer,[4] L. R. Donahue,[4] C. R. Rosen,[5] D. J. Baylink,[1,2] J. R. Farley[1,2]

[1]Jerry L. Pettis Memorial Veterans Medical Center, 11201 Benton St., Loma Linda, California 92357, USA
[2]Departments of Medicine and Biochemistry, Loma Linda University, Loma Linda, California, USA
[3]Department of Physical Education, Chukyo University, Toyota, Japan
[4]The Jackson Laboratory, Bar Harbor, Maine, USA
[5]Maine Center for Osteoporosis Research and Education, Bangor, Maine, USA

Received: 21 July 1999 / Accepted: 2 November 1999

Abstract. To identify the genes, and the mechanisms that account for the 53% higher peak bone density in C3H/HeJ (C3H) mice compared with C57BL/6J (B6) mice, we are performing quantitative trait locus and phenotypic analyses. The phenotypic studies revealed differences in bone formation and resorption, and showed that hindlimb immobilization (by sciatic neurectomy) caused a greater increase in endosteal resorption in the tibiae of B6 compared with C3H mice. The current studies were intended to examine the hypothesis that the bones of C3H mice are less sensitive to mechanical loading than the bones of B6 mice. To increase mechanical loading, 9-week-old female B6 and C3H mice (n = 10–13 mice/group) were subjected to a jumping exercise (20 jumps/day, 5 days/week, to heights of 20–30 cm) for a total of 4 weeks. Control mice did not jump. Osteocalcin, alkaline phosphatase (ALP) activity, and IGF-I were measured in serum. The left tibiae were used for histomorphometry (ground cross-sections prepared at the tibiofibular junction) and the right tibiae and femora were used for determinations of bone breaking strength (3-point bending). The results of these studies revealed (1) significant effects of both mouse strain (B6 and C3H) and the jumping exercise on tibial strength; (2) an exercise-dependent increase in serum IGF-I in C3H, but not B6 mice; and (3) no effects on serum ALP or osteocalcin. The histomorphometric analyses showed no effect of exercise on C3H tibiae, but significant exercise-dependent increases in total bone area, periosteal perimeter, periosteal mineral apposition rate (MAR), and periosteal bone formation ($P < 0.02$ for each) in B6 tibiae. There were no effects of exercise on periosteal resorption or any endosteal measurement in either C3H or B6 mice. Since the jumping exercise was designed to cause a two–three fold increase in muscular-skeletal loading at the tibio-fibular junction, and the calculated stress (g/mm^2) at this sampling site was only 16% greater for B6 compared with C3H mice, we had anticipated that both strains of mice would show exercise-dependent increases in periosteal bone formation, with a greater response in the B6 mice. The lack of a response in the C3H tibiae demonstrates that the bones of C3H mice are less sensitive to mechanical loading (and unloading) than the bones of B6 mice.

Correspondence to: J. Farley (151), J.L. Pettis Memorial VA Medical Center

Key words: Exercise and mechanical stress — Genetics — Bone formation.

Although adult bone density is affected by environmental factors (e.g., diet and skeletal loading), recent studies estimate that as much as 70% of peak bone density is genetically determined [1–7]. With the expectation that the genetic determinants of peak bone density are similar in mice and men, we are performing quantitative trait locus (QTL) analyses on two inbred strains of mice to identify and isolate the genes that determine peak bone density [8–15]. The two mouse strains that we have chosen—C3H/HeJ (C3H) and C57BL/6J (B6)—are similar in size and weight and have bones of similar external size, but differ greatly with respect to adult peak bone density [8, 9, 15].

To provide a physiological/mechanistic framework for our QTL analyses, we are also conducting phenotypic studies of bone formation and resorption in C3H and B6 mice. (A similar strategy combining QTL and phenotypic analyses has been applied to a murine model of accelerated skeletal senescence [16, 17]). To date, our studies have revealed evidence of more bone resorption in B6 with C3H mice [11, 14] and more bone formation in C3H mice compared with B6 mice [13]. Our phenotypic studies have also shown higher circulating levels of IGF-I in C3H compared with B6 mice [12], and this was consistent with previous findings of higher growth hormone levels [18]. Together, the results of these phenotypic studies have led us to hypothesize that C3H mice have higher peak bone density than B6 mice due to genes that determine both the rates of bone formation and resorption.

To gain more information on the phenotypic differences that determine peak bone density in these mice, we also tested *in vivo* responses to perturbations of skeletal metabolism (e.g., mechanical, dietary, pharmacologic). The first of these studies showed that hindlimb immobilization by sciatic neurectomy caused a greater increase in bone resorption and a greater decrease in bone formation in the tibiae of B6 mice compared with C3H mice [15]. Previous studies by Akhter et al. [19] have also revealed that the skeletons of B6 mice showed greater load-dependent increases in bone formation (both endosteal and periosteal, in response to 4-point bending) compared with C3H mice.

Together these data suggested that the skeletons of B6 mice are more sensitive to the effects of mechanical loading (and unloading) than the skeletons of C3H mice. (The general effects of exercise and loading are strain-related increases in bone formation and decreases in bone resorption, which result in increased bone volume [20–28]. The general effects of unloading and immobilization are increases in bone resorption and decreases in bone formation, which result in decreased bone volume [15, 26, 29, 30]). As a further test of this hypothesis, the current studies were designed to assess the effects of mechanical loading and, specifically, a regimen of jumping exercise on C3H and B6 mice. The jumping exercise, which forces axial loading (from muscular forces) on the femora and tibiae, has been shown to increase periosteal bone formation in rats, with a concomitant increase in bone-breaking strength [31, 32]. We assessed the effects of the jumping exercise (i.e., muscular loading) on the hindlimb skeletons of C3H and B6 mice with respect to bone-breaking strength; histomorphometric indices of bone formation and resorption; biochemical indices of bone formation—osteocalcin in serum and ALP activity in serum and extracts of bone; and serum IGF-I, which can increase (in humans) in response to exercise [33–36].

Materials and Methods

Chemicals and Supplies

Calcein, tetracycline, and PNPP were purchased from Sigma (St. Louis, MO). Radioimmunoassay (RIA) kit components for osteocalcin were from Biomedical Technologies, Inc. (Staughton, MA). Bio-Gel P-10 and Bio-spin disposable chromatography columns (for use in the Biospin separation of IGF-I from IGF-binding proteins) were purchased from Bio-Rad (Hercules, CA). Goat anti-rabbit antibody and nonimmune rabbit serum were from Chemicon (Temecula, CA), rabbit anti-IGF-I antibodies were from the NIH (Bethesda, MD), and recombinant human IGF-I was from Ciba Geigy (Toms River, NJ).

Animals and Treatment

Five-week-old female C3H mice and B6 mice were obtained from Dr. Beamer's research colony at the Jackson Laboratory (Bar Harbor, ME). The mice were housed in an accredited facility (Chukyo University, Toyota, Japan) on a 12-hour light/dark cycle, with food (standard chow) and water *ad lib.* The room temperature was kept at 23°C and the humidity was maintained at 55%. After 1 month of acclimation, the mice were randomly assigned to either the jump exercise or the nonexercised control groups (n = 10–13 mice/group). The design of this study did not include analysis of basal (pretreatment) controls.[1] The mice were 9 weeks old at the start of the experiment. The jumping exercise protocol has been described in detail [31, 32]. Briefly, each mouse in the jump groups was placed at the bottom of a special cage, 10 cm wide, 10 cm deep, and 20–30 cm high (the height of the cage was adjustable). The jumping exercise was initiated by applying electrical current (80 V) to the wire floor of the cage, applied only for the first 3 days of the 28-day exercise protocol because the mice learned to jump before the current was applied (i.e., avoidance behavior). Each mouse in the jump groups jumped 20 times per day, 5 days a week for 4 weeks. As the mice became accustomed to the jumping exercise, the height of the jump was increased from 20 cm in the first week to 25 cm in the second week, and 30 cm in the third and fourth weeks, by changing the height of the cage. Each mouse jumped from the floor of the cage to catch the top edge of the cage with its forepaws. The mouse was then returned to the floor of the cage to repeat the procedure.

All mice were triple-labeled with a series of tetracycline (20 mg/kg), calcein (20 mg/kg), and tetracycline injections 1, 14, and 28 days prior to sacrifice. At the end of the experiment, sera were collected and the tibiae and femora were dissected from both hindlimbs. The right femora and tibiae were used for mechanical testing (bone-breaking strength studies, conducted at Chukyo University). Frozen sera and dissected bones (including the fractured right femora and tibiae) were sent to the J L Pettis Memorial Veterans Medical Center for additional analyses including histomorphometry (left tibiae); bone levels of ALP activity (in extracts of the fractured right femora and tibiae); and serum levels of ALP activity, osteocalcin, and IGF-I. All procedures were approved by the Animal Subjects Committee of the Chukyo University Graduate School of Physical Education.

Mechanical Testing of Bone-Breaking Strength

Bone-breaking force was measured with the right femur and tibia from each mouse by 3-point bending using a servo-controlled electromechanical testing system (RX1600, I. Techno Corp., Tokyo, Japan), as described for previous studies [32]. Breaking force was measured at the midpoint of each bone. The distance between the two bottom supports was 4 mm (2 mm either side of center), and the crosshead speed was 10 mm/minute. After each bone was placed on the support, the crosshead was applied to the center of the bone, and the force was increased by the motion of the crosshead until a fracture occurred.

Histomorphometric Analyses

The left tibia from each mouse was used for histomorphometric analyses. Undecalcified ground cross-sections (30 μm thick) were prepared at the tibio-fibular junction. This method was selected because it is suitable for the analysis of cortical bone and because it had been used successfully in previous studies with rats [37, 38] and with these inbred strains of mice [11, 15]. Although the data obtained by this method are limited (i.e., compared with sagittal thin section data, which also provides measurements of trabecular, metaphyseal bone), the method allows measurements of medullary area, cortical bone, and both endosteal-and periosteal-forming and resorbing surfaces (i.e., fluorescent-labeled and eroded perimeters, respectively) and therefore was sufficient for this test of our hypothesis. From the ground sections, we determined total bone area (total cross-sectional area within the periosteal perimeter), total medullary, and the lengths of the periosteal and endosteal perimeters. We also measured the endosteal and periosteal bone-forming perimeters as (1) the absolute length of the non-eroded, single-labeled endosteal and periosteal perimeters; and (2) the ratio of non-eroded, single-labeled perimeter to total endosteal and periosteal perimeter. Endosteal and periosteal bone-resorbing perimeters were determined as (1) the absolute length of eroded surfaces on the endosteal and periosteal perimeters; and (2) the ratio of eroded perimeter to total endosteal and periosteal perimeter. The endosteal and periosteal mineral apposition rates (MAR) were calculated as the mean distance between the first and last fluorescent

[1] The design of this study did not include basal control groups (9-week-old C3H and B6 mice analyzed at the beginning of the jump-exercise regimen). Although this omission precluded an assessment of effects of growth druing the 4 weeks of exercise (and calculations that require basal values, such as net endosteal resorption), it did not affect our assessments of the effects of jumping exercise on the measured indices of bone formation and resorption and cortical and medullary areas at the tibio-fibular junction. We can assess effects of exercise by comparison with untreated controls, but without the pretreatment controls we cannot assess the possible significance of interactions between exercise and growth. (For example, the apparent effect of exercise to increase periosteal growth could represent a retardation of the age-dependent decrease in growth.)

labels divided by the interval (in days) between them. Periosteal bone formation was calculated as the product of periosteal MAR and the average length of forming surface on the periosteum. Histomorphometric indices are consistent with the recommendations of the American Society of Bone and Mineral Research [39], and histomorphometric measurements were made using the OsteoMeasure™ system (OsteoMetrics Inc., Atlanta, GA). The preparation and measurement of ground cross-sections of bone at the tibiofibular junction (along with relevant line drawings and photographs) have been described in detail [15, 37].

Extraction of Femora and Tibiae

The right femur and the tibiae (which had been fractured to determine breaking strength) were freed of adherent tissue, cut near the midpoint, and incubated overnight in phosphate-buffered-saline containing 0.01% azide at 4°C (1.5 ml/bone) to remove marrow and contaminating serum [13, 40]. Each bone was then extracted in 1.5 ml of 25 mmol/liter $NaHCO_3$ (pH 7.4) containing 0.01% azide and 0.01% Triton X-100 for 72 hours at 4°C. The extracts (centrifuged to remove insoluble material) were used for measurements of ALP activity. The extracted bones were dehydrated (24 hours in 70% ethanol, 1 ml/bone at 37°C), dried (18 hours at 37°C), and weighed using a Cahn microbalance (Model 7500, Cahn Instruments, Cerritos, CA).

Measurement of ALP Activity in Serum and Extracts of Femora and Tibiae

As in previous studies [12, 23, 15], ALP activity was measured by time-dependent formation of p-nitro-phenolate from PNPP (i.e., increased absorption of light at 405 nm) in alkaline solution, using a microtiter plate spectrophotometer (EAR400/340AT, Labinstruments, Vienna, Austria). Reactions were initiated by the addition of 0.005–0.025 ml of serum or bone extract to a total reaction volume of 0.3 ml (in 96-place microtiter plate wells) containing 10 mmol/liter PNPP, 1 mmol/liter $MgCl_2$, and 150 mmol/liter carbonate buffer, at pH 10. ALP activity was calculated as U/liter of serum and mU/mg dry weight of bone, where 1 unit is defined by the conversation of 1 μmol of substrate to product per minute at room temperature (25°C).

Measurement of Osteocalcin in Serum

Osteocalcin was measured in serum by RIA [15] using kit components purchased from Biomedical. Duplicate aliquots of each serum sample and extract were measured and the average value was used for the analyses. Serum osteocalcin was expressed as ng/ml of serum.

Measurement of IGF-I in Serum

Serum IGF-I was measured by RIA, after Biospin separation of IGF-I from serum IGF binding proteins [12, 41, 42]. The RIA used recombinant human IGF-I as a tracer and a standard, with polyclonal antiserum. The intra- and interassay variations for determination of IGF-I were <10%. The cross-reactivity of IGF-II in this RIA for IGF-I was <2%, and the sensitivity for IGF-I was 2–5 ng/ml.

Statistical Analysis of Data

All data are shown as averages of replicates (usually as mean ± SEM). Analytic methods included one- and two-way ANOVA, and nonparametric comparisons (e.g., Kruskal-Wallis one-way ANOVA), using Systat statistical software (Systat, Inc., Evanston, IL).

Results

Four weeks of jump exercise had no effect on body weight or longitudinal growth of the tibiae or the femora in either strain of mice and these parameters were similar in C3H and B6 mice (Table 1). Also summarized in Table 1 is our observation (by 2-way ANOVA and nonparametric comparison) that the dry weight of the tibiae was increased by 4 weeks of jumping exercise in the B6 mice. This effect was not observed with the C3H tibiae. The observations that the dry weights of femora and tibiae from C3H mice were greater than dry weights of bones prepared from B6 mice, irrespective of treatment (2-way ANOVA) were consistent with previous findings [13, 15].

Consistent with the effect of the jumping exercise to increase the dry weight of the tibiae in B6, but not C3H mice, the breaking strength studies revealed a jump-dependent increase in the breaking strength of the tibiae by 2-way ANOVA (Table 2). The effect of the jump exercise to increase the strength of the tibiae did not reach significance when the B6 tibiae were analyzed alone (i.e., $P = 0.053$ for jump versus control B6 mice, by Kruskal-Wallis test). These 3-point bending studies also demonstrated significantly greater breaking strength for both the femora and the tibiae from C3H, compared with B6 mice (i.e., an effect of the strain of mouse in our 2-way ANOVAs).

As shown in Table 3, the current data (i.e., 2-way ANOVAs) confirmed our previous reports of higher levels of ALP in extracts of C3H compared with B6, femora, and tibiae [12, 13, 15], and higher levels of IGF-I in the sera of C3H compared with B6 mice [12]. The only observed effect of the jumping exercise on any tested parameter was a jump-dependent increase in the serum level of IGF-I in the C3H, but not the B6 mice (a 17% increase that was significant by nonparametric comparison, $P < 0.05$). We should note, however, that the serum bone formation indices (e.g., ALP and osteocalcin) are systemic and therefore reflect contributions from the total skeleton, whereas the local indices (i.e., bone extract ALP activities) are specific for the tibiae and the femora. Since the effect of jump exercise is presumed to be local (i.e., muscular loading on the tibiae and femora), any change in serum ALP or osteocalcin would reflect a change in the contribution of the hindlimb that was sufficient to alter the circulating total.

Our histomorphometric studies showed a jump-dependent increase in periosteal perimeter ($P < 0.02$, by nonparametric comparison) in B6, but not C3H mice, with no effect of exercise on medullary area, endosteal perimeter, or endosteal MAR in either strain of mice. The results of these analyses of cross-sections prepared at the tibio-fibular junction are summarized in Table 4. These histomorphometric studies also confirmed our previous findings of greater medullary area and greater endosteal perimeter in B6 compared with C3H mice, with no difference in periosteal perimeter [15]. The observed effect of jumping to increase periosteal perimeter (at this tibio-fibular sampling site) in B6, but not C3H mice, was associated with a similar increase in total bone area (total area within the periosteal perimeter). The jumping protocol resulted in a 3.8% increase in total bone area in the B6 mice, which was significant by nonparametric comparison (Fig. 1). These two observations—jump-dependent increases in periosteal perimeter and total bone area in B6, but not C3H mice—are geometrically consistent, as the perimeter defines the total area.

Further histomorphometric analyses allowed for an assessment of the roles of bone formation and resorption as

Table 1. Effects of jump exercise on body weight and bone size

	B6 Mice		C3H Mice	
Parameter	Control	Jump	Control	Jump
Body weight (g)	20.8 ± 0.5	20.7 ± 0.2	21.6 ± 0.5	21.1 ± 0.4
Tibia dry weight (mg)	28.6 ± 0.5	30.4 ± 0.6[a]	31.2 ± 0.6	31.9 ± 1.1
Tibia length (cm)	1.78 ± 0.01	1.76 ± 0.01	1.80 ± 0.02	1.79 ± 0.02
Femora dry weight (mg)	31.2 ± 0.8	32.0 ± 2.8[b]	33.9 ± 0.8	36.0 ± 1.4
Femora length (cm)	1.56 ± 0.01	1.56 ± 0.01	1.51 ± 0.01	1.50 ± 0.01

Body weight was measured at the end of the experiment (i.e., after 4 weeks of jump exercise, 20 times per day, 5 days per week). The length and dry weight of the tibiae and femora were measured. All data shown as mean ± SEM (n = 10–13 per group)

[a] Significant effect of jumping (compared with control mice of same strain), by nonparametric analysis, $P < 0.05$

[b] Significant difference compared with C3H mice receiving the same treatment, $P < 0.05$, by 1-way ANOVA. Two-way ANOVA indicates significant effects of mouse strain (C3H vs B6) on tibial dry weight ($P = 0.011$) and femoral dry weight ($P = 0.002$), but no effect of jump exercise on either tibial or femoral dry weight. Neither ANOVA (1-way and 2-way) nor nonparametric comparisons revealed any significant intergroup differences in body weight, tibial length, or femoral length

Table 2. Effects of jump exercise on bone strength

		Breaking force/body weight (mN/g)		
Mouse strain	Bone	Control	Jump exercise	Effect of exercise
C3H	Tibia	48.78 ± 1.27	51.12 ± 1.56	$P = 0.258$
B6	Tibia	38.75 ± 1.14[a]	42.90 ± 1.58[a]	$P = 0.053$
C3H	Femur	63.46 ± 1.92	68.95 ± 2.45	$P = 0.09$
B6	Femur	36.58 ± 1.96[a]	36.73 ± 1.70[a]	$P = 0.96$

Body weight ranged from 20.74 ± 0.22 g for the B6 jump exercise group to 21.58 ± 0.47 g for the C3H control group, with no significant intergroup differences. N = 10, 12, 13, 13, for B6 control, B6 exercise, C3H control, and C3H exercise, respectively. Breaking force of tibiae and femora determined by 3-point bending and normalized to body weight (mN/g). Data shown as mean ± SEM. Effect of exercise indicates the significance of a nonparametric comparison (Kruskal-Wallis 1-way ANOVA). A standard (parametric) 2-way ANOVA indicates significant effects of both mouse strain ($P < 0.001$) and jump exercise ($P = 0.029$) for tibia load/body weight, and a significant effect of mouse strain ($P < 0.001$) but no effect of exercise ($P = 0.19$) on femur load/body weight

[a] Significant difference compared with C3H mice receiving the same treatment, $P < 0.001$

presumptive determinants of the observed, jump-dependent changes in tibial breaking strength and periosteal perimeter in B6, but not C3H mice. We found no effects of either the jump exercise or the strain of mice (B6 versus C3H) on the relative length of endosteal bone-forming surface (Table 5). We did, however, find that B6 mice had smaller percentages of their endosteal and periosteal surfaces involved in resorption, and a larger percentage of their periosteal surface involved in bone formation than the C3H mice. Two bone formation parameters were increased by the jump exercise (at our tibio-fibular junction sampling site) in B6, but not C3H mice. Figure 2 shows that the periosteal MAR was increased by 35% ($P < 0.02$ by nonparametric comparison) in the jump-exercised B6 mice but was not affected by jumping in the C3H mice. The rate of bone formation at the periosteum was similarly increased by jumping in B6 but not C3H mice (Fig. 3).

Discussion

The current studies demonstrate that musculoskeletal loading from a 4-week regimen of jumping exercise increased bone formation at our sampling site in the tibiae of B6 but not C3H mice. Our histomorphometric measurements, using ground cross-sections prepared at the tibio-fibular junction, revealed exercise-dependent increases in the periosteal perimeter (and both the total and cortical areas enclosed), the periosteal MAR, and the rate of bone formation at the periosteum in B6 but not C3H mice. The jumping exercise also affected the breaking strength of the tibiae, but did not yield detectable changes in endosteal parameters or systemic bone formation indices (i.e., ALP activity and osteocalcin in serum) in either strain of mice. Together, these data suggest that the jumping exercise caused a sufficient increase in periosteal loading in B6 but not C3H mice, to increase bone formation locally. Presumably, this resulted in an increase in periosteal osteoblast activity (as reflected by the increased MAR), and a consequent, adaptative, site-specific increase in periosteal bone volume, however, since we did not have a basal (pretreatment) control group, we cannot dismiss the possibility that exercise affected growth.

Our findings are consistent with the results of a previous

Table 3. Effects of jump exercise on ALP activity, osteocalcin, and IGF-1 in serum and ALP activity in extracts of bone

	B6 Mice		C3H Mice	
Parameter	Control	Jump	Control	Jump
Serum ALP (U/ml)	0.167 ± 0.010	0.147 ± 0.010	0.155 ± 0.007	0.168 ± 0.010
Serum osteocalcin (ng/ml)	4.79 ± 0.51	5.57 ± 0.41	3.74 ± 0.40	4.21 ± 0.36
Serum IGF-I (ng/ml)	231.6 ± 19.1	211.4 ± 14.2	391.1 ± 21.8[b]	459.3 ± 21.7[b,c]
Tibial ALP (mU/mg)	4.04 ± 0.28	3.56 ± 0.22	5.03 ± 0.30	5.07 ± 0.44[a]
Femoral ALP (mU/mg)	4.12 ± 0.51	4.04 ± 0.31	4.29 ± 0.24	4.38 ± 0.44

After 4 weeks of jump training (20 times a day, 5 days a week, n = 10–13 mice/group), sera were collected for measurements of ALP activity, osteocalcin, and IGF-I. In addition, the right tibiae and femora (which had been used for measurements of breaking strength) were extracted for measurements of ALP activity (expressed as mU/mg dry weight of bone). Data shown as mean ± SEM

[a] Significant difference (by I-way ANOVA), compared with B6 mice receiving the same treatment, $P < 0.01$

[b] $P < 0.001$

[c] Significant effect of jump exercise, $P < 0.05$ (by nonparametric, Kruskal-Wallis comparison). Two-way ANOVA revealed significant mouse strain-dependent differences in serum osteocalcin ($P < 0.005$), IGF-I ($P < 0.001$), and tibial ALP ($P < 0.001$), but no jump exercise-dependent differences in any listed parameter

Table 4. Effects of jump exercise on selected histomorphometric indices

	B6 mice		C3H mice	
Parameter	Control	Jump	Control	Jump
Periosteal perimeter (mm)	3.15 ± 0.01	3.22 ± 0.02[a]	3.19 ± 0.02	3.20 ± 0.03
Endosteal perimeter (mm)	1.91 ± 0.02	1.87 ± 0.02	1.44 ± 0.05[c]	1.46 ± 0.03[c]
Medullary area (mm^2)	0.281 ± 0.007	0.272 ± 0.006	0.166 ± 0.008[c]	0.163 ± 0.007[c]
Cortical area (mm^2)	0.474 ± 0.008	0.513 ± 0.017[a]	0.610 ± 0.013[c]	0.613 ± 0.015[c]
Endosteal MAR (μm/day)	1.84 ± 0.15	1.87 ± 0.13	1.18 ± 0.20[b]	1.46 ± 0.03[b]

After 4 weeks of jump training (20 times a day, 5 days a week), the mice were sacrificed to dissect the tibiae. Undecalcified ground cross-sections were made at the tibial-fibilar joint of the tibiae, followed by histomorphometric analyses

[a] Significant effect of jump exercise (by nonparametric compared with control mice of the same strain), $P = 0.015$

[b] Significant difference compared with B6 mice receiving the same treatment by 1-way (parametric) ANOVA, $P < 0.05$

[c] $P < 0.001$. Two-way ANOVA indicates no effect of mouse strain or jump exercise on periosteal perimeter, and significant effects of mouse strain ($P < 0.001$), but not jump exercise on medullary area, endosteal perimeter, and endosteal MAR

study by Akhter et al. [19] of external skeletal loading (by 4-point bending) applied to the tibiae of C3H and B6 mice. Those studies applied a lateral compression (about 9 N) to the periosteal tibial surface, proximal to the tibio-fibular junction, 36-times/day, 6 days/week for a total of 3 weeks, resulting in load-dependent increases in periosteal and endocortical bone-forming surfaces and endocortical mineral apposition in B6 but not C3H mice. Those studies also resulted in load-dependent increases in periosteal woven bone surface in both strains of mice, with greater increases in the B6 mice. Presumably, the observation of endocortical responses in the studies of Ahkter et al. reflects the effect of the 4-point bending to deform the entire bone (at both the periosteal and endocortical surfaces), whereas the skeletal loading with our jumping exercise was limited to the periosteum (to the points of muscle insertion). We might further speculate that our observation of an exercise-dependent increase in cortical area in the B6 but not the C3H mice, which was not evident in the studies of Akhter et al., was related to the fact that we used younger animals (9 weeks versus 16 weeks of age at the start of the studies).

Although the jumping exercise did not result in changes in serum ALP activity or serum osteocalcin in either strain of mice, that was not surprising inasmuch as those serum markers are presumed to reflect bone formation in the total skeleton, and the effect of the jump exercise was localized to the hindlimb. Although we were somewhat surprised to find a jump-dependent increase in the circulating level of IGF-1 in the C3H but not the B6 mice, that observation was consistent with previous findings of exercise-dependent increases in serum IGF-I in humans [33–36]. Since the systemic increase in IGF-I was associated with increased muscular activity but not with increased bone formation (in fact, the B6 mice, which showed a jump-dependent increase in bone formation, did not show a similar increase in serum IGF-I), it is interesting to speculate that IGF-I synthesis may be more sensitive to exercise in C3H than B6 mice. We might further speculate that a differential sensitivity to IGF-I synthesis in response to exercise could account (at least, in part) for the higher circulating level of IGF-I in C3H compared with B6 mice [12]. Further studies are required to resolve this issue and to answer the following

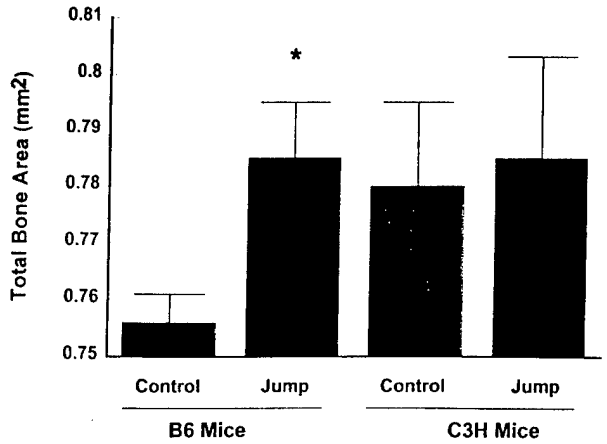

Fig. 1. Four weeks of jump exercise increases total bone area at the tibio-fibular junction in B6 but not C3H mice. Groups of 10–13 C3H and B6 mice subjected to jump exercise (shown as solid black bars) or not exercised (control groups, shown as solid gray bars). Total cross-sectional area was measured in ground sections prepared at the tibio-fibular junction (i.e., total area within the periosteal perimeter). Data are shown as mean ± SEM for each group. *Effect of jump exercise (a difference, compared with the control mice of the same strain), $P = 0.016$, by nonparametric comparison. Two-way ANOVA showed no effects of mouse strain or jump exercise on total bone area.

questions. Why didn't the 17% increase in serum IGF-I in jump-exercised C3H mice result in increased bone formation? (Was the basal level of IGF-I already saturating, with respect to bone formation?) Was the jump-dependent increase in serum IGF-I in the C3H mice a consequence of hepatic or muscular (or skeletal) IGF-I synthesis, and was it growth hormone dependent? Finally, did the C3H mice have increased muscle mass compared with the B6 mice before or after the regimen of jumping exercise?

Our observation of a higher basal level of serum IGF-I in C3H compared with B6 mice was consistent with previous findings [12], as were our observations of higher levels of ALP activity in tibial/femoral extracts of C3H compared with B6 mice [13, 15]. Our histomorphometric findings of a greater medullary area and a greater endosteal perimeter (at the tibio-fibular junction) in B6 versus C3H mice were also consistent with previous findings [15], as were our observations of increased dry weight for tibiae and femora prepared from C3H compared with B6 mice [13, 15]. The current observations of greater breaking strength in the tibiae and femora of C3H compared with B6 (the control, non-exercised mice) should be regarded as preliminary until they can be confirmed with a larger number of animals.

We believe the current findings are particularly interesting, because jump exercise provides a different method of skeletal loading than external bending [19] or compression. The forces applied to the bone result from muscular contraction (as opposed to impact loading), and they are periosteal (i.e., transmitted by tendon insertions on the periosteal surface of bone). Prior applications of this method have revealed that a jumping exercise can cause a significant increase in periosteal (but not endosteal) bone formation and breaking strength in the femora and tibiae of rats [31, 32]. Previous studies (with different exercise regimens) have also established that exercise can increase the strength of mouse bone [43, 44] and bone density in humans [24, 45, 46].

Although the current studies were not designed to measure jump-dependent stresses on the tibiae (or changes in the strength or mass of hindlimb muscles), we can estimate the peak strains at the tibio-fibular junction [37]. This calculation (which is, at best, approximate because it incorrectly assumes that the tibia is a hollow cylinder) indicates that the tibiae of B6 mice are subjected to a 16% greater load-related strain—at the tibio-fibular junction—than the tibiae of C3H mice[2]. Alternatively, we can calculate the peak strain at our sampling site by multiplying the cortical cross-sectional area (at the tibio-fibular junction) by a published estimate of the skeletal modeling threshold—about 20 N/mm^2 [47]. This calculation[3] predicts a somewhat greater difference of 28%. We can also estimate that the jumping exercise required muscular exertion equivalent to the potential energy gained by elevating a 21g mouse to heights of 20, 25, and 30 cm—0.0412, 0.0515, and 0.0617 J, respectively. If we assume that the mice ordinarily elevate/displace their bodies by 1–10 cm (with normal motion and jumping, within the confines of a plastic cage), we can further estimate that the jumping exercise would have increased the maximum load by as much as two-threefold at the higher elevations. Since the C3H and B6 mice appear to move and jump in a similar manner (and are similar in weight), it follows that the muscular forces would have placed similar loads on their hindlimb skeletons during the jump exercise. Together, these estimates indicate that the increase in tibial musculoskeletal loading, as a result of the jump exercise, should have been much greater (16–28% of the basal value) than the difference in the peak strain at the tibio-fibular junction between the C3H and B6 mice.

Recent studies have suggested that bone volume may be increased, in response to mechanical loading, when the load exceeds the normal range [23, 27]. Since the jump-related load should have exceeded the normal range in both the C3H and B6 mice, our results would not support this model, except for one further proviso—the model assumes an initial condition in which the skeleton has adapted to the range of normal loading, so that bone volume is sufficient for mechanical support, but not unnecessarily redundant (i.e., unloaded bone should be lost to resorption). Therefore, our

---

[2] This method [38] applies the formula

$$\sigma_{max} = WC[(R^2 + r^2)\cos\alpha + 4LbR\sin\alpha)]/\pi(R^4 + r^4)$$

where R is the radius of the total bone area, r is the radius of the medullary area, α is the angle at the sampling site between a vertical line and the long axis of the tibia when the knee is flexed (assumed to be 45°), Lb is the length of the tibia between the sampling site and its distal end, W is the final body weight, and C is the maximum portion of the body weight supported by the left hind limb—assumed to be half of the body weight. (This formula assumes that the skeletal structure can be modeled as a hollow column, and since the tibia is not a hollow cylinder, the calculated values should be regarded as approximate, at best). Application of this formula predicts peak stresses at our histomorphometric sampling site (the tibio-fibular junction), of 893 g/mm^2 for the B6 mice and 1031 g/mm^2 for C3H mice. (Although the maximal load at our sampling site occurs at an angle of 90°—1245 and 1439 g/mm^2 for C3H and B6 mice, respectively—the B6/C3H load ratio of 1.16 is invariant).

[3] This calculation would also predict that the increase in cortical area in the exercised B6 mice (from 0.474 to 0.513 mm^2) would have reduced the difference in peak strain at our sampling site (i.e., between the C3H and B6 mice) from 28% to 19%.

Table 5. Effects of jump exercise on bone-forming and resorbing surfaces

Parameter	B6 mice		C3H mice	
	Control	Jump	Control	Jump
Periosteal-forming surface	58.0 ± 2.1	65.2 ± 4.0	55.9 ± 1.4	54.7 ± 1.65[a]
Periosteal-resorbing surface	28.9 ± 1.9	26.6 ± 2.1	33.4 ± 2.0	31.3 ± 2.8
Endosteal-forming surface	67.8 ± 6.5	72.4 ± 7.1	65.4 ± 4.3	61.2 ± 2.1
Endosteal-resorbing surface	25.3 ± 2.8	19.6 ± 3.3	30.0 ± 1.6	27.0 ± 1.4

After 4 weeks of jump exercise (20 times a day, 5 days a week, n = 10–13 mice/group), undecalcified ground cross-sections, prepared at the tibio-fibilar junction, were used for histomorphometric measurements of forming and resorbing surfaces. Both resorbing (scalloped) and forming (single-labeled, nonscalloped) surfaces are shown as percent of total surface length (mean ± SEM). Absolute surface lengths may be determined by comparison with endosteal and periosteal perimeter lengths as specified in Table 4

[a] Difference (by 1-way ANOVA), compared with B6 mice receiving the same treatment, $P < 0.05$. Two-way ANOVA revealed no significant effect of either mouse strain or jump exercise on endosteal forming surface, and significant effects of mouse strain, but not jump exercise, on periosteal-forming surface ($P < 0.02$), periosteal-resorbing surface ($P < 0.05$), and endosteal-resorbing surface ($P < 0.01$). Nonparametric comparisons (Kruskal-Wallis 1-way ANOVA) revealed no effect of jump exercise on any listed parameter, in either strain of mice

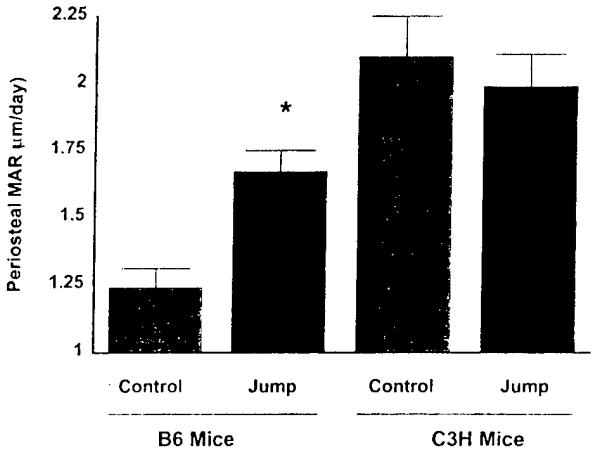

Fig. 2. Four weeks of jump exercise increases periosteal MAR in B6 but not C3H mice. Groups of 10–13 C3H and B6 mice subjected to jump exercise (shown as solid black bars) or not exercised (controls, shown as solid gray bars). Periosteal MAR measured as µm/day, using the first and third fluorescent labels, in ground sections prepared at the tibio-fibular junction. Data are shown as mean ± SEM for each group.* Effect of jump exercise (compared with the control mice of the same strain), $P = 0.012$, by nonparametric comparison. One-way ANOVA revealed a significant difference between the B6 and C3H control groups ($P < 0.001$), and two-way ANOVA revealed a significant effect of mouse strain ($P < 0.001$), but not jump exercise.

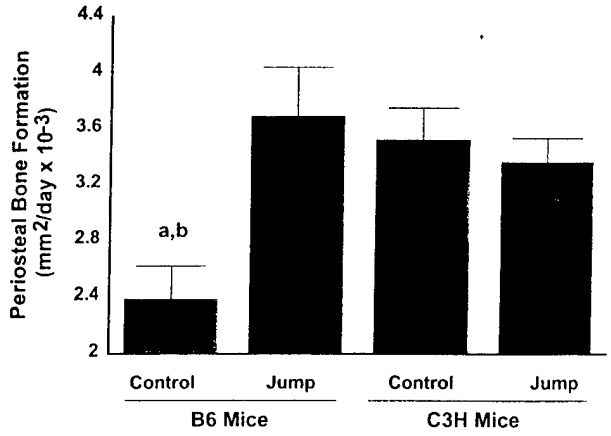

Fig. 3. Four weeks of jump exercise increase periosteal bone formation in B6 but not C3H Mice. Groups of 10–13 C3H and B6 mice subjected to jump exercise (shown as black bars) or not exercised (controls, shown as gray bars). Periosteal bone formation calculated as the product of MAR and the average length of periosteal-forming surface, and expressed as mm^2/day ($\times 10^{-3}$), in ground sections prepared at the tibio-fibular junction. Data are shown as mean ± SEM for each group.[a] Significant effect of jumping ($P = 0.011$ compared with the B6 control);[b] significant effect of mouse strain ($P < 0.04$ compared with the C3H control), by ANOVA. A nonparametric comparison confirms the effect of the jump exercise to increase bone formation in the B6 mice, $P = 0.034$.

data are consistent with the general hypothesis that C3H mice have more redundant bone (bone volume in excess of that required to prevent fracture within the normal range of loading) than B6 mice. This is consistent with previous findings that C3H mice are less sensitive than B6 mice to resorptive bone loss with disuse and/or unloading [15] and with a previous report that the adaptive response to loading can differ in different genetic strains of chicken embryos [48]. Indeed, since C3H and B6 mice are highly inbred strains, the results of these studies suggest that the mechanism(s) that result in more redundant bone and a decreased sensitivity to the effects of loading and unloading in C3H compared with B6 mice, are genetic and, therefore, amenable to QTL analysis.

It is interesting to speculate that the higher levels (compared with B6) of IGF-I in the serum of C3H mice may be involved in the preservation of some of the redundant bone and the insensitivity to immobilization-dependent resorption [15]. Two recent findings allow us to propose a role for IGF-I as an inhibitor of immobilization/unloading-dependent resorption: (1) bone loss from immobilization is

associated with apoptosis in osteocytes [49], and (2) IGF can inhibit apotosis [50, 51]. Therefore, we hypothesize that the higher levels of IGF-I in C3H (compared with B6) mice may inhibit apoptosis in osteocytes, preventing resorption of unloaded bone and thereby increasing bone volume beyond the normal level of redundancy. Additional studies are clearly required to examine this hypothesis.

Acknowledgments. The authors thank the secretarial staff of the Loma Linda University Mineral Metabolism Research Unit (which is located in the Jerry L. Pettis Memorial Veterans Medical Center) for assistance in the preparation of this manuscript. The authors also thank the staff members of the authors' laboratory staff of Chukyo University for practical work for jump exercise. These studies were supported by the National Institutes of Health, Grants AR-43618 and CA-34196 (one form WGB); a subcontract from US Army Medical Research Acquisition Activity Grant DAMD17-96-1-6306 (WGB and DJB); the Japan-North America Medical Exchange Foundation (YK); the Jackson Laboratory (WGB and LRD); Loma Linda University (DJB and JRF); and the Veterans Administration (DJB and JRF).

References

1. Evans RA, Marel GM, Lancaster EK, Kos S, Evans M, Wong YP (1988) Bone mass is low in relatives of osteoporotic patients. Ann Intern Med 109:870–873
2. Jouanny P, Guillemin F, Kuntz C, Jaendel C, Pourel J (1995) Environmental and genetic factors affecting bone mass. Arthritis Rheum 38:61–67
3. Kelly P, Harris M (1995) Genetic regulation of peak bone mass. Acta Paediatr Scand (suppl)411:24–29
4. Pocock NA, Eisman JA, Hooper JL, Yeates MG, Sambrook PN, Ebert S (1987) Genetic determinants of bone mass in adults. J Clin Invest 80:706–710
5. Slemenda CW, Christian JC, Williams CJ, Norton JA, Johnston CC (1991) Genetic determinants of bone mass in adult women: a reevaluation of the twin model and the potential importance of gene interaction on heritability estimates. J Bone Miner Res 6:561–565
6. Kelly PJ, Twomey L, Sambrook PN, Eisman JA (1990) Sex differences in peak adult bone mineral density. J Bone Miner Res 5:1169–1175
7. Pocock NA, Eisman JA, Hopper JL, Yeates MG, Sambrook PN, Ebert S (1991) Genetic determinants of bone mass in adults: a twin study. J Clin Invest 52:2800–2808
8. Baylink DJ, Donahue L, Rosen CJ, Gruber H, Lee JES, Farley J, Beamer W (1996) Novel genetic model of peak bone density: a polygenic trait. 10th Int Cong Endo, abstracts, vol 1:#P1-945
9. Beamer WG, Donahue LR, Rosen CJ, Baylink DJ (1996) Genetic variability in adult bone density among inbred strains of mice. Bone 18:397–403
10. Beamer WG, Donahue LR, Baylink DJ, Rosen CJ (1996) Mapping genes for normal bone density in inbred mice by quantitative trait locus analysis. J Bone Miner Res 11(suppl 1):S176
11. Baylink D, Farley J, Donahue L, Rosen C, Barr B, Lee J, Beamer W (1995) Evidence that high peak bone density is due to decreased resorption not increased formation in a murine model. J Bone Miner Res 10:S338
12. Rosen CJ, Dimai HP, Verault D, Donahue LR, Beamer WG, Farley J, Linkhart S, Linkhart T, Mohan S, Baylink DJ (1997) Circulating and skeletal insulin-like growth factor-I concentrations in two inbred strains of mice with different bone mineral densities. Bone 21:217–223
13. Dimai HP, Linkhart TA, Linkhart SG, Donahue LR, Beamer WG, Rosen CJ, Farley JR, Baylink DJ (1998) Alkaline phosphatase levels and osteoprogenitor cell numbers suggest bone formation may contribute to peak bone density differences between two inbred strains of mice. Bone 22:211–216
14. Linkhart T, Linkhart S, Kodama Y, Farley J, Dimai HP, Wright K, Wegedal J, Sheng M, Beamer W, Donahue LR, Rosen C, Baylink DJ (1999) Osteoclast formation in bone marrow cultures from two inbred strains of mice with different bone densities. J Bone Miner Res 14:39–46
15. Kodama Y, Dimai HP, Wergedal J, Sheng M, Malpe R, Kutilek S, Beamer W, Donahue LR, Rosen C, Baylink DJ, Farley J (1999) Cortical tibial bone volume in two strains of mice: effects of sciatic neurectomy and genetic regulation of bone response to mechanical loading. Bone 25 (in press)
16. Benes H, Dennis R, Zheng W, Weinstein R, Shelton R, Jilka R, Roberson P, Manolagas S, Shmookler R (1997) Genetic mapping of osteopenia-associated loci using crosses between closely related mouse strains with differing bone mineral density. J Bone Miner Res 12 (suppl 1):S375, #F598
17. Jilka RL, Weinstein RS, Takahashi K, Parfitt AM, Manolagas SC (1996) Linkage of decreased bone mass with impaired osteoblastogenesis in a murine model of accelerated senescence. J Clin Invest 97:1732–1740
18. Sinha YN, Vlahakis G, Vanlerlaan WP (1979) Serum, pituitary and urine concentrations for prolactin and growth hormone in eight strains of mice with varying incidence of mammary tumors. Int J Cancer 24:430–437
19. Akhter MP, Cullen DM, Pedersen EA, Kimmel DB, Recker RR (1998) Bone response to in vivo mechanical loading in two breeds of mice. Calcif Tissue Int 63:442–449
20. Lanyon LE, Goodship AE, Pye CJ, Mac Fie JH (1982) Mechanically adaptive bone remodelling. J Biomech 15:141–154
21. Rubin CT, Lanyon LE (1985) Regulation of bone mass by mechanical strain magnitude. Calcif Tissue Int 37:411–417
22. Carter DR, Wong M, Orr TE (1991) Musculoskeletal ontegeny, phylongeny, and functional adaptation. J Biomech 24(suppl 1):3–16
23. Turner CH, Forwood MR, Rho JY, Yoshikawa T (1994) Mechanical loading thresholds for lamellar and woven bone formation. J Bone Miner Res 9:87–97
24. Kerr D, Morton A, Kick I, Prince R (1996) Exercise effects on bone mass in postmenopausal women are site-specific and load-dependent. J Bone Miner Res 11:218–225
25. Gross TS, Edwards JL, McLeod KJ, Rubin CT (1997) Strain gradients correlate with sites of periosteal bone formation. J Bone Miner Res 12:982–988
26. Kaneps AJ, Stover SM, Lane NE (1997) Changes in canine cortical and cancellous bone mechanical properties following immobilization and remobilization with exercise. Bone 21: 419–423
27. Mosley JR, Lanyon LE (1998) Strain rate as a controlling influence on adaptive modeling in response to dynamic loading of the ulna in growing male rats. Bone 23:313–318
28. Pitsillides AA, Rawlinson SC, Mosley JR, Lanyon LE (1999) Bone's early responses to mechanical loading differ in distinct genetic strains of chick: selection for enhanced growth reduces skeletal adaptability. J Bone Miner Res 14:980–987
29. Globus RK, Bikle DD, Morey-Holton E (1984) Effects of simulated weightlessness on bone mineral metabolism. Endocrinology 114:2264–2270
30. Globus R, Bikle D, Morey-Holton E (1986) Temporal response of bone to unloading. Endocrinology 118:733–742
31. Umemura Y, Ishiko T, Tsujimoto H, Miura H, Mokushi N, Suzuki H (1995) Effects of jump training on bone hypertrophy in young and old rats. Int J Sports Med 16:364–367
32. Umemura Y, Ishiko T, Yamauchi T, Kurono M, Mashiko S (1997) Five jumps per day increase bone mass and breaking force in rats. J Bone Miner Res 12:1480–1485
33. Schwarz AJ, Brasel JA, Hintz RL, Mohan S, Cooper DM (1996) Acute effect of brief low- and high-intensity exercise on circulating insulin-like growth factor (IGF) I, II, and IGF-binding protein-3 and its proteolysis in young healthy men. J Clin Endocrinol Metab 10:3492–3497
34. Kiziris LP, Hickson RC, Chatterton RT Jr, Groseth RT, Christie JM, Goldflies DG, Unterman TG (1999) Serum levels of

total and free IGF-I and IGFBP-3 are increased and maintained in long-term training. J Appl Physiol 86:1436–1442
35. Bermon S, Rerrari P, Bernard P, Altare S, Dolisi C (1999) Responses of total and free IGF-I and IGF binding protein-3 after resistance exercise and training in elderly subjects. Acta Physiol Scand 165:51–56
36. Nguyen U, Mougin F, Simon-Rigaud M, Rouillon J, Marguet P, Regnard J (1998) Influence of exercise duration on serum IGF and its binding proteins in athletes. Eur J Appl Physiol 78:533–537
37. Baylink D, Stauffer M, Wergedal J, Rich C (1970) Formation, mineralization, and resorption of bone in vitamin D-deficient rats. J Clin Invest 49:1122–1129
38. Stauffer M, Baylink D, Wergedal J, Rich C (1972) Bone repletion in calcium-deficient rats fed a high calcium diet. Calcif Tissue Res 9:163–172
39. Parfitt AM, Drezner MK, Glorieux FH, Kanis JA, Malluche H, Meunier PJ, Ott SM, Recker RR (1987) Bone histomorphometry: standardization of nomenclature, symbols, and units. Report of the ASMBR Histomorphometry Nomenclature Committee. J Bone Miner Res 2:595–610
40. Farley JR, Hall SL, Herring S, Tarbaux NM (1989) Two biochemical indices of mice bone formation are increased, in vivo, in response to calcitonin. Calcif Tissue Int 45:214–221
41. Malpe R, Baylink DJ, Linkhart TA, Wergedal JE, Mohan S (1997) IGF-I, -II, IGF binding proteins-3, -4, and -5 levels in the conditioned media of normal human bone cells are skeletal site-dependent. J Bone Miner Res 12:423–430
42. Mohan S, Baylink DJ (1995) Development of a simple valid method for the complete removal of IGF-binding proteins from IGFs in human serum and other biological fluids: comparison with acid-ethanol treatment and C18 Sep-Pak separation. J Clin Endocrinol Metab 80(2):637–647
43. Gordon KR, Perl M, Levy C (1989) Structural alterations and breaking strength of mouse femora exposed to three activity regimens. Bone 10:303–312
44. Hoshi A, Watanabe H, Chiba M, Inaba Y (1998) Effects of exercise at different ages on bone density and mechanical properties of femoral bone of aged mice. Tohoku J Exp Med 185:15–24
45. Dalsky GP, Stocke KS, Ehsani AA, Slatopolsky E, Lee W, Birge SJ (1988) Weight-bearing exercise training and lumbar bone mineral content in postmenopausal women. Ann Intern Med 108:824–828
46. Snow-Harter C, Bouzsein ML, Lewis BT, Carter DR, Marcus R (1992) Effects of resistance and endurance exercise on bone mineral status of young women: a randomized exercise intervention trial. J Bone Miner Res 7:761–769
47. Frost HM (1999) Joint anatomy, design, and arthroses: insights of the Utah paradigm. Anat Rec 255:162–174
48. Pitsillides AA, Rawlinson SC, Mosley JR, Lanyon LE (1999) Bone's early responses to mechanical loading differ in distinct genetic strains of chick: selection for enhanced growth reduces skeletal adaptability. J Bone Miner Res 14:980–987
49. Noble BS, Stevens H, Mosley JR, Pitsillides AA, Reeve J, Lanyon L (1997) Bone loading changes the number and distribution of apoptotic osteocytes in cortical bone. J Bone Miner Res 12:S111
50. Hill P, Tumber A, Meikle M (1998) Multiple extracellular signals promote osteoblast survival and apoptosis. Endocrinology 138:3849–3858
51. Herrler A, Krusche CA, Beier HM (1998) Insulin and insulin-like growth factor-I promote rabbit blastocyst development and prevent apoptosis. Biol Reprod 59:1302–1310

JOURNAL OF BONE AND MINERAL RESEARCH
Volume 15, Number 6, 2000

Genetic Regulation of Cortical and Trabecular Bone Strength and Microstructure in Inbred Strains of Mice

CHARLES H. TURNER,[1] YEOU-FANG HSIEH,[1] RALPH MÜLLER,[2] MARY L. BOUXSEIN,[2] DAVID J. BAYLINK,[3] CLIFFORD J. ROSEN,[4] MARC D. GRYNPAS,[5] LEAH RAE DONAHUE,[6] and WESLEY G. BEAMER[6]

ABSTRACT

The inbred strains of mice C57BL/6J (B6) and C3H/HeJ (C3H) have very different femoral peak bone densities and may serve as models for studying the genetic regulation of bone mass. Our objective was to further define the bone biomechanics and microstructure of these two inbred strains. Microarchitecture of the proximal femur, femoral midshaft, and lumbar vertebrae were evaluated in three dimensions using micro-computed tomography (μCT) with an isotropic voxel size of 17 μm. Mineralization of the distal femur was determined using quantitative back-scatter electron (BSE) imaging. μCT images suggested that C3H mice had thicker femoral and vertebral cortices compared with B6. The C3H bone tissue also was more highly mineralized. However, C3H mice had few trabeculae in the vertebral bodies, femoral neck, and greater trochanter. The trabecular number (Tb.N) in the C3H vertebral bodies was about half of that in B6 vertebrae ($2.8^{-1} \pm 0.1$ mm^{-1} vs. $5.1^{-1} \pm 0.2$ mm^{-1}; $p < 0.0001$). The thick, more highly mineralized femoral cortex of C3H mice resulted in greater bending strength of the femoral diaphysis (62.1 ± 1.2N vs. 27.4 ± 0.5N, $p < 0.0001$). In contrast, strengths of the lumbar vertebra were not significantly different between inbred strains ($p = 0.5$), presumably because the thicker cortices were combined with inferior trabecular structure in the vertebrae of C3H mice. These results indicate that C3H mice benefit from alleles that enhance femoral strength but paradoxically are deficient in trabecular bone structure in the lumbar vertebrae. (J Bone Miner Res 2000;15:1126–1131)

Key words: biomechanics, bone density, osteoporosis, genetics

INTRODUCTION

ALTHOUGH MANY environmental factors (i.e., diet and exercise) affect bone accumulation during growth, studies in twins have determined that about 70% of the variability in bone density is genetically based.[1–3] Most researchers have assumed that variation in bone density is influenced by multiple genes, but there may be a set of genes that disproportionately influence peak bone density.[4] Inbred strains of mice make useful models for studies of genetic effects on bone structure. Beamer et al.[5] showed a large variation in the femoral bone mineral content and density among 11 inbred strains of mice. The largest difference was between C3H/HeJ (C3H) with 27.48 mg of

[1]Biomechanics and Biomaterials Research Center, Indiana University, Indianapolis, Indiana, U.S.A.
[2]Orthopedic Biomechanics Laboratory, Beth Israel Deaconess Medical Center and Harvard Medical School, Boston, Massachusetts, U.S.A.
[3]Loma Linda University and Jerry L. Pettis Memorial VA Medical Center, Loma Linda, California, U.S.A.
[4]Maine Center for Osteoporosis Research and Education, Bangor, Maine, U.S.A.
[5]Connective Tissue Research Group, Samuel Lunenfeld Research Institute, Mount Sinai Hospital, Toronto, Canada.
[6]The Jackson Laboratory, Bar Harbor, Maine, U.S.A.

femoral mineral and C57BL/6J (B6) with 18.62 mg. Although the C3H femoral lengths and volumes were very similar to B6, the C3H had substantially thicker cortices. Consequently, the total bone mineral densities (BMDs) of the femora, determined using peripheral quantitative computed tomography (CT), were 0.691 mg/mm^{3}and 0.450 mg/mm^3, respectively, for C3H and B6 females at 4 months of age.

The C3H and B6 mouse strains appear to be very good models for high and low bone mass, respectively. However, it is unclear how the single characteristic of femoral BMD reflects the bone mass at clinically important sites such as the femoral neck and lumbar vertebrae. One might presume that genes that control BMD have equal influence throughout the skeleton. However, this presumption has not been tested directly. Recently, Kline et al.[6] reported the inbred mouse strain DBA/2 had significantly lower whole body areal BMD by dual-energy X-ray absorptiometry than that in B6. Conversely, Beamer et al.[5] reported that femoral volumetric BMD in DBA/2 was significantly greater than that in B6. These contradictory results suggest that differences in phenotypic assessment may complicate studies of the genetic influence on skeletal BMD.

In the current study, we evaluated the bone microstructure and biomechanical properties of several regions of the skeleton in inbred mouse strains B6 and C3H. We hypothesized that for these inbred strains, phenotypic trends in bone structure and strength will vary with anatomic location.

MATERIALS AND METHODS

Animal care

Twenty-five female C3H mice and 25 female B6 mice were raised to 16 weeks of age at The Jackson Laboratory. These mice were group-housed in polycarbonate cages. Water was acidified with HCl to achieve a pH of 2.8–3.2 and was freely available. The diet used for all mice was pasteurized NIH 31 6% fat diet (vitamin and mineral fortified; Purina Mills, St. Louis, MO, U.S.A.) and was freely available. Use of mice in this research project was reviewed and approved by the Institutional Animal Care and Use Committee of The Jackson Laboratory.

Biomechanical tests

We measured bone strength at the midshaft of the femur and at two clinically relevant sites: the femoral neck and the lumbar spine. Femora were tested in three-point bending at room temperature. Load was applied midway between two supports that were 5 mm apart. Load-displacement curves were recorded at a crosshead speed of 0.5 mm/s using a microforce materials testing machine. Data were stored on a microcomputer. Ultimate force (F_u), stiffness (S), and work to failure (U) were calculated from the load-displacement curve as described elsewhere.[7] F_u reflects the strength of the bone, while S reflects the rigidity, and U is the energy necessary to cause a fracture. After the femur was fractured, cortical thickness was measured at the midshaft using digital calipers accurate to 0.01 mm, with a precision of ±0.005 mm (Mitutoyo, Aurora, IL).

L5 vertebrae were dissected free and the posterior elements were removed using a small clipper. The end plates of the vertebral body were cut parallel using a diamond wafering saw (Isomet, Buehler, Lake Bluff, IL, U.S.A.). Mechanical tests were performed in compression using a servohydraulic materials testing machine (810, MTS Corp., Minneapolis, MN, U.S.A.). All tests were done with the specimen submerged in 37°C saline using a displacement rate of 1 mm/s. From the resulting load-displacement curves F_u, S, and U were determined. There was some variation in the specimen height after the vertebral end plates were made parallel. Because stiffness and work to failure are affected by specimen height, these parameters were normalized by dividing U by specimen height and multiplying S by specimen height.

The proximal femora were mounted vertically in aluminum cylinders and fixed in place with cyanacrylate cement. Load was applied to the femoral head until fracture of the femoral neck occurred. Load-displacement curves were recorded at a crosshead speed of 0.5 mm/s using a microforce materials testing machine.

Microcomputed tomography

A subset of intact bone samples (multisegment vertebrae or whole femur) were measured using desktop microcomputed tomography (μCT; μCT 20, Scanco Medical AG, Bassersdorf, Switzerland). A microfocus X-ray tube with a focal spot of 10 μm was used as a source. To perform a measurement, the specimen was mounted on a turntable that could be shifted automatically in the axial direction. Six hundred projections were taken over 216° (180° plus-half the fan angle on either side). A standard convolution-backprojection procedure with a Shepp and Logan filter was used to reconstruct the CT images in 1024 × 1024 pixel matrices. For each sample, a total of 100–200 microtomographic slices, with a slice increment of 17 μm, were acquired. Measurements were stored in three-dimensional (3D) image arrays with an isotropic voxel size of 17 μm. A constrained 3D Gaussian filter was used to suppress partly the noise in the volumes. The bone tissue was segmented from marrow using a global thresholding procedure.[8] In addition to the visual assessment of structural images, morphometric indices were determined from the microtomographic data sets. Cortical and trabecular bone were separated using a semiautomated contour tracking algorithm to detect the outer and inner boundaries of the cortex. In trabecular bone, basic structural metrics including bone volume density (BV/TV), bone surface density (BS/TV), trabecular number (Tb.N), trabecular thickness (Tb.Th), and trabecular spacing (Tb.Sp), were measured in three dimensions using direct 3D morphometry.[9] Previous studies have shown trabecular structural metrics measured using μCT to closely correlate with those measured using standard histomorphometry.[10,11]

TABLE 1. BIOMECHANICAL MEASUREMENTS FOR C57BL/6J (B6) AND C3H/HEJ (C3H) MICE (MEAN ± SEM)

Variable	*B6 (n = 25)*	*C3H (n = 25)*
Femur		
F_u (N)	27.4 ± 0.5	62.1 ± 1.2[a]
S (N/mm)	157 ± 3	258 ± 3[a]
U (mJ)	5.3 ± 0.3	11.7 ± 0.5[a]
Femoral neck		
F_u (N)	19.0 ± 0.5[b]	16.2 ± 0.5
S (N/mm)	90 ± 5	118 ± 3[a]
U (mJ)	2.9 ± 0.2[b]	1.3 ± 0.1
Lumbar vertebra		
F_u (N)	61.2 ± 2.7	63.7 ± 2.5
Normalized S (N)	982 ± 58	1400 ± 81[a]
Normalized U (mJ/mm)	3.6 ± 0.3[b]	2.5 ± 0.2

[a,b] Significantly greater than B6 or C3H, respectively ($p < 0.01$ by unpaired t-test).

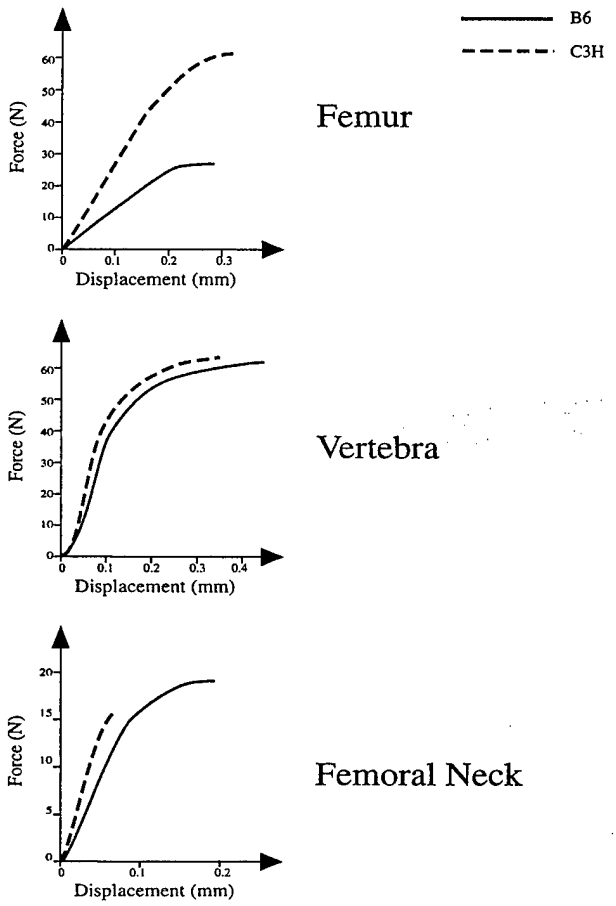

FIG. 1. Average load-displacement curves from mechanical tests at the different skeletal sites.

Quantitative back-scattering electron imaging

A subset of intact distal femoral samples were dehydrated in ascending grades of acetone and infiltrated in ascending grades of plastic/acetone (Spurr). Specimens were then embedded in Spurr resin and placed in a 60°C oven for 48 h to polymerize. The Spurr epoxy blocks were polished to 1 μm finish, mounted on a stub, and carbon coated. Multiple samples mounted on a large specimen holder were examined in a Hitachi S2500 scanning electron microscope (SEM, Hitachi, Japan) operated at 20 kV and at a 15-mm working distance. To collect back-scattering electron (BSE) images, a Link Tetra BSE detector (Oxford Instruments, U.K.) was calibrated of quantitative image analysis using Al, Al_2O_2, and C standards. Changes in beam current were corrected by remeasuring against the Al standard. Images were collected at magnification ×40. Images were separated into six equal bins of increasing intensity (gray levels) representing the mineralization level of the tissue and the percentage area of the specimen cross-section that fell in each bin was recorded. Comparison between the mineralization profiles was done using a cumulative logit function.[12]

Statistical tests

Comparisons between B6 and C3H strains were made using an unpaired t-test implemented by Statview software (Abacus Concepts, Berkeley, CA, U.S.A.).

RESULTS

Data from biomechanical tests are summarized in Table 1 and Fig. 1. C3H mice had greater femoral strength and cortical thickness compared with B6. F_u, S, and U for the femoral shaft were 2.2-fold, 1.6-fold, and 2.2-fold greater than B6, respectively (Table 1). The femoral neck of C3H mice was significantly stiffer than B6 (+31%; $p < 0.01$) but also was significantly weaker (−15%; $p < 0.001$) and absorbed less energy before fracture (−55%; $p < 0.001$). There was no difference between the two strains in vertebral strength (F_u), while stiffness (S) was 43% greater in C3H ($p < 0.01$) but work to failure (U) was 31% lower ($p < 0.01$).

The μCT images showed the substantially thicker femoral cortices in the C3H mice (Fig. 2A). μCT images of the femoral neck showed a thinning of the neck diameter distal to the capsule attachment in the C3H strain (Fig. 2B). This anatomical feature, which clearly weakened the femoral neck in C3H mice, was not present in B6 mice (Fig. 2B). The μCT further showed a lack of 3D trabecular bone structure in the lumbar vertebrae of C3H mice, compared with B6 mice (Fig. 2C). Femoral cortical thickness for C3H mice was 88% greater than in B6 mice, but the vertebral Tb.N was about 2-fold greater in B6 mice (Table 2). This reduction in Tb.N also was reflected in BS density, which was about 2-fold greater in B6 mice, and Tb.Sp, which was about 2-fold greater in C3H mice. Thus, C3H mice had ample cortical bone but were deficient in trabecular bone structure at the sites examined. Also, femoral cortical thickness was well correlated with femoral strength ($r = 0.94$; $p < 0.0001$) but had no correlation with vertebral strength ($r = 0.1$; $p = 0.48$).

The distal femoral bone of C3H mice was more highly mineralized than that from B6 mice ($p < 0.001$). The C3H

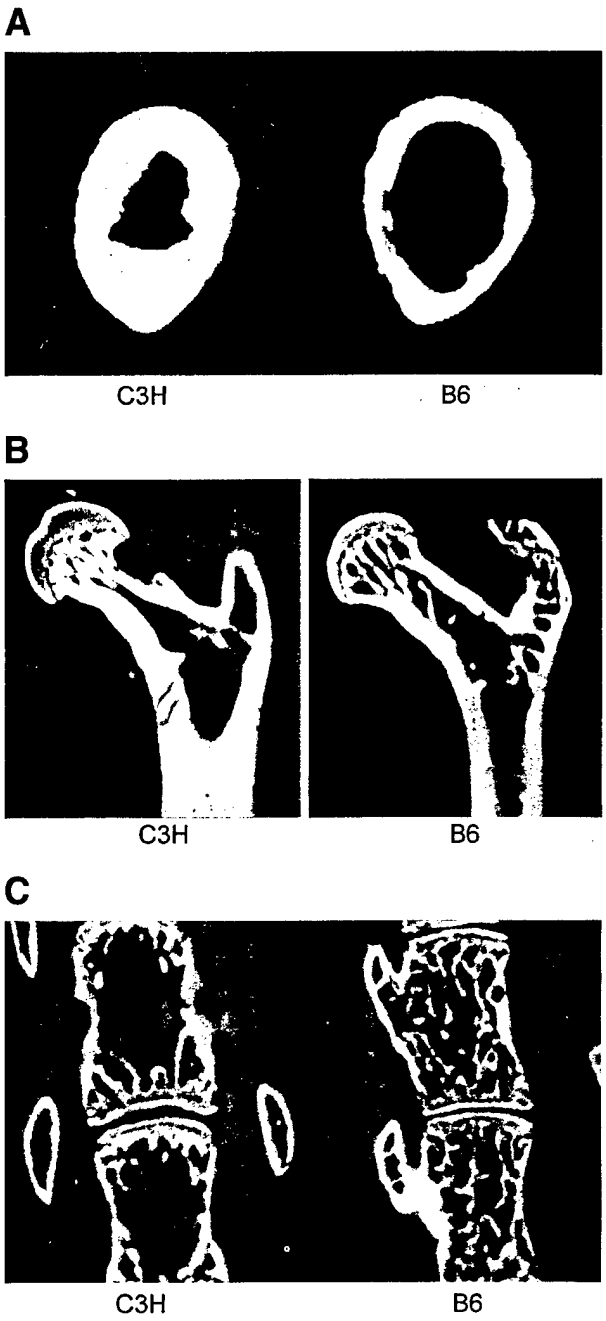

FIG. 2. μCT section of the (A) midshaft of the femur, (B) femoral neck, and (C) L5 vertebral body for C57BL/6J (B6) and C3H/HeJ (C3H) mice. The images were measured in 3D providing a 17-μm isotropic voxel size.

mineralization profile determined by BSE was shifted 15% to the right (higher mineralization; Fig. 3).

DISCUSSION

The results support our hypothesis that the genetic influence on skeletal bone structure and strength is site specific and complex. The enhanced cortical structure in C3H bone was coupled with inferior trabecular structure in the lumbar spine and proximal femur. It is possible that the C3H mice have a unique combination of alleles for improved cortical bone and impaired trabecular bone. Perhaps C3H mice have a defect in endochondral ossification so there is a failure of the normal development of spongiosa. Alternatively, the lack of trabecular bone structure in C3H mice could have resulted through a mechanical adaptation to thick cortices, that is, the enhanced cortical bone structure probably carries the majority of the mechanical load, which could cause a stress shielding effect and subsequent resorption of the trabecular bone. Further studies of the early development of trabecular bone structure in C3H and B6 mice are needed to provide more definitive conclusions about the biological mechanism for the skeletal heterogeneity. Regardless of mechanism, it is clear that the observation of enhanced

TABLE 2. MORPHOLOGICAL MEASUREMENTS FOR C57BL/6J (B6) AND C3H/HEJ (C3H) MICE (MEAN ± SEM)

Variable	*B6*	*C3H*
Femur		
Cortical thickness (mm)	0.294 ± 0.005	0.552 ± 0.010[a]
Length (mm)	16.13 ± 0.06	16.01 ± 0.05
Lumbar vertebra		
BV/TV (%)	24.1 ± 1.3[b]	16.0 ± 1.0
BS/TV (mm^{-1})	8.5 ± 0.2[b]	4.4 ± 0.2
Tb.N (mm^{-1})	5.1 ± 0.2[b]	2.8 ± 0.1
Tb.Th (μm)	61 ± 2	69 ± 4
Tb.Sp (μm)	199 ± 9	388 ± 11[a]

[a,b] Significantly greater than B6 or C3H, respectively ($p < 0.01$ by unpaired t-test).

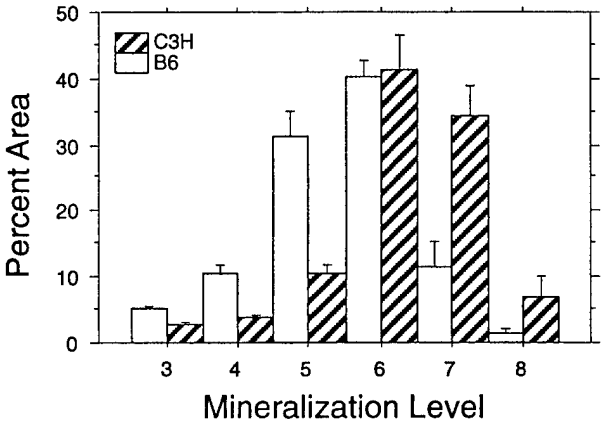

FIG. 3. Mineralization of the femoral cortical bone from C57BL/6J (B6) and C3H/HeJ (C3H) mice determined using quantitative BSE imaging. BSE images were separated into six equal bins of increasing intensity (gray levels) representing the mineralization level of the tissue and the percentage area of the specimen cross-section that fell in each bin was recorded to create a mineralization profile. The shift to the right of the C3H data indicates a significant increase in mineralization.

femoral BMD does not necessarily imply improved bone strength at clinically relevant sites. This was particularly evident for the femoral neck of C3H mice for which the mechanical properties clearly were inferior to B6 although C3H has greater femoral BMD.[5] The reason for this discrepancy appears to be an anatomical feature in the distal region of the C3H femoral neck. The C3H neck diameter distal to the capsule attachment was reduced greatly, compared with B6, resulting in a weakened structure. In addition, there was no correlation between the femoral cortical thickness and the vertebral strength, suggesting that femoral BMD is not related to vertebral mechanical properties. These findings suggest that the genes affecting BMD at a given skeletal site may not exert the most important regulation over bone strength or fragility at other skeletal sites.

An interesting finding of this study was the relative genetic influences of cortical and trabecular bone structure. The skeleton of the C3H mice seemed to be made up predominantly of cortical bone, whereas the B6 mice had a more typical balance of trabecular and cortical bone volume. As a result, C3H mice had superior mechanical properties of the femoral midshaft, which is predominantly cortical bone, yet did not have greater vertebral bone strength although the C3H vertebral stiffness was greater. In fact, the vertebral properties of C3H mice could be considered inferior to B6 because of the reduced work to fracture. This finding suggests that the C3H vertebral bone structure was more brittle. Consequently, it may be advantageous mechanically to have a greater proportion of trabecular bone mass in vertebral bodies because this increases the work to fracture, thus reducing vertebral fragility, and reduces vertebral stiffness. Also, load distribution through trabecular bone may allow more efficient stress transfer to the soft vertebral discs and consequently throughout the whole spine.

This study employed a relatively new and powerful μCT imaging technique. In fact, this represents the first use of this technique for analysis of inbred mouse strains. The results were very encouraging. The high-resolution images provided structural explanations for the measured biomechanical properties. This was best illustrated for the femoral neck, where the observation of a narrowing of the distal femoral neck explained the inferior C3H biomechanical properties. The μCT images of the C3H lumbar vertebrae illustrated a lack of trabecular structure, which explained why the "high bone mass" C3H mice did not have enhanced vertebral strength.

Beamer et al.[5] reported total femoral BMD in C3H mice was significantly greater than in B6 mice. They also reported that the femoral cortical tissue density was over 30% greater in C3H mice, suggesting that C3H cortical bone tissue was more highly mineralized, compared with B6. However, the XCT 960M peripheral quantitative CT instrument used by Beamer et al.[5] has partial volume averaging errors associated with measuring the middiaphyseal endosteal edge. This leads to inaccurate assessment of cortical bone shell volume and cortical density (W.G. Beamer and J. Wergedal, unpublished results, 1999). Our new findings using BSE, show that C3H femoral bone tissue is 15% more highly mineralized compared with B6. Consequently, the increased femoral BMD in C3H mice results from the combination of increased cortical thickness and increased mineralization.

In summary, the results from this study suggest the following:

(1) The elevated femoral cortical thickness in the C3H mice resulted in superior mechanical properties of the femoral shaft.
(2) The improved femoral cortical thickness, mineralization, and strength in C3H mice was combined with inferior vertebral trabecular bone microstructure. Thus, strength of the lumbar vertebrae, a predominantly trabecular bone site, was similar in C3H mice and B6 mice.

In addition, we found a difference in femoral neck strength that mainly was caused by an anatomical feature in the C3H femoral neck, rather than differences in bone mass between the strains.

ACKNOWLEDGMENTS

The authors thank Douglas Holmyard for technical assistance with the BSE imaging. This work was supported in part by the U.S. Public Health Service (USPHS) National Institutes of Health grants AR43618 (W.G.B.) and AR43730 (C.H.T.) and by the U.S. Army grant DAMD17–96-1–6306 (D.J.B.).

REFERENCES

1. Pocock NA, Eisman JA, Hopper JL, Yeates MG, Sambrook PN, Eberl S 1987 Genetic determinants of bone mass in adults: A twin study. J Clin Invest **80:**706–710.
2. Slemenda CW, Christian JC, Williams CJ, Norton JA, Johnston CC 1991 Genetic determinants of bone mass in adult women: A reevaluation of the twin model and the potential importance of gene interaction on heritability estimates. J Bone Miner Res **6:**561–567.
3. Smith DM, Nance WE, Kang KW, Christian JC, Johnston CC Jr 1973 Genetic factors in determining bone mass. J Clin Invest **52:**2800–2808.
4. Rogers J, Mahaney MC, Beamer WG, Donahue LR, Rosen CJ 1997 Beyond one gene-one disease: Alternative strategies for deciphering genetic determinants of osteoporosis. Calcif Tissue Int **60:**225–228.
5. Beamer WG, Donahue LR, Rosen CJ, Baylink DJ 1996 Genetic variability in adult bone density among inbred strains of mice. Bone **18:**397–403.
6. Klein RF, Mitchell SR, Phillips TJ, Belknap JK, Orwoll ES 1998 Quantitative trait loci affecting peak bone mineral density in mice. J Bone Miner Res **13:**1648–1656.
7. Turner CH, Burr DB 1993 Basic biomechanical measurements of bone: A tutorial. Bone **14:**595–608.
8. Müller R, Rüegsegger P Micro-tomographic imaging for the nondestructive evaluation of trabecular bone architecture 1997. In: Lowet G, Rüegsegger P, Weinans H, Meunier A (eds.), Bone Research in Biomechanics. IOS Press, Amsterdam, The Netherlands, pp. 61–79.
9. Hildebrand T, Müller R, Laib A, Dequeker J, Rüegsegger P 1999 Direct 3-D morphometric analysis of human cancellous bone: microstructural data from spine, femur, iliac crest, and calcaneus. J Bone Miner Res **14:**1167–1174.

10. Müller R, Van Campenhout H, Van Damme B, Van der Perre G, Dequeker J, Hildebrand T, Rüegsegger P 1998 Morphometric analysis of human bone biopsies: A quantitative structural comparison of histological sections and micro–computed tomography. Bone **23**:59–66.
11. Li XJ, Müller R, Stevens ML, Golden J, Seeherman H, Bouxsein ML 1998 Evaluation of trabecular bone morphometry: Comparison of micro-computed tomography and histomorphometry in the rat proximal tibia. Bone **23**:S635.
12. Bracci PM, Bull SB, Grynpas MD 1998 Analysis of compositional bone density data using log ratio transformations. Biometrics **54**:337–349.

Address reprint requests to:
Charles H. Turner, Ph.D.
Director of Orthopaedic Research
Indiana University
541 Clinical Drive, Room 600
Indianapolis, IN 46202, U.S.A.

Received in original form July 30, 1999; in revised form December 8, 1999; accepted January 12, 2000.

ELSEVIER

Bone Vol. 27, No. 3
September 2000:445–452

Effects of Dietary Calcium Depletion and Repletion on Dynamic Determinants of Tibial Bone Volume in Two Inbred Strains of Mice

Y. KODAMA,[1] N. MIYAKOSHI,[1] T. A. LINKHART,[1,2] J. WERGEDAL,[1,2] A. SRIVASTAVA,[1] W. BEAMER,[3] L. R. DONAHUE,[3] C. ROSEN,[4] D. J. BAYLINK,[1,2] and J. FARLEY[1,2]

[1]*Jerry L. Pettis Memorial Veterans Medical Center, Loma Linda, CA, USA*
[2]*Department of Medicine, Loma Linda University, Loma Linda, CA, USA*
[3]*The Jackson Laboratory, Bar Harbor, ME, USA*
[4]*Maine Center for Osteoporosis Research, St. Joseph Hospital, Bangor, ME, USA*

As an adjunct to our efforts to identify the genes that determine peak bone density, we examined phenotypic differences between two inbred strains of mice, C3H/HeJ (C3H) and C57BL/6J (B6), which are of similar size but differ with respect to peak bone density (e.g., C3H mice have 53% higher femoral bone density than B6 mice). The current studies were intended to compare the skeletal responses of C3H and B6 mice to 2 weeks of dietary calcium (Ca) depletion, followed by 2 weeks of Ca repletion. Initial studies showed that: (a) femur dry weight decreased during Ca depletion in both C3H and B6 mice (by 25% and 19%, respectively, $p < 0.001$) and most of this loss was recovered during Ca repletion; and (b) serum alkaline phosphatase (ALP) activity increased during Ca depletion, in both strains of mice ($p < 0.001$), and returned to normal after Ca repletion. Histological analyses of ground cross sections prepared at the tibiofibular junction showed that Ca-depletion increased medullary area in both C3H and B6 mice (indicating endosteal bone loss, $p < 0.01$), with reversal during Ca repletion. There were no effects of Ca depletion or repletion on periosteal bone growth. Endosteal bone forming surface and endosteal mineral apposition decreased during Ca depletion and increased during repletion in both C3H and B6 mice ($p < 0.05$). Net bone formation decreased during Ca depletion in C3H mice, but not B6 mice ($p < 0.01$), and was normal during Ca repletion in both strains. Endosteal bone resorbing surface and net bone resorption increased during Ca depletion and decreased during repletion in both strains ($p < 0.01$). A supplemental study (of Ca depletion without repletion) confirmed the effects of Ca depletion on femoral dry weight and serum ALP activity ($p < 0.001$ for each). This supplemental study also showed that Ca deficiency increased serum parathyroid hormone (PTH) ($p < 0.05$) and decreased (tibial) cortical bone area and cortical mineral content ($p < 0.05$ to $p < 0.001$) in both strains of mice. Together, these data demonstrate that the skeletal responses to Ca depletion and repletion are, qualitatively, similar in C3H and B6 mice.

Address for correspondence and reprints: Dr. John Farley, c/o Research Service (151), Jerry L. Pettis Memorial Veterans Medical Center, 11201 Benton Street, Loma Linda, CA 92357.

(Bone 27:445–452; 2000)

Key Words: Mouse; Bone density; Genetics; Calcium.

Introduction

Although bone density is influenced by environmental factors, epidemiological studies estimate that 70% of human peak bone density is determined by genetics.[11,15,16,23] To identify the genes responsible for the development of peak bone density, we are conducting a quantitative trait locus (QTL) analysis of two inbred strains of mice, C3H/HeJ (C3H) and C57BL/6J (B6), which differ with respect to peak bone density.[5] C3H mice have higher peak bone density than B6 mice (e.g., a constant 53% higher total femoral bone density between the ages of 4 and 12 months), although their body weights are similar and their bones are of similar external size.[5] To date, our QTL analyses have shown that >70% of the peak bone density difference between these inbred strains of mice is determined by a minimum of five genetic factors.[4,5,9,19,24]

As a supplement to these genetic studies, we are also characterizing the phenotypic differences between the skeletal tissues of the C3H and B6 mice. The goal of these phenotypic studies is to identify mechanistic, strain-specific differences in bone (and/or bone cells), which may reflect the actions of the bone density genes. To date, these studies have revealed: (a) decreased bone resorption in C3H mice; (b) in vitro evidence of fewer osteoclast progenitor cells in femoral bone marrow from C3H mice; and (c) lower levels of IL-6 production by C3H mice—all compared with B6 mice.[2,19] Our histomorphmetric and biochemical analyses have also shown higher rates of bone formation and a greater number of osteoblast progenitor cells in the femurs of C3H mice, compared to B6 mice.[9,24] Finally, our phenotypic studies have shown higher circulating levels of insulin-like growth factor (IGF-I) in C3H mice, as compared with B6 mice.[24] Together, these data suggest that the higher peak bone density in the C3H mice may be a composite consequence of more bone formation and less bone resorption, compared with B6 mice.

Our phenotypic studies of the C3H and B6 mice have also included assessments of the effects of mechanical loading. We found that hindlimb immobilization (by sciatic neurectomy) increased bone resorption and decreased bone formation in the

8756-3282/00/$20.00
PII S8756-3282(00)00340-9

Bone Vol. 27, No. 3
September 2000:445–452

tibiae of B6 mice, but had no effect on resorption, and a much smaller effect on formation, in the tibiae of C3H mice.[17] Additional studies have also revealed strain-specific differences in the skeletal responses of C3H and B6 mice to hormonal and load-related challenges. We have recently reported that increased musculoskeletal loading increased periosteal bone formation in B6 mice, but not C3H mice,[18] and other laboratories similarly have shown that mechanical loading (by external four-point bending) increased bone formation in B6 mice, but not C3H mice.[1]

Together, these data suggest that skeletal metabolism may be less sensitive to perturbations by mechanical and/or metabolic signals in C3H mice, as compared with B6 mice. This leads to the provocative hypothesis that the higher peak bone density in C3H mice, compared with B6 mice, may reflect the effect(s) of genes that determine sensitivities to these presumptive signals. The current studies were intended to extend our understanding of the regulation of bone volume in C3H and B6 mice by assessing the effect(s) of a metabolic challenge—dietary calcium (Ca) deficiency. The anticipated skeletal response to dietary Ca deficiency is increased serum parathyroid hormone (PTH), which affects an increase in endosteal bone resorption and an acute decrease in endosteal bone formation, allowing for a net removal of bone from the endosteal reservoir to compensate for the dietary deficiency.[10,20,21,26] The anticipated response to the restoration of Ca is a reversal of these effects, and the restoration of endosteal bone volume.[10,20] Because these metabolic skeletal responses are believed to be determined by systemic, endocrine factors (e.g., PTH), they are, in that sense, distinct from the local mechanisms that determine the effects of mechanical loading. Therefore, we reasoned that the current studies would allow us to extend our understanding of bone volume regulation in C3H and B6 mice. We elected to study young mice on the presumption that they would be more sensitive to Ca deficiency. As in previous studies of C3H and B6 mice,[17,18] we assessed the skeletal effects of Ca depletion and repletion by measurements of skeletal alkaline phosphatase activity (a presumptive index of the rate of bone formation), in serum and extracts of bone, and by histomorphometric measurements at the tibiofibular junction. Our initial findings were extended in a second protocol, which allowed us to determine the effects of dietary Ca depletion on serum PTH and tibial bone density (measured by peripheral quantitative computed tomography [pQCT]).

Materials and Methods

Animals and Treatments

Female C3H/HeJ (C3H) and C57BL/6J (B6) mice were purchased from the Jackson Laboratory (Bar Harbor, ME). The mice were housed on a 12 h light/dark cycle and fed standard laboratory chow and water (ad libidum) during a 1 week acclimation period, before assignment to a treatment group, as specified in what follows. Serum and tissue samples were collected at the time of killing. Killing of animals was done by CO_2 inhalation followed by decapitation. All protocols were reviewed and approved by the animal studies subcommittee (of the research and development committee) of the Jerry L. Pettis Memorial Veterans Medical Center.

Materials

The Ca-deficient diet (TD95027, <0.01% Ca by weight) and the control diet (TD97191, containing 0.6% Ca by weight) were purchased from Harlan Teklad (Madison, WI). Both diet formulations include 0.4% phosphorus, 17.5% protein (17.4% from casein, 0.1% from corn starch), and 6.3% fat (6% from soybean oil, 0.2% from casein, and 0.1% from corn starch) by weight. P-Nitrophenylphosphate (PNPP), calcein, tetracycline, and other chemicals were purchased from Sigma Co. (St. Louis, MO). Radioimmunoassay (RIA) kits for PTH were purchased from Nichols Institute (San Juan Capistrano, CA).

First Ca-deficiency Study

A total of 100 4-week-old female mice (50 C3H mice and 50 B6 mice) were purchased from the Jackson Laboratory. After 1 week, the mice were randomly assigned to one of the following five treatment groups (n = 10 mice of each strain per group): (1) the basal control group (killed at the start of the study); (2) the 2 week control group, which received the control diet (0.6% Ca) for 2 weeks; (3) the Ca-depletion group, which received the low-Ca diet (0.01% Ca) for 2 weeks; (4) the 4 week control group, which received the control diet (0.6% Ca) for 4 weeks; or (5) the Ca-repletion group, which received the low-Ca diet (0.01% Ca) for 2 weeks, and then the control diet (0.6% Ca) for an additional 2 weeks. Food and water were provided ad libidum. The mice were 5 weeks old at the start of the study and 5, 7, or 9 weeks of age at the end. Except for the basal group, all mice were triple-labeled with calcein, tetracycline, and calcein. The fluorescent labels were injected intraperitoneally 1, 7, and 14 days prior to killing.[3,10,17] Serum was collected for measurement of alkaline phosphatase activity. The left femora were dissected and extracted for measurement of bone-derived alkaline phosphatase and bone dry weight, and the left tibiae were dissected and used for quantitative histomorphometry.

Second Ca-deficiency Study

A total of 104 3-week-old female mice (52 C3H mice and 52 B6 mice) were purchased from the Jackson Laboratory. After 1 week, the mice were randomly assigned to one of the following two treatment groups (n = 26 mice of each strain per group): (1) the 2 week control group, which received the control diet (0.6% Ca) for 2 weeks; or (2) the Ca-depletion group, which received the low-Ca diet (0.01% Ca) for 2 weeks. These mice were 4 weeks old at the start of the study and 6 weeks of age at the end. Serum was collected for measurement of alkaline phosphatase activity and PTH. The right femora were dissected for preparation of osteoclasts from marrow cells. The left femora were dissected and extracted for measurement of alkaline phosphatase and bone dry weight. The left tibiae were used for absorptiometric measurements of density (at the tibiofibular junction).

Histomorphometry

In the first Ca-deficiency study, the left tibia from each mouse (except for the basal control group) was used for histomorphometry. Undecalcified ground cross sections (30 μm thick) were prepared at the tibiofibular junction for histological measurements of endosteal forming surface, mineral apposition rate (MAR), and endosteal bone formation. This method was selected because it was fast (i.e., compared with procedures required for the preparation and analysis of thin sections—decalcification, fixation, embedding, staining, etc.) and because it had been applied in previous studies with rats[3] and with mice.[2,17,18] This method allows measurements of medullary area and both forming and resorbing surfaces, and was, therefore, sufficient for the purpose of our studies. From the ground sections, we determined total bone area (B.Ar; i.e., total cross-sectional area within the periosteal perimeter) and total medullary area (Ma.Ar). We also measured the endosteal bone forming perimeter as the absolute

Table 1. First Ca-deficiency study: Effects of depletion/repletion on femoral dry weight

Mouse strain	Time	Femoral dry weight (mg)		Significance
		Control	Depletion-repletion	
B6	2 weeks (Ca depletion)	30.4 ± 0.2	24.8 ± 0.5	$p < 0.001$
B6	4 weeks (Ca depletion/repletion)	35.6 ± 0.6	33.7 ± 0.5	n.s.
C3H	2 weeks (Ca depletion)	30.5 ± 1.0	22.9 ± 1.1	$p < 0.001$
C3H	4 weeks (Ca depletion/repletion)	37.0 ± 2.8	34.1 ± 0.8	n.s.

Control mice received the normal Ca diet (0.6% Ca) for 2 or 4 weeks and treated mice received either the low-Ca diet (0.01% Ca) for 2 weeks or the low-Ca diet for 2 weeks followed by the normal Ca diet for 4 weeks. Data shown as mean ± SEM (n = 8–10). At the beginning of the study period (i.e., the 0 week basal controls), femur dry weight averaged 21.65 ± 0.78 and 19.41 ± 0.54 mg for B6 and C3H mice, respectively ($p < 0.05$ by one-way ANOVA). Significance indicates effect of treatment (i.e., effects of Ca depletion and repletion, as determined by one-way ANOVA). n.s. indicates no significance ($p > 0.05$). Two-way ANOVA indicates an overall effect of treatment ($p < 0.001$), but not mouse strain, on bone dry weight. Two-way ANOVA also showed a significant effect of time ($p < 0.001$) and mouse strain ($p < 0.02$) on bone dry weight in normal Ca controls (i.e., at 0, 2, and 4 weeks).

length of the noneroded, single-labeled perimeter (sL.Pm) and as the ratio of noneroded, single-labeled perimeter to total endosteal perimeter (sL.Pm/B.Pm). Endosteal bone resorbing perimeter was determined as the absolute length of eroded surface (E.Pm) and as the ratio of eroded perimeter to total endosteal perimeter (E.Pm/B.Pm). The MAR was calculated as the mean distance between fluorescent labels, divided by the interval (i.e., in days) between them. Net endosteal bone resorption was calculated as the difference between the observed changes in medullary area and net bone formation.[3] Our measurements were focused on the endosteal surfaces, because the skeletal mineral reservoir, which is accessed to compensate for dietary Ca deficiency, is primarily endosteal.[10] Histomorphometric indices were based on nomenclature recommended by the American Society of Bone and Mineral Research,[22] and histomorphometric measurements were made using the OsteoMeasure system (OsteoMetrics, Inc., Atlanta, GA). The methods related to the preparation and measurement of ground cross sections of bone at the tibiofibular junction (along with relevant line drawings and photographs) have been detailed in previous studies.[3,17] These procedures were only applied to tibiae obtained in the first Ca-deficiency study.

Measurement of Tibial Mineral Content

Cortical mineral content was measured in isolated tibiae, by pQCT (at the tibiofibular junction), using a Stratec XCT 960M (Normald, Fort Atkinson, WI) and the Stratec XMICE software. This program calculates cortical bone area as the cross-sectional region between the endosteal and periosteal perimeters and cortical mineral content as the density within that area. The machine was calibrated daily. Similar methods were used (with different equipment) in our previous studies of bone density in C3H and B6 mice.[2,5,24] This procedure was only applied to tibiae obtained in the second Ca-deficiency study.

Extraction of Femora

As in previous studies,[9,12] the left femora of each mouse was freed of adherent tissue, cut near the midshaft, and incubated overnight in phosphate-buffered saline containing 0.01% azide at 4°C (1.5 mL/bone) to remove marrow and contaminating serum. Each bone was transferred to 1.5 mL of 25 mmol/L $NaHCO_3$ (pH 7.4) containing 0.01% azide and 0.01% Triton X-100 for a 72 h extraction at 4°C. Each extract was centrifuged to remove insoluble material and the extracted bones were dehydrated (24 h in 70% ethanol, 1 mL/bone at 37°C), then dried (18 h at 37°C) for measurement of dry weight using a Cahn microbalance (Model 7500, Cahn Instruments, Cerritos, CA). This procedure was applied to femora obtained in both the first and second Ca-deficiency studies.

Measurement of ALP Activity in Serum and Bone Extract

As in our previous studies,[9,13,24] ALP activity was measured by time-dependent formation of *p*-nitrophenolate from PNPP (i.e., increased absorption of light at 405 nm) in alkaline solution, using a microtiter-plate spectrophotometer (Model EAR400/340AT, Labinstruments, Vienna, Austria). Reactions were initi-

Table 2. First Ca-deficiency study: Effects of depletion/repletion on alkaline phosphatase (ALP) activity

Treatment group	B6 mice		C3H mice	
	Serum ALP	Bone extract ALP	Serum ALP	Bone extract ALP
Baseline control	59.6 ± 6.4	2.58 ± 0.16	83.7 ± 7.5[a]	2.45 ± 0.11
2 week control	29.9 ± 1.8	2.10 ± 0.17	32.7 ± 1.5	2.11 ± 0.08
Ca depletion	48.4 ± 3.3[d]	2.01 ± 0.14	40.2 ± 1.6[a,d]	2.83 ± 0.17[a,c]
4 week control	24.1 ± 1.2	1.55 ± 0.16	27.9 ± 2.0	1.36 ± 0.08
Ca repletion	27.5 ± 1.6	1.23 ± 0.08	28.0 ± 2.3	2.00 ± 0.14[b,c]

All data expressed as mean ± SEM (n = 8–10). Serum ALP reported as milliunits per milliliter, and bone ALP as milliunits per milligram dry weight of femur. Two-way ANOVA shows significant effects of mouse strain and treatment on both serum and bone extract ALP activities, $p < 0.001$ for each.
[a]Significant difference, by one-way ANOVA, compared with B6 mice at $p < 0.05$, and at [b]$p < 0.005$.
[c]Significant difference (by one-way ANOVA), compared with normal Ca diet control group of the same age and mouse strain (i.e., an effect of treatment) at $p < 0.05$, and at [d]$p < 0.001$.

Bone Vol. 27, No. 3
September 2000:445–452

Table 3. First Ca-deficiency study: Effects of Ca depletion/repletion on endosteal mineral apposition rate (MAR) and medullary area

Mouse strain	Time	Endosteal MAR (μm/day)		Medullary area (mm^2)	
		Control	Depletion-repletion	Control	Depletion-repletion
B6	2 weeks	1.49 ± 0.10	1.50 ± 0.14	0.433 ± 0.018	0.493 ± 0.008[a]
B6	4 weeks	1.44 ± 0.11	1.91 ± 0.14[a]	0.420 ± 0.014	0.454 ± 0.021
C3H	2 weeks	2.69 ± 0.14[c]	3.16 ± 0.20[c]	0.253 ± 0.007[c]	0.378 ± 0.013[b,c]
C3H	4 weeks	2.73 ± 0.13[c]	3.18 ± 0.12[a,c]	0.231 ± 0.001[c]	0.279 ± 0.012[a,c]

Medullary area and endosteal MAR measured in ground cross sections of tibiae prepared at the tibiofibular junction. Control mice received the normal Ca diet (0.6% Ca) for 2 or 4 weeks and treated mice received either the low-Ca diet (0.01% Ca) for 2 weeks or the low-Ca diet for 2 weeks followed by the normal Ca diet for 4 weeks. All data expressed as mean ± SEM (n = 8–10).

[a]Effect of treatment (i.e., compared with control mice of same strain at the same time, by one-way ANOVA) at $p < 0.01$, and at [b] $p < 0.001$.

[c]Difference compared with B6 mice (i.e., at the same time and receiving the same treatment, by one-way ANOVA) at $p < 0.001$.

ated by the addition of 0.005–0.025 mL of serum or bone extract, to a total reaction volume of 0.3 mL (in 96-place microtiter plate wells) containing 10 mmol/L PNPP, 1 mmol/L $MgCl_2$, and 150 mmol/L carbonate buffer (pH 10.3). ALP activity was calculated as milliunits per milliliter of serum and milliunits per milligram dry weight of bone, where 1 unit is defined by the conversion of 1 μmol of substrate to product per minute at room temperature (25°C). This procedure was applied to serum and femoral extracts obtained in both the first and second Ca-deficiency studies.

Measurement of PTH in Serum

PTH was measured, in the second Ca-deficiency study, using a commercial kit (Nichols Institute), according to the manufacturer's instructions. Aliquots of serum—0.050 mL serum from each of four mice—were pooled to produce six different (aggregate) samples from the 26 mice in each of the four treatment groups (i.e., two groups for each strain of mice). Although this assay was developed for use in rats, the antibodies are cross reactive with mouse PTH, and the kit has been applied successfully to previous studies of mouse PTH.[7,14] This procedure was only applied to serum obtained in the second Ca-deficiency study.

Statistical Analysis of Data

All data are presented as the average of replicates, usually as mean ± SEM. Analytical methods included analysis of variance (one-way and two-way analysis of variance [ANOVA]), using SYSTAT statistical software (Systat, Inc., Evanston, IL).

Results

First Ca-deficiency Study

As shown in **Table 1**, 2 weeks of Ca depletion decreased femoral dry weight in both the C3H and B6 mice (i.e., compared with the normal dietary Ca control mice of each strain). Two weeks of Ca repletion was sufficient to correct this deficit. These observations suggest a net loss of bone from the femur during Ca depletion with bone volume recovery, during Ca repletion.*

The results of our ALP assays are summarized in **Table 2**. The baseline and normal dietary Ca control groups revealed that the C3H mice had higher serum levels of ALP activity than the B6 mice, at 5 weeks of age, and that serum ALP activity decreased with age in the control mice of both strains. The 2 weeks of Ca depletion resulted in higher levels of serum ALP activity in both the C3H and B6 mice (compared to the 2 week controls), and these values returned to normal (i.e., to levels seen in untreated controls) during the subsequent 2 weeks of Ca repletion. Our measurements of ALP activity in femoral bone extracts showed age-dependent decreases in ALP activity in the control mice of both strains. Femoral extract ALP activity (i.e., milliunits per milligram dry weight of bone) was increased by Ca depletion, and remained increased after 2 weeks of Ca repletion in the C3H mice, but not the B6 mice.†

Our histological analyses of ground cross sections (30 μm thick) prepared at the tibiofibular junction) showed that neither Ca depletion nor repletion had any effect on total cross-sectional area in either C3H or B6 mice. Total bone area increased in the C3H mice during the experiment (i.e., with growth) from 0.859 ± 0.026 mm^2 in the basal control to 1.056 ± 0.020 and 1.073 ± 0.017 mm^2 after 2 and 4 weeks, respectively. Total bone area increased in the B6 mice, from 0.960 ± 0.015 mm^2 in the basal control, to 1.062 ± 0.024 and 1.100 ± 0.020 mm^2 after 2 and 4 weeks, respectively.

*Although femoral dry weights did not differ between the C3H and B6 mice, at 2 weeks or at 4 weeks, they differed at the basal timepoint (i.e., an 11.5% higher dry weight for C3H as compared with B6, femora). Furthermore, two-way ANOVA of the data from the normal Ca controls (i.e., at 0, 2, and 4 weeks) showed a significant effect of mouse strain—a higher dry weight for the C3H bones. These findings were consistent with previous data[9] and with the presumption that femoral dry weight reflects total femoral mineral content and total femoral density (i.e., total mineral/total volume). Both total femoral mineral content and total femoral density are maximal and, relatively constant, in C3H and B6 mice (i.e., at a ratio of, about 1.5:1) between 4 and 12 months of age.[5]

†The apparent discrepancy between serum ALP and bone extract ALP in Table 2 is, in part, a consequence of the expression of bone extract ALP as milliunits per milligram dry weight of bone. In the normal Ca controls (i.e., at 0, 2, and 4 weeks), serum ALP is higher in C3H mice, as compared with B6 mice ($p < 0.005$ by two-way ANOVA). This is consistent with previous data.[9] Although bone extract ALP/unit bone dry weight did not show a similar difference, both ALP specific activity (ALP/mg protein) and total ALP/bone did ($p < 0.05$ for each, by two-way ANOVA, data not shown). Again, this was consistent with previous studies, which had also demonstrated a loose correlation ($r = 0.45$, $p < 0.002$) between ALP activities in serum and bone extracts.[9] We should also bear in mind that serum ALP reflects the net contribution of the entire skeleton (which may differ from the femora), as well as lesser contributions from the liver and intestine.

Table 4. First Ca-deficiency study: Effects of Ca-depletion/repletion on endosteal bone resorption and formation

Mouse strain	Time	Net resorption ($mm^2 \times 10^3$)		Net formation ($mm^2 \times 10^3$)	
		Control	Depletion-repletion	Control	Depletion-repletion
B6	2 weeks	12.3 ± 15.1	68.4 ± 9.5[a]	18.0 ± 1.8	13.5 ± 2.7
B6	4 weeks	0.4 ± 13.1	31.7 ± 21.5	19.5 ± 1.1	16.8 ± 1.6
C3H	2 weeks	26.0 ± 5.4	132.0 ± 12.6[b,c]	29.6 ± 2.2[c]	10.6 ± 2.6[b]
C3H	4 weeks	4.6 ± 5.5	57.2 ± 11.7[b]	30.4 ± 2.1[c]	35.6 ± 1.6[c]

Net endosteal resorption and formation calculated for ground cross sections of tibiae prepared at the tibiofibular junction. Control mice received the normal Ca diet (0.6% Ca) for 2 or 4 weeks and treated mice received either the low-Ca diet (0.01% Ca) for 2 weeks or the low-Ca diet for 2 weeks followed by the normal Ca diet for 4 weeks. All data expressed as mean ± SEM (n = 8–10). Net bone resorption calculated as the difference between the change in medullary area and net bone formation, during the final 2 week period (i.e., during the depletion or repletion phase for the 2 and 4 week groups, respectively). [a]Effect of treatment at $p < 0.01$ (compared with control group of same mouse strain and same time, by one-way ANOVA), and at [b]$p < 0.001$. [c]Difference compared with B6 mice (same time and treatment, by one-way ANOVA) at $p < 0.01$.

As shown in **Table 3**, 2 weeks of Ca depletion increased medullary area in both the C3H and B6 mice, and this effect was reversed (completely in the B6 mice) during the subsequent period of Ca repletion. Presumably, these changes reflected a net loss of endosteal bone during the 2 week period of dietary Ca deficiency with a compensatory restoration during the repletion period. Medullary area was greater in the B6 mice compared with the C3H mice for all times and treatments ($p < 0.001$ for each).

Our histomorphometric measurements of bone formation indices showed significant effects of Ca depletion and repletion on bone formation in both strains of mice. Endosteal bone forming surface (single-labeled surface) was decreased during Ca depletion and increased during Ca repletion (i.e., compared with untreated controls) in both C3H and B6 mice. These results are shown in **Figure 1**. Endosteal mineral apposition was unchanged during Ca depletion, but increased during Ca repletion in both strains of mice—this is shown in Table 3. Finally, as shown **Table 4**, net endosteal bone formation was decreased (i.e., at our sampling site at the tibiofibular junction) during Ca depletion, in the C3H mice, but not in the B6 mice. (The error involved in calculating net bone formation in our groups of ten mice precluded the possibility of statistical significance for a decrease of <25%.)

Our histomorphometric analyses of bone resorption indices showed effects of Ca depletion and repletion in both strains of mice. As shown in **Figure 2**, the relative length of endosteal resorbing surface (i.e., scalloped surface) was increased during Ca depletion and decreased during Ca repletion, in both C3H and B6 mice. As shown in Table 4, our calculations of net bone resorption (i.e., changes in medullary area less net bone forma-

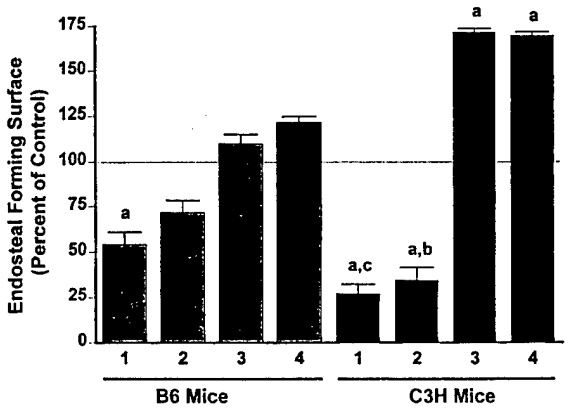

Figure 1. Time-dependent effects of Ca depletion and Ca repletion on endosteal bone forming surface in C3H and B6 Mice. Data from first Ca deficiency study. Length of endosteal labeled perimeter, expressed as percent of normal Ca control, is shown as a function of time (in weeks). Weeks 1 and 2 reflect the period of Ca depletion and weeks 3 and 4 reflect the period of Ca repletion. Data expressed as mean ± SEM (n = 8–10). [a]Difference, compared with control (by one-way ANOVA) at $p < 0.001$. [b]Difference, compared with B6 mice (by one-way ANOVA) at $p < 0.05$, and at [c]$p < 0.001$. Control values averaged 67.00 ± 5.68%, 48.86 ± 7.93%, 91.56 ± 3.40%, and 77.00 ± 6.46% forming surface for B6 mice at 1, 2, 3, and 4 weeks. Control values averaged 55.80 ± 4.01%, 47.00 ± 3.03%, 57.00 ± 3.29%, and 55.30 ± 4.02% forming surface for C3H mice at 1, 2, 3, and 4 weeks. Endosteal perimeter length was 2.42 ± 0.04, 2.57 ± 0.02, 2.30 ± 0.02, and 2.47 ± 0.05 mm for B6 2 week control, depletion, 4 week control, and repletion groups, respectively. Endosteal perimeter length was 1.86 ± 0.03, 2.25 ± 0.04, 1.76 ± 0.02, and 1.95 ± 0.05 mm for C3H 2 week control, depletion, 4 week control, and repletion groups, respectively.

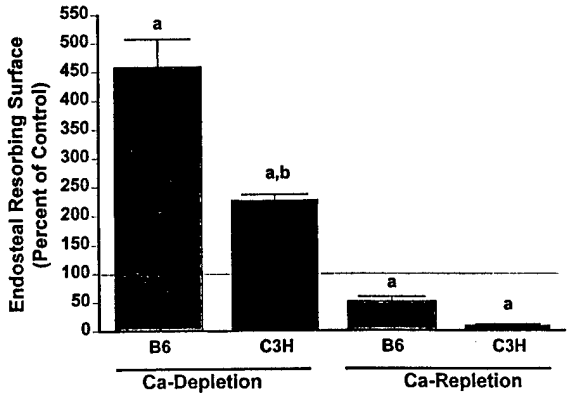

Figure 2. Effects of Ca depletion and Ca repletion on bone resorbing surface in C3H and B6 mice. Data from first Ca-deficiency study. Length of endosteal scalloped (nonlabeled) perimeter shown as percent of control (i.e., normal dietary Ca controls, of the same strain, at 2 weeks and 4 weeks). Data expressed as mean ± SEM (n = 8–10). Endosteal scalloped (i.e., resorbing) surface lengths averaged 11.63 ± 2.09% and 35.20 ± 2.71% of the total endosteal surface for the 2 week B6 and C3H controls, and 4.56 ± 1.65% and 37.30 ± 2.36% for the 4 week B6 and C3H controls, respectively. [a]Difference, compared with control (same strain and time, by one-way ANOVA), at $p < 0.01$. [b]Difference, compared with B6 mice (by one-way ANOVA), at $p < 0.001$. Two-way ANOVA indicates effects of mouse strain ($p < 0.001$) and treatment ($p < 0.01$).

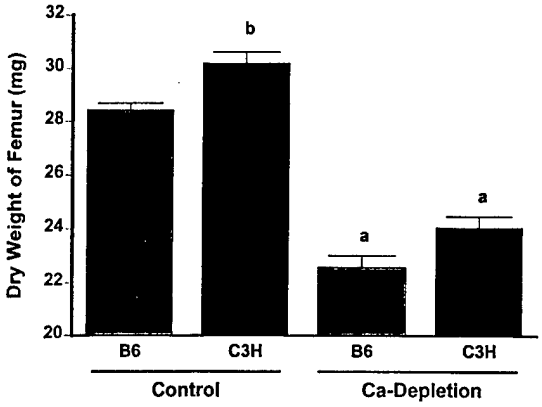

Figure 3. Effects of Ca depletion on femur dry weight in C3H and B6 mice. Data from second Ca-deficiency study. Dry weight of left femora shown as mean ± SEM (n = 26). [a]Difference, compared with control (same strain, by one-way ANOVA), at $p < 0.001$. [b]Difference, compared with B6 mice (same treatment, by one-way ANOVA), at $p < 0.05$. Two-way ANOVA indicates effects of mouse strain and treatment ($p < 0.001$ for each).

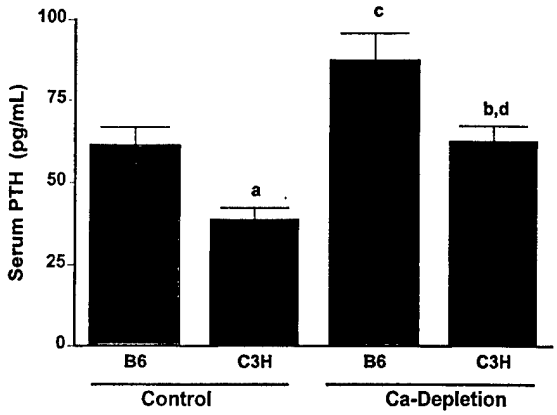

Figure 5. Effects of Ca-depletion on serum PTH. Data from second Ca-deficiency study, using pooled aliquots of serum, as described in *Methods*. Data expressed as mean ± SEM. [a]Difference, compared with B6 mice (same treatment, by one-way ANOVA), at $p < 0.05$, and at [b]$p < 0.03$. [c]Difference, compared with control mice of the same strain (i.e., an effect of treatment, by one-way ANOVA), at $p < 0.02$, and at [d]$p < 0.04$. Two-way ANOVA indicates effects of mouse strain and treatment ($p < 0.001$ for each).

tion) also showed increases during Ca depletion, in both C3H and B6 mice. Net endosteal resorption remained increased after Ca repletion in the C3H mice but not the B6 mice.

There were no effects of Ca depletion or Ca repletion on any measured periosteal parameter in either strain of mice, although the total periosteal forming surface was longer in the 4 week control B6 mice than in the 4 week control C3H mice ($p < 0.01$, data not shown). Periosteal MAR was not affected by Ca depletion or Ca repletion, but was higher in the C3H mice than in the B6 mice at each time and treatment condition ($p < 0.01$ for each, data not shown).

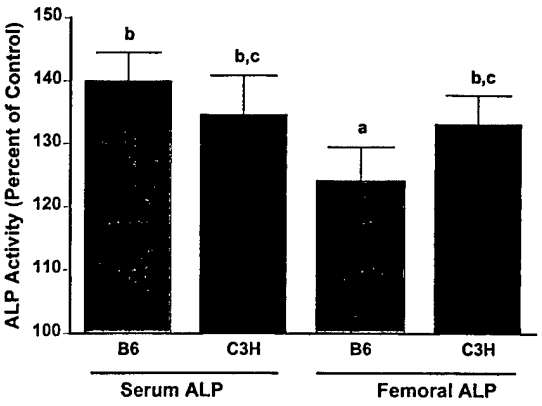

Figure 4. Effects of Ca-depletion on ALP activity in serum and extracts of femora. Data from second Ca-deficiency study. Data expressed as percent of control (i.e., for the same strain of mice). ALP activities calculated as milliunits per milliliter of serum and milliunits per milligram dry weight of bone. [a]Difference, compared with same-strain controls (i.e., an effect of treatment, by one-way ANOVA), at $p < 0.005$; and at [b]$p < 0.001$. [c]Difference, compared with B6 mice (same treatment, by one-way ANOVA), at $p < 0.005$. Two-way ANOVAs indicate effects of mouse strain and treatment on ALP in bone and serum ($p < 0.001$ for each). Control values for serum ALP averaged 165 ± 4 and 135 ± 3 mU/mL for B6 and C3H mice, respectively ($p < 0.01$). Control values for femoral ALP averaged 7.8 ± 0.3 and 8.6 ± 0.4 mU/mg dry weight for B6 and C3H mice, respectively.

Second Ca-deficiency Study

As shown in **Figure 3**, femoral dry weight was greater for the untreated C3H mice (i.e., compared with the untreated B6 mice) and 2 weeks of Ca depletion decreased femoral dry weight in both these inbred strains. This was consistent with the results of our initial study, as was the finding (summarized in **Figure 4**) that Ca depletion increased the serum levels of ALP activity in both strains of mice. Also shown in Figure 4 is the effect of 2 weeks of Ca-depletion to increase the amounts of ALP activity in the femora of both strains of mice.

As summarized in **Figure 5**, 2 weeks of Ca depletion increased serum PTH in both the C3H and B6 mice. These studies also indicated higher circulating levels of PTH in B6, compared with C3H mice, under basal conditions and in response to the Ca-deficient diet.

Table 5 shows the effects of Ca deficiency on densitometric measurements of cortical bone area and cortical mineral content, at the tibiofibular junction. Consistent with our earlier histological findings that 2 weeks of Ca depletion increased medullary area (i.e., at this sampling site—as shown in Table 3), we found that Ca depletion decreased cortical bone area and cortical mineral content in both C3H and B6 mice. Consistent with previous measurements of bone density at other skeletal sites,[5] these studies also revealed that cortical bone area and cortical mineral content were greater in the C3H than in the B6 mice.

Discussion

The results of these studies revealed that the skeletal responses to dietary Ca depletion and repletion are, qualitatively, similar in C3H and B6 mice. Both C3H and B6 mice showed decreases in femoral dry weight, with contrasting increases in the amount of ALP activity in serum, in response to dietary Ca deficiency. These changes were transient, returning to (or toward) the levels seen in untreated controls, after Ca repletion. The decrease in femoral dry weight was interpreted as evidence of a decrease in bone volume, and this inference was supported by our histological and absorptiometric measurements of tibial bone volume and density at the tibiofibular junction. Ca depletion was associated with an increase in medullary area in both C3H and B6 mice, and

Table 5. Second Ca-deficiency study: Effects on tibial cortical mineral content

Parameter	Mouse	Value of indicated parameter		Difference
		Control	Ca deficient	
Cortical bone area	B6	0.535 ± 0.009	0.485 ± 0.010	$p < 0.05$
Cortical mineral content	B6	0.532 ± 0.009	0.449 ± 0.011	$p < 0.005$
Cortical bone area	C3H	0.666 ± 0.015[b]	0.553 ± 0.18[a]	$p < 0.001$
Cortical mineral content	C3H	0.746 ± 0.018[b]	0.570 ± 0.023[b]	$p < 0.001$

Tibial cortical mineral content determined by peripheral quantitative computed tomography (pQCT) at the tibiofibular junction. Control mice received the normal Ca diet (0.6% Ca) for 2 weeks and treated mice received the low-Ca diet (0.01% Ca) for 2 weeks. Data expressed as mean ± SEM (n = 12/group). Difference refers to the comparison of control vs. Ca-deficient mice, with respect to each parameter (i.e., effects of treatment). Two-way ANOVA shows effects of mouse strain and treatment on both cortical area and cortical mineral content, $p < 0.001$ for each.

[a]Difference compared with B6 mice of same age and treatment (by one-way ANOVA) at $p < 0.005$, and at [b]$p < 0.001$.

corresponding decreases in tibial cortical mineral content. Histomorphometry further revealed that the net loss of endosteal bone was a composite consequence of increased bone resorption and decreased bone formation in both C3H and B6 mice. These effects on bone cell activities were associated with (and presumably determined by) the effect of Ca deficiency to increase serum PTH, again, in both strains of mice.

Together, these findings support the general hypothesis that bone volume regulation was similar in C3H and B6 mice, with respect to the metabolic processes involved in accessing the endosteal mineral reservoir for maintenance of normal serum Ca and restoring endosteal bone, when the dietary Ca was returned to normal levels. Although further studies are required to ensure that there are no fundamental defects in the way that C3H mice regulate the number and activity of osteoblasts and osteoclasts in response to PTH and 1,25-dihydroxyvitamin D, the current data suggest there are none. In this regard, it is of interest to compare our findings with those derived from two previous studies of Ca deficiency in these two strains of mice. Those studies[6,8] revealed that the greater cortical bone density of C3H mice was associated with higher serum levels of 1,25-dihydroxyvitamin D (i.e., compared with the levels observed in B6 mice), and with correspondingly higher efficiency of intestinal Ca absorption. Surprisingly, those studies also showed: (a) that low dietary Ca decreased serum 1,25-dihydroxyvitamin D (by about 50%) in both strains; (b) that, at normal (0.4%) dietary Ca, serum PTH was higher in C3H than B6 mice; and (c) that low dietary Ca increased serum PTH in B6 mice, but not C3H mice. Although we did not measure serum 1,25-dihydroxyvitamin D, the results of our studies showed: (a) that serum PTH was lower in C3H, compared with B6 mice, both under normal conditions and in response to a decrease in dietary Ca; and (b) that the decrease in dietary Ca was associated with increases in serum PTH, in both strains of mice. Although it is possible that the differences between the current data and the findings of Chen et al.[6,8] are age- and/or gender-related (i.e., we used 5- and 4-week-old female mice, they used 8-week-old male mice), further studies are required to resolve these issues.

Regarding the mechanism(s) that result in higher peak bone density in C3H mice, as compared with B6 mice, our previous studies suggested that the bones of C3H mice have greater cortical thickness within similar external volumes.[2,5,9,19,24] In other words, the bones of C3H mice have smaller medullary cavities than the bones of B6 mice, and that this appears to be a composite effect of more endosteal bone formation and less endosteal resorption.[2,9,19] Although the biochemical events that result in these differences have yet to be determined, we have obtained several clues. First, we know that B6 bones (e.g., tibiae) show increased periosteal formation in response to mechanical loading under conditions in which C3H bones do not.[1,18] In addition, we learned that skeletal disuse (i.e., unloading) causes bone loss due to increased bone resorption in B6 mice, but not in C3H mice.[17] Finally, previous studies have shown that C3H mice have higher levels of IGF-I in serum and in bone,[24] and higher growth hormone levels.[25] Together, these data are consistent with the general hypothesis that C3H mice may attain (and maintain) higher bone density than B6 mice because of genetic differences in the response to mechanical loading, if that phenomenon is broadened to include its inverse—bone loss in response to unloading.[17] This overview of the data also suggests that IGF-I may be involved in some aspect of the bone density difference between these inbred strains of mice. Although it is of interest to speculate that (at least, some of) the genes associated with the different bone densities in the C3H and B6 mice may reflect IGF-I regulation and/or skeletal responses to mechanical loading and unloading, we cannot dismiss the alternative of genetic differences in other aspects of osteoblast and/or osteoclast function. Further studies—including QTL analyses that are currently in progress[4]—are required to identify the genes and the associated physiological and biochemical mechanisms that account for the higher peak bone density in C3H mice, as compared with B6 mice.

Acknowledgments: The authors thank the secretarial staff of the Loma Linda University Mineral Metabolism Research Unit (which is located in the Jerry L. Pettis Memorial Veterans Medical Center) for assistance in the preparation of this manuscript. These studies were supported by: the National Institutes of Health, Grants AR-43618 and CA-34196 (W.B.); a subcontract from U.S. Army Medical Research Acquisition Activity, Grant DAMD17-96-1-6306 (W.B. and D.J.B.); the Japan–North America Medical Exchange Foundation (Y.K.); the Jackson Laboratory (W.B. and L.R.D.); Loma Linda University (D.J.B., T.L. and J.F.); and the Veterans Administration (D.J.B., T.L., and J.F.).

References

1. Akhter, M. P., Cullen, D. M., Pedersen, E. A., Kimmel, D. B., and Recker, R. R. Bone response to in vivo mechanical loading in two breeds of mice. Calcif Tissue Int 63:442–449; 1998.
2. Baylink, D., Farley, J., Donahue, L., Rosen, C. J., Barr, B., Lee, J. E. S., and Beamer, W. Evidence that high peak bone density is due to decreased resorption not increased formation in a murine model [abstract]. J Bone Miner Res 10(Suppl.):338; 1995.
3. Baylink, D., Stauffer, M., Wergedal, J., and Rich, C. Formation, mineralization,

and resorption of bone in vitamin D-deficient rats. J Clin Invest 49:1122–1129; 1970.

4. Beamer, W. G., Donahue, L. R., Baylink, D. J., and Rosen, C. J. Mapping genes for normal bone density in inbred mice by quantitative trait locus analysis [abstract]. J Bone Miner Res 11(Suppl. 1):S176; 1996.
5. Beamer, W. G., Donahue, L. R., Rosen, C. J., and Baylink, D. J. Genetic variability in adult bone density among inbred strains of mice. Bone 18:397–403; 1996.
6. Chen, C. and Kalu, D. N. Strain differences in calcium absorption, serum 1,25$(OH)_2$D and serum parathyroid hormone in response to dietary calcium restriction in C3H/HeJ and C57BL/6J mice [abstract]. J Bone Miner Res 12(Suppl. 1):S375; 1997.
7. Chen, C., Noland, K. A., and Kalu, D. N. Modulation of intestinal vitamin D receptor by ovariectomy, estrogen and growth hormone. Mech Ageing Devel 99:109–122; 1997.
8. Chen, C., Noland, K. A., and Kalu, D. N. Strain differences in bone density, calcium absorption, and intestinal calcium transport between C3H/HeJ and C57BL/6J mice [abstract]. J Bone Miner Res 12(Suppl. 1):S374; 1997.
9. Dimai, H. P., Linkhart, T. A., Linkhart, S. G., Donahue, L. R., Beamer, W. G., Rosen, C. J., Farley, J. R., and Baylink, D. J. Alkaline phosphatase levels and osteoprogenitor cell numbers suggest bone formation may contribute to peak bone density differences between two inbred strains of mice. Bone 22:211–216; 1998.
10. Drivdahl, R. H., Liu, C. C., and Baylink, D. J. Regulation of bone repletion in rats subjected to varying low-calcium stress. Am J Physiol 246:R190–R196; 1984.
11. Evans, R. A., Marel, G. M., Lancaster, E. K., Kos, S., Evans, M., and Wong, Y. P. Bone mass is low in relatives of osteoporotic patients. Ann Intern Med 109:870–873; 1988.
12. Farley, J. R., Hall, S. L., Herring, S., and Tarbaux, N. M. Two biochemical indices of mice bone formation are increased, in vivo, in response to calcitonin. Calcif Tissue Int 45:214–221; 1989.
13. Farley, J. R., Hall, S. L., Tanner, M. A., and Wegedal, J. E. Specific activity of skeletal alkaline phosphatase in human osteoblast like cell is regulated by phosphate, phosphate ester and phosphate analogs and release of alkaline phosphatase activity is inversely regulated by calcium. J Bone Miner Res 9:497–508; 1994.
14. Jilka, R. L., Weinstein, R. S., Takahashi, K., Parfitt, A. M., and Manolagas, S. C. Linkage of decreased bone mass with impaired osteoblastogenesis in a murine model of accelerated senescence. J Clin Invest 97:1732–1740; 1996.
15. Jouanny, P., Guillemin, F., Kuntz, C., Jaendel, C., and Pourel, J. Environmental and genetic factors affecting bone mass. Arthritis Rheum 38:61–67; 1995.
16. Kelly, P. and Harris, M. Genetic regulation of peak bone mass. Acta Paed Scand 411(Suppl.):24–29; 1995.
17. Kodama, Y., Dimae, H. P., Wergedal, J., Sheng, M., Malpe, R., Kutilek, S., Beamer, W., Donahue, L. R., Rosen, C., Baylink, D. J., and Farley, J. Cortical tibial bone volume in two strains of mice: Effects of sciatic neurectomy and genetic regulation of bone response to mechanical loading. Bone 25:183–190; 1999.
18. Kodama, Y., Umemura, Y., Nagasawa, S., Beamer, W. G., Donahue, L. R., Rosen, C. R., Baylink, D. J., and Farley, J. Exercise and mechanical loading increase periosteal bone formation and whole bone strength in C57BL/6J mice, but not C3H/HeJ mice. Calcif Tissue Int. In press.
19. Linkhart, T., Linkhart, S., Kodama, Y., Farley, J., Dimai, H. P., Wright, K., Wegedal, J., Sheng, M., Beamer, W., Donahue, L. R., Rosen, C., and Baylink, D. J. Osteoclast formation in bone marrow cultures from two inbred strains of mice with different bone densities. J Bone Miner Res 14:39–46; 1999.
20. Liu, C. C., Rader, J. I., Gruber, H., and Baylink, D. J. Acute reduction in osteoclast number during bone resorption. Metab Bone Dis Rel Res 4:201–209; 1982.
21. Murray, E. J. B., Song, M. K., Laird, E. C., and Murray, S. S. Heterogeneity of growth and turnover in the femurs and humeri of calcium-replete and -deficient C57BL/6 and SENCAR mice at sexual maturity. Growth Devel Aging 58:119–133; 1994.
22. Parfitt, A. M., Drezner, M. K., Glorieux, F. H., Kanis, J. A., Malluche, H., Meunier, P. J., Ott, S. M., and Recker, R. R. Bone histomorphometry: Standardization of nomenclature, symbols, and units. Report of the ASMBR Histomorphometry Nomenclature Committee. J Bone Miner Res 2:595–610; 1987.
23. Pocock, N. A., Eisman, J. A., Hooper, J. L., Yeates, M. G., Sambrook, P. N., and Ebert, S. Genetic determinants of bone mass in adults. J Clin Invest 80:706–710; 1987.
24. Rosen, C. J., Dimai, H. P., Verault, D., Donahue, L. R., Beamer, W. G., Farley, J., Linkhart, S., Linkhart, T., Mohan, S., and Baylink, D. J. Circulating and skeletal insulin-like growth factor-I concentrations in two inbred strains of mice with different bone mineral densities. Bone 21:217–223; 1997.
25. Sinha, Y. N., Vlahakis, G., and Vanlerlaan, W. P. Serum, pituitary and urine concentrations for prolactin and growth hormone in eight strains of mice with varying incidence of mammary tumors. Int J Cancer 24:430–437; 1979.
26. Tanimoto, H., Lau, K. H., Nishimoto, S. K., Wegedal, J. E., and Baylink, D. J. Evaluation of the usefulness of serum phosphatases and osteocalcin as serum markers in a calcium depletion-repletion rat model. Calcif Tissue Int 48:101–110; 1991.

Date Received: January 18, 2000
Date Revised: May 10, 2000
Date Accepted: May 10, 2000

JOURNAL OF BONE AND MINERAL RESEARCH
Volume 16, Number 2, 2001

Postnatal and Pubertal Skeletal Changes Contribute Predominantly to the Differences in Peak Bone Density Between C3H/HeJ and C57BL/6J Mice*

C. RICHMAN,[1] S. KUTILEK,[1] N. MIYAKOSHI,[1] A.K. SRIVASTAVA,[1] W.G. BEAMER,[2] L.R. DONAHUE,[2] C.J. ROSEN,[3] J.E. WERGEDAL,[1] D.J. BAYLINK,[1] and S. MOHAN[1]

ABSTRACT

Previous studies have shown that 60–70% of variance in peak bone density is determined genetically. The higher the peak bone density, the less likely an individual is to eventually develop osteoporosis. Therefore, the amount of bone accrued during postnatal and pubertal growth is an important determining factor in the development of osteoporosis. We evaluated the contribution of skeletal changes before, during, and after puberty to the development of peak bone density in C3H/HeJ (C3H) and C57BL/6J (B6) mice. Volumetric bone density and geometric parameters at the middiaphysis of femora were measured by peripheral quantitative computed tomography (pQCT) from days 7 to 56. Additionally, biochemical markers of bone remodeling in serum and bone extracts were quantified. Both B6 and C3H mice showed similar body and femoral weights. B6 mice had greater middiaphyseal total bone area and thinner cortices than did C3H mice. Within strains, males had thicker cortices than did females. C3H mice accumulated more minerals throughout the study, with the most rapid accumulation occurring postnatally (days 7–23) and during pubertal maturation (days 23–31). C3H mice had higher volumetric bone density as early as day 7, compared with B6 mice. Higher serum insulin-like growth factor I (IGF-I) was present in C3H mice postnatally at day 7 and day 14. Until day 31, B6 male and female mice had significantly higher serum osteocalcin than C3H male and female mice, respectively. Alkaline phosphatase (ALP) was found to be significantly higher in the bone extract of C3H mice compared with B6 mice at day 14. These data are consistent with and support the hypothesis that the greater amount of bone accrued during postnatal and pubertal growth in C3H mice compared with B6 mice may be caused by increased cortical thickness, increased endosteal bone formation, and decreased endosteal bone resorption. (J Bone Miner Res 2001;16:386–397)

Key words: bone density, puberty, insulin-like growth factor I, osteocalcin, C3H/HeJ and C57BL/6J mice

INTRODUCTION

THE RISK of developing senile osteoporosis in men and postmenopausal osteoporosis in women is in large measure determined by the amount of bone mass accumulated during the active growth phases early in life. This accumulation of bone mass determines the peak bone density attained during the third decade of life.[1,2] About 60–70% of variance in peak bone density is determined genetically,[3] and 40–50% of peak bone density is accumulated during puberty.[4] Elucidation of the mechanisms regulating this dramatic increase in skeletal mass during puberty is important in the effort to identify potential preventive or interventive measures that would lower the risk of developing osteoporosis.

*The view, opinions, and/or findings contained in this report are those of the author(s) and should not be construed as a position, policy, decision, or endorsement of the Federal Government or the National Medical Technology Testbed, Inc.

[1]J.L. Pettis Veterans Administration Medical Center and Loma Linda University, Loma Linda, California, USA.
[2]The Jackson Laboratories, Bar Harbor, Maine, USA.
[3]St. Joseph Hospital, Bangor, Maine, USA.

In humans, peak bone density is attained between 20 and 30 years of age.[1,2] The most rapid accumulation in bone mass occurs in postnatal growth, from birth roughly to 3 years of age, and during puberty, from 12 to 18 years of age.[5] This increase in bone mass closely correlates with an increase in body weight and height. Puberty is initiated 2 years earlier in girls than in boys and during this period of pubertal maturation, a sexual dimorphism is established. The pubertal growth spurt lasts roughly 2 years longer in boys than in girls, such that boys are taller, stronger, and exhibit higher peak bone mass than do girls.[6]

The most beneficial period for osteoporosis prevention may be during the rapid growth phases that occur within the first 20 years of life.[7] The attainment of higher peak bone mass during this period should lead to reduced risk for fracture later in life by increasing peak bone mass.

In this study we are particularly interested in the different rates of bone remodeling occurring before, during, and after puberty. In studies comparing bone mass accumulation, Slemenda et al. found that higher peak bone mass in black girls is associated with lower bone turnover during puberty compared with that of white girls.[8] During puberty, a complex series of events occurs that impacts the changes in bone turnover and attainment of peak bone mass, such as periosteal expansion and endosteal contraction, longitudinal growth, modeling-dependent remodeling,[9] and sex hormone–dependent reduction in bone turnover or remodeling.[10] With the development of assays for serum/urine levels of bone formation and resorption markers, the measurement of bone turnover in different conditions of growth or disease becomes possible. During growth and in osteolytic diseases, a high bone turnover rate exists.[11–14]

Studies using mice as a model system have shown that mice, like humans, attain a peak bone density (at 4–6 months of age). Some strains experience age-related bone loss (1 year and older) leading to osteopenia.[15,16] Different strains of inbred mice have been shown to exhibit different peak bone densities[17] and responded differently to ovariectomy.[18] Similar to human studies using monozygotic and dizygotic twins, different strains of inbred mice provide genetically identical animals to dissect out the role of individual genes and their products in the development of a trait or disease. However, unlike the design restraints on sample size and genetic diversity in humans, mice provide a relatively unlimited number of genetically identical subjects. Two inbred strains of mice, C3H/HeJ (C3H) and C57BL/6J (B6), which have the same body size and weight, previously have been shown to have very different peak bone densities.[17,19–21] Therefore, we chose to compare these two strains to study the following: (1) the relative contribution of postnatal (from birth until puberty), pubertal, and postpubertal growth to the final peak bone density of each strain; (2) the differences in bone remodeling between these two strains that may contribute to these different bone densities; (3) the differences in serum level of insulin-like growth factors (IGFs) between these two strains during postnatal, pubertal, and postpubertal growth; and (4) to determine if and when the sexual dimorphism in peak bone mass seen in humans after puberty also is seen in these mice.

MATERIALS AND METHODS

Recombinant human (rh) IGF-I (rhIGF-I) was a gift from Ciba-Geigy (Basel, Switzerland); rhIGF-II was purchased from BACHEM Chemicals (Torrance, CA, USA). Rabbit polyclonal antiserum against IGF-I (kindly provided by L.E. Underwood and J.J Van Wyk) was obtained form the National Hormone and Pituitary Program (Baltimore, MD, USA). Osteocalcin synthetic peptide was obtained from SynPep Corp. (Dublin, CA, USA). Paranitrophenol phosphate was purchased from Fluka (Buchs, Switzerland). All other chemicals were enzyme grade and purchased from Fisher Scientific (Tustin, CA, USA) or Sigma Chemical Co. (St. Louis, MO, USA).

In vivo work

Animals: Inbred C3H and B6 breeder mice were purchased from The Jackson Laboratory (Bar Harbor, ME, USA). On receipt, the mice were allowed to acclimate to the new environment for 7 days and were then mated to produce the pups used in this study.

Animal protocol: The female breeders were housed individually several days before expected parturition and fed a breeders' diet (10% fat content; Harlan Teklad, Placentia, CA, USA). The pups were weaned and weighed on postnatal day 21 using a digital scale (ACCULAB V-600) to the nearest 0.1 g. At weaning, the pups were fed regular rodent chow (4% fat content; Harlan Teklad) and housed 4–5 pups per cage with cages of females alternating with cages of males on each rack to eliminate uneven pheromone distribution. Pubertal maturation in B6 female mice begins when serum estradiol increases on day 26 and vaginal opening occurs by day 31.[22] In humans, puberty starts roughly 2 years later in males than in females and ends later in males than females.[23] We calculated that in mice, this difference would constitute a 2–3 day delay for males compared with females, so that puberty should be completed by day 35 in males. Based on this data, we chose to collect pups at days 7, 14, and 23 (before puberty starts); day 31 (at the end of puberty for the females); day 35 (at the end of puberty for the males); and on days 42, 49, and 56. Pups were killed by CO_2 inhalation (dry ice) followed by decapitation. Whole blood was collected, allowed to clot, and then centrifuged. The serum was skimmed off and stored at −70°C until assayed. The left femur was dissected free of soft tissue keeping the condyles and femoral neck intact. This bone was used for the bone extract assay to determine bone-specific alkaline phosphatase (ALP) activity and bone size data. The right femur and proximal tibia were dissected free and stored in 70% ethanol for volumetric bone density and geometric parameter determination by peripheral quantitative computed tomography (pQCT) using an XCT Research M instrument (Norland Medical Systems, Inc., Fort Atkinson, WI, USA). The experimental procedures performed in this study comply with the National Institutes of Health (NIH) guide for the Care and Use of Laboratory Animals. All animals studies were reviewed and monitored by the Animal Studies Subcommittee at the Jerry L. Pettis Veterans Administration Medical Center (Loma Linda, CA, USA).

Bone densitometry

Volumetric bone density and geometric parameters were determined by pQCT. Previously, pQCT has been validated as a reliable method of determining volumetric bone density and geometric parameters in mice.[17] Routine calibration was performed daily with a defined standard (cone phantom) containing hydroxyapatite embedded in lucite (Norland Medical Systems, Inc.). The voxel size was set at 0.07 mm and a half-millimeter-thick slice was scanned at the middiaphysis. Analysis of the scans was performed using the manufacturer-supplied software program (STRATEC MEDIZINTECHNIK GMBH Bone Density Software, version 5.40C; Norland Medical Systems). Volumetric bone density and geometric parameters were estimated with Loop analysis. For cortical analysis, the threshold was set at 350 mg/cm^3 for the 23- to 56-day-old mice. The 7- and 14-day-old mice had lower bone densities than did the 23- to 56-day-old mice and could not be measured at the 350 mg/cm^3 threshold. Therefore, we used a threshold of 150 mg/cm^3 for the 7- to 23-day-old mice in the cortical analysis. For cancellous analysis, the outer threshold was set at 250 mg/cm^3 and the inner threshold was set at 300 mg/cm^3 for 23- to 56-day-old mice, and 125 mg/cm^3 and 150 mg/cm^3 for 7-to 14-day-old mice, respectively. Values for 7- and 14-day-old mice may be less accurate than for the older mice because of the lower threshold used, but we have included them in this article because they show the rapid growth that occurs during the postnatal period (days 7–23).

Biochemical assays

Femoral bone extraction: The freshly dissected left femora were rinsed in 1× phosphate-buffered saline (PBS) for 24 h at 4°C and then transferred to 0.01% Triton X-100 (Sigma Chemicals) for 72 h at 4°C to extract the membrane bound ALP from the osteoblast cell surfaces. Bone-specific ALP activity and total protein content were determined for this extract. The femora were dehydrated in 75% ethanol and then allowed to dry out completely at 37°C. Once dry, the femoral length was measured to the nearest 0.01 mm using a caliper (Dial Caliper; Mitutoyo Corp., Japan) and the bones were weighed to the nearest 0.01 mg using a balance (Millibalance model 7500, Electrobalance DTL; Cahn Instruments, Inc., Cerritos, CA, USA).

ALP assay of bone extracts: ALP activity of the bone extract was determined using a paranitrophenol phosphate substrate as described previously.[24]

Protein assay: The total protein content of the bone extract was determined using Bradford assay (BioRad, Hercules, CA, USA)

Osteocalcin assay: Osteocalcin levels in serum were measured by specific radioimmunoassay (RIA) that was previously validated for mice. The mouse osteocalcin RIA had a CV of less than 8%.[25]

Separation of IGF binding proteins from IGFs: Because IGF binding proteins (IGFBPs) produce artifacts in IGF RIAs, complete separation of the IGFBPs from the IGFs is necessary in order for the IGF determinations to be valid. We have used previously validated BioSpin protocol to separate IGFs from IGFBPs.[26]

IGF-I RIA: IGF-I was measured by specific RIA as previously described.[27] The cross-reactivity of IGF-II in the IGF-I RIA was less than 0.5%. The sensitivity of the IGF-I RIA was less than 50 ng/liter; the intra- and interassay CVs were less than 10%.

IGF-II RIA: IGF-II was measured by specific RIA as previously described.[27] The cross-reactivity of IGF-I in the IGF-II RIA was less than 2%. The sensitivity of the IGF-II RIA was 0.1 μg/liter; the intra- and interassay CVs were less than 10%.

Statistics

Results are reported as mean ± SD for 7–9 animals per group and compared by two-tailed three-way analysis of variance (ANOVA) and Newman–Keuls post hoc test using commercially available statistical software (STATISTICA; StatSoft, Inc., Tulsa, OK, USA). Results were considered significantly different for $p < 0.05$.

RESULTS

The pattern of growth in body weight, femur weight, size, and mineral density have been determined for C3H and B6 mice for the postnatal, pubertal, and postpubertal growth periods. Although the general pattern of growth was similar for the two strains of mice, there were differences in femur bone growth. These differences were statistically significant as determined by three-way ANOVA (strain, sex, and day). The results of further analysis with Newman–Keuls post hoc testing are given in the tables and the figure legends.

Physical measurements

Body weight: Weight gain in all the mice was increased roughly 3-fold over day 7 during postnatal growth (days 7–23). There was no difference in body weights between females of C3H and B6 mice at any time points. Male C3H mice were heavier than B6 male mice at day 42 and day 56 (Tables 1 and 2). Within each strain, males gained more weight than females during pubertal growth (in B6, 161% for males and 133% for females; in C3H, 158% for males and 143% for females). Males were heavier than females at day 31 and thereafter for both strains (Tables 1and 2).

Femoral bone weight: The fastest rate of femoral growth was during the postnatal period (days 7–23) when dry femoral weight increased 8-fold in B6 and 7-fold in C3H mice. The C3H bones were significantly heavier than the B6 bones at day 42 and day 49 in male mice and at day 56 in female mice (Tables 1 and 2).

Femoral bone length: Femoral bone length increased more than 2-fold in both strains of mice during postnatal period. Although femora of B6 mice were shorter on day 7, the length increased more than in C3H mice during postnatal growth (days 7–23) so that there was no difference between strains from day 23 (Tables 1 and 2). Within strains, male femoral length was not different from that of females, either during or after puberty.

Middiaphysis geometric parameters

Area: Total area at the middiaphysis of the femur increased 2-fold during postnatal growth (days 7–23) in both

TABLE 1. AGE CHANGES IN MEASURED PARAMETERS FOR MALE C3H AND B6 MICE

Parameter		*Days*							
		7	*14*	*23*	*31*	*35*	*42*	*49*	*56*
Physical parameters									
Body weight (g)	C3H	3.5 ± 0.38	6.3 ± 1.1	11.6 ± 1.0	18.3 ± 2.4†	18.5 ± 2.6†	21.6 ± 2.0*,†	21.9 ± 2.1†	21.1 ± 1.4*,†
	B6	2.8 ± 0.39	7.1 ± 0.5	10.9 ± 0.6	17.5 ± 1.1†	18.2 ± 0.9†	19.2 ± 1.2*,†	20.4 ± 2.1†	22.8 ± 1.0*,†
Femur weight (mg)	C3H	2.2 ± 0.32	6.4 ± 1.4	15.9 ± 1.8	26.7 ± 3.0	29.0 ± 3.9	36.4 ± 2.6*,†	38.7 ± 3.7*,†	40.4 ± 4.4
	B6	1.8 ± 0.25	6.2 ± 0.7	14.5 ± 0.5	23.6 ± 2.4	26.6 ± 1.8	31.7 ± 2.3*,†	34.5 ± 3.7*,†	39.4 ± 2.1†
Femur length (cm)	C3H	0.47 ± 0.03*,†	0.8 ± 0.06	1.08 ± 0.03	1.25 ± 0.04	1.28 ± 0.05	1.36 ± 0.03	1.38 ± 0.05	1.43 ± 0.03
	B6	0.39 ± 0.03*,†	0.76 ± 0.03	1.05 ± 0.02	1.2 ± 0.04	1.27 ± 0.03	1.32 ± 0.04	1.37 ± 0.05	1.42 ± 0.04
Middiaphysis parameters									
Total area (mm^2)	C3H	0.61 ± 0.07	1.08 ± 0.17	1.32 ± 0.1	1.59 ± 0.15	1.65 ± 0.12	1.77 ± 0.11†	1.82 ± 0.13*,†	1.8 ± 0.16*
	B6	0.58 ± 0.06	1.15 ± 0.11	1.45 ± 0.06	1.75 ± 0.07	1.79 ± 0.12	1.9 ± 0.11	1.99 ± 0.17*	2.11 ± 0.11*,†
Cortical area (mm^2)	C3H	0.44 ± 0.06	0.72 ± 0.1	0.72 ± 0.08	0.99 ± 0.11*	1.04 ± 0.12*	1.18 ± 0.07*,†	1.25 ± 0.14*,†	1.26 ± 0.13*,†
	B6	0.35 ± 0.04	0.67 ± 0.1	0.63 ± 0.04	0.85 ± 0.05*,†	0.89 ± 0.06*	0.97 ± 0.04*	1.05 ± 0.1*	1.11 ± 0.05*,†
Total density (mg/cm^3)	C3H	224.6 ± 37.1*	274.6 ± 30.2*	421 ± 27.6*	572.8 ± 41.8*	589.4 ± 60.7*	680.5 ± 12.1*	715.4 ± 66.5*	758.1 ± 48.5*
	B6	159.8 ± 8.4	213 ± 34.8*	244 ± 11.8*	351.3 ± 22.1*	384.2 ± 27.2*	416.3 ± 17.6*	442.2 ± 11.4*	474.4 ± 14.2*
Serum parameters									
IGF-I (ng/ml)	C3H	193 ± 25.4*	293 ± 30.1	246.7 ± 70.6	293.3 ± 70.4	324.3 ± 93.4	390 ± 65	392 ± 73.2	337.7 ± 83
	B6	81.4 ± 22.6*	232 ± 53.5	226.3 ± 36	279.3 ± 51.9	248.3 ± 50.4	288 ± 56.2	258.3 ± 73.7	336.4 ± 51.7
Osteocalcin (ng/ml)	C3H	181 ± 25.4*	329.5 ± 64*,†	403 ± 56.6*	322 ± 51.1*	263 ± 35.3*	274 ± 45.7*	221.9 ± 27	180.6 ± 42.4
	B6	321.1 ± 43.5	422 ± 90.3*,†	496.3 ± 78.8*	471.7 ± 71*	369.8 ± 41.2*	365.6 ± 62.1*	287.1 ± 43.7	229.9 ± 45.3

Values presented as mean ± SD for 7–9 animals.
$^{*}p < 0.05$ versus opposite strain males; $^{\dagger}p < 0.05$ versus same strain females.

TABLE 2. AGE CHANGES IN MEASURED PARAMETERS FOR FEMALE C3H AND B6 MICE

Parameter		*Days* 7	14	23	31	35	42	49	56
Physical parameters									
Body weight (g)	C3H	3.2 ± 0.52	6.8 ± 1.2	10.5 ± 1.7	15.1 ± 1.2†	15.9 ± 0.6†	17.0 ± 1.4†	17.7 ± 1.2†	18.9 ± 1.2†
	B6	2.7 ± 0.24	6.4 ± 0.8	10.5 ± 0.4	14.0 ± 1.4†	14.5 ± 2.6†	15.6 ± 1.4†	17.6 ± 0.8†	18.6 ± 1.0†
Femur weight (mg)	C3H	2.1 ± 0.51	6.8 ± 1.5	15.3 ± 3.0	23.8 ± 3.9	27.2 ± 1.7	29.4 ± 3.2†	31.9 ± 4.4†	37.5 ± 3.2*
	B6	1.7 ± 0.23	5.6 ± 0.8	14.6 ± 0.7	22.5 ± 1.9	24.6 ± 2.5	26.9 ± 3.0†	31.2 ± 1.8†	33.9 ± 3.8*,†
Femur length (cm)	C3H	0.44 ± 0.03*,†	0.8 ± 0.06*	1.08 ± 0.05	1.2 ± 0.07	1.26 ± 0.02	1.29 ± 0.04	1.33 ± 0.04	1.39 ± 0.03
	B6	0.4 ± 0.02*,†	0.74 ± 0.03*	1.05 ± 0.02	1.19 ± 0.05	1.23 ± 0.03	1.27 ± 0.05	1.34 ± 0.04	1.37 ± 0.03
Middiaphysis parameters									
Total area (mm^2)	C3H	0.56 ± 0.11	1.05 ± 0.13	1.24 ± 0.11*	1.48 ± 0.14*	1.53 ± 0.07*	1.56 ± 0.05*,†	1.56 ± 0.11*,†	1.65 ± 0.14*
	B6	0.5 ± 0.14	1.07 ± 0.08	1.41 ± 0.07*	1.63 ± 0.11*	1.73 ± 0.14*	1.73 ± 0.10*	1.85 ± 0.10*	1.94 ± 0.13*,†
Cortical area (mm^2)	C3H	0.41 ± 0.1	0.71 ± 0.1	0.66 ± 0.08	0.89 ± 0.1*	0.95 ± 0.08	0.99 ± 0.06*,†	1.04 ± 0.1†	1.13 ± 0.11*,†
	B6	0.32 ± 0.1	0.59 ± 0.06	0.58 ± 0.04	0.74 ± 0.05*,†	0.86 ± 0.09	0.85 ± 0.05*	0.92 ± 0.06	0.98 ± 0.07*,†
Total density (mg/cm^3)	C3H	207.3 ± 27.3*	307 ± 35.8*	390.7 ± 34.8*	535.5 ± 34.3*	575.4 ± 48.1*	652.1 ± 51.1*	688 ± 53.1*	710.6 ± 109*
	B6	163.5 ± 12.4*	162.2 ± 36.7*	227.4 ± 33.1*	306.5 ± 23.4*	362.9 ± 29.8*	366.5 ± 20.1*	397.7 ± 25.3*	439.5 ± 20.7*
Serum parameters									
IGF-I (ng/ml)	C3H	182 ± 51.2*	305 ± 41.3*	282.2 ± 83.3	277.7 ± 63.3	295.7 ± 82.9	265.3 ± 46.5	288 ± 79	338.7 ± 83.1
	B6	87.3 ± 43.2*	176.3 ± 43.3*	260.3 ± 81.9	252 ± 69.5	177 ± 112.5	213 ± 45.8	296.7 ± 40.4	274 ± 42.6
Osteocalcin (ng/ml)	C3H	178 ± 46.5*	436 ± 156.5*,†	280 ± 33.6*	282.4 ± 35.7*	272.3 ± 12.5	251.4 ± 50.8	230.3 ± 42.4	206.3 ± 32.6
	B6	345.7 ± 49.2*	554.9 ± 154*,†	519.3 ± 49*	400.6 ± 56.2*	304.6 ± 98.8	270.1 ± 33.1	280.4 ± 39.5	276.3 ± 38.1

Values presented as mean ± SD for 7–9 animals.
*$p < 0.05$ versus opposite strain females; $^{\dagger}p < 0.05$ versus same strain males.

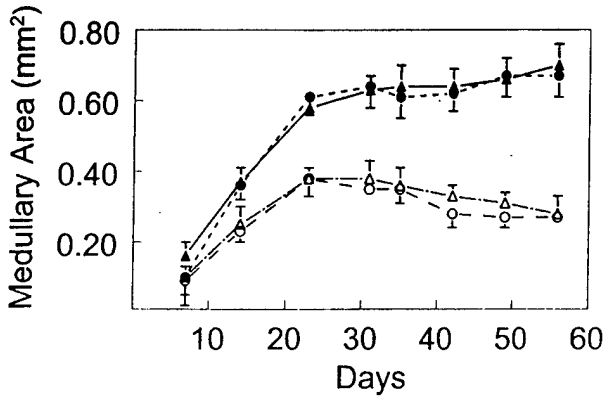

FIG. 1. Changes in medullary area in C3H and B6 mice from day 7 to day 56. Medullary area increased significantly between days 7 and 23 in both strains. Medullary area was greater by 45% or more in B6 mice compared with C3H mice for both sexes from day 14 onward. Medullary area was not significantly different in males versus females for either strain. Values expressed as mean of 7–9 animals ± SD; B6 male mice; closed triangles; B6 female mice, closed circles; C3H male mice, open triangles; C3H female mice, open circles.

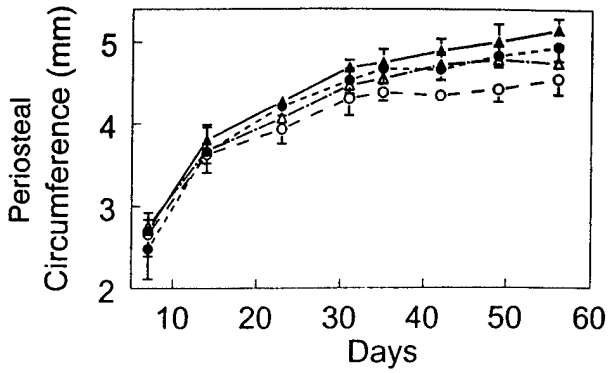

FIG. 2. Changes in periosteal circumference in C3H and B6 mice from day 7 to day 56. At day 23 periosteal circumference was 5% ($p = 0.03$) greater in B6 male mice and 7% ($p < 0.01$) in B6 female mice than in C3H male and female mice, respectively. On day 56, periosteal circumference was 8% ($p < 0.001$) greater in B6 male mice and 12% ($p < 0.01$) greater in B6 female mice than in C3H male and female mice, respectively. Within strain, B6 male mice had 5% ($p = 0.01$) greater periosteal circumference than B6 female mice on day 56 and C3H male mice had 8% ($p < 0.001$) greater periosteal circumference than C3H female mice on day 42. Values expressed as mean of 7–9 animals ± SD; B6 male mice, closed triangle; B6 female mice, closed circles; C3H male mice, open triangles; C3H female mice, open circles; SD = bars.

B6 and C3H mice. There was no difference by strain or sex in total area on day 7 and day 14. Total area in B6 male mice was 9% ($p = 0.028$) greater than that of C3H males on day 49 and 17% ($p < 0.001$) greater on day 56. B6 female mice had 13% ($p = 0.008$) greater total area than did C3H females from day 23 onward (Tables 1 and 2). The total area at the middiaphysis in B6 males was 9% ($p = 0.005$) greater than that of B6 females on day 56 and the value for C3H males was 16% ($p < 0.001$) greater than that of C3H females on day 49.

Cortical area: Cortical area at the middiaphysis of the femur was not different by strain or sex during rapid postnatal growth (days 7–23) but cortical area increased by 82% in B6 mice and 63% in C3H mice (Tables 1 and 2). C3H male mice had greater cortical area than did B6 male mice on day 31 (17%, $p = 0.02$) through day 56 (13%, $p = 0.005$). C3H female mice had greater cortical area than that of B6 female mice on day 31 (20%, $p = 0.007$), day 42 (16%, $p = 0.03$), and day 56 (15%, $p = 0.01$). Within strains, cortical area was 13% ($p = 0.03$) greater in B6 male mice than in B6 female mice by day 56, while cortical area was 19% ($p < 0.001$) greater in C3H male mice than in C3H female mice by day 42.

Medullary area: Medullary area increased dramatically during rapid postnatal growth (days 7–23) in both strains of mice (Fig. 1). Medullary area at the middiaphysis of the femur was significantly greater in B6 mice than in C3H mice from day 14 (45% in B6 male mice vs. C3H male mice [$p = 0.001$] and 55% in B6 female mice vs. C3H female mice [$p < 0.001$]). B6 mice had greater medullary area than did C3H mice for the duration of the study. At day 56, B6 male and female mice exhibited 149% and 108% greater medullary area than C3H male and female mice, respectively. Within strain, there was no difference between sexes at any time during the study.

Periosteal circumference: Periosteal circumference at the middiaphysis of the femur did not differ across strain or sex during rapid postnatal growth (days 7–14) (Fig. 2). B6 female mice had 12% ($p < 0.001$) greater periosteal circumference than that of C3H female mice at day 56, and B6 male mice had 8% ($p < 0.001$) greater periosteal circumference than that of C3H male mice at day 56. Within strains, periosteal circumference in B6 male mice was 5% ($p = 0.01$) greater than that of B6 female mice by day 56 and periosteal circumference was 8% ($p < 0.001$) greater in C3H male mice than that of C3H female mice by day 42.

Endosteal circumference: Endosteal circumference of the middiaphysis increased 65–90% during rapid postnatal growth (days 7–23) and a total of 7–10% during pubertal (days 23–31) and postpubertal growth (days 31–56) in B6 mice (Fig. 3). In C3H mice, endosteal circumference increased by 60–70% during rapid postnatal growth (days 7–23) but did not change significantly throughout the rest of the study. Endosteal circumference was significantly greater in B6 mice than in C3H mice for the entire study. Within strains, endosteal circumference did not differ across sex for the entire study (Fig. 3).

Cortical thickness: Cortical thickness at the middiaphysis of the femur was roughly 30% ($p < 0.01$) greater in C3H mice than in B6 mice throughout the study. Within strains, cortical thickness was 9% ($p < 0.05$) greater in C3H male mice than in C3H female mice from day 42. But no significant differences across sex were evident in B6 mice (Fig. 4). The greatest increase in cortical thickness occurred during rapid postnatal (days 7–23) and pubertal (days 23–31) growth, while the rate of change in cortical thickness decreased dramatically after puberty.

Bone densitometry

Mineral content: Total mineral content of the femoral middiaphysis increased 4-fold in both B6 mice and C3H

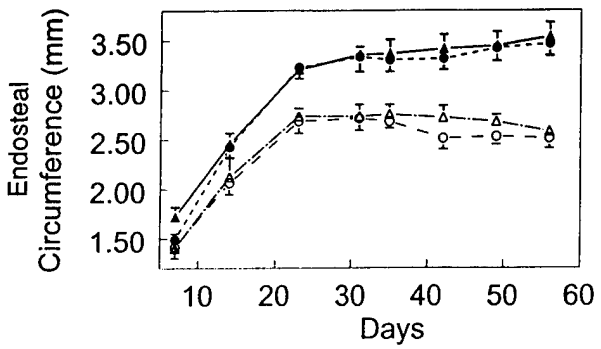

FIG. 3. Changes in endosteal circumference in C3H and B6 mice from day 7 to day 56. Endosteal circumference was significantly greater in B6 mice compared with C3H mice at all age groups except at day 7. Endosteal circumference was not significantly different in male versus female mice for either strain. Endosteal circumference increased significantly between days 7 and 23 after which there was no significant difference in endosteal circumference. Values expressed as mean of 7–9 animals ± SD; B6 male mice, closed triangles; B6 female mice, closed circles; C3H male mice, open triangles; C3H female mice, open circles; SD = bars.

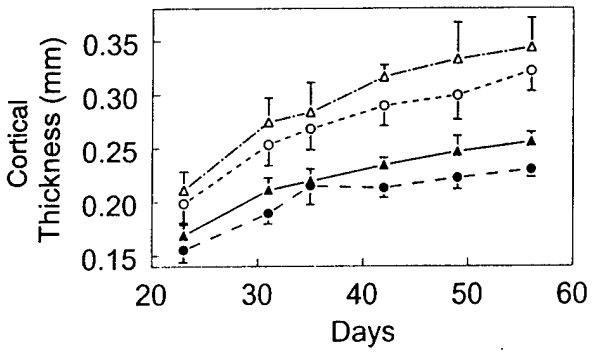

FIG. 4. Changes in cortical thickness in C3H and B6 mice from day 23 to day 56. Cortical thickness was significantly greater in C3H mice compared with B6 mice at all time points studied. Cortical thickness was significantly greater in male C3H mice compared with female C3H mice at days 42, 49, and 56. In B6 mice, the cortical thickness was significantly different in male mice compared with female mice. Cortical thickness increased significantly during puberty in both strains of mice. Values expressed as mean of 7–9 animals ± SD; B6 males mice, closed triangles; B6 female mice, closed circles; C3H male mice, open triangles; C3H female mice, open circles.

mice during rapid postnatal growth (days 7–23; Fig. 5). Total mineral content in C3H mice was roughly 40% ($p < 0.01$) greater than that of B6 mice throughout the study (44% on day 7, 54% on day 31, and 38% on day 56). Within strain, total mineral content of B6 male mice was 25% ($p = 0.01$) greater than that of B6 female mice and 23% ($p < 0.001$) greater in C3H male mice than in C3H female mice on day 42.

Density: Total volumetric bone density of the middiaphysis increased more in C3H mice (females, 81% and males, 83%) than in B6 mice (females, 37% and males, 51%) during rapid postnatal growth (days 7–23). Greater volumetric bone density was present in C3H mice on day 7

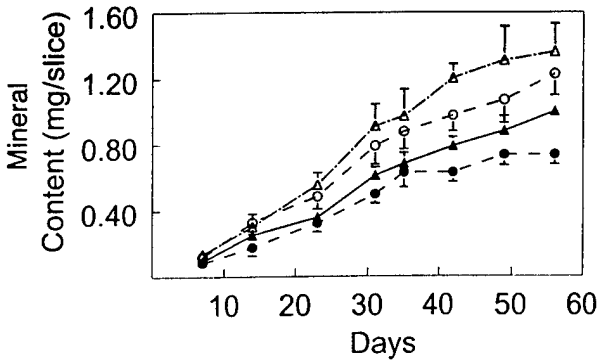

FIG. 5. Changes in middiaphyseal total mineral content in C3H and B6 mice from day 7 to day 56. On day 23, C3H male mice had 56% ($p < 0.001$) and C3H female mice had 51% ($p < 0.01$) greater total mineral content than B6 male and female mice, respectively. On day 35, C3H male mice had 42% ($p < 0.001$) and C3H female mice had 39% ($p < 0.001$) greater total mineral content than B6 male and female mice, respectively. On day 56, C3H males had 36% ($p < 0.001$) and C3H females had 40% ($p < 0.001$) greater total mineral content than B6 male and female mice, respectively. Within strain, B6 male mice had 25% ($p = 0.01$) greater mineral content than B6 female mice by day 42 and C3H male mice had 23% greater mineral content ($p < 0.001$) than C3H female mice on day 42. Values expressed as mean of 7–9 animals ± SD; B6 male mice, closed triangle; B6 female mice, closed circles; C3H male mice, open triangles; C3H female mice, open circles; SD = bars.

(C3H vs. B6 female mice, 27%; C3H vs. B6 male mice, 41%; $p < 0.05$), and by day 56, this difference was even greater (C3H vs. B6 female mice, 60%; C3H vs. B6 male mice 62%; $p < 0.001$). Within strain, there was no significant difference in volumetric bone density between sexes (Tables 1 and 2). The greatest difference in rate of total density accretion occurred during rapid postnatal (days 7–23) and pubertal (days 23–31) growth (Figs. 6 and 7). The rate of bone density gain in C3H mice during postnatal and pubertal growth was twice that of B6 mice, while it was not different after puberty.

Biochemical assays

Serum IGF-I: C3H female mice had significantly higher serum levels of IGF-I than did B6 mice on day 7 and day 14, whereas C3H male mice exhibited higher serum IGF-I levels at day 7 (Tables 1 and 2). In the pooled data from male and female mice, C3H mice had greater serum IGF-I levels than B6 mice at days 7, 14, 35, and 42 (data not shown).

Serum IGF-II: On day 7 and day 14, IGF-II levels were not different by strain or sex. By day 23, serum IGF-II was nearly undetectable and remained at low levels for the duration of the study (data not shown).

Serum osteocalcin: Serum osteocalcin was significantly higher in B6 mice compared with that of C3H mice from day 7 (77%, $p < 0.01$) to 42 (33%, $p < 0.01$) in males and from day 7 (94%, $p < 0.01$) to 31 (42%, $p < 0.01$) in females. Serum osteocalcin increased roughly 2-fold during postnatal growth (days 7–23) in male mice of both strains and then decreased steadily until day 56. However, in fe-

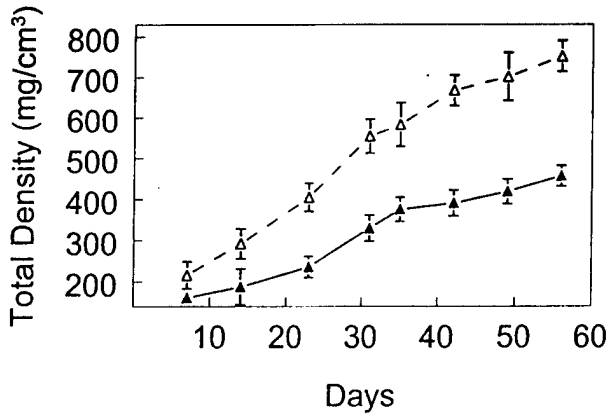

FIG. 6. Changes in bone density in C3H and B6 mice from day 7 to day 56. Because bone density was not different between male and female mice of either strain, the data for both sexes were pooled ($p < 0.01$). Total volumetric bone density of the middiaphysis was about 30% greater in C3H mice than in B6 mice at day 7. C3H mice exhibited 70% more bone density than did B6 mice after puberty (day 31). Bone density was significantly higher in C3H mice than B6 mice at all time points ($p < 0.01$). Bone density more than doubled during puberty in both strains of mice. Values expressed as mean of 7–9 animals ± SD; B6 mice, closed triangle; C3H mice, open triangles; SD = bars.

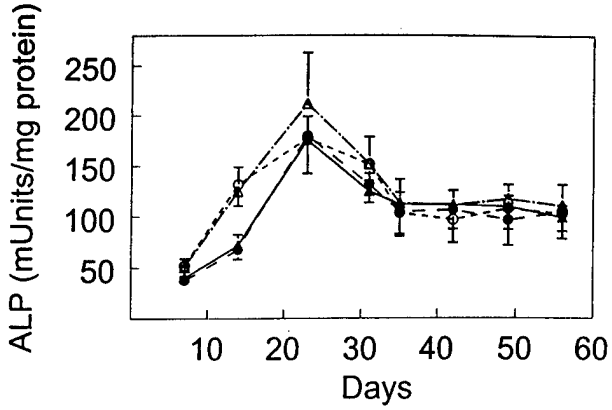

FIG. 8. Changes in bone-specific ALP activity in bone extracts for C3H and B6 mice from day 7 to day 56. On day 14, bone-specific ALP activity in C3H male mice was 75% ($p < 0.001$) and in C3H female mice was 95% ($p < 0.001$) greater than B6 male and female mice, respectively. On day 23, C3H male mice had 21% ($p < 0.01$) greater bone-specific ALP activity than B6 male mice, but C3H female mice were not different from B6 female mice. Values expressed as mean of 7–9 animals ± SD; B6 male mice, closed triangle; B6 female mice, closed circles; C3H male mice, open triangles; C3H female mice, open circles; SD = bars.

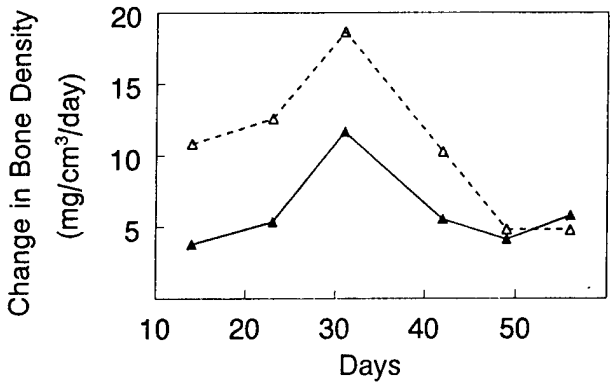

FIG. 7. Changes in the rate of volumetric bone density accretion per day in C3H and B6 mice from day 7 to day 56. C3H mice had a 2.8-fold and a 1.6-fold higher rate of bone accretion from day 7 to day 14 and from day 23 to day 31, respectively, compared with B6 mice. The gain in bone density for each time period was calculated from the mean value for each time period and was divided by the duration in days to obtain the rate. Male and female mice were calculated separately and used as replicate values for the calculation of significance. B6 mice, closed triangles; C3H mice, open triangles.

male mice, serum osteocalcin levels doubled from days 7–14 and then decreased steadily until day 56 (Tables 1 and 2). Serum osteocalcin levels in female mice of both strains were 32% higher than those in male mice on day 14 ($p < 0.01$), but were not different at other time points.

Bone extract ALP: Bone extract ALP normalized for total extractable protein showed a 4-fold increase in activity during the rapid-bone modeling associated with increased bone length and size during postnatal growth (days 7–23) in both strains, although bone extract from C3H mice contained 2-fold greater ALP activity on day 14 than that of B6 mice (Fig. 8). A decrease of 30% in ALP activity occurred during puberty (days 23–31). Within strains, there was no difference in ALP activity between sexes at any time.

Correlations: In both strains, body weight was highly correlated with all other physical, geometric, and densitometry measurements throughout the study (data not shown). Serum IGF-I levels were correlated positively with physical, geometric, and densitometry measurements in both strains, especially during postnatal growth but less so during pubertal and postpubertal growth (data not shown). In the pooled data from C3H and B6 strains of mice belonging to both sexes, multiple regression analyses were carried out using strain, sex, age, IGF-I, and osteocalcin as independent variables (Table 3). The β-coefficients, which represent the relative contribution of each independent variable in the prediction of the dependent variable, reveal that age is the most important predictor of various bone parameters, as expected. Furthermore, strain contributed predominantly to the differences in density, endosteal circumference, and cortical thickness. In addition, serum levels of IGF-I and osteocalcin provided statistically significant contributions to the prediction of various bone parameters (Table 3). To further evaluate the relative contribution of the previously mentioned five independent variables to predict the gender differences in bone size, we performed multiple regression analyses using data from prepubertal (days 7–23), pubertal (days 23–35), and postpubertal (days 35–56) periods. We found that the relative contribution of gender to differences in periosteal circumference was much greater during the postpubertal period than the prepubertal period (β-coefficient of 0.36 vs. 0.11). To determine if gender differences in periosteal circumference can be explained based on IGF-I, we determined the relative contribution of strain, sex, and age to differences in IGF-I using data from prepubertal (days 7–23) and postpubertal periods (days 35–56). We found that strain, sex,

TABLE 3. MULTIPLE REGRESSION ANALYSIS IN THE POOLED DATA FROM MALES AND FEMALES OF C3H AND B6 STRAINS OF MICE

	β-Coefficient for independent variable					
Dependent variable	*Strain*	*Sex*	*Age*	*IGF-I*	*Osteocalcin*	*Multiple* r
Body weight	0.04	0.16*	0.88*	0.14*	0.11*	0.95*
Bone length	0.11*	0.03	0.95*	0.09*	0.23*	0.94*
Total content	0.34*	0.14*	0.86*	0.07*	0.05*	0.95*
Total density	0.59*	0.08*	0.79*	0.01	0.08*	0.95*
Total area	0.18*	0.11*	0.85*	0.14*	0.16*	0.92*
Periosteal circumference	0.13*	0.09*	0.87*	0.14*	0.23*	0.91*
Endosteal circumference	0.45*	0.02	0.66*	0.09*	0.26*	0.86*
Cortical thickness	0.54*	0.16*	0.58*	0.12*	0.005	0.88*

* $p < 0.05$

and age nearly contributed equally (β-coefficient of 0.39, 0.3, and 0.26, respectively) during the postpubertal period. However, during the prepubertal period sex had no effect on serum IGF-I as expected (β-coefficient = 0.01).

DISCUSSION

In previous studies, two inbred strains of mice, C3H and B6, exhibited similar body weights but different volumetric peak bone densities.[17,19–21] To identify the growth period(s) in which this divergence in bone density becomes apparent, we evaluated temporal skeletal changes in C3H and B6 mice belonging to both sexes before, during, and after puberty. Our data show that although C3H mice exhibit slightly higher total bone density compared with B6 mice at 7 days of age (approximately 25%), total bone density is 69% greater in C3H mice compared with B6 mice at 31 days of age, despite similar body size, body weight, and bone length. Accordingly, the gain in bone density in C3H mice during postnatal (days 7–23) and pubertal (days 23–31) growth is more than twice that of B6 mice. In addition, the findings that the gain in bone density increases by more than 70% during puberty (days 23–31) attest that rapid skeletal changes occur during this period. Therefore, the postnatal (days 7–23) and pubertal (days 23–31) growth periods appear to be critical in the development of the difference in bone density between C3H and B6 mice. The difference in total bone density seen at day 35 between C3H and B6 mice was maintained during the rest of the study period.

The differences in cortical thickness between the two strains of mice reflect the greater accumulation of bone mineral in C3H mice compared with B6 mice during postnatal growth. This difference in cortical thickness between C3H and B6 mice developed during the rapid growth of the postnatal (days 7–23) and pubertal (days 23–31) periods. The difference in cortical thickness between C3H and B6 mice appeared to be caused by significantly smaller endosteal circumference in C3H mice (approximately 20% less) compared with B6 mice. The increase in cortical thickness of approximately 25% during puberty (days 23–35) in both strains of mice appeared mainly to be caused by increased periosteal circumference, because the endosteal circumference did not show significant change during this period (Fig. 3). Although neither the periosteal nor the endosteal circumference showed significant change during postpubertal growth (days 35–56) in C3H mice, both the periosteal and the endosteal circumference increased in B6 mice during this period, resulting in B6 mice having significantly greater periosteal circumference than C3H mice at 56 days of age. Consistent with these data, Sheng et al.[21] recently have shown, by histomorphometric analysis, that the total cross-sectional area of the femur at the middiaphysis is significantly greater in the B6 mice at 6 weeks of age compared with C3H mice.

The cellular mechanisms that contribute to the greater cortical thickness in C3H mice compared with B6 mice can only be speculated at this time. In this regard, the findings that endosteal but not periosteal circumference is significantly different between the two strains of mice during postnatal growth suggested that differences in endosteal bone formation and resorption could, in part, contribute to the observed differences in cortical thickness. Consistent with this idea were the findings that (1) C3H mice exhibited significantly higher ALP activity in the femoral bone extract than did B6 mice at the time when maximal differences in bone density between the two strains occur, (2) C3H mice exhibited greater endosteal bone formation rate than B6 mice by histomorphometric analysis,[21] and (3) there were fewer osteoclast precursors in the marrow of C3H mice than in B6 mice.[28] Further studies are needed to evaluate the relative contribution of endosteal bone formation versus endosteal bone resorption in contributing to differences in cortical thickness between the two strains of mice during postnatal growth.

The divergence in total volumetric bone density at the femoral middiaphysis between C3H and B6 strains during postnatal growth may, in part, be caused by greater bone area in the C3H mice than in the B6 mice because of differences in cortical thickness. However, the possibility that the bones of C3H mice during early postnatal growth may be more mineralized or less porous compared with B6 mice cannot be ruled out because C3H mice exhibit approximately 30% greater bone density than B6 mice despite similar bone area on day 7. Although the finding that C3H mice exhibit greater ash weight and calcium content compared with the B6 mice at 9 weeks of age[19] are consistent

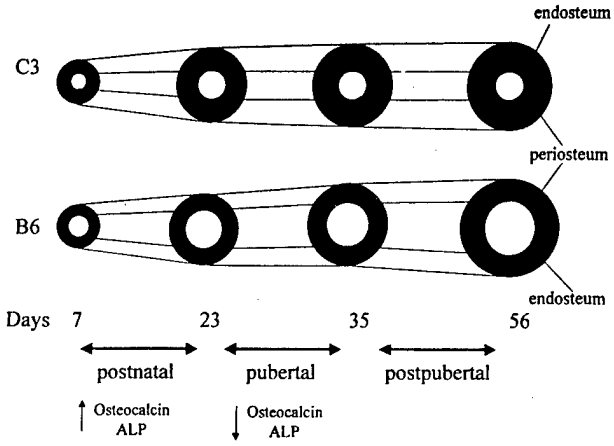

FIG. 9. A model of the changes in bone size during postnatal, pubertal, and postpubertal growth in C3H and B6 mice. On day 7, the periosteal circumference of C3H and B6 femora was similar; as illustrated by the cross-sectional diagram of the femur at the middiaphysis, B6 mice had a 20% greater endosteal circumference than did C3H mice, and C3H mice had 34% greater volumetric bone density than did B6 mice. Between days 7 and 23 periosteal circumference increased 50% in C3H mice and 58% in B6 mice, while endosteal circumference increased by 90% in both strains. On day 23, the periosteal circumference of C3H and B6 femora was similar; B6 mice had 16% greater endosteal circumference than did C3H mice, and C3H mice had 69% greater volumetric bone density than did B6 mice. On day 35, B6 mice had about 4% greater periosteal circumference than did C3H mice, B6 had a 22% greater endosteal circumference than did C3H mice, and C3H mice had 56% greater volumetric bone density than did B6 mice. On day 56, B6 mice had 8–12% greater periosteal circumference than did C3H mice, B6 had a 35% greater endosteal circumference than did C3H mice, and C3H mice had 61% greater volumetric bone density than did B6 mice.

with this idea, further studies are needed to evaluate whether or not C3H bones contain less porosity or more mineralization of the bone matrix compared with B6 mice during postnatal growth when the greatest difference in density was seen despite similarities in bone area.

The rapid increase in total mineral content during postnatal growth (days 7–23) appeared mainly to be caused by increased bone size, which increased by more than 50% during this period (Fig. 9). This increase in bone size appeared to be caused by increased periosteal bone formation rate because both osteocalcin levels in the serum and ALP activity in bone extract increased during this period. In terms of the individual factors that contribute to the increased periosteal bone formation, we postulate that IGF-I may be a potential candidate because: (1) serum levels of IGF-I increased dramatically during this period (Tables 1 and 2) and showed significant correlation with changes in periosteal circumference and biochemical measurements of bone formation during this period (Table 3); and (2) mice lacking IGF-I exhibit dramatic reduction in postnatal skeletal growth.[29] Consistent with a role for IGF-I, our findings also show significantly greater serum IGF-I levels in C3H mice than in B6 mice on days 7, 14, 35, and 42 in the pooled data from male and female mice. Consistent with these data, we have previously shown that the IGF-I differences are statistically significant up to 10 months of age.[20] Further studies are needed to evaluate the cause and effect relationship between changes in serum levels of IGF-I and skeletal changes in C3H and B6 mice during postnatal growth.

In contrast to postnatal growth, the mineral accumulation during puberty appears to be predominantly because of decreased bone resorption caused by increased male and female sex steroid hormones. There are a number of findings that support this idea. First, the increase in total bone density during puberty in both C3H and B6 mice was associated with a decrease in biochemical markers of bone remodeling in both serum and bone extracts. Second, we and others have shown that the increase in mineral accumulation during sexual development in girls is associated with decreased bone turnover.[8,10,30] Third, Slemenda et al.[8] have shown that black children accumulated 10% greater bone mass and had significantly reduced bone turnover, as measured by serum levels of osteocalcin and tartrate-resistant acid phosphatase, compared with white children during pubertal growth. Although sex steroid hormone–induced changes in cytokine production[31–33] have been implicated in the reduced bone turnover that occurs during puberty, the cause and effect relationship between cytokine production and the reduction in bone turnover during puberty remains to be established.

Surprisingly, we found that serum osteocalcin levels were significantly lower in C3H mice compared with B6 mice throughout the study. Because ALP activity in bone extract was significantly higher in the C3H mice than in the B6 mice during postnatal growth, we anticipated serum osteocalcin levels also to be higher during this period in C3H mice. There are a number of potential explanations for this discrepancy. It is possible that osteocalcin expression in osteoblasts is higher in C3H mice compared with B6 mice; however, a smaller proportion of synthesized osteocalcin was released into the extracellular fluid compared with the matrix compartment in C3H mice compared with B6 mice, resulting in reduced levels in serum. Metabolic differences in serum osteocalcin (e.g., half-life and clearance rate) between C3H and B6 mice also may contribute to the lower levels of serum osteocalcin in C3H mice compared with B6 mice. Alternatively, the higher level of osteocalcin produced in the B6 mice may act as an inhibitor of bone formation during postnatal growth because bone formation was increased at the endosteum in mice lacking osteocalcin.[34]

Our findings also show that sexual dimorphic skeletal changes occurred in mice during puberty as in the case of humans.[4] This sexual dimorphism may be attributed to greater bone size and cortical thickness in men than in women,[35] which in turn may be caused by a later start and a longer pubertal growth period in boys than girls.[5] However, volumetric bone mineral density (BMD) does not appear to be different between the two sexes in humans.[36–38] Within strains, we found that 8-week-old male mice had a greater total mineral content and a larger periosteal circumference than did female mice, despite similar endosteal circumference. Thus, male mice of both strains exhibited increased bone size and cortical thickness resulting in greater total mineral content compared with female mice. The molecular mechanisms that are responsible for the increased periosteal bone formation and/or reduction in periosteal bone resorption in the male mice compared with female mice have yet to be established.

In conclusion, the difference in bone density between C3H and B6 strains of mice is established early and maintained throughout the period of growth. Two growth periods, postnatal and pubertal, are particularly critical to the development of peak BMD. Although the difference in bone density is maintained throughout, there are differences in the pattern of growth between strains that suggest that the genes that contribute to the difference in BMD during each period of growth may be different. This is consistent with the evidence from quantitative trait loci studies[39] that multiple genes contribute to the difference in bone density. The genes that are expressed differentially in the skeleton of C3H and B6 mice during postnatal and pubertal growth may provide clues regarding the genes that contribute to the BMD differences between these two strains.

ACKNOWLEDGMENTS

The authors acknowledge the expert technical assistance provided by Daniel Bruch and Joe Rung-Aroon in this study. Support for this work was received from the NIH grant AR31062, the National Medical Technology Test Bed, and the U.S. Department of the Army.

REFERENCES

1. Lloyd T, Rollings N, Andon MB, Demers LM, Eggli DF, Kieselhorst K, Kulin H, Landis JR, Martel JK, Orr G, Smith P 1992 Determinants of bone density in young women. I. Relationships among pubertal development, total body bone mass, and total body bone density in premenarchal females. J Clin Endocrinol Metab **75**:383–387.
2. Theintz G, Buchs B, Rizzoli R, Slosman D, Clavien H, Sizonenko PC, Bonjour JP 1992 Longitudinal monitoring of bone mass accumulation in healthy adolescents: Evidence for a marked reduction after 16 years of age at the levels of lumbar spine and femoral neck in female subjects. J Clin Endocrinol Metab **75**:1060–1065.
3. Eisman JA, Kelly PJ, Morrison NA, Pocock NA, Yeoman R, Birmingham J, Sambrook PN 1993 Peak bone mass and osteoporosis prevention. Osteoporos Int 3(Suppl 1):56–60.
4. van der Meulen MCH, Carter DR 1999 Mechanical determinants of peak bone mass. In: Rosen CJ, Glowacki J, Bilezikian JP (eds.) The Aging Skeleton. Academic Press, San Diego, CA, USA, pp. 105–114.
5. Gertner JM 1999 Childhood and adolescence. In: Favus MJ (ed.) Primer on Metabolic Bone Diseases and Disorders of Mineral Metabolism, 4th ed. Lippincott Williams & Wilkins, Philadelphia, PA, USA, pp. 45–49.
6. Abbassi V 1998 Growth and normal puberty. Pediatrics **102**(2 Pt 3):507–511.
7. Seeman E, Tsalamandris C, Formica C 1993 Peak bone mass, a growing problem? Int J Fertil Menopausal Stud **38**(Suppl 2):77–82.
8. Slemenda CW, Peacock M, Hui S, Zhou L, Johnston CC 1997 Reduced rates of skeletal remodeling are associated with increased bone mineral density during the development of peak skeletal mass. J Bone Miner Res **12**:676–682.
9. Schiessl H, Frost HM, Jee WS 1998 Estrogen and bone-muscle strength and mass relationships. Bone **22**:1–6.
10. Cadogan J, Blumsohn A, Barker ME, Eastell R 1998 A longitudinal study of bone gain in pubertal girls: Anthropometric and biochemical correlates. J Bone Miner Res **13**:1602–1612.
11. Garnero P, Delmas PD 1998 Biochemical markers of bone turnover. Applications for osteoporosis. Endocrinol Metab Clin North Am **27**:303–323.
12. Ross PD, Knowlton W 1998 Rapid bone loss is associated with increased levels of biochemical markers. J Bone Miner Res **13**:297–302.
13. Weaver CM, Peacock M, Martin BR, McCabe GP, Zhao J, Smith DL, Wastney ME 1997 Quantification of biochemical markers of bone turnover by kinetic measures of bone formation and resorption in young healthy females. J Bone Miner Res **12**:1714–1720.
14. Garnero P, Delmas PD 1997 Bone markers. Baillieres Clin Rheumatol **11**:517–537.
15. Kalu DN 1999 Animal models of the aging skeleton. In: Rosen CJ, Glowacki J, Bilezikian JP (eds.) The Aging Skeleton. Academic Press, San Diego, CA, USA, pp. 37–50.
16. Ornoy A, Katzburg S 1995 Osteoporosis: Animal models for the human disease. In: Ornoy A (ed.) Animal Models of Human Related Calcium Metabolic Disorders. CRC Press, New York, NY, USA, pp. 105–126.
17. Beamer WG, Donahue LR, Rosen CJ, Baylink DJ 1996 Genetic variability in adult bone density among inbred strains of mice. Bone **18**:397–403.
18. Bain SD, Bailey MC, Celino DL, Lantry MM, Edwards MW 1993 High-dose estrogen inhibits bone resorption and stimulates bone formation in the ovariectomized mouse. J Bone Miner Res **8**:435–442.
19. Chen C, Kalu DN 1999 Strain differences in bone density and calcium metabolism between C3H/HeJ and C57BL/6J mice. Bone **25**:413–420.
20. Rosen CJ, Dimai HP, Vereault D, Donahue LR, Beamer WG, Farley J, Linkhart S, Linkhart T, Mohan S, Baylink DJ 1997 Circulating and skeletal insulin-like growth factor-I (IGF-I) concentrations in two inbred strains of mice with different bone mineral densities. Bone **21**:217–223.
21. Sheng MH, Baylink DJ, Beamer WG, Donahue LR, Rosen CJ, Lau KH, Wergedal JE 1999 Histomorphometric studies show that bone formation and bone mineral apposition rates are greater in C3H/HeJ (high-density) than C57BL/6J (low-density) mice during growth. Bone **25**:421–429.
22. Ahima RS, Dushay J, Flier SN, Prabakaran D, Flier JS 1997 Leptin accelerates the onset of puberty in normal female mice. J Clin Invest **99**:391–395.
23. Bonjour JP, Theintz G, Buchs B, Slosman D, Rizzoli R 1991 Critical years and stages of puberty for spinal and femoral bone mass accumulation during adolescence. J Clin Endocrinol Metab **73**:555–563.
24. Farley JR, Hall SL, Herring S, Tarbaux NM 1992 Two biochemical indices of mouse bone formation are increased, in vivo, in response to calcitonin. Calcif Tissue Int **50**:67–73.
25. Srivastava AK, Catillo G, Wergedal JE, Mohan S, Baylink DJ 2000 Development and application of a synthetic peptide based osteocalcin assay for the measurement of bone formation in mouse serum. Calcif Tissue Int **67**:255–259.
26. Mohan S, Libanati C, Dony C, Lang K, Srinivasan N, Baylink DJ 1995 Development, validation, and application of a radioimmunoassay for insulin-like growth factor binding protein-5 in human serum and other biological fluids. J Clin Endocrinol Metab **80**:2638–2645.
27. Mohan S, Bautista CM, Herring SJ, Linkhart TA, Baylink DJ 1990 Development of valid methods to measure insulin-like growth factors-I and -II in bone cell-conditioned medium. Endocrinology **126**:2534–2542.
28. Linkhart TA, Linkhart SG, Kodama Y, Farley JR, Dimai HP, Wright KR, Wergedal JE, Sheng M, Beamer WG, Donahue LR, Rosen CJ, Baylink DJ 1999 Osteoclast formation in bone marrow cultures from two inbred strains of mice with different bone densities. J Bone Miner Res **14**:39–46.
29. Baker J, Liu JP, Robertson EJ, Efstratiadis A 1993 Role of insulin-like growth factors in embryonic and postnatal growth. Cell **75**:73–82.
30. Mauras N, Rogol AD, Haymond MW, Veldhuis JD 1996 Sex steroids, growth hormone, insulin-like growth factor-1: Neu-

roendocrine and metabolic regulation in puberty. Horm Res **45**:74–80.
31. Manolagas SC, Bellido T, Jilka RL 1995 Sex steroids, cytokines and the bone marrow: New concepts on the pathogenesis of osteoporosis. Ciba Found Symp **191**:187–196.
32. Kimble RB, Srivastava S, Ross FP, Matayoshi A, Pacifici R 1996 Estrogen deficiency increases the ability of stromal cells to support murine osteoclastogenesis via an interleukin-1 and tumor necrosis factor-mediated stimulation of macrophage colony-stimulating factor production. J Biol Chem **271**: 28890–28897.
33. Hofbauer LC, Gori F, Riggs BL, Lacey DL, Dunstan CR, Spelsberg TC, Khosla S 1999 Stimulation of osteoprotegerin ligand and inhibition of osteoprotegerin production by glucocorticoids in human osteoblastic lineage cells: Potential paracrine mechanisms of glucocorticoid-induced osteoporosis. Endocrinology **140**:4382–4389.
34. Ducy P, Desbois C, Boyce B, Pinero G, Story B, Dunstan C, Smith E, Bonadio J, Goldstein S, Gundberg C, Bradley A, Karsenty G 1996 Increased bone formation in osteocalcin-deficient mice. Nature **382**:448–452.
35. Bonjour J-P, Rizzoli R 1995 Bone acquisition in adolescence. In: Marcus R, Feldman D, Kelsey J (eds.) Osteoporosis. Academic Press, San Diego, CA, USA, pp. 465–476.
36. Gilsanz V, Boechat MI, Roe TF, Loro ML, Sayre JW, Goodman WG 1994 Gender differences in vertebral body sizes in children and adolescents. Radiology **190**:673–677.
37. Kalender WA, Felsenberg D, Louis O, Lopez P, Klotz E, Osteaux M, Fraga J 1989 Reference values for trabecular and cortical vertebral bone density in single and dual-energy quantitative computed tomography. Eur J Radiol **9**:75–80.
38. Gilsanz V, Gibbens DT, Roe TF, Carlson M, Senac MO, Boechat MI, Huang HK, Schulz EE, Libanati CR, Cann CC 1988 Vertebral bone density in children: Effect of puberty. Radiology **166**:847–850.
39. Beamer WG, Rosen CJ, Shultz KL, Pung AE, Churchill GA, Donahue LR, Baylink DJ 1999 Mice congenic for bone density QTLs exhibit corresponding bone density changes. J Bone Miner Res **14**(Suppl 1):S174.

Address reprint requests to:
Subburaman Mohan, Ph.D.
Musculoskeletal Disease Center
J.L. Pettis Veterans Administration Medical Center
11201 Benton Street (151)
Loma Linda, CA 92357, USA

Received in original form December 28, 1999; in revised form June 13, 2000; accepted August 31, 2000.

Bone Vol. 27, No. 4
October 2000:521–528

ELSEVIER

Mapping Quantitative Trait Loci for Serum Insulin-like Growth Factor-1 Levels in Mice

C. J. ROSEN,[1,2] G. A. CHURCHILL,[2] L. R. DONAHUE,[2] K. L. SHULTZ,[2] J. K. BURGESS,[1] D. R. POWELL,[3] and W. G. BEAMER[2]

[1]*Maine Center for Osteoporosis Research and Education, St. Joseph Hospital, Bangor, ME, USA*
[2]*The Jackson Laboratory, Bar Harbor, ME, USA*
[3]*Department of Nephrology, Baylor University College of Medicine, Houston, TX, USA*

Serum insulin-like growth factor-1 (IGF-1) and femoral bone mineral density (BMD) differ between two inbred strains of mice, C3H/HeJ (C3H) and C57BL/6J (B6), by approximately 30% and 50%, respectively. Similarly, skeletal IGF-1 content, bone formation, mineral apposition, and marrow stromal cell numbers are higher in C3H than in B6 mice. Because IGF-1 and several bone parameters cosegregate, we hypothesize that the serum IGF-1 phenotype has a strong heritable component and that genetic determinants for serum IGF-1 are involved in the regulation of bone mass. We intercrossed (B6 × C3H)F1 hybrids and analyzed 682 F2 female offspring at 4 months of age for serum IGF-1 by radioimmunoassay and femoral BMD by peripheral quantitative computerized tomography (pQCT). Genomic DNA was assayed by polymerase chain reaction (PCR) to determine alleles for 114 Mit markers inherited in F2 mice at average distances of 14 centimorgans (cM) along each chromosome (Chr). Serum IGF-1 levels in the F2 progeny were relatively normal in distribution, but showed a greater range than either progenitor, indicating that serum IGF-1 level is a polygenic trait with an estimated heritability of 52%. Serum IGF-1 correlated with femoral length ($r = 0.266, p < 0.0001$) and femoral BMD ($r = 0.267, p < 0.0001$). Whole genome scans for main effects associated with serum IGF-1 levels revealed three significant QTLs (in order of significance) on mouse Chrs 6, 15, and 10. The QTL on Chr 6 showed a significant reduction in IGF-1 associated with increasing C3H allele number, whereas the Chr 15 and Chr 10 loci showed additive effects with increasing C3H allele number. A genome-wide search for interacting marker pairs identified a significant interaction between the Chr 6 QTL and a locus on Chr 11. This interactive effect suggested that when the Chr 11 locus was homozygous for C3H, there was no effect of the Chr 6 locus on serum IGF-1; however, the combination of C3H alleles on Chr 6 with B6 alleles on Chr 11 was associated with reduced serum IGF-1 concentrations. To test this in vivo, we tested congenic mice carrying the Chr 6 QTL region from C3H on a B6 background (B6.C3H-6). Both serum IGF-1 and femoral BMD were significantly lower in female congenic than progenitor B6 mice. In summary, we identified three major QTLs on mouse Chrs 6, 10, and 15, and noted a major locus-locus interaction between Chrs 6 and 11. We named these QTLs *IGF-1* serum *l*evels (*Igf1sl1* to *Igf1sl4*). Functional isolation of the *Igf1sl1* QTL on Chr 6 for IGF-1 in B6.C3H-6 congenic mice demonstrated effects on both the IGF-1 and BMD phenotypes. The genetic determinants of these *Igf1sl* QTLs will provide much insight into the regulation of IGF-1 and the subsequent acquisition of peak bone mass. (Bone 27:521–528; 2000)

Key Words: Insulin-like growth factor-1 (IGF-1); Bone mineral density (BMD); Quantitative trait loci (QTLs); Genotype.

Introduction

Insulin-like growth factor-1 (IGF-1) is a ubiquitous 7 kDa polypeptide synthesized by normal and neoplastic tissues. Besides its critical role as an autocrine and paracrine regulator of cell function, IGF-1 also circulates in large concentrations in an inactive storage form, bound to a family of high-affinity IGF-binding proteins (IGFBPs).[8] The primary origin of serum IGF-1 is liver, although skeletal cells synthesize and store both IGF-1 and IGF-2 in large quantities.[8] IGF-1 is a critical component for longitudinal growth and for coupling bone formation to resorption during adult skeletal remodeling. Moreover, autocrine and paracrine sources of IGF-1 are certain to be important in the process of peak bone acquisition. Several population studies have suggested that serum IGF-1 is related to adult bone mineral density (BMD), as well as fracture risk, and one longitudinal study has demonstrated that serum IGF-1 levels during puberty are associated with femoral cross-sectional area in both boys and girls.[4,11,13] These lines of preliminary evidence suggest that IGF-1 (serum and/or skeletal) may be an important intermediate phenotype for BMD.

Inbred, transgenic, and mutant mice provide model systems to define the genetic regulation of bone acquisition and its relationship to IGF-1. For example, generation of transgenic mice with targeted overexpression of IGF-1 in bone by means of the osteocalcin promoter results in a 30% increase in trabecular and cortical bone mass compared with wild-type mice.[18] Also, we demonstrated that serum IGF-1 differs in healthy inbred strains of mice in a pattern that parallels strain differences in femoral BMD.[14] Furthermore, in two inbred strains of the same size and weight, C3H/HeJ (C3H) and C57BL/6J (B6), serum IGF-1 levels from neonatal development through 12 months of age are con-

Address for correspondence and reprints: Dr. Clifford J. Rosen, Maine Center for Osteoporosis Research and Education, St. Joseph Hospital, 360 Broadway, Bangor, ME 04401. E-mail: rofe@aol.com

8756-3282/00/$20.00
PII S8756-3282(00)00354-9

Bone Vol. 27, No. 4
October 2000:521–528

sistently higher in C3H than B6, despite nearly identical levels of growth hormone (GH) and growth hormone-binding protein (GHBP).[1,14] In addition, we have shown that in vitro production of IGF-1 from cultured calvarial osteoblasts is higher in C3H than in B6 cells and the skeletal content of this peptide also differs by strain to the same degree as circulating levels.[14]

Previous studies in humans have established that the serum IGF-1 phenotype is an inherited quantitative trait with a polygenic inheritance.[8,16] In mice, the distributions for serum IGF-1 between C3H and B6 inbred strains are distinctly different, raising the possibility of using a mapping strategy with progenitor crosses, and F2 intercross progeny, to define the heritability of IGF-1 and the genetic loci that regulate the IGF-1 phenotype. In this study, we hypothesized that there would be several quantitative trait loci (QTLs) for IGF-1, and these determinants would be related to factors affecting acquisition of peak bone mass. To test this hypothesis, we generated a B6C3H-F2 population of mice and analyzed them for the correlation between genotype and IGF-1, then compared IGF-1 QTLs with genetic data for BMD, and finally tested the role of one QTL in shaping the IGF-1 and BMD phenotypes.

Materials and Methods

Generation of F2 Mice

Mice were produced and maintained in our research colony under 14:10 h light:dark cycles. Autoclaved diet NIH-31 (6% fat, 18% protein, Ca:P 1:1, vitamin and mineral fortified; PMI Richmond, IN) and HCl-acidified water (pH 2.8–3.2) were provided ad libitum. Females were housed in groups of four or five within polycarbonate boxes of 51 $in.^2$ area on sterilized shavings of Northern White Pine as bedding.

The inbred strains B6 and C3H were selected for QTL analysis of serum IGF-1 based on our previously reported marked differences in serum IGF-1 levels from ages 7 days to 12 months.[14] These inbred strains also differ in femoral BMD by at least 50%, as measured by peripheral quantitative computerized tomography (pQCT).[7] Progeny for genetic analysis of serum IGF-1 were produced by mating low-serum IGF-1 B6 females to high-serum IGF-1 C3H males, then intercrossing the (B6 × C3H)F1 hybrids to produce F2 offspring. A total of 682 F2 females were utilized in these genetic analyses. F2 males were not kept because of lethally aggressive behavior when group-housed. The F2 females were analyzed at 4 months of age when acquisition of adult BMD is maximal and peak adult serum IGF-1 levels are established. Body weights were recorded at necropsy, and partial carcass preparations were preserved in 95% ethanol as previously described.[1] Kidneys and spleens from each mouse were frozen in liquid N_2 and stored at −60°C for later extraction of genomic DNA. Subsequently, femurs were isolated and their lengths measured by digital calipers prior to densitometry (see later).

Congenic strains are valuable tools for genetically decomposing complex traits into simpler systems for testing the biological effects of individual QTLs and positional cloning the relevant gene(s) underlying a QTL. Congenic strains are established by ten cycles of backcrossing a specific chromosomal segment from a donor strain—in this case C3H—onto a recipient strain, which was B6. Mice chosen at each generation for matings to produce the next generation were genotyped by polymerase chain reaction (PCR) for strain-specific molecular makers to identify carriers of the chromosomal segment of interest. At the N10 generation, the genetic composition of the congenic strain is >99% identical to the original recipient strain, with only the transferred region being of the donor strain. Mice from one of a set of such strains, designated B6.C3H-(chromosome number), along with age- and gender-matched B6 controls, were compared for serum IGF-1 levels at 6–8 weeks of age.

Bone Densitometry

BMD of isolated femurs was measured by pQCT with a Stratec XCT 960M (Norland Medical Systems, Fort Atkinson, WI), as previously described.[1] Femurs were scanned at 2 mm intervals over their entire length, utilizing an X-ray attenuation threshold of 2000 units to define high-density bone, a threshold of 1300 to define low-density bone, and a unit volume for measurement of mineral set at 0.1 mm^3. The low-density threshold differentiated water, fats, and proteins from mineralized bone. The precision of this instrument for densitometry of mouse bones has been determined to be 1.2% by repeated placement and measurement of a single femur. Calibration of the densitometer was done with a set of hydroxyapatite standards and yielded a correlation of 0.997 between standards and pQCT estimation of bone density. In this study, femoral BMD is defined as total femoral mineral divided by total femoral volume.

Serum IGF-1

Serum IGF-1 in 4-month-old progenitors and all F2 mice was determined by a radioimmunoassay as previously described.[14] Blood was obtained at the time of necropsy and placed on ice for 3–4 h, then serum was harvested and stored frozen at −70°C prior to analysis. After a single defrost, 50 μL of serum was mixed with phosphate-buffered saline (PBS) to a final volume of 100 μL. IGF-binding proteins (IGFBPs) were removed prior to radioimmunoassay (RIA) by acid ethanol cryoprecipitation (AEC), according to previously established methods.[14,16] Following two extractions, serum IGF-1 was measured, in duplicate, by competitive protein binding using a polyclonal antibody (Nichols Institute, San Juan Capistrano, CA). In each assay, known concentrations of recombinant human IGF-1 (i.e., low, medium, and high levels of IGF-1), provided by the manufacturer, were used to construct a standard curve to delineate serum concentrations of IGF-1 for each sample. This RIA shows virtually no cross reactivity (<0.1%) with IGF-2 and the detection limit for this assay is 23 ng/mL of IGF-1. In our laboratory, the interassay coefficient of variation for the standard low concentration of IGF-1 is 6.2% and single intra-assay variation for the same standard is 3.6% for serum IGF-1 levels in range 150–200 ng/mL.

Because more than 700 F2 and progenitor serum samples were assayed, we established a series of control sera to correct for multiple testing and interassay variation. Pools combining C3H and B6 sera, as well as individual pools of C3H and B6 sera, were run in each assay and, subsequently, the F2 serum values were corrected for the combined B6 + C3H pool, whereas individual pools for the particular strain were used as an internal check to insure the assay results were consistent at various concentrations of serum IGF-1. For the combined pools, the mean value of serum IGF-1 was 373 ± 6 ng/mL in 20 assays. Hence, serum levels in the individual F2 mice were divided by the mean value of 373 and expressed as a normalized value, termed "adjusted" (adj) serum IGF-1. Individual serum samples from progenitor C3H and B6 female mice were also included in each assay to assess relative strain differences within assays. Both actual and adjusted serum IGF-1 concentrations were log-transformed for assessment of distribution characteristics. All serum values are reported as the mean of adj serum IGF-1 ± SEM.

Genetic Analyses

Genomic DNA was prepared from spleens of mice by standard chloroform-phenol extraction. Genotyping of individual mouse DNAs was accomplished by PCR using oligonucleotide primer pairs from Research Genetics (Birmingham, AL). Primer pairs identifying simple sequence length polymorphisms (SSLPs) that discriminate between alleles from B6 vs. C3H were selected from more than 6000 available. Details of PCR reactions have been described previously.[1] DNAs from B6 and C3H and (B6 × C3H)F1 hybrids were used as electrophoretic standards in every gel to identify the genotype of PCR products derived from F2 mice; for instance, homozygous B6 (*b6/b6*), C3H (*c3/c3*), and heterozygous (*b6/c3*). Nineteen autosomes in the F2 progeny were assessed for associations of PCR-based molecular markers with adj serum IGF-1 data. Chromosome (Chr) X alleles were not assessed because reciprocal F1 × F1 matings would be required to yield all possible allelic combinations necessary for meaningful genetic evaluations. Four to ten microsatellite DNA polymorphic markers were selected for testing each automosome at an average interval of 14 cM from centromere to telomere. Ten percent of the total population in either extreme of adj IGF-1 distribution was genotyped for 114 markers, and data inspected for correlations between segregating alleles and adj IGF-1. DNAs from the remaining F2 mice were prepared and genotyped for informative markers on chromosomes with putative IGF-1-related QTLs, as well as markers for upper, middle, and lower regions of all chromosomes, without initial evidence of correlation with adj serum IGF-1. There were 682 F2 included in the final data analyses, assuring that genetic radius swept per marker did not leave any chromosomal region untested for correlation of phenotype with genotype.

Statistical Analyses

Single marker genome scans. We computed a one-way analysis of variance (ANOVA) Fisher (*F*) statistic and LOD scores at each marker in the genotyping array. Statistical significance was assessed by permutation testing[5] using 10,000 permutations from the original trait data. Permutation test thresholds account for multiple testing implicit in the genome-wide search. For these data, the permutation threshold critical values are very close to the values proposed by Lander and Kruglyak.[10]

Pairwise genome scans. Some loci can affect a phenotype primarily through interaction effects. We developed an approach and implemented a software tool in MATLAB (Mathworks, Inc., Natick, MA) to conduct a simultaneous search for pairs of interacting loci. This search examines all pairs of marker loci for association with the trait in a two-dimensional genome scan. For each marker pair, the likelihood under a full regression model (with two main effects and an interaction) is compared with that under the null model of no genetic effects. This comparison generates an array of *F* statistics, which represents the primary screen for identifying locus pairs of interest. Significance is assessed by permutation analysis to account for the large number of pairs tested in the genome-wide search. If the *F* statistic for a locus pair is significant at $p < 0.05$, and genome-wide-corrected, we carry out several additional tests to determine if the pair represents a genuine interaction, two additive main effects, or is merely an artifact resulting from a strong association with only one of the two loci. A second *F* statistic (with 4 and 9 degrees of freedom) is computed that compares the full model likelihood to that of an additive model with two main effects but no interaction. If this test is significant ($p < 0.01$), we conclude that the loci interact. If this second *F* statistic is not significant ($p > 0.01$), we conclude that there is not strong evidence of interaction and proceed to the next level of testing. Two additional *F* statistics (with 2 and 5 degrees of freedom) are computed to compare each of the single locus models to the two-locus additive model. If either of these tests is not significant ($p > 0.01$), this indicates that one of the loci in the pair may not be contributing to the observed association. This could occur if one locus is carried by a much stronger effect at a second locus. Each of these secondary tests is carried out using nominal *p* values not corrected for the genome-wide search. Nominal *p* values are appropriate because we have already selected the locus pair using a stringent genome-wide criteria. The choice of a nominal level at 0.01 for significance is stringent.

Multiple regression. Genome scans are useful for detecting significant effects, but it is also important to assess the simultaneous effects of multiple QTLs on a trait. We use a general linear model, based on marker regression, to assess the joint effects of all loci (and interactions) that appear to be significant in the genome-wide scan. Multiple regression models were fit using MINITAB software (Minitab, Inc., State College, PA).

Other statistical analyses. Data for adj serum IGF-1, femoral length, and femoral total BMD were analyzed with the computer program STATVIEW version 4.5 (SAS Institute, Cary, NC). Comparisons among groups or between congenics and progenitors were made using ANOVA. Post hoc group-wise comparisons were done using a Fisher's protected least significant difference test with differences accepted as significant when $p < 0.05$.

Results

Adjusted IGF-1 Distribution in the F2 Population

In this study, we confirmed significant interstrain differences for serum IGF-1 in 4-month-old female progenitors: C3H, n = 11, 415 ± 19 ng/mL (adj IGF-1 = 1.11 ± 0.05); and B6, n = 12, 300 ± 13 ng/mL (adj IGF-1 = 0.80 ± 0.03); $p < 0.0001$ C3H vs. B6). For 20 B6C3 pools, in which sera from both strains were mixed and then assayed, the mean serum IGF-1 level was 373 ± 6 ng/mL. For all 671 F2 mice, the mean serum IGF-1 level was 369 ± 9 ng/mL (adj IGF-1: 0.99 ± 0.02). The range of serum IGF-1 was 180–576 ng/mL (adj IGF-1: 0.48–1.54). The distribution of serum IGF-1 in the F2 mice is noted in **Figure 1** along with arrows indicating mean values for B6 and C3H progenitors. The general heritability (h^2) of serum IGF-1 in this model was estimated to be 52% based on the variances in IGF-1 levels of the progenitors and F2 progeny.

Initial genotyping was performed for 10% of the F2 progeny located at the extremes of the IGF-1 phenotype distribution (Figure 1) to identify major effect loci. Subsequently, the remaining F2 population was genotyped for additional informative markers related to putative IGF-1 QTLs and for testing of gene interactions. Inspection of the actual data vs. the theoretical normal curve showed that the adj IGF-1 distribution in the F2 mice was skewed slightly to the left. A modest number of values were lower or greater than the mean of either progenitor strain (denoted by arrows). Mean femur length for the B6 progenitors was 16.06 ± 0.15 mm and for C3H was 15.71 ± 0.08 mm, which indicated a significant difference ($p < 0.001$). Mean femoral BMD for progenitor B6 was 0.458 ± 0.004 mg/mm^3, and for progenitor C3H was 0.707 ± 0.007 mg/mm^3 ($p < 0.0001$). The mean femoral BMD for all F2 mice was 0.584 ± 0.002 mg/mm^3. By simple linear correlation, significant relationships were noted between adj IGF-1 and femoral BMD ($r = 0.267$, $r^2 = 0.07$; $p < 0.0001$) (**Figure 2**). Differences in adj IGF-1 predicted approx-

Bone Vol. 27, No. 4
October 2000:521–528

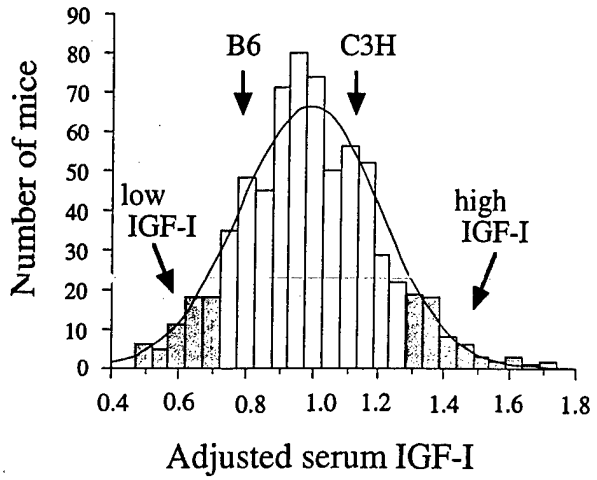

Figure 1. Frequency distribution for adjusted serum IGF-1 in 682 B6C3H-F2 mice. Serum IGF-1 levels were adjusted to values for control sera (pooled sera of C3H and B6 progenitors) included in each assay. An adjusted (adj) IGF-1 of 1.0 represents a serum value of 373 ng/mL, and all other levels are ratios of that value. Arrows indicate the mean values for groups of progenitor strain mice. Shaded tails of the distribution represent "extremes" samples chosen for initial genotyping; all mice were genotyped for the final analysis.

imately 7% of the differences in femoral BMD. Similar regression analyses were also performed for adj IGF-1 and: (a) body weight ($r = 0.260$, $r^2 = 0.067$, $p < 0.0001$); (b) femoral length ($r = 0.266$, $r^2 = 0.069$; $p < 0.0001$); and (c) periosteal circumference ($r = 0.131$, $r^2 = 0.017$, $p = 0.009$).

Mapping QTLs for Serum IGF-1 Phenotype

The results of genome-wide scans are presented in **Figure 3A**. Whole genome scans with marker regression revealed highly significant peaks on Chr 6 (*D6Mit150*), Chr 10 (*D10Mit95*), and Chr 15 (*D15Mit209*) after genome-wide correction by permutation analysis, according to criteria defined previously by Churchill and Doerge.[5] A suggestive peak was also noted on Chr 1 and was additive for serum IGF-1, although it did not achieve genome-wide significance. In Figure 3B, the interval maps for Chrs 6, 10, and 15 are presented along with the specific Mit markers used to genotype these chromosomes. The radii swept by these markers along each chromosome in the 682 F2 mice assured that significant correlations with the IGF-1 phenotype were detected. Genome-wide corrected LOD scores exceeded the threshold of 4.3 established by Lander and Krugliak[10] for significant linkage.

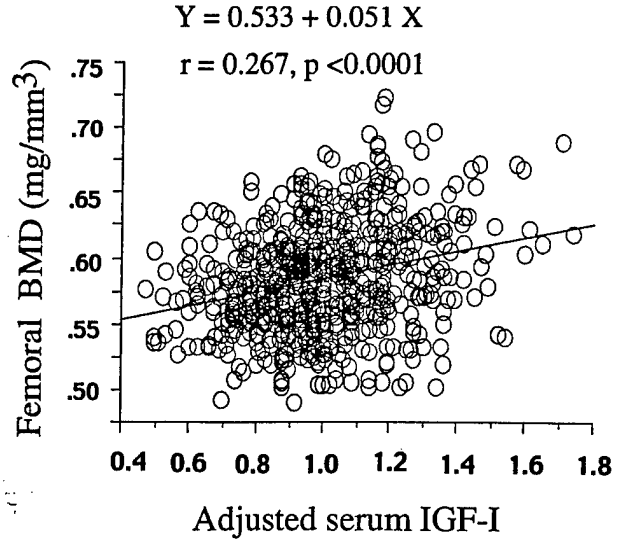

Figure 2. The adjusted serum IGF-1 data were regressed against femoral total BMD (mg/mm^3). The regression equation describing the relationship is included, along with the correlation coefficient and its significance level.

A pairwise genome scan was carried out as described in *Materials and Methods* to identify potentially interacting QTLs. A significant interaction was detected between loci on Chrs 6 and 11, represented by markers *D6Mit150* and *D11Mit71*. The overall F statistic for the pairwise comparisons was $F = 8.52$, which exceeded the genome-wide threshold of $F > 5.5$ for genome-wide significance at the $p = 0.01$ level. The interaction F statistic was $F = 4.52$, which has a nominal p value of 0.0013 based on tabulated F distribution with 4 and 673 degrees of freedom. To further characterize the joint contributions of significant QTLs detected by whole genome scans, we constructed a multiple regression model with each of the main effects and the Chr 6 × Chr 11 interaction. **Table 1** presents the complete ANOVA table for main and interaction effects. We found that the entire model explains 12.8% of the variance in serum IGF-1. After the other QTLs were taken into account, the Chr 6 × Chr 11 interaction explained 5.8% of the adjusted variance, the Chr 10 QTL explained 1.3% of the adjusted variance, and the Chr 15 QTL explained 2.4% of the adjusted variance. The difference between the entire model variance accounted for and the sum of individual QTL contributions was imperfect (12.8% vs. 9.5%) due to chance correlations among QTLs.

Analyses of QTL Effects

To determine if allelic variation at each of the QTLs on Chrs 6, 10, and 15 would affect adj serum IGF-1 levels, F2 mice were partitioned into groups that were *b6/b6*, *b6/c3*, or *c3/c3* for each chromosome. The data presented in **Figure 4A** show that, with respect to the Chr 6 QTL, serum IGF-1 was reduced significantly as the number of *c3* alleles increased from zero to two. On the other hand, in Figure 4B,C, serum IGF-1 rose significantly as the number of *c3* alleles increased at both Chrs 10 and 15. Frequencies of each allelic class were tested and found to not differ from the expected 1:2:1 ratio for single biallelic genes. Thus, the QTL alleles segregated normally and demonstrated additive effects.

The interaction between Chr 6 and Chr 11 can be described as an interaction between the additive effect at Chr 6 (i.e., lower serum IGF-1 levels with more *c3* alleles) with a dominant B6 modifier locus at Chr 11. To illustrate this interaction on serum IGF-1 levels, the F2 data were partitioned into allele groups (*b6/b6*, *b6/c3*, and *c3/c3*) for *D11Mit71*, then the *b6/b6* group was subdivided by *D6Mit150* alleles (**Figure 5A**), the *b6/c3* group was subdivided by *D6Mit150* alleles (Figure 5B), and the *c3/c3* group subdivided by *D6Mit150* alleles (Figure 5C). Significant lowering of IGF-1 levels was detected for the Chr 6 QTL only when the Chr 11 QTL carried one ($F = 26.94$; $p < 3.7 \times 10^{-7}$) or two ($F = 4.19$; $p < 0.017$) B6 alleles. The effect of the Chr 6 locus was essentially null when Chr 11 carried two *c3* alleles ($F = 1.43$; $p = 0.243$).

Testing the Relationship Between Serum IGF-1 and BMD

Because several studies have suggested a relationship between BMD and serum IGF-1 in humans, and we noted a statistically

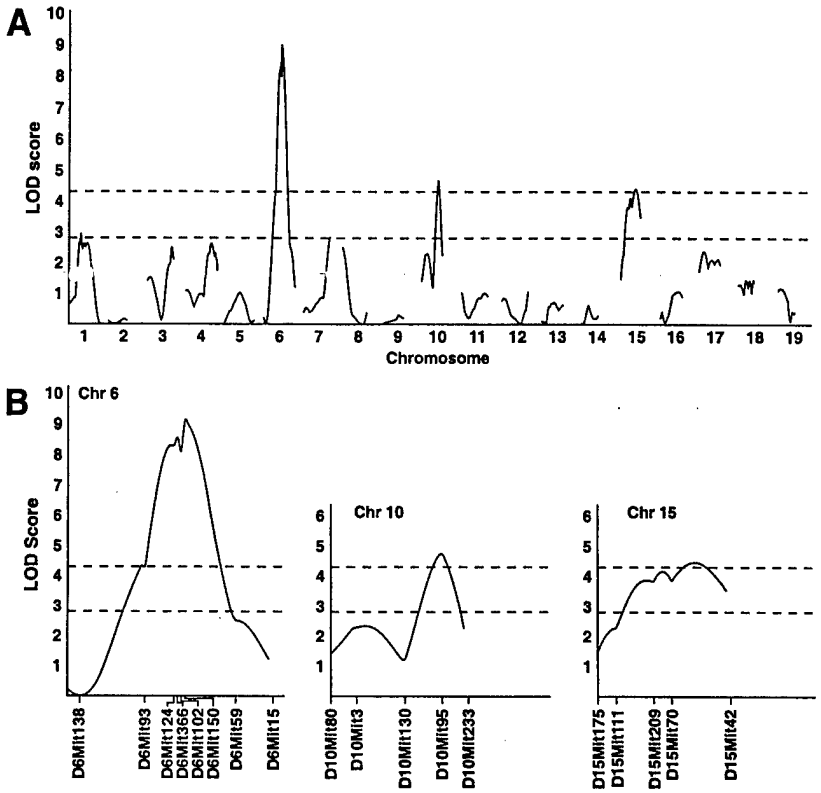

Figure 3. (A) Genome-wide scanning for Mit markers across all 19 autosomes that correlated with adjusted serum IGF-1 levels was performed as described in *Materials and Methods*. The abscissa shows relative location of marker loci with respect to each other on every chromosome. The ordinate shows the LOD score derived from the ANOVA obtained at each marker. The horizontal lines are threshold values for genome-wide significance at 0.10 (lower dashed line) and 0.01 (upper dashed line) as estimated by 10,000 permutations of the trait data.[5] (B) Interval mapping figures for each of the chromosomes (6, 10, and 15) with independent QTLs affecting adjusted serum IGF-1 levels. The lower and upper dashed lines in each panel represent the threshold LOD score (2.8 and 4.3) required to declare suggestive or significant linkage, respectively.

significant albeit modest correlation in the F2 mice between these two phenotypes, we performed additional studies to further define the interaction, if any, between serum IGF-1 and bone mass.[4,11,13] First, we compared the results of our QTL analysis for serum IGF-1 to preliminary data generated in our laboratory for a QTL analysis on femoral BMD in the same B6C3H-F2 mice.[2] Only principle QTLs on Chrs 6 and 11 are common to both phenotypes (Beamer et al., unpublished data). Second, we tested the hypothesis that the QTL on Chr 6 from C3H would, if placed on a B6 background, lower both serum IGF-1 and femoral bone mineral density. Using the available B6.C3H-6 congenic strain, we found that serum IGF-1 concentrations were 16% lower in the B6.C3H-6 congenic mice at 6–8 weeks than in age- and gender-matched B6 progenitors (B6.C3H-6-*c3/c3*: IGF-1 = 232 ± 8 ng/mL vs. B6 +/+ progenitors: IGF-1 = 278 ± 12 ng/mL, $p = 0.0001$). This is nearly identical to the estimated size effect of this QTL, derived from regression analyses, noted in Figure 4A. Moreover, the congenics exhibited nearly 4% lower femoral BMD by pQCT than homozygous B6 mice (i.e., B6C3H-6 *c3/c3*: BMD, 0.469 ± 0.006 mg/mm^3 vs. B6 +/+ progenitors, 0.485 ± 0.010 mg/mm^3). Thus, the presence of two C3H alleles at the Chr 6 QTL, and two B6 alleles at Chr 11 QTL, resulted in significantly lower BMD and lower serum IGF-1 values than mice homozygous for B6 alleles at all loci.

Table 1. One-way analysis of variance (ANOVA) summary of a general linear model for adj IGF-1 levels, utilizing all Mit markers with effects detected by genome-wide scans

Source	Degrees of freedom	Adjusted sum of squares	*F*	*p*
D6Mit150	2	0.88425	11.42	0.000013
D10Mit95	2	0.37815	4.88	0.0079
D15Mit209	2	0.71700	9.26	0.00011
D11Mit71	2	0.17229	2.22	0.109
D11Mit71 D6Mit150*	4	0.64827	4.19	0.0023
Error	669	25.90699		
Total	681	29.69496		

F represents the Fisher statistic, based on the adjusted (type III) sum of squares and *p* values obtained from the tabulated *F* distribution.

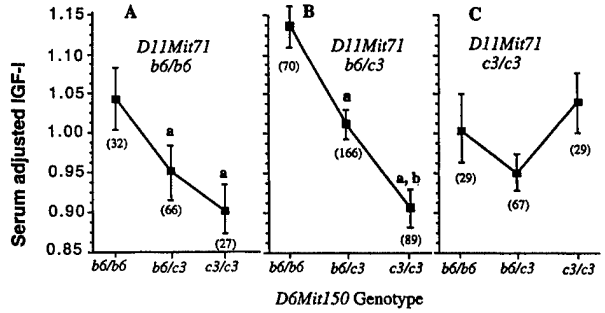

Figure 4. The interactive effects of QTLs marked by *D6Mit150* and *D11Mit71* are presented in three panels, each giving the allelic combinations for *D6Mit150* on the abscissa. Data are presented as mean ± SEM; numbers in parentheses represent group size. (A) Net effect of *b6/b6* alleles for *D11Mit71* when *D6Mit150* alleles were *b6/b6*, *b6/c3*, or *c3/c3* was significant ($p = 0.017$). Bold "**a**" indicates significant difference from *b6/b6* group ($p < 0.05$). (B) Net effect of *b6/c3* alleles for *D11Mit71* when *D6Mit150* alleles were *b6/b6*, *b6/c3*, or *c3/c3* was significant ($p < 10^{-7}$). Bold "**a**" and "**a,b**" indicate significant differences among all three groups ($p < 0.0001$). (C) Net effect of *c3/c3* alleles for *D11Mit71* when *D6Mit150* alleles were *b6/b6*, *b6/c3*, or *c3/c3* was not significant; thus, individual means were not compared.

Bone Vol. 27, No. 4
October 2000:521–528

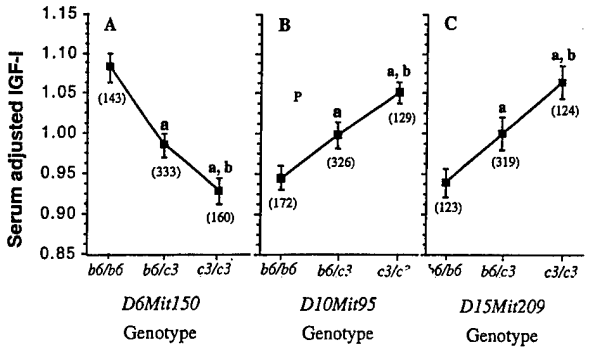

Figure 5. The effect of genetic alleles on the adjusted serum IGF-1 levels are shown for marker *Mit150* on Chr 6 (A), *Mit95* on Chr 10 (B), and *Mit209* on Chr 15 (C). All three QTLs behave in an additive fashion, with *b6/c3* heterozygotes and *c3/c3* homozygotes significantly different from each other as well as from *b6/b6* homozygotes ($p < 0.01$). Data presented as mean ± SEM; numbers in parentheses represent group sizes.

Candidates Genes

Last, we suggest provisional locus names of *Igf1sl1* to *Igf1sl4* for the QTLs mapped on Chrs 6, 10, 15, and 11 in relation to IGF-1 serum levels. These *Igf1sl* loci along with the best markers are presented in diagrammatic form in **Figure 6**, wherein genetic lengths of chromosomes and mapped locus positions are maintained. In addition, we examined whether the QTLs identified in this experimental analysis are near chromosomal regions for the major regulatory factors involved in the generation and activity of serum IGF-1. It is apparent that growth hormone (GH), GH receptors, GH binding proteins, GHRH, somatostatin, the six somatostatin receptors, and the Ghrhr receptor do not map to regions identified by these QTLs. However, two IGF binding protein genes, *Igfbp1* and *Igfbp3*, are located within 1 cM of the Mit marker correlated with *Igf1sl4* on proximal Chr 11. Furthermore, the mouse *Igf1* gene is located within 3 cM of the Mit marker correlated with *Igf1sl2* on Chr 10. The *Igf1sl1* QTL on Chr 6 and *Igf1sl3* QTL on Chr 15 have yet to be related to any genes.

Discussion

In previous studies with these two inbred strains, we demonstrated that: (a) C3H mice have greater bone mass at several skeletal sites (spine, femur, tibia, phalange), despite similar body size and weight, than B6 mice; and (b) the BMD phenotype in B6 and C3H mice is principally a function of heritable determinants.[1] Furthermore, we established several mechanistic properties related to both bone formation and resorption, which account for differences in this skeletal phenotype. For example, we have shown that C3H mice have decreased bone resorption, in vitro evidence of fewer osteoclast progenitor cells, and lower levels of interleukin-6 (IL-6) production compared with B6 mice.[12] With respect to bone formation, we demonstrated greater rates of bone formation and mineral apposition in the tibia and femur, a larger number of osteoblast progenitor cells, and higher circulating and skeletal levels of both IGF-1 and alkaline phosphatase compared with B6 mice.[6,9,17] Also, there was a consistent correlation between serum IGF-1 and femoral BMD in both F1 and F2 progeny, and calvarial osteoblasts from C3H mice were shown to secrete more IGF-1 than B6 cells in vitro.[14] These lines of evidence suggest that the bone density phenotype can be influenced by heritable determinants that might modulate bone formation either by regulating IGF-1 expression, or through common signaling pathways for the IGFs, which are also shared by other skeletal growth factors. To appreciate the importance and interaction of these determinants, we initiated QTL for an intermediate skeletal phenotype, serum IGF-1, in the F2 offspring of C3H and B6 progenitors.

In this study, we showed that the serum IGF-1 variation in B6C3H-F2 mice has a strong heritable component ($h^2 = 52\%$),

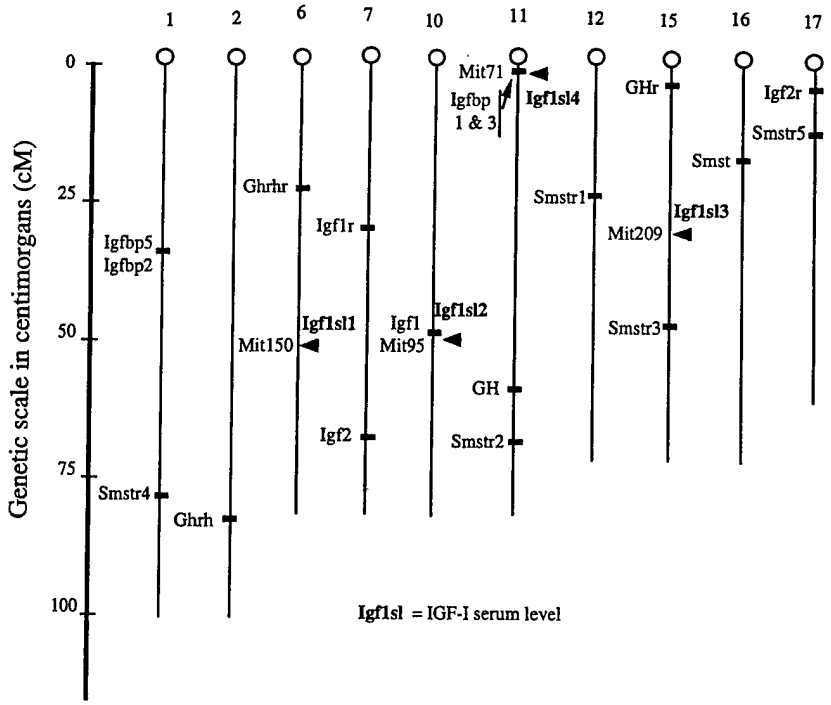

Figure 6. Diagram represents the location on ten different mouse chromosomes (numbers shown at top of each stick drawing) of several components of the GH/IGF axis. The vertical axis represents the distance from the centromere; chromosome lengths are relative to known genetic length. Arrow heads represent QTLs for the IGF-1 phenotype. *Igf1sl1* denotes the provisional term for the QTL on Chr 6 (IGF-1 serum level 1), *Igf1sl2* the QTL on Chr 10, *Igf1sl3* the QTL on Chr 15, and *Igf1sl4* the interactive QTL on Chr 11.

and the expression of IGF-1 is regulated by three independent *IGF1sl* QTLs (Chrs 6, 10, and 15). In addition, we found an important epistatic interaction between the *IGF1sl* QTL on Chr 6 and another *IGF1sl* QTL on Chr 11. The combined genetic effects by Chrs 6, 10, 11, and 15 partially account for the distribution of adj IGF-1 observed in Figure 1, including values less than B6 progenitors as well as those greater than the C3H progenitors. This transgressive effect indicates that both progenitors carry genes that result, independently or interactively, in very low or high serum IGF-1 concentration. For example, F2 mice carrying alleles for B6 at both *IGF1sl* QTLs on Chrs 15 and 11, but C3H alleles at *Igf1sl1* Chr 6, have 25% lower serum adj IGF-1 concentrations (0.888 ± 0.088) than those mice homozygous for C3H alleles at all three loci (1.137 ± 0.031). Similarly, the newly constructed B6.C3H-6 congenic is genetically $Igf1sl1^{c3}/Igf1sl1^{c3}$ and exhibited 16% lower serum IGF-1 than B6 progenitors, which are genetically $Igf1sl1^{b6}/Igf1sl1^{b6}$.

As predicted by whole genome scanning, the *Igf1sl1* QTL on Chr 6 has a significant effect on serum IGF-1, although the direction of change was contrary to our a priori predictions, which were based solely on the large differences in serum IGF-1 of the progenitors (i.e., C3H has serum IGF-1 concentrations 30% higher than B6 across all ages). Even though this finding was, at first glance, surprising, we found support for these data from a recent QTL analysis in mice performed by another laboratory,[3] as well as a closer examination of our own data. First, as noted earlier, there were numerous mice among the F2 progeny with circulating IGF-1 levels lower than concentrations noted for the B6 progenitors. Indeed, the distribution of serum IGF-1 levels in the F2 mice was shifted slightly toward mean B6 levels (see Figure 1), consistent with a strong effect from the *Igf1sl1* QTL alleles from C3H on Chr 6 in a mixed background including homo- or heterozygosity for B6 alleles at the *Igf1sl4* QTL on Chr 11. Similarly, like Benes et al.,[3] we noted that at least one set of C3H alleles from a high-bone-density strain is associated with lower, rather than higher, BMD. Further studies, including the evaluation of more congenic animals with different alleles at various loci, and recombinant inbred strains, will be necessary to define the functional aspects of the *Igf1sl1* QTL on Chr 6 and to delineate how the *Igf1sl4* QTL on Chr 11 can so strongly interact with a major genetic determinant of serum IGF-1.

Several lines of evidence from this study and preliminary work in our laboratory have revealed that heritable determinants of serum IGF-1 probably include regulatory elements other than growth hormone.[14] First, there are large differences in circulating IGF-1 levels in the progenitor strains despite similar serum GH and growth hormone binding proteins (GHBP) concentrations.[14] Furthermore, femoral length, periosteal diameter, and overall size are remarkably similar between the two strains at 16 weeks of age (this report).[1] The lack of anthropomorphic differences in these two strains, despite serum IGF-1 concentrations differing by at least 30%, argues against major alterations in the secretion of growth hormone. Second, little (*lit/lit*) mice (i.e., mutants with a spontaneous recessive mutation in the GHRH receptor) have low serum IGF-1 levels and reduced BMD.[7] As we have shown previously, when *lit* is moved from a B6 to a C3H background (B6.C3H-*lit/lit*), serum IGF-1 levels and hepatic IGF-1 mRNA increase threefold, while femoral BMD is also increased compared with B6 *lit/lit*, despite the virtual absence of GH.[15] Third, in this study, we found three *Igf1sl* QTLs for serum IGF-1 on Chrs 6, 10, and 15, as well as an interactive *Igf1sl4* QTL on Chr 11, all of which reside in regions of their respective chromosomes totally distinct from chromosomal locations for GH, the GH receptor, somatostatin, its six receptors, GHRH, or the GHRH receptor (Figure 6). Finally, in vitro studies with calvarial osteoblasts from the two strains demonstrate a nearly twofold greater secretion of IGF-1 in C3H than B6 mice.[14] Thus, changes in GH secretion are not likely to be responsible for heritable differences in the IGF-1 phenotype.

It is likely that the *Igf1sl* QTLs noted in this study include regulatory factors for IGF-1 that play a role in any or all of three processes: (1) intracellular signaling cascades for GH or IGF-1; (2) transcriptional control of the IGF-1 gene; or (3) posttranslational processing of IGF-1. With respect to the signalling process, the *Igf1sl1* QTL on Chr 6 is in a 24 cM region that contains as many as 2500 hundred genes. But, one gene located in very close proximity to *D6Mit150* (Figure 6) is *Raf-1*, a protooncogene, which is critical for induction of MAP kinase, a necessary component of GH, IGF-1, and other growth factor signaling. With regard to the second process, it is conceivable that interstrain differences in the structure of the IGF-1 gene could lead to alterations in transcription, and account for the disparity in circulating IGF-1 noted between C3H and B6 mice. Indeed, the QTL on Chr 10 is in very close proximity to the location of the mouse IGF-1 gene. We now have begun to sequence the IGF-1 promoter regions in the two mouse strains and have already identified several sequence differences. These differences may or may not be related to the *Igf1sl1* QTL on Chr 10, and to serum IGF-1 levels, although it is important to point out that at least one polymorphic dinucleotide repeat in humans within the *IGF1* gene has been associated with significant differences in serum IGF-1.[16] Further studies, including fine mapping of the Chr 10 region containing the *Igf1sl1* QTL, transient transfection analysis, and deletional studies of the IGF-1 promoters, should help determine whether there is a functional relationship between single nucleotide differences and IGF-1 expression.

Finally, posttranslational effects on IGF-1, including changes in IGF-binding protein (IGFBP) expression or proteolysis, can profoundly affect circulating concentrations of IGF-1 as well as the biological activity of this peptide. Interestingly, the interactive *Igf1sl4* on Chr 11 is in very close proximity to a set of highly conserved IGFBPs, IGFBP-3, and IGFBP-1. Although it is only speculation as to whether one of these IGFBPs is a candidate for *Igf1sl4* on Chr 11, this possibility raises some very provocative questions. In particular, it is conceivable that the presence of at least one B6 allele at this locus in a mouse with two C3H alleles at the Chr 6 QTL could alter IGFBP production, binding affinity, or degradation, thereby effectively changing the availability of IGF-1 in the circulation. Alternatively, one of the IGFBPs could regulate IGF-1 expression through a host of IGF-independent mechanisms. In sum, the results of this QTL analysis provide opportunities to examine novel mechanisms of IGF-1 regulation, and their role in acquisition of peak bone mass.

We recognize there are some potential limitations to this study. First, it is important to appreciate that, in the generation of F2 progeny from the two progenitor strains, the only QTLs we would expect to find are those in which there are allelic differences between B6 and C3H. Because these strains have been shown to be polymorphic at only about 50% of the Mit markers, there are likely to be other genetic determinants not detectable in this study. Crosses with different mouse strains may reveal additional QTLs for serum IGF-1. Second, even though the *Igf1sl* QTLs on Chrs 6, 10, and 15 contribute substantially to the variability in serum IGF-1 concentrations, there is still a large component of variance for this particular phenotype that is not heritable. For example, changes in several hormonal variables can have a profound effect on circulating levels of IGF-1.[8] Moreover, there are likely to be gene-environment interactions that are critical in determining serum IGF-1 levels. Third, we chose the serum IGF-1 phenotype because of its ease of measurement and its potential relationship to peak bone acquisition.

Bone Vol. 27, No. 4
October 2000:521–528

However, it is clear that skeletal IGF-1 is regulated by numerous factors, some of which are likely to be similar or identical to determinants of circulating (or hepatic) IGF-1, whereas others are unique to calcified tissues (e.g., parathyroid hormone). Notwithstanding, at least in this model of interstrain IGF-1 differences, we noted changes in skeletal content and in vitro production of IGF-1 from osteoblasts that parallel strain-specific differences in serum concentrations.[14] These data suggest there are shared regulatory factors for hepatic and skeletal IGF-1 expression that are heritable and may be completely independent of growth hormone. Fourth, we appreciate that the relationship between IGF-1 and BMD is more complex than a simple correlation. Indeed, serum IGF-1 accounts for only about 7% of the variance in femoral BMD in the F2 progeny. Yet F2 mice classically exhibit independent segregation of alleles; hence, our model reflects the nature of genetic heterogeneity, a characteristic property observed in human studies examining determinants of BMD. Still, like previous human studies, we found a statistically significant relationship between serum IGF-1 and BMD in the F2 and congenic mice.[4,8,11,13,14,18] Finally, we phenotyped and genotyped only female F2 and congenic mice. Therefore, our conclusions must be tempered by the possibility that there is a gender effect on IGF-1 and/or BMD that could not be revealed in this analysis.

In summary, we have shown in B6C3H-F2 mice that serum IGF-1 levels are inherited as a polygenic trait and this phenotype contributes to acquisition of peak BMD. Specifically, we identified three independent *Igf1sl* QTLs and one epistatic *Igf1sl1-Igf1sl4* interaction underlying the serum IGF-1 phenotype. Two of these QTLs are distinct from known genes in the GH axis; whereas one interactive locus may include genes for IGFBP-1 or IGFBP-3, and one locus resides in close proximity to the IGF-1 gene. Preliminary studies in the B6.C3H-6 congenic strain suggest that the *Igf1sl1* locus has a definitive effect on serum IGF-1 at 6 weeks of age, with parallel actions on the femoral BMD phenotype. Fine mapping of these putative QTLs will help discern IGF-1 regulatory genes and provide the tools necessary for functional studies relating IGF-1 to acquisition of bone mass.

Acknowledgments: This work was funded by PHS Grants AR 45433, AR 43618, and CA34196 (CORE support from the Jackson Laboratory).

References

1. Beamer, W. G., Donahue, L. R., Rosen, C. J., and Baylink, D. J. Genetic variability in adult bone density among inbred strains of mice. Bone 18:397–405; 1996.
2. Beamer, W. G., Rosen, C. J., Donahue, L. R., Frankel, W. N., Churchill, G. A., Shultz, K. L., and Baylink, D. J. Location of genes regulating volumetric bone mineral density in C57B1/6J and C3H/HeJ inbred strains of mice. Bone 23(Suppl. 162); 1998.
3. Benes, H., Weinstein, R. S., Zheng, W., Thaden, J. J., Jilka, R. L., Manolagas, S. C., and Rei-Shmookler, R. J. et al. Chromosomal mapping of osteopenia associated QTL using closely related mouse strains. J Bone Miner Res 15: 626–633; 2000.
4. Cadogan, J., Blumsohn, A., Barker, M. E., and Eastell, R. A longitudinal study of bone gain in pubertal girls: Anthropometric and biochemical correlates. J Bone Miner Res 13:1602–1612; 1998.
5. Churchill, G. A. and Doerge, R. W. Empirical threshold values for quantitative trait mapping. Genetics 138:963–971; 1994.
6. Dimai, H. P., Linkhart, T. A., Linkhart, S. G., Donahue, L. R., Beamer, W. G., Rosen, C. J., Farley, J. R., and Baylink, D. J. Alkaline phosphatase levels and osteoprogenitor cell numbers suggest that bone formation may contribute to peak bone density differences between two inbred strains of mice. Bone 22:211–216; 1998.
7. Donahue, L. R. and Beamer, W. G. Growth hormone deficiency in "little" mice results in aberrant body composition, reduced insulin-like growth factor-I (IGF-I) and reduced insulin-like growth factor binding protein-3 (IGFBP-3), but does not effect IGFBP-2, -1, or -4. J Endocrinol 136:91–104; 1993.
8. Donahue, L. R. and Rosen, C. J. IGFs and bone: The osteoporosis connection revisited. Proc Soc Exp Biol Med 219:1–7; 1998.
9. Kodama, Y., Dimai, H. P., Wergedal, J., Sheng, M., Malpe, R., Kutilek, S., Beamer, W. G., Donahue, L. R., Rosen, C. J., Baylink, D. J., and Farley, J. Tibial cortical bone volume in two strains of mice: A study of the effect of sciatic neurectomy and the genetic regulation of bone response to mechanical loading. Bone 25:183–190; 1999.
10. Lander, E. S. and Kruglyak, L. Genetic dissection of complex traits: Guidelines for interpreting and reporting linkage results. Nature Genet 11:241–247; 1995.
11. Langlois, J. A., Rosen, C. J., Visser, M., Hannan, M., Harris, T., Wilson, P. F. W., and Kiel, D. The association between IGF-I and bone mineral density in women and men: The Framingham heart study. J Clin Endocrinol Metab 83:4257–4262; 1998.
12. Linkhart, T. A., Linkhart, S. G., Farley, J. R., Dimai, H. P., Beamer, W. G., Donahue, L. R., Rosen, C. J., and Baylink, D. J. Osteoclast formation in bone marrow cultures from two inbred strains of mice with different bone densities. J Bone Miner Res 13:35–42; 1999.
13. Mora, S., Pitukcheewanonot, P., Nelson, J. C., and Gilsanz, V. Serum levels of IGF-I and the density, volume, and cross-sectional area of cortical bone in children. J Clin Endocrinol Metab 84:2780–2783; 1999.
14. Rosen, C. J., Dimai, H. P., Vereault, D., Donahue, L. R., Beamer, W. G., Farley, J., Linkhart, T., Linkhart, S., Mohan, S., and Baylink, D. J. Circulating and skeletal IGF-I concentrations in two inbred strains of mice with different bone densities. Bone 21:217–223; 1997.
15. Rosen, C. J., Friez, J., Donahue, L. R., Shultz, K. L., and Beamer, W. G. Determination of a major quantitative trait locus (QTL) for IGF-I in mice: Association with peak bone mass and implication for identification of potential IGF-I regulatory genes. J Bone Miner Res 14:(Suppl.); S175; 1999.
16. Rosen, C. J., Kurland, E. S., Vereault, D., Adler, R. A., Rackoff, P. J., Craig, W. Y., Witte, S., Rogers, J., and Bilezikian, J. P. An association between serum IGF-I and a simple sequence repeat in the IGF-I gene: Implications for genetic studies of bone mineral density. J Clin Endocrinol Metab 83:2286–2290; 1998.
17. Sheng, M. H., Baylink, D. J., Beamer, W. G., Donahue, L. R., Rosen, C. J., Lau, K. H., and Wegedal, J. E. Histomorphometric studies show that bone formation and bone mineral apposition rates are greater in C3H/HeJ (high density) than C57BL/6J (low density) mice during growth. Bone 25:421–429; 1999.
18. Zhao, G., Monier-Faugere, M. C., Langub, M. C., Geng, Z., Nakayama, T., Pike, J. W., Chernausek, S. D., Rosen, C. J., Donahue, L. R., Malluche, H. H., Fagin, J. A., and Clemens, T. L. Osteoblast-specific overexpression of IGF-I in transgenic mice increases cancellous bone volume. Endocrinology 2000;141: 2674–2682.

Date Received: February 16, 2000
Date Revised: May 5, 2000
Date Accepted: June 7, 2000

JOURNAL OF BONE AND MINERAL RESEARCH
Volume 16, Number 7, 2001

Quantitative Trait Loci for Femoral and Lumbar Vertebral Bone Mineral Density in C57BL/6J and C3H/HeJ Inbred Strains of Mice

WESLEY G. BEAMER,[1] KATHRYN L. SHULTZ,[1] LEAH RAE DONAHUE,[1] GARY A. CHURCHILL,[1] SAUNAK SEN,[1] JON R. WERGEDAL,[2] DAVID J. BAYLINK,[2] and CLIFFORD J. ROSEN[1,3]

ABSTRACT

Significant differences in vertebral (9%) and femoral (50%) adult bone mineral density (BMD) between the C57BL/6J (B6) and C3H/HeJ (C3H) inbred strains of mice have been subjected to genetic analyses for quantitative trait loci (QTL). Nine hundred eighty-six B6C3F2 females were analyzed to gain insight into the number of genes that regulate peak BMD and their locations. Femurs and lumbar vertebrae were isolated from 4-month-old B6C3F2 females at skeletal maturity and then BMD was determined by peripheral quantitative computed tomography (pQCT). Estimates of BMD heritability were 83% for femurs and 72% for vertebrae. Genomic DNA from F2 progeny was screened for 107 polymerase chain reaction (PCR)–based markers discriminating B6 and C3H alleles on all 19 autosomes. The regression analyses of markers on BMD revealed ten chromosomes (1, 2, 4, 6, 11, 12, 13, 14, 16, and 18) carrying QTLs for femurs and seven chromosomes (1, 4, 7, 9, 11, 14, and 18) carrying QTLs for vertebrae, each with $\log_{10}$ of the odds ratio (LOD) scores of 2.8 or better. The QTLs on chromosomes (Chrs) 2, 6, 12, 13, and 16 were unique to femurs, whereas the QTLs on Chrs 7 and 9 were unique to vertebrae. When the two bone sites had a QTL on the same chromosome, the same marker had the highest, although different, LOD score. A pairwise comparison by analysis of variance (ANOVA) did not reveal significant gene × gene interactions between QTLs for either bone site. BMD variance accounted for by individual QTLs ranged from 1% to 10%. Collectively, the BMD QTLs for femurs accounted for 35.1% and for vertebrae accounted for 23.7% of the F2 population variances in these bones. When mice were homozygous *c3/c3* in the QTL region, 8 of the 10 QTLs increased, while the remaining two QTLs on Chrs 6 and 12 decreased, femoral BMD. Similarly, when mice were homozygous *c3/c3* in the QTL region for the vertebrae, five of the seven QTLs increased, while two QTLs on Chrs 7 and 9 decreased, BMD. These findings show the genetic complexity of BMD with multiple genes participating in its regulation. Although 5 of the 12 QTLs are considered to be skeleton-wide loci and commonly affect both femurs and vertebrae, each of the bone sites also exhibited unique QTLs. Thus, the BMD phenotype can be partitioned into its genetic components and the effects of these loci on normal bone biology can be determined. Importantly, the BMD QTLs that we have identified are in regions of the mouse genome that have known human homology, and the QTLs will become useful experimental tools for mechanistic and therapeutic analyses of bone regulatory genes. (J Bone Miner Res 2001;16:1195–1206)

Key words: **quantitative trait loci, bone mineral density, acquisition of peak bone density, peripheral quantitative computed tomography, inbred mice**

[1]The Jackson Laboratory, Bar Harbor, Maine, USA.
[2]Musculoskeletal Disease Center, J.L. Pettis Veterans Affairs Medical Center and Loma Linda University, Loma Linda, California, USA.
[3]Research and Education, Maine Center for Osteoporosis, Bangor, Maine, USA.

INTRODUCTION

BONE MINERAL density (BMD), an accurate and precise measure of bone mass, has been identified in several epidemiological studies as being the single most important risk factor for osteoporotic fractures.[1,2] Hence, research efforts over the past three decades have focused on defining major environmental and hormonal determinants of bone mass and its subsequent loss. Such factors include age, gender, calcium intake during adolescence and senescence, estrogen deficiency in both men and women, glucocorticoid excess, physical activity, and demographic factors.

Recently, it has become apparent from a series of longitudinal studies that BMD at any time is a function of the rate of acquisition of peak bone mass in late adolescence and the subsequent rate of bone loss during adulthood. Although environmental and hormonal factors affect bone turnover, 60–70% of final adult BMD is determined by the process referred to as "peak bone acquisition,"[3,4] and it is this phase of skeletal accumulation, which occurs over a short time period during puberty in humans and other animals, that is influenced predominantly by genetic factors.[4–6] However, unlike the identification of established environmental risk factors for osteoporosis, progress in delineating specific heritable determinants of BMD has been relatively slow.

Several lines of evidence confirm the thesis that peak BMD is influenced strongly by heritable factors. Estimates of heritability for bone mass in humans have ranged from 40% to 90%, depending on the model. In general, twin studies have indicated that the proportion of variance of BMD accounted for by genetic factors approaches 80%.[4,5,7] However, this estimate may be exaggerated by the confounding influence of shared environmental factors that are common in monozygotic twins but more diverse for nontwins.[8] Indeed, sibling studies have yielded somewhat lower estimates of heritability of approximately 50–60%.[4] Moreover, there are certain to be gene by environment interactions and site specificity with respect to BMD measurements, which preclude absolute estimates of the overall genetic influence on bone mass from any population study.[9–11] Notwithstanding these concerns, it is apparent that peak BMD has a major genetic component in humans, and from a public health perspective, the significance of this is immense, because identifying these factors could have huge medical and social implications in terms of targeting susceptible individuals for simple preventive measures.

Animal models are critical for experimentally defining the genetic regulation of bone density. Inbred mice represent an animal model with a short lifespan, rapid generation time, and lower maintenance costs than other mammals. Mice of a given inbred strain represent unlimited numbers of genetically identical "twins" whose genes can be analyzed experimentally and whose environments can be controlled strictly. Equally important, each inbred strain is genetically different from every other inbred strain, making possible planned matings and studies of segregating genes. The mouse genome has become highly defined, especially with respect to protein and molecular polymorphic differences among the various inbred strains. This detailed mapping of chromosomes greatly facilitates rapid location of new genes. In addition, segments of many mouse and human chromosomes have been identified with homologous linked loci.[12] As the human and mouse genome sequences become available, identification and testing of candidate genes will be even more easily accomplished.

In this report, we present the quantitative trait locus (QTL) analyses conducted with B6C3F2 intercross progeny from normal progenitor inbred strains C57BL/6J (B6) and C3H/HeJ (C3H), which differ in BMD of femurs by 50% and of vertebrae by 9%.

MATERIALS AND METHODS

Animals

The study used two inbred strains of mice1–B6 and C3H—previously shown to differ widely in BMD of femurs, with lesser differences found in tibias, vertebrae, and phalanges.[13] Mice were produced and maintained in our research colony under 14:10 h light/dark cycles. Females were housed in polycarbonate cages (51 in^2) in groups of three to five on bedding of sterilized Northern White Pine shavings. Water was acidified with HCl to achieve a pH of 2.8–3.2 (to prevent bacterial growth) and was freely available. The diet used for all mice was autoclaved National Institutes of Health (NIH) 31 (6% fat diet, Ca/P of 1.15: 0.85, 19% protein, vitamin, and mineral fortified; Purina Mills International, Richmond, IN, USA) and was freely available. Use of mice in this research project was reviewed and approved by the Institutional Animal Care and Use Committee of The Jackson Laboratory (Bar Harbor, ME, USA).

Progenitor B6, C3H, and their (B6 × C3H)F1 hybrid strain females used in these studies ranged in age from 1 to 12 months. Progeny for genetic analysis of BMD was produced by mating low BMD B6 females to high BMD C3H males and then intercrossing this B6C3F1 hybrid to produce F2 offspring. A total of 1012 F2 females were raised, 986 of which eventually contributed to the genetic analyses. The F2 females were analyzed at 4 months of age when acquisition of adult BMD was achieved. Body weights were recorded at necropsy, and partial carcass preparations were preserved in 95% ethanol as previously described.[13] Kidneys and spleens from each mouse were frozen in liquid N_2 and stored at −60°C for later extraction of genomic DNA. Femurs were isolated and their lengths were measured by digital calipers (Stoelting, Wood Dale, IL, USA) before densitometry. The F2 males were not kept because of losses due to aggressive behavior when group housed.

BMD measurements by peripheral quantitative computed tomography

Isolated femora and lumbar vertebrae were assessed using peripheral quantitative computed tomography (pQCT; Stratec XCT 960M, Norland Medical Systems, Ft. Atkinson, WI, USA) as described previously.[13] Briefly, bones were isolated and stored in 95% ethyl alcohol (EtOH) until measured for bone parameters by XCT 960M. Thresholds of

1.300 attenuation units differentiated mouse bone from water, adipose tissue, muscle, and tendon; a threshold of 2.000 differentiated high-density cortical bone from low-density bone. Calibration of the densitometer was done with a set of hydroxyapatite standards (0.050–1.000 mg/mm^3) yielding a correlation of 0.997 between standards and pQCT estimation of density. Daily confirmation of that calibration was confirmed using a phantom of known density. Precision of the XCT 960M for repeated measurement of femoral BMD was 1.2%. Isolated femora were scanned at 2-mm intervals over their entire lengths. Total and cortical BMD values were calculated by dividing the total or cortical mineral content by the appropriate bone volume and expressed as milligrams per cubic millimeter. The XCT 960M does not have sufficient resolution to resolve accurately trabecular bone volume; thus, such data are not presented. Femoral periosteal circumferences and cortical thicknesses were calculated at the mid-point of the diaphysis. The CV for progenitor strain femoral parameters at 4 months were (a) 2.8–3.1% for density, (b) 8.4–9.8% for mineral, (c) 7.0–7.4% for volume, (d) 2.1–3.6 for middiaphyseal periosteal circumference, and (e) 3.4–5.0% for middiaphyseal cortical thickness.

Isolated L5 lumbar vertebrae also were evaluated with the XCT 960M, with precision for repeated measurement of vertebral BMD of 1.4%. Vertebrae were scanned at 0.7-mm intervals along their anterior-posterior lengths. The total and cortical BMD values were calculated for entire vertebrae. For the L5 vertebrae, the coefficients of variation for progenitor strain parameters were (a) 3.4–4.0% for density, (b) 5.5–12.4% for mineral, (c) 4.8–15.4% volume, and (d) 10.5–17.2% for cortical mineral.

Genetic analyses

Genomic DNA was prepared by two methods. First, kidney samples were digested with proteinase K and extracted by chloroform/phenol. Second, 20–25 mg of kidney or spleen tissues were heated to 95°C in 0.5 ml of 50 μM NaOH for 10 minutes, and then pH was adjusted to 8.0 with 0.05 mM Tris-HCl. Genotyping of individual mouse DNAs was accomplished by polymerase chain reaction (PCR) using oligonucleotide primer pairs from Research Genetics (Birmingham, AL, USA). These primer pairs amplify simple CA repeated sequences of anonymous genomic DNA that are of different length and via gel electrophoresis can uniquely discriminate between B6 and C3H genomes. Primer pairs identifying simple sequence length polymorphisms between B6 and C3H were selected from more than 6000+ available.[14] Details of standard PCR reaction conditions have been described previously.[15] PCR products from B6, C3H, and (B6 × C3H)F1 hybrids were used as electrophoretic standards in every gel to identify the genotypes of F2 mice (that is, homozygous B6 [*b6/b6*] or C3H [*c3/c3*] and heterozygous [*b6/c3*]). Nine hundred eighty-six F2 progeny provided data for the genetic analyses.

All F2 progeny were tested for correlations of BMD data with segregation of 107 PCR-based simple sequence length polymorphic markers on the 19 autosomes. Four to nine polymorphic DNA markers, spaced at approximately 15 cM intervals from centromere to telomere, were selected for each autosome. The 15-cM genetic distance is easily capable of detecting major loci for bone density in this experimental design, given the large F2 population size. Chromosome (Chr) *X* alleles were not assessed because reciprocal F1 × F1 matings would be required to yield all possible allelic combinations necessary for genetic evaluation of the BMD phenotype in females.

Statistical analyses

Biological measurements: Statistical analyses of progenitor and F1 hybrid femoral and vertebral data were performed with StatView 4.5 software from Macintosh (Cary, NC, USA). These data were analyzed first by analysis of variance (ANOVA) to detect major genotype effects. Individual group means were assessed for significant differences by Fisher's Protected least significant difference (LSD) test. Differences were judged statistically significant when $p < 0.05$.

Genomewide analyses: The genome scans described in this study were carried out using a software implementation of the pseudomarker algorithm.[16] Software and additional details can be found at http://www.jax.org/research/churchill. The genome scans for QTL main effects produce $\log^{10}$ of the odds ratio (LOD) score curves identical to the standard MapMakerQT package[17] for a univariate normally distributed phenotype. Pairwise genome scans were carried out to search simultaneously for QTL pairs that were associated with the femoral and vertebral BMD traits. These scans allowed us to assess the possibility of gene × gene interactions, in which the combined effects of allelic substitutions at two loci are not equal to the sum of the two individual loci.[18]

Multiple regression: We used a multiple linear model, based on marker regression, to assess the joint effects of all loci (and interactions) that appeared to be significant in the genomewide scan. Multiple regression models were analyzed using Minitab software (Minitab, Inc., State College, PA, USA).

RESULTS

Inbred and hybrid F1 mice

To define the optimum time at which to conduct a genetic analysis of peak bone density, the progenitor B6 and C3H strains, plus B6C3H-F1 hybrid progeny, were measured for their developmental patterns of femoral and lumbar vertebral BMD. The results presented in Fig. 1A indicated that C3H femoral BMD levels were consistently greater than those of the B6 mice. Both progenitor strains developed maximal adult femoral BMD at 4 months and then generally maintained those levels through 12 months of age. The F1 hybrids achieved their maximum femoral BMD at approximately 8 months, followed by a decline at 12 months of age. BMD levels in the F1 progeny were always higher than those of B6 and were lower than those of C3H from 4 months onward. In Fig. 1B, the lumbar vertebrae of C3H mice reached greater values than observed in B6 at 4, 8, and

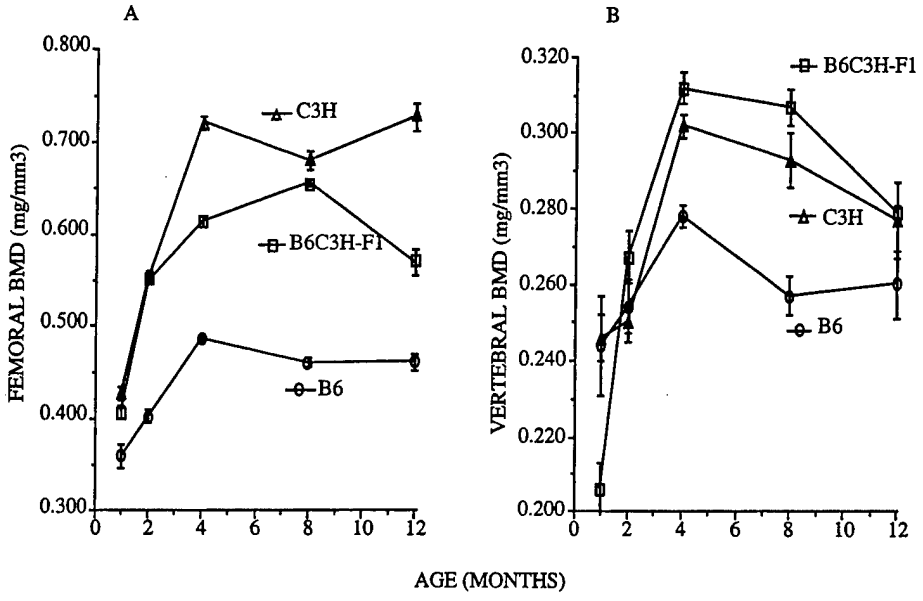

FIG. 1. Acquisition of adult peak BMD in B6, C3H, and B6C3F1 (F1) females. Means ± SEM are presented from groups of 7–12 mice that donated femurs and L5 lumbar vertebrae at the indicated ages for pQCT assessment of BMD. (A) Femoral data; (B) vertebral data.

12 months. Both progenitors and F1 females showed highest BMD levels at 4 months, followed by a significant decline in BMD levels by 12 months of age. In contrast with femoral BMD, the lumbar vertebral BMD levels were greater in F1 progeny at 2, 4, and 8 months than in either progenitor strain, following a remarkable growth spurt occurring between 1 and 2 months of age. Collectively, these results suggested that peak adult BMD in the femora and lumbar vertebrae were achieved at 4 months of age, making possible genetic analyses of peak BMD data gathered on both bone sites from the same mice.

Descriptive statistics for the bones in the 4-month-old progenitor and F1 hybrid mice are found in Tables 1 and 2. After determination of a significant "F" for each main effect, comparisons were made between the progenitor means, and then the F1 hybrid means were compared with each progenitor mean. Inspection of B6 and C3H data in Table 1 shows that the body weights of the progenitors did not differ from each other, whereas the C3H femur lengths were significantly shorter by 1.9% than those of B6 mice. The mineral contents of the B6 progenitor mice were markedly reduced compared with those of C3H mice, whereas femur volumes did not differ between B6 and C3H progenitors. Differences in these components result in the characteristic low femoral density of the B6 strain compared with the C3H strain. At the middiaphyseal region, periosteal circumference was larger in B6 than in C3H mice, whereas cortical thickness and cortical density were less than those values in C3H mice. Body weights, femur lengths, and volumes of the F1 mice were greater than those of the progenitors. For other measures, except periosteal circumference, the F1 mice showed femoral values significantly greater than B6. When F1 data are compared with C3H, measures of bone size (length, volume, and periosteal circumference) were greater than C3H while mineral content, density, and cortical thickness were smaller than these values for C3H mice.

Comparisons of the L5 vertebral data are presented in Table 2. Considering the B6 and C3H progenitors first, it can be seen that both the total mineral content and the volume of the L5 lumbar vertebrae of the B6 mice were lower than those of the C3H mice. Consequently, total lumbar vertebral density was significantly lower in B6 than in C3H; however, the percent difference was modest (~9%) when compared with the percent difference observed for femurs (~51%). As would be predicted, the cortical mineral content of the B6 vertebrae was significantly less than that of the C3H vertebrae. The F1 hybrid vertebral measurements were intermediate between the B6 and C3H progenitors, with the exception of BMD as discussed previously.

F2 progeny

BMD was measured by pQCT in femurs and lumbar vertebrae for the F2 progeny obtained from B6C3H-F1 intercross matings. nine hundred eighty-six F2 females contributed DNA that could be scored for the genetic analyses of the femoral BMD phenotype. The distributions of femoral and lumbar vertebral BMD data are presented in Fig. 2. The femoral BMD data in Fig. 2A approximate a normal distribution with a grand mean of 0.585 mg/mm^3 (minimum = 0.451 mg/mm^3; maximum = 0.751 mg/mm^3). Heritability of femoral BMD was calculated to be 83%.[19] The position of mean values for the B6 and C3H progenitor strains, as well as the B6C3H-F1 parental mice at 4 months of age, are indicated by arrows at appropriate locations. It is noteworthy that the distribution did not reveal significant numbers of F2 progeny with femoral BMD values less than that of B6 (0.487 ± 0.005 mg/mm^3) or greater than that of C3H (0.738 ± 0.006 mg/mm^3) progenitor values.

In Fig. 2B, the distribution of vertebral BMD from 938 F2 females having intact L5 vertebrae (48 damaged at necropsy or during subsequent isolation) is presented. The positions of mean values for B6 and C3H progenitors as well as for

TABLE 1. DATA FOR FEMURS FROM C3H, B6, AND F1 FEMALES AGED 4 MONTHS

Strain	Body weight (g)	Femur length (mm)	Total			Periosteal circumference (mm)	Cortical	
			Mineral (mg)	Volume (mm^3)	Density (mg/mm^3)		Thickness (mm)	Density (mg/mm^3)
B6 (8)	22.64 ± 0.46	15.54 ± 0.05	14.81 ± 0.21	31.09 ± 0.62	0.487 ± 0.005	4.720 ± 0.021	0.312 ± 0.003	0.616 ± 0.004
C3H (8)	23.06 ± 1.89	15.24* ± 0.14	22.94‡ ± 1.07	31.13 ± 1.51	0.738‡ ± 0.006	4.384‡ ± 0.013	0.509‡ ± 0.008	0.781‡ ± 0.006
F1 (10)	27.48† ± 0.58	16.31†,‡ ± 0.78	20.57*,‡ ± 0.60	33.57† ± 1.07	0.614‡ ± 0.006	4.488‡ ± 0.069	0.388‡ ± 0.002	0.714†,‡ ± 0.003

Total mineral, volume, and density data are for entire femur, while periosteal circumference, cortical thickness, and density data are from midpoint of the diaphysis. Data presented are mean ± SEM; number in parentheses indicates mice in each group.
* $p < 0.05$; † $p < 0.005$; ‡ $p < 0.0005$.

B6C3F1 parental genotypes are indicated by arrows. The overall distribution of vertebral BMD in Fig. 2B was normal in shape, with a grand mean of 0.306 mg/mm^3 (minimum = 0.195 mg/mm^3; maximum = 0.416 mg/mm^3). Heritability of L5 vertebral BMD was calculated to be 72%. In contrast with the femoral data in Fig. 2A, the B6 and C3H progenitor vertebral BMD means were close to each other in the central region of the F2 distribution. Some F2 progeny had vertebral BMD values that were lower than those of B6 progenitor, and there were many more F2 progeny with vertebral BMD greater than that of the C3H progenitor. These transgressive patterns of F2 values suggest that both B6 and C3H strains carry alleles for high and low lumbar vertebral BMD. The mean vertebral BMD for the F1 hybrids was greater, although not significantly so, than for the C3H progenitor.

Genetic analyses

QTLs with LOD scores indicating suggestive (>2.8) or significant (>4.3) linkage for the femoral and vertebral density traits were identified by the whole genome scans.[20] In addition, pairwise genome scans were carried out to detect gene × gene interactions. In Fig. 3, each chromosome is represented on the abscissa, and the percent of the BMD variance accounted for in the F2 population is presented on the ordinate. Dashed lines represent permutation analysis-based thresholds for genomewide significance at levels of $p < 0.05$ and $p < 0.01$, according to criteria defined previously by Churchill and Doerge.[21] In Fig. 3A, multiple regression analysis results show that the femoral QTLs on Chrs 1, 2, 4, 6, 11, 12, 13, 14, 16, and 18 collectively accounted for approximately 35.1% of the BMD variance in the F2 population. Similar analyses for vertebral BMD are shown in Fig. 3B where QTLs on Chrs 1, 4, 7, 9, 11, 14, and 18 account for 23.7% of the variance in vertebral density in the F2 population. The QTLs with the greatest effect on both femoral and vertebral variances were those on Chrs 1, 4, and 18. These accounted for 22.34% (femurs) and 16.24% (vertebrae) of the total variances for each skeletal site. The QTLs specifically associated with femurs (Chrs 2, 6, 12, 13, and 16) accounted for 8.36%, while QTLs specifically associated with vertebrae (Chrs 7 and 9) accounted for 4.31% of the F2 population variance by skeletal site.

Table 3 gives the Mit marker most highly associated with each BMD QTL, as well as the Mouse Genome Database (MGD) map position for that marker. In addition, the LOD score for each marker and the percent of F2 variance accounted for are presented for each femoral and vertebral QTL detected. Each BMD QTL is named sequentially by Chr number, beginning with *Bmd5* on Chr 1.[22] *Bmd1–4* were located in the B6CAST-F2 cross reported earlier.[15] A genomewide search for pairwise interaction effects on BMD between markers was carried out but failed to reveal significant interactions when the test statistics were compared with a genomewide permutation threshold.

Interval maps with Mit markers, associated LOD scores, and minimum critical level ($p = 0.05$, dashed line) for three QTLs accounting for the largest variance in BMD are presented in Fig. 4. These QTLs affected both femoral (solid

TABLE 2. DATA FOR ENTIRE LUMBAR L5 VERTEBRAE FROM C3H, B6, AND F1 FEMALES AGED 4 MONTHS

Mouse strain	Total L5			
	Mineral (mg)	Volume (mm^3)	Density (mg/mm^3)	Cortical mineral (mg)
B6 (8)	3.798 ± 0.074	13.688 ± 0.233	0.278 ± 0.003	1.648 ± 0.061
C3H (12)	5.688† ± 0.178	18.824‡ ± 0.470	0.302† ± 0.003	3.164† ± 0.157
F1 (8)	5.221†,‡ ± 0.178	16.739‡ ± 0.435	0.312† ± 0.004	2.850†,‡ ± 0.146

Data presented are mean ± SEM; number in parentheses is number of mice in group.
† $p < 0.005$; ‡ $p < 0.0005$.

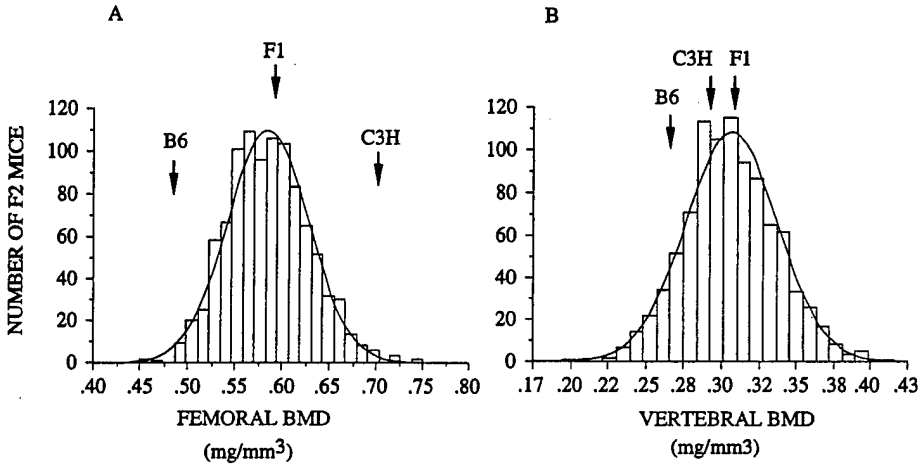

FIG. 2. Distributions of femoral and vertebral BMD obtained from B6C3F2 progeny. (A) Femoral BMD in female mice at 4 months of age. Positions of mean BMDs for the inbred progenitors and F1 parentals are indicated by arrows, while the bell-shaped line depicts a normal distribution of data. (B) L5 vertebral BMD from the same F2 mice. Location of mean values for the progenitors are markedly different than for the femoral BMD shown in panel A.

line) and vertebral (dotted line) BMD, as shown for Chrs 1, 4, and 18. The 95% CIs (femora = black bars; vertebrae = open bars) were estimated from a 1.5 LOD reduction from the peak LOD score generated by MapMakerQT. Overlapping CIs support the possibility that both femora and vertebrae are regulated by the same gene within the QTL region on the respective chromosomes. Two of the remaining 9 QTLs, Chrs 11 and 14, also had overlapping CIs for femoral and vertebral BMD. The interval map for femoral BMD on Chr 1 QTL suggested more than one locus may be present. Accordingly, we carried out additional analyses of F2 QTL models for Chr 1 but could not develop convincing statistical evidence for a second femoral QTL. Resolution of possible tightly linked QTLs will require further decomposition of this region via construction and testing of congenic strains. Finally, interval maps prepared for the remaining chromosomes showed that genetic regions containing BMD QTLs varied in size up to 35 cM of recombination distance.

In Figs. 5A and B, we present the main effects of C3H (*c3*) alleles for four selected QTLs on femoral and vertebral BMD. These include the three major effect QTLs on Chr 1, 4, and 18, plus an illustrative site-specific QTL for each bone. Inspection of these figures shows that the *c3* alleles for QTLs on Chrs 1, 4, and 18 are additive in action and the presence of one or more *c3* alleles significantly increased BMD at both skeletal sites. We also found that *c3* alleles on Chrs 6 and 12 significantly decreased femoral BMD, as exemplified by Chr 6 in Fig. 5A. Likewise, *c3* alleles on Chrs 7 and 9 significantly decreased vertebral BMD, as exemplified by Chr 7 in Fig. 5B. All remaining QTLs for both skeletal sites had additive effects with *c3* alleles increasing BMD (data not presented).

DISCUSSION

In this study, we found that heritability for femoral and vertebral BMD was high (83% and 74%, respectively), and that at least 10 QTLs for femoral and 7 QTLs for vertebral BMD had LOD scores greater than 2.8. These loci are distributed widely across the genome, and they accounted for 35% and 23%, respectively, of the variance in BMD among these B6C3F2 female mice. In addition, we have shown that the developmental patterns of peak bone acquisition in both progenitor B6 and C3H, as well as their F1 hybrids, are very similar for both bone sites, and that overall, the maximum differences in BMD values were evident at 4 months of age. Progenitor strain peak femoral BMD was maintained through 12 months of age, whereas vertebral BMD appears to decline after 4 months of age. Thus, we chose 4 months as the time to measure both femoral and vertebral BMD and to perform genetic analyses. The femoral F1 data were intermediate between those of C3H and B6, suggesting that heterozygosity for B6 alleles was suppressive for achievement of the high BMD observed in the C3H progenitor. For the vertebrae, F1 data were different

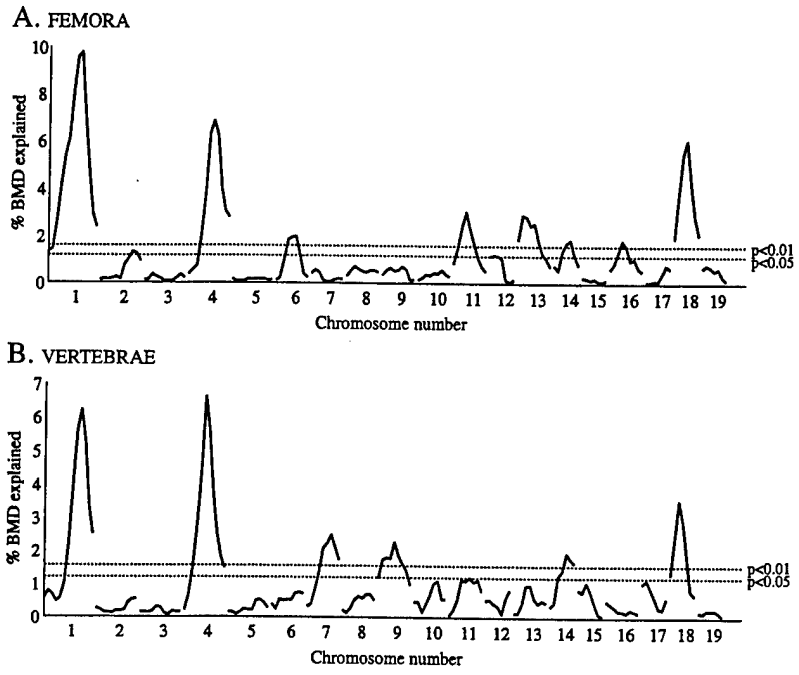

FIG. 3. Genomewide scans for correlations of BMD and molecular markers on each of the 19 autosomes. (A) Percentage of femoral BMD variance accounted for by each marker tested on the 19 autosomes. Horizontal lines represent the 1% (upper; nominal $p = 8 \times 10^{-4}$) and 5% (lower; nominal $p = 3 \times 10^{-3}$) permutation thresholds correcting for multiple testing. (B) Percentage of vertebral BMD variance accounted for by each marker tested on the 19 autosomes; details of presentation same as for panel A.

from those of both progenitors with low BMD at one month and higher BMD at adulthood. This suggests that heterozygosity for alleles of bone density genes, rather than homozygosity for either progenitor allele, may result in reduced bone formation, relative to bone resorption, before the first month of age. This delay in bone acquisition was reversed by a remarkable increase in vertebral BMD between 1 and 2 months of age. At 4 and 8 months of age, the F1 BMD was significantly higher than that of the C3H progenitor strain. We also observed F1 values exceeding progenitor strain values for three additional measures: body weight, femoral length, and femoral volume. These phenotypes also have polygenic regulation with individual loci that are dominant or additive in their main effects (Beamer and Donahue, unpublished data, 1998). The hybrid vigor in these phenotypes observed in the F1 progeny simply represents the sum of these main effects when all loci are heterozygous.

Acquisition of a large sample size of one gender was undertaken in this investigation to allow an in-depth look at the genetic regulation of bone density in appendicular and axial bone sites. A single sex was examined for economic reasons as noted in the Material and Methods section. The outcome of the genomewide analyses, judged by percent variance accounted for, clearly revealed three QTLs with major effects on both femoral and vertebral BMD and several QTLs with minor effects that were either unique to one skeletal site or common to both sites. The data for allele effects indicated that C3H and B6 alleles at each locus interacted in an additive fashion. Although we were not surprised by the number of QTLs regulating BMD, the lack of evidence supporting the existence of gene × gene interaction was unanticipated. Thus, we conclude from these findings that loci contributing to BMD are relatively independent.

The total variance for BMD in the B6C3F2 population explained by the QTLs for either femurs or vertebrae was 35% and 23%, respectively. The genomewide analyses (Fig. 3) showed a few additional chromosomes with effects on BMD in which LOD scores were below the minimum critical value established by permutation analyses for statistical significance at $p < 0.05$.[21] Even if these chromosomes with small effects were considered to harbor putative BMD QTLs, they would offer very little additional contribution to the percent BMD explained in these genetic analyses. Several other sources contributing to the BMD variance are readily discernible. For example, the maternal environment, pre- and postpartum or both, could exert effects via number of pups in a litter, litter number (e.g., first litter vs. fourth litter), or even gender distribution within a litter. Recently, Reifsnyder et al.[23] showed that maternal effects via *NZO* alleles significantly increased body weight gain in backcross progeny, most likely through elevation of milk lipid levels.

It also is possible that genes regulating variation in other phenotypes could have secondary effects on BMD. In our B6C3F2 females, regression analyses revealed that body weight had a significant effect on both femoral and vertebral BMD (6.3% and 5.7%, respectively). Analyses in progress indicate four body weight QTLs (Chrs 1, 6, 17, and 18) that achieved LOD scores >2.8 (Beamer and Donahue, unpublished observations, 2001). The body weight QTLs on Chr 1, 6, and 18 overlap regions that contain QTL for BMD. However, QTL for the regions are quite large and it can only be speculated as to whether the QTL for both body weight and BMD are the same or different. Another genetically complex phenotype correlated with B6C3F2 mice is serum levels of insulin-like growth factor I (IGF-I), for which we have reported four QTLs (Chrs 6, 10, 11, and 15).[24]

TABLE 3. SUMMARY OF GENOMEWIDE SCANS OF B6C3F2 MICE FOR BONE DENSITY QTLS

Chromosome locus and MGD position (cM)	*BMD QTL name*	*Femoral BMD LOD score*	*Percent of F2 variance*	*Vertebral BMD LOD score*	*Percent of F2 variance*
D1Mit14 (81.6)	*Bmd5*	24.44	9.98	14.02	6.18
D2Mit456 (86.3)	*Bmd6*	3.14	1.06	NS	—
D4Mit124 (57.4)	*Bmd7*	16.30	6.71	14.85	6.54
D6Mit150 (51.0)	*Bmd8*	4.56	1.84	NS	—
D7Mit332 (65.6)	*Bmd9*	NS	—	5.01	2.13
D9Mit196 (48.0)	*Bmd10*	NS	—	5.12	2.18
D11Mit242(31.0)	*Bmd11*	6.76	2.65	2.98	1.21
D12Mit215 (2.0)	*Bmd12*	2.89	1.07	NS	—
D13Mit13 (35.0)	*Bmd13*	7.73	2.96	NS	—
D14Mit160(40.0)	*Bmd14*	4.30	1.72	4.48	1.94
D16Mit12 (27.6)	*Bmd15*	4.07	1.43	NS	—
D18Mit36 (24.0)	*Bmd16*	13.67	5.65	8.35	3.52

Femoral and L5 vertebral volumetric BMD obtained by pQCT. Maximum LOD scores and associated percent variance explained are given for the best marker (LOD score > 2.8 suggestive linkage; >4.3 significant linkage). Bone mineral density QTLs named in sequence following *Bmd1–Bmd4*.[15]

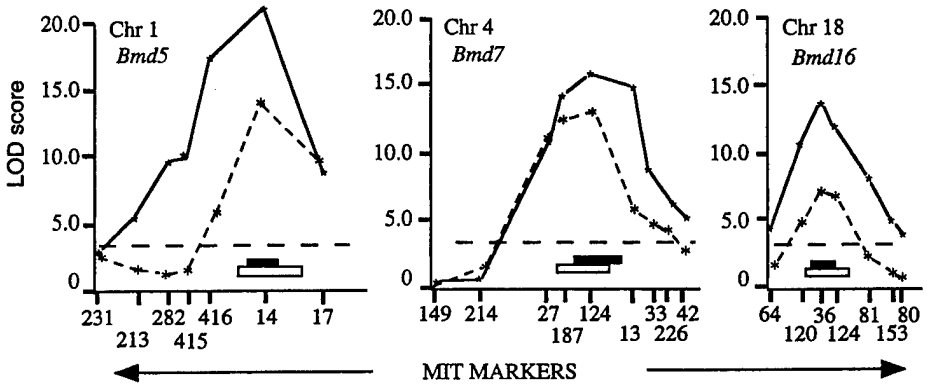

FIG. 4. Representative interval maps for three major QTLs (Chrs 1, 4, and 18) affecting both femoral (solid line) and vertebral (dotted line) BMD. Intermarker intervals and chromosome lengths in recombination distances are scaled. Statistical analyses are presented as LOD scores calculated for molecular markers beginning with the centromeric end of each chromosome on the left and extending toward the telomeric end. The 95% CI derived from a change of 1.5× LOD unit is shown by a black bar for femoral BMD (Chr 1 = 12 cM; Chr 4 = 19 cM; Chr 18 = 9 cM) and by an open bar for vertebral BMD (Chr 1 = 22 cM; Chr 4 = 22 cM; Chr 18 = 19 cM). The horizontal dashed line indicates the critical LOD score of 2.8 for each QTL. Locus names, *Bmd5, 7,* and *16* are assigned to each QTL based on Table 3.

Chromosomes 10, 11, and 15 are not shared with BMD, whereas Chr 6 QTLs for serum IGF-I and BMD are shared. The implication is clearly that other phenotypes we are not measuring with X-ray attenuation may have significant roles in peak BMD.[26]

Another source of genetic variability could be Chr X. Our F2 progeny was derived strictly from intercrosses of (B6 × C3H)F1 female with (B6 × C3H)F1 male mice. This design yields the expected genotypic classes of *b6/b6, b6/c3,* and *c3/c3* for autosomal loci, but only *b6/b6* and *b6/c3*, not the *c3/c3* genotype, for Chr X loci needed to unambiguously assign phenotype-genotype relationships between Chr X allelic combinations and BMD. From preliminary data analyzing strain distribution patterns for BMD among the 12 BXH recombinant inbred strains,[25,26] we detected a suggestive association between BMD and the proximal third of Chr X[27] (Beamer et al., unpublished observations, 2001). Therefore, it is very likely that a QTL accounting for significant variance in BMD is located on Chr X. This possibility could be analyzed by intercrossing (B6 × C3H) F1 females with (C3H x B6)F1 males and combining evaluation of both sets of F2 progeny for BMD and Chr X allelic segregation.

Finally, our statistical analyses were capable of evaluating interactions between two genes, but not interaction among three or more genes. If several of the BMD QTLs are within the same biochemical pathway leading to the same cellular change (e.g., mineralization), this multicomponent interaction would remain undetected. Finally, social interactions among individuals sharing the same cage may lead to behavioral consequences that affect acquisition of peak bone mass. Thus, additional experimental work plus new statistical tools are needed to improve our understanding of all genetic factors regulating the BMD variance in this cross.

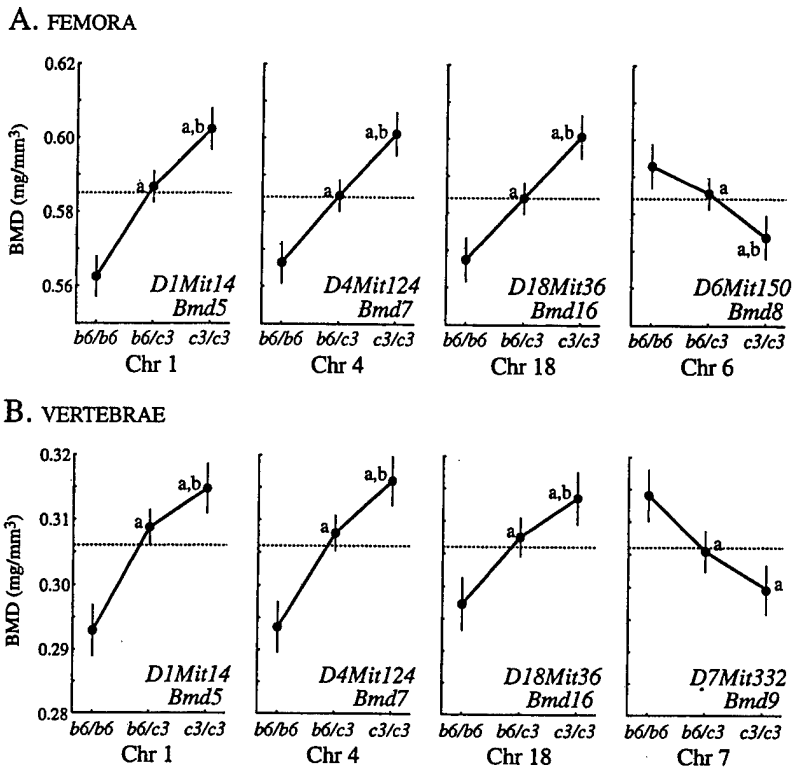

FIG. 5. The effects of C3H (*c3*) alleles at three major QTLs (Chrs 1, 4, and 18; *Bmd5*, *7*, and *16*) affecting both (A) femoral and (B) vertebral BMD. Lower case letters in each panel indicate significant difference at $p < 0.01$: a indicates mean differs from that for *b6/b6* mice; b indicates mean for *c3/c3* mice differs from that for *b6/c3* mice. In addition, a representative QTL (Chr 6, *Bmd8*) for femoral BMD not detected in the vertebral genome scan is presented in panel A. Likewise, a representative QTL (Chr 7, *Bmd9*) for vertebral BMD not detected in the femoral genomewide scan is presented in panel B.

Defining the exact location of a QTL for BMD or any other trait is limited even in a very large F2 intercross population. Limitations include the number of polymorphic markers available, chromosomal structural features that affect genetic recombination, and random characteristics of meiotic events. Based on our data, 95% CIs for regions containing BMD QTLs ranged from 12 to 35 cM in genetic distance. Any of these regions could contain a single locus or a cluster of linked genes, in which their net effect represents the percent variance accounted for by a given QTL. Because of the large number of genes within our QTLs, it is possible that even regions with overlapping CIs (Fig. 4) may contain more than one BMD regulatory gene. One solution to this complex locus challenge is congenic strains with single BMD QTLs isolated in a common genetic background.[27] Such congenic strains and sublines thereof can be used to confirm the presence of a QTL, narrow the genetic distance containing the putative gene, and decompose the genetic complexity of the region, that is, determine if more than one gene contributes to the difference in BMD caused by distinct parental alleles. Congenic sublines also can be used as bioassays to narrow the QTL regions and to identify candidate genes. For example, if one congenic subline responds to an experimental manipulation, such as ovariectomy, and a second subline for the same QTL does not, then certain candidate genes for the BMD phenotype such as steroid regulatory genes could be included or eliminated for a given QTL region. This would also indicate more than one gene is present within the QTL region.

Although some regions of the genome are more or less gene rich, it is commonly estimated that there are up to 60–70 genes per cM of mouse chromosome recombinational distance. This large number of potential genes argues against speculation about candidate genes, although attractive candidates have been proposed from human association or sib-pair studies. These candidates yield proteins such as (a) calcium sensing receptor,[28] (b) bone osteocalcin,[29] (c) apolipoprotein E,[30] (d) IGF-I,[31] (e) interleukin-1 receptor antagonist,[32] (f) calcitonin receptor,[33] (g) vitamin D receptor,[34] (h) collagen Ia1,[35] (i) interleukin-6,[36] (j) high bone mass,[37] or (k) estrogen and androgen receptors.[38] It is the case that our QTLs for regulation of normal BMD reported here map to other chromosomal regions more than the human genes cited previously, suggesting new loci regulating BMD. Although we are reluctant to offer a selection of candidate genes for any of the BMD loci described in the B6C3F2 cross at this time, it is clear that candidates will become obvious as incipient congenic strains because several of these QTL regions manifest anticipated changes in BMD.[39]

In a previously reported F2 intercross between B6 and CAST/Ei, we found four QTLs for femoral BMD located on Chrs 1, 5, 13, and 15 that exceeded the threshold for statistical significance.[15] In concert with the B6C3F2 data in this report, the proportion of variance explained by the four QTLs was low (13.1%) and the data were statistically devoid of detectable gene by gene interaction. Two of the QTLs—Chrs 5 and 15—were not detected in the B6C3F2 data reported here. Therefore, different crosses will reveal both similar and different BMD QTLs because of differences in alleles carried by particular strains. This is supported by studies from other investigators using a variety of genetic models combined with different measurement meth-

TABLE 4. SUMMARY OF QTLS FOR BMD IN MICE FROM FOUR DIFFERENT LABORATORIES

Chromosome	*Marker or gene*	*Map position*	*Method and bone site*	*Human homologous chromosomal region*	*Laboratory source*
Chr 1	*Mit14*	81.6	pQCT; femur, L5	1q21-q31	This report
Chr 1	*Mit15*	87.9	pQCT; femur	1q21-q31	Beamer et al.[15]
Chr 2	*Mit464*	9.5	DXA; spine	10p13-p11; 2q14; 9q34	Klein et al.[42]
Chr 2	*Mit456*	86.3	pQCT; femur	20q11	This report
Chr 2	*Ncvs42*	87.0	DEXA; whole body	20q11-q12	Devoto et al.[43]
Chr 3	*Mit23*	4.6	pQCT; femur	1q24-q32; 8q12-q22	Beamer et al.[15]
Chr 4	*Mit124*	57.4	pQCT; femur, L5	13q14-q21	This report
Chr 5	*Mit112*	42.0	pQCT; femur	4p14-p12; 4q11-q13	Beamer et al.[15]
Chr 6	*Mit150*	51.0	pQCT; femur	3p26-p25; 3q21-q24; 19q13; 10q11	This report
Chr 7	*Mit210*	11.0	DXA; spine	19q12-q13	Klein et al.[42]
Chr 7	*Mit234*	44.0	DXA; whole body	15q24-q26; 11q13-q21	Devoto et al.[43]
Chr 7	*Mit332*	65.6	pQCT; L5	10q25-q26	This report
Chr 9	*Mit196*	48.0	pQCT; L5	6q12-q16; 15q24	This report
Chr11	*Mit242*	31.0	pQCT; femur	5q31-q32; 17p12-p11	This report
Chr11	*Mit90*	42.0	CTI; femur	17p-pter; 17q-qter	Benes et al.[41]
Chr11	*Mit284*	52.0	DXA; spine	17q21-q22	Devoto et al.[43]
Chr12	*Mit215*	2.0	pQCT; femur	2p25-p22	This report
Chr13	*Mit135*	10.0	CTI; femur	7p15-p13; 6p22; 9q22	Benes et al.[41]
Chr13	*Mit16*	10.0	pQCT; femur	7p15-p13; 6p22; 9q22	Beamer et al.[15]
Chr13	*Mit266*	16.0	pQCT; femur	6p25-p21	This report
Chr13	*Mit13*	35.0	pQCT; femur, L5	5pq22-q35	This report
Chr13	*Mit20*	35.0	DXA; spine	6p24-22	Klein et al.[42]
Chr14	*Ptprg*	2.0	DXA; whole body	3p14; 10q21-q24; 8p23	Devoto et al.[43]
Chr14	*Mit160*	40.0	pQCT; femur, L5	13q14-q21	This report
Chr15	*Mit29*	42.8	pQCT; femur	8q24; 22q12-q13	Beamer et al.[15]
Chr16	*Mit12*	27.6	pQCT; femur	3q13-q29	This report
Chr16	*Mit39*	29.1	DXA; spine	3q13-q29	Klein et al.[42]
Chr18	*Mit36*	24.0	pQCT; femur, L5	5q21-q33	This report

Map position given in centiMorgans (cM); human homologous regions corresponding to ±3 cM of published marker or gene location.[12]

odologies to the study of density. Thus, the osteopenic senescence accelerated mouse (SAM)P6 plus the related normal P2, R1, and AKR inbred strains have been studied with F2 analyses by femoral Cortical Thickness Index[40] and by dual-energy X-ray absorptiometry (DXA) of the spine.[41] The BXD recombinant inbred strain set (26 strains) derived from an intercross between B6 and DBA/2J has been exploited by DXA for analyses of whole body BMD.[42] We have chosen to use F2 intercrosses: one between B6 and CAST[15] and a second between B6 and C3H strains—both assessed by pQCT. Accordingly, insights are emerging about BMD as a complex trait associated with a manageable number of genes amenable to study. Table 4 summarizes the available mouse data on (a) chromosomal locations with genomewide LOD scores suggestive of linkage (i.e., >2.8), (b) measurement techniques, (c) bone sites, and (d) homologous human chromosome locations. Given that CIs were not available for all data sets, it is uncertain how many QTLs or clusters of linked QTLs are represented by multiple markers such as on Chr 7. In general, the closer the markers are to each other, the more likely it is that the same locus is being detected. Collectively, the QTL data found by these groups indicate (a) some of the same loci are being detected by different methods in different crosses, (b) there are some loci with multiple alleles (and thus detectable in different crosses) and some loci with rare allelic differences (and not detectable in every cross), and (c) some loci are site specific.

The future of these studies lies in greater refinement of map positions, testing of candidate genes for BMD QTLs, sequencing of BMD genes, and prediction of BMD gene location in the human genome via linkage homology. This will in turn facilitate functional studies to define genes and their roles in bone biology and their potential as therapeutic targets. For example, the QTLs on mouse Chrs 1 and 4 are within regions that share linkage homology with human Chr 1. The importance of this relationship is illustrated by the studies of (a) Devoto et al.,[43] who reported a locus associated with human BMD linked to 1p36; (b) Reed et al.,[44] who described a syndrome of hypercalciuria and low bone mass linked to 1q25; and (c) Koller et al.,[45] who found a significant association in a large sib-pair study with spinal BMD linked to 1q21. Genome sequencing for *Homo sapiens* is nearly complete, and the B6 mouse sequence will be completed within the next year. Direct comparison of gene sequences from homologous regions will sharpen choice of candidate genes for testing and determining

whether, in fact, genes regulating BMD are the same or different between the two species.

In summary, our genetic analyses have shown that (1) BMD is a polygenic trait with a substantial number of genes supporting this bone parameter, (2) the QTL alleles are additive in their actions with respect to BMD, (3) the adult peak bone density in a given strain is the net result of QTLs with both positive and negative effects on BMD, and (4) there appear to be QTLs acting on multiple bone sites, as well as QTLs with site-specific effects. These data show that mouse models with a skeletal phenotype such as congenic strains, induced mutation strains (transgenics, gene knockout[46]), and spontaneous mutant gene-bearing strains[12] are going to be powerful tools for biological investigation of gene effects, as well as for fine mapping and candidate gene testing.

ACKNOWLEDGMENTS

The authors thank Dr. G. Cox and Dr. K. Johnson for critical review of this article. We appreciate the dedicated assistance provided by R. Donahue, V. Haynes, K. Leibwohl, T. Leidy, K. Smith, and C. Wishcamper in the pursuit of this work. The research was supported by grants from the NIH (AR43618 and CA34196) and the U.S. Army (DAMD17–96-1–6306).

REFERENCES

1. Hui SL, Slemenda CW, Johnston CC 1988 Age and bone mass as predictors of fracture in a prospective study. J Clin Invest **81:**1804–1809.
2. Black DM, Cummings SR, Genant HK, Nevitt MC, Palermo L, Browner W 1992 Axial and appendicular bone density predict fractures in older women. J Bone Miner Res **7:**633–638.
3. Lloyd T, Cusatis DC 1999 Nutritional determinants of peak bone mass. In: Rosen CJ, Glowacki J, Bilezikian JP (eds.) The Aging Skeleton. Academic Press, San Diego, CA, USA, pp. 95–103.
4. Nguyen TV, Blangero J, Eisman JA 2000 Genetic epidemiological approaches to the search for osteoporosis genes. J Bone Miner Res **15:**392–401.
5. Pocock NA, Eisman JA, Hopper JL, Yeates MG, Sambrook PN, Eberl S 1987 Genetic determinants of bone mass in adults: A twin study. J Clin Invest **80:**706–710.
6. Ferrari S, Rizzoli R, Slosman D, Bonjour JP 1998 Familial resemblance for bone mineral mass is expressed before puberty. J Clin Endocrinol Metab **83:**358–361.
7. Smith DM, Nance WE, Kang KW, Christian JC, Johnston CC 1973 Genetic factors in determining bone mass. J Clin Invest **52:**2800–2808.
8. Slemenda CW, Christian JC, Williams CJ, Norton JA, Johnston CC Jr 1991 Genetic determinants of bone mass in adult women: A reevaluation of the twin model and the potential importance of gene interaction on heritability estimates. J Bone Miner Res **6:**561–567.
9. Lutz J, Tesar R 1990 Mother-daughter pairs: Spinal and femoral bone densities and dietary intakes. Am J Clin Nutr **52:** 872–877.
10. Krall EA, Dawson H 1993 Heritability and life style determinants of bone mineral density. J Bone Miner Res **8:**1–9.
11. Harris M, Nguyen TV, Howard GM, Kelly PJ, Eisman JA 1998 Genetic and environmental correlations between bone formation and bone mineral density: A twin study. Bone **22:**141–145.
12. Mouse Genome Informatics Project TJL, Bar Harbor, ME 2000 Mouse Genome Database (MGD). http://www.informatics.jax.org/.
13. Beamer WG, Donahue LR, Rosen CJ, Baylink DJ 1996 Genetic variability in adult bone density among inbred strains of mice. Bone **18:**397–403.
14. Dietrich WF, Miller J, Steen R, Merchant MA, Damron-Boles D, Husain Z, Dredge R, Daly MJ, Ingalls KA, O'Connor TJ, Evans CA, DeAngelis MM, Levinson DM, Kruglyak L, Goodman N, Copeland NG, Jenkins NA, Hawkins TL, Stein L, Page DC, Lander ES 1996 A comprehensive genetic map of the mouse genome. Nature **380:**149–152.
15. Beamer WG, Shultz KL, Churchill GA, Frankel WN, Baylink DJ, Rosen CJ, Donahue LR 1999 Quantitative trait loci for bone density in C57BL/6J and CAST/EiJ inbred mice. Mamm Genome **10:**1043–1049.
16. Sugiyama F, Churchill GA, Higgins DC, Johns C, Makaritsis KP, Gavras H, Paigen B 2001 Concordance of murine quantitative trait loci for salt-induced hypertension with rat and human loci. Genomics **71:**70–77.
17. Lander ES, Green P, Abrahamson J, Barlow A, Daly MJ, Lincoln SE, Newburg L 1987 MAPMAKER: An interactive computer package for constructing primary genetic linkage maps of experimental and natural populations. Genomics **1:**174–181.
18. Chevrud JM, Routman EJ 1995 Epistasis and its contribution to genetic variance components. Genetics **139:**1455–1461.
19. Jenkins JB 1990 Human Genetics. HarperCollins, New York, NY, USA, pp. 392–423.
20. Lander E, Kruglyak L 1995 Genetic dissection of complex traits: Guidelines for interpreting and reporting results. Nat Genet **11:**241–247.
21. Churchill GA, Doerge RW 1994 Empirical threshold values for quantitative trait mapping. Genetics **138:**963–971.
22. Jackson I 2000 International Committee on Standardized Genetic Nomenclature for Mice. Rules and Guidelines for Gene, Allele, and Mutation Nomenclature. http://www.informatics.jax.org/mgihome/nomen.
23. Reifsnyder PC, Churchill G, Leiter EH 2000 Maternal environment and genotype interact to establish diabesity in mice. Genome Res **10:**1568–1578.
24. Rosen CJ, Churchill GA, Donahue LR, Shultz KL, Burgess JK, Powell DR, Beamer WG 2000 Mapping quantitative trait loci for serum insulin-like growth factor-I levels in mice. Bone **27:**521–528.
25. Taylor BA 1996 Recombinant inbred strains. In: Lyon MF, Brown S (ed.) Genetic Variants and Strains of the Laboratory Mouse, 3rd ed., vol. 2. Oxford University Press, New York, NY, USA, pp. 1597–1659.
26. Turner CH, Hsieh Y-F, Mueller R, Bouxsein ML, Rosen CJ, McCrann ME, Donahue LR, Beamer WG 2001 Variation in bone biomechanical properties, microstructure, and density in BXH recombinant inbred mice. J Bone Miner Res **16:**206–213.
27. Silver LM 1995 Recombinant inbred strain. In: Mouse Genetics. Oxford University Press, New York, NY, USA, pp. 207–227.
28. Tsukamoto K, Orimo H, Hosoi T, Miyao M, Ota N, Nakajima T, Yoshida H, Watanabe S, Suzuki T, Emi M 2000 Association of bone mineral density with a polymorphism of the human calcium-sensing receptor locus. Calcif Tissue Int **66:** 181–183.
29. Raymond MH, Schutte BC, Torner JC, Burns TL, Willing MC 1999 Osteocalcin: Genetic and physical mapping of the human

gene BGLAP and its potential role in postmenopausal osteoporosis. Genomics **60**:210–217.
30. Shiraki M, Shiraki Y, Aoki C, Hosoi T, Inoue S, Kaneki M, Ouchi Y 1997 Association of bone mineral density with apolipoprotein E phenotype. J Bone Miner Res **12**:1438–1445.
31. Rosen CJ, Kurland ES, Vereault D, Adler RA, Rackoff PJ, Craig WY, Witte S, Rogers J, Bilezikian JP 1998 Association between serum insulin-like growth factor-I (IGF-I) and a simple sequence repeat in IGF-I gene: Implications for genetic studies of bone mineral density. J Clin Endocrinol Metab **83**:2286–2290.
32. Keen RW, Woodford-Richens KL, Lanchbury JS, Spector TD 1998 Allelic variation at the interleukin-1 receptor antagonist gene is associated with early postmenopausal bone loss at the spine. Bone **23**:367–371.
33. Masi L, Becherini L, Colli E, Gennari L, Mansani R, Falchetti A, Becorpi AM, Cepollaro C, Gonnelli S, Tanini A, Brandi ML 1998 Polymorphisms of the calcitonin receptor gene are associated with bone mineral density in postmenopausal Italian women. Biochem Biophys Res Commun **248**:190–195.
34. Morrison NA, Qi JC, Tokita A, Kelly PJ, Crofts L, Nguyen TV, Sambrook PN, Eisman JA 1994 Prediction of bone density from vitamin D receptor alleles. Nature **367**:284–287.
35. Uitterlinden AG, Burger H, Huang Q, Yue F, McGuigan FE, Grant SF, Hofman A, van Leeuwen JP, Pols HA, Ralston SH 1998 Relation of alleles of the collagen type Ialpha1 gene to bone density and the risk of osteoporotic fractures in postmenopausal women. N Engl J Med **338**:1016–1021.
36. Murray RE, McGuigan F, Grant SF, Reid DM, Ralston SH 1997 Polymorphisms of the interleukin-6 gene are associated with bone mineral density. Bone **21**:89–92.
37. Johnson ML, Gong G, Kimberling W, Recker SM, Kimmel DB, Recker RR 1997 Linkage of a gene causing high bone mass to human chromosome 11 (11q12–13). Am J Hum Genet **60**:1326–1332.
38. Sowers M, Willing M, Burns T, Deschenes S, Hollis B, Crutchfield M, Jannausch M 1999 Genetic markers, bone mineral density, and serum osteocalcin levels. J Bone Miner Res **14**:1411–1419.
39. Beamer WG, Donahue LR, Shultz KL, Rosen CJ, Churchill GA, Baylink DJ 2000 Genetic regulation of BMD in low density C57BL/6J mice carrying donated QTLs from high density C3H/HeJ mice. J Bone Miner Res 15:S1,S186 (abstract 1192).
40. Shimizu M, Higuchi K, Bennett B, Xia C, Tsuboyama T, Kasai S, Chiba T, Fujisawa H, Kogishi K, Kitado H, Kimoto M, Takeda N, Matsuchita M, Okumura H, Serikawa T, Nakamura T, Johnson TE, Hosokawa M 1999 Identification of peak bone mass QTL in a spontaneously osteoporotic mouse strain. Mamm Genome **10**:81–87.
41. Benes H, Weinstein RS, Zheng W, Thaden JJ, Jilka RL, Manolagos SC, Smookler-Reis RJ 2000 Chromosomal mapping of osteopenia-associated quantitative trait loci using closely related mouse strains. J Bone Miner Res **15**:626–633.
42. Klein RF, Mitchell SR, Phillips TJ, Belknap JK, Orwoll ES 1998 Quantitative trait loci affecting peak bone mineral density in mice. J Bone Miner Res **13**:1648–1656.
43. Devoto M, Shimoya K, Caminis J, Ott J, Tennenhouse A, Whyte MP, Sereda L, Hall S, Considine E, Williams CJ, Tromp G, Kuivaniemi H, Ala-Kokko L, Prockop DJ, Spotilla LD 1998 First-stage autosomal genome screen in extended pedigrees suggests genes predisposing to low bone mineral density on Chromosomes 1p, 2p, and 4q. Eur J Hum Genet **6**:151–157.
44. Reed BY, Heller HJ, Gitomer WL, Ruml LA, Lemke M, Padalino PK, Poindexter JR, Pak CYC 1999 Location of a gene for absorptive hypercalciuria with bone loss to 1q24. J Clin Endocrinol Metab **84**:3907–3913.
45. Koller DL, Econs MJ, Rodriguez LA, Christian JC, Hui SL, Morin P, Conneally PM, Joslyn G, Peacock M, Johnston CC 1999 Genome screen for QTLs contributing to normal variation in bone mineral density and osteoporosis. J Bone Miner Res **14**:S1;S141.
46. Lian J, Stein G, Canalis E, Robey P, 1999 Primer on the metabolic bone diseases and disorders of mineral metabolism, 4th ed. Lippincott Williams & Wilkins, Philadelphia, PA, USA, pp. 14–29.

Address reprint requests to:
Wesley G. Beamer
The Jackson Laboratory
600 Main Street
Bar Harbor, ME 04609, USA

Received in original form November 1, 2000; in revised form March 5, 2001; accepted April 9, 2001.

Calcif Tissue Int (1997) 60:225–228

Calcified Tissue International

Editorial

Beyond One Gene–One Disease: Alternative Strategies for Deciphering Genetic Determinants of Osteoporosis

Received: 2 May 1996 / Accepted: 3 May 1996

Osteoporosis is a chronic disorder that is characterized by low bone mass and fragility fractures, which affects more than 25 million people in the United States alone [1]. Since the clinical syndrome of osteoporosis represents a spectrum from low bone mineral density (BMD) to multiple fractures and disability, identification of risk factors prior to the onset of fractures has become a major focus of investigation [2]. Although several hormones and environmental influences have been associated with osteoporotic fractures, low BMD represents the most important risk factor for fracture [3]. Moreover, peak BMD is the principal determinant of bone mass at any subsequent age [4]. Consequently, factors that affect the acquisition of BMD have received considerable attention [5, 6]. It is not surprising that there has been increasing interest in genetic differences among individuals that may influence variation in BMD and therefore that may influence variation in fracture risk [7–10]. Because there is mounting evidence that genes may be important in the pathogenesis of osteoporosis, a major effort has begun to identify the specific genes responsible for predisposing some people to low bone mass. Although investigators have reported significant associations between nucleotide base differences in several "candidate" genes and BMD [11, 12], most researchers have assumed that variation of BMD is influenced by multiple genes. Furthermore, it is anticipated that many of those genes exert relatively small additive effects on BMD whereas a few contribute substantially to variation in this trait. Although the genetic influences on BMD are commonly referred to as "polygenic," meaning that the phenotypic variation is caused by the effects of those many genes with small, additive effects, a complete description of the genetic influences on BMD would probably include a mixture of polygenic and oligogenic (several single loci with important effects) determinants [13, 14]. When the known environmental contributors to the variance in BMD are added into our models, the trait becomes a more complex, multifactorial one–not unlike the risk for osteoporosis itself.

Given the initial enthusiasm generated by positive-candidate gene-association studies [11, 12], and the subsequent confusion caused by major studies that failed to confirm those associations [13], a review of the brief history of genetic strategies for mapping osteoporosis genes is warranted. We review that history and offer suggestions for additional methodological approaches to this question.

Correspondence to: C. J. Rosen

Current Genetic Approaches and Their Limitations

Ultimately, the goals of research efforts that intend to elucidate the genetic basis of osteoporosis should include: (1) identification of specific genes that affect fracture risk and (2) demonstration of the mechanisms by which these genes influence that risk. The two genetic strategies most frequently employed in this field have been *studies of human twin pairs* and *genetic association studies* involving unrelated people. The former has resulted in confirmation of familial aggregation, thereby supporting the thesis that there is an underlying hereditary basis to some traits correlated with the onset of osteoporosis [7–9]. However, these investigations have methodological limitations because of their inability to elucidate the overall structure of specific genetic effects on a trait. A complete understanding of the genetic basis of variation in risk for osteoporosis should include information describing the number of loci exerting influence, the magnitude and nature of the effects of these loci, and the patterns of interaction among genes and between genes and the environment. For complex traits such as BMD or bone turnover (as measured through biochemical markers of bone metabolism), such a description cannot be achieved through detailed analysis of twins.

Genetic association studies have tested relationships between DNA polymorphisms in known candidate genes and osteoporosis-related phenotypes. Properly conducted, this approach can identify genes with large effects on the phenotype of interest. However, this is true only if a) the DNA polymorphism marks or is in strong linkage disequilibrium with the actual functional mutation responsible for a large proportion of the phenotypic variation in the trait studied, b) the effect is not modified by epistatic and/or pleiotropic effects of other genes, and c) there is no genotype-by-environment interaction. In cases where a selected polymorphism does mark a functional gene relevant to the phenotype being studied, failure to employ research strategies that accommodate these conditions will usually lead to a decrease in the power to detect the effects of genes that actually influence the trait of influence [13, 14, 15]. Paradoxically, in cases where the polymorphisms do *not* mark a significant functional gene, the probability of false positive genetic signals may increase, whereas the power to detect effects of previously unknown genes becomes nil [16].

Several strategies are available that can accommodate the complex interactions listed above. One strategy employs inbred strains of mice differing in the trait of interest. Well designed crosses between strains that differ in this way al-

low the investigator to isolate the effects of individual genetic loci, to observe the effects of varying combinations of genes on the phenotype, and to measure the effects of changing environmental variables on animals of similar genotype. There is also another approach that can be viewed as doing the same thing in a natural context rather than in a controlled experiment. Analysis of quantitative traits in individuals from large, multigenerational families allows the investigator to quantify the effects of individual genes, polygenic backgrounds, and environmental factors on a complex trait. Unlike studies of strains of mice where analytical power comes from the intentional manipulation of genetic relationships among study subjects, study of extended families provides genetic power through the analysis of data from individuals with varying degrees of genetic similarity (i.e., parents vs. offspring, siblings, half siblings, and more distantly-related subjects). The analysis of many quantitative traits has benefited from studies of the traits' transmission within multigenerational families. Through the quantitative analysis of a given phenotype in extended families, genetic epidemiologists have developed detailed descriptions of the genetic architecture of numerous traits of biomedical significance. Both of these approaches—inbred mice and family studies—provide much greater statistical power to assess the relationships between genes and complex phenotypes than do twin studies or association studies.

Analysis of BMD as a Complex Multifactorial Trait

Genetic analyses of complex quantitative traits have followed closely on the heels of the breathtaking expansion in molecular genetics over the past decade. Several strategies *using animal models* can be employed to measure the effects of genes on phenotypic variation in complex traits as well as to localize these genes to specific chromosomal regions. Methods of genotyping the extreme subjects in a quantitative trait distribution, a vast array of available genetic markers and computerized statistical programs (MapMaker, MapManager QT, QTLCartographer), have made inbred strains of mice an obvious experimental choice for exploiting an ever-expanding knowledge base [17, 18]. The determinants of quantitative traits, such as cancer, type II diabetes, epilepsy, atherosclerosis, hypertension, and obesity, are being successfully dissected into both genetic and other biological causes using crosses between inbred strains of mice. Given that inbred strains differ in peak bone mass [19], bone turnover [20], age-related fracture [21], and response to physical activity [22], the use of mice also will prove fruitful for partitioning the genetic regulation of bone into its constituent loci.

Quantitative genetics also provides maximum-likelihood methods for the analysis of complex traits in multigenerational families. These methods include variance decomposition and mixture analysis [23, 24, 25, 26, 27], and allow the investigator to specify and test hypotheses concerning the relative contributions of different genetic effects (e.g., those of additive polygenes and single loci). The same analyses can measure the environmental influences on variations in a trait. An important feature in maximum likelihood-based pedigree approaches is that they are of equal utility for tests of hypotheses concerning the influence of known candidate genes and for the detection of the effects of previously unknown loci. Although there are notable exceptions, the immediate and obvious candidate genes (or structural loci) for many complex traits rarely have been proven to influence significant proportions of quantitative variation in any but the most extreme expressions of the trait. Therefore, methods such as variance decomposition and complex segregation analysis, which enable the detection of previously unmeasured genes, are especially helpful in the genetic dissection of complex traits.

These methods have been applied to data from human families and extended pedigrees to enable the genetic dissection of a number of phenotypes that are associated with risk of complex, multifocal diseases, such as atherosclerosis, noninsulin-dependent diabetes, and obesity. Examples of these applications include the detection of single-locus effects on plasma concentrations of high-density lipoprotein cholesterol [27], on one of its subfractions [28] and on fat mass [29]. In addition, multivariate extensions [25] to these methods have enabled new insights into the effects of single genes or sets of genes on variation in several traits (i.e., pleiotropy), such as lipids, lipoproteins, adiposity [27] and thyroid-hormone and cholesterol-transport phenotypes [30].

Studies of Multigenerational Pedigrees of Baboons

Whereas quantitative genetic methods have been successfully applied to the genetic dissection of complex phenotypes that are related to several common diseases, these methods have not been widely applied to the analyses of osteoporosis-associated phenotypes. This is unfortunate because properly applied statistical genetic analyses can provide important insights into the genetic and environmental determinants of variation in osteoporosis-related traits. For example, Kammerer et al. [31] and Mahaney et al. [32] used maximum likelihood-based pedigree analysis methods to investigate genetic and environmental determinants of BMD in a large pedigree of captive baboons (*Papio hamadryas*). In the former analyses, Kammerer et al. [31] quantified the effects of genes on phenotypic variation in cortical thickness of baboon metacarpals [30]. In the latter study, Mahaney et al. [32] detected the effects of genes on BMD (determined by DEXA) at three vertebral bodies and three forearm skeletal sites for 500 pedigreed baboons. From that study, Mahaney et al. found significant genetic correlations for BMD in the three vertebrae of the spine. Phenotypic correlations between vertebral and forearm sites were positive, but there were no significant genetic correlations. This would suggest that variation in BMD in the three vertebral bodies is caused largely by the effects of genes that exert lesser effects on BMD in the forearm. Thus, whereas variation in BMD is moderately heritable in both regions of the baboon skeleton, different genes are probably responsible for BMD in each of these two skeletal sites.

Genome Scans for Mapping QTLs

Successes in studies of muscular dystrophy, breast cancer, and cystic fibrosis demonstrate that an important step in identifying genes related to human disease is the identification of a chromosomal region that contains a currently unknown disease gene. High resolution genetic linkage maps of the human genome are now available [33]. The application of variance components analysis of quantitative traits and high-resolution linkage maps in extended families can

map unknown osteoporosis-related genes to tightly defined chromosomal regions. The next step is a challenging one—the cloning and identification of the unknown gene. But linkage mapping of unknown functional genes will almost certainly play a major role in the genetic analysis of fracture risk. The vitamin D receptor, the estrogen receptor, and insulin-like growth factor-I are all genes that probably do exert some influence on fracture risk in some populations. We have little doubt that other genes that have as great or greater effects await mapping and identification.

Conclusions

Even though point mutations in a single gene can lead to a single disease state, and polymorphisms in untranslated regions of candidate genes can be associated with phenotypes such as low BMD, osteoporosis-related traits are clearly regulated by numerous genetic determinants. Locating and identifying those genes and their interactions will be a tremendous undertaking that is certainly attainable within the foreseeable future, given proper application of newer advances in molecular genetics and genetic epidemiology.

J. Rogers[1]
M. C. Mahaney[1]
W. G. Beamer[2]
L. R. Donahue[2]
C. J. Rosen[3]
[1]Southwest Foundation for Biomedical Research
Department of Genetics
San Antonio, Texas, USA
[2]The Jackson Laboratory
Bar Harbor, Maine, USA
[3]St. Joseph Hospital and the Maine Center for
Osteoporosis Research and Education
176 Mt. Hope Avenue
Bangor, Maine 04401, USA

References

1. Melton LJ, Chrishilles EA, Cooper CC, Lane AW, Riggs BL (1992) Perspective: how many women have osteoporosis? J Bone Min Res 7:1005–1010
2. Cummings SR, Black DM, Rubin SM (1989) Lifetime risks of hip, Colles', or vertebral fracture and coronary heart disease among white postmenopausal women. Arch Int Med 149: 2445–2448
3. Melton LJ, Atkinson EJ, O'Fallon WM, Wahner HW, Riggs BL (1993) Long term fracture prediction by bone mineral assessed at different skeletal sites. J Bone Min Res 8:1227–1233
4. Hui SL, Slemenda CS, Johnston CC (1988) Age and bone mass as predictors of fracture in a prospective study. J Clin Invest 81:1804–1809
5. Kroger H, Kotaniemi E, Kroger L, Alhava E (1993) Development of bone mass and bone density of the spine and femoral neck: a prospective study of 65 children and adolescents. Bone Miner 23:171–182
6. Teegarden D, Proulx WR, Martin BR, Zhao J, McCabe GP, Lyle RM, Peacock M, Slemendat C, Johnston CC, Weaver CM (1995) Peak bone mass in young women. J Bone Miner Res 10:711–715
7. Pocock NA, Eisman JA, Hopper JL, Yeates MG, Sambrook PN, Eberl S (1987) Genetic determinants of bone mass in adults: a twin study. J Clin Invest 80:706–710
8. Hansen MA, Hassager C, Jensen SB, Christiansen C (1992) Is heritability a risk factor for postmenopausal osteoporosis? J Bone Miner Res 9:1037–1043
9. Seeman E, Hopper JL, Bach LA, Cooper ME, Parkinson E, McKay J, Jerums G (1989) Reduced bone mass in daughters of women with osteoporosis. N Engl J Med 320:554–558
10. Slemenda CW, Christian JC, Williams CJ, Norton JA, Johnston CC (1991) Genetic determinants of bone mass in adult women: a reevaluation of the twin model and the potential importance of gene interaction on heritability estimates. J Bone Min Res 6:561–567
11. Morrison NA, Qi JC, Tokita A, Kelley PJ, Crofts L, Nguyen TV, Sambrook PN, Eisman JA (1994) Prediction of bone density from vitamin D receptor alleles. Nature 367:284–287
12. Fleet JC, Harris SS, Wood RW, Dawson-Hughes B (1995) The BsmI vitamin D receptor restriction fragment length polymorphism predicts low bone density in premenopausal black and white women. J Bone Min Res 10:985–990
13. Peacock M (1995) Vitamin D receptor gene alleles and osteoporosis: a contrasting view. J Bone Min Res 10:1294–1297
14. Mahaney MC, Jaquish CE, Comuzzie AG (1995) Statistical genetics of normal variation in family data for oligogenic diseases. Genet Epidemiol 12:783–787
15. Blangero J (1995) Genetic analysis of a common oligogenic trait with quantitative correlates: Summary of GAW 9 results. Genet Epidemiol 12:689–707
16. Goldin LR, Bishop DT, Meyers DA, Morgan K, Rice JP, MacCluer JW (eds) (1995) Genetic analysis workshop 9: analysis of complex oligogenic traits. Genet Epidemiol 12:ix–894
17. Lander ES, Botstein D (1989) Mapping mendelian factors underlying quantitative traits using RFLP linkage maps. Genetics 121:185–199
18. Dietrich WF, Miller J, Steen R, Merchant MA, Damron-Boles D, Husain A, et al. (1996) A comprehensive genetic map of the mouse genome. Nature 380:140–152
19. Beamer WG, Donahue LR, Rosen CJ, Baylink DJ (1996) Genetic variability in adult bone density among inbred strains of mice. Bone (in press)
20. Murray EJB, Song MK, Laird EC, Murray S (1993) Strain dependent differences in vertebral bone mass, serum osteocalcin, and calcitonin in calcium replete and deficient mice. Proc Soc Exp Biol Med 203:64–73
21. Tsuboyama T, Takashashi K, Yamamuro T, Hosokawa M, Takeda T (1993) Cross mating study on bone mass in the spontaneously osteoporotic mouse (SAM/P6). Bone Miner 23: 57–64
22. Kaye M, Kusy RP (1995) Genetic lineage, bone mass, and physical activity in mice. Bone 17:131–135
23. Lange K, Weeks D, Boehnke M (1988) Programs for pedigree analysis: Mendel, Fisher, and dGene. Genet Epidemiol 5:471–472
24. Hasstedt SJ (1989) Pedigree analysis package V 3.0. Department of Genetics, University of Utah, Salt Lake City, Utah
25. Blangero J, Konigsberg LW (1991) Multivariate segregation analysis using the mixed model. Genet Epidemiol 8:299–316
26. S.A.G.E. Statistical analysis for genetic epidemiology (1992) Computer program package available from the Department of Biostatistics, Case Western Reserve University School of Medicine, Cleveland, Ohio
27. Mahaney MC, Blangero J, Comuzzie AG, Vandeberg JL, Stern MP, MacCluer JW (1995) Plasma HDL cholesterol, triglycerides, and adiposity: a quantitative genetic test of the conjoint trait hypothesis in the San Antonio family heart study. Circulation 92:3240–3248
28. Coresh J, Beaty TH, Prengar VL, Xu J, Kwiterovich PO Jr (1995) Segregation analysis of HDL3-C levels in families of patients undergoing coronary arteriography at an early age. Arterioscler Thromb Vasc Biol 15:1307–1313
29. Comuzzie AG, Blangero J, Mahaney MC, Mitchell BD, Hixson JE, Samallow MP, Stern MP, MacCluer JW (1995) Major gene with sex-specific effects influences fat mass in Mexican Americans. Genet Epidemiol 12:475–488

30. Comuzzie AG, Blangero J, Mahaney MC, Sharp RM, Vandeberg JL, Stern MP, MacCluer JW (1996) Triiodothyronine exerts a major pleiotropic effect on reverse cholesterol transport phenotypes. J Arterioscler Thromb Vas Biol 16:289–293
31. Kammerer CM, Sparks ML, Rogers J (1995) Effects of age, sex, and heredity on measures of bone mass in baboons. J Med Primat 24:236–242
32. Mahaney MC, Kammerer CM, Whittam H, Hodgson WJ, Dyer T, Lichter JB, Rogers J (1995) Genetic and environmental correlations between bone mineral densities at six vertebral and long-bone sites in pedigreed baboons. J Bone Min Res 10(S1):364 (abstract)
33. Dib C, Faure S, Fizames C, Samson D, Druout N, Vignal A, Millasseau P, Marc S, Hazan J, Seboun E, Lathrop M, Gyapay G, Morissette J, Weissenbach J (1996) A comprehensive genetic map of the human genome based on 5,264 microsatellites. Nature 380:152–154

14

IGF-1 and Osteoporosis: Lessons from Mice and Men

CLIFFORD J. ROSEN, LEAH RAE DONAHUE, WESLEY G. BEAMER, ROBERT A. ADLER, ETAH S. KURLAND, AND JOHN P. BILEZIKIAN

The insulin-like growth factors (IGF-1 and -2) are ubiquitous polypeptides that mediate the activity of growth hormone. In many tissues they serve as paracrine or autocrine factors (1). Second only to the liver, the skeleton is an exceptionally rich source of IGF-1 where it is both synthesized and stored. During bone remodeling, both systemic and skeletal IGF-1 play a major role in the recruitment and differentiation of osteoblasts (2, 3). In the course of bone resorption, the initiating bone remodeling event, matrix-bound IGFs are released and become critical coupling agents linking the processes of bone resorption and bone formation (2). Efforts to establish a relationship between synthesis of rapid bone loss or impaired bone formation and changes in the skeletal or circulatory IGF system have led to several hypotheses suggesting that IGF-1 is of pathophysiologic significance (2). Two recent studies, one showing an age-associated decline in skeletal IGF-1, and the other relating serum IGF-1 to bone density, have strengthened the view that the skeletal IGF regulatory system is important in states of impaired bone remodeling (4, 5). Two additional studies have demonstrated a strong relationship between serum IGF-1 and bone mineral density in men with idiopathic osteoporosis (6, 7). Based on these lines of evidence and the concept that bone density at any age is strongly dependent on peak bone mass, our group has considered IGF-1 to be a key factor in the acquisition of peak bone mass. In this paper, data will be presented which suggest that in several inbred strains of mice and in humans, osteoporotic male idiopathic IGF-1 is an important determinant of bone mineral density (BMD).

Materials and Methods

Mice

Two inbred strains of healthy mice with low and high bone mineral density (as reported previously) were studied at 4, 8, and 12 months of age (8). Female

C57BL/6J (B6; n=49) and C3H/HeJ (C3H; n=28) progenitor mice had bone mineral density of the femur (F-BMD) and serum IGF-I measured. Progenitor matings yielded F1 B6C3 (n=11) mice and F1 x F1 intercrosses produced F2 (n=35) females. Both F1 and F2 females had F-BMD and serum IGF-I measurements.

Human Subjects

Twenty-four men (mean age 50.5 ± 1.9 years) with low spine bone mineral density (mean t-score -3.5) and previous spinal fractures, but no known secondary causes of osteoporosis, were studied. A group of 30 similarly aged, healthy men were recruited as normal controls. Both groups of men had serum IGF-1 measured, as well as BMD at several sites (spine, hip, and forearm).

Bone Mineral Density

Femoral volumetric BMD in mice was determined by pQCT (XCT 960M; Nordland Medical Systems, Ft. Atkinson, WI USA) specifically modified for use on small bone specimens as described previously (8). Isolated femurs are measured at 2-mm intervals over their entire lengths, the unit volume within which mineral was detected was set at 0.1 cubic millimeter. The precision of this method for the mid-femur in two inbred strains of mice is <1.2%. F-BMD was performed on progenitors, F1, and F2 females at 4 or in some cases 8 months of age. Areal BMD in human subjects was determined by DEXA measurements of the hip, spine, and forearm, using a Hologic 4500 standardized by use of the same phantom employed for other clinical studies.

Serum IGF-I

IGF-1 was measured by RIA after extraction of IGFBPs using acid-ethanol cryoprecipitation as described previously in our laboratory (9). The inter- and intra- assay cv is approximately 4% and 6% for both mouse and human serum. All samples were obtained in the fasting state for both mice and humans. Serum in from men were assayed in the same run to minimize interassay differences.

Statistics

Differences between strains for IGF-I and F-BMD were assessed for statistical significance by Student's t test. Differences across ages and strains for serum IGF-1 were analyzed by two way ANOVA. Regressions for IGF-1 versus F-BMD were reported as Pearson correlations. Differences were considered significant if the p value was <0.05.

Results

In the female progenitor C3H and B6 mice, F-BMD were markedly different from each other (n=16: C3H=0.699±0.010 mg/mm^3 versus B6=0.443±0.004 mg/mm^3, p<0.001). Similarly, in 8-month-old mice, the high-density strain (C3H) had serum IGF-I levels which were significantly higher than the low density strain (B6) (serum IGF-I in C3H: 609±16 ng/ml versus B6 455±14 ng/ml, p<0.001). Similar differences (35% greater serum IGF-I in C3H versus B6, p<0.001) were also noted for 2, 4 and 12-month old mice. For B6C3F1 progeny (n=19) serum IGF-I was intermediate between the two progenitor strains (522±48 ng/ml). In the F2 generation, groups of mice with high (n=12), intermediate (n=12), and low (n=11) F-BMD had serum IGF-I measurements performed. F2 progeny with the highest F-BMD also had the highest IGF-I levels, whereas the F2 progeny with the lowest F-BMD also had the lowest serum IGF-I levels. Figure 14.1 illustrates the strong correlation between F-BMD and serum IGF-I in these 36 F2 mice (r=0.62, p<0.0001). More than 38% of the variance in F-BMD can be attributed to serum IGF-I.

In 24 middle-aged white men (mean age 50.5±1.9 years) with low bone mass and previous spinal fractures, serum IGF-I was 157.9±7.6 ng/ml (normal range 140-260 ng/ml). In 30 normal, nonosteoporotic men (mean age 48.1±1.0 years) serum IGF-I was 197±14 ng/ml (p<0.04 versus osteoporotics). When IGF-I in the osteoporotic men was expressed as a Z-score (derived from age- and sex-matched references from our laboratory), the mean IGF-I Z-score was -0.75±0.9. The mean IGF Z-score in the normal men was -0.11, not significantly different from the expected values of x=0. The distribution for IGF-I was unimodal with a disproportionate number (n=20) below the normal mean (Fig. 14.2). A univariate description of the IGF-I Z-score revealed that when tested against the hypothesis that the Z-score should be equal to 0, this shift to the left was statistically very significant (p=0.0002). In addition, among osteoporotic males, serum IGF-I was positively related to lumbar BMD (r=0.39, p<0.0001).

Discussion

Using two distinct model systems we present evidence in this paper to support our working hypothesis that IGF-I is an important factor in the acquisition or maintenance of bone mass. In two inbred strains of mice, IGF-I cosegregates with bone mass across two generations and accounts for a significant proportion of the variance in femoral BMD. These data also help to confirm preliminary findings from two earlier studies, which suggested a causal relationship between serum IGF-I and bone mass in the syndrome of male idiopathic osteoporosis (6, 7).

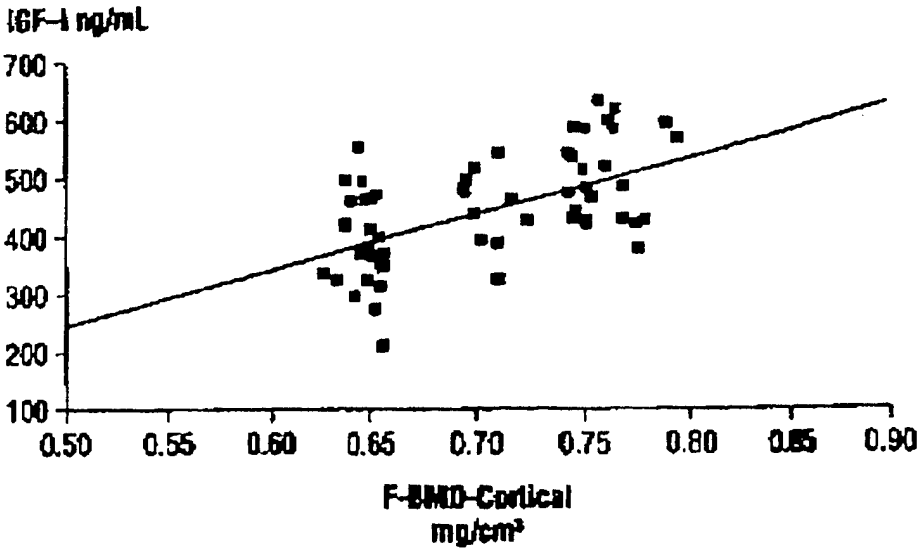

FIGURE 14.1. In F2 mice born from F1 x F1 crosses, high intermediate and low femoral bone mineral densities (F-BMD) are plotted against serum IGF-1 measured in the same mice. The Pearson correlation (r) was 0.68, $p<0.0001$, and $r^2=0.39$.

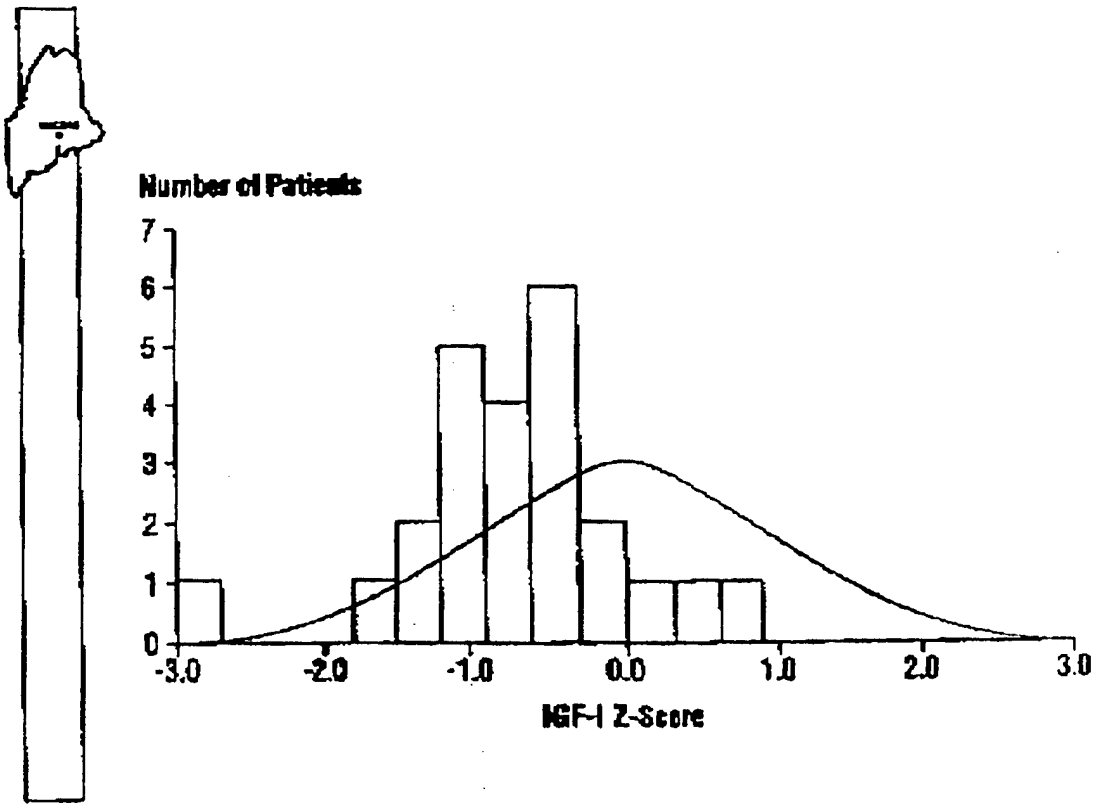

FIGURE 14.2. Distribution of IGF-1 Z-scores in men with idiopathic osteoporosis. The graph shows the mean Z-score of -0.75 is significantly lower ($p<0.0002$) than the normal expected Gaussian distribution (mean=0).

Several lines of evidence from earlier work also support the importance of IGF-1 in the determination of adult bone mass. First, two recent cross-sectional studies of postmenopausal women have shown a very strong correlation between serum IGF-1 and lumbar bone mineral density (4, 5). Second, age-associated changes in serum IGF-1 are mirrored by similar age related changes in skeletal IGF-1 content (4). Third, in growth hormone deficient patients, serum IGF-1 correlates closely with bone mineral density, and long-term growth hormone replacement increases both serum IGF-1 and bone mineral density (9). Finally, studies in the growth hormone releasing hormone receptor (Ghrhr) deficient mouse, *little*, have shown that low levels of serum IGF-1 are associated with low bone mineral density (10).

These data from mice are similar to clinical observations, despite obvious differences in the two species. But mice exhibit 60% linkage homology with man and demonstrate many hormonal processes that closely mirror physiologic events in the human organism. Although the life span of a mouse is much shorter than that of humans, work in our laboratory has convincingly demonstrated that peak bone mass in mice is acquired by 16 weeks of age and is maintained at that level for at least one year. Moreover, not unlike humans, regulation of peak bone mass in mice is predominantly genetic. Differences in serum IGF-1 between strains of mice are present by one month of age and are maintained throughout the first year of murine life. Our work suggest that two distinct phenotypes (IGF-1 and BMD) in mice cosegregate and are likely to be interrelated. Although it is premature to conclude that this is the case in humans, there remains abundant experimental evidence that IGF-1 is at least one factor which could mediate peak bone mass acquisition.

The data on serum-IGF1 and bone mass in men and mice are provocative for several reasons. First, two preliminary studies suggested that serum IGF-1 levels were low in relatively young males afflicted with osteoporosis (6, 7). Second, in this condition characterized by very low bone mass, reduced bone formation, and spinal fractures, bone resorption is not increased and other secondary causes have not been identified. Finally, there is preliminary evidence to suggest this could be a heritable disorder. Although the pathophysiology of this syndrome remains poorly defined, our findings are consistent with earlier reports that have suggested a causative link between reduced bone formation and low serum IGF-1. But the cross-sectional design of previous studies limit definitive conclusions (4–7). For example, it is not possible to know with certainty whether relatively low serum IGF-1 levels in men or mice are causally associated with low BMD. Nor can we know if changes in IGF-1 affect the process of bone mass acquisition or maintenance of adult bone density. But our data from inbred strains of mice suggest strongly that IGF-1 exerts a major influence on peak bone mass. In fact, the failure of earlier studies to find an association between IGF-1 and BMD in older subjects might relate more to a host of environmental influences on serum IGF-1 in later life rather than the absence of a relationship between these two variables. Still, longitudinal studies will be necessary to confirm the hypothesis that

IGF-I changes affect peak bone mass and thereby predispose men to future osteoporosis

In summary, we have presented data from two studies that suggest that IGF-I may play a critical role in determining bone mineral density in men and mice. More extensive studies that focus on the genetic relationship between BMD and IGF-I in mice are currently ongoing in our laboratory and promise to provide more data as we continue to test the working hypothesis that IGF-I is a key determinant of bone mass acquisition.

Acknowledgment. This study was supported in part by a grant from the U.S. Army Medical Research Acquisition Activity Grand DAMD17-96-1-6306 (WGB).

References

1. Jones JI, Clemmons DR. Insulin-like growth factors and their binding proteins: biological actions. Endocr Rev 1995;16:3–32.
2. Rosen CJ, Donahue LR, Hunter SJ. IGFs and bone: the osteoporosis connection. Proc Soc Exp Biol Med 1994;206:83–102.
3. Hayden JM, Mohan S, Baylink DJ. The insulin-like growth factor system and the coupling of formation to resorption. Bone 1995;17:93–8S.
4. Nicholas V, Prewett A, Bettica P, Mohan S, Finkleman RD, Baylink DJ, et al. Age-related decreases in IGF-1 and transforming growth factor-β in femoral cortical bone from both men and women: implications for bone loss in aging. J Clin Endocrinol Metab 1994;78:1011–6.
5. Mohan S, Baylink DJ. Development of a simple valid method for the complete removal of IGF binding proteins from IGFs in human serum and other biological fluids: comparison with acid-ethanol treatment and C18 Sep-Pak separation. J Clin Endocrinol Metab 1995;80:637–47.
6. Ljunghall S, Johansson AG, Burman P, Kampe O, Lindh E, Karlsson FA. Low plasma levels of IGF-1 in male patients with idiopathic osteoporosis. J Intern Med 1992;232:59–64.
7. Reed BY, Zerwekh JE, Sakhaee K, Breslau NA, Gottschalk F, Pak CYC. Serum IGF-I is low and correlated with osteoblastic surface in idiopathic osteoporosis. J Bone Miner Res 1995;10:1218–24.
8. Beamer WG, Donahue LR, Rosen CJ, Baylink DJ. Genetic variability in adult bone density among inbred strains of mice. Bone 1996;18:397–403.
9. Jorgensen JOL, Thuesen L, Ingemann-Hansen T, Pedersen SA, Jorgensen JU, Skakkebaek NES, et al. Beneficial effects of GH treatment in GH deficient adults Lancet 1989;1:1221–5.
10. Donahue LR, Beamer WG, Rosen CJ. Parathyroid hormone improves bone density in mice with growth hormone deficiency and IGF-1 deficiency. J Bone Miner Res 1995;10:523.

American Journal of Pathology, Vol. 155, No. 1, July 1999

Deficiency of SHP-1 Protein-Tyrosine Phosphatase Activity Results in Heightened Osteoclast Function and Decreased Bone Density

Syuji Umeda,* Wesley G. Beamer,* Katsumasa Takagi,† Makoto Naito,‡ Shin-Ichi Hayashi,§ Hiroyuki Yonemitsu,¶ Taolin Yi,‖ and Leonard D. Shultz*

From the Jackson Laboratory, Bar Harbor, Maine; the Department of Orthopaedic Surgery,† Kumamoto University of Medicine, Kumamoto, the Second Department of Pathology,‡ Niigata University School of Medicine, Niigata, the Department of Immunology,§ School of Life Science, Faculty of Medicine, Tottori University, Yonago, and Kumamoto Kinoh Hospital,¶ Kumamoto, Japan; and Department of Cancer Biology,‖ Cleveland Clinic Foundation, Cleveland, Ohio*

Mice homozygous for the motheaten (*Hcph*^{me}) or viable motheaten (*Hcph*$^{me\text{-}v}$) mutations are deficient in functional SHP-1 protein-tyrosine phosphatase and show severe defects in hematopoiesis. Comparison of femurs from *me*^{v}/*me*^{v} mice revealed significant decreases in bone mineral density (0.33 ± 0.03 mg/mm^3 for *me*^{v}/*me*^{v} *versus* 0.41 ± 0.01 mg/mm^3 for controls) and mineral content (1.97 ± 0.36 mg for *me*^{v}/*me*^{v} *versus* 10.64 ± 0.67 for controls) compared with littermate controls. Viable motheaten mice also showed reduced amounts of trabecular bone and decreased cortical thickness. These bone abnormalities were associated with a 14% increase in numbers of multinucleated osteoclasts and an increase in osteoclast resorption activity. In co-cultures of normal osteoblasts with mutant or control bone marrow cells, numbers of osteoclasts developing from mutant mice were increased compared with littermate control mice. Although *me*^{v}/*me*^{v} osteoclasts develop in the absence of colony-stimulating factor (CSF)-1, nevertheless cultured osteoclasts show increased size in the presence of CSF-1. CSF-1-deficient osteopetrosis (*op/op*) mutant mice develop severe osteosclerosis. However, doubly homozygous *me*^{v}/*me*^{v} *op/op* mice show an expansion of bone marrow cavities and reduced trabecular bone mass compared with *op/op* mice. Western blot analysis showed that several proteins that were markedly hyperphosphorylated on tyrosine residues were detected in the motheaten osteoclasts, including a novel 126-kd phosphotyrosine protein. The marked hyperphosphorylation of a 126-kd protein in motheaten osteoclasts suggests that this protein depends on SHP-1 for dephosphorylation. These findings demonstrate that the decreased SHP-1 catalytic activity in *me/me* and *me*^{v}/*me*^{v} mice results in an increased population of activated osteoclasts and consequent reduction in bone density. *(Am J Pathol 1999, 155:223–233)*

Osteoporosis is a major public health problem and is characterized by fragility fractures of the skeleton, most notably of the spine, wrist, and hip.[1] The maintenance of bone mass is a dynamic process requiring a balance between bone resorption and bone formation.[2] This process requires the coordinated regulation of bone-forming cells (osteoblasts) and bone-resorbing cells (osteoclasts). Increased osteoclast activity and/or decreased osteoblast activity may contribute to the development of osteoporosis. Osteoclasts are derived from hematopoietic progenitors and are members of the monocyte/macrophage family, whereas osteoblasts are derived from mesenchymal stem cells.[3–6]

The autosomal recessive motheaten mutation (*Hcph*^{me}) and the less severe allelic viable motheaten mutation (*Hcph*$^{me\text{-}v}$) cause aberrant splicing of the hematopoietic cell phosphatase (*Hcph*) gene transcript. The *Hcph* gene encodes the cytoplasmic protein-tyrosine phosphatase (PTP) Src-homology domain-2 phosphatase 1 (SHP-1) (also known as hematopoietic cell phosphatase, PTP-1C, src homology PTP-1, or PTP nonreceptor type 6).[7–11] The finding that the *me* and *me*^{v} mutations disrupt the *Hcph* structural gene encoding SHP-1 has illustrated the role of SHP-1 as a negative regulator in many signaling pathways in the hematopoietic and immune systems.[12,13] SHP-1 is a member of the family of PTPs that contain SH2 domains and is a cytoplasmic PTP expressed primarily in hematopoietic cells.[7,8,10,14,15] The *me* and *me*^{v} mutations result in a complete or partial loss, respectively, of SHP-1 catalytic activity.[16,17] These two mutant alleles generate phenotypes that are qualitatively similar but of different severity (Table 1).[18–21]

Supported by NIH grants CA20408 (L.D. Shultz), AR43618 (W.G. Beamer), and CA79891 and GM58893 (T. Yi) and NIH Cancer core grant CA34196 to the Jackson Laboratory.

Accepted for publication March 11, 1999.

Address reprint requests to Dr. Leonard D. Shultz, The Jackson Laboratory, Bar Harbor, ME 04609. E-mail: lds@jax.org.

Table 1. Phenotypes of Mutant Mice

Mutation (gene symbol)	Affected gene	Characteristic phenotype
Motheaten (*Hcph*^{me})	Hematopoietic cell phosphatase	Complete loss of SHP-1 catalytic activity Skin lesions appear at 3 to 5 days of age Mean life span of 3 weeks Impaired immunological function: Reduced proliferative response to B cell and T cell mitogens Absence of cytotoxic T cell responses Severely reduced NK cell function Systemic autoimmunity: Polyclonal B cell activation Expression of multiple autoantibodies
Viable motheaten (*Hcph*$^{me\text{-}v}$)	Hematopoietic cell phosphatase	Partial activity of SHP-1 (10–20%) Skin lesions appear at 3 to 5 days of age Mean life span of 9 weeks Impaired immunological function, similar to *me/me* mice Systemic autoimmunity but develops in a chronic fashion
Osteopetrosis (*Csfm*^{op})	Macrophage CSF	Complete loss of CSF-1 activity Osteopetrosis Absence of incisors Monocyte/macrophage deficiency Osteoclast deficiency

Our preliminary experiments showed that *me/me* and *me*^{v}*/me*^{v} mice had fragile bones. Although previous studies demonstrated hematopoietic abnormalities in these mice, little is known about the effect of deleterious alleles at the motheaten mutation on osteoclast development or function. The work described in this paper was carried out to test the hypothesis that SHP-1 protein-tyrosine phosphatase activity is required for the regulation of osteoclastogenesis and osteoclast function. First, we assessed bone density in *me*^{v}*/me*^{v} mice by radiography and by peripheral quantitative computed tomography (pQCT). Second, we carried out light microscopic and histochemical studies of bone tissue in *me/me* and *me*^{v}*/me*^{v} mice. Third, we measured the function of osteoclasts by pit formation in dentine slices and examined osteoclast differentiation in co-culture using bone marrow cells from *me/me* and *me*^{v}*/me*^{v} mice. Fourth, to define the potential role and mechanism of SHP-1 in the regulation of osteoclastogenesis and osteoclast function, we localized SHP-1 in osteoclasts from normal and *me*^{v}*/me*^{v} mice and analyzed possible SHP-1 substrates in these cells.

Colony-stimulating factor 1 (CSF-1 or macrophage colony-stimulating factor (M-CSF)) is known to be essential in the development and differentiation of osteoclasts and certain macrophages. The essential role of CSF-1 in development and differentiation of osteoclasts and certain macrophages is evidenced by the effects of the osteopetrosis mutation (*csfm*^{op}, hereafter termed *op*), which causes a total absence of CSF-1 production.[22] The CSF-1 deficiency in *op/op* mice causes widespread defects in development of the monocyte/macrophage lineage, including defects in osteoclast development. The failure of osteoclast development and differentiation in osteopetrosis (*op/op*) mice results in impaired bone resorption and leads to systemic osteopetrosis (Table 1).[6,23–25] Immunohistochemical staining and flow cytometry analyses revealed increased numbers of macrophages in the spleen, thymus, lungs, and liver of *me*^{v}*/me*^{v} mice.[26] It has been reported that macrophages from SHP-1-deficient mice show increased proliferation in response to CSF-1.[27] We also produced *me*^{v}*/me*^{v} mice that genetically lacked CSF-1 because of homozygosity for the osteopetrosis mutation to determine the role of CSF-1 in the bone disease observed in *me*^{v}*/me*^{v} mice. The doubly homozygous *me*^{v}*/me*^{v} *op/op* mice displayed less severe osteopetrosis than *op/op* mice.

This article shows that SHP-1-deficient mice develop osteoporosis that is due to increased numbers of osteoclasts and heightened osteoclast function. Thus, SHP-1 plays an important role as a negative regulator in osteoclastogenesis and osteoclast function.

Materials and Methods

Mice

C57BL/6J-*me/me* and *me*^{v}*/me*^{v} mice were produced in our research colony from matings of +/*me* or +/*me*^{v} heterozygotes, respectively. Homozygous *me/me* and *me*^{v}*/me*^{v} mice were identified by their characteristic skin lesions at 3 to 5 days of age. Littermate controls included both heterozygotes (+/*me* or +/*me*^{v}) and +/+ mice. The (C57BL/6J × B6C3FeJ)F2-*op/op me*^{v}*/me*^{v} mice were produced as follows: (C57BL/6J × B6C3FeJ)F1-+/*op* +/*me*^{v} doubly heterozygous mice were made from C57BL/6J-+/*me*^{v} × B6C3FeJ-+/*op* matings. The (C57BL/6J × B6C3FeJ)F2-*op/op me*^{v}*/me*^{v} mice were produced from matings of (C57BL/6J × B6C3FeJ)F1-+/*op* +/*me*^{v} double heterozygotes. Homozygous *op/op me*^{v}*/me*^{v} mice were identified by the characteristic (motheaten) skin lesions and characteristic (osteopetrosis) absence of incisors at 10 days of age. The femurs of *op/op me*^{v}*/me*^{v} and *op/op* +/? mice were studied by light microscopy and histochemical analyses.

Radiography

For conventional radiography, mice were anesthetized by intraperitoneal injection with tribromoethanol (0.2 ml/10 g body weight of 1.2% solution).[28] The mice were radiographed at 45 kV for 20 seconds at a focal distance of 35 cm with a cabinet x-ray system (Hewlett Packard, Wilmington, DE).

Bone Densitometry

Isolated femurs from 2-month-old *me^v/me^v* and littermate control mice were analyzed by peripheral quantitative computed tomography (pQCT) with a Stratec XCT 960M (Norland Medical Systems, Ft. Atkinson, WI) specifically modified for use on small bone specimens to measure bone mineral and volume as described previously.[29] Briefly, isolated femurs from *me^v/me^v* and littermate control mice were scanned at 2-mm intervals over their entire lengths, and the unit volume within which mineral was measured was set at 0.1 mm^3. The density values were calculated by dividing the mineral content by volume. The femur lengths were divided by body weights.

Light Microscopy, Histochemistry, and Immunohistochemistry

Femurs and tibias from 2-month-old *me^v/me^v* and littermate control mice and from 3- to 4-week-old *me^v/me^v op/op*, *me^v/me^v* +/?, +/? *op/op*, and +/? +/? mice were fixed and demineralized in Bouin's fixative, processed routinely, and then embedded in paraffin. Sections were cut at 6-μm thickness and stained with hematoxylin and eosin (H&E) for histological examination. For detection of osteoclasts, paraffin sections were processed for the histochemical localization of tartrate-resistant acid phosphatase (TRAP) as described previously.[6] Numbers of TRAP-positive cells per millimeter of bone edge were counted in the distal metaphysis of femurs. The bone surface lengths were measured by using the Quantimet Q600HR system (Leica, Deerfield, IL). In addition, tissue sections in *me/me* and normal littermate mice were stained by indirect immunoperoxidase using rabbit polyclonal antibody against SHP-1.[25,30] Briefly, the paraffin sections were incubated for 15 minutes in 10% hydrogen peroxide to quench endogenous peroxidase activity. After blocking for 10 minutes with donkey serum, the sections were incubated with rabbit anti-SHP-1 polyclonal antibody. Anti-rabbit immunoglobulin horseradish-peroxidase-linked whole antibody (Amersham, Little Chalfont, UK) was used as secondary antibody. After visualization with 3,3′-diaminobenzidine, the sections were counterstained with hematoxylin and coverslipped.

Measurement of Bone Resorption by Osteoclasts

Dentine slices from elephant tusk were the kind gift of Dr. I. Itonaga (Oita, Japan).[31,32] Dentine slices (4 mm diameter × 0.5 mm) were cut with a low-speed saw. The slices were sterilized by autoclaving and placed in 96-well culture plates. Bone marrow cells were harvested by scraping from the distal metaphysis of femurs and proximal metaphysis of tibias in 1-month-old *me/me*, *me^v/me^v*, and littermate control mice. A suspension (10^4 cells) of bone marrow cells from mutant or control mice was added to individual wells of 96-well culture plates. After 48 hours, the dentine slices were sonicated to remove the osteoclasts, and resorption lacunae formed on the slices were detected using a JSM-35C scanning electron microscope (Jeol, Tokyo, Japan). Four to six pits were measured for each animal, and six mice were examined. Pit areas were measured by using NIH Image 1.60 (National Institutes of Health, Bethesda, MD).

Co-Culture of Osteoblasts and Bone Marrow Cells

Osteoblasts were isolated from the calvariae of 3-day-old C57BL/6J-+/+ mice. The calvariae were collected and digested with a solution of phosphate-buffered saline (PBS) containing 0.1% collagenase (Wako Chemical, Dallas, TX) and 0.2% dispase (Boehringer Mannheim, Indianapolis, IN). Isolated cells were cultured until they became confluent in α-minimal essential medium (αMEM) containing 10% heat-inactivated fetal bovine serum (FBS; GIBCO, Grand Island, NY) in 25-cm^2 culture flasks at 10^6 cells/flask. Cells were then detached from the flasks by the addition of 0.05% trypsin in PBS, collected by centrifugation (1500 rpm for 5 minutes), suspended in αMEM containing 10% FBS, and plated in 75-cm^2 flasks (Corning Labware and Equipment, Corning, NY) or eight chamber Lab Tek chambers (Nalge Nunc International, Naperville, IL) at 1×10^4 cells/cm^2. The *me/me, me^v/me^v*, and littermate control mice (8 weeks old) were killed by CO_2 asphyxiation, and tibias and femurs were aseptically removed. The bone ends were cut off with scissors, and marrow cavities were flushed with 1 ml of αMEM by using syringes and 27-gauge needles. The bone marrow cells were then filtered through nylon mesh and washed once with αMEM. Bone marrow cells (2.5×10^4/cm^2) from the mutant or control mice were cultured with C57BL6J-+/+ osteoblasts in αMEM containing 10% FBS and 10 nmol/L $1,25(OH)_2D_3$ (Calbiochem, San Diego, CA) without or with 1.0 μg/ml human CSF-1 (Cetus, Emeryville, CA) or 10 μg/ml anti-mouse CSF-1 receptor antibody.[33] Medium was replaced every 3 days. After 8 days, the cells cultured in eight-well Lab Tek chambers were washed twice with PBS and fixed with 10% neutral buffered formalin, permeabilized with 1:1 (v/v) acetone/ethanol for 1 minute, and stained for histochemical localization of TRAP. Numbers of TRAP-positive cells (>2 nuclei/cell) per square millimeter were counted. The cells cultured in 75-cm^2 flasks were collected after treating with trypsin and prepared for immunoblotting.

Antibodies, Immunoprecipitation, Binding Assays, and Western Blotting

Antibodies against SHP-1 have been described previously.[30] Antibodies against phosphotyrosine (anti-ptyr; UBI, Lake Placid, NY) and β-actin (Amersham) were purchased from commercial sources. Immunoprecipitation and Western blotting were performed as described previously.[16,34,35] Briefly, total cell lysates (TCLs) were prepared by lysing the cell samples in cold lysis buffer (50 mmol/L Tris, pH 7.4, 150 mmol/L NaCl, 0.5% sodium deoxycholate, 0.2 mmol/L Na_3VO_4, 20 mmol/L NaF, 1% Nonidet P-40, 2 mmol/L phenylmethylsulfonyl fluoride, 20 μg/ml aprotinin, and 10% glycerol). The cell lysates were clarified by centrifugation, and Western blotting for SHP-1 protein and phosphotyrosine proteins was carried out as previous described.[16] For immunoprecipitation experiments, the TCLs were incubated with antibodies at 4°C for 60 minutes. Immune complexes were then collected with protein A/Sepharose beads (Pharmacia, Piscataway, NJ). TCLs and immune complexes were separated by SDS-polyacrylamide gel electrophoresis, blotted onto nitrocellulose membrane (Schleicher & Schuell, Keene, NH), probed with specific antibodies, and detected using an enhanced chemiluminescence kit (ECL, Amersham).

Statistical Analyses

Data are presented as means ± SEM. Statistical analyses were performed with Stat View software for Macintosh. All data were analyzed first by ANOVA to detect major effects due to genotype. When a significant F ratio was identified, groups were compared using Fisher's protected least significant difference *post hoc* test. Differences were judged as statistically significant when $P < 0.05$.

Results

Assessment of the Bone Density by Radiography and by pQCT

Four pairs of *me*^{v}/*me*^{v} and littermate control mice at 2 months of age were examined by radiography. The *me*^{v}/*me*^{v} mice at 2 months of age were smaller than littermate control mice, and there was no marked disproportion of the limbs and tail. However, absorption of x-rays by bone in *me*^{v}/*me*^{v} mice was markedly decreased, and the cortical bone was thinner compared with littermate control mice (Figure 1). The mid-diaphyseal scans for femurs

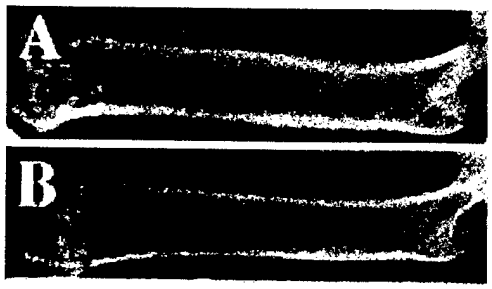

Figure 1. Femoral bone from *me*^{v}/*me*^{v} mice shows reduced cortical density by radiography of a femur in a 2-month-old littermate control mouse (A) and a *me*^{v}/*me*^{v} mouse (B). A: The femur of the littermate control mouse has clearly distinguishable cortical areas. B: In contrast, the femoral bone mass of the *me*^{v}/*me*^{v} mouse is decreased, and cortical bone density is reduced compared with that of the littermate control mouse.

from littermate control (Figure 2A) and *me*^{v}/*me*^{v} (Figure 2B) mice were obtained simultaneously and correspond to the XCT 960M measurements of bone parameters. High-density bone is represented by white and blue-green color; low-density bone and trabecular bone appear yellow and red in these images. The scan from the femur of a littermate control mouse (Figure 2A) shows more higher-density bone than the scan from a *me*^{v}/*me*^{v} mouse (Figure 2B). The thickness of cortical bone measured at the mid diaphysis of femurs in *me*^{v}/*me*^{v} and normal littermate control mice was 0.20 ± 0.01 mm and 0.25 ± 0.02 mm, respectively ($P < 0.02$). The body weight and femur parameters (length, density, mineral content, volume, and proportion of femur length to body weight) obtained from 2-month-old *me*^{v}/*me*^{v} and littermate control mice are shown in Table 2. There was no effect of sex on femur parameters in *me*^{v}/*me*^{v} or in littermate control mice (data not shown). The mineral content and bone volume of *me*^{v}/*me*^{v} mice were significantly

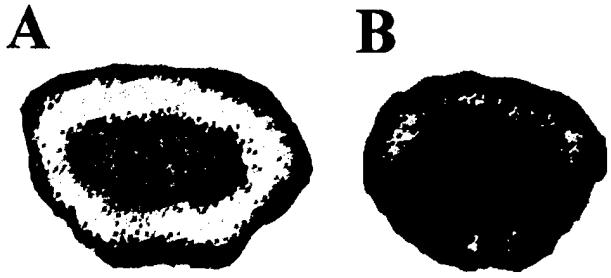

Figure 2. Decreased levels of high density bone in *me*^{v}/*me*^{v} mice, as shown by mid-diaphyseal pQCT tomograms of femurs from a 2-month-old littermate control mouse (A) and *me*^{v}/*me*^{v} mouse (B). High-density bone is represented by white and blue-green color, whereas low-density bone is represented by red/yellow color. Littermate control femur (A) shows substantially more high-density cortical bone compared with femur from a *me*^{v}/*me*^{v} mouse (B).

Table 2. Body Weight and Femur Measurements from 2-Month-Old Mice

Genotype	Body weight (g)	Length (mm)	Density (mg/mm^3)	Mineral (mg)	Volume (mm^3)	Length (mm)/ body weight (g)
me^v/*me*^{v} (n=11)	10.80 ± 0.52	12.55 ± 0.18	0.33 ± 0.03	1.97 ± 0.36	5.78 ± 0.84	1.18 ± 0.05
+/? (n = 12)	20.28 ± 0.69*	14.77 ± 0.12*	0.41 ± 0.01†	10.64 ± 0.67*	25.60 ± 1.35*	0.74 ± 0.20*

Mean ± SEM are presented for groups.
*$P < 0.0001$.
†$P < 0.02$.

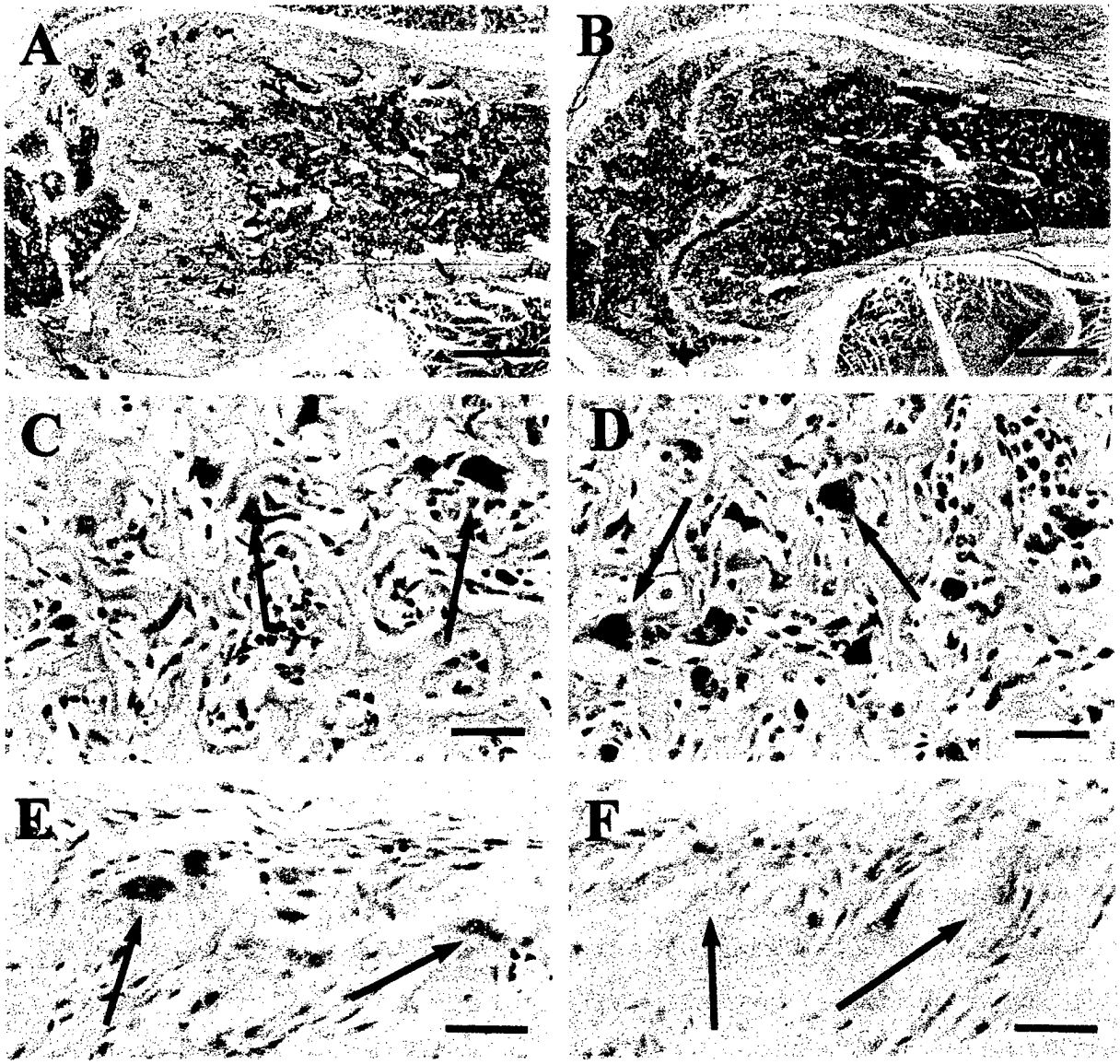

Figure 3. Reduced cortical and trabecular bone accompanied by increased numbers of multinucleated osteoclasts in bones from *me^v/me^v* mice, as shown by histological analyses of bone tissue in mice at 2 months of age: littermate control (A, C, and E) and *me^v/me^v* (B and D) and me/me (F) mice. A: Sagittal section of the femur in littermate control mouse shows abundant trabecular bone and thick cortical bone (H&E). Scale bar, 0.5 mm. B: Prominent loss of trabecular bone is seen in the metaphysis and the thickness of cortical bone is reduced in *me^v/me^v* mouse (H&E). Scale bar, 0.5 mm. C and D: Transverse section of the tibia in littermate control (C) and *me^v/me^v* mouse (D) were stained for TRAP. TRAP-positive cells are observed on the endosteal surfaces as indicated by arrows. TRAP-positive cells in *me^v/me^v* mouse (D) are larger in size and have increased numbers of nuclei compared with those from littermate control mouse (C). Scale bar, 0.03 mm. E and F: Immunohistochemical stain with anti-SHP-1 polyclonal antibody. SHP-1-positive multinucleated osteoclasts are detected on the endosteal surface in littermate control mouse (E). There are no SHP-1-positive multinucleated cells in *me/me* mouse, which lack SHP-1 protein (F). Scale bar, 0.03 mm. The arrows indicate multinucleated osteoclasts.

lower than in littermate control mice ($P < 0.001$). Bone density of femurs in *me^v/me^v* mice were also lower than in littermate control mice ($P < 0.02$). Finally, the femur lengths were divided by body weight. The femur length/body weight ratios in *me^v/me^v* mice were larger than in littermate control mice.

Histopathological Changes and Distribution of Osteoclasts in me^v/me^v *Mice*

Histological analysis of femurs revealed a marked reduction of trabecular bone and reduced thickness of cortical bone in *me^v/me^v* mice compared with littermate control mice (Figure 3, A and B). Similar histological changes were detected in femurs of *me/me* mice (data not shown). To determine the numbers and distribution of osteoclasts in *me^v/me^v* mice, we prepared sagittal sections of the distal metaphysis in femurs and transverse sections of proximal metaphysis in tibias for enumeration of TRAP-positive cells. Numbers of TRAP-positive cells per millimeter of bone edge in the distal femur of 8-week-old *me^v/me^v* mice were significantly increased compared with littermate control mice ($P < 0.05$; Figure 4A). Transverse sections of the proximal metaphysis in tibias from mutant and control mice were made to compare numbers of multinucleated TRAP-positive cells (Figure 3, C and D).

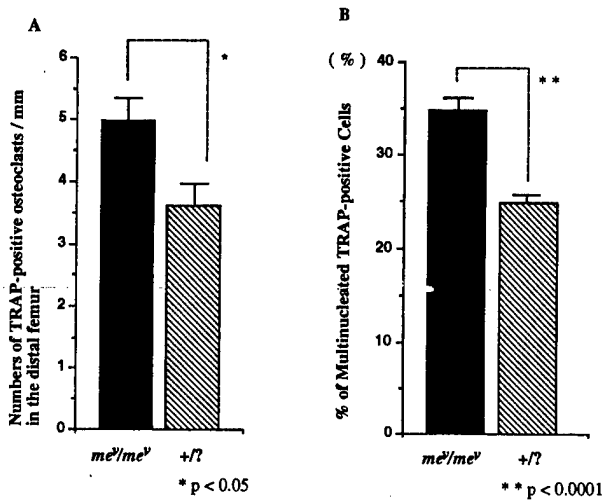

Figure 4. Increased numbers of multinucleated TRAP-positive cells in bones from me^v/me^v mice. Shown are numbers of TRAP-positive cells per millimeter in the distal femur (A) and percentage of TRAP-positive multinucleated (>4 nuclei) cells in the proximal tibia (B). A: Numbers of TRAP-positive cells per millimeter in the distal femur of 8 week-old me^v/me^v mice were significantly increased compared with littermate control mice. B: The percentage of multinucleated TRAP-positive cells was significantly increased in me^v/me^v mice compared with littermate control mice. Data are presented as mean ± SEM. $^*P < 0.05$; $^{**}P < 0.0001$, significantly different from the control group.

These data show the multinucleated TRAP-positive cells (>4 nuclei/cell) as a percentage of total TRAP-positive cells (Figure 4B). Numbers of multinucleated TRAP-positive cells were significantly increased in me^v/me^v mice compared with littermate control mice ($P < 0.0001$). Similar increased numbers of multinucleated TRAP-positive cells were observed in the distal femurs of me^v/me^v mice (data not shown). Immunohistochemical staining using anti-SHP-1 polyclonal antibody demonstrated the expression of SHP-1 in osteoclasts in the littermate control mice (Figure 3E). However, as expected, we could not detect SHP-1-positive osteoclasts in *me/me* mice, which lack SHP-1 protein and serve as a negative control for SHP-1 localization (Figure 3F).

Determination of Osteoclast Function by Analyses of Pit Formation in Dentine Slices

Histological data suggested that osteoclast activities in me^v/me^v and *me/me* mice were increased compared with littermate control mice. We examined osteoclast function directly by the isolated osteoclast resorption pit assay on dentine slices. Table 3 shows that pit area/osteoclast in dentine slices incubated with osteoclasts from *me/me* mice and me^v/me^v mice were significantly larger than pit area/osteoclast in dentine slices incubated with osteoclasts from littermate control mice ($P < 0.0001$).

Table 3. Osteoclast Pit Area in Bone Slices Incubated with Osteoclasts from *me/me*, me^v/me^v, or Normal Control Mice at 1 Month of Age

Genotype	Pit area ($\times 10^3$ μm^2/osteoclast)
me^v/me^v	13.25 ± 1.08
me/me	7.97 ± 2.16
+/?	1.15 ± 0.41

Mean ± SEM are presented for groups; $n = 6$. $P < 0.0001$ between all groups.

Assay of Osteoclastogenesis by Osteoblast/ Bone Marrow Cell Co-Cultures

As me^v/me^v mice showed increased numbers of TRAP-positive cells and increased percentages of multinucleated TRAP-positive cells compared with littermate control mice, we next examined osteoclastogenesis *in vitro* from bone marrow cells isolated from *me/me*, me^v/me^v, or littermate control mice. Osteoclastogenesis was determined by measuring numbers of osteoclasts produced in co-culture using normal C57BL/6J-+/+ osteoblasts co-cultured with bone marrow cells from *me/me*, me^v/me^v, or littermate control mice. The results are reported as numbers of TRAP-positive multinucleated cells (>2 nuclei/cell) per square millimeter of eight-chamber Lab Tek chambers. TRAP-positive cells from me^v/me^v mice were larger in size compared with those from littermate control mice (Figure 5, A and B). Numbers of TRAP-positive cells in me^v/me^v mice were significantly increased compared with those in littermate control mice. However, there was no significant difference in numbers of TRAP-positive cells between *me/me* and littermate control mice (Table 4).

CSF-1 or neutralizing monoclonal antibody to mouse CSF-1 receptor was added to stimulate or inhibit osteoclast formation, respectively. Addition of anti-CSF-1 receptor antibody completely inhibited the formation of multinucleated TRAP-positive cells from bone marrow cells of *me/me*, me^v/me^v, or littermate control mice (Table 4). Addition of CSF-1 stimulated development of TRAP-positive cells in *me/me*, me^v/me^v, and littermate control mice, but there was no significant difference in numbers of CSF-1-stimulated TRAP-positive cells among *me/me*, me^v/me^v, and littermate control mice (Table 4). TRAP-positive cells from *me/me* and me^v/me^v mice were larger in size and had increased numbers of nuclei compared with those from littermate control mice (Figure 5, C and D).

Histopathological Changes of Femurs in Doubly Homozygous me^v/me^v op/op *Mice*

We produced doubly homozygous me^v/me^v *op/op* mice to determine the effects of CSF-1 deficiency *in vivo* on osteoporosis in me^v/me^v mice. Histological analysis of femurs from me^v/me^v *op/op* mice showed increased bone thickness compared with me^v/me^v mice. However, an expansion of bone marrow cavities and reduced trabecular bone were exhibited me^v/me^v *op/op* compared with +/? *op/op* mice (Figure 6, A and B). Although there were no observable TRAP-positive osteoclasts in +/? *op/op* mice (Figure 6C), osteoclasts on the endosteal surface of femoral bones in me^v/me^v *op/op* mice were detected by positive histochemical reaction for TRAP (Figure 6D). However, these endosteal TRAP-positive cells were small and mononuclear.

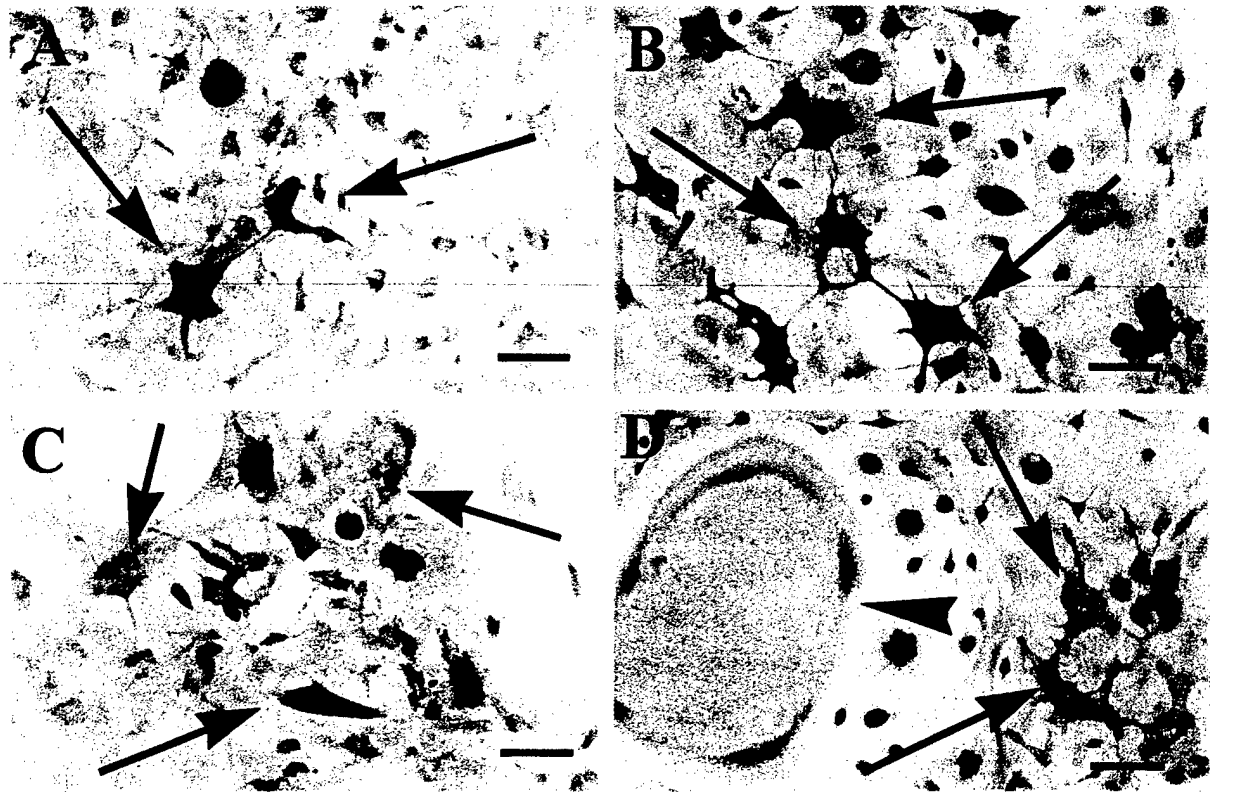

Figure 5. Increased size of me^v/me^v osteoclasts. Osteoclast cultures from littermate control (A and C) and me^v/me^v mice (B and D) were fixed and stained for TRAP. A and B were cultured without CSF-1. C and D were cultured with CSF-1. The arrows indicate TRAP-positive cells. A and B: Cultured osteoclasts from me^v/me^v mice (B) in the absence of exogenous CSF-1 are larger than those from littermate control mice (A). Numbers of TRAP-positive cells in me^v/me^v mice were increased compared with those in controls. C and D: After addition of CSF-1, osteoclasts from me^v/me^v mice (D) are larger in size than that from littermate control mice (C) and have increased numbers of nuclei (arrowhead). Scale bar, 0.05 mm.

Western Blotting Analysis of SHP-1 Protein

Osteoclasts isolated from osteoblast/bone marrow cell co-cultures were analyzed for the expression of SHP-1 protein. Osteoclasts from littermate control and me^v/me^v bone marrow cells treated with $1,25(OH)_2D_3$ expressed SHP-1 protein (Figure 7A). Although me^v/me^v mice are deficient in SHP-1 functional activity, these mice, nevertheless, express normal levels of SHP-1 protein. As is shown in Figure 7A, lane 3, those mice produce two SHP-1 bands on Western blotting. One band is slightly lower than normal and is slightly smaller. However, as expected, osteoclasts isolated from *me/me* mice did not express SHP-1 (Figure 7A). This is consistent with our previous finding that me^v/me^v hematopoietic cells express SHP-1 protein with severely reduced catalytic activity whereas *me/me* hematopoietic cells lack SHP-1 protein.[16] To identify potential SHP-1 substrates, we examined the total cell lysate (TCL) of cultured osteoclasts from *me/me*, me^v/me^v, and littermate control mice. Several distinct protein bands in TCLs from *me/me* and me^v/me^v osteoclasts were found to be hyperphosphorylated on tyrosine residues, including proteins of approximately 47, 60, and 126 kd (Figure 7A). We next looked for phosphotyrosine proteins that were associated with SHP-1 in osteoclasts. A phosphotyrosine protein of approximately 126 kd (p126) was detected in the anti-SHP-1 immune complex from me^v/me^v osteoclasts (lane 3) but not in osteoblasts (lane 1), littermate control osteoclasts (lane 2), or *me/me* osteoclasts, which lack SHP-1 protein (lane 4; Figure 7B).

Table 4. Numbers of TRAP-Positive Cells in Co-Culture in the Presence or Absence of CSF-1 Growth Factor or Neutralizing Anti-CSF-1 Receptor Antibody

Genotype	Numbers of cells × 10^2/mm^2		
	No treatment	CSF-1	Anti-CSF-1
+/?	1.74 ± 0.26	2.81 ± 0.32*	0 ± 0
me^v/me^v	3.56 ± 0.61†	3.85 ± 0.87	0 ± 0
me/me	2.66 ± 0.45	2.98 ± 0.54	0 ± 0

Data are presented as mean ± SEM. In the no-treatment group, there was no significant difference between +/? and *me/me* or between *me/me* and me^v/me^v. In the CSF-1 treatment group, there was no significant difference between +/? and me^v/me^v or *me/me*. There was no significant difference between the presence and absence of CSF-1 in *me/me* and me^v/me^v mice.

*$P < 0.05$ *versus* no treatment.

†$P < 0.05$ *versus* +/? group.

Discussion

This study shows that the absence or severe reduction of SHP-1 activity in *me/me* and me^v/me^v mice, respectively, caused marked abnormalities in the development and activity of osteoclasts *in vitro* and *in vivo*. Histological studies demonstrated increased numbers of TRAP-posi-

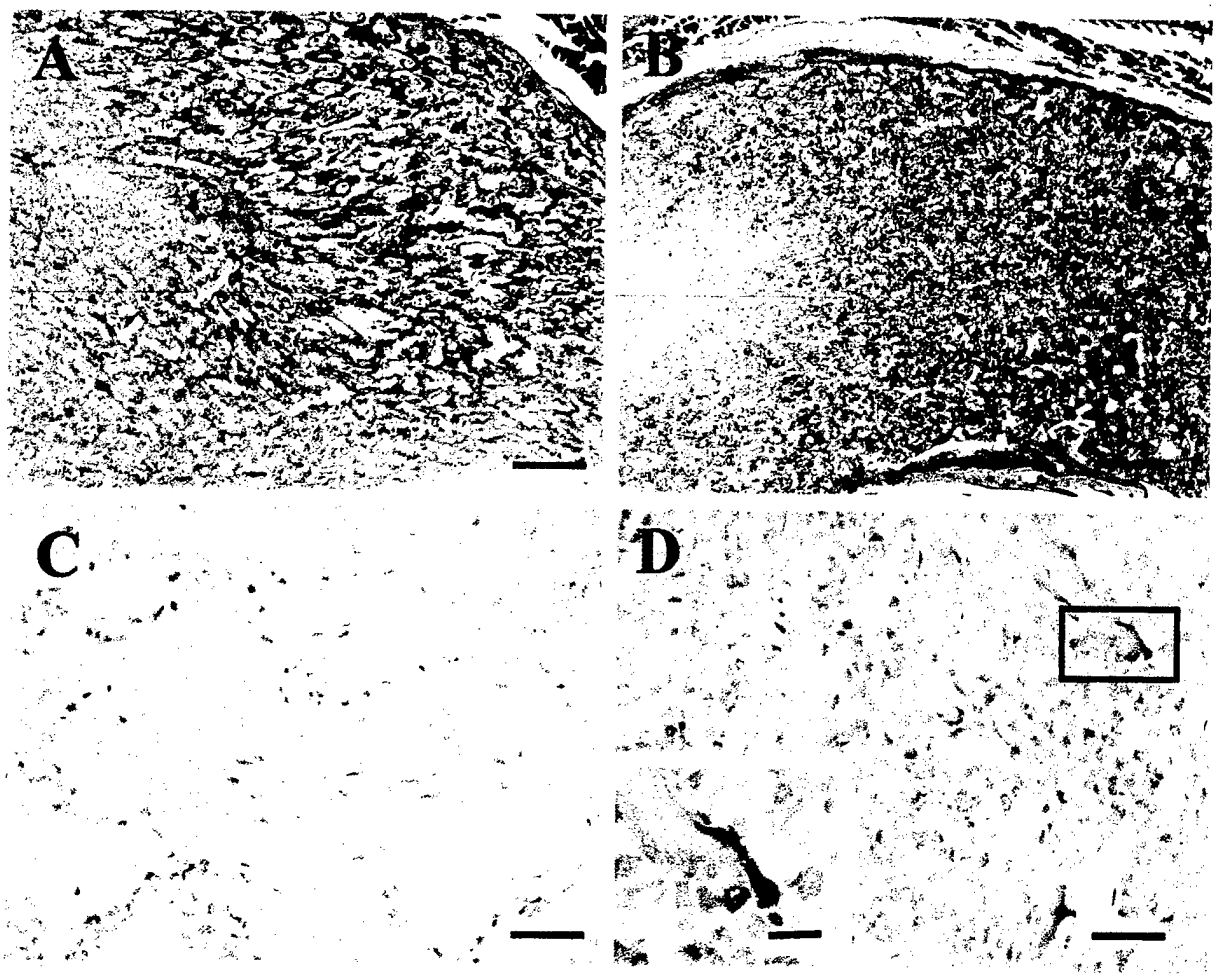

Figure 6. Reduction of osteopetrosis in CSF-1-deficient me^v/me^v *op/op* mice, as shown by histological analyses of bone tissue in mice at 4 weeks of age. A and C: +/? *op/op* mice. B and D: me^v/me^v *op/op* mice. A and C: Sagittal section of +/? *op/op* femur shows prominent osteosclerosis, marked reduction of bone marrow cellularity, and lack of TRAP-positive cells. B and D: Decreased trabecular bone and increased bone marrow cellularity are seen in me^v/me^v *op/op* mouse. Although TRAP-positive cells are detected, they are small and mononuclear. Inset: A high magnification of TRAP-positive mononuclear cell indicated by box. Scale bar, 0.01 mm. The arrows indicate the TRAP-positive cells. H&E (A and B); TRAP stain (C and D). Scale bar, 0.1 mm (A and B) and 0.03 mm (C and D).

tive cells and increased percentages of multinucleated osteoclasts (>4 nuclei/cell) in me^v/me^v mice When osteoclasts from *me/me*, me^v/me^v, and littermate control mice were incubated on dentine slices, the areas of pit formation caused by osteoclasts from the mutant mice were substantially increased compared with pit areas from littermate control osteoclasts. SHP-1 was found to be expressed in osteoclasts, but not in osteoblasts as determined by immunohistochemical staining and Western blotting with anti-SHP-1 antibody. In our previous studies, it was shown that treatment of motheaten mice with 500 R γ-irradiation followed by reconstitution with normal bone marrow cells resulted in increased life span.[36] The density of femoral bone in these treated mutant mice was normal (unpublished data). This result indicates a primary defect in hematopoietic progenitor cells. It has been reported that the turnover rate of bone in *me/me* mice was increased compared with that in littermate control mice.[37] As bone turnover rate is increased in the *me/me* mutant mice, osteoblast activity is not likely to be impaired, and increased osteoclast activity is likely the major factor contributing to osteoporosis in the mutant mice. These data clearly suggest that the osteoporotic changes observed in these mutant mice resulted from increased osteoclast numbers and heightened osteoclast function.

To determine the role of SHP-1 in osteoclastogenesis, we have used *in vitro* culture systems. Co-culture using normal osteoblasts and bone marrow cells from *me/me*, me^v/me^v, or littermate control mice showed that numbers of TRAP-positive cells generated from bone marrow cells from *me/me* and me^v/me^v mice were increased compared with those from littermate control mice. These data suggest that the abnormal growth of osteoclasts in the mutant mice may be due to impaired negative regulation of cytokine signaling by SHP-1 *in vitro*. Similarly, in the erythroid lineage, activation of SHP-1 by binding to the erythropoietin receptor plays a major role in terminating proliferative signals.[18,20,38,39] Likewise, absence or reduction of enzymatic activity of SHP-1 results in hyperresponsiveness to erythropoietin. Our data show that absence or reduction of functional SHP-1 in *me/me* and me^v/me^v mice, respectively, results in increased osteoclastogenesis. First we examined effects of CSF-1, which play an important role in osteoclast development and differentiation. It has been reported that SHP-1 is rapidly phosphorylated in macrophages after binding of

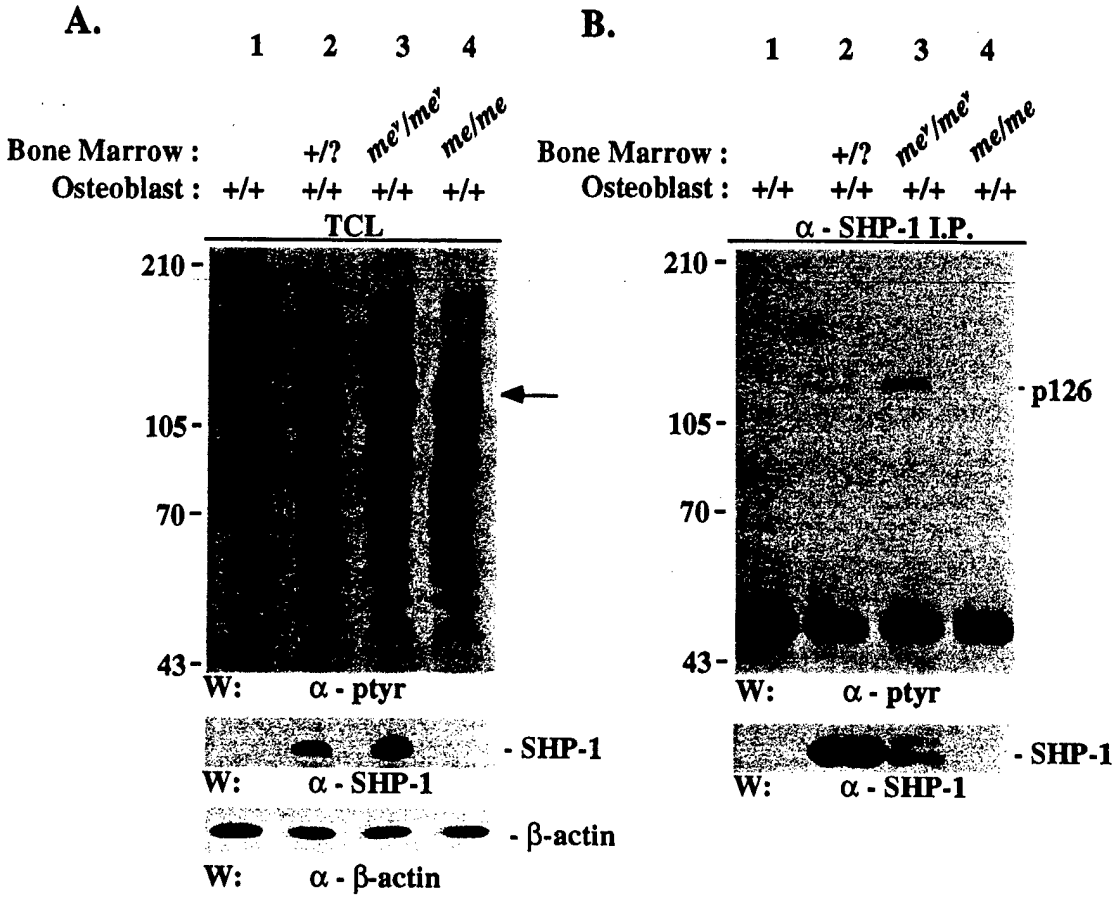

Figure 7. Hyperphosphorylation of phosphotyrosine proteins in *me^v/me^v* osteoclasts, as shown by Western blotting analysis of SHP-1 and proteins that were hyperphosphorylated on tyrosine residues (A) and immunoprecipitation with anti-SHP-1 antibody (B). Osteoclasts were obtained from co-culture of normal osteoblasts (+/+) and bone marrow cells from *me/me*, *me^v/me^v*, or littermate control mice (+/?). A: The cells were lysed to prepare total cell lysate (TCL). The positions of protein size markers, SHP-1, β-actin, and several hyperphosphorylated proteins are indicated. The arrow indicates a 126-kd protein. B: TCL was used for immunoprecipitation with anti-SHP-1 antibody. The immune complexes were analyzed by SDS-PAGE/Western blotting with anti-phosphotyrosine protein. A phosphotyrosine protein of 126 kd was detected in TCL anti-SHP-1 immunoprecipitates from *me^v/me^v* osteoclasts (lane 3) but not in osteoblasts (lane 1), littermate control osteoclasts (lane 2), or *me/me* osteoclasts (lane 4). Lane 1 shows the +/+ osteoblast culture without bone marrow cells.

CSF-1 to its receptor.[27] Addition of neutralizing monoclonal antibody to CSF-1 receptor completely blocked multinucleated TRAP-positive cell development *in vitro*. We expected that osteoclasts from *me/me* and *me^v/me^v* mice would show increased proliferation in response to CSF-1. Although addition of CSF-1 (1.0 μg/ml) stimulated increased numbers of TRAP-positive cells in littermate control mice, there were no significant effects of adding exogenous CSF-1 on numbers of TRAP-positive cells in *me/me* and *me^v/me^v* mice. We found that TRAP-positive cells in *me/me* and *me^v/me^v* mice were larger than those in normal mice and were multinucleated after incubation with CSF-1. In a recent *in vitro* study, it was shown that CSF-1 induced the formation of large multinucleated osteoclasts in rats.[40] This may explain why there were increased TRAP-positive multinucleated cells in *me/me* and *me^v/me^v* mice and suggests that SHP-1 is a negative regulator of CSF-1 signaling in osteoclasts.

We performed genetic crosses with CSF-1-deficient osteopetrosis (*op*) mutant mice to determine the role of CSF-1 in the bone disease observed in *me^v/me^v* mice. Doubly homozygous *me^v/me^v op/op* mice showed poor survival associated with overgrowth of granulocytes in the lungs, skin, and elsewhere. However, *me^v/me^v op/op* mice manifested improved development of lymphoid follicles compared with *me^v/me^v* +/? mice, suggesting that the overgrowth of macrophages in the spleen of *me^v/me^v* mice may play a suppressive role in follicle development (data not shown). Although *me^v/me^v op/op* mice displayed osteopetrosis, mononucleated TRAP-positive cells developed in these mice, and osteopetrosis in *me^v/me^v op/op* mice was less severe than in +/? *op/op* mice. These observations suggest that differentiation of osteoclasts is supported by CSF-1-independent mechanisms in *me^v/me^v op/op* mice to compensate for the absence of functional CSF-1 activity. It is known that osteopetrosis in aged *op/op* mice is partially reversed with a spontaneous increase of numbers of mononuclear osteoclasts and expansion of bone marrow cavities.[41,42] Bcl-2 overexpression in monocytes of *op/op* mice results in replenishment of tissue macrophages and partial reversal of long bone osteopetrosis.[43] The partial reversal of osteopetrosis with age in *op/op* mice may be associated with increased levels of granulocyte/macrophage colony-stimulating factor (GM-CSF) and interleukin-3 as these cytokines are increased in aged *op/op* mice.[42] Although

studies by Wiktor-Jedrzeijczak et al[44] suggested that short-term administration of GM-CSF to *op/op* mice failed to cure osteopetrosis, studies by Myint et al[42] suggested that injection of rmGM-CSF induced osteoclast development in *op/op* femurs. In previous *in vitro* studies, the effects of GM-CSF on osteoclast formation were controversial. In contrast to most known cytokines, osteoprotegrin ligand (OPGL) stimulates osteoclast differentiation directly.[45] The signaling pathways of the OPGL receptor are not clear. We sought to define the potential role and mechanisms of SHP-1 in osteoclasts.

It was reasoned that protein tyrosine phosphorylation, which is down-regulated by SHP-1 in normal mice, would be altered in osteoclasts from SHP-1-deficient motheaten mice. To identify potential SHP-1 substrates, we examined proteins that were hyperphosphorylated on tyrosine residues in the total cell lysates (TCLs) of osteoclast co-cultures from *me/me* and *me^v/me^v* mice. Several distinct protein bands were found to be hyperphosphorylated on tyrosine residues compared with littermate control TCLs, indicating that dephosphorylation depends on SHP-1. The identities of these hyperphosphorylated proteins have not yet been determined. We also examined phosphotyrosine proteins associated with SHP-1 in osteoclasts. A phosphotyrosine protein of approximately 126 kd (p126) was detected in the anti-SHP-1 immune complexes from *me^v/me^v* osteoclasts. We have previously reported that p126 is a novel phosphoprotein in macrophages.[30] The marked hyperphosphorylation of p126 in *me^v/me^v* osteoclasts suggests that it is a major SHP-1 substrate in these cells. One of the most significant advances in the study of osteoclast differentiation was the development of a co-culture system for production of osteoclasts in tissue culture. Although the murine osteoclast-like cells produced in this manner are well characterized, it is difficult to obtain purified osteoclast preparations. Although we used a co-culture system to produce osteoclasts, there is a possibility that the lysates were contaminated by a proportion of non-osteoclastic cells, including osteoblasts and adherent bone marrow cells. Thus, our findings reported here must be considered as preliminary. Recently, it has been reported that OPGL stimulates osteoclast differentiation directly without osteoblasts.[45] OPGL would provide improvement in the study of osteoclast biochemical characterization.

In conclusion, *me/me* and *me^v/me^v* mice show markedly lowered bone density due to increased numbers and function of multinucleated osteoclasts. Thus, SHP-1 plays an important role in the regulation of osteoclastogenesis and osteoclast function. The association of p126 with SHP-1 suggests that p126 plays an important role in osteoclast signaling pathways. However, it is not clear from the current data whether p126 mediates the heightened osteoclastogenesis or osteoclast function. Additional studies to identify and characterize the hyperphosphorylated proteins in motheaten osteoclasts are not only important for defining SHP-1 substrates but will also help to elucidate the signaling pathways for osteoclastogenesis and osteoclast function.

Acknowledgments

We thank Bruce Gott, Sherri Christianson, Rebecca McCabe, Pamela Lang, Holly Savage, and Lesley S. Bechtold for excellent technical assistance. We also thank Drs. Leah Rae Donahue and John P. Sundberg for critical reading of the manuscript and Shin-Ichi Nishikawa, M.D. (Department of Molecular Genetics, Faculty of Medicine, Kyoto University, Kyoto, Japan), for providing anti-CSF-1 receptor antibody and Ichiro Itonaga, M.D. (Department of Orthopaedic Surgery, Oita Medical University, Oita, Japan), for providing dentine slices.

References

1. Khosla S, Riggs L, Melton L: Clinical spectrum. Osteoporosis: Etiology, Diagnosis and Management. Edited by L Riggs, L Melton. New York, Raven Press, 1995, pp 133–160
2. Parfitt AM: The cellular basis of bone remodeling: the quantum concept reexamined in light of recent advances in the cell biology of bone. Calcif Tissue Int 1984, 36(Suppl 1):S37–S45
3. Walker DG: Osteopetrosis cured by temporary parabiosis. Science 1973, 180:875
4. Kahn AJ, Simmons DJ: Investigation of cell lineage in bone using a chimaera of chick and quail embryonic tissue. Nature 1975, 258:325–327
5. Ibbotson KJ, Roodman GD, McManus LM, Mundy GR: Identification and characterization of osteoclast-like cells and their progenitors in cultures of feline marrow mononuclear cells. J Cell Biol 1984, 99:471–480
6. Umeda S, Takahashi K, Naito M, Shultz LD, Takagi K: Neonatal changes of osteoclasts in osteopetrosis (op/op) mice defective in production of functional macrophage colony-stimulating factor (M-CSF) protein and effects of M-CSF on osteoclast development and differentiation. J Submicrosc Cytol Pathol 1996, 28:13–26
7. Shen SH, Bastien L, Posner BI, Chretien P: A protein-tyrosine phosphatase with sequence similarity to the SH2 domain of the protein-tyrosine kinases. Nature 1991, 352:736–739
8. Plutzky J, Neel BG, Rosenberg RD: Isolation of a src homology 2-containing tyrosine phosphatase. Proc Natl Acad Sci USA 1992, 89:1123–1127
9. Plutzky J, Neel BG, Rosenberg RD, Eddy RL, Byers MG, Jani-Sait S, Shows TB: Chromosomal localization of an SH2-containing tyrosine phosphatase (PTPN6). Genomics 1992, 13:869–872
10. Yi TL, Cleveland JL, Ihle JN: Protein tyrosine phosphatase containing SH2 domains: characterization, preferential expression in hematopoietic cells, and localization to human chromosome 12p12–p13. Mol Cell Biol 1992, 12:836–846
11. Zhao Z, Bouchard P, Diltz CD, Shen SH, Fischer EH: Purification and characterization of a protein tyrosine phosphatase containing SH2 domains. J Biol Chem 1993, 268:2816–2820
12. McCulloch J, Siminovitch KA: Involvement of the protein tyrosine phosphatase PTP1C in cellular physiology, autoimmunity and oncogenesis. Adv Exp Med Biol 1994 365:245–254
13. Ihle JN: Cytokine receptor signalling. Nature 1995, 377:591–594
14. Matthews RJ, Bowne DB, Flores E, Thomas ML: Characterization of hematopoietic intracellular protein tyrosine phosphatases: description of a phosphatase containing an SH2 domain and another enriched in proline-, glutamic acid-, serine-, and threonine-rich sequences. Mol Cell Biol 1992, 12:2396–2405
15. Adachi M, Fischer EH, Ihle J, Imai K, Jirik F, Neel B, Pawson T, Shen S, Thomas M, Ullrich A, Zhao Z: Mammalian SH2-containing protein tyrosine phosphatases. Cell 1996, 85:15
16. Shultz LD, Schweitzer PA, Rajan TV, Yi T, Ihle JN, Matthews RJ, Thomas ML, Beier DR: Mutations at the murine motheaten locus are within the hematopoietic cell protein-tyrosine phosphatase (Hcph) gene. Cell 1993, 73:1445–1454
17. Tsui HW, Siminovitch KA, de-Souza L, Tsui FW: Motheaten and viable motheaten mice have mutations in the haematopoietic cell phosphatase gene. Nat Genet 1993, 4:124–129

18. Green MC, Shultz LD: Motheaten, an immunodeficient mutant of the mouse. I: Genetics and pathology. J Hered 1975, 66:250–258
19. Shultz LD: Pleiotropic effects of deleterious alleles at the "motheaten" locus. Curr Top Microbiol Immunol 1998, 137:216–222
20. Shultz LD, Coman DR, Bailey CL, Beamer WG, Sidman CL: "Viable motheaten," a new allele at the motheaten locus. I. Pathology. Am J Pathol 1984, 116:179–192
21. Shultz LD: Hematopoiesis and models of immunodeficiency. Semin Immunol 1991, 3:397–408
22. Yoshida H, Hayashi S, Kunisada T, Ogawa M, Nishikawa S, Okamura H, Sudo T, Shultz LD, Nishikawa S: The murine mutation osteopetrosis is in the coding region of the macrophage colony stimulating factor gene. Nature 1990, 345:442–444
23. Marks SC, Lane PW: Osteopetrosis, a new recessive skeletal mutation on chromosome 12 of the mouse. J Hered 1976, 67:1–18
24. Naito M, Hayashi S-I, Yoshida H, Nishikawa S-I, Shultz LD, Takahashi K: Abnormal differentiation of tissue macrophage populations in 'osteopetrosis' (op) mice defective in the production of macrophage colony-stimulating factor. Am J Pathol 1991, 139:657–667
25. Umeda S, Takahashi K, Shultz LD, Naito M, Takagi K: Effects of macrophage colony-stimulating factor on macrophages and their related cell populations in the osteopetrosis mouse defective in production of functional macrophage colony-stimulating factor protein. Am J Pathol 1996, 149:559–574
26. Nakayama K, Takahashi K, Shultz LD, Miyakawa K, Tomita K: Abnormal development and differentiation of macrophages and dendritic cells in viable motheaten mutant mice deficient in haematopoietic cell phosphatase. Int J Exp Pathol 1997, 78:245–257
27. Chen HE, Chang S, Trub T, Neel BG: Regulation of colony-stimulating factor 1 receptor signaling by the SH2 domain-containing tyrosine phosphatase SHPTP1. Mol Cell Biol 1996, 16:3685–3697
28. Papaioannou VE, Fox JG: Efficacy of tribromoethanol anesthesia in mice. Lab Anim Sci 1993, 43:189–192
29. Beamer WG, Donahue LR, Rosen CJ, Baylink DJ: Genetic variability in adult bone density among inbred strains of mice. Bone 1996, 18:397–403
30. Jiao H, Yang W, Berrada K, Tabrizi M, Shultz L, Yi T: Macrophages from motheaten and viable motheaten mutant mice show increased proliferative responses to GM-CSF: detection of potential HCP substrates in GM-CSF signal transduction. Exp Hematol 1997, 25:592–600
31. Fujikawa Y, Shingu M, Torisu T, Itonaga I, Masumi S: Bone resorption by tartrate-resistant acid phosphatase-positive multinuclear cells isolated from rheumatoid synovium. Br J Rheumatol 1996, 35:213–217
32. Raynal C, Delmas PD, Chenu C: Bone sialoprotein stimulates in vitro bone resorption. Endocrinology 1996, 137:2347–2354
33. Sudo T, Nishikawa S, Ogawa M, Kataoka H, Ohno N, Izawa A, Hayashi S, Nishikawa S: Functional hierarchy of c-kit and c-fms in intramarrow production of CFU-M. Oncogene 1995, 11:2469–2476
34. Tabrizi M, Yang W, Jiao H, DeVries EM, Platanias LC, Arico M, Yi T: Reduced Tyk2/SHP-1 interaction and lack of SHP-1 mutation in a kindred of familial hemophagocytic lymphohistiocytosis. Leukemia 1998, 12:200–206
35. Yang W, Tabrizi M, Berrada K, Yi T: SHP-1 phosphatase C-terminus interacts with novel substrates p32/p30 during erythropoietin and interleukin-3 mitogenic responses. Blood 1998, 91:3746–3755
36. Shultz LD, Bailey CL, Coman DR: Hematopoietic stem cell function in motheaten mice. Exp Hematol 1983, 11:667–680
37. Vignery A, Silverglate A, Horowitz M, Shultz L, Baron R: Abnormal bone remodeling activity in the immunodeficient nude (nu/nu) and motheaten (me/me) mutant mice. Calcif Tissue Int 1981, 33:301
38. Klingmuller U, Lorenz U, Cantley LC, Neel BG, Lodish HF: Specific recruitment of SH-PTP1 to the erythropoietin receptor causes inactivation of JAK2 and termination of proliferative signals. Cell 1995, 80:729–738
39. Van Zant G, Shultz L: Hematologic abnormalities of the immunodeficient mouse mutant, viable motheaten (me^v). Exp Hematol 1989, 17:81–87
40. Amano H, Yamada S, Felix R: Colony-stimulation factor-1 stimulates the fusion process in osteoclasts. J Bone Miner Res 1998, 13:846–853
41. Takatsuka H, Umezu H, Hasegawa G, Usuda H, Ebe Y, Naito M, Shultz LD: Bone remodeling and macrophage differentiation in osteopetrosis (op) mutant mice defective in the production of macrophage colony-stimulating factor. J Submicrosc Cytol Pathol 1998, 30:239–247
42. Myint YY, Miyakawa K, Naito M, Shultz LD, Oike Y, Yamamura K-I, Takahashi K: Granulocyte/macrophage colony-stimulating factor, and interleukin-3 correct osteopetrosis in mice with osteopetrosis mutation. Am J Pathol 1999, 154:553–566
43. Lagasse E, Weissman IL: Enforced expression of Bcl-2 in monocytes rescues macrophages and partially reverses osteopetrosis in op/op mice. Cell 1997, 89:1021–1031
44. Wiktor-Jedrzejczak W, Urbanowska E, Szperl M: Granulocyte-macrophage colony-stimulating factor corrects macrophage deficiencies, but not osteopetrosis, in the colony-stimulating factor-1-deficient op/op mouse. Endocrinology 1994, 134:1932–1935
45. Lacey DL, Timms E, Tan HL, Kelley MJ, Dunstan CR, Burgess T, Elliott R, Colombero A, Elliott G, Scully S, Hsu H, Sullivan J, Hawkins N, Davy E, Capparelli C, Eli A, Qian YX, Kaufman S, Sarosi I, Shalhoub V, Senaldi G, Guo J, Delaney J, Boyle WJ: Osteoprotegrin ligand is a cytokine that regulates osteoclast differentiation and activation. Cell 1998, 93:165–176

Bone Vol. 27, No. 5
November 2000:619–626

ELSEVIER

Spontaneous Fracture (*sfx*): A Mouse Genetic Model of Defective Peripubertal Bone Formation

W. G. BEAMER,[1] C. J. ROSEN,[1,2] R. T. BRONSON,[1,4] W. GU,[3] L. R. DONAHUE,[1] D. J. BAYLINK,[3] C. C. RICHARDSON,[3] G. C. CRAWFORD,[1] and J. E. BARKER[1]

[1]*The Jackson Laboratory, Bar Harbor, ME, USA*
[2]*Maine Center for Osteoporosis Research and Education, St. Joseph Hospital, Bangor, ME, USA*
[3]*J. L. Pettis Veterans Administration Medical Center, Loma Linda, CA, USA*
[4]*School of Veterinary Medicine, Tufts University, Boston, MA, USA*

A new mouse model of stage-specific bone growth failure and fracture has been recovered as an autosomal recessive mutation, designated spontaneous fracture (*sfx*). The *sfx/sfx* mice are phenotypically normal until shortly after weaning, when reduced mobility and impaired somatic growth are first noted. By 6 weeks of age, body, spleen, and thymus weights, as well as hematocrits and serum calcium, inorganic phosphate, total alkaline phosphatase, insulin-like growth factor-I, and osteocalcin levels are decreased. The *sfx/sfx* mice also show reduced femoral cortical density and diaphyseal circumference, as well as a paucity of mature osteoblasts on bone surfaces. Histological analyses of the femur and tibia in the mutants show subtle reduction of chondrocyte numbers in epiphyseal-plate columns, reduction of matrix, and near absence of osteoid below the differentiated chondrocytes. Trabeculae in proximal tibiae, iliacs, and vertebral bodies are sparse and thin. Cortical bone thickness of mutants is markedly thinned in all sites examined. By 7–8 weeks, radiographic films routinely show spontaneous impact fractures of the distal femur accompanied by callus formation, whereas complete fractures are less commonly observed. Volumetric bone mineral density (BMD) of mutant femurs is similar to +/? littermates in the center of the femoral diaphysis, but BMD declines as either end of the femoral diaphysis is approached. We have mapped the gene responsible for this phenotype to central Chromosome 14. Reduced bone mass, impaired bone formation, abnormalities of bone architecture, and a disposition to spontaneous fracture identify *sfx/sfx* mice as a useful model for understanding the mechanisms responsible for peripubertal bone formation. (Bone 27:619–626; 2000)

Key Words: Mice; Mutation; Bone formation; Spontaneous fracture.

Introduction

Spontaneous mouse mutants with a skeletal phenotype have long been the focus of investigation in developmental biology and comparative morphology. Currently, there are more than 120 known and genetically mapped mutant genes, plus nearly 50 additional ones not yet mapped (Mouse Genome Database at http://www.informatics.jax.org). These mutant genes affect the broadest imaginable range of endochondral and membranous skeletal biology, with many representing analogous and homologous models of human bone disorders. As experimental tools, these mouse mutations are particularly useful not only for dissecting biochemical pathways, but also for mapping previously unknown genes that affect structure and bone turnover. In this report, we describe a new spontaneous mouse genetic model, designated spontaneous fracture (gene symbol *sfx*), that is inherited as an autosomal recessive locus and maps near the center of mouse Chromosome 14. Mice homozygous for the mutation appear normal until weaning; however, by 28–30 days of age, they fail to maintain pubertal growth and display reduced serum insulin-like growth factor-I (IGF-I), osteocalcin, calcium (Ca), inorganic phosphate (Pi), total alkaline phosphatase, and hematocrits. By 49–56 days of age, mutants show radiographic evidence of compression fractures of the distal femur, and a striking histological pattern of diminished bone formation in long bones, axial skeleton, and calvaria. This mutation was initially reported at the 1997 annual meeting of the American Society for Bone and Mineral Research.[3]

Materials and Methods

Mice

Mice exhibiting the *sfx* phenotype appeared in a BALB/cBy inbred strain segregating for another mutation, *s*evere *c*ombined *a*nemia and *t*hrombocytopenia (gene symbol *scat*[12]). The *scat* and *sfx* mutations were separated from one another by backcrossing to BALB/cBy wild-type mice and obtaining normal N1F1 progeny. These F1 mice were intercrossed to identify pairs that carried *sfx* by reappearance of the spontaneous fracture phenotype in their offspring, but not that of *scat*. This separation of the two mutant phenotypes in the intercross N1F2 offspring confirmed *sfx* as a unique mutant gene that was inherited as a recessive gene and not genetically linked to *scat*. Both male and female spontaneous fracture mice are equally affected; heterozygous (*sfx*/+) mice are indistinguishable from homozygous (+/+) wild-type animals.

All mice were housed in groups of two to four in polycarbonate boxes (130 cm^2) with sterilized White pine shavings as

Address for correspondence and reprints: Dr. Jane E. Barker, The Jackson Laboratory, Bar Harbor, ME 04609. E-mail: jeb@jax.org

8756-3282/00/$20.00
PII S8756-3282(00)00369-0

Bone Vol. 27, No. 5
November 2000:619–626

bedding. Diet consisted of pelleted and autoclaved NIH 31 diet (Rat and Mouse Diet #5K52, 6% fat; PMI Mills, Inc., St. Louis, MO) fed ad libitum. Water was acidified with HCl to a pH of 2.8–3.2 to retard bacterial growth. When mutants were present in a weaned litter, they were supplemented daily with a watered slurry of ground diet in a 60 mm plastic tissue culture dish. Lighting schedule was 14:10 h light:dark with an ambient temperature of 20 ± 2°C. Mice were exsanguinated by decapitation to rapidly obtain blood samples for serum assays of osteocalcin and IGF-I, as well as blood chemistry analyses. Samples of bone, muscle, and organs were preserved as described below for histological analyses.

The BALB/cBy *sfx* colony was maintained by test mating normal littermate progeny from litters produced by known carriers of *sfx* and by transplantation of ovaries from *sfx/sfx* into congenic C.B-$c^{+}Hbb^{s}$ hosts. Ovary transplanted females were mated to BALB/cBy +/+ males to produce heterozygous (*sfx*/+) mice. The physiological data reported below are for mice from the BALB/cBy colony. All procedures were approved by the institutional animal care and use committee of The Jackson Laboratory.

Genetic Mapping

Genetic localization of the *sfx* gene was undertaken by first mating *sfx/sfx* ovary-grafted females to CAST/Ei males to obtain (BALB/c × CAST/Ei)F1-*sfx*/+ progeny. These F1-*sfx*/+ mice were intercrossed to produce F2 progeny segregating the mutant *sfx* and wild-type + alleles at this locus. Nearly 900 mice were weaned, of which 217 were phenodeviants at 30–40 days of age and judged to be mutants. At necropsy, kidneys and spleens were collected from the 217 *sfx/sfx* and 55 +/? mice, snap frozen in liquid N_2, and stored at −60°C. DNA was prepared from F2 spleens with Qia-amp kits (Qiagen, Inc., Valencia, CA) following the manufacturer's instructions. Genotyping was accomplished with oligonucleotide primer pairs (MapPairs, Research Genetics, Birmingham, AL) that amplified simple sequence length polymorphisms (SSLPs) from known regions of mouse chromosomes.[5] These primers distinguish between sequences on the same chromosome in different strains of mice based on the size of the product generated. Polymerase chain reaction (PCR) products were generated under standard conditions. Amplified PCR products were separated on 4% NuSieve agarose gels (FMC, Rockland, ME) and visualized by ethidium-bromide staining. Two to six Mit markers per chromosome were used to establish the frequency of allelic combinations present at each marker; that is, homozygous for CAST (*cast/cast*) or BALB/cBy (*balb/balb*) progenitor alleles, or heterozygous for progenitor alleles (*cast/balb*). DNAs from BALB/cBy, CAST, and (BALB × CAST)F1 hybrids were used as electrophoretic standards in every gel to identify the genotype of PCR products derived from F2 mice. Possible linkage of the *sfx* locus to the markers was indicated when the recombination frequency between marker and phenotype decreased to below 20%.

Histology

Soft tissues removed from mice were preserved in Bouin's fixative for 24 h, then processed by routine paraffin-embedded methodology, sectioned at 5 μm, and stained by hemotoxylin and eosin (H&E) for histological study. Skeletal specimens were decalcified by 3 week fixation in multiple changes of Bouin's solution, then paraffin embedded, and sectioned at 5 μm thickness. Sections were stained with H&E for morphological analyses or with naphthol-AS-BI-phosphate and counterstained with hemotoxylin for tartrate-resistant acid phosphatase (TRAP) detection of osteoclasts.

Radiographic Analysis

Animals were anesthetized with Avertin (2,2,2-tribromoethanol in amylenehydrate; Aldrich Chemicals, St. Louis, MO[10]) at a dose of 250 mg/kg and placed in both dorsal recumbent and lateral positions with legs extended as much as possible. Radiographs were taken with a Faxitron Cabinet X-ray System (Model MX-20, Faxitron X-ray Corp., Wheeling, IL). Mice were exposed at 22 kVp for 3 sec. Images of mutant and normal mice were recorded on Kodak mammography-grade film.

Bone Densitometry

Measurement of bone mineral density was undertaken by peripheral quantitative computerized tomography (pQCT) utilizing a Stratec XCT 960M (Norland, Medical Systems, Ft. Atkinson, WI) as previously described.[1] Whole femurs were measured at 1 mm intervals and the unit volume within which mineral was measured was set at 0.1 mm^3. Attenuation data were analyzed by a manufacturer-supplied software package, XMICE v5.1. The data for two sections located 1 mm apart at the middiaphysis were averaged and analyzed for total bone mineral content, total mineralized volume, and total bone density. Normal and mutant mice were gender-matched littermates at approximately 40 days of age. Six sets of animals were analyzed in each group.

Biochemical Assays

Chemical analyses of *sfx/sfx* and +/? serum samples were performed on separate sets of trunk blood samples collected from mice aged 34–40 days. Serum calcium, potassium, sodium, phosphorus, alkaline phosphatase, magnesium, and chloride values were measured (13–25 mice/group) with a Synchron CX5 Clinical System (Beckman Instruments, Fullerton, CA) following the manufacturer's instructions. Prior to each assay, calibration standards were assessed to establish validity and accuracy of measurements. Serum IGF-I was measured in separate sets of blood samples (50 μL/sample; five to nine mice per genotype) from mice aged 5–7 weeks using a commercially available radioimmunoassay kit (Nichols Institute, San Juan Capistrano, CA) as previously described.[14] Serum IGF binding proteins were dissociated from IGF-I by acid-ethanol treatment, then cryoprecipitated. Serum osteocalcin levels were assayed in 12 pairs of *sfx/sfx* and +/? age- and gender-matched mice by Immunoradiometric assay (IRMA) using a commercially available kit (Immunotopics, Inc., San Clemente, CA). This assay requires 25 μL of serum and detects levels as low as 50 ng/mL. Hematocrit values were obtained from three separate groups of mutant and normal littermate mice contributing serum for osteocalcin or serum electrolyte measurements.

Statistical Analyses

Mapping data are expressed as percent recombination frequency ± SEM, with linkage of segregating markers with the mutant *sfx* phenotype evaluated by chi-square analysis. All physiological data are expressed as mean ± SEM, with differences between means analyzed by analyses of variance (ANOVAs) or by unpaired Student *t*-tests, using the computer program STAT VIEW 4.5 (SAS Institute, Cary, NC).

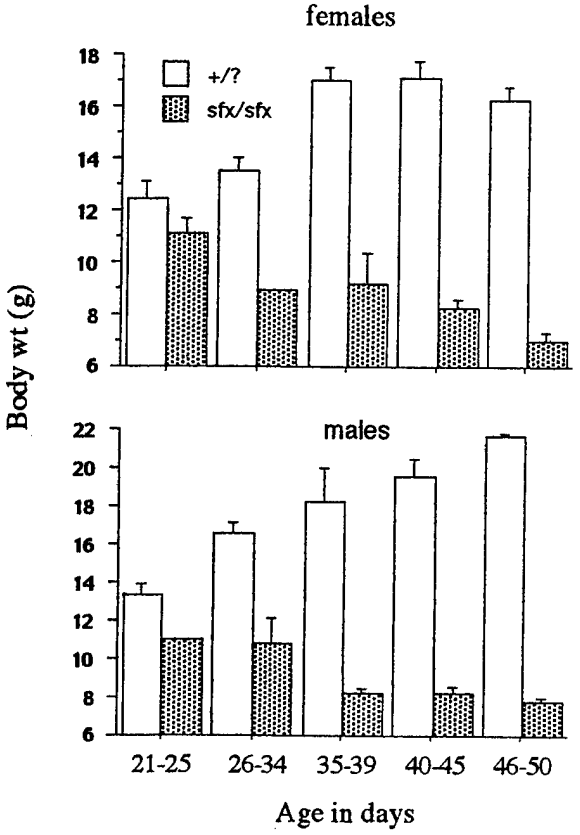

Figure 1. Patterns of growth for female and male *sfx/sfx* and *+/?* littermate mice. Body weights of the *sfx/sfx* mice were lower than the *+/?* littermates at every age, although the mutant mice at the 21–25 day period were identified retrospectively after phenotyping at 35–40 days of age. Mutants of both genders lose body mass between 5 and 7 weeks, and die between 7 and 8 weeks of age. Number of mice per group ranged from three to nine.

Results

Phenotypic Characterization

Growth. At 20–24 days of age, the progeny of tested BALB/cBy *sfx/+* breeder pairs appeared unremarkable in size and movement. At 26–30 days of age, *sfx/sfx* mice demonstrated increasing difficulty moving about in their cages and failed to maintain the rate of body weight gain observed in normal littermates (**Figure 1**). The mutants' coats appeared scruffy, possibly as a result of difficulties with self-grooming behavior. Postweaning, the mutants were fed a slurry of ground NIH 31 diet and water in 60 mm tissue culture dishes because of difficulty in obtaining food and water from suspended dispensers and bottles. At necropsy, inspection of gastrointestinal tracts showed that mutants fed in this manner had food in their stomachs and small intestines, plus fecal pellets in their colons.

Assessment of allometric measurements at 35 days of age revealed that the *sfx/sfx* mice had significantly smaller ($p < 0.01$) spleens (*sfx/sfx* = 0.0036 ± 0.0002 vs. *+/?* = 0.0062 ± 0.0005) and thymus glands (*sfx/sfx* = 0.0017 ± 0.0003 vs. *+/?* = 0.0069 ± 0.0004), whereas brain (*sfx/sfx* = 0.0381 ± 0.0011 vs. *+/?* = 0.0231 ± 0.0011) and kidney (*sfx/sfx* = 0.017 ± 0.000 vs. *+/?* = 0.014 ± 0.001) weights were significantly larger. Relative heart, liver, and testes weights did not differ between mutant and normal littermates. Heterozygous (*sfx/+*) mice were

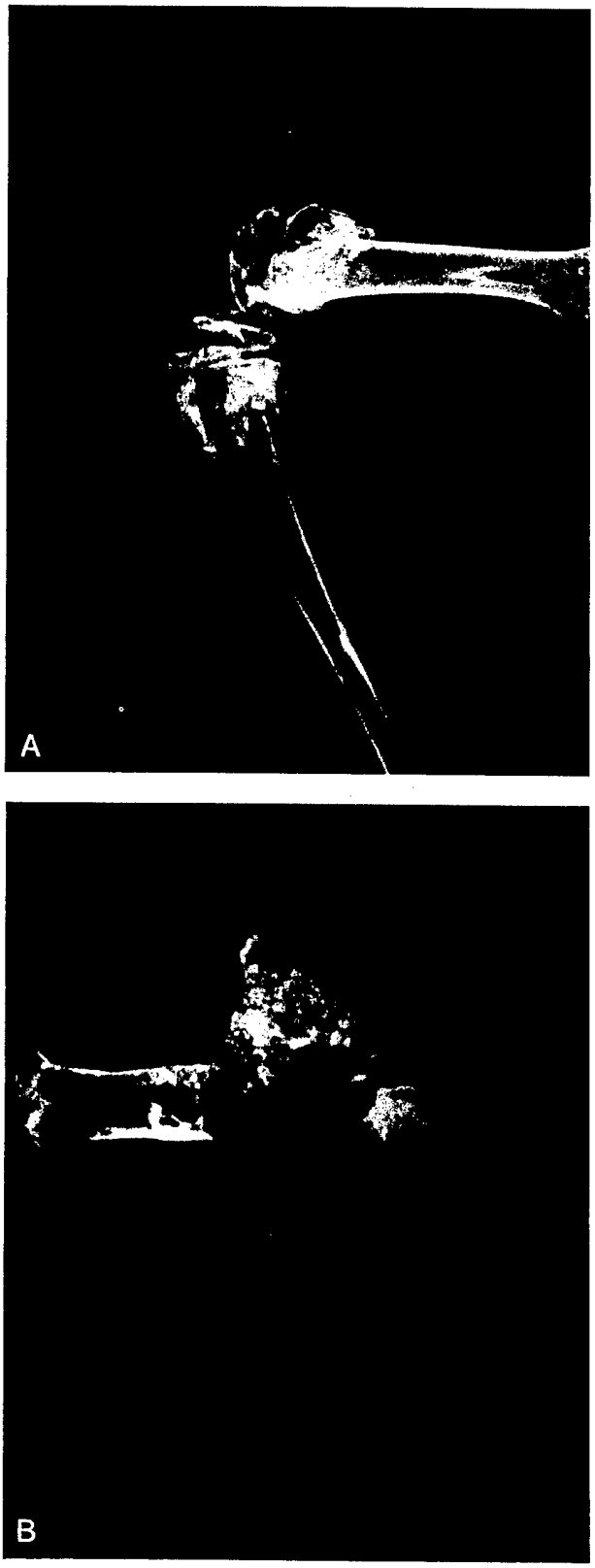

Figure 2. (A) Radiograph of *sfx/sfx* mouse at 40 days showing the common characteristic impact fracture of the knee joint. The distal diaphysis penetrated into the metaphysis. (B) Radiograph of *sfx/sfx* mouse at 47 days showing infrequent complete fracture of the distal femur.

Bone Vol. 27, No. 5
November 2000:619–626

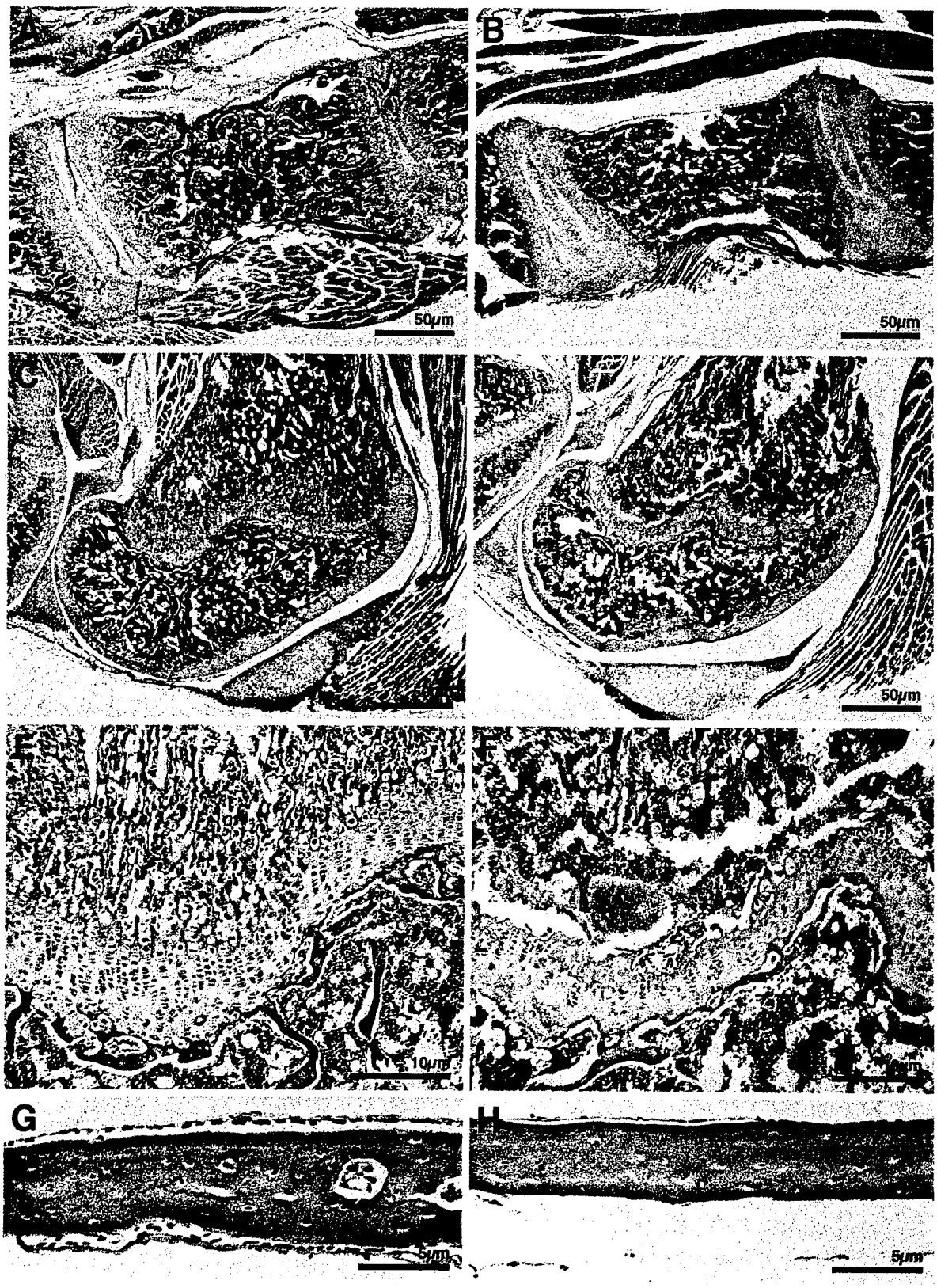

Figure 3. Histology of bone tissues from +/? (A,C,E,G) compared with *sfx/sfx* (B,D,F,H) littermate mice at 40 days of age. Scale bars represent 50, 10, or 5 μm for comparative purposes. (A,B) Proximal lumbar vertebrae of +/? and *sfx/sfx* mice, respectively. Note the virtual absence of trabeculae and the thin growth plate with minimal osteoid in the mutant bone. (C,D) Distal femur of +/? and *sfx/sfx* mice, respectively. Note reduction of trabeculae in metaphysis, reduced osteoid distal to the growth plate, and reduced thickness of the growth plate in the mutant bone. (E,F) Higher power of distal femur growth plates shown in (C) and (D). Osteoid deficiency is very apparent, while the columns of chondrocytes are present but do not appear very active. (G,H) Calvarial bone shows osteocytes within *sfx/sfx* cortical bone; however, the thickness of the mutant bone averages approximately 60%–65% of +/? littermate bone. Cells in the *sfx/sfx* calvaria bone lining are sparse compared with those of +/? mice.

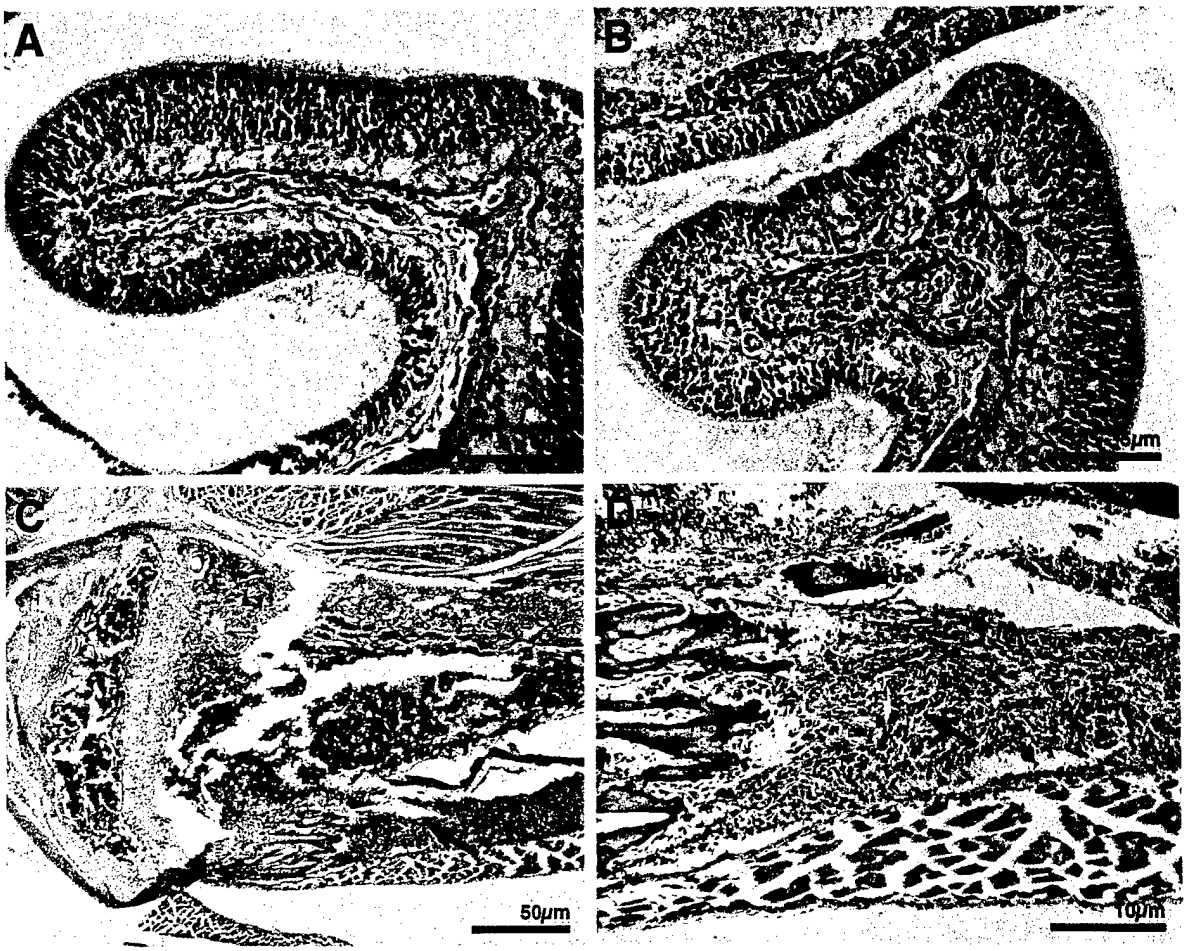

Figure 4. Cellular hyperplasia found on surfaces of *sfx/sfx* bones at 40 days of age. (A) Nasal turbinate of +/? mouse. Supportive bone for olfactory epithelia is indicated by arrow. (B) Nasal turbinate of *sfx/sfx* littermate that shows reduced supportive bone and proliferation of a cell type of uncertain origin indicated by arrow. (C,D) Low- and high-power photomicrographs of proximal tibia from *sfx/sfx* mouse showing a proliferative cell type similar to that in (B) of uncertain lineage. Such proliferative masses of cells were also observed on iliac surfaces and in mandibles.

indistinguishable from homozygous +/+ wild-type animals at all ages. No defects at the gross or light-microscopic levels were found in heart, thymus, spleen, thyroid gland, parathyroid gland, pituitary gland, liver, kidneys, gastrointestinal tract, pancreas, adrenal gland, or brain.

Bone parameters. Spontaneous fractures of the femur were identified in both male and female F2 and BALB/cBy *sfx/sfx* mice. Radiographs and histology revealed numerous impact fractures wherein the femoral diaphyseal shaft was driven into the distal metaphysis in mice aged 6–7 weeks (**Figure 2**A). Occasionally, a mouse showed bilateral transverse fracture of the distal metaphyses at about 7–8 weeks of age (**Figure 2**B). Fractures were also identified in radiographs of the smaller bones in *sfx/sfx* mice, such as the metacarpals. Due to the fragile nature of this mutant's skeleton, handling of mice for any reason from weaning onward was done with the greatest possible care.

Bone specimens for histological analyses were collected at 5–6 weeks of age from BALB/cBy +/? and *sfx/sfx* littermates when mutants showed significant weight loss and increased reluctance to move about their cages. Significant abnormalities were observed in various skeletal sites. (**Figure 3**A,B) shows that lumbar vertebral bodies of *sfx/sfx* mice were essentially devoid of osteoid and trabeculae, and fewer chondrocytes could be seen in the growth plates. Growth plate arrest was also apparent when long bones such as distal femurs were examined, as shown in Figure 3C,D. Osteoid was markedly deficient or absent in re-

Table 1. Body weight and femoral middiaphyseal data for BALB/cBy +/? and *sfx/sfx* littermates at 40 days of age

Genotype (n)	Body weight (g)	Total density (mg/mm^3)	Cortical density (mg/mm^3)	Periosteal circumference (mm)
+/? (6)	17.06[a] ± 0.83	0.416 ± 0.008	0.601[a] ± 0.012	4.053[a] ± 0.108
sfx/sfx (6)	7.89 ± 0.45	0.401 ± 0.016	0.461 ± 0.012	1.858 ± 0.389
Percent difference	46%	96%	77%	46%

[a] $p < 0.0001$.

Bone Vol. 27, No. 5
November 2000:619–626

Table 2. Serum data for *sfx/sfx* and *+/?* littermate mice

Genotype	Calcium	Pi	Alkaline phosphatase (total)	Osteocalcin	Insulin-like growth factor-I
+/?	9.14 ± 0.09 (38)	9.08 ± 0.19 (38)	194 ± 4 (38)	326 ± 31 (12)	200 ± 22 (16)
sfx/sfx	8.56[c] ± 0.05 (25)	8.15[b] ± 0.20 (24)	178[a] ± 9 (24)	96[c] ± 30 (12)	123[b] ± 22 (19)

Data presented as mean ± SEM. Numbers in parentheses indicate number of observations.
[a]$p < 0.05$; [b]$p < 0.01$; [c]$p < 0.0001$.

gions adjacent to growth plates in long bones, whereas remnants of mineralized osteoid were observed distal to the growth plates. We also observed necrosis beneath the epiphyseal growth plate and neovascularization of the same region as shown in Figure 3E,F. The cells lining the endosteum in the *sfx/sfx* long bones were less abundant, thinner, and more variable than the cells lining the osteoid-covered surfaces in the wild-type mice. Although TRAP-stained osteoclasts were observed in both *sfx/sfx* and normal mice, the numbers were very modest (data not shown). Figure 3G,H shows coronal sections of *+/?* and *sfx/sfx* calvariae that reveal the thickness of the mutant bone was approximately 65% that of normal littermates. Osteoblast-like cells lining the dorsal and ventral calvarial bone surfaces were very sparse in the *sfx/sfx* mice. The periosteum was thickened and fibrous in many of the sections examined. An unusual observation made in *sfx/sfx* skeletal specimens is detailed in **Figure 4**. Inspection of nasal turbinates shows that mature bone supporting the olfactory epithelium was deficient in amount, as seen in Figure 4A vs. B. Most enigmatic was the presence of unidentified cellular masses within the *sfx/sfx* turbinate structures (arrow in Figure 4B). Other skeletal sites (i.e., mandibles, iliacs) in the *sfx/sfx* mice also showed accumulations of large eosinophilic cells with heterochromatic nuclei surrounding fragments of mineralized bone. Formation of molars and incisors appeared normal (data not presented). In Figure 4C,D an *sfx/sfx* proximal tibia is presented that shows callus-like masses of cells on the periosteal surfaces. These cells appeared to be similar to osteoblasts, but lacked the cytoplasmic basophilia associated with active protein production and ribosomes.

Data for femoral bone parameters measured at the midpoint of the diaphysis by pQCT are presented in **Table 1**. We found that the middiaphyseal total bone density was not significantly lower in *sfx/sfx* than in *+/?* littermates; however, as measurements were made toward either end, mineral density levels characteristic of cortical bone rapidly disappeared. Periosteal circumference, an approximation of bone size, was reduced in proportion to body mass. However, cortical density was significantly reduced in the mutant mice to 77% of the value in normal littermates.

Metabolic Parameters

Selected serum mineral and protein parameters were assessed in 27 *sfx/sfx* (14 males, 13 females) and 44 *+/?* (19 males, 25 females) mice aged 33–44 days. Because no gender differences were seen, the data for males and females were combined for presentation of genotype effects in **Table 2**. We found that each of the measures (Ca, Pi, total alkaline phosphase, osteocalcin, and IGF-I) was significantly reduced in the *sfx/sfx* mice compared with *+/?* mice. Given that mutant mice had food in their gastrointestinal tracts, the serum changes observed were not a consequence of failure to consume nutrients. Nevertheless, we did find that serum Na and Cl were significantly elevated in female but not male mutants, suggesting the likelihood of a modest degree of dehydration. No differences were detected in serum Mg levels.

Hematocrits were measured in mutant and normal littermate mice and grouped by age in weeks. Two-way ANOVA of these data show that packed cell volumes did not differ by age, but did differ by genotype ($p < 0.0001$) with *sfx/sfx* mice having a consistently lower percent red blood cells than *+/?* littermates. Comparative values for mutants and normals at 5 (a), 6 (b), and 7 (c) weeks were: (a) *sfx/sfx* (8) = 45.6 ± 0.4 vs. *+/?* (7) = 48.6 ± 1.4; (b) *sfx/sfx* (6) = 43.5 ± 1.4 vs. *+/?* (9) = 49.3 ± 1.2; and (c) *sfx/sfx* (5) = 43.4 ± 1.0 vs *+/?* (3) = 49.3 ± 1.8. White blood cell counts were assessed in the 5–6-week-old mice and found to be significantly reduced ($p < 0.0001$) in the mutants vs. *+/?* littermates (*sfx/sfx* [14] = 0.82 ± 0.07 × 10^9/L vs. *+/?* [15] = 2.16 ± 0.15 × 10^9/L).

Genetic Mapping

When a sampling of BALB/cBy *sfx/+* matings was evaluated for the ratio of mutant:normal siblings, we found 25 affected mice (13 females, 12 males) out of a total of 93 offspring. Similarly, matings between (BALB/c × CAST/Ei)F1 *sfx/+* parents produced 217 affected mice among nearly 900 total offspring. Collectively, these ratios of affected:normal progeny demonstrate that a single autosomal recessive gene was responsible for the mutant phenotype. To localize the gene to a chromosomal region, a genome-wide scan of 217 F2 *sfx/sfx* progeny was performed using two to six MIT markers per chromosome. By exploiting the polymorphic differences between the BALB/cBy parental inbred background of the *sfx* mutation and CAST/Ei strain carrying the wild-type allele, recombination events that occurred in the gametes of the F1 generation could be scored in the F2 generation. Nonrandom association between the mutant phenotype and the molecular genetic markers was found for chromosome 14. Data presented in **Table 3** show that *D14Mit203* yielded the lowest recombination frequency. Analy-

Table 3. Mapping data locating the *sfx* mutation to chromosome 14 of the mouse

Genetic distance (cM)	8.0	13.5	15.0	26.0	28.5	40.0	44.0	48.0	54.0
D14Mit SSLP marker	*252*	*139*	*141*	*66*	*203*	*34*	*35*	*265*	*75*
Recombination fraction	10	39	39	8	4	25	12	16	18
	34	217	217	190	210	212	35	35	35
	(29%)	(18%)	(18%)	(4%)	(2%)	(12%)	(34%)	(46%)	(53%)

Genetic map distances were obtained from the Mouse Genome Database (http://www.informatics.jax.org). The recombination frequencies are given for nine informative markers. The *sfx* locus is genetically linked to *D14Mit203* and *D14Mit34* and lies between these markers.

sis of recombination events along chromosome 14 indicated a gene order of: centromere–*D14Mit203*–(1.9 ± 0.9 cM)–*sfx*–(11.8 ± 2.2 cM)–*D14Mit34*.

Discussion

In this article we described a new mouse model with reduced bone mass that is almost certainly a function of impaired bone formation. The phenotype was named "spontaneous fracture," and given the gene symbol *sfx*. The skeletal phenotype, which is unique to *sfx/sfx* mice, does not appear until after weaning. At 40 days, femoral cortical bone mineral content and cortical BMD in *sfx/sfx* mice is reduced compared with their normal littermates. There is histological evidence of significantly reduced cortical matrix, paucity of trabeculae at both axial and appendicular sites, and a marked deficiency of mature osteoblasts, whereas osteoclasts were sparse but demonstrable by TRAP staining. The histological analyses of mutant bones did not reveal osteomalacia. On the contrary, there is a striking deficiency of osteoid rather than defective mineralization of osteoid. These morphologic observations suggest a defect in osteoblast-mediated bone formation.

Multiphasic screening assessments in the serum of *sfx/sfx* mice revealed that serum levels of Ca and Pi were below those of *+/?* littermates. This reduction in mineral levels in *sfx/sfx* mice was significant; however, the absolute levels should be considered "low normal," because the means were within 1 SD of the mean for a reference population of adult (C57B1/6 × DBA/2)F1 mice.[7]

Osteocalcin levels, a phenotypic marker of differentiation and activity of osteoblasts in young animals, were also low in *sfx/sfx* serum. In adults, osteocalcin levels more accurately reflect bone turnover.[2] One possible explanation for the reduced serum osteocalcin levels in mutant mice is that the product of the *sfx* gene downregulates the osteocalcin genes. This seems unlikely, however, based on observations by other investigators: First, it has been demonstrated that the osteocalcin-deficient knockout mouse does not show an alteration in the number of osteoblasts.[6,8] Second, unlike *sfx/sfx* mice, the osteocalcin −/− mice showed increased bone formation in the absence of osteocalcin gene expression. These findings suggest that the reduction in serum osteocalcin observed in the *sfx/sfx* mouse is reflective of defective osteoblastogenesis, as opposed to a regulatory effect of *sfx* on the osteocalcin gene. These data are further supported by the histological examination of other bones as well as the pQCT data for cortical density.

The mutation is inherited as a recessive gene that maps to the middle of Chromosome 14. At this time, the region containing *sfx* includes up to 14 cM of genetic distance and possibly as many as a 1000 genes, effectively precluding a closer examination of specific candidate genes. It is likely that the *sfx* phenotype results from abnormalities in osteoblast differentiation or proliferation, because few osteoblasts were noted histologically and also there was a generalized reduction in osteoid production. Although a similar phenotype has been reported in several induced mutant mouse strains, the genetic loci were different. For example, the *sfx* phenotype is not caused by the absence of the gene for the osteoblast transcription factor, *cbfa1*, which maps to mouse chromosome 17. The phenotype of the *cbfa1* homozygote also differs from *sfx* in that the *cbaf1* knockout (−/−) lacks mineralized bone and dies soon after birth,[9] whereas *sfx/sfx* mice are undetectable until shortly after weaning. Another regulatory factor for osteoblast differentiation and proliferation is IGF-I. Serum IGF-I levels in the *sfx/sfx* mice were moderately, but significantly, lower than their age- and gender-matched littermates, despite similarities in environmental conditions and evidence of adequate dietary intake. However, neither the IGF-I gene locus nor the genetically mapped major IGF binding proteins (IGFBP-1, -2, -3, -5) are located on Chromosome 14. The product of the insulin receptor substrate-1 (*irs-1*) gene, Irs-1, an intracellular signaling molecule required for both insulin and IGF-I intracellular action, has recently been causally linked to the process of bone formation. Specifically, *irs* −/− mice have shown reduced osteoblast proliferation and differentiation, plus severe osteopenia.[11] However, these −/− mice do not have anemia or a reduced lifespan, two phenotypes characteristic of *sfx*. Because the chromosomal location of the *irs-1* gene has not been established, it is unclear whether this is a possible candidate gene for the *sfx* mutation. Finally, two matrix-associated genes that yield reduced bone formation in knockout −/− mice that are excluded by chromosomal location include biglycan (*bgn*) located on chromosome X[15] and osteonectin (*Sparc*) located on chromosome 11.[4]

The *sfx* phenotype is indistinguishable from normal littermates through the neonate-to-juvenile period of development. Shortly thereafter, a constellation of changes develops, which have been described in this report. One of the major difficulties in defining the phenotype imposed by the *sfx* mutant gene is separating the phenotype dictated directly by the mutation in the gene from those secondarily created by impaired mobility and a catabolic state. Thus, many questions remain unanswerable at this time. For example, what happened to the osteoblasts that appeared to normally form bone prior to weaning of the *sfx/sfx* mice? Likewise, do the characteristic deficiencies in osteoblasts and hemopoietic cells (reduced white and red blood cells) represent pleiotropic effects of the *sfx* mutation on a bone marrow stem cell?[13] Fine mapping of the locus on Chromosome 14 may provide the best way to address whether this represents a novel gene that regulates transcriptional activity in the osteoblast, or defines a protein that controls other critical factors in the lifecycle of the osteoblast. Understanding the actions and structure of a single gene with such a dramatic phenotype will most likely have important ramifications for elucidating the molecular mechanisms involved in the acquisition and retention of bone mass and for devising therapeutic protocols that might be useful in the treatment of osteoporosis.

Acknowledgments: The authors appreciate the critical reviews of the manuscript provided by Dr. K. Johnson and Dr. T. O'Brien, and the proficient technical assistance of C. Ackert and J. Burgess. This work was supported by NIH DK27726 and HL49761 (to J. E. B.), AR43618 (to W. G. B.), CA34196 (CORE support, The Jackson Laboratory), and AR45433 (to C. J. R.), and the Musculoskeletal Disease Center, J. L. Pettis VAMC, and Loma Linda University (to D. J. B.).

References

1. Beamer, W. G., Donahue, L. R., Rosen, C. J., and Baylink, D. J. Genetic variability in adult bone density among inbred strains of mice. Bone 18:397–403; 1996.
2. Calvo, M. S., Eyre, D. R., and Gundberg, C. M. Molecular basis and clinical application of biological markers of bone turnover. Endocrine Rev 17:333–368; 1996.
3. Crawford, G., Beamer, W., Rosen, C. J., Baylink, D. J., Richman, C. C., and Barker, J. E. A new mouse model for osteoporosis maps to mouse chromosome 14 [Abstract 67]. J Bone Miner Res 12(Suppl.):S119; 1997.
4. Delany, A. M., Amling, M., Priemel, M., Howe, C., Baron, R., and Canalis, E. Osteopenia and decreased bone formation in osteonectin-deficient mice. J Clin Invest 105:915–923; 2000.
5. Dietrich, W. F., Miller, J., Steen, R., Merchant, M. A., Damron-Boles, D., Husain, Z., Dredge, R., Daly, M. J., Ingalls, K. A., O'Connor, T. J., Evans, C. A., DeAngelis, M. M., Levinson, D. M., Kruglyak, L., Goodman, N.,

Copeland, N. G., Jenkins, N. A., Hawkins, T. L., Stein, L., Page, D. C., and Lander, E. S. A comprehensive genetic map of the mouse genome. Nature 380:149–152; 1996.

6. Ducy, P., Desbois, C., Boyce, B., Pinero, B., Story, B., Dunstan, C., Smith, E., Bonadio, J., Goldstein, S., Gundberg, C., Bradley, A., and Karsenty, G. Increased bone formation in osteocalcin-deficient mice. Nature 382:448–452; 1996.
7. Everett, R. M. and Harrison, S. D., Jr. Clinical biochemistry. In: Foster, H. L., Small, J. D., Fox, J. G., Eds. The Mouse in Biomedical Research. Normative Biology, Immunology, and Husbandry. New York: Academic; 1983; 313–326.
8. Hofbauer, L. C. and Heufelder, A. E. Less can be more—at least in mice: Osteocalcin deficiency associated with increased bone formation. Eur J Endocrinol 136:586–587; 1997.
9. Komori, T., Yagi, H., Nomura, S., Yamaguchi, A., Sasaki, K., Deguchi, K., Shimizu, Y., Bronson, R. T., Gao, Y.-H., Inada, M., Sato, M., Okamoto, R., Kitamura, Y., and Kishimoto, T. Targeted disruption of *cbfa1* results in a complete lack of bone formation owing to maturational arrest of osteoblasts. Cell 89:755–764; 1997.
10. Lumb, W. Small Animal Anesthesia. Philadelphia: Lea & Febiger; 1963.
11. Ogata, N., Chikazu, D., Kubota, N., Terauchi, Y., Tobe, K., Azuma, Y., Ohta, T., Kadowaki, T., Nakamura, K., and Kawaguchi, H. Insulin receptor substrate-1 in osteoblast is indispensable for maintaining bone turnover. J Clin Invest 105:935–943; 2000.
12. Peters, L. L. and Barker, J. E. Novel inheritance of the murine severe combined anemia and thrombocytopenia (*scat*) phenotype. Cell 74:135–142; 1993.
13. Prockop, D. J. Marrow stromal cells as stem cells for nonhematopoietic tissues. Science 276:71–74; 1997.
14. Rosen, C. J., Dimai, H. P., Verault, D., Donahue, L. R., Beamer, W. G., Farley, J., Linkhart, S., Linkhart, T., Mohan, S., and Baylink, D. J. Circulating and skeletal insulin-like growth factor-I (IGF-I) concentrations in two inbred strains of mice with different bone mineral densities. Bone 21:217–223; 1997.
15. Xu, T. and Fisher, L. W. Targeted disruption of the biglycan gene leads to an osteoporosis-like phenotype in mice. Nature Genet 20:78–82; 1998.

Date Received: July 12, 1999
Date Revised: May 30, 2000
Date Accepted: July 11, 2000

JOURNAL OF BONE AND MINERAL RESEARCH
Volume 16, Number 1, 2001

Atherogenic High-Fat Diet Reduces Bone Mineralization in Mice

FARHAD PARHAMI,[1] YIN TINTUT,[1] WESLEY G. BEAMER,[2] NIMA GHARAVI,[1] WILLIAM GOODMAN,[3] and LINDA L. DEMER[1,4]

ABSTRACT

The epidemiological correlation between osteoporosis and cardiovascular disease is independent of age, but the basis for this correlation is unknown. We previously found that atherogenic oxidized lipids inhibit osteoblastic differentiation in vitro and ex vivo, suggesting that an atherogenic diet may contribute to both diseases. In this study, effects of an atherogenic high-fat diet versus control chow diet on bone were tested in two strains of mice with genetically different susceptibility to atherosclerosis and lipid oxidation. After 4 months and 7 months on the diets, mineral content and density were measured in excised femurs and lumbar vertebrae using peripheral quantitative computed tomographic (pQCT) scanning. In addition, expression of osteocalcin in marrow isolated from the mice after 4 months on the diets was examined. After 7 months, femoral mineral content in C57BL/6 atherosclerosis-susceptible mice on the high-fat diet was 43% lower (0.73 ± 0.09 mg vs. 1.28 ± 0.42 mg; $p = 0.008$), and mineral density was 15% lower compared with mice on the chow diet. Smaller deficits were observed after 4 months. Vertebral mineral content also was lower in the fat-fed C57BL/6 mice. These changes in the atherosclerosis-resistant, C3H/HeJ mice were smaller and mostly not significant. Osteocalcin expression was reduced in the marrow of high fat-fed C57BL/6 mice. These findings suggest that an atherogenic diet inhibits bone formation by blocking differentiation of osteoblast progenitor cells. (J Bone Miner Res 2001;16:182–188)

Key words: osteoporosis, oxidized lipids, bone, atherosclerosis, high-fat diet

INTRODUCTION

EPIDEMIOLOGICAL EVIDENCE links osteoporosis with cardiovascular disease, independently of age.[1,2] Osteoporosis and the subsequent 1 million fractures in the United States each year[3] results from a combination of increased bone resorption and decreased bone formation. Low bone mineral density (BMD) is associated closely with cardiovascular disease mortality,[4–6] cardiovascular calcification,[7–9] atherosclerosis,[10,11] and high lipid levels.[10–13] Such correlations raise the possibility of a common underlying factor or mechanism.

We previously found that minimally oxidized low-density lipoprotein (MM-LDL), and other bioactive oxidized lipids that promote atherogenesis and are increased in atherosclerotic lesions,[14–19] also inhibit osteoblastic differentiation of bone- and marrow-derived preosteoblasts in vitro.[20,21] Preosteoblasts harvested from the marrow of mice fed a high-fat, atherogenic diet showed significantly less osteoblastic differentiation.[21] Others have shown a paucity of cells committed to the bone lineage in osteoporotic bone marrow and with aging.[22,23] These links between lipids, vascular disease, and bone suggest the novel hypothesis that oxidized lipids are the biological link.

[1]Division of Cardiology, University of California, Los Angeles School of Medicine, Los Angeles, California, USA.
[2]The Jackson Laboratory, Bar Harbor, Maine, USA.
[3]Division of Nephrology, University of California, Los Angeles School of Medicine, Los Angeles, California, USA.
[4]Departments of Medicine and Physiology, University of California, Los Angeles School of Medicine, Los Angeles, California, USA.

In this study, effects of a high-fat atherogenic diet versus control chow diet on bone mineral content (BMC) and BMD were tested in two strains of mice with genetically different susceptibility to oxidized lipids and atherogenesis. In 1985, Paigen et al. showed differences in the susceptibility of two inbred strains of mice to development of hyperlipidemia and atherosclerotic lesions when fed an atherogenic diet[24,25]; C3H/HeJ were identified as a resistant strain and C57BL/6 as a sensitive strain. Several years later, Liao et al. reported the induction of inflammatory genes by an atherogenic diet in the C57BL/6 but not in the C3H/HeJ strain,[26] and Navab et al.[27] and Shih et al.[28] found differences in the antioxidant defense systems between the susceptible and resistant mouse strains. In the present study, we have compared the susceptibility and resistance of these two strains of mice to the effects of high-fat diet-induced hyperlipidemia on bone. We report that in the atherosclerosis-susceptible C57BL/6 mice, BMC and BMD were significantly lowered by the high-fat diet versus chow diet. These changes were smaller in the atherosclerosis-resistant C3H/HeJ mice. In addition, marrow cells from the high-fat–fed C57BL/6 mice showed reduced osteocalcin expression.

Altogether these results suggest that oxidized lipids adversely affect bone by inhibiting osteoblastic differentiation. If applicable to humans, these studies may result in new therapeutic approaches to osteoporosis.

MATERIALS AND METHODS

Mice and diets

At 1 month of age, male C57BL/6 (atherosclerosis-susceptible strain) and C3H/HeJ (atherosclerosis-resistant strain) mice (The Jackson Laboratory, Bar Harbor, ME, USA) were placed on either a control chow diet (National Institutes of Health [NIH]-31 Mouse/Rat Diet 7013 containing 6% fat) or a high-fat (atherogenic) diet (Teklad TD90221; Harlan Teklad, Madison, WI, USA; including 1.25% cholesterol, 15.8% fat, and 0.5% cholate). This atherogenic diet has been found to cause significant hypercholesterolemia in C57BL/6 mice.[24,25] Femurs and lumbar vertebrae were harvested from 8 animals after 4 months and 14 animals after 7 months. The bones were cleared of soft tissue and fixed in 95% ethanol.

Quantitative computed tomographic scanning

Peripheral quantitative computed tomographic (pQCT) scans were performed on individual bones (left femur, L4 vertebrae) from each mouse. Scanning was done with a STRATEC XCT 960M unit (Norland Medical Instruments, Ft. Atkinson, WI, USA) specifically configured for small bone specimens. Mineral thresholds were set at 1.30 for low-density bone and 2.00 for high-density bone. These thresholds excluded mouse fat, water, muscle, and tendon from true bone. Daily calibration was performed with a manufacturer-supplied phantom (hydroxyapatite in Lucite) of defined density. Calibration with a set of known hydroxyapatite standards (0.05–1000.0 mg/mm^3) yielded a correlation of 0.998 with XCT 960M estimation of volumetric density. Estimates of measurement precision of mineral and volume of femurs and vertebrae were obtained from the middiaphyseal shaft of a B6C3H-F1 femur and from the midbody scans of a B6C3H-F1 L5 vertebra. Six replicate measurements for each bone yielded average values of 1.6, 2.1, and 2.8% for femoral density, mineral, and volume, respectively, and 3.2, 5.9, and 4.7% for L5 vertebral density, mineral, and volume, respectively.

Femurs were scanned full length at 2-mm intervals with a resolution of 0.100 mm/voxel, yielding eight 1-mm-thick cross-sections representing eight axial levels of the femur. Vertebrae were scanned full length at 0.7-mm intervals with the same resolution, yielding three to four 1-mm-thick cross-sections. The center-most scan (based on image morphology) or the mean of two scans sharing the center position was selected for data analyses.

Marrow isolation

After 4 months on the diets, mouse marrow cells were isolated from both femurs from 2 animals in each group as previously described.[21,29,30] Marrow from both femurs was pooled for each animal and RNA was isolated and analyzed separately by reverse-transcriptase polymerase chain reaction (RT-PCR). RNA was isolated as previously described using the RNA isolation kit from Stratagene (La Jolla, CA, USA).[28]

RT-PCR

RNA in 3-μg quantities was reverse-transcribed, and PCR was performed using primers as described previously.[31] Thermal cycling was carried out for 21 cycles (glyceraldehyde-3-phosphate dehydrogenase [GAPDH]) or 34 cycles (osteocalcin) at 60°C annealing temperature for both GAPDH and osteocalcin. Amplified fragments were isolated on a 6% polyacrylamide gel (29:1 acrylamide to bis-acrylamide), and the autoradiographs were scanned with an AGFA ARCUS II scanner and semiquantitated with NIH Image software, version 1.59, public domain program (National Institutes of Health, Bethesda, MD, USA).

Lipoprotein preparation and oxidation

Human LDL was isolated by density-gradient centrifugation of serum and stored in phosphate-buffered 0.15 M NaCl containing 0.01% EDTA. MM-LDL was prepared by iron oxidation of human LDL as previously described.[20] Minimal oxidation of LDL resulted in a 2- to 3-fold increase in conjugated dienes and 2–3 nmol of thiobarbituric acid reactive substances per milligram of cholesterol after dialysis. The concentrations of lipoproteins used in this study are reported in micrograms of protein. The pre- and postoxidation lipopolysaccharide levels in these lipoprotein preparations were <30 pg/ml.

Statistical analysis

Differences in BMC and BMD were assessed using Student's two-tailed *t*-test, allowing for unequal variances and unequal sample sizes where appropriate.

TABLE 1. QCT BONE PARAMETERS FOR FEMURS FROM C57BL/6 MICE AFTER 7 MONTHS ON A CONTROL CHOW OR HIGH-FAT DIET

	Mineral content (mg)		*Chow versus high fat*	*Mineral density (mg/mm³)*		*Chow versus high fat*
Slice	*Chow*	*High fat*	p	*Chow*	*High fat*	p
1	2.29 ± 0.82	0.74 ± 0.19	0.002	0.502 ± 0.05	0.441 ± 0.04	0.01
2	1.05 ± 0.21	0.53 ± 0.20	0.001	0.365 ± 0.05	0.355 ± 0.05	0.70
3	1.02 ± 0.08	0.77 ± 0.10	0.0001	0.447 ± 0.05	0.400 ± 0.06	0.02
4	0.99 ± 0.07	0.72 ± 0.06	0.0003	0.440 ± 0.02	0.391 ± 0.02	0.05
5	1.19 ± 0.14	0.78 ± 0.07	<0.0001	0.520 ± 0.04	0.410 ± 0.03	0.01
6	1.26 ± 0.12	0.86 ± 0.10	<0.0001	0.573 ± 0.04	0.465 ± 0.05	<0.0001
7	1.32 ± 0.16	0.75 ± 0.19	0.0008	0.515 ± 0.05	0.416 ± 0.04	0.1
8	1.13 ± 0.43	0.71 ± 0.31	0.001	0.538 ± 0.03	0.476 ± 0.05	0.01
Mean ± SD	1.28 ± 0.42	0.73 ± 0.09	0.008	0.488 ± 0.07	0.419 ± 0.04	0.03

Scans were performed at 8 longitudinal axis positions (slices) for each femur with 1 being most proximal and 8 most distal. Values of BMC and BMD are expressed as mean ± SD over all animals in each diet group.

TABLE 2. QCT BONE PARAMETERS FOR FEMURS FROM C3H/HeJ MICE AFTER 7 MONTHS ON A CONTROL CHOW OR HIGH-FAT DIET

	Mineral content (mg)		*Chow versus high fat*	*Mineral density (mg/mm³)*		*Chow versus high fat*
Slice	*Chow*	*High fat*	p	*Chow*	*High fat*	p
1	2.73 ± 0.79	2.00 ± 0.84	0.12	0.596 ± 0.06	0.542 ± 0.06	0.11
2	1.60 ± 0.24	1.26 ± 0.15	0.01	0.510 ± 0.06	0.426 ± 0.06	0.016
3	1.72 ± 0.16	1.40 ± 0.13	0.002	0.800 ± 0.03	0.720 ± 0.05	0.005
4	1.88 ± 0.24	1.66 ± 0.16	0.07	0.883 ± 0.07	0.909 ± 0.03	0.39
5	2.01 ± 0.18	1.73 ± 0.16	0.009	0.853 ± 0.03	0.846 ± 0.02	0.63
6	2.28 ± 0.27	2.06 ± 0.14	0.09	0.922 ± 0.06	0.911 ± 0.02	0.68
7	2.01 ± 0.41	1.95 ± 0.15	0.75	0.694 ± 0.11	0.807 ± 0.09	0.05
8	1.47 ± 0.40	1.55 ± 0.21	0.67	0.612 ± 0.07	0.562 ± 0.04	0.15
Mean ± SD	1.96 ± 0.40	1.70 ± 0.29	0.59	0.734 ± 0.15	0.715 ± 0.19	0.26

Scans were performed at 8 longitudinal axis positions (slices) for each femur with 1 being most proximal and 8 most distal. Values of BMC and BMD are expressed as mean ± SD over all animals in each diet group.

RESULTS

Femoral BMC and BMD

After 4 months, femoral BMD was significantly lower in fat-fed C57BL/6 mice at three of the eight levels scanned ($p <$ 0.04; from 0.488 ± 0.038 mg/mm^3 to 0.423 ± 0.043 mg/mm^3). All three levels were in the middiaphyseal region where variance caused by anatomic complexity is minimized. BMC was not significantly different between the two groups.

After 7 months, femoral BMC was significantly lower in fat-fed C57BL/6 mice compared with control chow-fed mice at all eight levels scanned. Mean mineral content was lowered 43% (from 1.28 ± 0.42 mg to 0.73 ± 0.09 mg; $p \leq$ 0.002; Table 1) on the high-fat diet. Changes in mineral content were most significant ($p \leq 0.0003$) at the four middiaphyseal levels (scans 3–6). Femoral mineral density was also significantly lower in fat-fed C57BL/6 mice compared with chow-fed mice at six of eight levels, with a 14.5% mean difference (from 0.488 ± 0.066 mg/mm^3 to 0.419 ± 0.035 mg/mm^3; $p = 0.03$; Table 1).

In C3H/HeJ mice, which are resistant to the atherogenic effects of a high-fat diet and lipid oxidation products,[24,25] the high-fat diet had less effect on bone mineralization. After 4 months on the diet, C3H/HeJ mice showed no significant difference in femoral BMC at any of the eight levels examined (data not shown); BMD was significantly lower at one of eight scanned sites ($p = 0.01$).

After 7 months on the diet, the fat-fed C3H/HeJ mice had significantly ($p \leq 0.01$) lower BMC compared with chow-fed mice at only three of eight levels (Table 2). However, the overall mean difference for all eight levels did not reach statistical significance ($p = 0.59$). There also was no significant effect of the high-fat diet on femoral mineral density ($p = 0.26$; Table 2).

Lumbar vertebral mineral content and mineral density

At 4 months, there was no significant difference between chow and high-fat diet groups in either vertebral mineral content or density in either mouse strains. However, at 7

TABLE 3. QCT BONE PARAMETERS FOR L4 VERTEBRAE FROM C57BL/6 AND C3H/HeJ MICE AFTER 7 MONTHS ON A CONTROL CHOW OR HIGH-FAT DIET

Total bone				*Cortical bone*			
Mineral content (mg)		*Mineral density (mg/mm³)*		*Mineral content (mg)*		*Mineral density (mg/mm³)*	
Chow	*High fat*	*Chow*	*High fat*	*Chow*	*High fat*	*Chow*	*High fat*
C57BL/6							
1.20 ± 0.10	0.77 ± 0.10	0.229 ± 0.02	0.212 ± 0.03	0.317 ± 0.08	0.088 ± 0.05	0.455 ± 0.01	0.445 ± 0.01
p	<0.001	0.30		<0.001		0.09	
C3H/HeJ							
1.41 ± 0.35	1.31 ± 0.14	0.248 ± 0.03	0.217 ± 0.01	0.624 ± 0.25	0.445 ± 0.13	0.481 ± 0.02	0.474 ± 0.01
p	0.49	0.03		0.12		0.48	

Values are for the central slice or slices for each of the L4 vertebrae and are expressed as mean ± SD over all animals in each diet group.

months, vertebral mineral content was significantly lower in the C57BL/6 fat-fed mice (Table 3). Total mineral content of the central section or sections was lower by a mean of 35% (from 1.2 ± 0.1 mg to 0.77 ± 0.1 mg; $p < 0.001$), primarily because of changes in high-density cortical bone (i.e., a 72% decrease). Total mineral density decreased 7% on the high-fat diet, but this change was not statistically significant. In C3H/HeJ mice, a 7% decrease in total mineral content was found, as well as a 29% decrease in cortical mineral content. These changes did not reach statistical significance. Total mineral density of vertebrae from C3H/HeJ mice decreased 12.5% on the high-fat diet (from 0.248 ± 0.03 to 0.217 ± 0.01 mg/mm^3; $p = 0.03$).

Gene expression in marrow cells

After 4 months on the high-fat or chow diets, the marrow isolated from 2 C57BL/6 mice on each diet was analyzed for the expression of three markers of osteoblastic differentiation: alkaline phosphatase, bone sialoprotein, and osteocalcin. All three markers were expressed by the marrow cells. Of the three, only osteocalcin expression was affected by diet, showing a 35% reduction with the high-fat diet when normalized to GAPDH values (Fig. 1).

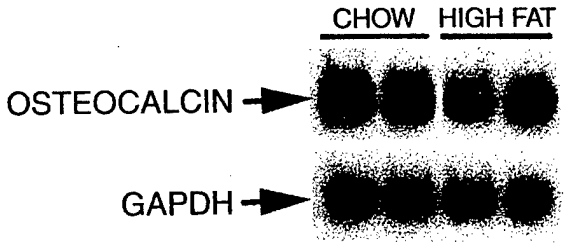

FIG. 1. Effects of a high-fat diet on osteocalcin expression in marrow cells. One-month-old C57BL/6 mice were placed on a high-fat or chow diet for 4 months. The animals were killed and femoral marrow was isolated from each mouse and used to isolate total RNA. RT-PCR analysis showed an expected size band of 360 base pairs (bp). Expression of GAPDH was used for normalization. Each lane represents RNA isolated from an individual mouse.

DISCUSSION

The present study is the first to show that 7-month treatment with an atherogenic high-fat diet lowers BMD and BMC in vivo in atherosclerosis-susceptible C57BL/6 mice, with much smaller effects in the atherosclerosis-resistant C3H/HeJ mice. The atherogenic diet resulted in a significantly lower femoral mineral content and femoral mineral density in the C57BL/6 mice. Smaller changes were seen in the C3H/HeJ mice. The differential effects of the atherogenic diet on bones in the two strains of mice are similar to the effects of that diet on the development of atherosclerosis. Previous reports showed differences in genetically determined factors in response to diet-induced hyperlipidemia and lipid oxidation in these mouse strains to be the underlying reason for their degree of susceptibility to atherosclerosis. These differences include: (1) the level of induction of inflammatory genes such as monocyte chemotactic protein-1, colony-stimulating factors, heme oxygenase, and serum amyloid A and activation of nuclear factor κB (NFκB) transcription factor in response to atherogenic diet[26,27,32] and (2) the ability of high-density lipoprotein (HDL) to protect against the effects of atherogenic diet, because of variability in the level of antioxidant enzyme paraoxonase.[28] The latter difference is important in light of the observation that the protective effect of HDL appears to correlate inversely with atherosclerosis,[33] and a direct correlation between HDL levels and BMD in fat-fed mice has been shown (T. Drake, University of California, Los Angeles [UCLA], Department of Pathology, personal communication, 1999). It is intriguing to speculate that similar genetically regulated factors, involved with defense against atherogenic oxidized lipids, also determine susceptibility to osteoporosis.

Because femoral mineral content was more substantially changed by the atherogenic diet than mineral density, the effect may be caused by quantitatively less bone formation

and/or shorter bones in the high-fat–fed mice. Although we did not measure femoral size after 7 months in this study, in a separate study, we found no significant change in the femoral or tibial length between chow-fed versus high-fat–fed C57BL/6 mice after 4 months on the diet (F. Parhami, unpublished observations, 1999). Because our previous in vitro and in vivo studies showed inhibition of osteoblastic differentiation and bone formation by marrow stromal cells isolated from C57BL/6 mice on the high-fat diet versus chow diet, we speculate that bone formation is inhibited by the atherogenic diet. More direct future studies will further validate this speculation. It is important to note that the mice used in the present study were in their growing stage when peak bone mass is achieved. Inhibition of bone formation during growth stage also would have adverse consequences by reducing peak bone mass. The reducing effects of the dietary fat on BMC and BMD would translate into a reduction in this important determinant of bone strength.

The present results also suggest that increased dietary lipids interfere with osteoblast maturation in vivo, based on dietary inhibition of osteocalcin messenger RNA (mRNA) expression. Although the effect of the high-fat diet on the expression of osteocalcin alone is not sufficient to draw definitive conclusions about differentiation of osteoblasts, this inhibition is consistent with previous ex vivo evidence that exposure to a high-fat diet reduced marrow preosteoblastic maturation in culture,[21] as well as in vitro evidence that lipid and lipoprotein oxidation products inhibit osteoblast differentiation and function.[20,21] Previous studies using the same atherogenic diet in C57BL/6 mice have shown 2- to 3-fold increases in cholesterol levels after 3–4 weeks on this diet, as well as a significant drop in the HDL levels.[24,25] We therefore speculate that the adverse effects of the high-fat diet on bone in the C57BL/6 mice are caused by dyslipidemia and subsequent increases in lipid oxidation. The diet-induced hyperlipidemia in circulation further translates into increased lipid accumulation in highly vascular tissues and the artery wall because of the diffusion of lipoproteins across the vascular endothelium. Once apart from the protective, antioxidant environment of serum, these lipoprotein particles are oxidized further into biologically active forms responsible for inflammatory processes in atherosclerosis and vascular calcification.[19,20] Because bone and marrow are both vascularized, circulating lipids can access both sites of active bone remodeling where osteoprogenitor cells are present: (1) the subendothelial space of the osteons and (2) the marrow stroma at the trabecular surface or endosteum. Lipid accumulation[34] and monocyte accumulation and plaquing[35] have been observed in the vessels of osteons in osteoporotic and aging bone. The presence of circulating lipoproteins in the marrow is expected because marrow is a site for clearance of chylomicrons and chylomicron remnants derived from dietary fat,[36] and dietary fat has been found to alter the lipid profile in the marrow.[37] Thus, lipid oxidation products may underlie the paradoxical association of cardiovascular disease with osteoporosis.

The findings in the present report are consistent with a preliminary report showing a significant correlation between dietary cholesterol intake and vertebral bone loss in women,[38] as well as with population studies showing an association of cholesterol levels with osteoporosis in women[13] and, preliminarily, in men.[39] Recent evidence suggests that 3-hydroxy-3-methylglutaryl coenzyme A (HMG-CoA) reductase inhibitors (statins), lipid-lowering agents commonly used to treat cardiovascular disease, have potent positive effects on bone formation in rodents,[40] and statin therapy in humans correlates with reduced osteoporosis.[41–45] Although the mechanism is proposed to be a direct stimulation of osteoblasts, an equally likely mechanism is an indirect effect through lipid-lowering, given that the dominant site of action of these agents, in both humans and rodents,[46] is in the liver where statins are mostly cleared from circulation.

Evidence suggests that the atherogenic nature of the high-fat diet is essential for effects on bone. Wohl et al. previously showed a minimal effect on BMC of a noncholesterol, 8% fat diet in adult roosters.[47] Because cholesterol feeding is necessary to induce atherosclerosis in roosters,[48] this finding suggests that a nonatherogenic high-fat diet is not sufficient to induce bone changes.

Collectively, these observations suggest the adverse effects of lipids on bone. The possibility that lipid oxidation products are the biologically active factors linking a high-fat diet with reduced bone formation is supported by the finding of substantially reduced effects in mice that are resistant to the effects of oxidized lipids and by the anabolic effects of the antioxidant vitamin E on bone.[49] Because cardiovascular disease is the highest risk cause of death for patients with osteoporotic fracture[4,5] and low BMD is associated with mortality independent of fractures,[50] elucidation of common lipid- and lipid oxidation–mediated mechanisms has great importance for identifying new preventive measures for both osteoporosis and cardiovascular disease. The possibility that high lipid levels are a common underlying factor in atherosclerosis and bone loss may explain the epidemiological evidence for correlation between cardiovascular disease and osteoporosis.

ACKNOWLEDGMENTS

The authors are grateful to Vien Le and Jeanenne O'Connor for technical assistance and Alan Han for manuscript preparation. They also thank Dr. Theodore J. Hahn, Dr. Judith A. Berliner, and Dr. Robert Marcus for their input on this manuscript. F. Parhami is a recipient of a Career Development Award from the Claude D. Pepper Older American Independence Center at UCLA. This work was funded in part by NIH grants HL30568, AR43618, DK52905, DK35423, and RR00865 as well as the Laubisch Fund.

REFERENCES

1. Boukhris R, Becker KL 1972 Calcification of the aorta and osteoporosis. JAMA **219:**1307–1311.
2. Frye MA, Melton LJ, Bryant SC, Fitzpatrick LA, Wahner HW, Schwartz RS, Riggs BL 1992 Osteoporosis and calcification of the aorta. Bone Miner **19:**185–194.

3. Riggs BL, Melton LJ 1992 The prevention and treatment of osteoporosis. N Engl J Med **329**:620–627.
4. von der Recke P, Hansen MA, Hassager C 1999 The association between low bone mass at the menopause and cardiovascular mortality. Am J Med **106**:273–278.
5. Browner WS, Seeley DG, Vogt TM, Cummings SR 1991 Nontrauma mortality in elderly women with low bone mineral density. Lancet **338**:355–358.
6. Naito S, Ito M, Sekine I, Ito M, Hirano T, Iwasaki K, Niwa M 1993 Femoral head necrosis and osteopenia in stroke-prone spontaneously hypertensive rats (SHRSPs). Bone **14**:745–753.
7. Jie KG, Bots ML, Vermeer C, Witteman JC, Grobbee DE 1996 Vitamin K status and bone mass in women with and without aortic atherosclerosis: A population-based study. Calcif Tissue Int **59**:352–356.
8. Barengolts EI, Berman M, Kukreja SC, Kouznetsova T, Lin C, Chomka EV 1998 Osteoporosis and coronary atherosclerosis in asymptomatic postmenopausal women. Calcif Tissue Int **62**:209–213.
9. Ouchi Y, Akishita M, deSouza AC, Nakamura T, Orimo H 1993 Age-related loss of bone mass and aortic/aortic valve calcification—reevaluation of recommended dietary allowance of calcium in the elderly. Ann NY Acad Sci **676**:297–307.
10. Laroche M, Pouilles JM, Ribot C, Bendayan P, Bernard J, Boccalon H, Mazieres B 1994 Comparison of the bone mineral content of the lower limbs in men with ischaemic atherosclerotic disease. Clin Rheumatol **13**:61–64.
11. Laroche M, Moulinier L, Bon E, Cantagrel A, Mazieres B 1994 Renal tubular disorders and arteriopathy of the lower limbs: Risk factors for osteoporosis in men? Osteoporos Int **4**:309–313.
12. Pinals RS, Jabbs JM 1972 Type-IV hyperlipoproteinemia and transient osteoporosis. Lancet **2**:929.
13. Broulik PD, Kapitola J 1993 Interrelations between body weight, cigarette smoking and spine mineral density in osteoporotic Czech women. Endocr Reg **27**:57–60.
14. Yla-Hertualla S 1998 Is oxidized low density lipoprotein present in vivo? Curr Opin Lipidol **9**:337–344.
15. Watson AD, Leitinger N, Navab M, Faull KF, Horkko S, Witztum JL, Palinski W, Schwenke D, Salomon RG, Sha W, Subbanagounder G, Fogelman AM, Berliner JA 1997 Structural identification by mass spectrometry of oxidized phospholipids in minimally oxidized low density lipoprotein that induce monocyte-endothelial interactions and evidence for their presence in vivo. J Biol Chem **272**:13597–13607.
16. Haberland ME, Fong D, Cheng L 1988 Malondialdehyde-altered protein occurs in atheroma of Watanabe heritable hyperlipidemic rabbits. Science **241**:215–218.
17. Morrow JD, Minton TA, Mukundan CR, Campbell MD, Zackert WE, Daniel VC, Badr KF, Blair IA, Roberts LJ 1994 Free radical-induced generation of isoprostanes in vivo. Evidence for the formation of D-ring and E-ring isoprostanes. J Biol Chem **269**:4317–4326.
18. Rosenfeld ME, Khoo JC, Miller E, Parthasarathy S, Palinski W, Witztum JL 1991 Macrophage-derived foam cells freshly isolated from rabbit atherosclerotic lesions degrade modified lipoproteins, promote oxidation of low-density lipoproteins, and contain oxidation-specific lipid-protein adducts. J Clin Invest **87**:90–99.
19. Berliner JA, Navab M, Fogelman AM, Frank JS, Demer LL, Edwards PA, Watson AD, Lusis AJ 1995 Atherosclerosis: Basic mechanisms. Oxidation, inflammation, and genetics. Circulation **91**:2488–2496.
20. Parhami F, Morrow AD, Balucan J, Leitinger N, Watson AD, Tintut Y, Berliner JA, Demer LL 1997 Lipid oxidation products have opposite effects on calcifying vascular cell and bone cell differentiation. A possible explanation for the paradox of arterial calcification in osteoporotic patients. Arterioscler Thromb Vasc Biol **17**:680–687.
21. Parhami F, Jackson SM, Tintut Y, Le V, Balucan JP, Territo MC, Demer LL 1999 Atherogenic diet and minimally oxidized low density lipoprotein inhibit osteogenic and promote adipogenic differentiation of marrow stromal cells. J Bone Miner Res **14**:2067–2078.
22. Mullender MG, van der Meer DD, Huiskes R, Lips PP 1996 Osteocyte density changes in aging and osteoporosis. Bone **18**:109–113.
23. Bergman RJ, Gazit D, Kahn AJ, Gruber H, McDougall S, Hahn TJ 1996 Age-related changes in osteogenic stem cells in mice. J Bone Miner Res **11**:568–577.
24. Paigen B, Morrow A, Brandon C, Mitchell D, Holmes P 1985 Variation in susceptibility to atherosclerosis among inbred strains of mice. Atherosclerosis **57**:65–73.
25. Paigen B, Mitchell D, Reue K, Morrow A, Lusis AJ, LeBoeuf RC 1987 Ath-1, a gene determining atherosclerosis susceptibility and high density lipoprotein levels in mice. Proc Natl Acad Sci USA **84**:3763–3767.
26. Liao F, Andalibi A, de Beer FC, Fogelman AM, Lusis AJ 1993 Genetic control of inflammatory gene induction and NF-kB-like transcription factor activation in response to an atherogenic diet in mice. J Clin Invest **91**:2572–2579.
27. Navab M, Levy-Hama S, Van Lenten BJ, Fonarow GC, Cardinez CJ, Castellani LW, Brennan ML, Lusis AJ, Fogelman AM 1997 Mildly oxidized LDL induces an increased apolipoprotein J/paraoxonase ratio. J Clin Invest **99**:2005–2019.
28. Shih DM, Gu L, Hama S, Xia YR, Navab M, Fogelman AM, Lusis AJ 1996 Genetic-dietary regulation of serum paraoxonase expression and its role in atherogenesis in a mouse model. J Clin Invest **97**:1630–1639.
29. Maniotopoulos C, Sodek J, Melcher A 1988 Bone formation in vitro by stromal cell obtained from bone marrow of young adult rats. Cell Tissue Res **254**:317–330.
30. Malaval L, Modrowski D, Gupta AK, Aubin JE 1994 Cellular expression of bone related proteins during in vitro osteogenesis in rat bone marrow stromal cultures. J Cell Physiol **158**: 555–572.
31. Tintut Y, Parhami F, Bostrom K, Jackson SM, Demer LL 1998 Cyclic AMP stimulates osteoblast-like differentiation of calcifying vascular cells: Potential signaling pathway for vascular calcification. J Biol Chem **273**:7547–7553.
32. Liao F, Lusis AJ, Berliner JA, Fogelman AM, Kindy M, de Beer MC, de Beer FC 1994 Serum amyloid A protein family. Differential induction by oxidized lipids in mouse strains. Arterioscler Thromb Vasc Biol **14**:1475–1479.
33. Gordon DJ, Probstfield JL, Garrison JR, Neaton JD, Castelli WP, Knoke JD, Jacobs DR Jr, Bangdiwala S, Tyroler HA 1989 High-density lipoprotein cholesterol and cardiovascular disease: Four prospective American studies. Circulation **79**:8–15.
34. Ramseier E 1962 Untersuchungen uber arteriosklerotische Veranderungen der Knochenarterien. Virchows Arch Path Anat **336**:77–86.
35. Nyssen-Behets C, Duchesne PY, Dhem A 1997 Structural changes with aging in cortical bone of the human tibia. Gerontology **43**:316–325.
36. Hussain MM, Mahley RW, Boyles JK, Fainaru M, Brecht WJ, Lindquist PA 1989 Chylomicron-chylomicron remnant clearance by liver and bone marrow in rabbits. J Biol Chem **264**: 9571–9582.
37. Li Y, Watkins BA 1998 Conjugated linoleic acids alter bone fatty acid composition and reduce ex vivo prostaglandin E2 biosynthesis in rats fed n-6 or n-3 fatty acids. Lipids **33**:417–425.
38. Lin YC, Lyle RM, Weaver CM, Teegarden D 1999 Impact of diet variables on changes in spine bone mineral density. FASEB J **13**:A244 (abstract).
39. Semmler JC 1992 Risk factors for osteoporosis in men. ICCRH, Florence (abstract).

40. Mundy G, Garrett R, Harris S, Chan J, Chen D, Rossini G, Boyce B, Zhao M, Gutierrez G 1999 Stimulation of bone formation in vitro and in rodents by statins. Science **286:**1946–1949.
41. Bauer DC, Mundy GR, Jamal SA, Black DM, Cauley JA, Harris F, Duong T, Cummings SR 1999 Statin use, bone mass and fracture: An analysis of two prospective studies. J Bone Miner Res **14:**S179 (abstract).
42. Meier CR, Schlienger RG, Kraenzlin ME, Schlegel B, Jick H 2000 HMG-CoA reductase inhibitors and the risk of fractures. JAMA **283:**3205–3210.
43. Wang PS, Solomon DH, Mogun H, Avorn J 2000 HMG-CoA reductase inhibitors and the risk of hip fractures in elderly patients. JAMA **283:**3211–3216.
44. Chan KA, Andrade SE, Boles M, Buist DSM, Chase GA, Donahue JG, Goodman MJ, Gurwitz JH, LaCroix AZ, Platt R 2000 Inhibitors of hydroxymethylglutaryl-coenzyme A reductase and risk of fracture among older women. Lancet **355:** 2185–2188.
45. Edwards CJ, Hart DJ, Spector D 2000 Oral statins and increased bone mineral density in postmenopausal women. Lancet **355:**2218–2219.
46. Hamelin BA, Turgeon J 1998 Hydrophilicity/lipophilicity: Relevance for pharmacology and clinical effects of HMG-CoA reductase inhibitors. Trends Pharmacol Sci **19:**1–38.
47. Wohl GR, Loehrke L, Watkins BA, Zernicke RF 1998 Effects of high-fat diet on mature bone mineral content, structure, and mechanical properties. Calcif Tissue Int **63:**74–79.
48. Lucas A, Dai E, Liu LY, Nation PN 1998 Atherosclerosis in Marek's disease virus infected hypercholesterolemic roosters is reduced by HMGCoA reductase and ACE inhibitor therapy. Cardiovasc Res **38:**237–246.
49. Xu H, Watkins BA, Seifert MF 1995 Vitamin E stimulates trabecular bone formation and alters epiphyseal cartilage morphometry. Calcif Tissue Int **57:**293–300.
50. Center JR, Nguyen TV, Schneider D, Sambrook PN, Eisman JA 1999 Mortality after all major types of osteoporotic fracture in men and women: An observational study. Lancet **353:**878–882.

Address reprint requests to:
Farhad Parhami, Ph.D.
Division of Cardiology
47–123 CHS
Box 951679
University of California, Los Angeles School of Medicine
Los Angeles, CA 90095-1679, USA

Received in original form April 24, 2000; in revised form July 26, 2000; accepted August 24, 2000.

Bone Vol. 27, No. 4
October 2000:471–478

ELSEVIER

ORIGINAL ARTICLES

Comparison of Bone Formation Responses to Parathyroid Hormone(1-34), (1-31), and (2-34) in Mice

S. MOHAN,[1] S. KUTILEK,[1] C. ZHANG,[1] H. G. SHEN,[1] Y. KODAMA,[1] A. K. SRIVASTAVA,[1] J. E. WERGEDAL,[1] W. G. BEAMER,[2] and D. J. BAYLINK[1]

[1]*Musculoskeletal Disease Center, Jerry L. Pettis VA Medical Center, Loma Linda, CA, USA*
[2]*The Jackson Laboratory, Bar Harbor, ME, USA*

In this study we used a mouse model system to compare the in vivo effects of parathyroid hormone(1-34) [PTH(1-34)] with that of PTH(1-31) or PTH(2-34) analogs. Daily subcutaneous administration of PTH(1-34) for 15 days caused a dose-dependent increase in the serum osteocalcin level and bone extract alkaline phosphatase activity, markers of bone formation. PTH(2-34) was much less potent, whereas PTH(1-31) was equipotent in stimulating bone formation parameters in mice. PTH(1-34) caused significant increases in serum calcium (after 4 h) and tartrate-resistant acid phosphatase activity in bone extract (after 4 h), whereas PTH(2-34) and PTH(1-31) were less potent. Because PTH(1-31) caused a smaller increase in bone resorption parameters compared to PTH(1-34), despite similar effects on bone formation parameters, we evaluated the long-term anabolic effects of PTH(1-31) and PTH(1-34) in mice. Weekly evaluations of serum osteocalcin levels demonstrated that daily injections of PTH(1-34) and PTH(1-31) at 80 μg/kg body weight increased serum osteocalcin levels within 1 week of the start of treatment, which were maintained during the entire 22 week treatment. Assessment of bone density at the end of the treatment period with peripheral quantitated computed tomography (pQCT) revealed that PTH(1-34) caused a significantly greater increase in femoral bone density compared to PTH(1-31) at the middiaphysis (18% vs. 9% over vehicle control; $p < 0.001$). Both PTH(1-34) and PTH(1-31) increased periosteal circumference compared to vehicle ($p < 0.01$) without a significant difference between the two treatments. In contrast, PTH(1-34) caused a significantly greater reduction in endosteal circumference than PTH(1-31) ($p < 0.001$). Both analogs significantly increased maximum load and area of moment of inertia over the vehicle group. In conclusion, our findings suggest that PTH(1-34) and PTH(1-31) may exhibit different anabolic effects at the periosteum vs. endosteum in the long bones of mice. (Bone 27:471–478; 2000)

Key Words: Bone formation; Bone resorption; Bone strength; Osteoblasts; Parathyroid hormone (PTH) analogs; PTH signaling.

Address for correspondence and reprints: Subburaman Mohan, Ph.D., Musculoskeletal Disease Center (151), Loma Linda University, Jerry L. Pettis VA Medical Center, 11201 Benton Street, Loma Linda, CA 92357. E-mail: mohans@lom.med.va.gov

Introduction

Osteoporosis is a disease characterized by low bone mass and microarchitectural deterioration of bone tissue that leads to increased bone fragility and consequent increased risk of fractures.[2,35] Studies on the pathogenesis of osteoporosis have revealed that osteoporosis occurs mainly because of: (1) low peak bone density, which occurs at the end of sexual maturity; and (2) increased bone resorption that occurs as a result of estrogen deficiency, not compensated by a corresponding increase in bone formation.[2,35] Currently available therapies for the treatment of osteoporosis are based on inhibition of bone resorption to prevent further bone loss. Because many osteoporotic patients who come for treatment have already lost a substantial amount of bone, there is a need for developing treatments that increase bone mass by stimulating new bone formation. Of the potential candidates for anabolic therapies for osteoporosis, parathyroid hormone (PTH) has received much attention in the recent years based on the findings that intermittent treatment with PTH causes a significant increase in bone mass in animals and humans, improves mechanical strength, and preserves trabecular bone connectivity in an animal model of osteoporosis.[23,24,26,27,30,31,34,40,52]

The osteoblasts are the primary target cells for the anabolic effects of PTH on bone tissue. Effects of PTH on osteoblasts are known to be mediated via binding of PTH to the seven-membrane-spanning G-protein-coupled receptor and activation of both the 3,5-cyclic adenosine monophosphate (cAMP)-dependent protein kinase A (PKA) pathway and the phospholipase C (PLC)-dependent protein kinase C (PKC) pathway.[20] Although the mechanisms of the anabolic action of PTH are still not totally understood, stimulation of cAMP production has been shown to be involved, based on previous in vivo studies using the N-terminal-truncated PTH fragment, which lacks PKA activity.[1,5,16,20,37] The involvement of the PKC pathway in mediating the anabolic effects of PTH is controversial.[10,12,13,19,39,44–46,50,51] To elucidate the signaling pathways for the anabolic effects of PTH on bone, aminoterminal- and carboxyterminal-truncated PTH analogs have been used frequently based on previous findings that some of these analogs activate one but not both of the signaling pathways.[1,5,16,20,37] In this regard, it is fairly well established that PTH(2-34) is much less potent than PTH(1-34) in stimulating adenylate-cyclase activity.[1,5] However, the issue of whether or not PTH(1-31) can activate PLC/PKC activity with a potency similar to that of PTH(1-34) is controversial at this time, based on recent findings.[10,12,19,44–46] Much less is also known about the involvement of the PKC pathway in mediating the bone resorbing effects of PTH.

Earlier studies on the in vivo effects of PTH have most often

8756-3282/00/$20.00
PII S8756-3282(00)00355-0

Bone Vol. 27, No. 4
October 2000:471–478

utilized ovariectomized rats as the experimental model system. Although the mouse model has been used extensively in transgenic overexpression and knockout studies, little is known about the anabolic effects of PTH in mice. Therefore, we investigated the effects of PTH(1-34) on bone formation and bone resorption parameters in mice and found that PTH increased both bone formation and resorption, as shown in humans. We next evaluated the relative contribution of PKA- and PKC-signaling pathways in mediating the bone forming and bone resorbing effects of PTH by comparing the in vivo effects of PTH(1-34) with those of PTH(2-34) and PTH(1-31). Finally, the long-term effects of PTH(1-34) and PTH(1-31) on bone density and bone strength were evaluated.

Materials and Methods

Materials

PTH(1-34), PTH(2-34), and PTH(1-31) were synthesized as amides by SynPep (Dublin, CA). The purity of all three analogs was >95% by amino acid analysis and mass spectrometry. The calculated molar concentrations of 40 μg PTH(1-34), PTH(1-31), and PTH(2-34) were 9.7, 10.7, and 9.9 nmol/L, respectively. Adult female Swiss/Webster mice were purchased from the Jackson Laboratory (Bar Harbor, ME). Antibodies to mouse osteocalcin were produced in our laboratory. Mouse osteocalcin standard and tracer were purchased from Biomedical Technologies (Stoughton, MA).

Animals and Treatment

Six- to 8-week-old Swiss/Webster mice were purchased from the Jackson Laboratory (Bar Harbor, ME) and maintained at the Animal Research Facility of the Jerry L. Pettis VA Medical Center (Loma Linda, CA) for 7–10 days prior to the start of the experiment. They were housed in a room maintained at 20°C on a 12 h light/12 h dark cycle and fed ad libitum with standard rat/mouse diet containing normal calcium. The animals were given daily subcutaneous injections of vehicle (phosphate-buffered saline [PBS]) or PTH(1-34), PTH(2-34), or PTH(1-31). PTH was prepared in PBS prior to administration. Twenty four hours after the last injection, blood and femurs were collected and used for various analyses. Study procedures were approved by the institutional animal research subcommittee at the Jerry L. Pettis VA Medical Center.

Bone Densitometry

Bone mineral density (BMD) of left femur was measured by peripheral quantitative tomography (pQCT) using a pQCT system (Stratec XCT 960M) with version 5.20 software (Norland, Madison, WI). Total BMD was calculated at the middle diaphysis as described elsewhere.[3,38] Trabecular density was determined at the distal metaphysis. The precision for total bone density is 1.2%.

Mechanical Testing

After pQCT measurements, the samples were subjected to mechanical testing using a Model 8841 mechanical tester (Instron, Canton, MA). Three-point bending strength was measured at the middiaphysis. The bone was placed horizontally with the anterior surface upward, centered on the supports, and the pressing force was directed vertically to the midshaft of the bone. Each bone was compressed at a constant rate of 2 mm/min until failure. Breaking force was defined as bending load at failure. Stiffness was calculated as the slope of the linear (elastic) part of the load-displacement curve. Stress (σ) and elastic or Young's modulus (E) were calculated as previously described.[17] Maximal stress was defined as stress at breaking force.

Biochemical Assays

Serum. Osteocalcin levels were measured by radioimmunoassay (RIA) using rabbit antimouse osteocalcin antiserum and purified mouse osteocalcin as standard and tracer.[36] The sensitivity of the mouse osteocalcin assay was 0.5 ng/mL and intra- and interassay variations were <8%. A recently developed enzyme-linked immunoassay (ELISA) was used to measure serum C-telopeptide levels.[43] Serum calcium levels were measured by a colorimetric assay.[4]

Bone. Alkaline phosphatase (ALP, a potential measure of bone formation) and tartrate-resistant acid phosphatase (TRAP, potential measure of bone resorption) activities were measured in bone extracts by previously established methods.[6,36]

Statistical Analysis

Six to nine animals were used for each treatment group. Values are expressed as mean ± SEM. Multiple comparisons between treatment groups were made by Fisher's protected least significant difference method (post hoc test) with a one-way analysis of variance (ANOVA). The Student's t-test was used for comparisons between the two groups.

Results

PTH(1-34) Effects on Bone Formation and Bone Resorption Parameters in Mice

Daily subcutaneous injections of PTH(1-34) at 80 and 160 μg/kg caused a significant increase in serum osteocalcin levels as compared with the control group. Statistically significant increases in serum osteocalcin levels occurred as early as day 5, with maximum increases occurring at day 10 (**Figure 1**a). PTH(1-34) treatment also caused a dose-dependent increase in ALP activity in the femoral bone extract. A maximal increase in ALP activity of 100% over control was seen at a dose of 160 μg/kg per day (Figure 1b). PTH-induced increases in serum osteocalcin and bone ALP activity in mice are consistent with previous reports in humans and rats that PTH treatment causes an acute increase in bone formation.

To determine if PTH treatment causes an acute increase in bone resorption in mice, we measured serum calcium levels and TRAP activity in the femoral bone extract. At 4 h after injecting PTH at a dose of 320 μg/kg, serum calcium concentration was increased to 121 ± 7% of control ($p < 0.05$). Serum calcium concentration was not statistically different from the control group at other timepoints (Figure 1c). The TRAP activities of the bone extract from mice treated with 80 and 160 μg/kg PTH for 10 days were significantly higher than the control group (Figure 1d).

Effect of PTH Analogs on Bone Formation and Bone Resorption Parameters in Mice

To investigate the role of the PKA pathway in the bone forming effects of PTH, mice were injected with two different doses (80 and 800 μg/kg) of PTH(2-34), an analog with reduced cAMP activity. Treatment of mice with 80 μg/kg PTH(1-34), but not PTH(2-34), caused significant increases in serum osteocalcin and

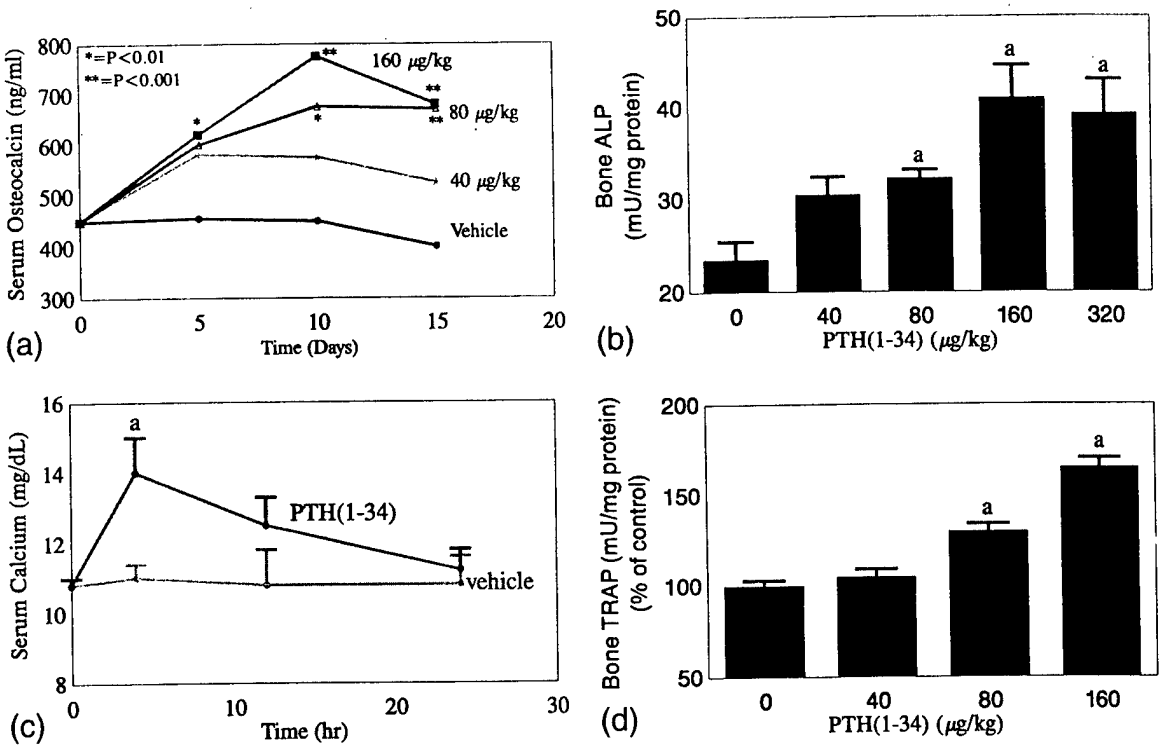

Figure 1. (a) Dose and time effects of PTH(1-34) on serum osteocalcin levels in mice. Swiss/Webster mice were injected subcutaneously each day with various doses (40, 80, and 160 μg/kg) of PTH subcutaneously. Vehicle (PBS) was used as a control. At 5, 10, and 15 days, one group (n = 9) of mice for each dose was killed and blood samples were collected for osteocalcin measurements. One group was killed at the beginning of the experiment for use as a baseline group. $*p < 0.01$ vs. baseline; $**p < 0.001$ vs. baseline. (b) Effect of PTH(1-34) treatment on ALP activity in the femoral bone extract of mice. Swiss/Webster mice (n = 8) were treated with various doses (40, 80, 160, and 320 μg/kg) of PTH for 15 days. ALP activity was extracted from the femurs with 0.1% Triton X-100 and used for measurement of ALP activity. $^{a}p < 0.01$ vs. vehicle-treated control group. (c) Effect of PTH(1-34) treatment on serum calcium levels in mice. Mice were treated with PTH (320 μg/kg) or vehicle. At 4, 12, and 24 h (n = 6) after treatment, animals were killed and blood was collected and used for calcium measurements. $^{a}p < 0.01$ vs. baseline; (d) Effect of PTH(1-34) treatment on TRAP activity in the femoral bone extract of mice. Mice were treated for 10 days with daily subcutaneous injections of vehicle or with various doses (40, 80, and 160 μg/kg) of PTH (n = 6) prior to determination of TRAP activity in the skeletal extracts. $^{a}p < 0.01$ vs. vehicle group.

bone ALP activity. PTH(2-34) at 800 μg/kg caused significant increases in serum osteocalcin and bone ALP activity compared with control (**Figure 2**a). These data suggest that cAMP activity may be essential for the bone forming effects of PTH in mice.

To investigate the role of PKC in the bone forming effects of PTH, mice were injected with various doses (40, 80, or 160 μg/kg) of PTH(1-31) daily for 10 days prior to serum osteocalcin and bone ALP determinations. Figure 2b shows that PTH(1-31) increased serum osteocalcin and bone ALP activity in a dose-dependent manner. Comparison of dose effects of PTH(1-34) and PTH(1-31) on serum osteocalcin and bone ALP activity revealed no significant difference between the two treatment groups (Figures 1a, 1b, and 2b).

To evaluate the role of PKA- and PKC-signaling pathways on the bone resorbing effects of PTH, mice were treated with either PBS or PTH(1-34), PTH(2-34), or PTH(1-31) at various doses (40–800 μg/kg) and used for biochemical measurements of bone resorption at 4 h after injection. All three analogs increased serum calcium at high doses (Figure 2c). PTH(1-34) was much more potent than PTH(1-31) or PTH(2-34) in increasing serum calcium levels. Consistent with these data we found that PTH(1-34) was more potent than the other two analogs in increasing TRAP activity in the femoral bone extracts. Figure 2d shows that PTH(1-34) at 320 μg/kg increased TRAP activity to 265% of control, whereas PTH(1-31) and PTH(2-34) at 320 and 400 μg/kg, respectively, increased TRAP activity to 146% of control. In contrast to TRAP activity, ALP activity was not different in any of the treatment groups at 4 h after a single injection.

Long-term Effects of PTH(1-34) and PTH(1-31) in Mice

To examine if the bone forming effect of PTH persists over a long period of time, mice were treated daily with vehicle, PTH(1-34), or PTH(1-31) at a dose of 80 μg/kg for 22 weeks. Blood samples were collected weekly through tail bleeding and used for serum osteocalcin determinations. Both PTH(1-34) and PTH(1-31) increased serum osteocalcin levels to a maximum within 2 weeks of the start of treatment (**Figure 3**a). The increases in serum osteocalcin levels were maintained during the entire treatment period. There was no significant difference in the serum osteocalcin level between the PTH(1-34) and PTH(1-31) groups. In contrast to serum osteocalcin, serum C-telopeptide level was increased significantly at the end of the experimental period in PTH(1-34)-treated, but not PTH(1-31)-treated, mice compared to vehicle-treated control mice (Figure 3b). These data suggest that long-term treatment with PTH does not induce resistance in mice.

PTH(1-34) and PTH(1-31) treatments increased dry weight of the femur by 22% and 16%, respectively, compared to the vehicle-treated group (**Table 1**). Femur length was not significantly different between the treatment groups. Total bone density at the middiaphysis was increased by 18%, in the PTH(1-34)-

Bone Vol. 27, No. 4
October 2000:471–478

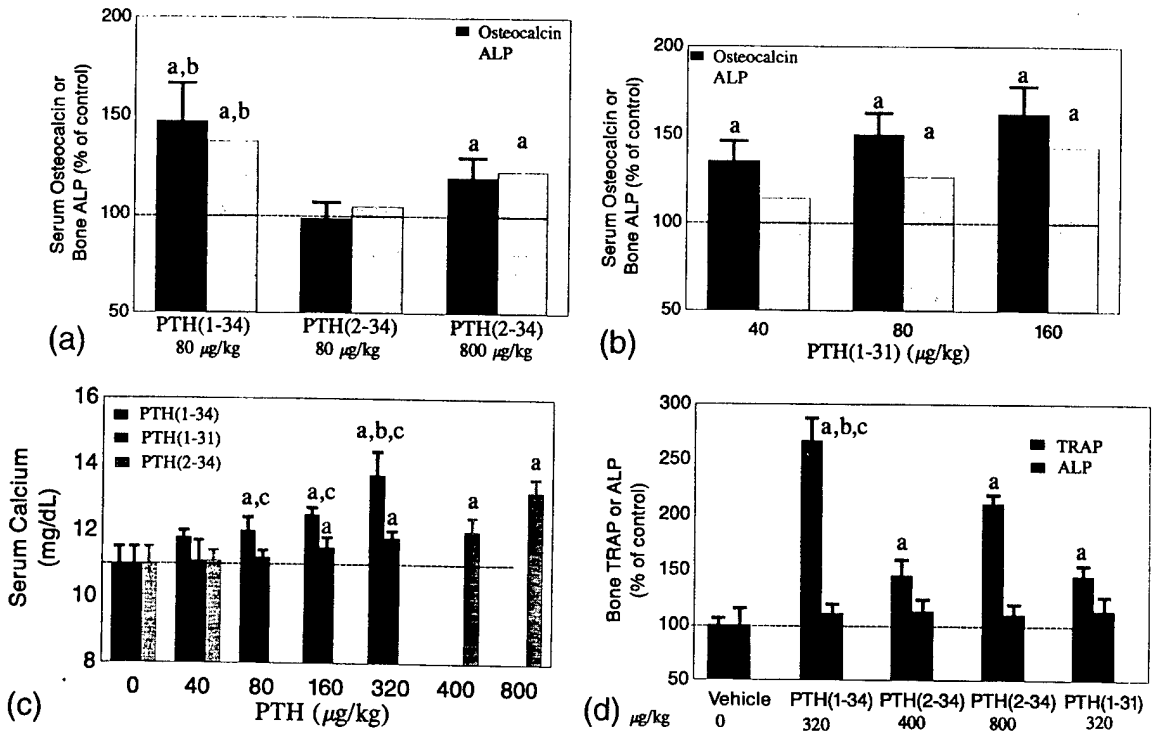

Figure 2. (a) Effect of PTH(2-34) on serum osteocalcin and ALP activity in the femoral bone extract of mice. Mice were injected with two different doses (80 and 800 μg/kg) of PTH(2-34), an analog with reduced cAMP activity. PBS and PTH(1-34) were used as controls (n = 6). At day 10, serum osteocalcin and bone ALP activity were measured. [a]$p < 0.01$ vs. vehicle group; [b]$p < 0.01$ vs. PTH(2-34) at a similar dose. (b) Effect of PTH(1-31) on serum osteocalcin and ALP activity in the femoral bone extract of mice. Mice were injected with various doses (40, 80, and 160 μg/kg) of PTH(1-31) daily for 10 days prior to serum osteocalcin and bone ALP determinations (n = 6). [a]$p < 0.01$ vs. vehicle group. (c) Effect of PTH analogs on serum calcium levels in mice. Mice were treated with either PBS or PTH(1-34), PTH(2-34), or PTH(1-31) at the doses indicated (n = 6). Four hours after injection, mice were killed and serum samples were used for calcium determinations. [a]$p < 0.01$ vs. vehicle group; [b]$p < 0.01$ vs. 400 μg/kg PTH(2-34); [c]$p < 0.01$ vs. similar dose of PTH(1-31). (d) Effect of PTH analogs on TRAP activity in the femoral bone extract of mice. Four hours after injection with PTH at doses indicated, or vehicle, mice were killed and femurs removed and used for determination of TRAP activity (n = 6). [a]$p < 0.01$ vs. vehicle group; [b]$p < 0.01$ vs. a similar dose of PTH(2-34); [c]$p < 0.01$ vs. a similar dose of PTH(1-31).

treated group and by 9% in the PTH(1-31) treated group, over vehicle-treated control mice (Figure 3c). Consistent with these data, total bone mineral content at the middiaphysis was increased by 41% with PTH(1-34) and 26% with PTH(1-31) administration, respectively, over the vehicle-treated group. The PTH(1-34)-induced increase in bone density and bone mineral content at middiaphysis was significantly greater than that induced by PTH(1-31) (Figure 3c and Table 1). Trabecular bone density at the distal metaphysis was increased by 39% with PTH(1-34) and 27% with PTH(1-31) treatment, respectively, compared to the vehicle group (Table 1).

Periosteal and endosteal circumference measurements by pQCT revealed that cortical thickness was increased by 25% with PTH(1-34) and by 13% with PTH(1-31) treatment, respectively (Figure 3d). Both PTH(1-34) and PTH(1-31) increased periosteal circumference and decreased endosteal circumference compared to the vehicle-treated group. Although there was no difference in the increase in periosteal circumference between PTH(1-34) and PTH(1-31), the reduction in endosteal circumference was significantly greater in the PTH(1-34) group compared to the PTH(1-31) group (Figure 3d). These data suggest that the greater increase in bone density in the PTH(1-34) group compared to the PTH(1-31) group may be due to a greater increase in cortical thickness in the PTH(1-34) group compared to the PTH(1-31) group.

PTH(1-34) and PTH(1-31) Effects on Mechanical Strength

Treatment with PTH(1-34) and PTH(1-31) caused a 46% and 37% increase in load-bearing capacity, respectively, compared to the vehicle-treated group (**Table 2**). Although both load-bearing capacity and area of moment of inertia were 7% and 10% higher, respectively, in the PTH(1-34) group compared to the PTH(1-31) group, these values were not statistically significant compared to the PTH(1-31) group. Neither analog had any significant effect on maximal stress or elastic modulus compared to the vehicle-treated group. In the pooled data from three groups, breaking strength of bone correlated positively with periosteal circumference ($r = 0.91$, $p < 0.001$). The correlation between breaking strength of bone and endosteal circumference, however, was not significant ($r = -0.33$). As expected, breaking strength of bone correlated positively with bone density ($r = 0.46$, $p < 0.01$) and serum osteocalcin level ($r = 0.65$, $p < 0.01$). In addition, serum C-telopeptide level correlated positively with endosteal circumference ($r = 0.70$, $p < 0.01$) in the pooled data from all three groups. The correlation between serum C-telopeptide and breaking strength of bone, however, was not significant ($r = -0.18$).

Discussion

The findings of this study using PTH(1-34) and aminoterminal- and carboxyterminal-truncated PTH analogs suggest that PTH

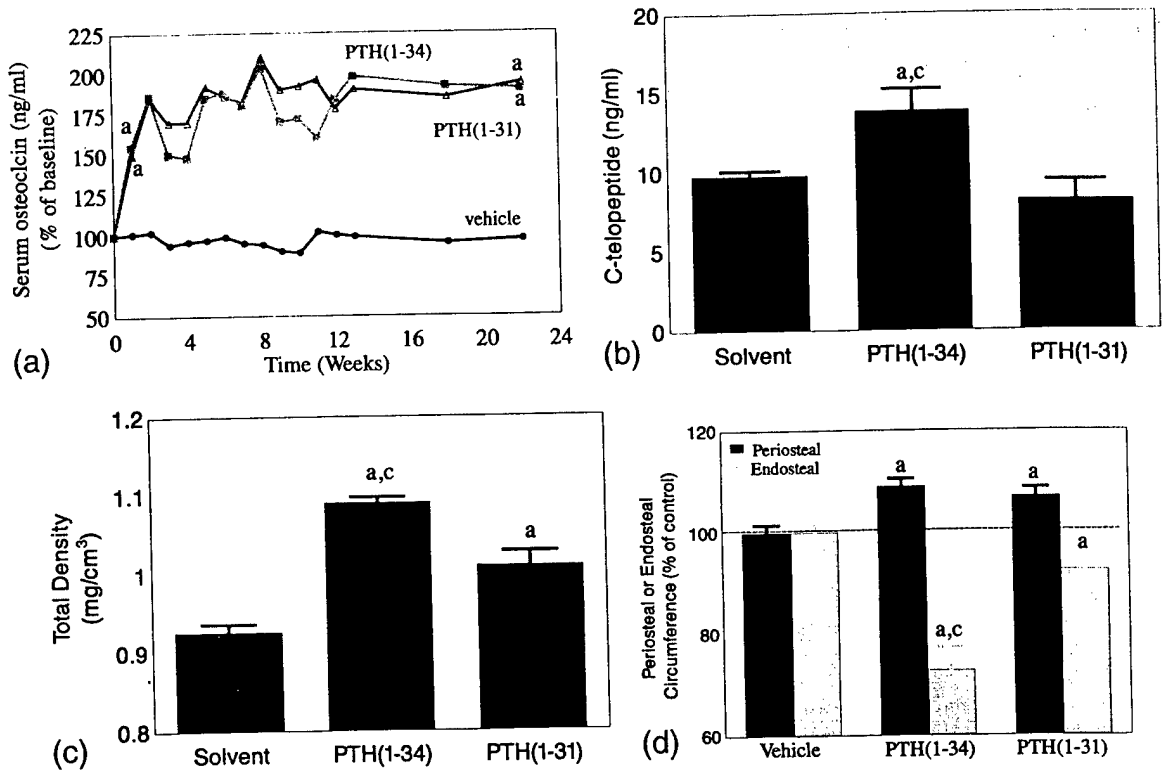

Figure 3. (a) Effect of long-term PTH treatment on serum osteocalcin levels. To examine if the bone forming effect of PTH persists over a long period of time, mice were treated daily with vehicle, 80 μg/kg PTH(1-34), or 80 μg/kg PTH(1-31) for 22 weeks (n = 7 or 8). Blood samples were collected weekly through tail bleeding and used for serum osteocalcin determinations. The values are expressed as percent of baseline. $^{a}p < 0.01$ vs. vehicle. (b) Effect of long-term PTH treatment on serum C-telopeptide levels. The mice were treated with vehicle, 80 μg/kg PTH(1-34), or 80 μg/kg PTH(1-31) for 22 weeks as described in (a), and serum was collected at the end of the experiment and used for C-telopeptide measurements (n = 7). To evaluate the effect of PTH(1-34) and PTH(1-31) on bone resorption, we measured C-telopeptide levels in serum samples collected after 22 weeks of treatment at the end of the study (n = 7). $^{a}p < 0.01$ vs. vehicle; $^{c}p < 0.01$ vs. PTH(1-31). (c) Effect of long-term PTH treatment on bone density in mice. Mice were treated with vehicle, 80 μg/kg PTH(1-34), or 80 μg/kg PTH(1-31) for 22 weeks, as described in (a), and the femur was excised and used for bone density measurements by pQCT (n = 7). $^{a}p < 0.01$ vs. vehicle; $^{c}p < 0.01$ vs. PTH(1-31). (d) Long-term effect of PTH treatment on periosteal and endosteal circumference in the femoral bone of mice. Mice were treated with vehicle, 80 μg/kg PTH(1-34), or 80 μg/kg PTH(1-31) for 22 weeks, as described in (a), and used for periosteal and endosteal circumference measurements by pQCT (n = 7). The periosteal and endosteal circumferences for vehicle-treated mice at the end of the treatment period were 4.99 ± 0.08 mm and 1.58 ± 0.03 mm, respectively. $^{a}p < 0.01$ vs. vehicle; $^{c}p < 0.01$ vs. PTH(1-31).

analogs exhibit different effects at the periosteum and endosteum of middiaphysis of long bones in the mouse model. Although PTH(1-34) and PTH(1-31) caused similar increases in periosteal circumference, PTH(1-34) caused a significantly greater reduction in endosteal circumference than PTH(1-31). Consistent with the differential effects of these two analogs on cortical thickness, PTH(1-34) caused a significantly greater increase in BMD than PTH(1-31). Both PTH(1-34) and PTH(1-31) treatment significantly increased mechanical strength in the femur of mice. Our data on the anabolic effects of PTH(1-34) in mice are consistent with a recent report by Jilka et al.,[18] which demonstrated that daily subcutaneous administration of PTH(1-34) over a 4 week period increased BMD in adult mice with normal bone mass or in mice with osteopenia. Our observations on the middiaphyseal site of the femur indicate cortical bone is not being lost, but rather is increasing, at this site. This argues against the possibility

Table 1. Effect of parathyroid hormone (PTH) treatment on various parameters in the femur of mice

	Control	PTH(1-34)	PTH(1-31)
Dry weight (mg)	63.7 ± 2.3	77.5 ± 2.8[c]	73.9 ± 2.3[c]
Length (mm)	16.0 ± 0.16	15.7 ± 0.18	15.9 ± 0.16
Cortical thickness[a] (mm)	0.56 ± 0.025	0.70 ± 0.035[c,d]	0.63 ± 0.026[a]
Total mineral content[a] (mg/slice)	1.94 ± 0.07	2.73 ± 0.009[c,d]	2.44 ± 0.11[c]
Total density[a] (mg/cm²)	926 ± 10	1090 ± 7[c,d]	1010 ± 18[c]
Trabecular density[b] (mg/cm²)	242 ± 18	336 ± 15[c]	307 ± 13[c]

[a]Measurement at middiaphysis of femur.
[b]Measurement at distal metaphysis of femur.
[c]$p < 0.01$ vs. control.
[d]$p < 0.01$ vs. PTH(1-31).

Bone Vol. 27, No. 4
October 2000:471–478

Table 2. Effects of long-term treatment of mice with two parathyroid hormone fragments [PTH(1-34) and PTH(1-31)] on mechanical strength parameters in the femur of mice

Group	Maximum load (N)	Area moment of inertia (mm^4)	Maximal stress (MPa)	Elastic modulus (GPa)
Control	46.7 ± 3.0	0.34 ± 0.021	191.1 ± 6.0	5.63 ± 0.3
PTH(1-34)	68.6 ± 2.9[a]	0.52 ± 0.019[a]	204.0 ± 9.0	6.06 ± 0.041
PTH(1-31)	63.9 ± 3.9[a]	0.47 ± 0.026[a]	205.6 ± 5.2	6.18 ± 0.15

[a] $p < 0.01$ vs. control (n = 7 per group).

that the increase in trabecular bone is associated with a loss of cortical bone, although further studies of other sites are needed to establish that bone loss is not occurring in other locations.

Long-term treatment of mice with either PTH(1-34) or PTH(1-31) increased periosteal circumference to a similar extent over vehicle-treated control mice. Based on the findings that both of these PTH analogs increased biochemical markers of bone formation in serum and bone extracts similarly, we speculate that the effect of PTH to increase periosteal circumference is mediated via increased periosteal bone formation. In addition, both PTH(1-34) and PTH(1-31) significantly decreased endosteal circumference compared to the control group. An increase in bone formation and/or decrease in bone resorption could mediate the decrease in endosteal circumference by these two analogs. Based on the findings that PTH(1-34) treatment significantly increased the bone formation rate at both the periosteum and endosteum in the femoral middiaphysis of rats,[33,37,42] we speculate that the PTH-induced increase in bone formation at the endosteum may, in part, contribute to the decreased marrow cavity in PTH-treated mice. In contrast to the similar potency of the PTH(1-34) and PTH(1-31) analogs at the periosteum, PTH(1-31) was found to be less effective than PTH(1-34) in decreasing endosteal circumference. The differential effects of PTH(1-34) and PTH(1-31) at the endosteum is not specific to mice, because previous studies by Rixon et al.[37] have shown that daily injections of PTH(1-31) stimulated bone growth less effectively than PTH(1-34) in ovariectomized rats, but it stimulated cortical bone growth as rapidly and as dramatically as PTH(1-34). Thus, the effects of PTH(1-34) and PTH(1-31) appear to be site-specific in both mice and rats.

In this study, treatment of mice with PTH(1-34) and PTH(1-31) caused similar increases in bone formation parameters (i.e., serum osteocalcin and bone alkaline phosphatase activity), whereas PTH(2-34) was much less active. These data are consistent with previous studies in rats, which demonstrated that PKA activity is crucial for bone forming effects of PTH.[5,20,21] In contrast to the similar potencies of PTH(1-34) and PTH(1-31) to increase bone formation parameters, PTH(1-31) treatment caused a much smaller increase in bone resorption as measured by serum calcium level and TRAP activity in bone extract. Consistent with our findings, Fraher et al.[10] recently showed that daily infusion of PTH(1-34) for 10 days in 10 healthy individuals caused significant increase in bone resorption as measured by changes in serum-ionized calcium and urinary aminoterminal telopeptides of type I collagen (NTx). On the contrary, PTH(1-31) infusion was an ineffective stimulator of bone resorption as indicated by a failure to increase the blood calcium and urinary NTx, although PTH(1-31) was as effective as PTH(1-34) in increasing plasma and urinary cAMP levels. Because PTH can regulate serum calcium by acting on kidney and intestine in addition to bone,[7,11] further studies are needed to evaluate whether the lack of increase in serum calcium by PTH(1-31) is caused by its inability to increase bone resorption and/or calcium uptake by intestine and kidney. PTH(2-34) was also found to be much less potent than PTH(1-34) in stimulating bone resorption parameters. These data suggest that the bone resorbing effect of PTH may require both aminoterminal and carboxyterminal regions of PTH(1-34).

Because PTH(1-31) increased bone formation parameters to a level similar to that of PTH(1-34), and because PTH(1-31) caused a much smaller increase in TRAP activity compared to PTH(1-34), we anticipated PTH(1-31) to increase bone density to a greater extent than PTH(1-34). On the contrary, we found that PTH(1-31) caused a smaller increase in bone density compared to PTH(1-34). We have no experimental data to explain why PTH(1-31) is less anabolic than PTH(1-34), although both of these analogs increased bone formation markers to a similar extent. There are several potential explanations for this discrepancy: (1) Activation of PKC and PLC by PTH(1-34) and PTH(1-31) have not been tested in target cells from the mouse; therefore, it is possible that the mouse PTH receptor at the periosteum and endosteum of long bones of mice might respond differently to these analogs than the receptor from other species. (2) The differences in the anabolic activity of PTH(1-34) and PTH(1-31) analogs may be related to the differences in the pharmacokinetic properties or potencies of these two analogs in the mouse rather than the differences in their ability to activate signaling pathways. (3) Based on the findings that PTH(1-34), but not PTH(1-31), caused an increase in bone resorption at the dose used in long-term in vivo studies, and that PTH(1-34) produced a greater reduction in endosteal circumference than PTH(1-31), it is possible that the bone resorbing activity of PTH at the endosteum may be required for PTH-mediated decreases in endosteal circumference in mice. Although the mechanism by which PTH(1-34) and PTH(1-31) elicit different responses at the endosteum cannot be ascertained, these data are consistent with a number of previous studies demonstrating that the magnitude of anabolic response to PTH may vary at different sites within the skeleton.[23,24,27,30,31,40]

The effect of PTH on bone formation may involve direct action of PTH on osteoblast line cells or indirect action via modulation of local growth factor production. Based on the finding that PTH treatment causes an acute increase in several potential second messenger signaling molecules, such as c-*fos*, MAPK, and cyclin-dependent kinase, which are implicated in cell proliferation, it has been proposed that the effects of PTH on osteoblasts are direct.[9,14,22,32,47] Recent findings by Jilka et al.[18] have also indicated that prevention of osteoblast apoptosis is a crucial mechanism for the anabolic effects of PTH on bone. In addition to the direct effects of PTH, it has been shown that PTH treatment increases production of insulin-like growth factor-I (IGF-I) in rat and mouse osteoblasts in vitro,[25,28,48] and rat osteoblasts in vivo.[49] Although studies by Gunness and Hock[15] demonstrated that PTH treatment increases bone formation in hypophysectomized rats, suggesting that growth hormone is not essential for anabolic effects of PTH, the implications whether or not the effects of PTH on bone formation require local IGF production by osteoblasts requires further study. In any case, based on past findings that PTH actions are complex and involve both direct and indirect actions on osteoblasts, it is possible to speculate that different receptors or signaling molecules could mediate the differential effects of PTH at the periosteum vs. endosteum. Further studies are needed to evaluate if the observed site-specific effects of PTH(1-34) and PTH(1-31) also occur at other skeletal sites as well as in other animal models.

The findings of this study also demonstrated that PTH treatment causes a significant increase in mechanical strength of the bones without altering the quality of the bone in mice. The effect of PTH to increase biomechanical competence of the cortical bone is consistent with previous reports using

rats.[8,23,24,29,31,40,41] Because PTH(1-34) caused a significantly greater increase in bone density (18% vs. 9%) compared to PTH(1-31), we anticipated PTH(1-34) treatment to produce a greater increase in mechanical strength than PTH(1-31). We found that, although PTH(1-34)-induced increases in load-bearing capacity and area of moment of inertia were higher than that those found using PTH(1-31), these results were not significant. In this regard, the lack of difference in bone strength between PTH(1-34) and PTH(1-31) could be due to similar increases in periosteal circumference, which appears to be the major determinant of bone strength. Further studies are also needed to evaluate if these two analogs caused a similar increase in trabecular number and thickness, which could have contributed to similar changes in mechanical strength.

In conclusion, our findings demonstrate that: (1) PTH(1-31) was as potent as PTH(1-34), whereas PTH(2-34) was less potent in stimulating bone formation parameters in mice; and (2) both PTH(1-31) and PTH(2-34) were less potent than PTH(1-34) in stimulating bone resorption parameters in mice. Although both PTH(1-34) and PTH(1-31) caused similar increases in periosteal circumference and mechanical strength, PTH(1-34) was more effective than PTH(1-31) in increasing bone density and decreasing endosteal circumference. Future studies are needed to determine whether PTH increases bone formation at the periosteum and endosteum in mice via similar or different molecular mechanisms.

Acknowledgments: The authors acknowledge the technical assistance provided by Daniel Bruch and Joe Rung-Aroon, as well as the secretarial assistance provided by Joyce Ciechanowski. This work was supported by funds from the NIH (AR31062 and AR07543), the Veterans Administration, and Loma Linda University.

References

1. Armamento-Villareal, R., Ziambaras, K., Abbasi-Jarhomi, S. H., Dimarogonas, A., Halstead, L., Fausto, A., Avioli, L. V., and Civitelli, R. An intact N terminus is required for the anabolic action of parathyroid hormone on adult female rats. J Bone Miner Res 12:384–392; 1997.
2. Baylink, D. J., Strong, D. D., and Mohan, S. The diagnosis and treatment of osteoporosis: Future prospects. Mol Med Today 5:133–140; 1999.
3. Beamer, W. G., Donahue, L. R., Rosen, C. J., and Baylink, D. J. Genetic variability in adult bone density among inbred strains of mice. Bone 18:397–403; 1996.
4. Chapoteau, E., Czech, B. P., Zazulak, W., and Kumar, A. New reagent for colorimetric assay of calcium in serum. Clin Chem 39:1820–1824; 1993.
5. Cole, J. A., Carnes, D. L., Forte, L. R., Eber, S., Poelling, R. E., and Thorne, P. K. Structure-activity relationships of parathyroid hormone analogs in the opossum kidney cell line. J Bone Miner Res 4:723–730; 1989.
6. Dimai, H. P., Hall, S. L., Stilt-Coffing, B., and Farley, J. R. Skeletal response to dietary zinc in adult female mice. Calcif Tissue Int 62:309–315; 1998.
7. Dobnig, H. and Turner, R. T. The effects of programmed administration of human parathyroid hormone fragment (1-34) on bone histomorphometry and serum chemistry in rats. Endocrinology 138:4607–4612; 1997.
8. Ejersted, C., Andreassen, T. T., Nilsson, M. H. L., and Oxlund, H. Human parathyroid hormone(1-34) increases bone formation and strength of cortical bone in aged rats. Eur J Endocrinol 130:201–207; 1994.
9. Evans, D. B., Hipskind, R. A., and Bilbe, G. Analysis of signaling pathways used by parathyroid hormone to activate the c-fos gene in human SaOS-2 osteoblast-like cells. J Bone Miner Res 11:1066–1074; 1996.
10. Fraher, L. J., Avram, R., Watson, P. H., Hendy, G. N., Henderson, J. E., Chong, K. L., Goltzman, D., Morley, P., Willick, G. E., Whitfield, J. F., and Hodsman, A. B. Comparison of the biochemical responses to human parathyroid hormone-(1-31)NH_2 and hPTH-(1-34) in healthy humans. J Clin Endocrinol Metab 84:2739–2743; 1999.
11. Friedman, P. A., Coutermarsh, B. A., Kennedy, S. M., and Gesek, F. A. Parathyroid hormone stimulation of calcium transport is mediated by dual signaling mechanisms involving protein kinase A and protein kinase C. Endocrinology 137:13–20; 1996.
12. Friedman, P. A., Gesek, F. A., Morley, P., Whitfield, J. F., and Willick, G. E. Cell-specific signaling and structure-activity relations of parathyroid hormone analogs in mouse kidney cells. Endocrinology 140:301–309; 1999.
13. Fujimori, A., Cheng, S. L., Avioli, L. V., and Civitelli, R. Structure-function relationship of parathyroid hormone: Activation of phospholipase-C, protein kinase-A and -C in osteosarcoma cells. Endocrinology 130:29–36; 1992.
14. Goltzman, D. Interactions of PTH and PTHrP with the PTH/PTHrP receptor and with downstream signaling pathways: Exceptions that provide the rules. J Bone Miner Res 14:173–177; 1999.
15. Gunness, M. and Hock, J. M. Anabolic effect of parathryoid hormone is not modified by supplementation with insulin-like growth factor I (IGF-I) or growth hormone in aged female rats fed an energy-restricted or ad libitum diet. Bone 16:199–207; 1995.
16. Hilliker, S., Wergedal, J. E., Gruber, H. E., Bettica, P., and Baylink, D. J. Truncation of the amino terminus of PTH alters its anabolic activity on bone in vivo. Bone 19:469–477; 1996.
17. Jamsa, T., Jalovaara, P., Peng, Z., Vaananen, K., and Tuukkanen, J. Comparison of three-point bending test and peripheral quantitative computed tomography analysis in the evaluation of the strength of mouse femur and tibia. Bone 23:155–161; 1998.
18. Jilka, R. L., Weinstein, R. S., Bellido, T., Roberson, P., Parfitt, A. M., and Manolagas, S. C. Increased bone formation by prevention of osteoblast apoptosis with parathyroid hormone [see comments]. J Clin Invest 104:439–446; 1999.
19. Jouishomme, H., Whitfield, J. F., Gagnon, L., MacLean, S., Isaacs, R., Chakravarthy, B., Durkin, J., Neugebauer, W., Willick, G., and Rixon, R. H. Further definition of the protein kinase C activation domain of the parathyroid hormone. J Bone Miner Res 9:943–949; 1994.
20. Kronenberg, H. M., Lanske, B., Kovacs, C. S., Chung, U. I., Lee, K., Segre, G. V., Schipani, E., and Juppner, H. Functional analysis of the PTH/PTHrP network or ligands and receptors. Recent Progr Horm Res 53:283–301; 1998.
21. Lane, N. E., Kimmel, D. B., Nilsson, M. H. L., Cohen, F. E., Newton, S., Nissenson, R. A., and Strewler, G. J. Bone-selective analogs of human PTH(1-34) increase bone formation in an ovariectomized rat model. J Bone Miner Res 11:614–625; 1996.
22. Lee, K., Deeds, J. D., Chiba, S., Un-No, M., Bond, A. T., and Segre, G. V. Parathyroid hormone induces sequential c-fos expression in bone cells in vivo: In situ localization of its receptor and c-fos messenger ribonucleic acids. Endocrinology 134:441–450; 1994.
23. Li, M., Liang, H., Shen, Y., and Wronski, T. J. Parathyroid hormone stimulates cancellous bone formation at skeletal sites regardless of marrow composition in ovariectomized rats. Bone 24:95–100; 1999.
24. Li, M., Mosekilde, L., Sogaard, C. H., Thomsen, J. S., and Wronski, T. J. Parathyroid hormone monotherapy and cotherapy with antiresorptive agents restore vertebral bone mass and strength in aged ovariectomized rats. Bone 16:629–635; 1995.
25. Linkhart, T. A. and Mohan, S. Parathyroid hormone stimulates release of insulin-like growth factor-I (IGF-I) and IGF-II from neonatal mouse calvaria in organ culture. Endocrinology 125:1484–1491; 1989.
26. Ma, Y., Jee, W. S., Chen, Y., Gasser, J., Ke, H. Z., Li, X. J., and Kimmel, D. B. Partial maintenance of extra cancellous bone mass by antiresorptive agents after discontinuation of human parathyroid hormone (1-38) in right hindlimb immobilized rats. J Bone Miner Res 10:1726–1734; 1995.
27. Ma, Y. F., Ferretti, J. L., Capozza, R. F., Cointry, G., Alippi, R., Zanchetta, J., and Jee, W. S. Effects of on/off anabolic hPTH and remodeling inhibitors on metaphyseal bone of immobilized rat femurs. Tomographical (pQCT) description and correlation with histomorphometric changes in tibial cancellous bone. Bone 17(Suppl.):321S–327S; 1995.
28. McCarthy, T. L., Centrella, M., and Canalis, E. Parathyroid hormone enhances the transcript and polypeptide levels of insulin-like growth factor I in osteoblast-enriched cultures from fetal rat bone. Endocrinology 124:1247–1253; 1989.
29. Mosekilde, L., Danielsen, C. C., and Gasser, J. The effect of vertebral bone mass and strength of long term treatment with antiresorptive agents (estrogen and calcitonin), human parathyroid hormone-(1-38), and combination therapy, assessed in aged ovariectomized rats. Endocrinology 134:2126–2134; 1994.
30. Mosekilde, L., Danielsen, C. C., Sogaard, C. H., McOsker, J. E., and Wronski, T. J. The anabolic effects of parathyroid hormone on cortical bone mass, dimensions and strength—assessed in a sexually mature, ovariectomized rat model. Bone 16:223–230; 1995.
31. Mosekilde, L., Thomsen, J. S., and McOsker, J. E. No loss of biomechanical

Bone Vol. 27, No. 4
October 2000:471–478

effects after withdrawal of short-term PTH treatment in an aged, osteopenic, ovariectomized rat model. Bone 20:429–437; 1997.

32. Onishi, T., Zhang, W., Cao, X., and Hruska, K. The mitogenic effect of parathyroid hormone is associated with E_2F-dependent activation of cyclin-dependent kinase 1 (cdc2) in osteoblast precursors. J Bone Miner Res 12:1596–1605; 1997.
33. Oxlund, H., Ejersted, C., Andreassen, T. T., Torring, O., and Nilsson, M. H. L. Parathyroid hormone (1-34) and (1-84) stimulate cortical bone formation both from periosteum and endosteum. Calcif Tissue Int 53:394–399; 1993.
34. Qi, H., Li, M., and Wronski, T. J. A comparison of the anabolic effects of parathyroid hormone at skeletal sites with moderate and severe osteopenia in aged ovariectomized rats. J Bone Miner Res 10:948–955; 1995.
35. Raisz, L. G. Osteoporosis: Current approaches and future prospects in diagnosis, pathogenesis, and management. J Bone Miner Metab 17:79–89; 1999.
36. Richman, C., Baylink, D. J., Lang, K., Dony, C., and Mohan, S. Recombinant human insulin-like growth factor binding protein-5 (rhIGFBP-5) stimulates bone formation parameters in vitro and in vivo. Endocrinology. 140:4699–4705; 1999.
37. Rixon, R. H., Whitfield, J. F., Gagnon, L., Isaacs, R. J., MacLean, S., Chakravarthy, B., Durkin, J. P., Neugebauer, W., Ross, V., Sung, W., and Willick, G. E. Parathyroid hormone fragments may stimulate bone growth in ovariectomized rats by activating adenylyl cyclase. J Bone Miner Res 9:1179–1189; 1994.
38. Rosen, C. J., Dimai, H. P., Vereault, D., Donahue, L. R., Beamer, W. G., Farley, J., Linkhart, S., Linkhart, T., Mohan, S., and Baylink, D. J. Circulating and skeletal insulin-like growth factor-I (IGF-I) concentrations in two inbred strains of mice with different bone mineral densities. Bone 21:217–223; 1997.
39. Sabatini, M., Lesur, C., Pacherie, M., Pastoureau, P., Kucharczyk, N., Fauchere, J.-L., and Bonnet, J. Effects of parathyroid hormone and agonists of the adenylyl cyclase and protein kinase C pathways on bone cell proliferation. Bone 18:59–65; 1996.
40. Sato, M., Zeng, G. Q., and Turner, C. H. Biosynthetic human parathyroid hormone (1-34) effects on bone quality in aged ovariectomized rats. Endocrinology 138:4330–4337; 1997.
41. Shen, V., Birchman, R., Liang, X. G., Wu, D. D., Dempster, D. W., and Lindsay, R. Accretion of bone mass and strength with parathyroid hormone prior to the onset of estrogen deficiency can provide temporary beneficial effects in skeletally mature rats. J Bone Miner Res 13:883–890; 1998.
42. Shen, V., Dempster, D. W., Birchman, R., Xu, R., and Lindsay, R. Loss of cancellous bone mass and connectivity in ovariectomized rats can be restored by combined treatment with parathyroid hormone and estradiol. J Clin Invest 91:2479–2487; 1993.
43. Srivastava, A. K., Bhattacharyya, S., Castillo, G., Miyakoshi, N. Mohan, S., and Baylink, D. J. Development and evaluation of a c-telopeptide ELISA for measurement of bone resorption in mouse serum. Bone 27:529–533; 2000.
44. Takasu, H. and Bringhurst, F. R. Type-1 parathyroid hormone (PTH)/PTH-related peptide (PTHrP) receptors activate phospholipase C in response to carboxyl-truncated analogs of PTH(1-34). Endocrinology 139:4293–4299; 1998.
45. Takasu, H., Gardella, T. J., Luck, M. D., Potts, J. T., Jr., and Bringhurst, F. R. Amino-terminal modifications of human parathyroid hormone (PTH) selectively alter phospholipase C signaling via the type 1 PTH receptor: Implications for design of signal-specific PTH ligands. Biochemistry 38:13453–13460; 1999.
46. Takasu, H., Guo, J., and Bringhurst, F. R. Dual signaling and ligand selectivity of the human PTH/PTHrP receptor. J Bone Miner Res 14:11–20; 1999.
47. Tyson, D. R., Swarthout, J. T., and Partridge, N. C. Increased osteoblastic c-fos expression by parathyroid hormone requires protein kinase A phosphorylation of the cyclic adenosine 3′,5′-monophosphate response element-binding protein at serine 133. Endocrinology 140:1255–1261; 1999.
48. Verheijen, M. H. G. and Defize, L. H. K. Parathyroid hormone inhibits mitogen-activated protein kinase activation in osteosarcoma cells via a protein kinase A-dependent pathway. Endocrinology 136:3331–3337; 1995.
49. Watson, P., Lazowski, D., Han, V., Fraher, L., Steer, B., and Hodsman, A. Parathyroid hormone restores bone mass and enhances osteoblast insulin-like growth factor I gene expression in ovariectomized rats. Bone 16:357–365; 1995.
50. Whitfield, J. F. and Morley, P. Small bone-building fragments of parathyroid hormone: New therapeutic agents for osteoporosis. Trends Pharmacol Sci 16:382–386; 1995.
51. Whitfield, J. F., Morley, P., Willick, G., MacLean, S., Ross, V., Isaacs, R. J., and Barbier, J.-R. Comparison of the abilities of human parathyroid hormone (hPTH)-(1-34) and [Leu27]-cyclo(Glu22-Lys26)-hPTH-(1-31)NH_2 to stimulate femoral trabecular bone growth in ovariectomized rats. Calcif Tissue Int 63:423–428; 1998.
52. Wronski, T. J., Pun, S., and Liang, H. Effects of age, estrogen depletion, and parathyroid hormone treatment on vertebral cancellous wall width in female rats. Bone 25:465–468; 1999.

Date Received: November 19, 1999
Date Revised: March 6, 2000
Date Accepted: May 25, 2000

JOURNAL OF BONE AND MINERAL RESEARCH
Volume 16, Number 2, 2001

Variation in Bone Biomechanical Properties, Microstructure, and Density in BXH Recombinant Inbred Mice

CHARLES H. TURNER,[1] YEOU-FANG HSIEH,[1] RALPH MÜLLER,[2] MARY L. BOUXSEIN,[2] CLIFFORD J. ROSEN,[3] MARGARET E. McCRANN,[4] LEAH RAE DONAHUE,[4] and WESLEY G. BEAMER[4]

ABSTRACT

To test the hypothesis that factors associated with bone strength (i.e., volumetric bone mineral density [vBMD], geometry, and microstructure) have heritable components, we exploited the 12 BXH recombinant inbred (RI) strains of mice derived from C57BL/6J (B6; low bone mass) and C3H/HeJ (C3H; high bone mass) progenitor strains. The femurs and lumbar vertebrae from each BXH RI strain were characterized for phenotypes of vBMD, microstructural, biomechanical, and geometrical properties. Methods included bending (femur) and compression (vertebra) testing, peripheral quantitative computed tomography (pQCT), and microcomputed tomography (μCT). Segregation patterns of femoral and vertebral biomechanical properties among the BXH RI strains suggested polygenic regulation. Femoral biomechanical properties were strongly associated with femoral width in the anteroposterior (AP) direction and cortical thickness—geometric properties with complex genetic regulation. Vertebral vBMD and biomechanical properties measured in BXH RI strains showed a greater variability than either B6 or C3H progenitors, suggesting both progenitor strains have independent subsets of genes that yield similar vBMD and strength. The μCT and pQCT data suggested that the distribution of vertebral mineral into cortical and trabecular compartments is regulated genetically. Although the B6 and C3H progenitors had similar vertebral strength, their vertebral structures were markedly different: B6 had good trabecular bone structure and modest cortical bone mineral content (BMC), whereas C3H had high cortical BMC combined with a deficiency in trabecular structure. These structural traits segregated independently in the BXH RI strains. Finally, vertebral strength was not correlated consistently with femoral strength among the BXH RI strains, suggesting genetic regulation of bone strength is site specific. (J Bone Miner Res 2001;16:206–213)

Key words: biomechanics, bone density, osteoporosis, genetics

INTRODUCTION

OSTEOPOROSIS IS primarily a disease of bone fragility resulting from decreased bone mass, altered microarchitecture, and possibly impaired bone quality. Key among the factors contributing to the prevalence of osteoporosis is reduced skeletal density.[1] Studies in twins have determined that approximately 70% of the variability in bone density is genetically based.[2–4] This variation in bone density probably is influenced by multiple genes, which have not yet been identi-

[1]Biomechanics and Biomaterials Research Center, Indiana University, Indianapolis, Indiana, USA.
[2]Orthopedic Biomechanics Laboratory, Beth Israel Deaconess Medical Center and Harvard Medical School, Boston, Massachusetts, USA.
[3]Maine Center for Osteoporosis Research and Education, Bangor, Maine, USA.
[4]The Jackson Laboratory, Bar Harbor, Maine, USA.

fied.[5] Beamer et al.[6] showed a large difference in the femoral volumetric bone mineral density (vBMD) and bone mineral content (BMC) between the inbred mouse strains C3H/HeJ (C3H) and C57BL/6J (B6). Thus, these strains appear to be very good models for the analyses of high and low bone mass, respectively. However, the genetic influence on skeletal bone microstructure and strength in these mice is site specific and complex. For example, C3H mice have thicker femoral cortices and stronger femoral shafts when compared with B6 but are deficient in trabecular bone structure in the proximal femur and lumbar spine.[7] Although C3H mice have significantly stronger femurs compared with B6, their lumbar vertebrae are not stronger, but instead are more brittle,[7] suggesting that the genes contributing to improved femoral strength have no effect or even a negative effect on trabecular bone structure in the spine. These findings led us to hypothesize that multiple genes contribute independently to cortical and trabecular bone microstructures and bone fragility in the C3H and B6 strains.

In the current study, we evaluated the bone microstructure, vBMD, and biomechanical properties of femurs and vertebrae in BXH recombinant inbred (RI) mouse strains. RI strains were created by first crossbreeding two different inbred strains, intercrossing the resulting F1 hybrids and then inbreeding pairs of F2 progeny for 20 subsequent generations.[8] This breeding strategy creates a set of RI strains. The mice within each RI strain are "twins" and thus contain the same genetic alleles, half of these alleles come from each of the two progenitor strains. A set of 12 RI strains (denoted BXH) were previously created from B6 and C3H progenitor strains. Each of the BXH RI strains contains a unique combination of genetic alleles from the B6 and C3H strains that can be phenotyped for genetically based polymorphic traits that differ between the B6 and C3H progenitors. Comparison among strains of the distribution pattern for a quantitative trait can be used to gain chromosomal location of genes responsible for the trait of interest.[9] Originally, RI strains were developed for mapping single genes with major effects; mapping precision rapidly degenerates with increasing genetic complexity of a trait.[10] Nevertheless, such strains can be exploited to discriminate between single versus polygenic inheritance, as well as to gain clues about subsets of regulatory genes and possible locations of major genes.[11]

We hypothesized that factors associated with bone strength (i.e., BMD, geometry, and microstructure) have heritable components. To test this hypothesis, we measured femoral and vertebral bone strength in the 12 BXH RI strains and the progenitor B6 and C3H strains. In addition, we measured femoral and vertebral geometry, vBMD, and trabecular microstructure in the lumbar spine. The resultant phenotypic segregation patterns differed from each other, indicating distinct inheritance patterns and a complexity of genetic regulation for these traits.

MATERIALS AND METHODS

Animal care

The study involved 12 BXH RI strains of mice (n = 7–13) and the B6 and C3H progenitor strains. All mice used in the study were female and 8 months of age. Adult femoral density is achieved at about 4 months of age in mice and maintained until about 8–12 months of age.[6] Consequently, the mice in this study are mature adults with peak bone mass. These mice were group-housed in polycarbonate cages at The Jackson Laboratory (Bar Harbor, ME, USA). Water was acidified with HCl to achieve a pH of 2.8–3.2 for suppression of bacteria and was freely available. The diet used for all mice was pasteurized National Institutes of Health (NIH) 31 (6% fat diet, vitamin and mineral fortified; PMI, Richmond, IN, USA) and was freely available. Use of mice in this research project was reviewed and approved by the Institutional Animal Care and Use Committee of The Jackson Laboratory.

BMD measurements

Isolated femurs and vertebrae were assessed using peripheral quantitative computed tomography (pQCT; Stratec XCT 960M; Norland Medical Systems, Ft. Atkinson, WI, USA) as described previously.[6] Briefly, bones were isolated and stored in 95% EtOH until assessed by pQCT for vBMD. Thresholds of 1.300 attenuation units differentiated mineralized bone from water, adipose tissue, muscle, and tendon; a threshold of 2.000 differentiated high-density cortical bone from bone of lower density. Precision of the pQCT for femoral, tibial, and vertebral vBMD were 1.2, 1.5, and 1.4%, respectively. Isolated femurs were scanned at 2-mm intervals over their entire lengths. Total vBMD was calculated by dividing the total mineral content by the total bone volume. Femoral cortical thickness was calculated at the midpoint of the diaphysis. Isolated lumbar vertebrae (L5) were scanned at their measured midpoints and vBMD was calculated as described previously. Cortical BMC values also are presented for the L5 vertebrae.

Bone microstructure measurements

The L5 vertebra from BXH RI strains with the highest and lowest bone strength were analyzed using a desktop micro-CT (μCT 20; Scanco Medical AG, Bassersdorf, Switzerland). A microfocus X-ray tube with a focal spot of 10 μm was used as a source. To perform a measurement, the specimen was mounted on a turntable that could be shifted automatically in the axial direction. Six hundred projections were taken over 216° (180° plus half the fan angle on either side). A standard convolution-backprojection procedure with a Shepp and Logan filter was used to reconstruct the CT images in 1024 pixel × 1024 pixel matrices. For each sample, a total of 100–200 microtomographic slices, with a slice increment of 17 μm, were acquired. Measurements were stored in three-dimensional (3D) image arrays with an isotropic voxel size of 17 μm. A constrained 3D Gaussian filter was used to partly suppress the noise in the volumes. The bone tissue was segmented from marrow using a global thresholding procedure.[12] In addition to the visual assessment of structural images, morphometric indices were determined from the microtomographic data sets. Cortical and trabecular bone were separated using a semiautomated contour tracking algorithm to detect the outer and inner boundaries of the cortex. In trabecular bone, basic structural metrics were measured using direct 3D morphometry.[13]

TABLE 1. BODY WEIGHT AND FEMUR GEOMETRY, INCLUDING LENGTH, WIDTH IN AP AND ML DIRECTIONS, AND MIDDIAPHYSEAL THICKNESS, FOR B6, C3H, AND BXH RI STRAINS

Inbred strain	n	*Body weight (g)*	*Femur length (mm)*	*Width ML (mm)*	*Width AP (mm)*	*Cortical thickness (mm)*
B6	8	28.4 ± 1.5	16.1 ± 0.11	1.80 ± 0.05[a]	1.23 ± 0.02[a]	0.40 ± 0.01[a]
C3H	10	27.7 ± 1.0	16.0 ± 0.08	1.60 ± 0.01[b]	1.31 ± 0.02[b]	0.56 ± 0.01[b]
BXH-2[c]						
BXH-3	10	25.6 ± 1.0	16.0 ± 0.09	1.54 ± 0.04[b]	1.11 ± 0.02[a,b]	0.36 ± 0.01[a]
BXH-4	11	31.4 ± 1.3	**17.2 ± 0.07**[a,b]	1.81 ± 0.02[a]	1.28 ± 0.02[b]	0.49 ± 0.01[a,b]
BXH-6	13	25.7 ± 1.3	16.1 ± 0.04	1.73 ± 0.03[a]	1.02 ± 0.01[a,b]	0.45 ± 0.01[a,b]
BXH-7	8	26.9 ± 2.3	15.9 ± 0.08	**1.90 ± 0.05**[a,b]	1.16 ± 0.03[a,b]	0.37 ± 0.01[a]
BXH-8	10	24.3 ± 1.3	16.1 ± 0.09	1.84 ± 0.03[a]	1.20 ± 0.01[a]	0.44 ± 0.02[a,b]
BXH-9	8	31.9 ± 1.9	**16.4 ± 0.05**[a,b]	1.82 ± 0.04[a]	1.26 ± 0.02[a]	0.46 ± 0.02[a,b]
BXH-10	10	26.6 ± 0.7	15.1 ± 0.06[a,b]	1.52 ± 0.02[b]	1.07 ± 0.01[a,b]	0.37 ± 0.01[a]
BXH-11	7	24.5 ± 1.8	16.3 ± 0.14[a]	1.84 ± 0.02[a]	1.27 ± 0.03	0.41 ± 0.01[a]
BXH-12	10	28.9 ± 2.5	16.0 ± 0.09	1.60 ± 0.02[b]	1.15 ± 0.02[a,b]	0.44 ± 0.01[a,b]
BXH-14	9	26.2 ± 1.4	**16.6 ± 0.10**[a,b]	1.66 ± 0.03[b]	1.10 ± 0.01[a,b]	0.49 ± 0.02[a,b]
BXH-19	8	21.7 ± 0.4[a,b]	16.2 ± 0.07	1.72 ± 0.03[a]	1.08 ± 0.01[a,b]	0.46 ± 0.02[a,b]

Data presented are mean ± SEM.
Boldface indicates significantly greater than both C3H and B6; underline indicates significantly less than both C3H and B6.
[a] Significantly different from C3H.
[b] Significantly different from B6.
[c] BXH-2 developed early onset leukemia and were excluded from the study.

The measurements included bone volume density (BV/TV), bone surface density (BS/TV), trabecular number (Tb.N), trabecular thickness (Tb.Th), and trabecular spacing (Tb.Sp). Previous studies have shown that trabecular structural metrics measured using μCT closely correlate with those measured using standard histomorphometry.[14,15] Average height and width of the L5 vertebrae were measured directly on midcoronal μCT images.

Biomechanical tests

We measured bone strength of the femur and the L5 lumbar vertebrae. Femurs were tested at the mid-shaft by three-point bending at room temperature. Load was applied in the anteroposterior (AP) direction midway between two supports that were 5 mm apart. Load-displacement curves were recorded at a crosshead speed of 0.5 mm/s using a microforce materials testing machine (Vitrodyne 2000). Data were stored on a microcomputer. Ultimate force (F_u), stiffness (S), and work to failure (U) were calculated from the load-displacement curve as described elsewhere.[16] F_u reflects the strength of the bone, while S reflects the rigidity and U is the energy necessary to cause a fracture. Widths of the cortical midshaft in the mediolateral (ML) and anteroposterior (AP; a.k.a. cranial-caudal) directions were measured using digital calipers accurate to 0.01 mm, with a precision of ±0.005 mm (Mitutoyo, Aurora, IL, USA).

The L5 vertebrae were dissected free and the posterior elements were removed using a small clipper. The endplates of the vertebral body were cut parallel using a diamond wafering saw (Isomet, Buehler, Lake Bluff, IL, USA). Mechanical tests were performed in compression using a servohydraulic materials testing machine (810; MTS Corp., Minneapolis, MN, USA). All tests were done with the specimen submerged in 37°C saline using a displacement rate of 1 mm/s. The standard parameters of F_u, S, and U were calculated from the resulting load-displacement curves. Variation was noted in the specimen height resulting from both genetic differences and effects of making the endplates parallel. Because stiffness and work to failure are affected by specimen height, these parameters were normalized by dividing U by specimen height and by multiplying S by specimen height.

Statistical tests

Comparisons among the BXH RI strains and the B6 and C3H progenitors were made using analysis of variance (ANOVA) implemented by StatView software (Abacus Concepts, Berkeley, CA, USA). Post hoc comparisons between groups were accomplished using a Fisher's protected least significant difference test. Statistical significance was assumed at $p < 0.05$.

RESULTS

The average body weights for BXH RI strains were not significantly different from the B6 and C3H progenitor strains, with the exception of BXH-19 mice, which were significantly lighter than both progenitor strains (Table 1). The C3H mice had greater femoral strength (F_u), stiffness (S), and work to failure (U) compared with B6, as previously reported.[7] For most RI strains, femoral biomechanical properties fell between those of the progenitor strains (Fig. 1, note that mice from the BXH-2 RI strain developed early onset leukemia and were excluded from the study). However, five RI strains (BXH-3, -6, -7, -10, and -11) had

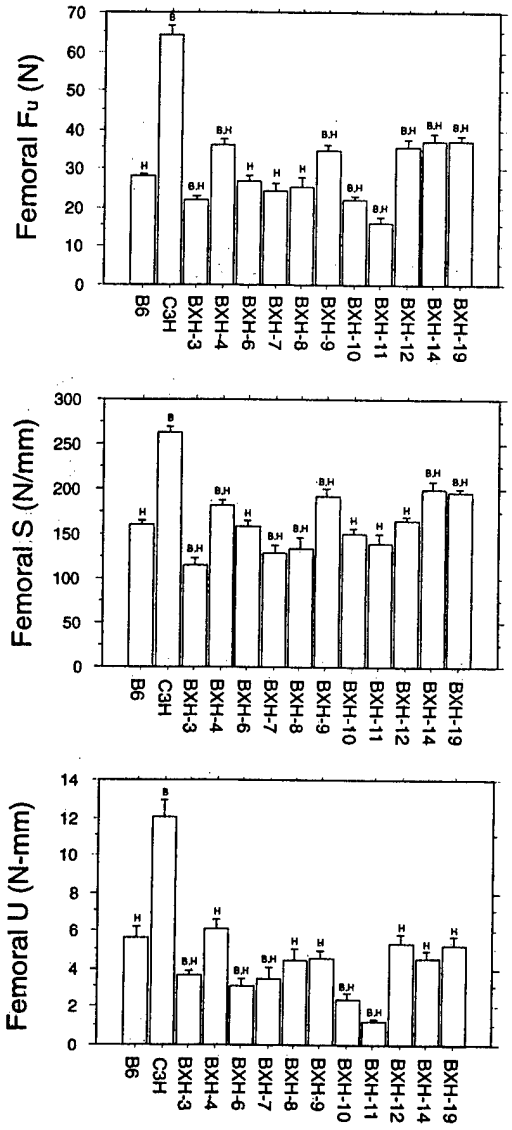

FIG. 1. Femoral biomechanical properties for B6, C3H, and BXH RI inbred strains of mice. Data presented are mean ± SEM (n = 7–13). B indicates a significant difference from B6 and H indicates a significant difference from C3H; F_u is ultimate force, S is stiffness, and U is work to failure.

significantly reduced U compared with either of the progenitor strains. Three of these strains (BXH-3, -10, and -11) also had significantly reduced F_u compared with progenitors. This indicates that these strains had femurs that are more fragile. For the most part, the increased femoral fragility was caused by a combination of reduced cortical thickness and reduced femoral width in the AP direction (Table 1). A remarkable exception was BXH-11, where cortical thickness and AP femoral width were not different from B6, yet F_u and U were only 60% and 25% of B6, respectively. These results suggest that BXH-11 mice had diminished femoral bone quality. We explored this issue further by calculating femoral toughness, which is a measure of the bone tissue integrity corrected for the size and shape of the bone.[16] Femoral toughness in BXH-11 mice (2.0 ± 0.2 mJ/mm^3) was significantly lower than all other RI strains ($p < 0.001$) and considerably less than the toughness of B6 (8.1 ± 0.5 mJ/mm^3; $p < 0.0001$) or C3H (17.2 ± 0.6 mJ/mm^3; $p < 0.0001$) progenitors.

There was variation among the strains in femoral geometry. Femoral length was not significantly different between C3H and B6 progenitor strains but varied greatly among BXH RI strains (Table 1). In particular, mice from BXH-4, -9, and -14 strains had femoral lengths that exceeded those from either progenitor strain, whereas mice from the BXH-10 strain had significantly shorter femurs. Femoral width varied greatly among the progenitor and RI strains, particularly in the ML direction as presented in Table 1. Femurs from the B6 progenitor mice were 15% wider in the ML dimension compared with C3H measurements. Among the RI strains, ML width values distributed rather uniformly as intermediate, B6-like, or C3H-like.

Total vBMD values for femurs were higher in C3H mice, compared with B6 (Table 2). The total femoral vBMD values for BXH RI strains fell between those of the progenitor strains and in all instances were significantly different from both progenitors. The femoral cortical BMC values for the RI strains tended to segregate into low B6-like levels (BXH-3, -7, and -10), intermediate levels (BXH-6, -8, -11, and -12), or high C3H-like levels (BXH-4, -9, -14, and -19).

There were no differences in vertebral bone strength (F_u) between these 8-month-old C3H and B6 mice, yet there was considerable variation in bone strength among the BXH RI strains. Four RI strains (BXH-3, -7, -10, and -12) had significantly weaker vertebrae than either B6 or C3H progenitors, while one RI strain—BXH-4—had significantly greater vertebral bone strength than both progenitors (Fig. 2). Normalized stiffness (S^*h) and normalized work to failure (U/h) tended to distribute more normally with values similar to, as well as between, those of the B6 and C3H progenitors.

The total vBMD values for L5 vertebrae distributed differently from vBMD in femurs: five of the BXH RI strains (BXH-3, -7, -8, -10, and -11) were statistically below both progenitor strains, whereas BXH-4, -6, -9, and -19 were like the B6 and C3H progenitors, and only BXH-14 exceeded the high-density C3H value. C3H mice had substantially more vertebral cortical BMC when compared with B6 values. The vertebral cortical BMC (Table 2) showed that six of the RI strains (BXH-3, -6, -7, -8, 10, and -11) had significantly lower BMC values than both progenitor strains and two RI strains (BXH-9 and -12) were statistically identical with B6 progenitors, whereas three RI strains (BXH-4, -14, and -19) showed BMC values like that of the C3H progenitors. None of the BXH RI strains had vertebral BMC values statistically greater than C3H mice.

μCT analyses revealed marked differences between the vertebrae with highest (BXH-4) and lowest (BXH-3) bone strength (Fig. 3). BXH-4 had superior bone microstructure compared with BXH-3 and progenitor strains, including significantly higher trabecular bone volume and thickness (Table 3). Both BXH-3 and C3H mice had poor trabecular bone structure with reduced Tb.N and increased Tb.Sp compared with B6 or BXH-4 mice. There were no significant differences in trabecular structure between BXH-3 and C3H; however, the vertebral bone strength for BXH-3 was

TABLE 2. BONE PARAMETERS DETERMINED BY pQCT FOR THE FEMUR AND LUMBAR VERTEBRAE FOR B6, C3H, AND BXH RI STRAINS OF MICE

Strain	n	*Femoral total vBMD (mg/mm^3)*	*Femoral cortical BMC (mg)*	*Midvertebral total vBMD (mg/mm^3)*	*Midvertebral cortical BMC (mg)*
B6	8	0.459 ± 0.009^{a}	7.77 ± 0.25^{a}	0.228 ± 0.007^{a}	0.45 ± 0.07^{a}
C3H	10	0.680 ± 0.010^{b}	11.9 ± 0.83^{b}	0.240 ± 0.007^{b}	0.69 ± 0.06^{b}
BXH-2[c]					
BXH-3	10	$0.511 \pm 0.013^{a,b}$	6.78 ± 0.43^{a}	$\underline{0.189 \pm 0.008^{a,b}}$	$\underline{0.09 \pm 0.02^{a,b}}$
BXH-4	11	$0.601 \pm 0.006^{a,b}$	12.7 ± 0.16^{b}	0.246 ± 0.008	0.57 ± 0.07
BXH-6	13	$0.602 \pm 0.012^{a,b}$	$9.69 \pm 0.41^{a,b}$	0.220 ± 0.006	$\underline{0.29 \pm 0.05^{a,b}}$
BXH-7	8	$0.524 \pm 0.012^{a,b}$	7.61 ± 0.38^{a}	$\underline{0.200 \pm 0.009^{a,b}}$	$\underline{0.19 \pm 0.03^{a,b}}$
BXH-8	10	$0.548 \pm 0.016^{a,b}$	$9.95 \pm 0.58^{a,b}$	$\underline{0.213 \pm 0.007^{a,b}}$	$\underline{0.20 \pm 0.04^{a,b}}$
BXH-9	8	$0.585 \pm 0.007^{a,b}$	11.0 ± 0.46^{b}	0.229 ± 0.006	0.39 ± 0.05^{a}
BXH-10	10	$0.551 \pm 0.004^{a,b}$	7.01 ± 0.11^{a}	$\underline{0.188 \pm 0.004^{a,b}}$	$\underline{0.10 \pm 0.01^{a,b}}$
BXH-11	7	$0.522 \pm 0.008^{a,b}$	$9.66 \pm 0.46^{a,b}$	$\underline{0.189 \pm 0.005^{a,b}}$	$\underline{0.20 \pm 0.04^{a,b}}$
BXH-12	10	$0.594 \pm 0.008^{a,b}$	$9.50 \pm 0.36^{a,b}$	0.226 ± 0.007	0.32 ± 0.05^{a}
BXH-14	9	$0.613 \pm 0.013^{a,b}$	11.2 ± 0.40^{b}	$\mathbf{0.279 \pm 0.010^{a,b}}$	0.82 ± 0.11^{b}
BXH-19	8	$0.604 \pm 0.008^{a,b}$	10.9 ± 0.33^{b}	0.256 ± 0.010^{b}	0.67 ± 0.07^{b}

Data are presented as mean ± SEM.
Boldface indicates significantly greater than both C3H and B6; underline indicates significantly less than both C3H and B6.
[a] Significantly different from C3H.
[b] Significantly different from B6.
[c] BXH-2 developed early onset leukemia and were excluded from the study.

only 54% of C3H. These results apparently are caused by the very low vertebral cortical BMC of BXH-3, compared with C3H (Table 2). B6 vertebrae were shorter than those from C3H, whereas C3H vertebrae were more narrow. The selected BXH RI strains tended to retain the height of C3H and the width of B6 (Table 3).

Because of the independent variation of cortical and trabecular bone microstructures among progenitor and RI strains, the variance in vertebral strength was not reflected consistently in the femoral strength (Fig. 4). The solid symbols in Fig. 4 denote the inbred strains that are particularly useful to illustrate the point that genetic regulation of vertebral strength is sometimes independent of regulation of femoral strength. The BXH-12 and BXH-4 strains showed a difference in vertebral strength of almost 2-fold with no corresponding difference in femoral strength. Likewise, the B6 and C3H strains showed a 2.2-fold difference in femoral strength with no difference in vertebral strength.

DISCUSSION

It is widely recognized that loss of bone strength is accompanied by a corresponding rise in risk for osteoporotic fracture. Critical insight to osteoporotic fracture will follow from a better understanding of factors regulating biomechanical properties. In this report, we have hypothesized that factors associated with bone strength (i.e., BMD, size, and microstructure) have heritable components. To test this concept, we exploited a unique genetic model system in the form of the BXH RI strains derived from B6 and C3H progenitors known to differ in many aspects of bone biology.[6,7,17–22] By phenotyping each BXH RI strain for the traits that differ between the B6 and C3H progenitors, analyses of resultant patterns yield insights about genetic regulation underlying each trait. The evidence reported here shows a remarkable complexity to the biological basis for differences in bone strength between B6 and C3H mice.

The segregation patterns of values of biomechanical properties for BXH RI femurs lead to the following conclusions. First, none of the investigated properties segregated the RI strains into subsets that simply resembled either the B6 or the C3H progenitors. In the absence of such a simple segregation pattern, we conclude that each of the phenotypes represented by F_u, S, and U of these skeletal sites is regulated by more than one gene. The modest numbers of RI strains available in this BXH set will not support linkage analyses of traits with more than one gene. Therefore, we have not compared the BXH RI strain distribution patterns recorded for any of the phenotypes reported here with published data in search of single genes. Second, several BXH RI had significantly lower femoral F_u and U values than those found in the low-strength B6 strain and none of the BXH RI strains achieved values that approached those observed in the high-strength C3H strain. This phenomenon of transgenesis suggests that (a) the C3H strain carries genetic alleles contributing to low bone strength and (b) the high bone strength of C3H may result from the interaction of specific genes in C3H but, by chance, none of the BXH RI strains contain the correct combination of C3H genes supporting high femoral strength.

Femoral geometry (overall length and ML and AP widths) also showed complex genetic regulation. Although the length of the B6 and C3H femurs were not different, half of the BXH RI strains had femurs that were either shorter or longer than the progenitor strains. Middiaphyseal ML

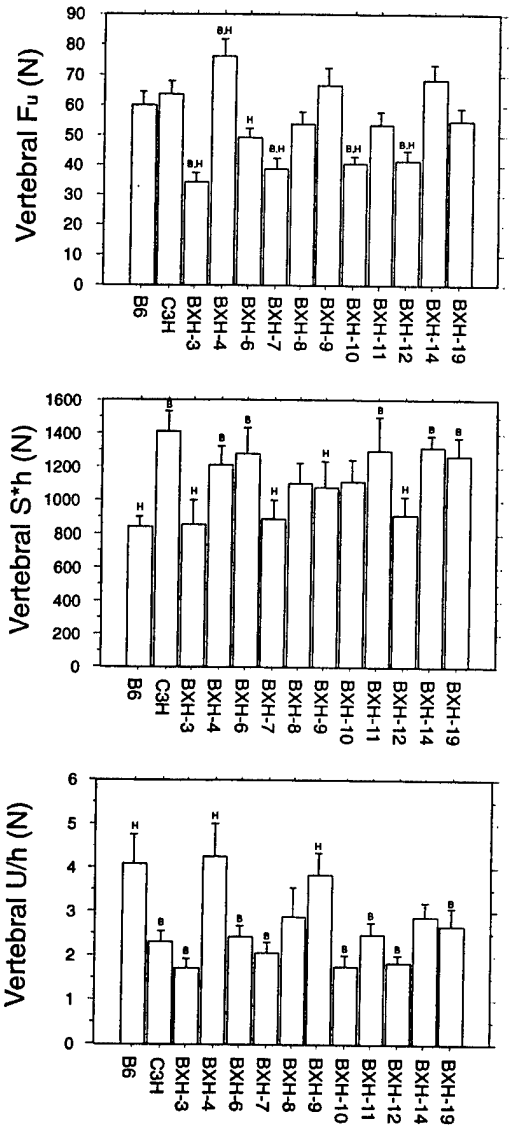

FIG. 2. Vertebral biomechanical properties for B6, C3H, and BXH RI inbred strains of mice. Data presented are mean ± SEM (n = 7–13). B indicates a significant difference from B6 and H indicates a significant difference from C3H; F_u is ultimate force, S^*h is normalized stiffness, and U/h is normalized work to failure.

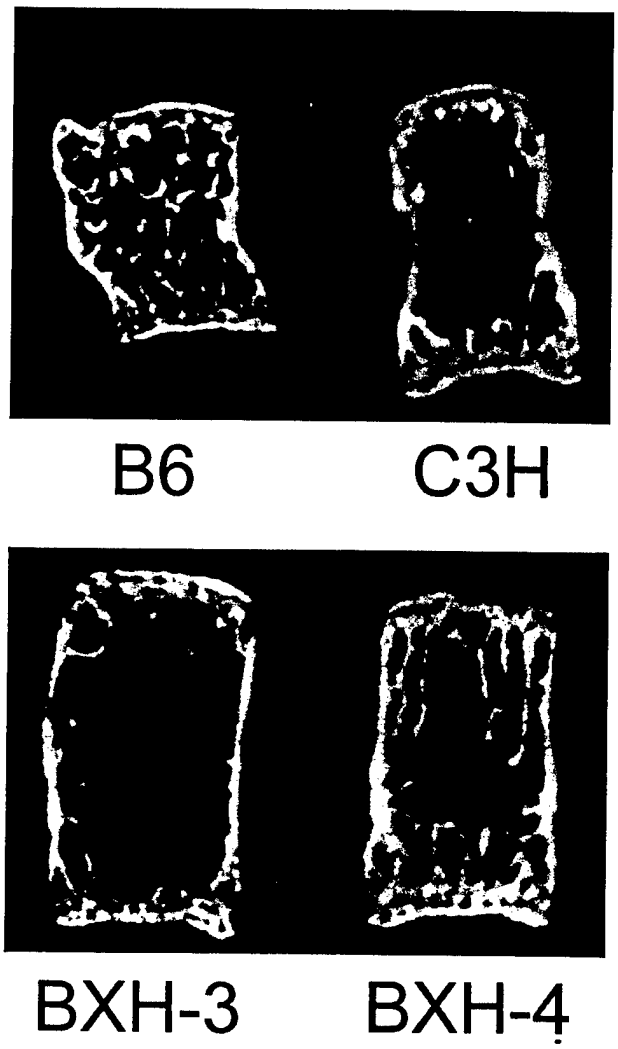

FIG. 3. μCT section of the L5 vertebral body for progenitor strains (B6 and C3H) and the BXH RI strains with maximum (BXH-4) and minimum (BXH-3) vertebral strength. The images were measured 3-D providing a 17-μm isotropic voxel size.

widths distributed into either progenitor and intermediate categories, while the majority of the RI strain AP widths were less that those of the smaller B6 progenitor. As was noted for the femoral strength properties, the thicker femoral cortex of the C3H femurs was not observed in the BXH RI strains. Collectively, these data argue cogently for complex genetic regulation of parameters for femoral size.

The RI strain BXH-11 was remarkable because apparently it had robust femoral shaft geometry, yet with weaker and more fragile femurs. The femoral toughness of the BXH-11 mice was substantially lower than other strains, indicating a deficit in bone quality. These results suggest that one of the B6 and C3H progenitor strains contains a genetic allele(s) that influences some aspect of bone quality. It is unclear, based on the present data, exactly what alteration in the BXH-11 femoral tissue caused the deficit in toughness; nevertheless, the BXH RI strains may be useful for studying genetic influences on bone quality.

As was true for biomechanical and morphology properties, segregation of total vBMD and cortical BMC for femurs was consistent with conclusions of polygenic regulation. Femoral vBMD values from the BXH RI strains were distributed between those of the progenitor strains and no BXH RI replicated either progenitor strain value, again arguing for the fact that combinations of specific genes are required to achieve the respective densities of the progenitor strains.

The biomechanical properties of the L5 vertebrae, particularly F_u, in BXH RI strains, showed a greater range of variation than either B6 or C3H progenitors, suggesting regulation by multiple genes. Likewise, patterns for vertebral vBMD values were noteworthy in that the B6 and C3H progenitors were marginally different from each other, whereas the BXH RI strains showed a much greater range of

TABLE 3. μCT ANALYSIS OF LUMBAR VERTEBRAE FOR B6, C3H, AND BXH RI STRAINS WITH THE GREATEST (BXH-4) AND LEAST (BXH-3) VERTEBRAL STRENGTH (MEAN ± SEM)

	Inbred strain			
Variable	*B6*	*C3H*	*BXH-3*	*BXH-4*
	Vertebral geometry			
Height (mm)	2.60 ± 0.05[a]	3.22 ± 0.10[b]	3.51 ± 0.11[b]	3.45 ± 0.22[b]
Width (mm)	1.95 ± 0.13[a]	1.66 ± 0.08[b]	2.03 ± 0.06[a]	1.98 ± 0.06[a]
	Trabecular structure			
BV/TV (%)	24.1 ± 1.3[a]	16.0 ± 1.0[b]	10.8 ± 1.3[a,b]	**30.0 ± 3.6**[a,b]
BS/TV (mm^{-1})	8.5 ± 0.2[a]	4.4 ± 0.2[b]	3.3 ± 0.4[a,b]	6.7 ± 0.2[a,b]
Tb.N (mm^{-1})	5.1 ± 0.2[a]	2.8 ± 0.1[b]	2.6 ± 0.2[b]	4.1 ± 0.2[a,b]
Tb.Th (μm)	61 ± 2	69 ± 4	73 ± 1	**93 ± 8**[a,b]
Tb.Sp (μm)	199 ± 9[a]	388 ± 11[b]	415 ± 38[b]	255 ± 13[a,b]

Boldface indicates significantly greater than both C3H and B6; underline indicates significantly less than both C3H and B6.
[a] Significantly different from C3H.
[b] Significantly different from B6.

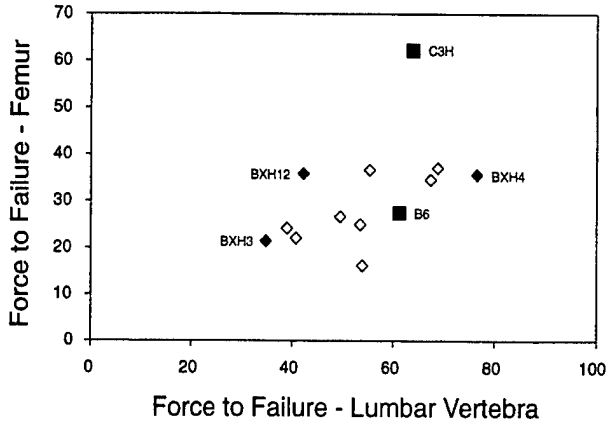

FIG. 4. Relationship between femoral strength (ultimate force) and vertebral strength for B6, C3H, and BXH RI strains. The progenitor strains (B6 and C3H) show a large variation in femoral strength with no difference in vertebral strength. Likewise, selected BXH RI strains (BXH-3, BXH-4, and BXH-12) show large variation in vertebral strength with little or no variation in femoral strength.

values. This distribution of values supports the conclusion that both progenitor strains have independent subsets of genes that yield very similar mean values. Recombination of those genes in the BXH RI strains yields a broader range of values.

Not only is vertebral vBMD under genetic control, but it appears that the distribution of vertebral mineral into cortical and trabecular compartments also is regulated genetically. Trabecular structure in the lumbar vertebra tended to vary independently of cortical BMC of the vertebra, and both trabecular and cortical bone contributed to vertebral strength. BXH-4 mice had alleles that contributed to superior vertebral strength by increasing Tb.N, reducing Tb.Sp, improving Tb.Th, and increasing cortical BMC, while BXH-3 vertebrae were osteopenic with diminished trabecular and cortical bone structure. As for the progenitor strains, B6 had good trabecular bone structure and poorer cortical BMC, whereas C3H had the opposite combination, resulting in intermediate biomechanical properties. However, the correlation between vertebral structure and biomechanical properties was not perfect because the RI strain with the highest total vertebral vBMD and cortical BMC (BXH-14) did not have the greatest vertebral strength. This observation suggests that although the measured densitometry and geometric variables explain much of the variation in vertebral strength, other important structural variables that contribute to vertebral integrity remain.

It was noteworthy that the variation in vertebral strength was not correlated consistently with femoral strength. In particular, the B6 and C3H strains indicated over a 2-fold difference in femoral strength with no difference in vertebral strength while BXH-12 and BXH-4 strains were vastly different in vertebral strength with no corresponding difference in femoral strength. These results strongly suggesting site-specific genetic regulation of bone strength.

Although the ultimate goal of our studies is to better understand the pathogenesis of human osteoporosis, the mouse model used does not mimic osteoporotic humans. We chose 8-month-old female mice, which model middle-aged, premenopausal women. Our aim was to study the variation in bone microstructure and biomechanical properties in animals with peak bone density. In women, the peak bone density achieved during childhood, adolescence, and young adulthood protects against osteoporosis in later years.[23] A further limitation of mice in the study of skeletal biology is their lack of osteonal remodeling in compact bone tissue. This key difference between mice and humans can lead to confounding results. These limitations not withstanding, mice remain one of the best animal models for studying genetic influences on human diseases and disorders, skeletal or otherwise.

In conclusion, we found that the regulation of femoral and vertebral biomechanical properties in BXH RI mice involved multiple genes and was both site specific and com-

partment specific. Independent genetic regulation of femoral geometry, cortical BMC, and vertebral trabecular microstructure contributed to the variation in biomechanical properties among the strains. The genetic control of bone strength appears to be rich and complex with many puzzles to be solved before the genetic mechanisms are understood.

ACKNOWLEDGMENTS

This work was supported in part by the United States Department of Health and Human Services National Institutes of Health grants AR43618 (W.G.B.), CA34196 CORE (The Jackson Laboratory), and AR43730 (C.H.T.). M.E.M. received support from the Alumni Fund of The Jackson Laboratory.

REFERENCES

1. Cummings SR, Black DM, Nevitt MC, Browner W, Cauley J, Ensrud K, Genant HK, Palermo L, Scott J, Vogt TM 1993 Bone density at various sites for prediction of hip fractures. The Study of Osteoporotic Fractures Research Group. Lancet **341:**72–75.
2. Pocock NA, Eisman JA, Hopper JL, Yeates MG, Sambrook PN, Eberl S 1987 Genetic determinants of bone mass in adults: A twin study. J Clin Invest **80:**706–710.
3. Slemenda CW, Christian JC, Williams CJ, Norton JA, Johnston CC 1991 Genetic determinants of bone mass in adult women: A reevaluation of the twin model and the potential importance of gene interaction on heritability estimates. J Bone Miner Res **6:**561–567.
4. Smith DM, Nance WE, Kang KW, Christian JC, Johnston CC Jr 1973 Genetic factors in determining bone mass. J Clin Invest **52:**2800–2808.
5. Rogers J, Mahaney MC, Beamer WG, Donahue LR, Rosen CJ 1997 Beyond one gene-one disease: Alternative strategies for deciphering genetic determinants of osteoporosis. Calcif Tissue Int **60:**225–228.
6. Beamer WG, Donahue LR, Rosen CJ, Baylink DJ 1996 Genetic variability in adult bone density among inbred strains of mice. Bone **18:**397–403.
7. Turner CH, Hsieh Y-F, Müller R, Bouxsein ML, Baylink DJ, Rosen CJ, Grynpas MD, Donahue LR, Beamer WG 2000 Genetic regulation of cortical and trabecular bone strength and microstructure in inbred strains of mice. J Bone Miner Res **15:**1126–1131.
8. Taylor BA 1979 Established and incipient recombinant inbred strains of mice. In: Green MC (ed.) Genetic Variants and Strains of the Laboratory Mouse. Fischer, Stuttgart, Germany, p. 397.
9. Bailey DW 1981 Recombinant inbred strains and bilinear congenic strains. In: Foster HS, Small JK, Fox JG (eds.) The Mouse in Biomedical Research. Academic Press, New York, NY, USA, pp. 223–239.
10. Silver LM 1995 Mouse Genetics: Concepts and Applications. Oxford University Press. New York, NY, USA, pp. 207–227.
11. Beamer WG, Shultz KL, Tennent BJ, Nadeau JH, Churchill GA, Eicher EM 1998 Multigenic and imprinting control of ovarian granulosa cell tumorigenesis in mice. Cancer Res **58:**3694–9.
12. Müller R, Rüegsegger P 1997 Micro-tomographic imaging for the nondestructive evaluation of trabecular bone architecture. In: Lowet G, Rüegsegger P, Weinans H, Meunier A (eds.) Bone Research in Biomechanics. IOS Press, Amsterdam, The Netherlands, pp. 61–79.
13. Hildebrand T, Müller R, Laib A, Dequeker J, Rüegsegger P 1999 Direct 3-D morphometric analysis of human cancellous bone: Microstructural data from spine, femur, iliac crest, and calcaneus. J Bone Miner Res **14:**1167–1174.
14. Müller R, Van Campenhout H, Van Damme B, Van der Perre G, Dequeker J, Hildebrand T, Rüegsegger P 1998 Morphometric analysis of human bone biopsies: A quantitative structural comparison of histological sections and micro-computed tomography. Bone **23:**59–66.
15. Li XJ, Müller R, Stevens ML, Golden J, Seeherman H, Bouxsein ML 1998 Evaluation of trabecular bone morphometry: Comparison of micro-computed tomography and histomorphometry in the rat proximal tibia. Bone **23:**S635.
16. Turner CH, Burr DB 1993 Basic biomechanical measurements of bone: A tutorial. Bone **14:**595–608.
17. Dimai HP, Linkhart TA, Linkhart SG, Donahue LR, Beamer WG, Rosen CJ, Farley JR, Baylink DJ 1998 Alkaline phosphatase levels and osteoprogenitor cell numbers suggest bone formation may contribute to peak bone density differences between two inbred strains of mice. Bone **22:**211–216.
18. Kodama Y, Dimai HP, Wergedal J, Sheng M, Malpe R, Kutilek S, Beamer W, Donahue LR, Rosen C, Baylink DJ, Farley J 1999 Cortical tibial bone volume in two strains of mice: Effects of sciatic neurectomy and genetic regulation of bone response to mechanical loading. Bone **25:**183–190.
19. Chen C, Kalu DN 1999 Strain differences in bone density and calcium metabolism between C3H/HeJ and C57BL/6J mice. Bone **25:**413–420.
20. Linkhart TA, Linkhart SG, Kodama Y, Farley JR, Dimai HP, Wright KR, Wergedal JE, Sheng M, Beamer WG, Donahue LR, Rosen CJ, Baylink DJ 1999 Osteoclast formation in bone marrow cultures from two inbred strains of mice with different bone densities. J Bone Miner Res **14:**39–46.
21. Rosen CJ, Dimai HP, Vereault D, Donahue LR, Beamer WG, Farley J, Linkhart S, Linkhart T, Mohan S, Baylink DJ 1997 Circulating and skeletal insulin-like growth factor-I (IGF-I) concentrations in two inbred strains of mice with different bone mineral densities. Bone **21:**217–223.
22. Sheng MH, Baylink DJ, Beamer WG, Donahue LR, Rosen CJ, Lau KH, Wergedal JE 1999 Histomorphometric studies show that bone formation and bone mineral apposition rates are greater in C3H/HeJ (high-density) than C57BL/6J (low-density) mice during growth. Bone **25:**421–429.
23. Riis BJ, Hansen MA, Jensen AM, Overgaard K, Christiansen C 1996 Low bone mass and fast rate of bone loss at menopause: Equal risk factors for future fracture: A 15-year follow-up study. Bone **19:**9–12.

Address reprint requests to:
Charles H. Turner, Ph.D.
Director of Orthopedic Research
Indiana University
541 Clinical Drive, Room 600
Indianapolis, IN 46202, USA

Received in original form May 16, 2000; in revised form August 10, 2000; accepted September 5, 2000.

Effects of Dietary Restriction on Appendicular Bone in the SENCAR Mouse

Elsa J. Brochmann Murray, Wesley G. Beamer, Maria Eugenia Duarte, Keyvan Behnam, Mario S. Grisanti, and Samuel S. Murray

Peptide hormones, cytokines, and growth factors regulate cellular metabolism by stimulating second messenger signal transduction cascades in target tissues. A mutation in the regulatory domain of protein kinase C (PKC) in SENCAR (*sen*sitive to *car*cinogenesis) mice renders them extremely sensitive to diacylglycerol and phorbol esters, resulting in rapid growth, high free radical generation, carcinogenesis, and metabolic bone disease. Dietary restriction (DR) normalizes PKC and ameliorates adverse downstream effects, including carcinogenesis, in SENCAR mice. We hypothesized that DR sufficient to ameliorate carcinogenesis would prevent or delay the early onset of metabolic bone disease in SENCAR mice. Male mice were assigned to 1 of 4 feeding groups from 10 to 16 weeks of age (the critical period when metabolic bone disease develops): ad libitum (AL)-fed; AL antioxidant (0.07% thioproline)-fed; 40% DR; or 40% DR antioxidant-fed. Femoral bone mass was determined gravimetrically. Tibial total, cortical, and trabecular bone mineral density (BMD) were determined by quantitative computed tomography. Body weight, femoral bone mass, and tibial cortical BMD were lower in DR than in AL mice. However, tibial total and trabecular BMD were higher in DR than in AL mice. Serum calcitonin, the hormone that inhibits the osteoclastic bone resorption that is most notable in trabecular bone, was 2-fold higher in DR than in AL-fed mice. Dietary thioproline had no major effects. Thus, DR sufficient to ameliorate carcinogenesis in SENCAR mice did not prevent early-onset metabolic bone disease, but it had a beneficial effect on tibial trabecular BMD that occurred at the apparent expense of cortical BMD. DR in SENCAR mice was also associated with elevated serum calcitonin, which may inhibit osteoclastic resorption and account for trabecular bone conservation in this model. In conclusion, PKC or the downstream metabolic processes regulated by it appear to play previously unrecognized roles in the regulation of tibial trabecular BMD and serum calcitonin in SENCAR mice.

INBRED AND MUTANT mice, with their defined genetic backgrounds and short life spans, are useful models for determining the effects of diet and heredity on bone and mineral metabolism.[1,2] The SENCAR (*sen*sitive to *car*cinogenesis) mouse is a model of elevated free radical generation,[3-6] oxidative damage,[7-9] and carcinogenesis[10-12] that can be ameliorated by defined total dietary or calorie (fat or carbohydrate) restriction and exacerbated by high dietary fat intake.[13-21] The primary genetic defect in SENCAR mice is a mutation in the regulatory domain of a protein kinase C (PKC) isozyme that renders it exquisitely sensitive to diacylglycerol and phorbol ester stimulation.[22,23] Enhanced PKC signal transduction induces 8-lipoxygenase activity and arachidonic acid synthesis in SENCAR mice, resulting in elevated hydroperoxide and superoxide anion production by many cells, including peritoneal macrophages and peripheral blood leukocytes,[5,6,8,9] and a 5- to 10-fold increase in free radical–mediated oxidative DNA damage.[10] Phorbol esters induce high levels of granulocyte-macrophage colony-stimulating factor (GM-CSF),[24,25] epidermal growth factor receptor, transforming growth factor-α and -β (TGF-α and -β),[26,27] and interleukin-1 (IL-1)[28,29] mRNA, protein expression, and activity in SENCAR mice.

Previously, we reported that SENCAR mice rapidly grow to a large size and have higher vertebral and long bone and body mass at sexual maturity[30,31] than most other mouse strains.[2] However, sexually mature SENCAR mice develop histologic features of metabolic bone disease (low numbers of osteoblasts and osteoclasts, fatty infiltration of the marrow cavity, low mineral apposition rate, and low osteoid volume) by 14 weeks of age,[1] while similar characteristics are not observed in control strains until about 2 years of age.[32,33] These results suggest that the mutation in the regulatory domain of PKC that enhances oxidative metabolism, arachidonic acid synthesis, and cytokine and growth factor protein and receptor levels in SENCAR mice may also have important downstream effects on bone metabolism.

Since defined total dietary or calorie restriction regimens can normalize PKC activity or ameliorate its adverse downstream biologic consequences, such as carcinogenesis, in SENCAR mice,[15,17-19,34] we tested the hypothesis that dietary restriction (DR), alone or in combination with antioxidant feeding, will prevent the development of metabolic bone disease in this unique, well-defined murine model of elevated free radical generation, oxidative damage, and growth factor induction. During the critical period from about 10 to 16 weeks of age, when metabolic bone disease develops,[1,30,31] SENCAR mice were subjected to 40% DR,[15] antioxidant feeding, or 40% DR plus antioxidant feeding. The effects of dietary treatment on the appendicular skeleton were assessed by classical gravimetric

From the Geriatric Research, Education and Clinical Center, Veterans Affairs Greater Los Angeles Healthcare System, Sepulveda, CA; Department of Medicine, University of California, Los Angeles, CA; The Jackson Laboratory, Bar Harbor, Maine; and the Departamento de Patologia, Universidade Federal Fluminense, Rio de Janeiro, Brazil.

Submitted May 5, 2000; accepted October 23, 2000.

Supported in part by the Geriatric Research, Education, and Clinical Center of the VA Greater Los Angeles Healthcare System, Sepulveda, CA (E.J.B.M. and S.S.M.) and the National Institutes of Health (W.G.B.; NIAMS AR43618).

Presented in part at the annual meetings of the Gerontological Society of America, November 17-21, 1996, Washington, DC, and the American Society for Bone and Mineral Research, September 10-14, 1997, Cincinnati, OH.

Address reprint requests to Elsa J. Brochmann Murray, PhD, 11-E (GRECC), Sepulveda Ambulatory Care Center and Nursing Home, VA Greater Los Angeles Healthcare System, 16111 Plummer St, Sepulveda, CA 91343.

0026-0495/01/5004-0011$35.00/0
doi:10.1053/meta.2001.21694

and morphometric methods, as well as by high-resolution peripheral quantitative computed tomography (pQCT). In addition, 2 serum parameters (calcitonin and osteocalcin) germane to mineral metabolism were measured by radioimmunoassay.

MATERIALS AND METHODS

Mice and Dietary Treatments

All experiments were approved by the Animal Subjects Subcommittee and the Research and Development Committee. A SENCAR mouse colony was maintained as outlined in the Guide for the Care and Use of Laboratory Animals (DHEW Publication 86-23). Deionized, distilled water and Richmond standard 9F mouse breeding chow (Diet #5020, Purina Mills, St Louis, MO) were provided ad libitum to the breeding colony. Housing facilities were maintained at 20° to 23°C and 50% to 60% relative humidity with a 12-hour light:12-hour dark cycle.

To permit comparison with previously published studies of bone metabolism in SENCAR mice,[1,30,31] experimental mice were fed modified rodent basal test diet #5755 (Purina Mills, Richmond, IN) from 10 to 16 weeks of age. Modified test diet #5755 for AL-fed experimental mice contained 0.8% calcium and 0.6% phosphorus. Modified test diet #5755 for DR mice contained 1.33% calcium, and 1.0% phosphorus, so that the total dietary calcium and phosphorus intakes of AL-fed and 40% DR mice were equal. Where indicated, modified basal test diet #5755 also contained 0.07% (wt/wt) thioproline (Sigma, St Louis, MO), a natural intracellular antioxidant derivative of the amino acid proline.[35]

At 10 weeks of age, 51 male mice were randomly assigned to 1 of 5 groups: time-zero (t_0) control; AL/−T (ad libitum-fed, no thioproline); AL/+T (ad libitum fed, 0.07% thioproline); DR/−T (40% dietary restriction, no thioproline); or DR/+T (40% dietary restriction, 0.07% thioproline). Time-zero control mice were killed at 10 weeks of age, and the remaining AL-fed or DR mice were killed at 16 weeks of age. The mice in each of the AL-fed and DR groups were weighed weekly from 10 to 16 weeks of age. Food consumption was determined on a daily basis for the AL-fed (0.00% or 0.07% thioproline) mice, and the mice in the 40% DR groups received 60% of the amount of food consumed by their respective AL-fed control groups on the previous day[15] beginning on day 2 of the 6-week dietary treatment.

Quantification of Bone Mass and Density

At the end of the experimental period, the mice were killed by carbon dioxide inhalation followed by exsanguination. The femurs were removed and defleshed, and their maximum lengths and widths were measured with a #5921 micro caliper (Manostat, Geneva, Switzerland).[31] The dry, fat-free and ash weights of the femur were determined as previously reported.[31] Briefly, the femurs were defatted for 48 hours in diethylether:ethanol (1:1; vol/vol), dried at 105°C for 18 hours to obtain constant dry, fat-free weights, and heated at 550°C for 18 hours to obtain constant ash weights.[31] The tibias were excised, lightly defleshed, and stored at 4°C in 95% ethanol until subjected to pQCT with a Stratec XCT 960M (Norland Medical Systems, Ft Atkinson, WI) specifically modified to measure bone mineral and volume in small specimens.[2] Briefly, isolated intact tibias were scanned at 1-mm intervals beginning approximately 0.6 mm from the proximal end. The unit volume within which mineral was measured was set at 0.1 mm^3.[2] Attenuation data for scans through the spongiosal region at the proximal end of the marrow cavity were used to generate values for bone mineral content, volume, and density using XMICE software (version 1.3; Norland).[2] Data are presented for total bone parameters defined by an attenuation threshold ≥ 500 and for cortical bone parameters defined by an attenuation threshold ≥ 2,000.[2] Total bone density values were calculated by dividing the total mineral content by the total volume.[2] The precision for midshaft total cortical bone mineral density is 1.2%.[2] The resolution of detection is 0.05 mm.[2] The total mass of mineral per femur calculated from pQCT data using the XMICE software algorithms ranged from 15.3 mg to 27.4 mg in 11 strains of inbred mice, which is in excellent agreement with the range of 16.9 mg to 27.4 mg obtained by directly ashing and weighing bone from mice of similar ages.[2]

Serum Osteocalcin and Calcitonin Assays

Blood samples were collected by heart puncture between 8 AM and noon on the day the mice were killed. Serum was obtained by centrifuging heparinized unhemolyzed whole blood in a microfuge for 3 minutes at 4°C. The serum was stored at −20°C until assayed for calcitonin and mouse osteocalcin using commercial radioimmunoassay (RIA) test kits and reagents (Incstar, Stillwater, MN, and Biomedical Technologies, Stoughton, MA, respectively).[30] All assays were conducted in triplicate in multiple dilutions of serum, as well as in control serum containing high or low levels of osteocalcin or calcitonin.[30] The osteocalcin antibody is specific for highly purified intact murine osteocalcin, and the RIA has an intra-assay coefficient of variation (CV) of 7% and inter-assay CV of 12%. The antibody to synthetic human calcitonin (1-32) (a highly conserved mammalian sequence) exhibits excellent cross-reactivity (≥99%) with rodent calcitonins. The calcitonin RIA has an intra-assay CV of 11% and an inter-assay CV of 15%. Assay results were calculated using the four-parameter spline fit option of RIACALC software (Wallac, Turku, Finland).[30]

Statistical Analysis

Data are expressed as the mean ± SEM (n) for all groups. Data were subjected to 2-way multiple ANOVA using dietary food intake and antioxidant feeding as the main effects and testing for interaction using StatView 512$^+$ software (BrainPower Software, Agoura Hills, CA). Where indicated, data for individual groups were analyzed by 2-tailed Student's t test for parametric data or Mann-Whitney test for nonparametric data. Results were considered significant at $P \leq .05$.

RESULTS

Food Consumption and Body Mass

Altering the calcium and phosphorus content or adding 0.07% thioproline to Purina test diet #5755 did not affect its palatability, assessed as food consumption (Fig 1), or the apparent health status and activity levels of 10- to 16-week-old SENCAR mice, relative to that observed in previous studies of bone metabolism in this mouse strain.[1,30,31] No consistent statistically significant differences in food consumption were observed when AL/−T mice were compared with AL/+T mice (Fig 1). Since the palatability of the thioproline-supplemented diet had not been determined for AL-fed mice prior to these experiments, the mice in the 40% DR/−T group were fed 60% of the amount of food consumed by the mice in the AL/−T group,[15] while the mice in 40% DR/+T group were fed 60% of the amount of food consumed by the mice in the AL/+T group. The mice in both of the 40% DR groups (DR/−T and DR/+T) consumed all the food supplied to them each day, and the total food intake was essentially the same for both DR groups (DR/−T and DR/+T) for the 6-week test period from 10 to 16 weeks of age. It should be noted that such a 40% total dietary restriction regimen reduced the incidence and number of skin tumors in SENCAR mice seen 16 and 20 weeks after treatment with the tumor initiator 7,12-dimethylbenzanthracene and the tumor promoter 12-*O*-tetradecanoylphorbol-13-acetate.[15] Therefore, this dietary regimen was specifically chosen

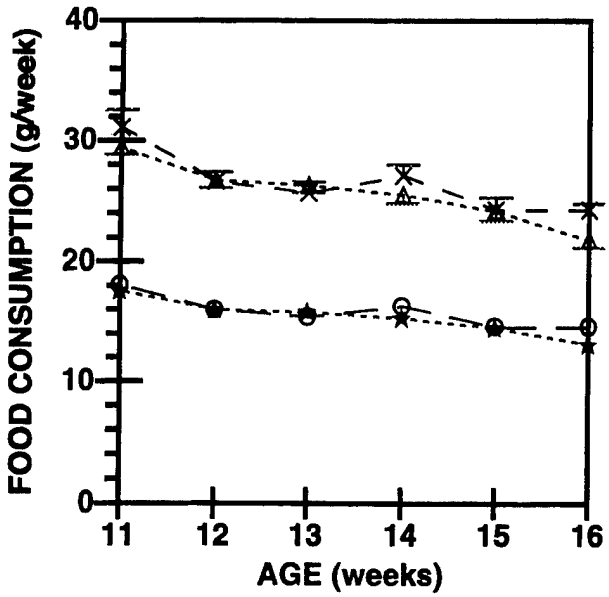

Fig 1. Food consumption by SENCAR mice. Mice were randomly assigned to 1 of 4 experimental feeding groups from 10 to 16 weeks of age, and food consumption was recorded daily. AL/−T (X); AL/+T (△); 40% DR/−T (○); 40% DR/+T (★). Data are the mean ± SEM (n = 10).

for the present studies because it was associated with a statistically significant improvement in a downstream biologic effect (carcinogenesis) of PKC stimulation in SENCAR mice.[15]

AL-fed (AL/−T and AL/+T) SENCAR mice weighed more than 40% DR (DR/−T and DR/+T) mice from 11 to 16 weeks of age ($P < .001$) (Fig 2). The average weight of SENCAR mice in the AL/−T group was not significantly different from that of mice in the AL/+T group. Similarly, the average weight of mice in the 40% DR/−T group was not different from that of 40% DR/+T group, confirming that this natural intracellular antioxidant has no overt adverse effects on food consumption or energy utilization in SENCAR mice.

Femoral Bone Size, Mass, and Ash Content

Six weeks of DR and antioxidant feeding had no statistically significant effects on the maximum external length or width of the femur (Table 1). As previously reported,[31] the dry, fat-free and ash weights of femurs from 10-week old t_0 control mice were equal to or greater than those observed in older mice. In addition, the dry, fat-free and ash weights of the femurs of 16-week-old AL-fed mice were significantly greater ($P = .0008$ and $P = .001$, respectively) than those of DR mice by ANOVA (Table 1). The data demonstrating that AL-fed mice had heavier femurs than DR mice are consistent with preliminary observations that the cortical width (eg, the width of both cortices measured at 7 equidistant sites) of the femurs was 20.7 μm (−T) to 28.2 μm (+T) greater in AL-fed mice than it was in the corresponding group of DR mice. This corresponds to a cortical thickness that was 17% (−T) to 25% (+T) greater in AL-fed mice than in the respective group of DR mice. In addition, the cortical width of the femur was lower in 16-week-old DR mice than in 10-week-old t_0 control mice, while the cortical widths of the femurs were similar in t_0 and AL-fed mice (data not shown). Since the cortices were thicker in AL-fed mice, but the exterior dimensions of the femur were similar in AL-fed and DR mice, the higher dry, fat-free and ash weights observed in AL-fed mice can be attributed to reduced endosteal remodeling, enhanced endosteal deposition, or a combination of both in AL-fed mice, relative to DR mice. DR did not prevent the fatty infiltration of the marrow cavity that develops in sexually mature SENCAR mice[1] (data not shown).

The dry, fat-free and ash weights of the femurs of the DR mice that received no thioproline (DR/−T) were 13.9% (dry, fat-free weight) and 12.6% (ash weight) lower than those of AL/−T control mice (Table 1). In contrast, when thioproline was added to the diet, the femoral bone masses of 40% DR/+T SENCAR mice were only 4.3% (dry, fat-free weight) to 4.5% (ash weight) lower than those of the respective AL/+T control group (Table 1). However, although it appears that there was a trend toward higher femoral bone dry, fat-free and ash weights in thioproline-fed DR mice than in DR mice that did not receive dietary thioproline supplementation (DR/−T), compared with their respective AL-fed control groups, the trend was not statistically significant. Finally, the degree of mineralization, assessed as the percentage ash, was not significantly affected by DR or antioxidant feeding (Table 1).

Tibial Bone Density

When 16-week-old AL-fed and DR SENCAR mice were compared, DR mice had significantly greater tibial trabecular bone density than AL-fed mice ($P = .0002$ by ANOVA) (Table 2). In contrast, 16-week-old AL-fed SENCAR mice had significantly higher tibial cortical bone density than DR mice ($P =$

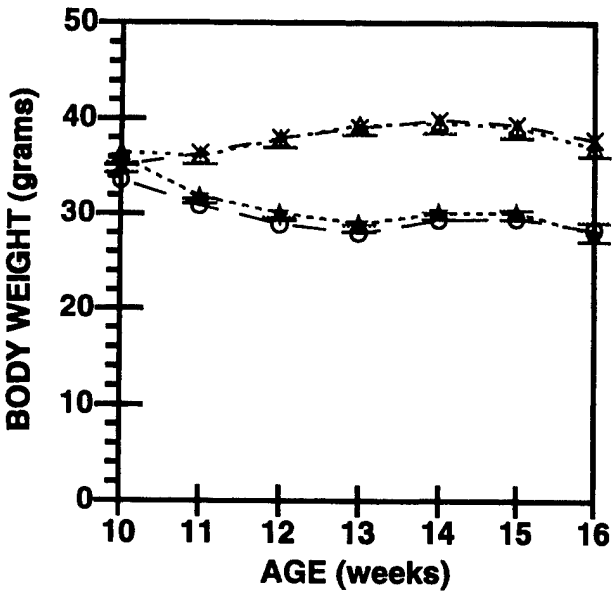

Fig 2. Body weights of 10- to 16-week old SENCAR mice. AL/−T (X); AL/+T (△); 40% DR/−T (○); 40% DR/+T (★). Data are the mean ± SEM (n = 10). Addition of the dietary antioxidant thioproline had no effect on body mass over the course of the experiment.

Table 1. Femoral Bone Length, Width, Mass, and Ash Content in 10- and 16-Week-Old SENCAR Mice

Parameter*	Dietary Group†					ANOVA (*P* values)‡		
	t_0	AL/−T	AL/+T	DR/−T	DR/+T	Effect of DR	Thioproline	Interaction
Age (wk)	10	16	16	16	16			
Length (mm)	17.2 ± 0.11 (11)	17.6 ± 0.06 (9)§	17.4 ± 0.09 (10)	17.1 ± 0.05 (8)§	17.5 ± 0.12 (10)	NS	NS	NS
Width (mm)	2.59 ± 0.03 (11)	2.38 ± 0.04 (9)§	2.43 ± 0.04 (10)	2.38 ± 0.06 (8)§	2.44 ± 0.04 (10)	NS	NS	NS
Dry, fat-free weight (mg)	49.1 ± 1.2 (11)	48.8 ± 0.8 (10)	46.2 ± 1.3 (10)	42.0 ± 1.7 (9)¶	44.2 ± 0.9 (10)	.0008	NS	NS
Ash weight (mg)	32.8 ± 0.8 (11)	31.8 ± 0.4 (10)	30.8 ± 0.9 (10)	27.8 ± 1.03 (9)¶	29.4 ± 0.6 (10)	.001	NS	NS
% Ash‖	66.7 ± 0.2 (11)	65.3 ± 0.7 (10)	66.7 ± 0.4 (10)	66.3 ± 0.3 (9)¶	66.5 ± 0.4 (10)	NS	NS	NS

Abbreviation: NS, not significant.

*All values are expressed as the mean ± SEM (n).

†All mice received Richmond standard 9F mouse breeding chow ad libitum from weaning to 10 weeks of age (t_0). To permit comparison to previous studies of bone metabolism,[1,30,31] DR,[15] and thioproline,[35] AL-fed mice received Purina basal test diet #5755 containing 0.8% Ca and 0.6% Ca; 40% DR mice received test diet #5755 containing 1.33% Ca and 1.0% P; and thioproline-fed (+T) mice received 0.07% (wt/w) thioproline from 10 to 16 weeks of age.

‡All data for 16-week-old mice were subjected to ANOVA, with DR and antioxidant feeding as the major variables.

§The lengths and widths of intact unbroken femurs are reported.

¶The bone from 1 mouse fragmented during cleaning and was lost from the study.

‖% Ash = (Ash weight)/(Dry, fat-free weight) × 100.

.0001). The net result was that total tibial bone density was greater in DR mice than in AL-fed mice ($P = .047$).

When 10-week-old t_0 control mice were compared with 16-week-old AL-fed and DR SENCAR mice, total and trabecular tibial bone density were preserved in 40% DR mice, relative to 10-week-old t_0 controls, while 16-week-old AL-fed SENCAR mice had 40% to 42% lower tibial trabecular bone density than t_0 controls (Table 2). In contrast, tibial cortical bone density in 16-week-old AL-fed mice was conserved, relative to 10-week-old t_0 control values, and the lowest tibial cortical bone densities were observed in 40% DR mice. In summary, there was conservation of tibial total and trabecular bone density in 40% DR SENCAR mice, relative to 10-week-old t_0 control mice, that occurred at the apparent expense of cortical density, while trabecular bone density declined significantly in AL-fed mice. The greatest change in tibial bone density that occurred between 10 and 16 weeks of age in SENCAR mice was the decline observed in the trabecular bone of AL-fed mice, and addition of dietary thioproline had no protective effect on this parameter. Finally, the higher cortical bone density observed in the tibias of AL-fed SENCAR mice (Table 2) is consistent with the greater cortical width (data not

Table 2. Tibial Bone Densities in 10- and 16-Week-Old SENCAR Mice

Parameter*	Dietary Group†					ANOVA (p values)‡		
	t_0	AL/−T	AL/+T	DR/−T	DR/+T	DR	Thioproline	Interaction
Age (wk)	10	16	16	16	16			
Total density (mg/mm^3)	0.439 ± 0.014 (10)	0.413 ± 0.011 (10)	0.411 ± 0.017 (10)	0.429 ± 0.015 (10)	0.453 ± 0.011 (10)	.047	NS	NS
Cortical density (mg/mm^3)	0.515 ± 0.006§¶ (10)	0.538 ± 0.012 (10)	0.524 ± 0.005 (10)	0.497 ± 0.005§ (10)	0.495 ± 0.005¶ (10)	.0001	NS	NS
Trabecular density (mg/mm^3)	0.233 ± 0.030‖,# (10)	0.135 ± 0.017‖ (10)	0.140 ± 0.018# (10)	0.198 ± 0.025 (9)**	0.240 ± 0.018 (8)**	.0002	NS	NS

*Experimental values are expressed as the mean ± SEM (n).

†The diets are described in Table 1.

‡All data for 16-week-old mice were subjected to ANOVA, with DR and antioxidant feeding as the major variables.

¶Cortical bone density in 10-week-old t_0 control mice was significantly higher than that observed in 16-week-old 40% DR mice at § $P = .0272$ (DR/−T) and ¶ $P = .0197$ (DR/+T) by Student's *t* test.

‖,#Trabecular bone density in 10-week-old t_0 t_0 control mice was significantly greater than that observed in 16-week-old AL-fed mice at ‖ $P = .0108$ (AL/−T) and # $P = .0151$ (AL/+T) by Student's *t* test.

**The attenuation by trabecular bone could not be distinguished in 3 samples.

shown) and mass observed in their femurs (Table 1), when compared with DR mice.

Serum Osteocalcin and Calcitonin

When 16-week-old AL and DR mice were compared, there was no statistically significant difference in serum osteocalcin (one of the major noncollagenous proteins of bone synthesized and secreted by the osteoblast) (Table 3).[36] Calcitonin, the systemic peptide hormone that inhibits osteoclastic bone resorption,[37] was significantly higher ($P = .0001$) in the serum of 16-week-old 40% DR SENCAR mice than in 16-week-old AL-fed controls (Table 3).

DISCUSSION

The SENCAR mouse is a novel, well-defined model of 2-stage carcinogenesis characterized by enhanced PKC activation[22,23] and the downstream consequences of this activation, including elevated free radical generation,[5,6,8,9] oxidative damage,[10] and growth factor (GM-CSF, TGF-α and -β, and IL-1) and growth factor receptor transcription, synthesis, and activity in epidermal cells, monocytes, and macrophages.[24-29] In addition, the metabolic regulation of bone development, growth, and maintenance is disordered in SENCAR mice. Specifically, the SENCAR mouse rapidly grows to a large size, and its vertebrae and long bones are larger and heavier at sexual maturity than those of 10 other strains of mice.[2,30,31] Although the biochemical mechanisms underlying this robust bone growth have not been elucidated, it is consistent with the high levels of growth factor and growth factor receptor synthesis and activity observed in the nonskeletal tissues of SENCAR mice.[24-29] For example, osteoblasts secrete TGF-β, which is deposited in the extracellular matrix during bone formation.[37] TGF-β, which has previously been shown to be upregulated by phorbol esters in SENCAR mouse skin,[26,27] is an autocrine/paracrine upregulator of osteoblast anabolism when it is subsequently released from the bone matrix by osteoclastic resorption.[37] Enhanced expression and activity of local growth factors that affect bone, such as TGF-β, in immature SENCAR mice would favor the development of high peak bone mass.

The vertebrae[30] and femurs[1,31] of SENCAR mice stop growing significantly by the time they are sexually mature ($\geq$10 weeks of age). By 14 weeks of age, SENCAR mice exhibit severe histologic abnormalities in bone and cartilage, including the development of architectural disarray and focal discontinuities in the growth plate, low bone and osteoid volume, low mineral apposition rate, fatty infiltration of the marrow cavity, and very low numbers and biosynthetic activity of osteoblasts and osteoclasts.[1] Although the pathophysiologic mechanisms of bone loss in SENCAR mice have not been elucidated, the perforation of structural elements, increased marrow cavity size, and discontinuities in bone structure that are observed[1] are consistent with an osteoclast-mediated imbalance in focal remodeling.[38] GM-CSF and IL-1 (which are upregulated in phorbol ester-stimulated macrophages and skin in SENCAR mice[24,25,28,29] and induce osteoclastogenesis in bone[39]) may initiate cycles of osteoclast-mediated remodeling[38] that result in the unique histologic features of metabolic bone disease that are observed in this model.[1] In addition, reactive oxygen species, including superoxide and peroxide (which are produced at high levels by the leukocytes and macrophages of phorbol ester-treated SENCAR mice[5,6,8,9,11]) stimulate osteoclastogenesis in bone marrow stem cell cultures.[40] Since the dietary antioxidant thioproline had no statistically significant beneficial effects on femoral bone mass or basic morphometry or on tibial bone density in 16-week-old SENCAR mice (Tables 1 and 2), the results presented here suggest that autocrine and paracrine cytokines and growth factors, such as IL-1 and GM-CSF, probably play a more important role in the development of bone and cartilage abnormalities in mature SENCAR mice than do free radicals. Earlier implementation of antioxidant feeding or the substitution of other antioxidants for thioproline may have greater effects, but this remains to be determined empirically.

Since defined total dietary or calorie (fat or carbohydrate) restriction regimens are sufficient to normalize PKC activity and ameliorate its downstream biologic consequences in SENCAR mice,[15,17-19,34] the present studies were undertaken to test the hypothesis that DR would prevent the development of metabolic bone disease if it were instituted during the critical period of the life span when metabolic bone disease developed. Long bones were analyzed by classical gravimetric and morphometric methods,[30,31] as well as by pQCT, which is extremely sensitive to regional changes in cortical and trabecular bone mass, volume, and density.[2] The results obtained in 16-week-old AL-fed SENCAR mice confirmed previous reports that bone growth slows or stops at about 10 weeks of age (Table 1) and that early-onset metabolic bone disease develops within weeks of achieving sexual maturity (Table 2).[1,31] When

Table 3. Serum Osteocalcin and Calcitonin Levels in 16-Week-Old SENCAR Mice

Parameter*	Dietary Group				ANOVA (P value),† DR Effect
	AL/−T	AL/+T	DR/−T	DR/+T	
Serum osteocalcin (ng/mL)	3.19 ± 0.40 (9)‡	3.46 ± 0.33 (9)‡	4.87 ± 0.71 (10)	3.82 ± 1.07 (10)	NS
Serum calcitonin (pg/mL)	83.9 ± 5.5 (9)‡	91.4 ± 14.3 (9)‡	214.9 ± 25.8 (9)§	175.9 ± 18.5 (8)§	.0001

*All experimental results are expressed as the mean ± SEM (n).

†All data for AL-fed and DR mice were subjected to ANOVA, with DR and antioxidant feeding as the major variables. No significant ($P < .05$) antioxidant effects or interactive effects between DR and antioxidant feeding were observed.

‡Hemolyzed samples were not assayed.

§There was not enough serum available to assay calcitonin in multiple dilutions in 3 mice.

assessed by pQCT, 16-week-old AL-fed SENCAR mice were found to have lower tibial total and trabecular bone mineral density (BMD) than 10-week-old t_0 controls (Table 2). Trabecular bone has a much larger surface area to volume ratio than cortical bone.[37-39] Since osteoclastic resorption occurs on the surfaces of bone, trabecular bone is much more labile to osteoclast-mediated imbalances in remodeling and bone loss than is cortical bone.[37-39] The novel observation that decrements in trabecular BMD, but not cortical BMD, are observed at an early age in SENCAR mice (Table 2) supports a major role for the osteoclast in the evolution of metabolic bone disease in this model.

Our findings also suggest that the effects of DR appear to vary depending on the type of bone (cortical *v* trabecular) examined and the sensitivity and selectivity of the method of analysis (gravimetric or morphometric *v* pQCT) employed (Tables 1 and 2). Specifically, 40% DR did not affect gross femoral morphometry (maximum external length and width) (Table 1), but it was associated with reduced cortical width, relative to 10-week-old control and 16-week-old AL-fed mice. Although the external dimensions of the femur were unchanged, the decrease in cortical width in DR mice resulted in lower femoral bone mass in DR mice than in t_0 control and AL-fed mice (Table 1). In conclusion, the observations that 40% DR did not prevent femoral bone loss (assessed gravimetrically as dry, fat-free and ash weights, or morphometically as cortical width) (Table 1) between 10 and 16 weeks of age in SENCAR mice appear to refute the initial hypothesis that DR sufficient to correct the underlying biochemical defect would also prevent bone loss. However, when the bones were analyzed by pQCT, 40% DR was associated with a relative conservation of tibial total and trabecular BMD that occurred at the apparent expense of cortical BMD (Table 2). The mechanisms by which DR effects the preservation of trabecular bone, relative to cortical bone, in SENCAR mice have not been determined. Diacylglycerol-regulated growth factor or growth factor receptor synthesis may be reduced by DR in SENCAR mice, thus reducing the rates of osteoclastogenesis and bone resorption, and preferentially preserving trabecular bone. This hypothesis could be tested in several ways. For example, the rate of bone metabolism (anabolism + catabolism) in AL-fed and DR SENCAR mice could be assessed by measuring bone resorption and formation markers in the blood and urine. The levels, rates of synthesis, and turnover of specific growth factors and growth factor receptors could be measured in vitro in osteoblast-enriched cultures or osteoblast and osteoclast cocultures derived from AL-fed and DR control (eg, C57BL/6 or DBA/2) and SENCAR mice. The rates of bone resorption in calvariae or long bones from AL-fed and DR control and SENCAR mice could be tested ex vivo in the absence or presence of vehicle, phorbol esters, diacylglycerol, or regulatory hormones, such as calcitonin or PTH.

DR was also associated with 2-fold increase in serum calcitonin levels (Table 3). Calcitonin is the calcitropic hormone that inhibits osteoclastic bone resorption and enhances urinary calcium reabsorption.[37] If PKC-mediated increases in GM-CSF,[24,25] IL-1,[28,29] superoxide and hydroperoxide[3-6] documented in nonskeletal tissues in SENCAR mice also induce osteoclastogenesis and osteoclast activation in bone, as suggested above, then the increased circulating calcitonin levels observed in DR mice may account for preservation of tibial total and trabecular BMD. However, further research will be required to determine the physiologic mechanism responsible for increased circulating calcitonin levels in DR SENCAR mice. In conclusion, more detailed and longer-term studies of bone and mineral metabolism, bone cell biology, and the hormonal regulation of bone remodeling in SENCAR mice will be required to determine the mechanistic bases for the development of metabolic bone disease and the beneficial effects of DR on total and trabecular BMD.

REFERENCES

1. Murray EJB, Murray SS, Grisanti M, et al: Effect of low dietary calcium on bone metabolism in the SENCAR mouse. J Orthop Res 15:585-592, 1997

2. Beamer WG, Donahue LR, Rosen CJ, et al: Genetic variability in adult bone density among inbred strains of mice. Bone 18:397-403, 1996

3. Fischer SM, Cameron GS, Baldwin JK, et al: Reactive oxygen in the tumor promotion stage of skin carcinogenesis. Lipids 23:592-597, 1988

4. Lewis JG, Adams DO: Divalent cation requirements for mounting a respiratory burst in response to phorbol diesters by macrophages from SENCAR and C57BL/6 mice. Chem Biol Interact 66:1-11, 1988

5. Sirak AA, Beavis AJ, Robertson FM: Enhanced hydroperoxide production by peripheral blood leukocytes following exposure of murine epidermis to 12-*O*-tetradecanoylphorbol-13-acetate. Carcinogenesis 12:91-95, 1991

6. Yoon HL, Marcus CB, Pfeifer RW: Induction of superoxide by 12-*O*-tetradecanoylphorbol-13-acetate and thapsigargin, a non-phorbol-ester-type tumor promoter, in peritoneal macrophages elicited from SENCAR and B6C3F1 mice: A permissive role for the arachidonic acid cascade in signal transduction. Mol Carcinog 7:116-125, 1993

7. Lewis JG, Adams DO: Inflammation, oxidative DNA damage, and carcinogenesis. Environ Health Perspect 76:19-27, 1987

8. Fischer SM, Baldwin JK, Jasheway DW, et al: Phorbol ester induction of 8-lipoxygenase in inbred SENCAR (SSIN) but not C57BL/6J mice correlated with hyperplasia, edema, and oxidant generation but not ornithine decarboxylase induction. Cancer Res 48:658-664, 1988

9. Czerniecki BJ, Witz G: Arachidonic acid potentiates superoxide anion radical production by murine peritoneal macrophages stimulated with tumor promoters. Carcinogenesis 10:1769-1775, 1989

10. Wei L, Wei H, and Frenkel K: Sensitivity to tumor promotion of SENCAR and C57BL/6J mice correlates with oxidative events and DNA damage. Carcinogenesis 14:841-847, 1993

11. Wei H and Frenkel K: Relationship of oxidative events and DNA oxidation in SENCAR mice to in vivo promoting activity of phorbol ester-type tumor promoters. Carcinogenesis 14:1195-1201, 1993

12. Slaga TJ, Budunova IV, Gimenez-Conti IB, et al: The mouse skin carcinogenesis model. J Invest Dermatol Symp Proc 1:151-156, 1996

13. Birt DF, Pelling JC, Tibbels MG, et al: Acceleration of papilloma growth in mice fed high-fat diets during promotion of two-stage skin carcinogenesis. Nutr Cancer 12:161-168, 1989

14. Birt DF, White LT, Choi B, et al: Dietary fat effects on the initiation and promotion of two-stage skin tumorigenesis in the SENCAR mouse. Cancer Res 49:4170-4174, 1989

15. Birt DF, Pelling JC, White LT, et al: Influence of diet and caloric

restriction on the initiation and promotion of skin carcinogenesis in the SENCAR mouse model. Cancer Res 51:1851-1854, 1991

16. Belury MA, Leyton J, Patrick KE, et al: Modulation of phorbol ester-elicited events in mouse epidermis by dietary n-3 and n-6 fatty acids. Prostaglandins Leukot Essent Fatty Acids 44:19-26, 1991

17. Birt DF, Kris ES, Choe M, et al: Dietary energy and fat effects on tumor promotion. Cancer Res 52:2035s-2039s, 1992 (suppl)

18. Birt DF, Pinch HJ, Barnett T, et al: Inhibition of skin tumor promotion by restriction of fat and carbohydrate calories in SENCAR mice. Cancer Res 53:27-31, 1993

19. Kris ES, Choe M, Luthra R, et al: Protein kinase C activity is reduced in epidermal cells from energy-restricted SENCAR mice. J Nutr 124:485-492, 1994

20. Birt DF, Barnett T, Pour PM, et al: High-fat diet blocks the inhibition of skin carcinogenesis and reductions in protein kinase C by moderate energy restriction. Mol Carcinog 16:115-120, 1996

21. Mouat MF, Locniskar MF: Dietary lipid varying in corn and coconut oil influences protein kinase C in phorbol ester-treated mouse skin. Nutr Cancer 30:108-117, 1998

22. Choe M, Kris ES, Luthra R, et al: Protein kinase C is activated and diacylglycerol is elevated in epidermal cells from SENCAR mice fed high fat diets. J Nutr 122:2322-2329, 1992

23. Imamoto A, Wang XJ, Fujiki H, et al: Comparison of 12-*O*-tetradecanoylphorbol-13-acetate and teleocidin for induction of epidermal hyperplasia, activation of epidermal PKC isozymes, and skin tumor production in SENCAR and C57BL/6 mice. Carcinogenesis 14:719-724, 1993

24. Updyke LW, Yoon HL, Pfeifer RW: Induction of granulocyte-macrophage colony-stimulating activity by 12-*O*-tetradecanoylphorbol-13-acetate in SENCAR and B6C3F1 mice. Carcinogenesis 12:735-739, 1991

25. Robertson FM, Bijur G, Oberyszyn AS, et al: Granulocyte-macrophage colony stimulating factor gene expression and function during tumor promotion. Carcinogenesis 15:1017-1029, 1994

26. Rho O, Beltran LM, Gimenez-Conti IB, et al: Altered expression of the epidermal growth factor receptor and transforming growth factor-alpha during multistage skin carcinogenesis in SENCAR mice. Mol Carcinog 11:19-28, 1994

27. Patamalai B, Burow DL, Gimenez-Conti I, et al: Altered expression of transforming growth factor-beta 1 mRNA and protein in mouse skin carcinogenesis. Mol Carcinog 9:220-229, 1994

28. Oberyszyn TM, Sabourin CL, Bijur GN, et al: Interleukin-1 alpha gene expression and localization of interleukin-1 alpha protein during tumor promotion. Mol Carcinog 7:238-248, 1993

29. Lee WY, Lockniskar MF, Fischer SM: Interleukin-1 alpha mediates phorbol ester-induced inflammation and epidermal hyperplasia. FASEB J 8:1081-1087, 1994

30. Murray EJB, Song MK, Laird EC, et al: Strain-dependent differences in vertebral bone mass, serum osteocalcin, and calcitonin in calcium-replete and -deficient mice. Proc Soc Exp Biol Med 203:64-73, 1993

31. Murray EJB, Song MK, Laird EC, et al: Heterogeneity of growth and turnover in the femurs and humeri of calcium-replete and -deficient C57BL/6 and SENCAR mice at sexual maturity. Growth Dev Aging 58:119-133, 1994

32. Bar-Shira-Maymon B, Coleman R, Cohen A, et al: Age-related bone loss in lumbar vertebrae of CW-1 female mice: A histomorphometric study. Calcif Tissue Int 44:36-45, 1989

33. Kahn A, Gibbons R, Perkins S, et al: Age-related bone loss: A hypothesis and initial assessment in mice. Clin Orthop 313:69-75, 1995

34. Birt DF, Copenhaver J, Pelling JC, et al: Dietary energy restriction and fat modulation of protein kinase C isozymes and phorbol ester binding in Sencar mouse epidermis. Carcinogenesis 15:2727-2732, 1994

35. de la Fuente M, Ferrandez D, Munoz F, et al: Stimulation by the antioxidant thioproline of the lymphocyte functions of old mice. Mech Ageing Dev 68:27-36, 1993

36. Termine JD, Gehron Robey P: Bone matrix proteins and the mineralization process, in Fauvus M (ed): Primer on the Metabolic Bone Diseases and Disorders of Mineral Metabolism. (ed 3). Philadelphia, PA, Lippincott Williams & Wilkins, 1996, pp 24-28

37. Strewler GJ, Rosenblatt M: Mineral metabolism, in Felig P, Baxter JD, Frohman LA (eds): Endocrinology and Metabolism (ed 3). New York, NY, McGraw-Hill, 1995, pp 1407-1516

38. Parfitt AM: Bone remodeling and bone loss: Understanding the pathophysiology of osteoporosis. Clin Obstet Gynecol 30:789-811, 1987

39. Mundy G: Bone remodeling, in Fauvus M (ed): Primer on the Metabolic Bone Diseases and Disorders of Mineral Metabolism. (ed 4). Philadelphia, PA, Lippincott Williams & Wilkins, 1999, pp 30-38

40. Suda N, Morita I, Kuroda T, et al: Participation of oxidative stress in the process of osteoclast differentiation. Biochim Biophys Acta 1157:318-323, 1993

Bikle D, Majumdar S, Laib A, Powell-Braxton L, Rosen CJ, Beamer WG, Nauman E, Leary C and Halloran B. 2001. The skeletal structure of insulin-like growth factor-I deficient mice. J Bone Miner Res. **in press** Fall 2001.

Growth Hormone & IGF Research 2000, **Supplement B**, S103–S105

Insulin-like growth factor I and bone: from mouse to man

W. G. Beamer[1], L. R. Donahue[1] and C. J. Rosen[1,2]

[1]The Jackson Laboratory, Bar Harbor, and [2]Maine Center for Osteoporosis Research and Education, St Joseph Hospital, Bangor, Maine, USA

Summary Serum insulin-like growth factor I (IGF-I) is regulated by numerous variables, including growth hormone (GH), nutritional status, gonadal steroids and other hormones. However, the circulating IGF-I phenotype is also under heritable regulation, and several genetic determinants may be important in defining tissue-specific expression of the gene encoding this peptide. A very strong correlation has been found between serum IGF-I concentration and bone acquisition in both mice and humans. Based on previous studies as well as ongoing work with mice, it has been hypothesized that regulation of the serum IGF-I phenotype includes non-GH-dependent factors and, furthermore, that these determinants are also involved in the acquisition of bone mass. This paper reports that, by performing intercrosses between two inbred strains of mice of similar age, size and length, but with different serum levels of IGF-I, we have identified regulatory loci for serum IGF-I and established their relationship to putative quantitative trait loci for bone mineral density. Mapping these quantitative trait loci will help refine our understanding of disorders related to IGF-I.

Key words: Bone mineral density, genes, insulin-like growth factor I.

INTRODUCTION

Insulin-like growth factor I (IGF-I) is a ubiquitous polypeptide synthesized by virtually all cells of the body. IGF-I also circulates in large quantities bound to a series of six IGF-specific binding proteins (IGFBPs). Serum levels of IGF-I mirror tissue levels in certain disorders such as growth hormone (GH) deficiency states and acromegaly[1]. With advancing age, serum levels of IGF-I decline significantly, as do tissue levels in cortical and trabecular bone[2]. Moreover, recent epidemiological studies have suggested that serum IGF-I concentration reflects the rate of epithelial turnover and may be considered a surrogate for the potential risk of cancer of the prostate, breast and colon[2]. Hence, understanding the regulation of serum IGF-I levels is essential to defining the role of this peptide in several disorders, including osteoporosis, heart disease and malignancy.

GH is the principal regulator of hepatic *IGF-I* gene expression, although malnutrition and metabolic imbalances can depress the production of IGF-I[3]. Still, the majority of circulating IGF-I is synthesized in the liver. However, the skeleton is also a major depot for the IGFs, and it is likely that there is a relationship between the skeletal and serum concentrations of these peptides[4]. Even among healthy individuals of the same age and stature, serum IGF-I levels can vary by a factor of 5. The reasons for this disparity are not entirely clear, but recent studies in humans have demonstrated a strong heritable component to the serum IGF-I phenotype[5]. Studies in inbred strains of mice also reveal characteristic differences in serum IGF-I levels, despite similarities in body size, shape and length[4]. Because there are also genetic differences in the peak rate of bone acquisition, which occurs during a time of enhanced GH activity (hence peak serum IGF-I concentration), several investigators have suggested there must be a relationship between the genetic determinants of each phenotype. We have hypothesized that the serum IGF-I phenotype is under the regulation of several non-GH-dependent heritable factors, and these determinants may also be important for the acquisition of peak bone mass. Hence, using healthy inbred strains of mice, we have developed a strategy to map quantitative trait loci (i.e. the genetic factors) that regulate the serum IGF-I phenotype.

Correspondence to: C. J. Rosen, Maine Center for Osteoporosis Research and Education, St Joseph Hospital, 360 Broadway, Bangor, ME 04401, USA. Tel: +1 207 262 1176; Fax: +1 207 262 2060; E-mail: kershjcd@mint.net

1096–6374/00/030103+03 $35.00/0

Table 1 Quantitative trait loci for serum IGF-I concentration and femoral BMD

Quantitative trait loci for IGF-I			Quantitative trait loci for BMD		
Chromosome	MIT marker	*P*	Chromosome	MIT marker	*P*
1[a]	215–416	1×10^{-4}	1[a]	416	3×10^{-15}
4	124–187	5×10^{-5}	4[a]	187	2×10^{-10}
6[a]	93	6×10^{-6}	6	93	4×10^{-4}
6[a]	124–150	1.2×10^{-5}	6[a]	124	4×10^{-4}
			11	242	3×10^{-4}
12	233	5×10^{-5}			
			13	13	3×10^{-5}
			14	62	4×10^{-4}
			18[a]	36	4×10^{-5}

[a]Quantitative trait loci contributing > 5% of variance for IGF-I or BMD

MATERIALS AND METHODS

Serum IGF-I concentration is 35% higher in 4-month-old C3H/HeJ mice than in C57BL6 mice of similar age and size[4]. This difference exists across all age groups and genders. Similarly, bone mineral density (BMD), measured by peripheral quantitative computed tomography (QCT) of the femur, differs by the same magnitude between these two inbred strains[6]. Hence, we performed intercrosses between 4-month-old male C57BL6 mice and 4-month-old female C3H/HeJ mice to produce F1 heterozygotes. These F1 mice were then intercrossed to yield F2 mice. A total of 636 F2 female mice were studied using the following methodology.

Genotyping

Genomic DNA from the kidneys and spleen of all 636 animals was analysed. Polymerase chain reaction amplification was performed using oligonucleotide primer pairs (Research Genetics, Huntsville, Alabama, USA) to identify highly polymorphic microsatellite allelic variance between C57BL6 and C3H/HeJ mice.

Phenotyping

Serum IGF-I from all 636 animals was evaluated by radioimmunoassay after acid–ethanol cryoprecipitation to remove residual IGFBPs[4]. To correct for interassay variation, pools of B6 and C3 progenitor strains were assayed during each run as a standard.

Bone mass measurements

BMD was measured by peripheral QCT of the mid-shaft of the femur in all 636 animals. Previous studies have demonstrated a coefficient of variation of 0.6% for measurements at this site[6].

Association

Associations between the serum IGF-I phenotype and the genotype of the F2 mice were assessed using MATLAB and MapMaker QTL computer software (Mathworks, Natick, Massachusetts, USA), and 107 MIT genetic markers were examined. Statistical significance was defined as *P* values of less than 0.0001. Correlations between serum IGF-I concentration and femoral BMD were determined by simple Pearson's correlation coefficients. Results are presented as means ± SEM.

RESULTS

In the 4-month-old progenitor strains (11 C3H mice, 13 B6 mice), the mean IGF-I serum levels of the two strains differed by approximately 30% (C3H mice, 415 ± 19 μg/l; B6 mice, 300 ± 13 μg/l; $P < 0.0001$). In the 636 F2 mice, the mean serum IGF-I level was 360 ± 5 μg/l (range, 187–634 μg/l). The distribution of serum IGF-I levels in the F2 mice was Gaussian. Serum IGF-I level correlated with femoral BMD, as measured by peripheral QCT, and accounted for 10% of the variance in BMD ($r = 0.30$, $P < 0.0001$). Analysis of the entire genome identified three putative quantitative trait loci with *P* values less than 0.0001, according to the criteria of Lander and Kruglyak[7]: one on chromosome 1 and two on chromosome 6. Table 1 identifies the other loci that were statistically significant for the IGF-I phenotype and delineates the major quantitative trait loci for the BMD phenotype. The three major loci for serum IGF-I concentration are also shared with quantitative trait loci for BMD, although the strength of the association varied for each trait.

While none of the tentative loci for the IGF-I phenotype mapped to the locus of the gene encoding GH or GH-releasing hormone (GHRH), one of the chromosome 6 loci is in the region of the gene locus for the GHRH receptor. However, the major quantitative trait loci for

serum IGF-I is located between MIT markers 124 and 150 on chromosome 6. This region is approximately 4 centimorgans. One of the candidate genes in this area is the gene that encodes Raf-1, a serine threonine kinase that is essential in the signalling pathway for MAP kinase. GH, IGF-I and other growth factors signal through this pathway and activate Fos and Jun as well as other peptides that enhance cell proliferation.

DISCUSSION

In this study, we have defined several quantitative trait loci for the serum IGF-I phenotype. These putative regions are also shared by the femoral BMD phenotype. In addition, for all the F2 mice studied, serum IGF-I level closely correlated with bone mass. These lines of evidence suggest that there is a link between IGF-I concentration and bone mass. Previous studies have suggested there is a relationship between IGF-I and BMD, and this study provides further evidence for this relationship and implies there may be shared genetic determinants of these two phenotypes[8,9]. More importantly, this study also suggests there must be non-GH-dependent factors that regulate the expression of genes encoding IGF-I. Although it has long been known that parathyroid hormone and other cyclic AMP analogues can induce expression of the gene encoding IGF-I in bone, these data suggest there must be other factors that presumably regulate hepatic IGF-I synthesis[10].

In the two progenitor mice strains, serum IGF-I concentrations differ by a significant magnitude, yet the levels of GH secretion, GH-binding protein and the IGFBPs do not differ. Very recently, we have shown that, in mutant *lit/lit* GHRH receptor-deficient mice in which the background strain has been switched from C57BL6 to C3H but the phenotype of a little mouse is maintained, hepatic transcription of the gene encoding IGF-I is enhanced four-fold, despite the absence of GH. This finding suggests there are genetic determinants in C3H mice that regulate transcription of *Igf-I* but are independent of GH. Our strategy of mapping quantitative trait loci may provide important new information about potentially novel transcription factors.

In summary, we have defined several quantitative trait loci for the IGF-I phenotype. These putative loci may also be important in the acquisition of peak bone mass in mice. Further studies should definitely map these regions as well as any interactive loci, and could produce candidate genes for transgenic or knockout studies.

ACKNOWLEDGEMENTS

This work was funded by a grant from the National Institutes of Health (AR45433).

REFERENCES

1. Donahue LR, Rosen CJ. IGFs and bone: the osteoporosis connection revisited. Proc Soc Exp Biol Med 1998; 219: 1–7.
2. Donahue LR, Hunter SJ, Sherblom AP, Rosen CJ. Age-related changes in serum insulin-like growth factor binding proteins in women. J Clin Endocrinol Metab 1990; 71: 575–579.
3. Thissen JP, Ketelslegers JM, Underwood LE. Nutritional regulation of the insulin-like growth factors. Endocr Rev 1994; 15: 80–101.
4. Rosen CJ, Dimal HP, Vereault D *et al.* Circulating and skeletal insulin-like growth factor-I (IGF-I) concentrations in two inbred strains of mice with different bone mineral densities. Bone 1997; 21: 217–223.
5. Kao PC, Matheny AP, Lang CA. IGF-I comparisons in healthy twin children. J Clin Endocrinol Metab 1994; 78: 310–312.
6. Beamer WG, Donahue LR, Rosen CJ, Baylink DJ. Genetic variability in adult bone density among inbred strains of mice. Bone 1996; 18: 397–403.
7. Lander E, Kruglyak L. Genetic dissection of complex traits: guidelines for interpreting and reporting linkage results. Nat Genet 1995; 11: 241–247.
8. Langlois JA, Rosen CJ, Visser M *et al.* The association between IGF-I and bone mineral density in women and men: the Framingham heart study. J Clin Endocrinol Metab 1998; 83: 4257–4262.
9. Cadogan J, Blumsohn A, Barker ME, Eastell R. A longitudinal study of bone gain in pubertal girls: anthropometric and biochemical correlates. J Bone Miner Res 1998; 13: 1602–1612.
10. Rosen CJ, Pollak MF. IGF-I and aging: a new perspective for a new century. Trends Endocrinol Metab 1999; 10: 136–142.

Ms Patricia Modrow,
Grant Officer's Representative
Fort Detrick,
Frederick MD 21702-5012

31 August 2000

RE: Grant number DAMD17-96-1-6306
Request for extension and supplement
Title: "Genetic and morphometric analyses of bone density, a polygenic trait"
PI: Wesley G. Beamer, PhD

Request

The above US Army grant co-sponsors our bone genetics program in conjunction with NIH AR43618. We have requested a 12 month no-cost extension, while our application for renewal of the NIH program support is reviewed by the NIAMS review system. This is a request for a companion extension for DAMD17-96-1-6306, and for consideration of a supplement for equipment specifically to capitalize on existing progress in our bone program.

The Bone Program at The Jackson Laboratory

The Jackson Laboratory is a not-for-profit biomedical research institution specializing in genetic studies utilizing inbred and mutant gene-bearing strains of laboratory mice for investigation of biomedical problems. Major human health problems currently being studied are cardiovascular disease, hematologic disorders, cancer, immunology, neurological disorders, reproductive disorders, diabetes and adiposity, dermatologic disease, and prenatal developmental errors.

Rationale for Analyses of Bone Mineral Density and Strength Genes

In humans, peak bone density is essentially completed at the end of the second decade of life after pubertal growth ceases and adult rates of bone turnover have been established. When an adult acquires a low peak bone density, this is recognized as a risk factor for osteoporotic fracture in the elderly. Genetic factors that each individual possesses orchestrates the effect of exogenous and endogenous factors leading to the final adult bone status. Although studies have shown that 60-70% of the normal variability in bone mineral density is genetically determined, identifying genes participating in maintenance of normal skeletal mass is in a rudimentary state.

With the timely assistance of the US Army financial support provided by DAMD17-96-1-6306, we have developed a unique program in bone and osteoporosis as a powerful addition to the Institution's repertoire of scientific endeavor. The bone program focuses on four areas of genetic regulation: 1) bone mineral density, 2) IGF-I, 3) bone size, and 4) bone strength. Inbred strains of mice represent excellent systems for genetic analyses of polygenic traits such as bone density, because within each strain all genetic loci are homozygous, while matings between strains allow unambiguous correlation between phenotype and genotype. Highlights of current genetic studies with animal models include: 1) definition of proportion of bone density regulated by genes is remarkably similar to human twin studies (~70%); 2) location of approximately 14 genes participating in density ; 3) successful isolation of 10 density regulatory loci in congenic strains; 3) distinct regulatory loci also demonstrable for bone strength and geometry; 4) regulation of serum Insulin-like Growth Factor-I (important in bone formation) by 4 loci - at least one gene common to density regulation; 5) mineral packing density properties, as well as biochemical correlation of bone formation and resorption markers with specific genes are emerging; and 6) very few known candidate genes are associated with normal regulation of bone density or strength. This latter point means that many new genes are being identified and much hard work lies ahead.

Instrumentation request

Continued pursuit of fundamental advances in locating genes, mapping, and sequencing, requires the full combination of today's technology in the bone field. Essential to further genetic analyses is the instrumentation to accurately measure the subtle phenotypes associated with gene-induced changes in bone formation and resorption. Three specific instruments have been identified with technological

characteristics that will facilitate additional progress on genetic analyses of bone density and strength at The Jackson Laboratory. There instruments are synopsized as follows:

• *Bone Histomorphometry.* Undecalcified bone sectioning instrumentation consists of the model 300 CP band (saw) system and the model 400 CS grinding system from EXAKT Technologies, Inc., (Dallas, TX; Instruments made in Hamburg, Germany). This instrument permits examination of bone at the cellular level. Cost: approximately $90,000. This equipment is designed and intended to address the static (single point in time) and dynamic (changes with time) patterns of biochemically active sites in bone. Typically experimental animals are treated with tetracycline compounds that are rapidly deposited with mineral in bone; these compounds fluoresce under polymerized UV light. The advantage of histomorphometry is accurate assessment in a 2-dimensional plane of dynamic changes in bone formation and bone resorption via measurements of amount of mineral deposited, specific bone surface mineralized, and bone formation rates. Accomplishment of these objectives requires specialized equipment designed to cut and polish undecalcified bone sections that are approximately 50 microns in thickness. Serial sections, however, are not practical.

• *Micro computerized tomography.* MicroCT 20 manufactured by SCANCO Medical AG (Scanco USA, Inc.; Bern, Switzerland). Cost: approximately $150,000 per recent quote. This instrument has a detection resolution of approximately 17 micrometers. This is more than sufficient to visualize bone at the trabecular as well as cortical level, permitting assessment of properties of shape, thickness, connectivity, volumes, etc. Routinely, this instrument obtains user defined, multiple serial scans of individual bones that can be assembled in 3-dimensional reconstructions to demonstrate the actual structure and geometry of bone specimens. Data on structure and geometry are crucial for interpretation of experiments aimed at how mineral density, geometry, and quality related to the overall property of bone biomechanical strength.

• *Skeletal phenotyping by whole body computer assisted tomography.* MicroCAT manufactured by ImTek, Inc. (Knoxville, TN 37939) This instrument produces 3-dimensional transverse images of the body of small experimental animals (such as mice) at any plane desirable. Cost of system components: approximately $180,000. The instrument produces an image with 50 mm diameter, with a resolution of 50 micrometers. The value of this instrument is that it will be possible to detect skeletal aberrations at the whole bone level with a high through put. This will greatly facilitate the detection of mutant gene actions on bone parameters such as number of vertebrae, cross-section size, joint configurations, etc. Given that multiple 'slices' with the MicroCAT are user defined, available software will permit 3-dimensional reconstruction of any portion of the skeleton shown to be of special interest.

Publications from our group and close collaborators are contributing to a broader understanding of normal bone, in addition to goals of identifying new genes through studies of spontaneous models of skeletal aberrations caused by mutant genes. In short, we are poised to link our genetic findings with specific phenotypes measured by the above technologies to gain the insights to biochemical mechanisms responsible for maximal density, strength, shape, and growth of bone. We would appreciate any consideration for possible supplement toward acquiring these technologies. Without question, such would accelerate our ability to pursue the functional relevance needed to apply our newly discovered genetic insights to bone biology.